CRANFIELD UNIVERSITY

SCHOOL OF MECHANICAL ENGINEERING

PhD THESIS

Academic Year 1994 to 1995

Peter David Smout

THE MEASUREMENT OF NEAR WALL FLOWS USING PNEUMATIC WEDGE PROBES

Academic Supervisor: P C Ivey
Industrial Supervisor: P Loftus

January 1995

VOLUME CONTAINS CLEAR OVERLAYS

OVERLAYS HAVE BEEN SCANNED SEPERATELY AND THEN AGAIN OVER THE RELEVANT PAGE

ABSTRACT

The three hole, wedge-type pneumatic pressure probe represents a robust traverse probe design which is widely used for total and static pressure and yaw angle measurements in turbomachinery. However, unsteady flows are incorrectly averaged due to pneumatic meaning errors in the pressure pipes. Wedge probes also fail to measure the correct static pressure when operating in close proximity to a wall through which the probe is inserted. Thirdly, the aerodynamic calibration obtained for a wedge-type probe in a closed wind tunnel differs appreciably from that obtained in an open jet. If not corrected, these errors will corrupt any calculation of turbomachinery blade row performance.

In this investigation, the second and third effects described above have been addressed. A factorial experiment was completed in which the influence of seven variables on the wall proximity effect was quantified. Flow visualisation studies were performed to understand the responsible flow mechanisms. Two regions of re-circulating flow were identified in the probe wake, the structure of which depended on the probe immersion. Similar re-circulatory flows were resolved from three-dimensional computational fluid dynamics (CFD) calculations of the flow over a wedge probe. A link between the probe wake re-circulations and flow over the wedge faces was established. Based on this understanding of the flow structures, a model was developed from which the wall proximity effect could be predicted for a given set of conditions.

Wedge probe calibrations were completed in a closed wind tunnel and in two open jets. Discrepancies in the static pressure coefficient and yaw angle sensitivity results were found. These were partially explained in terms of modifications to the probe wake structure which occurred when the probes were calibrated in the open jet facilities. Procedures for correcting the wall proximity effect and for avoiding the facility dependence of wedge probe calibrations were developed from this understanding of the flow mechanisms involved.

Based on the findings of this investigation, a novel wedge probe was designed to minimise the wall proximity effect. This probe demonstrated a reduction in the wall proximity effect, from 20% dynamic head with current designs, to 3% dynamic head at flows typical of high speed turbomachinery.

ACKNOWLEDGEMENTS

The author wishes to thank Dr. S. C. Cook and Dr. J. W. H. Chivers for the original encouragement to pursue this investigation, and Professor R. L. Elder for his support throughout the project. Particular thanks go to Dr. P. Ivey and Mr. P. Loftus for their supervision on a day-to-day basis, and to all members of the Total Technology PhD support panel.

The author is grateful to his local and senior management at Rolls-Royce for the opportunity and funding to pursue this work as a three year Ph.D. Financial support from the E.P.S.R.C. is also acknowledged. The advice and support of the author's colleagues at Rolls-Royce has been greatly appreciated on many occasions. Particular thanks go to Mr. C. Haxell for his assistance with the laser anemometry work, and to Dr .J. Northall and Dr. L. Lapworth for their advice and interest in the CFD calculations. Expert assistance was also received from the Rolls-Royce photographic department. This, together with the support of technicians at Rolls-Royce, Cranfield University and Sheffield University, contributed significantly to the success of this project.

The author would like to thank his family and friends for their encouragement throughout the study. The selfless support of the author's wife Sara has been unfailing throughout, and is most gratefully acknowledged.

CONTENTS **PAGE**

LIST OF TABLES

LIST OF PLATES

LIST OF FIGURES

NOMENCLATURE

			UNITS
A	-	Frontal area of wedge head	-
B	-	Probe static pressure coefficient (=$(S_m-p_s)/(p_t-p_s)$)	-
B2	-	Probe static pressure coefficient for left hand tapping, S2	-
B3	-	Probe static pressure coefficient for right hand tapping, S3	-
BCR	-	Benefit Cost Ratio	-
c	-	Wedge head chord	-
C	-	Local speed of sound	m/s
C_D	-	Drag coefficient	-
C_t	-	Probe total pressure coefficient (=$(P1-p_t)/(p_t-p_s)$)	-
C_{yaw}	-	Probe yaw angle coefficient (=$(S2-S3)/(p_t-p_s)$)	-
d	-	Probe stem diameter	m
F	-	Scaling factor	-
F_D	-	Drag force	N
h	-	Height of wedge head	m
H	-	Four stage rig annulus height	m
i	-	Cylindrical stem immersion from wall of introduction	m
I	-	Probe immersion from wall of introduction	m
k	-	Dynamic pressure head scaling factor	-
l	-	Length of probe interface piece	m
L	-	Length of wedge face	m
p	-	Pressure measured in calibration tunnel	Pa
P1	-	Pressure indicated by probe total pressure tapping	Pa
q	-	Forced vortex tangential velocity	m/s
r	-	Forced vortex radius	m
S2	-	Pressure indicated by probe left hand static tapping	Pa
S3	-	Pressure indicated by probe right hand static tapping	Pa
S_m	-	(S2+S3)/2	-
v	-	velocity	m/s
x	-	Distance back over wedge face from leading edge	m

X	-	Distance back from boundary layer transition point	m
y	-	Displacement of static tappings from probe end	m
24LF	-	24° wedge probe, long interface piece, fillet fitted	-
24LS	-	24° wedge probe, long interface piece, no fillet fitted	-
24SF	-	24° wedge probe, short interface piece, fillet fitted	-
24SS	-	24° wedge probe, short interface piece, no fillet fitted	-
30MS	-	30° wedge probe, medium interface piece, no fillet fitted	-

Greek Symbols

α	-	Wedge probe included angle	°
γ	-	Ratio of specific heats	-
δ	-	Boundary layer thickness	m
ε	-	Wedge probe semi-included angle	°
ρ	-	Density	kg/m^3
ω	-	Rotational speed of forced vortex	rad/s

Subscripts

bc	-	Value of parameter at base of cylinder
bw	-	Value of parameter at base of wedge head
c	-	Value of parameter in wake of cylinder
ce	-	Equilibrium value of parameter in wake of cylinder
LE	-	Value at leading edge
o	-	Free stream value
s	-	Static value
t	-	Total value
w	-	Value of parameter in wake of wedge head
we	-	Equilibrium value of parameter in wake of wedge head
WF	-	Value at wedge face

CHAPTER 1: INTRODUCTION

1.1 BACKGROUND

The popularity of the gas turbine engine, both as an industrial power unit and as an aircraft propulsor, owes much to the pioneering work of Whittle, whose turbo-jet engine first flew in 1941, (Rolls-Royce, 1969). Although the concept of using a reaction jet had interested aircraft engineers at least since the early design of Rene Lorine in 1913, progress was hampered by the available technology, and the competing requirements for low weight, high reliability and optimum efficiency. Whittle effectively demonstrated that the gas-turbine was viable as an aircraft power unit, and engines based on similar thermodynamic cycles are still being developed today.

Essential in this development process is an ability to measure the condition of the mechanical components to ensure design integrity. Equally important is an accurate knowledge of the working fluid properties at various positions throughout the engine. As the gas-turbine has been developed to operate at higher temperatures, pressures and gas velocities, so the available measurement techniques have had to be developed. The highly competitive nature of today's aeroengine market demands that the fuel efficiency and performance of a given engine design be optimised; this requirement makes further demands of the aerodynamic instrumentation in terms of high accuracy.

The high by-pass ratio, triple spool gas turbine engine produced by the author's company, Rolls-Royce plc for the civil aeroengine market, and pictured in figure 1.1, exemplifies the complexity of design and technology which is now incorporated by the major producers world-wide. Mechanical and aero-thermal testing of the component parts of such engines is essential in quantifying the individual performance of each component, and in understanding the overall engine performance. Within Rolls-Royce, compressor and turbine rig testing forms an integral part of a new engine development programme. This is a cheaper approach to turbomachinery development than exclusive

testing of the whole engine. It also simplifies the application of measurement techniques, and can present a less harsh environment, particularly for measurements in the turbine.

The measurement requirements depend on the type of turbomachine, and on the purpose of the test. Where the overall machine performance is required, inlet and exit total temperature and pressure measurements are usually made using radially supported arrays, or rakes, of sensors at various circumferential positions. A shaft torquemeter (compressor) or dynamometer (turbine) may be used to measure the work input or extracted from the machine respectively. This can be combined with a measure of the inlet massflow to calculate the temperature change through the machine. Where the performance of individual blade rows or stages of a multi-stage machine are needed, then the gas properties up and downstream of the blade row in question must be determined by traversing the annulus with a suitable probe. The stage efficiency and reaction can then be calculated, and compared with other stages in the machine. Adjustments to optimise matching at design and off-design conditions, either by changing the blading completely or by varying stator blade setting angles, are then possible.

1.2 PRESSURE PROBES IN TURBOMACHINERY RIG TESTING

The earliest aerodynamic traverse probes for turbomachinery application drew heavily on wind tunnel probe design practices of the time. They included pitot tubes for total pressure measurement, a variety of differential pressure measuring devices for yaw and pitch angle determination, and probe mounted thermocouples or resistance temperature devices for total temperature sensing. The narrow confines of turbomachinery passages lead to miniaturisation, and the combination of several sensors into a single probe head. The literature contains much research into both the sensor technology and the aerodynamic characteristics of such probes, as summarised by Bryer and Pankhurst (1971).

Figure 1.2 shows three widely used types of combination probe, namely the cylindrical, cobra and wedge-type designs. All are intended to measure total and static pressure and yaw angle using three air-filled pressure lines. Total pressure is measured by the centre tapping when facing directly into the prevailing flow. This is achieved by rotating the probe until the pressures read from the two outer tappings are equal, whereupon the probe is said to be 'nulled'. Static pressure is then inferred from the side tappings via an aerodynamic calibration, and yaw angle is taken to be the probe setting angle relative to the rig axis. Alternatively, the probe setting angle can be fixed, and the required parameters inferred from the three individual pressure readings via a probe calibration. There is no provision for measuring pitch angle. Although the principal of operation is the same for each probe, their geometrical differences result in distinct characteristics. The requirements are for a mechanically robust probe the calibration of which is insensitive to mechanical damage and to changes in the prevailing flow conditions. Although less compact than the cobra probe, previous investigators have found that the wedge-type probe design generally meets these requirements, and many applications of wedge probes for turbomachinery research are reported in the literature.

Because pneumatic pressure probes rely on long lengths of pipe to transmit pressures sensed in the test vehicle to remote pressure transducers, such probes have a response time described by a primary time constant of several seconds, depending on the detailed geometry. The measured pressure is therefore a pneumatic average of the highly unsteady pressure field characteristic of turbomachinery flows. In recent years it has become necessary to measure these pressure fluctuations directly in order to understand the unsteady loss generating mechanisms which currently limit turbomachinery efficiency levels. The wedge probe has proved a suitable vehicle for achieving this, by installing miniature pressure transducers into the wedge faces in order to resolve the time-dependent pressure variations. A review of this work is given in section 4.4.

However, it is also clear from the literature, and from studies undertaken within Rolls-Royce, that the performance of wedge-type pressure probes even in steady flow is compromised in two ways. Firstly, wedge-type probes fail to sense the correct static

pressure when operating in close proximity to a wall through which the probe is introduced, yet well outside the boundary layer. Figure 1.3 is taken from Cook (1988), and shows the experimentally determined variation in static pressure coefficient, B, with immersion from the wall of introduction for four wedge probes with different wedge head included angles. Static pressure coefficient is defined as the difference between probe indicated static pressure, S_m, and actual free stream static pressure, p_s, non-dimensionalised by the dynamic pressure head (p_t-p_s). Immersion, I, is defined as the distance from the probe tip to the wall through which the probe is inserted, and is non-dimensionalised by the probe stem diameter, d. In general, the static pressure coefficient decreases monotonically with increasing immersion until a plateau is reached at a negative value of B. This implies that, in each case, the static pressure indicated by the probe is less than the free stream static pressure. The shape of the curve and the level of the plateau depends on the probe wedge head included angle, α. This effect was reviewed by the author (Smout, 1990) and is termed the wall proximity effect. Because the determination of gas velocity at a given plane in a turbomachine relies on an accurate knowledge of the free stream static pressure at that plane, the velocities, and hence the blade loading and reaction calculated in the near wall region are thought to be compromised by the wall proximity effect.

Secondly, the aerodynamic calibration of a given wedge probe performed in a closed section wind tunnel may differ significantly from that conducted in an open jet, (Fransson, 1983). Errors may be introduced into both static pressure and yaw angle measurements in consequence.

Alternative designs of static pressure probe are discussed in the literature, and illustrated in figure 1.4. The Prandtl probe, (Prandtl et al., 1934), comprises a tube bent through 90°, the upstream end of which is closed in a semi-elliptical form, (figure 1.4a). A ring of pressure tappings is judiciously placed so that the probe nose and stem effects cancel, giving a direct static pressure reading. This approach was developed by Smith and Bauer (1970), who used potential flow theory to re-design the probe head cross-section, (figure 1.4b). They experimentally demonstrated probes for which the

indicated static pressure was independent of incidence angle and Mach number within useful limits. Needle probes (Huey, 1978) and disc probes (Walshe et al., 1960) are shown in figures 1.4c) and 1.4d) respectively. Both comprise multiple tappings symmetrically arranged and manifolded into a single internal cavity. The design intent is that tappings on opposite sides of the probe will compensate for each other if the probe is yawed or pitched into the flow. In practice, significant incidence and turbulence sensitivity resulting from three-dimensional flow effects is reported. Finally, Rossow (1991) reports on a probe system shown in figure 1.4e) which aims to deliver the correct time-averaged static pressure in laminar or turbulent flow by summing the various contributions from several probe heads.

However, 95% of all turbomachinery traversing undertaken at Rolls-Royce involves inserting the probe through a hole or slot 6.35mm wide in order to access the narrow rotor/stator gaps typical of such machines. None of the probe designs above offer a viable alternative to the miniaturised cobra or wedge probes for static pressure measurement in these situations. Given the company's commitment to both steady-state and dynamic embodiments of the wedge-type probe, together with the advantages given above, a research programme aimed at overcoming the wall proximity effect and calibration facility dependence of wedge-type probes was considered necessary to realise the true potential of this type of probe for both steady and unsteady flow measurements in turbomachinery.

1.3 DEFINITIVE PROJECT OBJECTIVES

Based on the arguments above, a set of four definitive objectives were defined for the project. These are stated below:

i) An investigation of the 'wall proximity effect' experienced with three hole wedge probe designs, in order to understand the physical mechanisms responsible for this phenomena.

ii) The removal of 'wall proximity effects', either through probe re-design, and/or through the derivation of suitable calibration methods.

iii) Insight in to the physical cause of differences frequently experienced between aerodynamic calibrations of a given three hole wedge probe, one conducted in a bounded flow and the other in an open jet.

iv) The elimination of such differences through both probe re-design and the specification of an appropriate aerodynamic calibration methodology.

In addition, to avoid potentially extensive modifications to existing turbomachinery, it was required that any re-design of probe must still be contained within a cylindrical envelope of 6.35mm diameter, and be sufficiently rugged to survive the arduous environment of a turbomachine test, including exposure to temperature, vibration, air-borne particulates, and minor mechanical impact through handling. These objectives were established from the start of the project, and it was always recognised that they were targets to be aimed at, rather than goals that would necessarily be achieved. Because the background information available on wall proximity effects was limited at the project launch, more specific and quantified objectives could not realistically be set at this stage.

1.4 DESIGN OF THE INVESTIGATION

An investigation was planned in which experimental and numerical methods were applied in parallel to realise the project objectives. The structure of this dissertation reflects the major elements of this plan, and is now described.

Chapter 2 considers in detail the economic justification for the project. A detailed cost benefit analysis is given, based on the assumption that all of the project objectives would be achieved in full. Recognising that research projects of this nature are inherently

'high-risk', the cost benefit analysis is then revised to include a critical assessment of the risks associated with the research work. This process is documented, and includes a review of risk analysis techniques found in the literature, together with recommendations for the routine application of risk analysis to projects undertaken within the author's department at Rolls-Royce. Details of the project management process, including sections on planning, resource management, documentation and communication are given in Chapter 3. Chapters 2 and 3 are included in fulfilment of the Total Technology PhD scheme requirements.

A thorough review of relevant work reported in the open literature, and undertaken within Rolls-Royce, was completed at project launch. This is included as chapter 4, and concentrates on the two specific effects addressed by this thesis, namely the wall proximity effect and the calibration facility dependence of wedge-type probes. A general overview of the performance of wedge probes, and how this depends on the detailed probe geometry and prevailing flow conditions, is also given.

From the review of previous work, it was clear that the wall proximity effect was influenced by the probe shape, by the prevailing flow conditions, and by the way in which the probe was presented to the flow. Because the background information was limited, and because turbomachinery flows are typically complex, effort was concentrated on establishing the relative importance of variables in a steady flow environment only. Seven dependent variables were identified, and a factorial experiment designed to quantify the effect and interaction of these variables. Wedge probes of 6.35mm diameter were traversed in a 200mm diameter, closed section wind tunnel, as reported in chapter 5. A truncated series of traverses was completed in a low-speed compressor annulus to determine the influence of casing shape on the wall proximity effect. A definitive data set was also required on which to base the investigation of calibration facility dependence. This was achieved by calibrating each of four wedge probes in a closed flow, and two open jet flows of different diameter. This is also reported in chapter 5.

Whilst the actual probe experiments were essential in quantifying the two effects, they were not expected to provide much insight into the physical cause. A series of large scale model tests were arranged for this purpose, and are reported in chapter 6. Smoke flow visualisation tests were completed with various two-dimensional wedge shapes, and with an eight times scale model of a 30° included angle wedge probe. Pressure measurements at the probe model surfaces were also made.

Chapter 7 discusses the numerical modelling element of the project. The main thrust of this work was in establishing an understanding of the physical flow mechanisms responsible for the two effects. Details of the computational fluid dynamics (CFD) code are given, and some examples of test cases to validate the code predictions are included. Effort was concentrated on modelling the cases for which flow visualisation data were available. This enabled the code predictions to be validated against experiment before attempting a detailed interpretation.

In chapter 8, the findings from each stage of the investigation are combined to develop an understanding of the highly three-dimensional flow structure which forms around the probe head and stem under steady flow conditions. It is argued that this flow structure governs the probe's calibration, and that modifying the structure, by moving the probe close to a wall or by changing its calibration environment, will in turn modify the probe's characteristics. A simple one-dimensional model of the near-probe flow field is developed from which the characteristics of a given probe in a given flow environment can be calculated quite accurately. A prototype probe designed to incorporate the findings of this investigation was built and tested; the success of this exercise in removing the wall proximity effect through probe re-designed is also discussed. Conclusions to the project are drawn in chapter 9, and aspects of the work which require further attention are summarised in chapter 10.

CHAPTER 2: PROJECT JUSTIFICATION

2.1 INTRODUCTION

The overall aim of this chapter is to consider the economic justification for the investigation presented in this thesis. A brief summary of the costs and benefits associated with the project were included with the original project submission, and are explained in section 2.2. A more detailed but retrospective cost-benefit analysis is included as section 2.3, based on the assumption that all project aims would be accomplished successfully. Because research projects are inherently 'risky' however, an indication of the risk should be reflected in the benefit assessment. Thus a discussion of 'risk analysis' techniques based on the available literature is given in section 2.4, and followed in section 2.5 by a re-analysis of the cost-benefit ratio to include realistic estimates of the probability of successfully completing each stage of the project. Section 2.6 summarises the conclusions reached in each preceding section.

2.2 PRELIMINARY COST BENEFIT ANALYSIS

2.2.1 Introduction

In its fullest sense, a cost-benefit analysis aims to quantify the totality of change that would result from the successful completion of the project under scrutiny. It achieves this by systematically comparing the cost of the project with the benefits that society will derive from a successful project outcome. All benefits are considered, be they direct, indirect, economic or social in nature, and are quantified in monetary terms. The timescales over which it is expected to realise these benefits are also considered, and their monetary value discounted accordingly. The ratio of discounted benefit to project cost then becomes a characteristic ratio which may be used in comparing a number of different projects analysed on the same basis. In this way, cost-benefit analysis can make

a useful contribution in comparing projects which compete for the same limited resource, although it is by no means the only tool available to the decision maker.

Such a formalised approach to cost benefit analysis came to be adopted only as recently as the mid 1960's. However it has since been used in assessing projects as diverse as underground railway construction, disease control methods, reservoir building and airport siting, (Mishan, 1988). A cost-benefit analysis is an essential element of all applications for private venture (PV) project funding within Rolls-Royce; that compiled for this project is given below, followed by a more thorough analysis in section 2.3.

2.2.2. Research Brochure Cost-Benefit Analysis.

The original cost-benefit analysis for this project was summarised on a single sheet, and is included as Figure 2.1. Benefits are stated under section 3, "Engine Applicability". Although not quantified, these claims were supported by practitioners in the fields of compressor and turbine development, whose judgement of the relative merits of the value of this project when weighed against turbomachinery research projects of the same value was sought. The estimated project costs were quantified and are tabulated under section 5 as internal and external expenditure, (in pounds sterling), plus engineering time, (in man years), for each year of the three year project duration. One of the claimed benefits was the requirement for fewer builds of a component turbomachinery rig such as a high pressure compressor, at a typical saving of £150,000 per build. Even from this very simple analysis therefore it was apparent that the benefits would outweigh the costs if just one fewer rig-build was required as a result of the research.

This analysis is limited in a number of respects however. Only a few choice benefits are sighted, rather than a complete list including direct, in-direct, social and economic benefits. Nor is consideration given to the timescales over which these benefits are expected to be realised. The costing is incomplete in that it omits the overhead charges associated with use of the company computing facilities. It also fails to split the

pure research costs from the costs of implementing the research results. Finally, the analysis inherently assumes a completely successful outcome, thus failing to recognise the risks involved, or to quantify the probability of success. These deficiencies are addressed in the more detailed analysis of section 2.3.

2.3 DETAILED COST BENEFIT ANALYSIS

2.3.1 General Approach

The 'baseline scenario' approach was adopted in analysing the benefits associated with this project, (Sassone, 1978). In the general case, this involves identifying the problems that the project aims to solve, and computing the costs associated with these problems. These costs are then taken to be the realisable benefits. In this case, the problems concern the measurement of near wall static pressure and yaw angle in a turbomachinery environment, and the associated costs fall into three categories which are considered below in detail. The scope of the analysis is confined to turbomachinery testing at Rolls-Royce sites; whilst a considerable amount of Rolls-Royce sponsored turbomachinery testing is conducted within Universities and other independent research establishments, attempts to collect a consistent set of information from each proved unrealistic.

2.3.2 Benefit Categories

Category 1: Alternative Approach

By radially traversing a turbomachinery annulus with either a laser or hot-wire anemometer, the radial velocity profile at that plane may be determined. This may then be combined, via the isentropic flow equation, with the radial total pressure profile determined from a pitot tube traverse to give the required static pressure profile, and the need for direct measurement of static pressure is avoided. In practice, laser anemometry

would be preferred, being more accurate and robust than hot-wire anemometry in this environment. However additional effort is demanded by this approach as summarised in table 2.1 and expanded below.

Relative to a single probe traverse, the user of laser anemometry involves additional technical support and more rig running hours. Up to 50 hours of specialist technical support is required to set-up, conduct and dismantle a laser anemometry test. At the 1994 hourly rate for technical support to engine development projects, this equates to an additional £1615 per test. Then in table 2.2, the cost per hour of running the two compressor test facilities and two turbine test facilities sited at Rolls-Royce Derby are determined by averaging across all the turbomachinery rig tests conducted on these facilities during 1993. Assuming that the laser traversing requires an additional four hours rig running time, this adds £2647 to the cost of a compressor rig test for example.

The provision of optical access at the plane of interest will involve design time plus the manufacturing costs associated with modifying the rig and producing the window, although this is generally a one-off modification for a given test vehicle. The post-test data analysis procedure is also more involved, incurring an estimated additional cost of £1000 per test through man-hours and computer overheads. If the laser anemometry approach were to be adopted as a standard technique, a dedicated system would be required to support typically 20 plus turbomachinery rig tests per year. Suitable systems currently cost approximately £150,000, a capital expenditure which should be depreciated over five years. Assuming that the depreciation costs are spread on the basis of 20 tests per year, this equates to a further £1500 per test. Summing all these individual contributions in table 2.1, the additional cost of exclusively adopting the laser anemometry approach would be approximately £6,800 per test, or £136,000 per annum.

A second alternative to direct measurement is to predict the radial static pressure distribution at a plane using computational tools. Available techniques range from simple radial equilibrium calculations to full numerical modelling of the flow field via

Navier-Stokes equation solvers. However, although a given prediction may be checked in the near-wall region against wall static pressure tappings, the ability to validate such tools is compromised by the inadequacy of free-stream static pressure measurement techniques. Also, computational tools are generally only applicable to steady flows, rather than the highly unsteady flows generated between turbomachinery blade rows. Hence an unquantified level of uncertainty will be introduced into the overall turbomachine analysis by the use of predicted static pressure profiles. The implications and cost of measurement uncertainty are considered under the second category of benefits.

Category 2: Cost of Uncertainty

When evaluating a new or modified multi-stage turbomachine design through experiment, the individual performance of each stage as well as the overall characteristics of the complete machine are of interest. In particular for a given embedded stage, the efficiency, the degree of reaction and the matching between up and downstream stages are required. Whilst the isentropic stage efficiency may be determined from inlet and exit stagnation pressure and temperature measurements, (Cohen et al, 1988), stage loading and matching are calculated from the axial velocity and the inlet and exit blade relative flow angles. Measurements of all three of these parameters are compromised by the wall proximity effect, resulting in an incomplete understanding of the machine's performance.

This situation has a number of consequences varying in severity and cost. Firstly, effort will be required on behalf of the rig owner and his team to resolve inconsistencies in the measurements, and departures from the blading performance predictions. A survey of the compressor and turbine technology groups at Derby has shown that up to 6.5% of the time of thirty staff employees is devoted to this task annually. This equates to £100,000 per annum at the 1994 hourly cost rate. Secondly, if discrepancies in the measurements cannot be reconciled, an extra test of the machine may be ordered at an average cost per test of £200,000. This figure is made up of rig preparation costs, testing costs and technical support. Given that a particular component development programme

will typically take three years, and that at least three components will simultaneously be under test, it is reasonable to assume that one less test per year would be required given a reliable standard of interstage instrumentation. (This compares well with an analysis conducted by Cook (1989) of the high pressure compressor development programme for the RB211-535E4 engine during the mid 1980's. Cook concluded that 15%, or £225,000 of the compressor development budget could have been saved annually through the use of reliable interstage measurement methods.)

The performance of an aeroengine design has to be estimated up to three years before the final design standard is tested. Such predictions enable airframe compatibility to be checked, and form the basis of guarantees against which the engine is sold to the airline companies. Competition in the civil aeroengine market is intense, and the pressure to sell against the best possible prediction of performance is therefore very great. A third scenario is that erroneous performance characteristics will be derived from early component turbomachinery test data with a high level of associated uncertainty, resulting in overall engine performance guarantees which are unattainable. Failure to meet the fuel burn guarantees given on engine types currently in service has, and continues to cost Rolls-Royce in the order of £10million per year in fuel equivalence guarantee payments to engine operators, (Loftus et al, 1993). However, whilst the other potential benefits given so far have been quantified, it is not possible to reliably decide the reduction in fuel equivalence guarantee payments that would result from an improved standard of interstage instrumentation. This potential saving must therefore be considered as a 'soft' benefit, that is, a benefit that is real but which cannot be included in the quantified cost-benefit analysis.

Category 3: Enabling Benefits

In recent years the rate of turbomachinery efficiency improvement has decreased, with efficiency levels tending towards a plateau at around 90%. It has been consistently argued by Cherrett (1994) amongst others that further improvement will only follow an increased understanding of unsteady flow phenomena. Such understanding in turn

demands both numerical and experimental techniques with sufficient frequency response to reliably capture the unsteady effects.

As discussed in chapter 1, the last decade has brought several high-response pressure probe designs, including the dynamic yawmeter developed within Rolls-Royce by Cook (1988). However, because this instrument is based on the wedge-type probe, it also suffers from wall proximity effects, and the claimed benefits cannot be fully realised. Those originally claimed by Cook are summarised here on the assumption that probe design improvements resulting from the wall proximity study are incorporated into future embodiments of the dynamic yawmeter. Because wall proximity effects are not the sole cause of error in unsteady pressure measurements with such instruments, no attempt has been made to quantify the benefits attributable directly to overcoming this effect. However the benefits may legitimately be considered under the category of soft benefit.

The first benefit relates to establishing the correct mean pressure in a fluctuating pressure environment. A pneumatic pressure probe positioned downstream of a turbomachinery rotor will return a steady pressure which represents some sort of average pressure at that position. However the probe is incapable of responding to the rapid pressure changes that accompany a rotating wake for example, due to pneumatic damping of the signal within the first few mm's of piping. Thus the sensed, average pressure will be erroneously weighted towards the free-stream pressure level, ignoring the influence of the blade wakes. By careful probe design, such errors can be reduced to 0.5% dynamic head, (Grant, 1977). However by directly measuring the time-dependent unsteady pressure signal, and averaging this as required, the error can be further reduced to a claimed 0.3%.

Hot wire anemometry is used as an alternative dynamic flow measurement technique within Rolls-Royce. However only velocity information is available, which is inherently less useful than the pressure and angle information yielded by a dynamic pressure probe. Hot wire anemometers are notoriously fragile and offer an absolute uncertainty of, at best, 3% when operated in a turbomachinery environment. Apart from

determining performance characteristics, time-resolved pressure measurements in turbomachines are also required for validating computational fluid dynamics code predictions. A particularly important example, given the ever more stringent noise restrictions being imposed at international airports, is that of noise prediction models. These require detailed rotor wake and over-tip leakage measurements, such as provided by dynamic pressure probes, as an input.

A final benefit derives from the probe traverse procedure currently adopted. The rate of traversing a pneumatic probe is set by an operator who must balance the conflicting requirements of minimum test time against minimum uncertainty. Too quick a traverse rate will result in a 'smearing' of strong pressure gradients due to the response time of the pneumatic system. The high data acquisition rate achievable with a dynamic pressure measuring instrument would permit a more rapid traverse rate, and realise a slight overall reduction in testing time. More significantly, any danger of compromising the data would be avoided.

2.3.3 Cost-Benefit Summary

This section describes the procedure used in comparing the costs incurred with the hard benefits described above in order to derive a benefit cost ratio (BCR) for the project. A simple spreadsheet was constructed for tabulating the figures and calculating the BCR. Features of this include cost discounting and the ability to allow for less than 100% success in achieving the stated project aims. A typical output is given in figure 2.2 and discussed below, with the assumption that all the stated aims were successfully achieved. Following a risk analysis of the project in section 2.4, the validity of this assumption is questioned, and a new BCR is calculated including revised estimates of the probabilities.

The costs of conducting but not implementing the research over the three year project duration are given first, and allocated to the three areas of manufacture, fit and test, (M., F.& T.) man hours and computing overheads. All costs and benefits are quoted

in multiples of £1,000. From comparison with figure 2.1, it is seen that only the M., F.& T. costs were included in the original brochure submission. Further details of these costs are given in chapter 3. Having summed the costs for each year, they are then discounted, at a rate of 5% in this case, to the base year, i.e. the year in which the project commenced, (Department of the Environment Report, 1972). By discounting in this way, costs incurred and benefits derived over differing time spans can legitimately be compared. The choice of discount rate depends on numerous factors including the prevailing rates of interest and inflation. The sensitivity of the analysis to discounting rates between 0 and 15% was established by substituting various rates into the spreadsheet. Results are plotted in figure 2.3; the relationship is almost linear and indicates a reduction in BCR of 0.43 per 1% increase in discount rate. Facility for entering estimates of the probability of successfully achieving the project aims stated in chapter 1 is also provided.

Under the 'Benefits' section, the hard benefits discussed in section 2.3.2 are summed, and assumed to extend over the next five years. In general, this time period will vary depending on the nature of the project, subsequent advances in technology, and criteria adopted by the funding body. Given the rate at which technology develops, it is felt that at least some of the assumptions on which the benefit analysis has been based will not be valid beyond 1999. In some cases the successful completion of a project may bring dis-benefits as well as benefits. For example the 'hush-kits' fitted to in-service aeroengines successfully reduced noise levels to within the prevailing legislative levels at the time, but at the expense of fuel efficiency. Space for quantifying any dis-benefits is provided, but none have been identified in this case. The net-benefits are taken as the difference between benefits and dis-benefits, and discounted to the base year to give a final value for each year.

The implementation costs are considered separately from the research costs because the probabilities of successful completion are likely to be different. In this case, the implementation broadly involves three steps:

i) probe re-design based on the findings of the research,

ii) probe manufacture and evaluation,

iii) training in the use of the new probe, including suitable documentation.

The costs, categorised as before, are totalled and discounted to the base year. Again, the probability of successfully meeting each implementation aim can be inputted, the net implementation cost then being the product of the probability of success and the discounted implementation cost. The final row under the benefits section shows the net hard benefit of the project for each year, taking into account the probabilities of successfully achieving both the research and implementation aims. It is therefore the product of all the probability values and the discounted benefit.

Under the summary section, the yearly net benefits are added to give an estimate of the total project benefit. The research and implementation costs are similarly summed across the years in which they are incurred. A final BCR is computed, this being defined as:

$$BCR = \frac{\text{Benefits - Total Cost}}{\text{total cost}} \quad \ldots\ldots\ldots (2.1)$$

From figure 2.2, a total benefit over five years of £1.63million was calculated for this project, which exceeds the costs by a factor of 9.5 assuming complete success in achieving all the stated objectives. The validity of this assumption is examined below.

2.4 RISK ANALYSIS

2.4.1 Introduction

To a greater or lesser extent, an investigator embarking on a project of whatever nature will assess the risks involved. The rigour of this assessment might range from a

purely subjective view based on the individual's previous experience, to a thorough investigation involving extensive data and statistical analysis. In either extreme, the objective will be the same, namely to balance the likelihood of success against the consequences of failure. A decision as to whether or not the project proceeds as proposed, or is modified in some way, will then be based in part on the outcome of such an analysis.

The aim of this section is to illustrate ways in which a formal risk analysis, conducted as an integral step in the planning process, can influence a project outcome. To this end, a review of the literature that discusses risk analysis in the context of technological research and development projects is given. A simple set of guidelines for the application of risk analysis are drawn from this and used in conducting a retrospective risk analysis of the project discussed in this thesis.

2.4.2 Literature Review

A technological project will normally have associated targets expressed in terms of a job specification, time to completion, and costs. Ruffles (1993) defines a 'quality job' within Rolls-Royce as one which exactly meets these targets. However as the economic climate exerts ever increasing pressure on the aeroengine industry to improve productivity whilst simultaneously enhancing product reliability, a degree of uncertainty in meeting a customer's targets is inevitable. Such uncertainty may be embodied in the concept of 'risk'; the risk of an event occurring is defined by the Rolls-Royce Engineering Audit Department (King, 1993) as the product of the LIKELIHOOD of the event occurring and the CONSEQUENCE of the event occurring. It follows that the consequences will be expressed in terms of the specification, time or cost targets as appropriate.

Risk analysis in its fullest sense is defined by Cooper and Chapman (1986) as "the identification, evaluation, control and management" of the risks associated with a given project. More specifically, Vlay and Brekka (1990) divide this into three stages, i.e:

Stage 1: Risk Identification, where all the potential sources of uncertainty in the planned project are identified,

Stage 2: Risk Assessment, where the levels of uncertainty in achieving specification, time and cost targets are quantified to a degree of accuracy consistent with the project complexity, and

Stage 3: Risk Mitigation, where ways of reducing each risk to an acceptable level are identified.

The benefits of a formal risk analysis are given by the Rolls-Royce Audit Department as a sounder basis for decision making, a lower risk, more robust initial project plan, plus an early identification of likely contingent requirements. That an investor is likely to have more confidence in a 'risk managed' project is highlighted by Cooper and Chapman. Thomas (1973) notes the importance to a technologically based organisation of a balanced portfolio of projects, i.e. one comprising ventures ranging from high-risk, high-gain to low-risk, low-gain in nature. A formal and consistent risk assessment approach is an obvious pre-requisite in establishing such a portfolio. Risk management is also an essential element of the Total Quality Management (TQM) philosophy that originated in the U.S., was championed by the Japanese, and has now been adopted to a greater or lesser extent by many world-wide industries. In some cases, the requirement for TQM is laid down by law; for example, the United States Department of Defence mandated the TQM approach in 1988, (Vlay and Brekka). This example, amongst many others, indicates growing recognition of the benefits that formalised risk analysis has to offer. Details of techniques described in the literature for conducting a risk analysis are now discussed, in the framework of the three stages introduced above, i.e. risk identification, risk assessment, and risk mitigation.

Risk Identification

Any analysis is only as good as the information on which it is based. Whilst it will be seen in the following section that risk analysis tools are both available and often sophisticated, the omission of one important source of risk at the risk identification stage can severely flaw the analysis, and lead to inappropriate risk management decisions. This is recognised by Meldrum and Millman (1991) in an article discussing the marketing of high technology products. Although aimed primarily at the marketing profession, this article identifies ten potential sources of risk which relate directly to the planning of any high-technology project, be it research, development or production oriented. These are summarised below:

i) There is a risk that new technology will be inadequate. Research that relied on say a new, high-technology piece of analysis equipment could be severely compromised if the equipment fell short of specification. Alternatively, it may prove impossible to meet the original claims of a particular R&D project without unacceptable cost and timescale implications to the sponsoring company.

ii) The research may result in a product which, although meeting its specification, does not prove an acceptable substitute for the technology it is designed to replace, i.e. there is risk associated with assuming that successful implementation will automatically follow successful completion of the research.

iii) Any likelihood of alterations to the research specification must be assessed.

iv) Any risk of the underlying technology becoming obsolete before completion of the research or product development must be considered.

v) The complete or partial failure of a research package may damage the credibility of an organisation. Particularly in the civil aeroengine market place, a tarnished reputation for product quality and reliability could well endanger future orders.

vi) The risk of lengthening timescales associated with both product development and the selling cycle are shown from experience to be common to high-technology companies.

vii) Performance and quality standards for innovative projects or products may not be in-place. When debating the degree to which such a project should be funded for example, the funding body will be lacking standards against which comparisons can be drawn, and the work will be considered 'high-risk.'

viii) The full or partial failure of previous research into a particular area may generate a poor perception which in turn detracts from proposals for further work in the same area.

ix) Closely associated with point vi) above is the risk of overspending the available budget. In some cases, timescales can be recovered by additional spend, and Meldrum and Millman site examples to suggest that cost overruns will generally have less impact than time.

x) The final identified source of risk concerns the development of technology which lacks the infrastructure to support it effectively. Whilst successful in its own right, the benefits of the research cannot be fully implemented.

Meldrum and Millman conclude by stressing the importance of a structured approach to risk identification which is intrinsic to the company or research establishment make-up. Corti (1973) illustrates past failings in this regard by presenting a survey of private sector companies. When asked to describe their risk analysis strategy, the majority admitted relying predominantly on personal judgement, with little feel for when such analysis was appropriate, or by whom it should be conducted. Corti suggests that guidance for risk identification and classification should be provided by top management, accompanied by a clear allocation of responsibilities. Without this, there is a danger of multiple analysis leading to a pessimistic risk estimate, or no analysis at all.

Corti also stresses the importance of learning from previous projects about areas of risk which perhaps were not identified at the outset, but which proved significant as the project progressed. The most recent computer-based project and resource management system installed within Rolls-Royce recognises this fact, (Rolls-Royce, 1992). By monitoring the time and cost involved in completing a particular task, and comparing this with the time and cost estimates, the system will, in-time, build a database which can be interrogated as new projects are planned. Particularly for the repetition of similar design tasks, this should facilitate a more accurate identification of the risks involved, through a fully documented and quantified record of 'what happened last time.' The facility should also assist in the numerical assessment of risks, as discussed in the following section.

The danger when identifying risks is that an important area will be overlooked. King (1993) advocates the use of 'brain-storming' techniques, both by individuals and especially within a team, to identify all conceivable risk areas. Particular emphasis is placed on assembling the optimum team of people, including experts in branches of technology which are key to the project's success. King recommends a more structured approach to the brainstorming exercise than is usual, and suggests that five categories of risk should be considered; people, procedural, equipment, technical and programme. However the ten general areas identified by Meldrum and Millman might readily be substituted as a structure for brainstorming sessions.

An alternative technique for identifying risk is to separately approach individual members of a given project team for estimates of time and cost to complete the job in question. Those who submit the most optimistic and the most pessimistic replies are then asked to justify their estimates in a short written statement. Comparison of these statements may reveal areas of risk identified in the pessimistic response which were overlooked by the majority. Some measure of confidence in the predictions can also be judged from their distribution about a mean.

Risk Assessment

King defines the assessment stage of the risk analysis process as quantifying the uncertainty in the time, cost and specification estimates of a given project. This involves two stages; the mathematical expression of each of the risks identified above, followed by a combination of these expressions to determine a measure of risk for the project. The literature includes many techniques, of varying degrees of complexity, for realising both stages. The choice of technique will depend on the scope of the project in question, and these are summarised below in increasing complexity order.

An allowance for risk can be incorporated into a cost benefit analysis such as that given in section 2.3 by appropriate upward adjustment of the *discounting rate*, (Cooper and Chapman, 1986 and Thomas, 1973). However, this implies that risk increases into the future, where the opposite is more usual in practice. In cases where one factor has been identified as carrying the majority of the risk, Sullivan and Or (1982) suggest the use of *'break-even' analysis*. A 'break-even' value of the high risk factor is determined at which two alternative outcomes are equally attractive economically. By estimating the most likely value of the factor, and comparing this with the break-even value, the most likely-to-occur alternative is determined. A more general form of this is *sensitivity analysis*, (for example, Cooper and Chapman, 1986), applicable in cases where two or more risk areas have been identified. Based on a model of the situation, or simply on a priori knowledge, the sensitivity of a given project outcome to the high risk inputs is tested by sequentially varying each input by a fixed percentage. Such a sensitivity test may also be designed to reveal dependencies between the variables, (Walpole and Myers, 1993).

A further, simple assessment tool is that described by King as the *high/medium/low* technique. This involves categorising the likelihood and consequence attached to each identified risk into one of three pre-defined bands. For example a risk might be classified as 'high' if the likelihood of an event occurring was judged to be greater than 50%. Those risk areas which fall into the high likelihood and high

consequence bracket would then be viewed more seriously than those in the low/low bracket, etc. Increasing in complexity, the *decision* or *event tree* described by Buck (1989) is appropriate where time has been identified as playing an important part in the risk. King sites the example of a civil aeroengine development programme, involving a series of sequential tests. Less than complete success in one test can seriously delay or compromise the next, and an event tree is constructed to map the various possibilities. Again, the process can be quantified to arrive at likelihood and consequence measures for each route through the tree, (see section 2.4.5).

The high/medium/low approach is the simplest means of determining a probability distribution for a given identified risk. The triangular distribution proposed by Cooper and Chapman is a development of the high/medium/low approach and is illustrated in figure 2.4a) using as an example the probability of completing a particular task within a given time. Buck notes that in some cases, it is appropriate to extend the triangular distribution to a Gaussian one as shown in figure 2.4b). If the risk approximates to being normally distributed, it can then be described simply in terms of a mean and a variance, thus simplifying subsequent analysis. If not, then statistical tools including the semivariance, partial mean, partial deviation and linear loss integrals can be used to model skewness in the distribution, (figure 2.4c). Collins (1992) also suggests the use of cumulative probability distributions for modelling risk profiles, noting that they mathematically represent the way in which people generally think, and are therefore straightforward to construct. Explaining the example given in figure 2.4d), one might be confident of completing a task within six weeks, but equally certain that it won't be finished within four. Based on previous experience, there is a 50% chance of completing within five weeks; these three points are sufficient to fit the 'S' shaped cumulative probability curve as shown. Seyb (1992) applies this approach in predicting the efficiency level to be achieved when developing a typical axial compressor.

Having mathematically described each risk element to an appropriate degree of complexity, these must then be combined to determine an overall risk profile in terms of cost, time and specification. The high/medium/low approach is again the simplest

example of this, and easy to implement. Both the triangular and Gaussian distributions can be combined through direct analysis; the mean and variance of the combined Gaussian distribution will simply be the sum of the individual contributing means and variances respectively, (Walpole and Myers). Skewed distributions described using the tools listed above may also be combined analytically, as described by Buck.

Numerical methods of combination are also now widely used. Cooper and Chapman describe a method in which the probability distribution is discretised into an array of probablity/base variable pairs which are then combined by simple addition. However the most widely reported numerical method is the *Monte-Carlo* type analysis described by Sullivan and Or. They identify three steps in this type of analysis:

i) the construction of an analytical model which accurately represents the project in question,

ii) the modelling of the probability distribution of each identified risk using techniques described above, and

iii) repeated runs of the model, taking random combinations of points from all the input risk probability distributions, to arrive at an overall risk probability distribution for the project expressed in terms of time, cost and specification.

Buck describes the analytical model in stage i) as 'a decision tree consisting of choice and chance nodes and probabilistic branches'; this is illustrated in figure 2.5. The ease with which such models can be created and extended using modern computational techniques is seen as a major advantage of the simulation approach to risk assessment. Vlay and Brekka (1990) give just one example of a suite of software tools designed for modelling the most complex of projects, and conducting risk assessments via the Monte-Carlo approach. The number of simulation runs required under stage iii) to generate a reliable risk profile is difficult to judge, and depends on the characteristics of the project. Sullivan and Or advocate continuous monitoring of changes in the generated profile with repeated

running, until the change tends to zero. Buck stresses the importance of defining representative initial conditions for the model, and Thomas warns of the need for conditionality statements between risk areas which cannot be considered independent. However, given that Monte-Carlo simulation has been in use for at least thirty years, and that its implementation using contemporary computing tools is increasingly cheap and reliable, the more widespread use of simulation risk assessment is now possible and indeed probable.

Risk Mitigation

Completion of the analysis discussed so far will result in a quantified understanding of the risks involved. However this is of little more than academic interest unless the results are translated into positive actions. This process is termed risk mitigation, and involves modifying the project plan in the light of the risk analysis to minimise the likelihood and consequences of high risk events.

King suggests that this process should begin by reviewing the risk assessment to extract any main messages, and to identify the issues which contribute the most significant risk. The key question is then whether the risks posed by these hazards are acceptable or not. Baranson (1978) presents this question graphically by plotting 'noise factor' against production costs, as reproduced in figure 2.6. Taking the noise factor to be a measure of risk, the curve defines the trade-off between risk and rate of return. A tolerance level is then set at the considered maximum level of risk, thus defining the production cost. The shape of the trade-off curve depends on a composite of economic, commercial and technical factors. The tolerance level also depends on a number of factors, summarised by Baranson into three categories:

i) The technical sophistication of the project. Higher risks are generally associated with high technology projects, although the potential rate of return is high. In deciding whether to launch a new project, a given organisation will often consider the tolerance level against those of current programmes with a view to

establishing a balanced portfolio of high risk/high gain and low risk/low gain projects.

ii) The nature of the organisation. Private industry for example operates in a market where a higher level of risk is often necessary to remain competitive on cost and capability, and where profit maximisation is demanded. In contrast the emphasis within public enterprise is biased more towards service regardless of cost, i.e. a low tolerance level.

iii) Management's attitude towards risk. This in turn dictates a given organisation's cultural attitude towards risk, and a firm policy for its control.

Corti emphasises the latter point, recommending that rules should be in place against which conscious and traceable decisions can be drawn from the risk assessment. Baranson stresses that without this infrastructure, an organisation's approach to risk mitigation will be influenced by the natural inclinations and career aspirations of the technical managers. He suggests that an individual's personality profile may be characterised as a risk-taking index. An alternative measure is offered by Buck, who discusses the use of utility theory in describing rational human behaviour in economic decision making. In a situation where a number of decisions are possible, utility is the measure of relative preference between options. The application of utility theory will ensure rational consistency in decision making, and avoid the whimsical traits of individual managers.

The options available for mitigating the risk will depend on the nature of the risk itself, (King, 1993). For example, where a strong likelihood of timescale overrun is identified, then either the start date should be brought forward, parts of the work run in parallel, or more resource made available to accelerate the task. It may be possible to sub-contract packages of work identified as particularly high risk to an expert in the field, or as a last resort, to reject the project altogether. Even the latter option, although

extreme, could avoid wasted expenditure on a project which fails because the associated risks were too high.

2.4.3 Risk Analysis Guide-Lines

The aim here is to define the basis from which a simple set of guide-lines for the application of risk analysis to high-technology research and development projects could be formulated. The scope of projects envisaged are those typically undertaken within the author's department at Rolls-Royce. These might range from a new pressure transducer evaluation exercise, involving one man for a week at minimum expense, to the design, production and testing of a test-bed data collection and analysis system, requiring a team of people for up to two years with a multi-thousand pound budget. Typical three year, University based PhD projects also fall into this category. Although beyond the scope of this thesis, the intention is that the guide lines developed here should form the basis of an all-embrasing, computer based tool for the rapid risk-analysis of such projects. There exists a range of commercially available software packages for performing individual stages of the risk analysis, such as Monte-Carlo numerical analysis for example, and these are listed in appendix A. However no mention of an overall package which guides the user through the risk analysis process from start to end was found.

The risk analysis process was defined in three stages in section 2.4.2., the first stage being risk identification. Given the variety of assessment techniques available however, a preliminary step must be to decide on an appropriate level of analysis, given the size of job to be undertaken. To avoid subjectivity in this decision, a procedure including all the dependent variables is required, and some of the more important are listed below:

i) The anticipated resource commitment in terms of man-power and budget. The greater this is, then the higher the potential waste if the project fails, and the less the resource available for other work.

ii) The anticipated utilisation of facilities. If a project proposal relies heavily on a specialised item of high technology equipment which subsequently fails, the project may be put at risk. Alternatively, the equipment may already be well utilised by other projects such that the required access is difficult.

iii) The benefit-cost ratio. The higher the expected benefits then the less detailed the analysis need be on the basis that a partial failure would still reap some reward. This is of secondary importance against the resource considerations however.

iv) The 'company culture'. The attitude of an organisation to risk taking will depend on the nature of its business. It is also subjective, and difficult to quantify. What is important, as stated in section 2.4.2, is a consistent approach. Without this consistency, the job of weighing the merits of different project proposals becomes impossible.

This represents a general list of considerations which is not exhaustive, and which would require tuning to a given organisation. However it is useful as a basis for compiling a procedure for selecting the appropriate level of risk assessment. Taking x as a measure of appropriate analysis, the points made under i), ii) and iii) above may be expressed mathematically in a relationship of the form:

$$x = (r \times R) + (b \times B) + (a \div BCR) \quad \ldots\ldots\ldots\ldots \quad (2.2)$$

where:

a	=	0.01
b	=	budget weighting factor
r	=	resource weighting factor
BCR	=	benefit cost ratio
B	=	budget
R	=	man-power resource

The inclusion of b and r enables differing emphasis to be placed on man-power and budget, depending on the nature of the project. For example, a project proposal for which funding is being sought might place higher emphasis on the budget than in the case where funding is committed, and the risk analysis is aimed solely at modifying the project plan to minimise risk. However, recognising that the two are inextricably linked, a further condition is proposed, i.e:

$$(b + r) = 1 \qquad \text{..... (2.3)}$$

Secondary importance is attached to the BCR by imposing an arbitrary scaling factor of 0.01.

From consideration of the options in section 2.4.2., five levels of assessment may be identified, namely:

1. No assessment appropriate
2. likelihood/consequence analysis
3. event tree analysis
4. analytical modelling
5. simulation modelling

In table 2.3, five bands of funding levels and man-power resource appropriate to the scope of project considered here are allocated. Given the project budget and man-power requirements, values of B and R can be read from this table, and substituted into equation (2.2) along with the BCR to give a value for x. The appropriate level of assessment is then that corresponding to the next highest integer value of x.

It must be appreciated that the categories of table 2.3 are somewhat arbitrarily defined based on the experience of only one project, and would require modification to reflect the range of projects typically undertaken by a given organisation. This would be achieved in practice by monitoring and recording the performance of a range of projects

over a period of time against committed timescales and budgets. This information could then be used to refine a suitable set of criteria for use within the organisation.

The risk analysis process is summarised in flowchart form in figure 2.7. Having identified the appropriate level of assessment, this guide-line flow chart follows the stages identified in the original risk analysis framework. A computer based risk analysis tool would follow the logic presented in this chart, and prompt the user for the information required to proceed with a given stage. Rather than duplicate much of section 2.4.2 by developing a set of questions here, the process is illustrated first by considering its use within the author's department at Rolls-Royce, and then in section 2.4.5 by retrospectively analysing the risks associated with this project.

2.4.4 Use of Risk Analysis Within Rolls-Royce

The strategic planning and development of the Rolls-Royce product range involves a risk analysis the complexity of which is well outside the scope of this thesis. However the routine application of risk analysis as part of the planning process for every project undertaken within the author's department would be beneficial in several respects. Firstly, it would become possible to achieve and retain a demonstrateably balanced portfolio of projects, rather than one which is subjectively judged to be balanced. This balance could be altered if required, in line with the prevailing economic climate, i.e. support the higher risk projects when profits are high, and minimise the risk in times of recession. Secondly, in cases where management is forced to choose between a number of demands from external customers on the same limited resource, a knowledge of the relative risks involved would be an important and useful contributor to the decision making process. Thirdly, there are occasions when a choice between several possible solutions to a given measurement problem must be made. Again the relative risks of each solution could helpfully influence the choice. Finally, a rigorous appreciation of the risks involved in a given project would influence the attitude adopted if that project began to over-run or over-spend. It might be more prudent to halt a known high-risk project

which is running over budget, in the knowledge that a further injection of funds is by no means guaranteed to bring success, than to continue optimistically.

2.4.5 Retrospective Project Risk Analysis

The guide-line flow chart defined above is now applied in analysing the risks associated with the project discussed in this thesis. As previously seen, a risk analysis must be conducted at the project planning stage if the findings are to be used in mitigating risk successfully. This retrospective analysis is included by way of example to demonstrate the simplicity and potential effectiveness of the technique.

Risk Planning

Considering firstly the appropriate level of analysis, it was seen from section 2.3.3 (cost benefit summary) that the project had an estimated man-power resource of 4100 hours and a budget of £29,500. From table 2.3 therefore, both R and B are set to 5. At the time of planning, there was commitment to neither resource or budget, and so each is given equal weight by setting $b = r = 0.5$. Taking the BCR of 9.5 calculated in section 2.3.3, and substituting into equation (2.2) gives an 'x' value of 5.001. This suggests that a complete risk assessment including a Monte-Carlo type simulation of the overall risk profile is appropriate. In practice the computational tools required to realise a Monte-Carlo were not readily available to the author, and the assessment is limited to stages 1 to 4.

As discussed further in chapter 3, the definitive aims of the project were set in October 1992, on completion of one year's study. A definitive project plan (figure 2.8) was compiled at this stage, and represents an appropriate starting point for the risk analysis. It is seen that the research content of the project comprises five 'work packages,' whilst implementation of the research results is in three stages.

Risk Identification

Taking each of the five research work packages in turn, potential areas of risk were identified by thinking through the work involved. These were noted, and categorised under the five headings given in section 2.4.2. Table 2.4 summarises the risk areas identified for the computational modelling element of the project as an example. Although this activity was completed by the author alone, it would have been appropriate to seek the advice of experts in the various fields had the analysis been conducted at the start of the project.

Risk Assessment - Likelihood/Consequence

A likelihood/consequence analysis was completed initially, this being the quickest and simplest assessment to perform. Criteria for a low, medium or high likelihood of the risk occurring were set as shown in table 2.5. This also defines low, medium and high levels for the consequential impact on time, cost and specification. What were considered to be appropriate levels were then assigned to each risk area based on the author's experience, as shown in table 2.4. In fact the author had no prior experience of the computational modelling work included as an example, and the advice of experts would have had to be sought for a reliable 'up-front' analysis.

Simple inspection of table 2.4 shows a wide spread in perceived risk between a row of 'highs' for item 1, and a predominance of 'lows' for item 5. The assessment can be extended by quantifying the three categories; 1, 2 or 3 for low, medium or high risk respectively. The risk to time, cost and specification against each item is then the product of the likelihood and consequence value, shown in the bottom right hand corner of each consequence cell. An overall risk indicator was determined for every item by summing the individual contributions across each row to give the value in the right hand column. Values within the range 3 to 27 were possible; by arbitrarily defining scores above 20 to be high risk, and those below 10 to be low risk, an overall distribution of low, medium and high risks was assembled. In the numerical modelling example, only one of the eight

identified items, i.e. 12.5%, emerged as high risk, 50% as medium, and 37.5% as low risk. A similar analysis was conducted on each of the five research work-packages, and the final risk distributions are summarised in figure 2.9.

Because the same assessment categories were used for each of the five work-packages, figure 2.9 enables a rapid and direct comparison of the risks associated with each. Package 3, the high speed probe calibration activity, carries the highest overall level of risk, whilst packages 4 and 5 carry only medium and low risk items. However, this presentation masks the area where the consequence of an event occurring would be felt. Figure 2.10 was constructed by summing the risk indicators in each time, cost and specification column, and expressing them as a percentage of the total of all three columns. Consistently for each work-package, it can be seen that the anticipated timescales are most at risk of being exceeded, whilst the cost and specification are generally at equal risk. Having drawn this conclusion from the assessment so far, subsequent analysis concentrates on the timescale issues.

Risk Assessment - Event Trees

As discussed above, event trees are appropriate where a process which depends on several sequential events is to be assessed. Of the five research work-packages, only the computational modelling fell into this category, in that model validation relied on experimental results from the other four packages. An event tree was constructed over the timescales identified in the project plan, i.e. from December 1992 to October 1993. This period was represented as a horizontal time bar at the top of figure 2.11, on which the planned completion dates of the four experimental work-packages were marked as shown. Working from the left of figure 2.11, the first branch occurred on completion of the flow visualisation studies. The highest risk identified in the likelihood/consequence analysis concerned the use of an essentially steady-flow solving numerical code to model what was expected to be an unsteady flow problem. The flow visualisation was expected to indicate whether or not this was a concern; had a high level of unsteadiness been experienced, then the adoption of an alternative numerical model would have been

necessary. Against the criteria set for the likelihood/consequence analysis, a 'high' likelihood implies greater than 33% chance of occurrence. Hence three branches were defined, with 35% chance of needing to adopt a different code, 60% chance of retaining the original code, and 5% chance of completely failing to numerically model the problem at all. These likelihood values are marked on the appropriate branches in figure 2.11.

Each branch was then developed in-turn. It was hoped to numerically model probes in an open jet, and the suitability of the code for this purpose would be tested against actual results from the open-jet calibrations. Again a successful outcome relied on the assumption of pseudo-steady flow, plus the ability to model in three dimensions. Taken together, the overall likelihood of success was set at 60%, and branches drawn accordingly. The process was continued as shown for the remaining two work-packages. The likelihood of proceeding along a given path was calculated as the product of the individual likelihood values along that path. Crude estimates of the consequential extensions in timescales were also made by considering each possible combination of events.

Although the absolute values used in constructing the event tree are debatable, it can be concluded that the likelihood of proceeding along the optimum (upper-most) route is less than 33%, and that up to 13 weeks additional time could be required to achieve a successful outcome.

Risk Assessment - Analytical Modelling

The use of analytical modelling is illustrated here by taking Gaussian probability distributions to describe each identified risk. Again only timescale implications are considered, although the analysis could be extended to address the risks to cost and specification.

Continuing the numerical modelling example, estimates of the times required to complete each stage were made, as shown in table 2.6a), and taken to be mean values.

Any uncertainty in these estimates was also considered and taken as ±1 standard deviation from the mean. An overall mean and standard deviation for the modelling work was then calculated by summing and root sum squaring the individual means and standard deviations respectively. This process was repeated for the other four work-packages, and for the three implementation stages, and the results recorded in table 2.6b).

One aim in conducting the risk analysis was to determine a probability of success for inclusion in the cost-benefit analysis. To achieve this, it was necessary to relate the contributions of each of the five research work-packages to the declared objectives of the project. This relationship is mapped in figure 2.12, based on the project outline in chapter 1. For example, the first objective of successfully understanding and overcoming wall proximity effects is seen to depend on the outcome of work-packages 1, 2, 3 and 5. By combining the individual means and standard deviations of the timescale estimates for these packages from table 2.6b), an overall estimate of the time required to achieve the wall proximity aim was determined, together with an uncertainty in the estimate. In this way it was estimated that 114.6 days, ±8.3 days were required to complete the work necessary to meet the first objective. From figure 2.8, the total number of days allocated for these four packages was 130, which is 1.86 standard deviations more than the estimated time. From the area under a standard normal curve, this equates to a 96.9% chance of completing the work in the time allocated. This procedure was repeated for all work-packages and implementation steps, and the results summarised in table 2.6c).

In that the intention is to incorporate results from the risk analysis into the cost-benefit analysis, it might be argued that the risk to cost or specification would be more appropriate than the timescale risks considered here. However, a project overrun will generally delay the time from which benefits are realised, and reduce the period over which benefit is derived. Since timescales were identified as the major risk area by the likelihood/consequence analysis, it is reasonable in an illustrative analysis such as this to use timescale probability estimates in the cost-benefit analysis. A full risk analysis would

also consider the risks to cost and specification; by ignoring these, the current analysis is likely to be optimistic, and this point is addressed further in the following section.

Whilst the inherent assumption of normally distributed risk profiles makes the combination of these profiles straightforward, a particular operation might be better modelled by the skewed-normal type of distribution illustrated in figure 2.4c). For example, experience showed that the mean times estimated for experimental work tended to be the minimum time required for completion. A skewed distribution with the maximum turning point shifted towards the left and a greater area under the right hand tail would therefore have been more appropriate. Such distributions can be modelled and combined analytically, (Buck, 1989), but require far more computational effort. This is beyond the scope of the current discussion, but could be incorporated as a facility in a computer based risk-analysis tool. However, given the increasing commercial availability of risk simulation software based around the Monte-Carlo method, the relative effort in implementing the two techniques should be critically compared before committing to a complex analytical approach.

A second assumption inherent in this analysis is that the information yielded even from successfully completed work packages is sufficient to meet the project objectives. It is shown in chapter 8 that, although the contributing work packages were successfully completed according to the project plan, the resulting information was not sufficient to fully understand the facility dependence of wedge probe calibrations. Such a deficiency should be highlighted by a risk analysis completed at project launch, such that the specific content of the work packages can be altered accordingly.

Risk Mitigation

Because the analysis given here is retrospective, the risks involved in undertaking this project were accepted by default, without a quantified idea of what they were. From the likelihood/consequence analysis, six items were identified as of potentially high risk to the project timescales. In each case, means by which the risk might have been reduced

had the analysis been completed at project launch are considered. The potential impact on the project in terms of achieving the original objectives and savings in time and cost are also estimated.

Considering the numerical modelling work first, the choice of a steady flow code to model what was probably an unsteady flow problem was the single high risk item. However, although codes with an unsteady flow capability exist, no such code for modelling in three dimensions was available within Rolls-Royce. Hence there was little choice but to accept the associated risks, and acknowledge that failure was a possibility. Had the event tree of figure 2.10 been constructed at the outset, the likelihood and consequences of failure would have been better understood. As reflected in the risk analysis, converged solutions particularly of the three-dimensional geometries proved difficult to achieve, and some aspects of the numerical modelling, including a thorough investigation of the effects of turbulence, had to be curtailed in the interests of timely completion.

Two high risk areas were identified for the flow visualisation studies, namely the generation of suitable smoke as the visualised medium, and the necessary modification of a wind tunnel which was hired from another university. Had these areas been identified at the outset, the risks associated with the first would have been reduced significantly by organising a series of preliminary tests with a variety of smoke generators to determine the most suitable, and to gain experience in its use. This would have avoided one man-day of technical time and two days of wind tunnel hire charges, a total saving of approx. £420. The required modifications to the wind-tunnel were finished on time, but the project plan included no built-in contingency for other than 'right-first-time' completion. Contingency could have been included had the risk been identified. In addition, it was assumed at the project planning stage that an understanding of the flow structures responsible for the calibration facility dependence of wedge probes would result from the flow visualisation studies in a bounded flow. This proved not to be the case. Had the problem been recognised via an informed risk analysis at the project launch, appropriate mitigating action could have been taken. In the event, the calibration

facility dependence specifically of wedge probe yaw angle sensitivity has not been fully explained, and further investigation is required as discussed in chapter 10.

Three high risk areas in calibrating probes at high Mach numbers were identified. In practice, this work-package did prove the most problematic to complete satisfactorily, experience which has inevitably influenced the risk analysis. However two errors were made which could have been avoided if the risks had been analysed beforehand.

i) Laser anemometry, involving the installation of complex equipment and the technical support of a colleague, was attempted before the wind tunnel was fully commissioned. Problems in running the wind tunnel were encountered initially which absorbed approx. £2,430 of technical time, in taking measurements which were of no subsequent value, and five days elapsed time.

ii) Laser measurements of the wind tunnel flow field revealed strong radial pressure gradients when operating with an upstream turbulence grid. Two iterations of tunnel modification and laser flow measurement were required to eradicate the gradient. The potential for such problems would have been recognised in a risk analysis, realising further savings in laser anemometry time of approx. £2,000, and four days elapsed time.

In summary, it is estimated that £4,850 or 3% of the total project resource allocation could have been saved, and two weeks of work avoided had a risk analysis been included at the project planning stage. This time could have been profitably invested in extending the numerical modelling work as originally planned, although the original objectives have not been compromised through failure to complete the turbulence modelling work. The objectives relating to the calibration facility dependence of wedge probes could have been achieved more fully had the content of the work packages been extended following a risk analysis at project launch.

2.5 REVISED COST BENEFIT ANALYSIS

Returning to the spreadsheet used in calculating the benefit cost ratio of section 2.3.3, the revised probability of success estimates were substituted to determine a new ratio of 8.3 , a 13% reduction over the original value. Given the high sensitivity of BCR to probability of success implied by this result, the relationship was explored further by sequentially varying the probabilities of successfully completing both the research and the implementation. Results are plotted in figure 2.13 for probability values between 0.8 and 1 in each case. For this example, the BCR is halved if probabilities of success are set at 0.9, and reduced further to 20% of its original value with probabilities of 0.8. This serves to illustrate how misleading a BCR based on the assumption of complete success can be, and is further justification for conducting a formal risk analysis at the project planning stage.

2.6 CONCLUSIONS

The economic justification for this project was considered briefly in the original project proposal document, and has been expanded considerably by a more thorough, but retrospective cost benefit analysis. Although some difficulty was experienced in realistically attributing benefits to the results of this project alone, hard benefits totalling £1.6million over five years have been identified. Assuming complete success in realising all the research objectives and in implementing the results, an attractive benefit cost ratio of 9.5 was calculated using a simple spreadsheet to summarise the figures.

Recognising that complete success was unlikely, a wide range of techniques for quantifying the risks associated with any technological project have been identified from the literature. A simple framework involving the four stages of risk planning, identification, assessment and mitigation is proposed as a basis for conducting a risk analysis. The extent of analysis will depend on the nature of the project, and a procedure for deciding this has been developed. Software is now required, structured around the proposed framework, which guides the user through an analysis appropriate to his

project. Even without such a tool, a retrospective risk analysis of the project described in this thesis has been completed, and has highlighted steps that could have been taken when planning the project to reduce the associated risks. Specifically, it is estimated that 3% of the total budget, and two weeks of elapsed time were spent unnecessarily on activities which could have been avoided by completing a risk analysis during the project planning process. An overall probability of successfully meeting the imposed *timescales* has also been determined, and fed back into the cost-benefit analysis. This reduced the BCR by 13% to 8.3, which still represents an attractive return on investment. However this analysis does not recognise that the scope of the various aspects of the investigation was insufficient to enable all the stated objectives, i.e. the project *specification*, to be achieved in full. Substituting an estimate of the probability of successfully meeting the project objectives into the cost benefit analysis would probably have reduced the BCR by considerably more than 13%. A more thorough risk analysis would consider the potential impact on *costs*, *timescales* and *specification*.

It is recognised that, because the risk analysis reported here was completed retrospectively, the thinking behind it was inevitably influenced by experience. A degree of uncertainty must therefore be associated with the absolute values of potential savings and BCR reduction quoted above. The real value of this chapter to the work of the author's department within Rolls-Royce is more as an introduction to those who are unfamiliar with the risk analysis concept, as an indicator of the importance of the discipline, and as a pointer for further work, supported and illustrated by an applied example.

CHAPTER 3: PROJECT MANAGEMENT

3.1 INTRODUCTION

This chapter deals with the management aspects of the research programme which was planned and executed to meet the project aims stated in chapter 1. Section 3.2 records the background to the project, and summarises the original project submission document. Section 3.3 presents the original project planning and costing process, and justifies the use of the Gantt chart planning method which was adopted throughout. Details of the decision making process involved in setting the direction for the second and third years of research are also documented.

A budget of £29,500 was agreed against the original research brochure submission and the management of these funds, and of the available man-power resources is summarised in section 3.4. Section 3.5 considers the various means by which overall progress was monitored, recorded and communicated to other interested parties. This includes mention of the steps taken to keep abreast of on-going developments in the field at other U.K. and European research establishments. Conclusions are drawn in section 3.6.

3.2 ORIGINAL PROJECT SUBMISSION

3.2.1 Background

The wedge probe wall proximity effect explained in Chapter 1 was recognised by Cook (1988) as a serious threat to reliable free-stream static pressure measurement in turbomachines, affecting both steady state and dynamic pressure probe designs. Through personal contacts, it was known that others within the industry had observed similar effects. Realising the need for a well controlled experimental and theoretical approach to

this problem, a request for proposals for research programmes was prepared by the author, (Smout, 1988), and circulated to four United Kingdom research establishments known to possess the required test facilities and expertise.

Although replies were received from all the establishments approached, the most comprehensive and apparently cost effective programme was that proposed by Cranfield University. Compiled by Elder and Tan (1990), the proposed programme incorporated both experimental and numerical elements aimed at investigating the fundamental physical causes of the wall proximity effect, and overcoming the effect through probe re-design.

Given that the wedge probe wall proximity problem was first reported by Lewis in 1963, there was some concern that investigative work might already have been completed to which Rolls-Royce could be party, although no such evidence could be found in the literature. The opportunity of the 10th European Symposium on Measurement Techniques, held at the V.K.I. in September 1990, was taken to present what was believed to be the state-of-the-art, and to discuss the proposed programme. This forum was considered particularly appropriate given that the subject of pressure probe calibration, including the wall proximity effect, had been discussed at the 6th meeting of the same group in 1981, (Fransson, 1983). (The research institutions represented at the symposium are listed in appendix B, together with a summary of their research interests.)

The meeting was not able to offer any further insight into the problem and the Rolls-Royce Assistant Chief Engineer with responsibility for company sponsored University research was approached with a view to private venture funding for the programme. However despite considerable support for the technical aims and proposed approach, the programme as stated was turned-down on the grounds of cost.

3.2.2: Research Brochure Submission

An alternative course was therefore pursued, that of a research programme to be conducted by the author and registered with Cranfield University for a Total Technology PhD. Given that the author was already employed by Rolls-Royce, this scheme effectively avoided hiring additional man-power, although the overall costings were similar. Government funding through the Science and Engineering Research Council in the form of a student CASE award was successfully applied for, and converted to an industrial studentship which was paid directly to Rolls-Royce, and offset against the author's normal wage. The wedge probe research programme was re-written by the author as a research brochure in the standard form required by the company. This contained obligatory elements including a statement of the technical proposal, a list of the technical objectives and expected benefits, and a breakdown of costs and timescales.

Given that a 15 month timescale had originally been envisaged for the wedge probe research, the scope of the investigation was broadened and given the title, "High Accuracy Interstage Measurement in Multi-Stage Turbomachines." Structured broadly in two parts, part 1 related specifically to understanding and overcoming the wall-proximity problem with wedge probes. Part 2 then considered three measurement techniques where improvements were required in order to enhance the company's ability to achieve reliable measurements between the individual stages of multi-stage machines. The intention was to further develop one of these techniques on completion of the wedge probe work, the choice depending on the perceived company requirement at the time, the outcome of part 1, and the results of the literature survey.

The three options under part 2 of the brochure were as follows:

a) to develop further the dynamic yawmeter originally designed at Rolls-Royce by Cook (1988), and discussed in chapter 1. Steps to reduce the physical size of the probe, modifying its geometry in accordance with the findings of part 1 of the project and incorporating state of the art transducer technology were envisaged.

b) to continue the work initiated again by Cook in designing an intrusive probe such as the reverse-Kiel temperature probe for measuring the true mass-averaged temperature in an environment of fluctuating total temperature such as that generated downstream of a turbomachinery rotor.

c) to research the idea of using a 'sandwich' of appropriately arranged thin-film sensors to resolve instantaneous temperature variations at frequencies up to 30kHz.

Figure 3.1 shows the original project plan, with part 1 beginning in October 1991, and part 2 scheduled to begin in October 1992. On completion of the first year, it was decided to capitalise on the encouraging findings of the wedge probe research, in preference to diversifying into one of the part 2 options. Details of the process involved in making this decision are given in section 3.3.2. The definitive set of project objectives given in chapter 1 for the remaining two years of study were compiled in October 1992.

3.3 PROJECT PLANNING

Whilst four specific objectives are defined in chapter 1, it was envisaged that two separate but parallel investigations would be required to meet them, one to address the wall proximity effect, and a second to understand the calibration facility dependence of wedge probe performance. It was recognised that each investigation would involve a combination of experimental, numerical and analytical approaches in varying degrees, with the possibility of some commonality between investigations. Whilst the numerical and analytical work was to be conducted within the author's company, and was not expected to be resource limited, the majority of identified experimental facilities were situated at external sites and heavily used either by other students or for contract research. It was therefore clear that careful planning, scheduling and continuous monitoring would be necessary throughout.

3.3.1 Planning Tools

Given the author's relative inexperience in managing a project of this scale, suitable training was sought early in the planning process. Part of the total technology PhD course requirement is for a minimum level of training in non-technical, managerial subjects including inter-personnel skills, cost control and marketing. A series of suitable courses were identified and are summarised in appendix C. However these were necessarily spread over the first eighteen months of the project duration, and more immediate project management training was sought. The company adult training officer was consulted, and identified a computer based teaching package available at the Derby site Learning Resources Centre (L.R.C.). L.R.C.'s represent a relatively new, company wide training initiative designed to impart textbook knowledge through interactive, computer based software packages, rather than via the more traditional lecture courses previously offered by the company training schools. An engineer is able to attend the L.R.C. at a time convenient to him, and to learn at his own rate. Whilst the benefits of interaction with the lecturer and other students are obviously lost, the information is assimilated as and when required. The project management package took three hours to complete, and introduced the author to techniques for defining, overview planning, detailed planning and scheduling projects. This background knowledge was then extended by reference to suitable texts as required.

As a project planning tool, the Gantt chart (Woodgate, 1964) is perhaps the most familiar. Individual activities of a particular task are presented as horizontal bars, or blocks of work plotted against an appropriate time scale. Thus the planning and scheduling are combined, the relative positions of the blocks indicating the relationship between activities. Complex projects may be represented by several years of planning, and modifications to the plan are easily reflected in the Gantt chart. A limitation is that, for a given activity, the block length merely indicates the start and end dates, which do not necessarily reflect the actual time required for completion. Thus accurate planning of sequential events may be compromised. Although this can be overcome to some extent

by writing the time required for completion above the bar, a more powerful and flexible planning technique is that of Critical Path Analysis, (C.P.A.), (Barnetson, 1968).

Beginning with the project objectives, the C.P.A. approach involves identifying all necessary activities, and then networking them such that they lead logically to the terminating event, and show explicitly their relationships to one another. The resources and time required to complete each activity are estimated, assuming at this stage that resources are unlimited. These estimates are combined via a simple algorithm to compute an expected completion date which is then compared with the required completion date. Any mismatch is corrected by rescheduling activities or by redeploying resources. The 'critical path' is the route through the network which determines the completion date, critical because any extension to the associated time-scales will delay project completion. Thus the C.P.A. approach is more detailed and gives independent control of the planning and scheduling activities. The ability to more carefully control resources may lead to collectively reduced costs and time-scales, and computerised tools for the analysis of C.P.A. networks are now readily available.

However the success of any planning method relies on the accuracy of the time-scale forecasts, which for high technology research and development projects are notoriously unreliable. Chapter 2 illustrates the ways in which project plans may be modified to accommodate probability distributions for early, on-time or late completion via a project risk analysis. However the likelihood is that plans will undergo constant revision through the course of the programme, an argument in favour of the simple and readily modified Gantt chart approach. A further requirement of the Total Technology PhD scheme is that the student should devote 80% of his time at work to PhD studies. Hence the available man-power resource was effectively fixed for this project at one man for four days per working week on average. Overall therefore the advantages of greater resource and scheduling control offered by the C.P.A. approach were considered outweighed by the simplicity and adaptability of the Gantt chart method which was adopted throughout.

3.3.2 Choice of Project Direction

The project plan submitted with the original brochure is included as figure 3.1, and is a high level Gantt chart covering the whole three year project duration. More detailed planning was included for part 1, from which a time for completion of 18 months was anticipated. Detailed plans for the three options under part 2 were also included. The decision as to which option to pursue was taken in October 1992 following consideration of two primary factors, namely:

i) the progress made against the original plan for part 1, (the wall proximity investigation) and

ii) the strategic needs of the company for turbomachinery instrumentation.

The first factor impacts directly on the success of the PhD studies, and was taken as the need to achieve a positive result within three years. The second factor was split into three parts, these being the need for instrumentation with sufficient mechanical integrity, capable of returning the correct mean flow conditions in an unsteady flow environment, and with a high response capability for resolving time-dependent fluctuations. Taking these as the four objectives against which a decision should be made, the 'Churchman-Ackoff' decision analysis technique described by Thomas (1973) was chosen since it enables each objective to be weighted according to its perceived importance. Two matrices were assembled, (figure 3.2), the first being a 'k x n' matrix where k represents the available options, and n the decision objectives. Each option was assessed against the decision objectives and assigned a value between 0 (did not meet the objective in any way) and 1 (met the objective completely) in the appropriate position in the matrix. The second, 'k x 1' matrix contained the weighting factors for each objective, the sum of all weightings being unity. The strategic requirement for high response instrumentation was considered by the company compressor engineering group as secondary to the other objectives, which were weighted equally. Multiplying the matrices as in figure 3.2 resulted in the decision matrix 'D', from which continuing with the wall

proximity effect investigation emerged as the favourite option against the selected objectives.

The definitive project aims were reflected in a revised Gantt chart, (figure 2.8), comprising five research work packages and five implementation stages. Detailed Gantt charts were also constructed for each research activity. Because resources were limited to the author alone, these work packages were planned to follow each other sequentially. With the exception of the computational fluid dynamics modelling work, which was scheduled to run for the majority of the project, this also avoided substantial cross-linking between the work packages. The construction and modification of Gantt charts was considerably eased with the introduction of the personal computer based project planning software package 'Power-Project', which became available within the company from January 1992.

3.4 RESOURCE MANAGEMENT

Fundamentally, the resources available at the beginning of the project comprised 80% of the author's time for three years, a budget to cover manufacture, fitting and testing costs of £29,500 and largely unlimited use of the company main-frame computer for numerical modelling work. The management of each of these is now discussed in turn.

3.4.1 Time Management

Assuming a 38 hour working week, and that 45 weeks are worked in every year, this equates to 4,100 man-hours over three years for completion of the project. A task was raised on the company central time-booking system under the author's departmental overheads allocation, since it was expected that the ultimate benefits would be enjoyed by all the engine development projects, rather than by any one in-particular. The number of hours spent on the project was logged weekly onto the time-booking system, such that

the overall rate could be monitored against the required 80%. In fact a disappointingly low rate of only 70% was achieved in year 1, for three principal reasons:

i) work in which the author was already involved could not be completed before the PhD programme began, and therefore ran in parallel for some months,

ii) although additional resource was made available to help complete the existing tasks, the author was inevitably involved in familiarising and training the individuals concerned in the appropriate disciplines, and

iii) the author's advisory role as an aerodynamic instrumentation specialist within the company did not automatically cease as the PhD work began.

This 10% short fall equated to 171 hours in the first year; rather than slip the programme by a corresponding 5½ weeks, recovery actions were identified and executed, including:

i) additional time spent out of works hours, and

ii) the support of the company laser anemometry expert for the probe calibration wind tunnel characterisation work which was performed at Cranfield during the first year. It was originally anticipated that training in anemometry techniques would be undertaken at Rolls-Royce prior to using the equipment for the characterisation at Cranfield. By combining the training exercise with the actual testing, approximately 3 of the 5½ weeks deficit were recovered.

In January 1992, a new, computer based project and resource management system already operating at the Rolls-Royce Bristol site was extended to include the engineering organisation at Derby. Referred to as the 'Engineering COmmitment Monitoring' or ECOM system, this was designed to emphasise the accountability of individual engineers to their particular customers, and to more closely plan, monitor and record the performance of work packages against pre-determined milestones. Because of

the considerable research content, it was considered more appropriate for the company Advanced Engineering group to act as customer for the author's project. Thus a new task was raised in January 1992 as a component part of the Advanced Engineering work package. Weekly time bookings continued much as before, but improved access to the logged information via terminals networked to the company mainframe computer considerably eased the work rate monitoring process.

A work rate of 75% was achieved through the 1992 to 1993 academic year. The deficit was addressed this time by securing the services of a graduate trainee who had recently joined the company having completed an Engineering Sciences degree. Working directly under the author's supervision, the trainee successfully organised the preparation and characterisation of a small open-jet wind tunnel for wedge probe calibration purposes, part of the open jet calibration work identified as work package 4 in figure 2.8.

3.4.2 Budget Management

Considering next the control of costs, an approximate spend profile was prepared for the original brochure submission, and is included in figure 2.1. This was split between internal and external spend on a year by year basis, and was compiled without knowledge of which option would be pursued under part 2. Having chosen after the first year to pursue the wall proximity investigation for the remaining two years, a fresh manufacture, fit and test budget was prepared. This was plotted against the quarter in which the spend was expected to occur, based on the revised project plan, resulting in the predicted spend profile shown in figure 3.3. A total spend of £25,000 was predicted, comfortably within the original brochure estimate.

Actual spend within the company, for example to cover the manufacture of research probes, was controlled by issuing the appropriate order number to the department in question. Estimates for the technical time and material costs were obtained from a particular department before sanctioning any work, and the actual bookings against the order numbers were carefully monitored. Spend external to the company was

covered by Advanced Engineering External Agency Authorisation (EAA) sheets. Again the task of monitoring spend was eased with the introduction of the ECOM system, from which a summary of cumulative spend against project order numbers was obtained every four weeks. This information is summarised in table 3.1 which includes all the major spend items rounded to the nearest £100. The rate of spend is then compared with the predicted spend profile by over-plotting the information in table 3.1 on figure 3.3. Agreement between the two profiles is generally good, both approximating to a linear increase of cumulative spend with time which flattened out towards the project completion date. As such, the profiles tend towards the classic 'S' shaped curve for research and development project expenditure discussed by Norris (1971). The largest discrepancy occurred between the final quarter of 1993 and the first of 1994, and resulted from an un-planned spend of £7,900 for an additional series of probe calibrations. Because the budget was under-spent up to this time, the additional cost was absorbed without exceeding the brochure value. In fact the final spend corresponded exactly with the original brochure estimate, whilst the anticipated split between internal and external spend was achieved to within £400.

3.4.3 Computer Charge Management

The numerical modelling element of the project involved using a computational fluid dynamics code available on the company IBM mainframe computer. When the project began in October 1991, the costs associated with maintaining and administering this facility were born by the company as an overhead, and not allocated to particular projects. This situation altered following the introduction of the ECOM system in January 1992, with computer time being charged against a user's department. Hence although the author's use of computing facilities did not appear as a charge against the research brochure, it represented a real cost of the project which had to be added to the technical time and brochure spend when computing values for inclusion in the overall cost benefit analysis. Figure 3.4 plots, at four weekly intervals over the project duration, the cumulative costs incurred through running the code. These costs are automatically computed on completion of a successful run, and are based on the elapsed CPU time,

plus a fixed overhead charge. The code familiarisation and evaluation runs undertaken early in the programme involved simple two dimensional geometries and incurred little cost. The rapidly increasing rate of spend towards the end of the programme reflects the intensification of effort, and the extension of the modelled geometries into the third dimension.

3.4.4 Support Panel Monitoring

The importance of effective monitoring in the project management process has been eluded to above. Whilst the four weekly checks of time allocation and brochure spend were essential in monitoring the use of resources, the Support Panel assembled as a requirement of the Total Technology PhD scheme also played an invaluable role in this respect. The panel compromised a core membership of five, including the author's industrial and academic supervisors and an advisor from the Cranfield School of Management. Additional members were co-opted as and when required to advise generally on technical issues, and specifically on the selection of appropriate non-technical courses. Meetings were held at three monthly intervals throughout the three year programme, as summarised in appendix D, and were minuted by the author. An agenda compiled jointly by the author and his academic supervisor was circulated to every support panel member prior to each meeting. At a minimum, these always demanded a report of activities since the previous meeting on both technical and non-technical issues, and a critical review of progress against the project plan. The discipline of preparing for these meetings, and the value of expert comment on a regular basis were undoubtedly strong contributors to the task of managing the project to a successful conclusion.

3.5 PROJECT DOCUMENTATION AND COMMUNICATION

The minutes of the support panel meetings referred to above formed the most complete record of the project's progression, and proved a valuable reference source

when compiling this thesis. Up to fifteen hours were absorbed in preparing for each meeting which took a further five hours each on average, including travel. Being a fairly detailed review of three months work, each set of minutes took roughly ten hours to compile. This equates to a total of 360 hours, or 8.8% of the originally allotted time dedicated over three years to documenting the project via the Support Panel review procedure. In addition, full technical reports were required after the first nine months, (Smout, 1992) and after two years, (Smout, 1993), followed ultimately by the thesis.

At the other extreme, industrial research often demands timely answers to quite specific problems, and can not afford this level of investment in documentation. The minimum demanded of an engineer working on a PV funded research brochure is a full report at project completion, plus brief statements of achievement at quarterly intervals. Whilst this approach might achieve the immediate research objective, the danger is that intermediary material of future potential worth is lost. This may ultimately result in repeat work at further expense, which represents false economy in the long term. The experience from this project is that regular review and documentation pays dividends in terms of achieving maximum return on investment; it is suggested that, certainly for the research oriented projects supported by the company Advanced Engineering operation, an insistence on more detailed and regular reporting would be beneficial overall.

Apart from the documentation, details of the work were presented internally to members of the author's departments at both Cranfield University and Rolls-Royce, at various stages in the programme. A technical paper, (Smout and Ivey, 1994), based on the experimental work reported in chapter 5 was also prepared, accepted and presented at the 1994 Congress and Exposition organised by the American Society of Mechanical Engineers. Apart from this conference, the activities of other U.K. and European research establishments were monitored through conference proceedings and publications, particularly those of the 'European Symposium on Measuring Techniques for Transonic and Supersonic Testing,' (see appendix B). The current instrumentation research activities of a group at ETH, Zurich, and of the Osney laboratory in Oxford were of particular relevance to the author's work. Contact with the ETH group was

established through a direct meeting at Rolls-Royce in June 1991, and maintained by subsequent correspondence. Meetings with members of the Oxford group were held at roughly six monthly intervals throughout the project duration. More details of the work of these two establishments are included in the review of previous work in chapter 4.

3.6 CONCLUSIONS

Four principal conclusions are drawn from this discussion of the project management process. Firstly, the Gantt chart method of project planning chosen for this project proved effective and adaptable, and avoided the complexity of a network technique such as critical path analysis. It is recognised however that a more complex project involving input from more than one person would require the greater control and flexibility afforded by C.P.A. Secondly, careful monitoring of resource utilisation and progress to plan was essential in the timely identification of deficiencies, which could then be rectified through appropriate action. The availability of central, computer based records considerably eased this task.

The Total Technology requirement for quarterly review meetings and reports ensured that the project stayed on track, and resulted in comprehensive documentation which was of great value in reaching a successful conclusion. As a result, the project was completed within the originally defined time-scales and budget.

CHAPTER 4: REVIEW OF PREVIOUS WORK

4.1 INTRODUCTION

The wedge probe wall proximity effect, whereby the freestream static pressure is incorrectly sensed near to the boundary through which the probe is introduced, was known within Rolls-Royce before the current investigation began. A number of relevant research papers were therefore available within the author's department; literature searches of the NASA, Compendex, Inspec, Fluidex, SAE and Heat Transfer and Fluid Flow databases were commissioned to supplement this information, and to avoid important omissions.

A detailed study of literature relating more generally to wedge type probe characteristics was also completed to give a wide knowledge base from which to design the investigation. This study is presented in section 4.2, where geometry related probe characteristics are discussed, and in section 4.3, where compressibility, Reynolds number and turbulence sensitivities are considered. The wedge probe has been used by several investigators as the basis for dynamic pressure sensing instruments; although strictly beyond the scope of this thesis, a brief review of these developments is included in section 4.4 for completeness.

Information relating to the wall proximity effect is summarised in section 4.5, where results from previous experimental investigations of the effect undertaken within Rolls-Royce by Cook (1988) and by the author, (Smout, 1990), are also included. The aerodynamic calibration facility dependence of wedge probes is less well documented and had not specifically been investigated in-house prior to this study. Available information is summarised in section 4.6.

4.2 GEOMETRY RELATED WEDGE PROBE CHARACTERISTICS

The literature provides much information on how a wedge probe's characteristics are related to its geometry. This is considered with reference to the Rolls-Royce standard wedge probe design in figure 1.2c). Bryer and Pankhurst (1971) state that the wedge leading edge must be sharp if the indicated static pressure and flow direction are to be independent of Mach number. Morris (1961) concurs, and cautions careful handling to avoid leading-edge damage. Ferguson (1974) attempted a more mechanically robust wedge probe design with a blunt leading edge. Experimental evaluation proved the design to be unsatisfactory for yaw angle measurement, with more than one null point, and regions of yaw insensitivity. Recent investigations by Humm (1991) show that radiusing the leading edge to truncate the wedge chord by 10% has very little influence on the indicated static pressure coefficient and yaw sensitivity, but that a 20% truncation will substantially drop the static pressure coefficient and increase yaw sensitivity.

The effect on total pressure measurement of varying the pitot tube design was also investigated by Ferguson (1974), with the aim of improving spatial resolution by reducing the separation between pressure tappings. Several probes with total pressure tappings recessed into the leading edge were investigated. The optimum design in terms of pitot tube sensitivity to yaw and insensitivity to pitch is shown in figure 4.1. An increase in static pressure tapping yaw sensitivity also resulted from aligning the recessed pitot tube with the static tappings as shown. The pitot tube in the figure 1.2c) wedge probe design is positioned at the free end of the wedge. This removes the static tappings from the downstream influence of the pitot tube, but the radial separation of total and static tappings must be accounted for when analysing test data.

The influence of pressure tapping diameter on indicated static pressure is reported by Shaw (1960) in the general context of pipe flow. Ferguson investigated the influence for wedge probes, and detected no change in indicated static pressure for hole diameters between 0.2 and 0.5mm. However increasing the bore of the pitot tube from 0.5 to 1.0mm reduced the pitot tube yaw sensitivity and increased pitch sensitivity, in

accordance with established conventional pitot tube behaviour, (Benedict, 1984). This result was repeated by Hodson (1989) in calibrations of a 30° wedge probe over a wide range of sub-sonic Mach numbers.

Several researches have attempted to quantify the influence of wedge included angle on probe yaw sensitivity. This information is summarised in figure 4.2, which plots yaw sensitivity against non-dimensionalised static tapping position (x/L) for several probes with included wedge angles ranging from 23° to 60°. Definitions of x and L are given in figure 1.2c). Cook (1988) originally used this form of presentation, to which additional data from more recent sources has been added. The trend is for yaw sensitivity to increase as the static tappings are moved towards the wedge apex, and as the included wedge angle is increased. Both results were repeated by Ainsworth et al.(1992) in a low speed experimental study of large scale, two-dimensional wedge models. This presentation takes no account of the type of tunnel in which the calibration was conducted, which may explain some of the scatter, (see section 4.6 below). Figure 4.3 is taken from Ferguson (1967) and summarises the experimentally determined dependence of static pressure coefficient on wedge included angle and static tapping position. The shallow wedge face pressure gradient implied by the slope of these curves is often used to justify staggering the static pressure tappings in narrow angle wedge probes where internal space for pressure tubes is restricted, (Bryer and Pankhurst, 1971). Ferguson also studied the interaction between static pressure coefficient, static tapping position and yaw angle using long wedge-section models. By noting the conditions at which a unity static pressure coefficient occurred, he concluded that a stagnation point was formed on the pressure surface of a wedge probe running at incidence, which moved rearwards over the wedge surface as the yaw angle was increased. The rate of stagnation point movement as a function of yaw angle was reduced as the wedge included angle reduced, suggesting that the probe performance was governed more by the angle presented by the pressure surface to the flow, than by the wedge included angle as such. Pressure measurements made at three positions on the suction side of a 45° wedge model are plotted as static pressure coefficients against yaw angle in figure 4.4. Rapid changes in slope are seen at -5°, -11° and -16° yaw angles for (x/L) values of 0.27, 0.68 and 0.88

respectively. In explanation, Ferguson suggests that a separation bubble forms in the suction surface leading-edge region which grows along the wedge face as the yaw angle increases, until complete stall occurs. Al-Shamma (1967) and Hollis (1971) suggested that the stalling yaw angle corresponded to the minimum turning point in figure 4.4.

4.3 FLOW RELATED WEDGE PROBE CHARACTERISTICS

4.3.1 Velocity Dependence

An advantage of wedge-type probes over other designs according to Morris (1961) is superior in-sensitivity to velocity. Detailed calibrations by Cook of a probe design similar to that in figure 1.2c) showed that pitot tube yaw angle sensitivity reduces as the Mach number is increased from 0.6 to 0.85. This characteristic was also shown in Hodson's investigation of a 30° included angle wedge probe. The data of Cook and Hodson showed that an increase in yaw angle sensitivity based on the two static tappings also occurred as the Mach number increased.

Bryer and Pankhurst (1971) report, and Hodson's data confirms, that the static pressure tapping characteristics are velocity dependent. Up to 15% change in the static pressure coefficient based on one of the static tappings of a 30° included angle probe was observed as the Mach number was increased from 0.3 to 0.9. Hodson also shows an important increase in static pressure coefficient sensitivity to pitch angle that accompanies an increase in Mach number, (figure 4.5). This contradicts the conclusions drawn from previous investigations in incompressible flow, where the pitch sensitivity was found to be independent of velocity, (Ferguson, 1967).

4.3.2 Reynolds Number Dependence

Lewis (1963) investigated the Reynolds number dependence of wedge and cylindrical pressure probe designs, when selecting a probe for annular cascade tests over

a wide Reynolds number range. No change in the calibration characteristics of a 30° included angle wedge probe were observed for Reynolds numbers based on the probe stem diameter of up to $2x10^4$. The superior performance of the wedge probe over the cylindrical probe in this regard was related to the way in which the flow separates from the probe surfaces. Lewis noted that, at zero incidence, the flow separation points are fixed for the wedge at the rear corners regardless of the Reynolds number. However the separation point moves around the circumference of a cylinder from 80° to 120° back from the upstream stagnation point, depending on the Reynolds number, (Morkovin, 1964). Ferguson (1967) did not observe any calibration change for a variety of wedge probes tested at Reynolds numbers between $0.7x10^4$ and $1.5x10^4$. Bryer and Pankhurst (1971) state that the influence of Reynolds number on the performance of yawmeters with square or sharp leading edges is insignificant for values of Reynolds number above $0.1x10^4$, below which the static tapping yaw sensitivity decreases.

The effect of Reynolds number on the calibration of a 30° included angle wedge probe was investigated by Hodson (1989). The probe was calibrated at the exit of a transonic nozzle at turbomachinery representative Reynolds numbers of $4x10^4$ and $12x10^4$. Reynolds number was varied independently from the Mach number, to avoid the compressibility effects discussed in section 4.3.1. Within the limits of experimental uncertainty, the pitot tube calibration against yaw angle was independent of Reynolds number. The static pressure coefficient based on the pressure surface static tapping was also independent of Reynolds number regardless of the yaw angle. However the static pressure coefficient based on the suction surface static tapping was significantly different between the two Reynolds numbers. Consistent with this, the yaw angle sensitivity was greater by 12% at the higher Reynolds number. Whilst the earlier assertions that wedge probe calibrations are independent of Reynolds number may apply at zero yaw angle, Hodson's data shows that yaw angle measurement errors will result if the same is assumed at incidence.

4.3.3 Turbulence Sensitivity

Only two direct references to the turbulence sensitivity of wedge probes have been found. Meyer and Benedict (1952) claim that the measured static pressure is unaffected by the free stream turbulence intensity, but give no supporting evidence, whilst Ferguson (1967) observed a slight change in calibration for turbulence intensities ranging between 0.08% and 14%. However Christiansen and Bradshaw (1981) thoroughly investigated the effects of turbulence on other pressure probe designs including the Conrad three-hole yaw meter. This design consists of three parallel tubes, the outer two being chamfered at nominally 45° to form a blunt arrow head shape. The design is similar to the cobra type probe in figure 1.2b). Although the tubes are not surrounded by supporting metal work as in a wedge probe, the general calibration characteristics are at least qualitatively similar. Differences in the pitot tube performance were observed between calibrations of a Conrad probe at free stream turbulence intensities of 0.5% and 22%. A 2% increase in yaw angle sensitivity was also noted at the higher turbulence intensity. Dominy and Hodson (1992) investigated the turbulence dependence of various five hole pressure probes, and showed that design variants which were Reynolds number sensitive also exhibited a marked turbulence sensitivity. This was attributed to the influence of turbulence on low Reynolds number separation bubbles. Given the observation of Ferguson (section 4.2) that a separation bubble forms in the suction surface leading edge region of wedge probes run at incidence, some effect of turbulence on the yaw sensitivity of wedge probes might be expected, as observed by Christiansen and Bradshaw for the Conrad probe.

4.4 WEDGE PROBES FOR UNSTEADY PRESSURE MEASUREMENT

A pneumatic pressure probe operating in a periodically unsteady environment typical of turbomachinery flows will measure a time averaged pressure value. This may or may not approach the correct time averaged value, depending on the detailed arrangement of the pressure tappings and pipes within the probe and measurement

system. Grant (1977) provides a set of design criteria for minimising the error, which is due to the pneumatic damping characteristics of long, air filled pipes. However these are difficult to achieve within the confines of miniature pressure probe designs.

Errors introduced into the measurement will have direct bearing on the performance characteristics calculated for a given turbomachine. Also, unsteady loss-causing mechanisms are generated within turbomachines which limit performance. The prize for understanding and overcoming these phenomena is improved efficiency, and competitive advantage in the market place. Driven principally by these two factors, the last decade has seen considerable activity in the field of unsteady pressure probe development, (Cook, 1988). One approach has been to install miniature pressure transducers in aerodynamic probe geometries, and the literature contains at least four independent references to the use of wedge-type probe designs. These are summarised for their relevance to the wedge probe development work contained in this thesis.

Bubeck and Wachter (1985) developed a 'dynamic' wedge probe for application to rotor exit flow from an axial compressor, where the blade passing frequency was 5kHz. This comprised three, flush mounted transducers for time-resolved pressure measurement, and four conventional pressure tappings to measure the mean pressure level. Three of these were conventionally positioned for total and static pressure measurements; the fourth was sited on the end of the probe, which was inclined into the flow to give a pitch angle measurement capability. This approach for obtaining the absolute unsteady pressure, by combining the pneumatic, time-averaged signal with the unsteady component sensed by the transducers, is compromised for the reasons already given. However the probe proved to be robust in operation, and gave some insight into the unsteady flow phenomena.

The dynamic wedge probe developed within Rolls-Royce by Cook (1988) was aimed at overcoming the averaging errors introduced by the pressure tappings. Three absolute pressure transducers were incorporated into a 30° embodiment of the standard Rolls-Royce wedge probe design. The total signal was recorded onto analogue, magnetic

tape thus maximising resolution, and enabling a frequency response of 80kHz to be claimed. On-line, electronic compensation of each transducer output for temperature and pressure dependent zero drift, sensitivity change and non-linearity was provided to minimise the overall measurement uncertainty. Data recorded at the rotor exit plane of a model, high-pressure compressor enabled the time dependent variation of pressures and velocities to be resolved. Good mechanical integrity was demonstrated, but time-dependent drifting of the transducer calibrations compromised the absolute pressure levels and subsequent performance calculations.

Humm et al. (1994) adopted a similar approach to Bubeck and Wachter in developing a wedge probe for unsteady pressure measurements at the exit of a centrifugal compressor. However, the probe geometry was influenced by an investigation of wedge probe behaviour in unsteady flows. Sinusoidally oscillating probe models were towed relative to the water at rest in a 40m long channel. The models were scaled to give turbomachinery representative reduced frequencies and Reynolds numbers, and a number of dynamic effects were isolated. The most significant in terms of wedge probe design was a dynamic stall phenomena, associated with the formation of a separation bubble in the suction side, leading-edge region of a sharp nosed wedge probe inclined rapidly beyond its static stall angle. Differences between the steady-state and dynamically determined probe calibrations were observed which equate to dynamic yaw angle measurement errors of similar magnitude to the fluctuation being measured. This error source was substantially reduced when the probe leading edge was radiused by 20% probe chord. The static pressure sensing transducers were positioned towards the rear of the wedge faces to maximise the unambiguous yaw angle calibration range, (section 4.2).

The response of a 23° included angle wedge probe to periodically unsteady flow incident at 10° was studied numerically by Ainsworth and Stickland (1992) using the C.F.D. code 'UNSFLO', (Giles, 1991). Adopting a fully viscous, unsteady version of the code, a separated region in the suction surface leading edge region was modelled, as visualised experimentally by Humm. The extent of separation varied periodically with changing flow conditions. A von Karman vortex street shed from the rear of the probe

was also modelled which modulated the static pressure seen towards the rear of the wedge faces. In designing a dynamic wedge probe for application at the exit plane of a turbine rotor blown-down facility, Ainsworth et al. (1994) sited the static pressure transducers as far forward as possible both to maximise yaw sensitivity, and to avoid any adverse influence of the wake vortex modulated unsteady pressure field. This instrument is otherwise similar in appearance to the Cook design of dynamic wedge probe, but adopts the 'chip-on' method for embedding pressure transducer chips into metallic objects. (Ainsworth et al., 1990). Recent versions of the probe are fitted with state-of-the-art 'epitaxial' pressure transducers; the calibration of these devices has been shown to be far more stable, over a two week period, than that of the earlier standard of 'diffuse-gauge' transducers adopted by Cook, (Ainsworth et al., 1994).

To summarise, the wedge-type probe design has been used as the basis for dynamic pressure probes which have given some insight into unsteady turbomachinery flows. Investigators have modified features of the probe, including the leading edge shape and the static tapping position, in order to minimise undesirable probe/unsteady flow interactions. That these modifications are in some cases at opposite extremes to achieve the same goal suggests that unsteady flow effects are not fully understood. This, together with transducer related errors, results in unacceptable uncertainty in the indicated absolute pressure, at least for machine performance calculations.

4.5 WALL PROXIMITY EFFECTS

The first recorded observation of wall proximity effects with traversable pressure instruments was by Morris (1961) in connection with a cylindrical probe. 'Very large errors' in indicated static pressure and yaw angle when measuring close to boundaries are reported but not quantified. Lewis (1963) presents calibration data for a cylindrical probe, and a 30° included angle wedge probe of the type used by Keast (1951). A characteristic typical of the wall proximity curve in figure 1.3 was noted for both probe types. Specifically, the static pressure indicated by the cylindrical probe at 0.1 Mach number fell short of the calibration tunnel reference static by up to 18% dynamic head

over a region extending 65mm from the boundary. Under similar flow conditions, the wedge probe indicated static pressure was low by up to 7% dynamic head over 50mm immersion. Shreeve (1976) also presents calibration results again for cylindrical and wedge type probes. These were traversed across a 175mm diameter parallel free jet discharging to atmosphere, and across a 200mm diameter closed tunnel. The static pressure profiles in each flow had previously been checked with a Prandtl probe, (Bryer and Pankhurst, 1971), to ensure uniformity. In both the un-bounded and bounded flows, Shreeve noted that the probe indicated static pressures decreased as the length of probe immersed in the fluid increased. Immersions of up to 75mm were required, depending on the probe type, before the indicated static pressure reached a stable value. Wedge probes of the type reported by Glawe and Krause (1975) with included angles of 35° and greater were most affected; a cylindrical probe, in which the static pressure tappings were located further from the tip and in a shallow groove in the probe surface, indicated less total variation across the open jet flow. The least variation was achieved using a very narrow (8°) included angle wedge probe in which the static tappings were positioned forward of the probe stem axis.

Robinson (1991) observed the wall proximity effect when calibrating miniature wedge probes for use in low speed axial compressor traverse tests. In a previously unreported investigation, a total of seven variants of the basic wedge probe design shown in figure 1.2c) were traversed across a 150mm diameter closed flow of 0.1 Mach number. The wall proximity effect was minimised, but not altogether removed, for probes with narrow included wedge angles, and in which the wedge head was furthest removed from the main circular stem by a long interface piece. The detailed geometry of this interface piece had a secondary effect, particularly when run-out into the cylindrical stem as shown in figure 1.2c). In an extension of this work to higher flows of 0.5 Mach number, Cook (1988) similarly observed that the wall proximity effect reduced as the included wedge angle was decreased; the results of Cook's investigation are included as figure 1.3. An independent investigation by Kennewell (1988) on a 30° included angle wedge probe demonstrated a reduction in the wall proximity effected region from 70mm to 30mm by doubling the interface piece length.

The literature suggests causes of the wall proximity effect. Filbee (1990) noted that flow local to the tip of a cantilevered traverse probe will accelerate, reducing the static pressure at the sensing head relative to that at other positions along the probe stem. A pressure gradient is established along the probe length, resulting in stemwise flows which could interfere with the probe indicated static pressure. The influence of this mechanism will be a function of the probe tip proximity to the wall.

Shreeve et al. (1976) postulated that vortices shed from the probe tip may be responsible for wall proximity effects. Ferguson (1967) demonstrated the existence of a wedge probe tip vortex using low speed smoke flow visualisation techniques. He also shows experimental evidence of wedge tip cross flows from pressure to suction surface when the probe is yawed relative to the flow. It can be concluded that tip vortices and cross flows influence the static pressure sensed by a wedge probe, particularly when the static tappings are positioned near to the wedge free end. Takagi (1986) also used flow visualisation to examine the performance of miniature wedge probes at speeds up to Mach 1.5. From observation of Schlieren photographs, he suggested that at transonic Mach numbers, the shock formed ahead of the probe head interferes with that upstream of the probe stem. The probe stem bow shock wave was seen to strengthen as the probe immersion increased, resulting in calibrations which exhibited the typical wall proximity effect.

At sub-sonic Mach numbers, the wall proximity effect is in a sense that would result from probe blockage, i.e. as the probe immersion is increased, so the blockage in the plane of the probe increases, thus accelerating the flow and dropping the local static pressure. Gould (1971) studied experimentally the influence of probe blockage on the static pressure sensed both by the probe and at the wall through which the probe is introduced into the flow. For the geometries of wind tunnel and probe used for example by Cook, Gould's results show that the probe static pressure coefficient would be depressed by less than 2% for immersions of up to 100mm, whereas depressions of up to 25% were actually experienced. Probe blockage effects therefore account for but a small fraction of the overall wall proximity effect.

It was suggested by this author, (Smout , 1990), that the hole through which the probe is inserted may, at certain immersions, generate local disturbances which would alter the static pressure field around the probe head. Again, this mechanism can be but partly responsible, since the wall proximity effect persists well beyond the immersion at which the traverse hole is completely filled by the circular probe stem. Smout also investigated the influence of leakage at the hole through which the probe was introduced into the calibration flow. Leakage both into and out of the main flow was induced by pressurising or evacuating a chamber arranged around the probe stem, but no significant change in the wall proximity effect was observed.

Howard et al. (1993) used a narrow angle wedge probe to measure the radial distribution of static pressure downstream of the inlet guide vanes of a low speed research compressor. The distribution was also predicted by streamline curvature analysis. Good agreement between the two profiles was obtained over the majority of the traverse, but discrepancies of up to 4% dynamic head were observed over the outer 30% annulus height. The discrepancy was in a direction that would be explained by the wall proximity effect.

Three approaches to solving the problem of static pressure measurement in turbomachinery with probes that suffer from wall proximity effects are found in the literature.

i) Geometrical modifications to the probe have been attempted. Filbee (1990) reports a comprehensive study involving the attachment of extensions, end-plates and fins to a Glawe and Krause type wedge probe design, as shown in figure 4.6. However, whilst details of the wall proximity curve were altered, there is no evidence in this or any other study that geometrical modification has overcome the problem.

ii) Shreeve formulated a means of modifying the probe calibration coefficients used in analysing turbomachinery test data for the effects of wall proximity. The formulation was based on experimentally determined probe characteristics, and was used successfully in correcting static pressure measurements from research compressor tests.

iii) Predictions of the static pressure profile at a plane are used in place of measured data, (Howard et al. (1993) for example).

To summarise, the wall proximity effect has been reported for both cylindrical and wedge type probes by several investigators, and shown to depend on details of the probe geometry and possibly on the prevailing flow conditions. The majority of information concerns static pressure measurement errors, although there is some evidence to suggest that near wall yaw angle measurements may also be affected. The effect is manifest in both wind-tunnel and turbomachinery flows, and cannot be explained by blockage effects. Although several other explanations are offered, the literature does not contain a detailed study of the effect.

4.6 CALIBRATION FACILITY DEPENDENCE

Concern over the validity of pneumatic pressure probe measurements in the transonic flow domain were raised at the 1981 symposium, "Measuring Techniques for Transonic and Supersonic Flow in Cascades and Turbomachines," (Fransson, 1983). In response, a cross-calibration exercise of the same 46° included angle wedge probe was organised using eleven wind tunnels located throughout Europe. Calibrations at zero incidence over a Mach number range of 0.3 to 1.5 were completed in each facility. In collating the results, Fransson concluded that the probe read a higher static pressure in the free jet than in the closed duct type of facility at nominally the same flow condition. No explanation for this observation was offered, but it concurred with unreported Rolls-Royce experience of calibrating wedge probes in the two types of facility.

In a detailed investigation of pressure probe characteristics, Humm et al. (1994) present curves of yaw angle sensitivity vs. Mach number for several wedge probe designs, where yaw angle sensitivity is defined in appendix E. The yaw sensitivity of a 45° included angle wedge probe was higher in the closed tunnel than in the free jet. For example at Mach 0.6, yaw sensitivities of 0.65 and 0.52 were obtained in the closed tunnel and free jet respectively. Humm suggests that a three dimensional flow effect local to the probe tip may be responsible.

To summarise, significant differences between calibrations of the same probe in open jet and closed tunnel facilities are reported, in terms of both the static pressure coefficient and the yaw angle sensitivity. No record of an investigation into the cause of these differences has been found in the literature. In the following chapter, the design, execution and results of a set of experiments aimed at quantifying the wall proximity effect and the calibration facility dependence of actual wedge probes is reported.

CHAPTER 5: EXPERIMENTS WITH ACTUAL PROBES

5.1 INTRODUCTION

Four experiments to determine the characteristics of actual size, wedge-type probes under various conditions are reported in this chapter. Each of these experiments was aimed primarily at establishing a complete and consistent data set from which the wall proximity effect and calibration facility dependence of wedge probes could be defined and quantified. This was to form the basis from which further experiments to investigate the physical causes of these effects would be planned and executed.

Section 5.2 explains the factorial experiment which was designed to quantify the effect and interaction of several probe and flow variables on the wall proximity effect. Details of the wind tunnel characterisation and modifications which were necessary to achieve uniform flow conditions are included. A supplementary test to assess near wall yaw angle measurement errors with wedge probes is also described.

A truncated version of the factorial experiment was performed at the inlet to a low speed compressor rig, to determine whether the results obtained in the wind tunnel could be repeated in an annular duct. This is reported in section 5.3. Section 5.4 describes a series of tests on which the investigation of probe calibration facility dependence was based. Four wedge probes were calibrated in each of three facilities, a closed section wind tunnel, and two open jets of different size.

5.2 FACTORIAL EXPERIMENT

5.2.1 Design of Experiment

From the review of previous work in chapter 4, it emerged that the wall proximity effect depended on details of the wedge probe geometry, on the prevailing flow conditions, and on the way in which the probe was introduced to the flow. The wedge included angle, the length of the interface piece and the presence of a fillet at the base of the interface piece were seen to be influential geometric features. In turbomachinery flows, turbulence intensity, Reynolds number, air speed and direction relative to the probe are all variables. Resolving the flow direction into yaw and pitch components, a minimum of eight variables were identified for investigation.

An experiment was needed in which the relative importance of each of these variables, and any interaction between variables could be quantified. The 'Taguchi Method' described by Bissell (1989) was used to good effect by Bosworth (1989) in determining the relative influence of eight variables on road vehicle steering wheel vibration. The required number of experiments was reduced from 6561 to 18 through the use of a Taguchi orthogonal array. However, the choice of an appropriate array relied on considerable à priori knowledge of the problem, which was not available in the case of wall proximity effects.

The full factorial approach to experiment design was therefore adopted, (Davies, 1978). This technique requires a choice of 'high' and 'low' values for each variable, where chosen values bracket the practical range for each variable. Experiments are then conducted with all combinations of variables in their high and low states. A total of 2^n experiments are required where 'n' is the number of variables. Eight variables implied 256 separate experiments. However, experimental facilities for varying the test flow Reynolds number independently of the Mach number were not available, and it was not possible to include Reynolds number as an independent variable. (The implications of this on the overall result are discussed in chapter 8.) The required number of experiments was

further reduced to a manageable level by conducting two stand alone tests, each incorporating five variables. Test 1 was conceived as a preliminary investigation, the result of which would influence the choice of variables for a second, definitive test. Whilst limiting the applicability of factorial experiment analysis techniques, this approach reduced the required number of experiments to 64. Table 5.1 gives the final choice of variables for each test.

5.2.2 Wind Tunnel Selection and Characterisation

Five criteria were identified in selecting a suitable wind-tunnel for the factorial experiment. Firstly, a uniform static pressure field at the measurement plane was required under all flow conditions, against which the static pressure indicated by a given probe could be compared reliably. It was also required that the total pressure field at the measurement plane be uniform outside the boundary layer, to minimise shear effects. A minimum size of 150mm between opposite walls was set, this being twice the most severe wall proximity effect reported in the literature. Facility for varying the free stream Mach number and turbulence intensity over turbomachinery representative ranges was required. Finally, the selected wind tunnel had to be both cost effective to operate, and available within the project timescales.

A circular section, suction wind tunnel of 203mm internal diameter was available within the Turbomachinery Department at Cranfield, and is shown schematically in figure 5.1. This was fitted with an inlet scroll designed in accordance with McKenzie (1952) to avoid static pressure distortion at the measurement plane. An intake filter box was used to condition the flow. The literature contains examples of the wall proximity effect both in circular ducts and in turbomachinery annuli, implying that investigations conducted in a circular section tunnel would be representative of the turbomachinery annulus case. The tunnel was equipped with manually operable probe radial traverse, yaw and pitching mechanisms, and would operate stably over a Mach number range between 0.1 and 0.8.

A square mesh of circular wires was introduced at 20 mesh spacings upstream of the measurement plane to vary the flow turbulence intensity and length scale. Strong radial total pressure gradients generated by the turbulence grid near the tunnel walls were observed during early commissioning tests. These were overcome by incorporating a vertical plate at the half radius position as detailed in figure 5.2. Two holes were provisioned in the plate to facilitate probe traverses at both 0° and -10° of pitch, with removable guide tubes between the original tunnel wall and the plate to prevent leakage into the tunnel around the probe stem. Sign conventions adopted for yaw and pitch angle are given in figure 5.2. The plate leading edge was shaped as shown in figure 5.2, and manufactured as a separate part which was then doweled on to the square ended plate. A slight discontinuity at the join was left as a boundary layer trip, and ensured a turbulent boundary layer under all flow conditions. The complete facility is shown in plate 5.1.

The tunnel flow conditions at the measuring section were monitored using a fixed immersion pitot tube and two wall static pressure tappings which were manifolded together. Stand alone instruments of an appropriate range were used to measure the tunnel reference and probe indicated pressures; details of the pressure instruments and rigging arrangements used for all the experiments reported in this chapter are given in appendix E.

An experimental characterisation of the flow in this tunnel was undertaken to check the uniformity of the working section static pressure profile. This entailed traversing the measurement plane with a simple pitot tube to measure the total pressure profile out from the vertical plate. A 'Polytec' two-spot laser transit anemometer was used to measure the velocity profile on the same probe traverse axis, and under nominally the same tunnel operating conditions. Following suitable normalisation, the velocity and total pressure profiles were combined via the isentropic flow equation to derive the static pressure profile. For all tested flow conditions, the static pressure derived in this way agreed with the tunnel wall static pressure tappings to within 1.0% dynamic head at all positions across the measurement plane.

Figure 5.3 plots the laser measured velocity, normalised by the tunnel centre line value, against distance out from the vertical plate, for a flow of 0.75 Mach number and 0.8% turbulence. By spraying the plate matt-black, and by turning down the gain of the photomultiplier tubes in the laser anemometer to minimise glare induced noise, it proved possible to measure velocities to within 1.5mm of the plate. Schlicting (1960) contains the following correlation for turbulent boundary layer thickness (δ) as a function of distance back from the transition point (X), and of Reynolds number based on X, (Re_x):

$$\delta = 0.37.X.Re_x^{-0.2} \quad \ldots\ldots\ldots\ldots\ldots\ldots\ldots\ldots (5.1)$$

This gives a boundary layer thickness of 2.04mm for the case in figure 5.3. Excellent agreement between the measured velocity profile and that predicted assuming a (1/7) power law for the velocity distribution through a turbulent boundary layer (Massey, 1988) was obtained when using a boundary layer thickness of 2.04mm in the calculation. Similarly good agreement was obtained at other flow conditions.

Free stream turbulence measurements were made at the measuring plane using a single element, 5μm diameter hot wire with an 'M-series' anemometer bridge manufactured by Dantec Ltd. Data were recorded at 40kHz bandwidth onto magnetic tape, and subsequently replayed through a suitable r.m.s. meter. A background turbulence intensity of 0.8% was measured with no turbulence grid fitted, and was attributed to the inlet flow conditioning filter box. The turbulence grid used in all the 'high turbulence' tests had a mesh spacing of 8.5mm and a bar diameter of 1.6mm, and was chosen against criteria given by Townsend (1976) to ensure a full spectrum of turbulent eddies at the measurement plane. A radially uniform turbulence intensity of 4.5% was measured with this configuration. Frenkiel (1948) gives correlations which predict a turbulence intensity of 2.8% for a similar tunnel arrangement, but these are only valid for negligible levels of turbulent kinetic-energy upstream of the turbulence grid. A significantly higher turbulence intensity is to be expected given the relatively high level of background turbulence present in this tunnel, (Roach, 1987).

5.2.3 Experiments

The criteria in choosing high and low values for each variable in the factorial experiment was to ensure that values typically reported in the literature for turbomachinery rig testing were bracketed. Considering the probe itself, the smallest wedge included angle that can realistically be achieved on a 6.35mm diameter stem is 23°, being limited by the diameter of pressure tubing that must be inserted into the head. Larger wedge angles may be used in applications requiring greater sensitivity to flow incidence; a 60° angle was chosen, this being the largest value to find repeated use in turbomachinery tests reported in the literature.

Low and high values for the interface piece length were taken as 6mm and 20mm respectively, covering the range seen in practice. The shape of the fillet between the circular stem and the interface piece is defined in Figure 5.4. A high value was assigned to this variable in experiments with the fillet installed. Two 24° and two 60° included angle wedge probes based on a 6.35mm diameter stem were purpose built for this exercise. The fillet was built-up using a filled epoxy resin, and was added or removed as required. Each probe was assigned a unique four digit identification code of the form '24SS'. (The first two numbers signify the included wedge angle, the first letter indicates the interface piece length (Long or Short) and the second letter indicates whether a fillet was fitted (F) or not (S).) The two 24° probes are shown in plate 5.2.

All the experiments of test 1 were conducted at 0.1 Mach number, this being typical of low speed research compressor rig flows. Low and high Mach number values of 0.35 and 0.75 were chosen for the second test series to bracket the range experienced in high pressure compressors. Low and high free stream turbulence intensity values of 0.8% and 4.5% were achieved as explained in section 5.2.2. The higher value was believed to be representative of the purely random component typical of turbomachinery flows, as distinct from the periodic flow structures.

For turbomachinery applications, the range of flow incidence onto the probe is generally contained within ±10° of yaw, and 0° and 10° were taken respectively as low and high values of yaw angle. Similarly in an axial flow machine, it is usually assumed that the bulk flow does not deviate from the bounding walls by more than ±10° pitch. Ferguson (1967) and others have shown that the influence on the static pressure coefficient is up to eight times as great at negative than at positive pitch angles. Thus 0° and -10° were chosen as low and high values.

From the preliminary test 1, it was concluded that both the wedge head included angle and the length of the interface piece were statistically significant in influencing wall proximity effects. The wall proximity effect was reduced by decreasing the included wedge head angle, and by increasing the length of the interface piece, in good agreement with the literature. A significant interaction between interface piece length and pitch angle was observed, but yaw angle showed no statistically significant influence over the tested 0° to 10° range.

Although the included wedge angle was identified as an significant effect, it did not significantly interact with any of the other variables. This was considered sufficient justification to discard the included wedge angle as a variable, in order to limit the size of the definitive test 2 to a realistic number of experiments. It was recognised that the penalty of this decision would be failure to establish the significance of the included wedge angle relative to the other tested variables. The insignificance of yaw angle was a surprising result which apparently contradicted the observation by Morris (1961) that wedge probe yaw angle sensitivity could be influenced by the close proximity of a wall. However it is important to draw the distinction between yaw angle sensitivity, which is based on the *difference* between the static pressures S2 and S3 sensed at either side of the wedge head, and static pressure coefficient, which is based on the *mean* of S2 and S3. On the basis of the preliminary test 1 results, yaw angle was dropped as a variable in the definitive factorial experiment, leaving a set of five variables to be investigated as test 2. These are summarised in table 5.1. The influence of the wall on yaw angle sensitivity was investigated separately by calibrating wedge probes against yaw angle at several

different immersions; this experiment is reported in section 5.2.4, '*Near Wall Calibrations for Yaw Angle*.'

Table 5.2 summarises the combinations of high and low values for each variable with the corresponding experiment number. For a given experiment, the appropriate probe was installed in the traverse gear, and the wind tunnel stabilised at the required flow condition. The probe was traversed out from flush with the vertical plate to 100mm immersion in 5mm increments, and nulled into the flow at each immersion. In practice this involved yaw angle adjustments of less than ±0.5° over the entire traverse. A set of probe and tunnel reference pressures were recorded at each position. The experiments of test 2 were conducted in random order to reduce the risk of systematic error.

5.2.4 Results and Analysis

Factorial Experiment

Successful results were achieved for experiments 1 to 24 in table 5.2. The wind tunnel fan proved incapable of driving a 0.75 Mach number flow at high turbulence intensity, the pressure drop across the turbulence grid being prohibitively high. Experiments 25 to 32 were not therefore completed and the impact of this is discussed in chapter 8.

Results were plotted for each experiment as static pressure coefficient , B, against immersion non-dimensionalised by the probe stem diameter, (I/d), and exhibited a similar form. This is illustrated in figure 5.5 for probe 24SS at 0.75 Mach number, 0.8% turbulent flow and at 0° pitch, (experiment 9). The zero immersion position corresponds to the point at which the static tapping centres are aligned with the wall surface. The probe exhibits a positive value of B immediately adjacent to the wall which progressively decreases with increasing immersion. A point is reached beyond which increasing the immersion results in no further change in B. The stable B value of -0.15 at immersions greater than 65mm reflects the fact that, at the flow conditions set for experiment 9,

probe 24SS reads a static pressure which is less than the true freestream static pressure by 15% of the dynamic pressure head. The general form of curve shows good agreement with the wall proximity effect reported in the literature, and typified by figure 1.3. Error bars were calculated as shown in appendix E in accordance with the industry standard uncertainty analysis technique by Abernathy (1973). The uncertainty in each data point is one order of magnitude smaller than the effect itself, and the wall proximity effect is one order of magnitude greater than the variation in static pressure profile reported in section 5.2.2. Assuming that the value of static pressure coefficient obtained at 70mm immersion were applied in analysing radial traverse data from a turbomachine, the static pressure determined from the near wall measurements would be in error by up to +20% dynamic head.

Inspection of figure 5.5 suggests three options for quantifying the wall proximity effect:

i) the distance from the plate over which the effect is manifest, (referred to as the 'immersion' result),

ii) the maximum deviation in static pressure coefficient from the 'free-stream' value, (referred to as the 'deviation' result), or

iii) some combination of these two such as the area under the curve, (referred to as the 'area' result).

Analysis of all three sets of results was performed using 'Yates' technique, (Davies, 1978). This method compares the results of a suitable number of factorially designed experiments in a sequential manner in order to quantify the relative effect of each variable, and any interactions between variables. Experiments 1 to 16 inclusive were analysed together as sub-set 1 to fully define the effects of Mach number, interface piece length, interface fillet and pitch angle at 0.8% turbulence intensity. Experiments 9 to 24

were similarly combined as sub-set 2 to investigate interface piece length, interface fillet, pitch angle and turbulence intensity at 0.35 Mach number.

The results of the Yates analysis on the area results for sub-set 1 experiments are plotted in figure 5.6. Figure 5.6a) shows the relative effects of the four variables; the length of the interface piece and the freestream Mach number are the two most important variables, pitch angle has a relatively small effect, and the fillet has hardly any effect. A variable was taken as having a *positive* effect if increasing its value from low to high resulted in an *increase* in the wall proximity effect, and vice versa. Interactions between the variables are plotted in figure 5.6b). In this case, a *positive* interaction between two variables indicates that increasing the value of the second variable from low to high resulted in an *increase* in the effect of the first variable, and vice versa.

To establish which of these effects and interactions were statistically significant given the uncertainty associated with the experiment, it was assumed that interactions between three or more variables had no significance, such that the contributions from the five higher order interactions could be used as an error indicator. The method first involved computing the mean sum of squares from these five contributions. The ratio of variances for one and five degrees of freedom at 0.10, 0.05 and 0.01 probability levels were then obtained from one-sided 'F-test' tables, and multiplied by the error mean sum of squares to give the sum of squares values required for significance at the 10%, 5% and 1% levels respectively.

These values were compared with the sum of squares computed for each effect and interaction to ascertain the level of significance in each case. Variables whose effects were significant at the 1% level were thus more influential than those which showed significance at the 5% level, and so on. Tables 5.3 and 5.4 summarise this information for sub-sets 1 and 2 respectively, including the sense, (-ve or +ve) of the effect or interaction, for the area, immersion and deviation results. No entry against a given variable or pair of variables indicates a statistically insignificant effect or interaction. These results are discussed fully in chapter 8.

Near Wall Calibrations for Yaw Angle

The results of calibrating a 30° included angle wedge probe against yaw angle at 0.1 Mach number are plotted in figure 5.7 in the form C_{yaw} vs. yaw angle, (where C_{yaw} is defined in appendix E). Calibrations were completed at four probe immersions. In general, C_{yaw} is directly proportional to yaw angle over ±8° of yaw, beyond which the change in C_{yaw} is non-linear but still monotonic with yaw angle increasing up to at least ±20° of yaw. A marked difference between the four calibrations is apparent outside the linear region.

The slope of the linear region between ±8° yaw, (i.e. the probe yaw sensitivity), is plotted against immersion in figure 5.8, where yaw sensitivity is seen to increase by 12% between 15mm and 60mm immersion. Also plotted in figure 5.8 is the wall proximity effect curve for the same probe; yaw angle sensitivity is apparently affected over a similar immersion range to static pressure. Assuming that the calibration value at 60mm were applied in analysing radial traverse data from a turbomachine, at 0.1 Mach number and a probe setting angle of 5° relative to the flow, an error of +0.7° near the wall would result. Given that the current industry requirement is for yaw angle measurements of less than 0.5° uncertainty, this represents a significant error.

The same test was repeated with Probe 24SF at a higher flow of 0.35 Mach number, and at three immersions. Results are presented in figure 5.9. The same trend of increasing yaw sensitivity with increasing immersion was observed as in the previous experiment. In figure 5.10, the data from figure 5.9 is re-plotted as static pressure coefficient based on the S2 (left-hand side) static tapping only, against yaw angle for the three immersions. This indicates excellent agreement between the two higher immersion curves, but a significant departure at the lowest immersion, particularly at negative incidence when the S2 tapping is effectively on the wedge suction surface. These results are discussed fully in chapter 8.

5.3 COMPRESSOR RIG TRAVERSING

5.3.1 Design of Experiment

It was inherently assumed in the factorial experiment, with justification from the literature, that the wall proximity effect was independent of the precise geometry of flow ducting in which measurements were made, for duct heights greater than the extent of the wall proximity effect. Probe traverses in an annular section were required to check this assumption, and hence to demonstrate the applicability of the factorial experiment results to a turbomachinery environment.

The option of constructing a purpose designed, annular section wind tunnel was weighed against that of using an existing annulus in a suitable compressor or turbine rig. Of the turbomachines available at Cranfield University, the low speed, large-scale four stage compressor rig, with an annulus height of 100mm, was considered most suitable. This also emerged as the most cost effective option at least for a limited amount of running, and was adopted as the test vehicle.

The flow at the I.G.V. inlet plane of the four stage rig was expected to be both axial and steady, being conditioned by an inlet filter box and bell-mouth intake arrangement. This plane was therefore adopted for the probe traverse tests. Of the five independently varied parameters in test 2 of the factorial experiment, only the probe geometry could be altered in the four stage rig. The flow inlet velocity was fixed at the design point condition of 0.1 Mach number, the inlet turbulence intensity was also fixed by the inlet flow conditioning at a level to be determined, and the available traverse gear had no facility for varying pitch angle.

Probes 24SF and 24LF returned significantly different wall proximity curves in the factorial experiment at 0.35 Mach number. These probes were chosen for the four-stage rig tests, to determine whether the factorial experiment result was repeated in an annular facility at a lower flow.

5.3.2 Description of Facility

The four stage rig is a large-scale, low-speed research compressor with repeating stage blading designed to be representative of a multi-stage compressor subsonic middle stage. A cut-away drawing is shown in figure 5.11, and a full description was given by Howard et al., (1993). In this experiment, measurements were taken in the parallel section of the intake where the annulus height is 108mm. Total pressure rakes and wall static pressure tappings were available for reference measurements at the traverse plane. Pressures were sensed via a remote scani-valve and a temperature stabilised, high accuracy pressure transducer manufactured by 'Druck Ltd.'

A flow characterisation similar to that of the suction wind tunnel was completed. The total pressure profile at the traverse plane was measured using a pitot tube. A wedge probe operated in the 'null' reading mode was used to check for inlet swirl. Little change in swirl angle was found over the central part of the annulus, but variations of upto 2° over the outer 20%, and 3° over the inner 30% of the annulus were measured. The 'Polytec' laser anemometer was not available, and a single element hot-wire probe set perpendicular to the flow at mid-height was used instead to measure the radial velocity profile. The wire was calibrated at low Mach numbers up to 0.15 immediately prior to the four stage rig traverse, and checked again afterwards, to minimise and quantify errors associated with probe calibration drift. A velocity measurement uncertainty of 3% of reading (1.1m/s) was achieved, which compares acceptably with an absolute uncertainty of 1.0m/s associated with the laser anemometer. A free-stream turbulence intensity of 1.4% was determined from the hot wire measurements and was approximately uniform across the annulus.

Combining the total pressure and velocity profiles via the isentropic flow equation as before, the variation in static pressure across the annulus was calculated. This static pressure profile is shown in figure 5.12 relative to a mean of the hub and casing wall static pressures, non-dimensionalised by the dynamic head. In this case, the distance, I, from the outer annulus wall is normalised by the annulus height, H. Error

bars were determined according to the procedure in appendix E. Good agreement between wall static pressure and the freestream static pressure determined in this way was achieved at the inner and outer wall positions. A depression in static pressure at the mid-height position of 0.08 or 8% dynamic head was observed. Within the limits of experimental uncertainty, this is consistent with the measured variation in inlet swirl angle, as demanded by radial equilibrium. The static pressure profile in figure 5.12 was taken as the datum against which the two wedge probe indicated static pressures were compared.

5.3.3 Experiments

Having characterised the inlet flow, each wedge probe was rigged in turn to appropriate pressure transducers, (appendix E), and traversed from outer to inner annulus wall. In each case, with the rig stationary, a radial datum was established by immersing the probe until it touched the inner wall. The traverse gear was then backed off by an amount corresponding to the annulus height, to leave the probe tip flush with the outer annulus wall. The rig was then run up to the design point flow condition and stabilised. The outer 20% of the annulus was traversed in 2mm increments, the probe being nulled in to the flow at each radial height by rotating it until the pressures sensed by S2 and S3 were equivalent. This procedure was continued at 5mm increments over the remaining annulus, probe indicated total and static pressures being recorded at each radial position. Automated scans of the rig reference instrumentation were taken before, during and after every probe traverse. Reference pressure variations of no more than 0.12% dynamic head were recorded during any given traverse.

5.3.4 Results and Analysis

Plots of static pressure coefficient, B, against probe immersion non-dimensionalised in this case by the annulus height, H, are shown in figures 5.13 and 5.14 for probes 24SF and 24LF respectively. The reference static pressure at a given immersion was taken from the derived profile in figure 5.12, and the wall proximity effect is clear in each case. Error bars calculated as shown in appendix E are also plotted, and the results obtained in the factorial experiment for the same probes are over-layed in the appropriate figures for comparison. For each probe, the agreement between the wall proximity curves determined in the four-stage rig and in the original factorial experiment is within the limits of experimental uncertainty at all immersions. It was concluded from this that, at least at 0.1 Mach number, moving from a circular to an annular cross-section duct had no detectable impact on the probe performance.

5.4 CALIBRATION FACILITY DEPENDENCE

5.4.1 Design of Experiment

Although the information available on wedge probe calibration facility dependence was limited, (section 4.6), it was known that calibrations of static pressure coefficient vs. Mach number for a given wedge probe depended on whether a closed duct or a free jet calibration flow were used, (Fransson, 1983), and also possibly on the free jet diameter, (Shreeve, 1976). No information on the influence of probe geometry or incidence angle could be found.

An experiment was required to extend the database of relevant information, and to form the basis on which further investigation, via flow visualisation and numerical modelling, could build. For the probe itself, both included wedge angle and interface piece length were varied by using the four probes from the factorial experiment, thus bracketing the 45° wedge probe investigation discussed by Fransson. The closed section

wind tunnel flow had been thoroughly characterised for the factorial experiment and was selected together with two open jet facilities of differing jet cross-sectional areas. The maximum flow achievable on the smallest open jet was 0.35 Mach number; two flows of 0.1 and 0.35 Mach number were therefore selected. Full calibrations of each probe against yaw angle at each flow condition were planned on the three facilities, in order to investigate the importance of flow incidence.

5.4.2 Description of Facilities

The smaller of the two open jet facilities was assembled specifically for this experiment by a graduate trainee working directly under the author's supervision, and is shown in figure 5.15 and plate 5.3. The facility is subsequently referred to as 'Jet 1'. It is based around an existing plenum chamber housed within the company research laboratories at Derby. Compressed air is piped to the plenum chamber from the central site compressor, the flow rate being controlled by a series of upstream valves. Reference total pressure is measured in the plenum chamber using a pitot tube and a remote DPI140 pressure indicator. A bellmouth type intake is installed inside the plenum chamber downstream bulkhead to condition the flow into a two dimensional contraction which reduces to a rectangular nozzle measuring 50mm by 30mm at the exit plane. Due to the varying demands on the site air system throughout any one day, it was not possible to achieve steady flows of greater than 0.35 Mach number for the time required to complete a probe calibration. A probe traverse gear manufactured by 'Rotadata Ltd.', and mounted above the jet on a purpose built frame, gave automated variation of radial height and yaw angle, and manual adjustment in the axial direction, (plate 5.3).

The flow was characterised by traversing a 1.0mm O.D. pitot tube radially through the jet at six planes between 10mm and 40mm downstream of the nozzle front face. The jet total pressure measured in this way agreed with the plenum chamber reference pressure to within 0.2% dynamic head over the central 90% of the jet area at the 10mm axial position; this position was therefore selected as the traverse plane.

The larger of the two open jet facilities is similar in layout to the 'Jet 1' facility shown in figure 5.15, and is pictured in plate 5.4. Subsequently referred to as 'Jet 2', it is sited at the Rolls-Royce Derby test site and used routinely for calibrating aerodynamic instrumentation. Compressed air is delivered by a two-stage centrifugal blower to a plenum chamber in which reference measurements of stagnation pressure are made using a pitot tube and a remote DPI510 pressure indicator. The flow is then accelerated through a contraction and exhausts to atmosphere via an octagonal cross-section nozzle of 102mm across flats. It is assumed that no losses occur through the contraction, and that the jet static pressure equals ambient pressure. Stable flows of between 0.1 and 0.9 Mach number may be achieved at the measurement plane, 25mm downstream of the nozzle face. A fully automated traverse gear affords freedom in the radial, yaw and pitch modes.

A flow characterisation exercise was completed following installation of the current compressor in 1988. A pitot-static tube of the NPL type was traversed radially through the jet at various planes between 12mm and 150mm downstream of the nozzle front face. At the 25mm axial position, and over the central 90mm core of the jet, the indicated static pressure agreed with atmospheric pressure measured in the test cell to within the limits of experimental uncertainty at the tested Mach numbers of 0.1 and 0.35. Likewise the total pressure measured at the same plane agreed with that in the plenum chamber to within experimental uncertainty limits.

The closed duct wind tunnel was used in exactly the same configuration for this experiment as for the factorial experiment. A full description of the facility and its characterisation is given in section 5.2.2 above.

5.4.3 Experiments

Individual calibrations were completed in each tunnel in turn using the same procedure throughout. Probes were positioned in the open jets such that the plane of static tappings lay on the jet centre line, and at 100mm immersion in the closed wind

tunnel to avoid wall proximity effects. The standard of pressure instrumentation defined in appendix E was used for probe calibrations in Jet 1 and the closed tunnel , whilst the facility standard water and mercury manometers were adopted for the work in Jet 2. With the flow stabilised at the required condition, a given probe was first nulled to establish a zero yaw datum, and then yawed in 2° increments over a total range of ±20°. A complete set of probe and tunnel reference pressures were recorded at each angular position.

5.4.4 Results and Analysis

All the originally planned tests were completed successfully, giving a complete and consistent dataset on which to base further investigations. Probe indicated pressures were non-dimensionalised to form C_{yaw}, C_t, B2 (based on S2) and B3 (based on S3). Each coefficient was then plotted against yaw angle and summarised in a single sheet. Figure 5.16 exemplifies this form of presentation for probe 24LF at 0.35 Mach number in the larger open jet.

The specific characteristics of interest in comparing results between the three facilities were static pressure coefficient at zero yaw, and yaw angle sensitivity. The former were extracted from each of the calibration summary sheets and grouped as a function of the probe included wedge angle. This information is presented in bar chart form in figures 5.17a) and b) for the 24° and 60° probes respectively, and includes error bars computed in the usual way. Substantial differences particularly between the closed tunnel and open jet, but also between the two open jet calibrations are apparent.

Yaw angle sensitivities were similarly determined from each of the probe calibrations, over 10° and 20° yaw. Values obtained at each Mach number and in the three facilities were grouped together under probe type, and plotted in bar chart form to ease comparison. These are included as figures 5.18a) and b) for the 24° probes, and figures 5.19a) and b) for the 60° probes. Again, differences substantially in excess of the

experimental uncertainty are highlighted between calibrations of the same probe in the two types of facility. These are discussed fully in chapter 8.

To summarise this chapter, a 203mm diameter, closed section wind tunnel was modified and the flow fully characterised to achieve a facility in which a probe's ability to measure static pressure under a wide range of conditions could be tested reliably. The fully factorial approach to experiment design was used successfully in quantifying the relative effects and interactions of five independent variables on the near wall performance of wedge type traverse probes. The probe interface piece length and fillet geometry, the probe pitch angle, and the flow Mach number and turbulence intensity were all investigated. Good qualitative agreement was achieved with the limited information on wall proximity effects contained in the literature. In a supplementary experiment, two wedge probes were calibrated against yaw angle at various immersions. A significant increase in yaw sensitivity was observed as each probe was moved away from the tunnel wall.

From a truncated version of the factorial experiment at the I.G.V. inlet plane of a low speed compressor rig, the dependence of the wall proximity effect on duct geometry was assessed, and found to be insignificant, at least at low Mach numbers. The calibration facility dependence of wedge probe performance was investigated by calibrating four probes against yaw angle at two Mach numbers in three different wind tunnels. Significant differences between values of static pressure coefficient and yaw sensitivity were observed between results from the closed section tunnel and the two open jet flows.

Overall, the tests succeeded in establishing a complete and consistent data set appertaining to the wall proximity effect and calibration facility dependence of wedge probes. A fuller discussion is given in chapter 8, where the results are interpreted in the light of further experimental work reported in chapter 6, and numerical modelling work presented in chapter 7.

CHAPTER 6: EXPERIMENTS WITH MODEL PROBES

6.1 INTRODUCTION

Whilst the actual probe experiments discussed in chapter 5 aimed to quantify the wall proximity effect and the calibration facility dependence of wedge probes, the experiments reported in this chapter were designed to reveal the physical flow mechanisms responsible for these effects, primarily through the application of flow visualisation techniques. The experiments were planned against the following specific aims:

i) to generate a physical picture of the flow around a wedge probe design over a representative range of flow incidence angles,

ii) to study the alterations in this flow pattern as the probe was progressively immersed into the flow,

iii) to study the influence of probe geometry on the visualised flow pattern,

iv) to generate data with which to validate numerical predictions of the flow field using a computational fluid dynamics code, and against which to compare the findings of the chapter 5 experiments.

Three individual experiments were designed to meet these aims. The first, third and fourth aims were met in part using large scale, two dimensional wedge models. Low speed smoke flow visualisation was used to illustrate the influence of the wedge included angle and leading edge shape, the flow Reynolds number and the angle of incidence. The experiment design and technique is reported in section 6.2.

Section 6.3 describes a similar experiment in which the flow past a large scale, three dimensional model of a 30° included angle wedge probe was studied using smoke flow visualisation. The model installation in the wind tunnel was designed to give radial and angular movement such that the first two aims could be met in full. In an extension of this experiment, static pressure tappings were incorporated into the model surfaces in order to record the probe surface pressures as a function of probe immersion and yaw angle at various flows. This third experiment was included primarily to meet the fourth aim. Sample results from all three experiments are included. In chapter 8, these are used to develop an understanding of the physical flow mechanisms responsible for the results presented in chapter 5.

6.2 TWO DIMENSIONAL MODELS

6.2.1 Design of Experiment

Whilst it was recognised that two-dimensional model testing was unlikely to provide insight into the wall proximity effect, a detailed understanding of the flow over wedge shapes was required in interpreting the calibration facility dependence of wedge probes. Two dimensional models of simple construction offered a rapid and low cost means of achieving this for a range of geometries. In addition, flow visualisation of the complex flows expected around a fully three-dimensional probe model was likely to be more successful given some prior experience in the simpler two-dimensional case. All the explanations proposed in the literature for both the wall proximity effect and the calibration facility dependence were in terms of flow structures local to the probe, rather than phenomena such as boundary layer transition or separation at the probe surface. A tracer technique for visualising these structures was therefore required in preference to a surface flow visualisation method. Given that the experiments were to be conducted in air, a review of the literature highlighted the following options:

i) the direct injection of smoke particles sufficiently small to accurately follow the flow, and observation by eye and on film, (Nakayama et al., 1988),

ii) the smoke-wire method, whereby very fine smoke filaments are generated by vaporising oil from an electrically heated fine wire, and results again captured on film, (Mueller, 1983),

iii) the laser-light sheet method, where the intensity of light scattered from smoke particles passing through a coherent laser light sheet is recorded on video film, (Betts and Stanfield, 1992). (A single light source and electro-optic detector arrangement working on the same principle is reported by Dominy (1992)),

iv) the spark tracing method, where electric discharges are produced using a series of high voltage pulses between suitably shaped electrodes. A low resistance, ionised path results which moves with the flow, and along which the second and subsequent electric discharges propagate in a succession of trace time lines, (Nakayama et al., 1988),

A technique which was reliable, inexpensive and readily transportable between facilities was required, in that the use of at least two different wind tunnels possibly at different sites was envisaged. These criteria were best met by the fist option of direct injection and filming of smoke filaments. This method was selected for all the flow visualisation tests reported in this chapter, and effectively imposed a free-stream velocity limit of 15m/s, since the smoke filaments were expected to become unstable at appreciably higher flows, (Ewald, 1980).

Wedge probe models with included angles of 24° and 60° were chosen to simulate the actual probes tested in the factorial design experiment. For the tests to be representative, dynamic, kinematic and geometric similarity between the model and the actual situation had to be ensured as far as possible. Dynamic similarity requires that the ratio of forces at similarly located positions in two systems be equal in magnitude. In this

case, the inertial, viscous, pressure and elastic forces formed a closed force polygon, with the elastic component only becoming significant as the flow became compressible. Thus dynamic similarity could be ensured by simulating the actual Reynolds number, (the ratio of inertial to viscous forces), and the actual Mach number, (directly related to the ratio of inertial to elastic forces). In practice, turbomachinery representative Mach numbers could not be reproduced in the flow visualisation tests due to the velocity limit imposed by the smoke flow technique, and the results were strictly representative of the incompressible flow case only. The use of models scaled from the original by applying a uniform scaling factor as required for geometric similarity did offer the potential to achieve turbomachinery representative Reynolds numbers. A wedge probe based on a 6.35mm diameter stem and immersed in a Mach 0.8 flow has an associated Reynolds number of 11.2×10^4. This equates to a thirty times size model probe operated at 9.4m/s, comfortably within the 15m/s velocity limit set above. A uniform scaling factor of thirty was therefore adopted for the two-dimensional model designs.

6.2.2 Wind Tunnel Selection and Experimental Arrangement

The development of the smoke-flow wind tunnel from the earliest recorded design by Ludwig Mach in 1893 was reviewed by Mueller (1983), who identified a set of key features for successful smoke flow visualisation. Mueller noted that precise visualisation of detailed flow features would only be achieved if laminar to turbulent transition of the injected smoke filaments was avoided, and that this implied an upstream settling chamber, upstream damping screens and a large contraction from the inlet to the working section. Adequate optical access at the working section, and sufficiently intense lighting to illuminate the smoke particles for capture by eye or on film were also prerequisites.

A smoke flow visualisation wind tunnel which met these requirements was available in the Cranfield College of Aeronautics. Normally used for teaching purposes, this tunnel was already equipped with smoke generating and injection equipment, and was ideally suited to the two-dimensional model experiments. This tunnel is shown in

figure 6.1 and plate 6.1. Air is sucked through a rectangular section intake into a settling chamber which also houses the motor and fan. The flow is accelerated through a two dimensional contraction of 8:1 into the working section. A multi-point smoke rake is mounted vertically in the contraction and can be moved radially and laterally to align smoke filaments with features of interest on the model. The smoke rake design follows that of Ewald (1980) and comprises a two-dimensional airfoil section of 0.06 thickness to chord ratio, with tapered injectors protruding from the trailing edge; the smoke rake is shown in figure 6.2. Smoke is produced within a smoke generator mounted beneath the tunnel by vaporising a light, high purity machine oil. The oil is drip fed onto a disc spinning in the horizontal plane, and then flung onto heated plates arranged around the disc. Smoke is sucked into the rake by the tunnel depression, and the smoke generator is pressurised to assist this process. By varying the oil drip feed rate, the disc rotational speed and the feed pressure, the volume of smoke can be matched to the prevailing flow conditions in the tunnel.

Figures 6.3a) and b) detail the 24° and 60° included angle wedge models designed for this experiment. Dimensions were scaled directly from the equivalent actual probes as discussed. The wedge leading edges were made detachable at a transverse line 10% chord back from the wedge apex, such that rounded leading edges could be substituted. This enabled tests with sharp, rounded and square leading edges to be conducted with only two basic models. The wedges were constructed from pin board material, and equipped with brass bushes for rapid mounting and dismounting on to a plywood disc of 0.66m diameter. This then located in the tunnel back wall (figure 6.1) and could be rotated through up to 360° to present the model at any angle to the flow. All the tunnel internal walls and model surfaces were sprayed matt-black to maximise contrast with the smoke filaments, although it proved necessary to use a pale grey colour on the end of the model to distinguish it from the tunnel back wall.

A pitot-static tube (Bryer and Pankhurst, 1971) was used in calibrating the fan speed control unit against air velocity in the working section prior to introducing the models. Strip lights were arranged above and below the model to illuminate the smoke

flow patterns which were recorded using a black and white video camera. Additional halogen spot lighting, judiciously positioned to avoid shadows and reflections from the back wall, was necessary to give adequate contrast on film. A time code generator was used to superimpose the date and time in one corner of the video image. This subsequently enabled experiments to be identified , and particular frames of interest selected for printing as still photographs by the Rolls-Royce photographic department. Additional still photographs were shot to supplement the video.

6.2.3 Experiments

With a given wedge model mounted in the tunnel, the fan speed was set to give the required air velocity, and the smoke generator controls adjusted to achieve sufficiently dense smoke filaments. In practice this involved a considerable amount of fine tuning, both of the smoke generator, and of the lighting positions. Vertical adjustment of the smoke rake ensured that a smoke filament impinged on the model leading edge in the zero degrees yaw position. The video camera was then set to record continuously as the wedge was rotated from 0° to 44° yaw in discrete 2° steps. Whilst filming, the flow pictures were checked at a video monitor for contrast and consistency. Occasional fading of the smoke filaments was observed, but was rectified via minor adjustments to the smoke generator before proceeding with the next yaw angle point. A total of fourteen tests were completed in this way with different configurations of the wedge models and at three Reynolds numbers as summarised in table 6.1.

6.2.4 Results

A total of 3½ hours of video film was recorded during two test sessions in the Cranfield flow visualisation tunnel. Significant features of the visualised flow are described below, and illustrated by frames extracted from the video, or with original still photographs. A full discussion of these results in the light of other findings is reserved for chapter 8.

Figures 6.4a) and b) show the flows around the sharp nosed 24° wedge model inclined at 4° and 8° to the flow respectively, at a Reynolds number of 5.2×10^4. Well defined, laminar smoke filaments were clearly observed in the free stream flow away from the model, and near the model pressure surface. Although some detail of the suction surface flow was obscured by shadow, the flow lifted noticeably immediately downstream of the leading edge of the wedge at 8° incidence, before moving back towards the wedge face further downstream. Diffusion of the same suction surface smoke filament just downstream of the leading edge was apparent from the corresponding video film, indicative of a suction surface separation bubble in the leading edge region.

As the yaw angle of the 24° probe was increased, so the reattachment point moved progressively further back along the leeward wedge face until complete separation without re-attachment occurred at 20° yaw, (figure 6.5). A stagnation point was observed on the pressure surface, just downstream of the leading edge, about which the flow divided. Although the smoke filaments were not always ideally positioned, a progressive migration of this stagnation point away from the leading edge was observed as yaw angle was increased. Generally similar results were recorded for the 60° wedge model, with suction surface flow separation beginning at 18° yaw, followed by complete separation without re-attachment at 30° yaw.

The development of the flow structure in the wake of the model at increasing yaw angles was recorded on video film using the wide angle video camera lens. In general, smoke filaments crossed over each other in a helical pattern which propagated downstream by at least 4 wedge chords, (figure 6.6). The diameter of this helix and the amplitude of transverse oscillation of the wake both increased with increasing yaw angle. At yaw angles greater than 20°, transverse oscillations of the filaments near the wedge faces were also apparent. Both wedge models exhibited similar behaviour, although the frequency of wake oscillation was higher for the 24° wedge than for the 60° wedge.

Figure 6.7 shows the flow patterns around the 24° wedge model fitted with a radiused leading edge, again at a Reynolds number of $5.2x10^4$ and at 8° yaw. Radiusing the leading edge made little observable difference to the flow near the pressure or suction surface over the whole yaw angle range, although the suction surface separation bubble on the blunt nosed wedge formed at a lower yaw angle of 4°. Fitting a rounded leading edge to the 60° wedge had more effect, and delayed the onset of transition and complete separation without re-attachment to higher yaw angles. As with the 24° wedge, suction surface separation was evident in the blunt nosed model at 4° yaw. Results recorded at the three tested Reynolds numbers were broadly similar. From the literature survey, differences in the size and structure of the suction surface separation bubbles might have been expected as a function of Reynolds number, but the suction surface flow was not visualised in sufficient detail to detect any such differences.

6.3 THREE DIMENSIONAL MODELS

6.3.1 Design of Experiment

In order to fully meet the originally stated aims, a large scale experiment in which smoke flow visualisation techniques could be used, but which simulated the actual wedge probe calibrations reported in chapter 5 was required. The flow visualisation wind tunnel used for the two dimensional experiments was not suitable for this purpose, and a specification based on the recommendations of Mueller (1983) and Ewald (1980) was assembled. This is included as appendix F. In sizing the tunnel working section, it was assumed that the wall proximity effect would extend up to eight times the probe stem diameter, d, from the wall of introduction, regardless of the probe stem diameter. A minimum tunnel height of 16d was then specified to avoid any adverse influence of the opposite wall. Given that a x30 scaling factor would have required a prohibitively large wind tunnel, the lowest part of the Reynolds number range over which probes are typically used was specified as a minimum requirement. This introduced a degree of

flexibility into the specification, and extended the choice of wind tunnel. It was planned to use smoke as the visualising medium, recorded onto video film as before.

The specification was circulated to six U.K. research establishments known to operate potentially suitable wind tunnels. Four of these responded positively, and were visited by the author. Eight wind tunnels were inspected, five of which were considered to meet the specification; the pertinent details of these are summarised in table 6.2. Cost aside, the re-circulating "4ft x 3ft" tunnel at DRA (Farnborough) was the most suitable, with optical access to the working section from three sides, and a 30:1 area contraction between the settling chamber and the working section. The Sheffield University Portobello Road facility, although somewhat smaller, was placed second in terms of technical acceptability, and the quoted hire charges were just 7% of those at DRA. This tunnel was selected for the three dimensional experiments, and is described fully in section 6.3.2.

Given that the working section of the Sheffield tunnel was 610mm square, this implied a probe diameter based on the original specification of 38.1mm, or six times that of the actual probes. Given a maximum free stream velocity of 15m/s for successful flow visualisation, this corresponded to a Reynolds number of 3.7×10^4, significantly below the specified value of 5×10^4. This was overcome by selecting a uniform scaling factor of eight; although this then violated the probe sizing criteria, the factorial experiment results showed that the wall proximity effect extended significantly less than eight stem diameters from the wall of introduction for small angle wedge probes. It had been hoped to construct a set of large scale probes as in the factorial experiment, or one probe of modular construction in which the included wedge angle and interface piece length could be varied. This proved impractical on the grounds of cost and test time, and a single, 30° included angle wedge probe was chosen. The 30° included angle was necessary to give sufficient room in the wedge head to install static pressure tappings. A scaled interface piece length of 100mm was selected such that the design fell mid-way between the extremes of the factorial experiment probes, and represented the optimum compromise.

A detail drawing of the large scale probe is given in figure 6.8. Static pressure tappings were specified at various locations over the wedge faces and in the stem leading and trailing edge regions. These were intended for mapping the probe surface static pressure distribution as a function of probe immersion, yaw angle and flow condition, prior to conducting the smoke flow tests. Actual probe calibrations were used in calculating the anticipated surface pressures at free stream velocities of up to 15m/s. From consideration of the experimental uncertainties involved in using a bank of inclined water manometers to sense the individual pressures, it was concluded that worthwhile pressure measurements would result at flows greater than 10m/s. There was therefore opportunity for both pressure measurement and flow visualisation studies at velocities between 10 and 15m/s.

The probe was fabricated from stainless steel material in the instrumentation manufacturing cell at Rolls-Royce Derby. Low temperature braze was used in assembling the individual components. A hollow wedge head was constructed as shown in figure 6.9a), and precision drilled to accept 1.1mm O.D. pressure tubes. These were then assembled through the wedge head and brazed in position before being ground back flush with the wedge surfaces. These processes are illustrated in figures 6.9b) and c). This procedure ensured that the resulting pressure taps were square edged, and free of immediate up or downstream surface irregularities. The hollow cavity was filled with a low expansion, silica filled epoxy based casting resin, having previously jigged pressure tube No.10 in the required position. Once cured, this resin was ground back to form the second wedge face. The completed probe is shown in plate 6.2.

6.3.2 Description of Facility

The Sheffield University wind tunnel is shown in figure 6.10, and is similar to the Cranfield tunnel in overall layout. Air is drawn through a square section inlet into a settling chamber by an electrically driven fan at the tunnel exit. It is then accelerated through a 18:1 three-dimensional contraction to the working section before exhausting vertically to atmosphere. This arrangement, with the fan downstream of the working

section, is the preferred option for smoke flow visualisation tunnels, (Mueller, 1980), as it minimises the risk of fan induced flow instabilities in the plane of the model. In its original form, optical access was limited to the two vertical walls, although these windows and the tunnel roof could be removed and replaced as required. A traversable pitot-static tube was provided for reference pressure measurements.

Because the aim was to replicate, as far as possible, the environment in which the actual probe factorial experiments were conducted, a flat plate was designed to stand-off from one of the tunnel vertical walls by 100mm as illustrated in figure 6.11. The plate leading edge was shaped similarly to that installed in the 203mm diameter suction wind tunnel, (section 5.2.2), and a strip of tape was secured just downstream of the leading edge to ensure the development of a turbulent boundary layer. By positioning the probe traverse plane 0.71m downstream of the plate leading edge, a boundary layer thickness of 15mm was expected, almost eight times that in the Cranfield suction wind tunnel at a similar Reynolds number. The plate was secured to the original tunnel wall using streamlined struts, and a 50mm I.D. perspex tube was incorporated at the selected traverse plane through which the large scale probe was immersed into the flow. Because these modifications blocked one of the two original windows, a perspex panel was also constructed to replace the tunnel roof, such that the probe model could be viewed from the end and from above. All necessary modifications were completed to the author's instructions by the Rolls-Royce model shop at Derby.

A flow characterisation exercise was completed as the first experiment. The total and static pressure profiles at the traverse plane were measured directly by traversing a pitot static probe out from the flat plate to the opposite wall. Tuffnol sealing bushes were provided in the perspex guide tube through which the pitot-static probe would slide, whilst avoiding the ingress of air from outside the tunnel, (figure 6.12a)). Traverses completed at velocities of 5m/s and 24m/s showed less than ±1.5% dynamic head variation in both total and static pressure profiles from the flat plate out to the opposite tunnel wall, outside of the boundary layer. A single element hot wire probe was used to measure the boundary layer profile at four freestream velocities between 5m/s and 24m/s.

The anemometry equipment and wire calibration procedure was the same as that adopted for the compressor rig traverse reported in section 5.3. Figure 6.12b) shows the bushing arrangement designed to minimise flow disturbances near the wall through which the wire was introduced. The measured velocity profiles were typical of a turbulent boundary layer, and the measured boundary layer thicknesses agreed with those calculated from equation 5.1 to within 5% at both velocities. Measured and predicted boundary layer thicknesses are summarised for various flows in table 6.3. The freestream turbulence intensity calculated from hot wire measurements on the tunnel centre line varied between 0.5% to 0.6% depending on the tunnel speed.

6.3.3 Experiments

The test schedule shown in table 6.4a) was compiled with the aim of recording flow visualisation and pressure data at velocities between 10m/s and 15m/s, plus detailed pressure measurements as a function of both yaw angle and probe immersion at higher Reynolds numbers typical of the factorial experiment, i.e. within the range 4.6×10^4 to 10×10^4. In practice, smoke flow visualisation proved difficult to achieve at flows above 5m/s as discussed below; the schedule was modified to that of table 6.4b), which concentrated the pressure measurements at higher velocities to minimise experimental uncertainties.

Pressure Measurements

The probe surfaces and static pressure tubes were thoroughly cleaned with an appropriate solvent to remove any swarf or oil before attempting the pressure measurements. Each pressure tapping was piped individually to a bank of water manometers which were inclined to an extent depending on the pressure differences to be measured. For experiments in which the probe immersion was varied, the wind tunnel was first stabilised at the required condition based on the reference total and static pressure measurements, with the probe retracted as far as possible. A minor misalignment of the probe head relative to the stem meant that immersions of less than

50mm could not be achieved, immersion being defined as the distance from the tip of the probe to the flat plate surface. The probe was nulled into the flow by balancing the readings from tappings 4 and 10, the manometer water levels allowed to stabilise for approximately two minutes, and a set of readings taken. This procedure was repeated at 20mm increments for immersions between 50mm and 480mm. The tunnel speed was adjusted at each immersion to retain a constant dynamic head throughout the traverse, thus compensating for probe blockage effects. A number of tests were completed with a stem fillet in place, as reflected in table 6.4b). This was simply achieved by sculpturing a modelling compound to the form detailed in figure 5.4.

Experiments in which the probe yaw angle was varied were conducted at an immersion of 400mm, or eight times the probe stem diameter, to avoid wall proximity effects. The 0° datum was established by nulling the probe as before, prior to recording pressures at 5° intervals over a ±45° yaw angle range. Friction between the probe stem and the supporting perspex tube proved sufficient to hold the probe at the required yaw angle without recourse to mechanical clamping.

Smoke Flow Visualisation

Initial attempts to visualise the flows around the large scale probe model used a theatre type, 'Concept - Colt' smoke generator in conjunction with a rake of smoke injectors. Oil was supplied to the smoke generator from pressurised canisters, and vaporised within an electrically heated block before exhausting as a dense white smoke through a converging nozzle arrangement. The nozzle exit was piped to the smoke rake positioned 590mm upstream of the traverse plane. The smoke rake itself was designed by the author based on the Cranfield smoke rake, and manufactured by technicians within the Cranfield turbomachinery department. Preliminary tests with this arrangement were unsuccessful, as oil droplets tended to condense back out of the vapour within the tortuous passages of the smoke rake, blocking the injectors and generating turbulent smoke filaments. On the basis of advice from the Cranfield College of Aeronautics, it was considered that smoke generated from higher purity oil was required, and a smoke

generator such as that used at Cranfield for the two-dimensional model experiments was recommended. The practicalities and cost of installing such a smoke generator in the Sheffield wind tunnel were prohibitive, and an alternative was sought.

More success was achieved with a smoke generator and single point injector probe manufactured by Aerotech A.T.E. Ltd. This device avoids the problems described above by pumping medicinal quality white oil from the control unit to the tip of the probe, where a low voltage electrical coil heats it to produce a dense plume of smoke which can then be positioned as required. The stem of the smoke probe is shaped to minimise interference with the flow. A procedure was adopted whereby the large scale probe was set to the required immersion at a given flow condition, and the smoke wand traversed in the plane of the probe through a hole in the plate upstream of the traverse plane, whilst continually recording the resulting flow patterns on video film. The wedge probe was then incremented to the next immersion and the procedure repeated, thus avoiding the potential disadvantage of only a single smoke filament. Mounted above the wind tunnel, the video camera was pointed vertically down towards the tunnel floor which was lined with a black velvet material to maximise contrast and to avoid reflections. Two halogen spot lights were required to illuminate the smoke sufficiently, their optimum position being established by trial and error. The final experimental arrangement is shown in figure 6.13 and plate 6.3. By carefully adjusting the smoke generator oil pumping rate and the heater coil supply voltage, good quality flow patterns were recorded at freestream velocities of 5m/s. Flow features particularly in the probe wake became less well defined at higher velocities approaching 10m/s; given that the time available in the wind tunnel was limited, efforts were concentrated at lower flows.

6.3.4 Results

Pressure Measurements

Pressure data required to complete all the calibrations and probe traverses detailed in table 6.4b) were successfully recorded. The pressure readings from each

tapping were non-dimensionalised in the usual form of static pressure coefficient, B, and plotted against yaw angle or probe immersion as appropriate, for each flow condition. A sample of results recorded at 25m/s are presented below.

In figure 6.14, the variation of B with yaw angle for the six wedge face static pressure tappings is plotted. At positive incidences, the curves bunch together in three groups, the lower group comprising the curves for the two rear most tappings, (3 and 6), and the upper group the curves for the two near-most leading edge tappings, (5 and 8). At positive incidence, B increases monotonically with increasing yaw angle over the tested 0° to 45° yaw angle range. Departure from the monotonic variation of B with yaw angle is observed at negative incidences where the instrumented wedge face becomes the wedge suction surface. Quantitatively, these results show similar trends to those of Ferguson (1967) included in section 4.4. Qualitatively, they indicate that a probe in which the static tappings are positioned near the wedge leading edge will be more sensitive to yaw angle than one in which the tappings are sited towards the rear of the wedge faces.

In figure 6.15, B for each of the wedge face static tappings is plotted against the normalised probe immersion (I/d), at a freestream velocity of 25m/s. The probe is drawn to scale against the absisca of this plot such that the correspondence between a set of data points and the probe position relative to the flat plate can easily be visualised. (For example, at two stem diameters immersion, the probe wedge head and half of the interface piece were immersed in the flow, etc.). Tapping no.4 is the closest in position to the static tappings of the actual probes used in the factorial experiment; this tapping exhibits a drop in indicated static pressure with increasing immersion which is characteristic of the wall proximity effect, and of a similar magnitude. Like behaviour is observed with the other tappings, the magnitude of change in B depending primarily on the distance back from the leading-edge, and to a lesser extent on the stemwise displacement of the tapping from the probe tip. A discontinuity in the curves for tappings 3 and 6 at three stem diameters immersion is observed, and corresponds with the emergence of the circular probe stem into the flow. The variation of static pressure at the

back of the probe as a function of probe immersion at a freestream velocity of 25m/s is plotted in figure 6.16, the beginning of each curve corresponding with the emergence of each successive pressure tapping. Broadly similar calibrations and traverse results were recorded at the other two flow conditions.

Flow Visualisation

Video film running to three hours of playing time was recorded from three separate days of testing in the Sheffield wind tunnel, the majority of which was with the Aerotech smoke generator, and significant features of the visualised flow at 5m/s are presented. With little more than the wedge head immersed in the flow, figure 6.17 illustrates the formation of a re-circulation at the lip of the probe hole of introduction. Previous investigation into the wall proximity effect had suggested that flow disturbances in this region might contribute to the effect, (section 4.2.). A second, stable re-circulatory region was visualised at the probe tip, in the wake of the wedge head and in the plane of the probe, by aligning the smoke wand with the end of the probe, (figure 6.18.).

As the probe immersion was increased to three stem diameters, so the hole of introduction was filled by the circular stem, and the local re-circulation in this region was replaced by a horse-shoe vortex around the 'U' shaped interface piece, as shown in figure 6.19. An increase in diameter of the wedge tip vortex was observed, and faint traces of smoke in the wake of the interface piece suggested flow out of the bottom of the wedge tip re-circulation and down the back of the probe towards the wall. The tip re-circulation could be visualised by aligning the smoke probe with either the top or bottom end of the wedge shape, indicating that flow was sucked in to the wedge wake region from both the free and supported ends.

By four stem diameters immersion, the formation of a re-circulatory flow structure at the base of the cylindrical stem and in the plane of the probe was noted. The stemwise flow along the back of the probe is captured in figure 6.20, and had intensified.

A horse-shoe vortex structure was observed around the cylinder leading edge. The wedge head wake re-circulation was still clearly visible, and had stabilised at a constant diameter as shown in figure 6.21. As the probe immersion was increased further, the re-circulation in the wake of the cylinder continued to grow until stabilising at a constant diameter of approximately 200mm at seven probe stem diameters immersion. Beyond this immersion, the structure of the re-circulatory regions in the wake of the wedge head and the cylindrical stem showed little change, with a continual transfer of fluid from the former to the latter along the back of the interface piece.

Flow over the central part of the wedge head was visualised in a plane perpendicular to the probe as the probe yaw angle was varied. Detail of the wake structure downstream of the probe was captured using a wide angle lens, although the flow local to the probe was less well resolved as a result. The process of transferring photographic images from the video to still prints tended to obscure important detail altogether, and a description of the main features is given here in preference. At 0° yaw angle, a pair of contra-rotating vortices were observed in the wake of the wedge head which extended downstream from the base of the wedge by approximately one wedge chord. As yaw angle was increased, so the wake flow became more obviously three-dimensional, with flow from the wedge pressure surface spiralling over the top of that leaving the suction surface as illustrated schematically in figure 6.22. This observation agreed qualitatively with the two-dimensional wedge model flow visualisation experiments. Smoke particles were also observed passing over the tip of the probe from pressure surface to suction surface, although the video image was not sufficiently well resolved to ascertain the yaw angle at which this over-tip flow began. Nor was the flow visualisation sufficiently detailed to confirm the formation of a separation bubble in the leading edge region of the wedge suction surface at yaw angles greater than 8°, as noted in the two-dimensional model studies.

In summary, smoke flow visualisation experiments with simple, two-dimensional models were successful in picturing the flow around six wedge shape variants over a wide range of yaw angles and at turbomachinery representative Reynolds numbers. The

development, with increasing immersion, of flow structures in the plane of the probe was visualised using a large scale model of a narrow-angle wedge probe, at Reynolds numbers representative of low-speed turbomachines. Static pressures at the probe surfaces were successfully measured using static pressure tappings and an inclined water manometer, over a wide range of turbomachinery representative Reynolds numbers. The variation in wedge face pressure as a function of yaw angle was qualitatively similar to that previously reported by Ferguson (1967). The variation in wedge face pressure as a function of probe immersion followed the characteristic wall proximity trend observed with actual probes.

Although it was not feasible to study the influence of different three-dimensional probe geometries on the visualised flow patterns beyond the effect of fitting a stem fillet, all other aspects of the originally defined experiment aims were met. The results are discussed further in the context of validating the numerical modelling work reported in chapter 7, and in developing an understanding of the physical flow mechanisms responsible for the results reported in chapter 5.

CHAPTER 7: NUMERICAL MODELLING

7.1 INTRODUCTION

The motion of a small element of fluid may be described mathematically in terms of expressions for mass, momentum and energy conservation. If viscosity is allowed for by including shear stress terms, the Navier-Stokes partial differential equations result. Apart from very simple, laminar flow cases, these equations have never been solved analytically. However numerical schemes, where a solution to the Navier-Stokes equations is converged upon iteratively, now offer a viable alternative to solving practical fluid dynamics problems.

The application of numerical methods in solving all but the simplest of cases has only become a realistic proposition with the advent of digital computers. The work of Kopal (1947) in compiling tables for supersonic flow over sharp cones is an early example of the use of digital machines for numerically solving the governing differential equations. Since then, numerical scheme developments have paralleled rapid advances in computing technology. Noteworthy examples include the solution of inviscid flow problems by Hall et al.(1962), and the modelling of boundary layers by Blottner (1964). The solution of increasingly complex problems involving transonic, separated or re-circulatory flows became possible during the mid-1960's with the development of time-dependent techniques for solving the full Navier-Stokes equations, (Anderson, 1992).

Between 1953 and 1979, the relative cost of computing reduced by one order of magnitude every eight years, (Chapman, 1979), and has continued to fall ever since. This contrasts with the ever increasing costs of experimental work, and explains the adoption by industry of numerical methods to compliment the more established experimental and analytical approaches. For economic reasons, modern airframe manufacturing companies use computational fluid dynamics exclusively for preliminary design, before final

refinement in the wind tunnel, (Anderson, 1992). Recent examples of turbomachinery research projects in which a combined experimental and numerical approach was adopted include an investigation of over-tip leakage flows in a swept, transonic fan by Copenhaver et al.(1994), and the optimisation of the flow field within a centrifugal compressor reported by Strazisar, (1994). In these and many other cases, the two approaches were used to compliment, rather than duplicate each other.

Fawcett (1991) summarised the benefits and limitations of CFD. techniques as they currently stand. Because they solve the governing equations, numerical methods should provide fundamental insight into a given problem, together with a complete picture of the flow. Because it is readily adaptable, the CFD. approach has great potential in design optimisation exercises, or for determining trends. However the quality of solution depends heavily on the grid used in defining the problem. This must be sufficiently detailed to accurately represent the modelled geometry, and to resolve important flow structures. A poor appreciation of the physical nature of the flow in any given problem may lead to an inappropriate choice of turbulence or chemical reaction model. Such flow phenomena cannot be solved absolutely at present, and rely on empirical models with limited application. Numerically induced, artificial flows can occur under certain conditions and require a suitably trained and experienced operator to detect and rectify them. Fawcett recommends that at least six months should be allowed to move an inexperienced person sufficiently far up the learning curve to achieve reliable predictions from CFD codes.

The numerical modelling content of this wedge probe investigation was included to complement the experimental work. The ultimate aim was to compute the three-dimensional flow field around a wedge probe immersed by differing amounts from the wall of introduction, to qualitatively compare the predictions with the flow-visualisation pictures, and to validate the predictions quantitatively against the factorial experiment results. The intention was then to examine the CFD whole flow field solution to more fully understand the flow mechanisms responsible for the wall proximity effect. By re-defining the flow boundary conditions, it was also hoped to model the open

jet probe calibration situation to more fully understand the calibration facility dependence of wedge probes. This problem was tackled by Depolt and Koschel (1992) using panel numerical methods. Although the characteristics of various pressure probes were predicted, the facility dependence was not resolved. No other attempts at numerically modelling the steady flow behaviour of pressure probes have been found in the literature.

The process involved in selecting a suitable CFD code for this project is documented in section 7.2. The Moore's Elliptic Flow Program (MEFP) pressure correction code was chosen, and this is described in section 7.3. In section 7.4, the modelling of flow around a circular cylinder at low Reynolds numbers with both structured and embedded meshes is described. This exercise was completed partly to familiarise the author with the technique, and partly to test the ability of the code to model a well-documented flow. The solutions from the two different gridding methods are critically compared.

As a further step towards modelling the complete probe, the two-dimensional flow visualisation experiments were simulated by modelling the flow around a 24° included angle wedge shape at three yaw angles of 0°, 4° and 8°. This was included particularly to resolve detail of the suction surface separation bubble at higher incidence angles, and is described in section 7.5.

Predictions of the flow around a fully three-dimensional model of the probe at three different immersions were completed and are reported in section 7.6. Comparisons are made with the experimental results to determine the extent to which the predictions can be relied upon.

7.2 CFD CODE SELECTION

Modern CFD codes generally adopt one of two alternative strategies for solving the governing flow equations, either a time-marching technique or a pressure correction

method, (Anderson, 1992). In the former, the mass, momentum and energy conservation equations are taken in their complete (Navier-Stokes) or simplified formulation, and discretised to give a system of algebraic difference equations for the dependent variables at grid points throughout the flow domain. A time marching approach to solving these equations is adopted whereby the dependent variables at time $(t + \Delta t)$ are obtained explicitly from their value at time t. Generally, the governing equations are formulated such that the momentum components form the dependent variables, and absolute pressures are derived from the density via the equation of state.

This approach is well suited to compressible flow problems, but becomes computationally inefficient and potentially unstable when modelling incompressible flows. Pressure correction methods avoid these problems by expressing the governing equations in terms of pressure differences. The velocity components are taken as the dependent variables, and a solution is reached by progressively correcting the pressure field until the velocity components determined from the momentum equations simultaneously conserve mass. Whilst best suited to incompressible flows, this approach may be extended to cover transonic flow regimes.

For the purposes of wedge probe modelling, a pressure correction code was considered more appropriate given that the turbomachinery environments in which probes operate are generally subsonic. From the large scale probe flow visualisation studies, it was known that flows local to the probe were highly three-dimensional and potentially unsteady. The complex wedge probe geometry also demanded that a code with sufficiently flexible grid point structuring and classification be chosen. Of the CFD codes available within Rolls-Royce, only the 'UNSFLO' solver developed by Giles and Haimes (1991) was capable of resolving time dependent fluctuations. However, this code was not designed to model three-dimensional geometries and was not a viable option for investigating the wall proximity effect. However, given that at least the re-circulatory regions in the wake of the probe appeared from the flow visualisation experiments to be stable, the risks involved in using a steady flow code were judged to

be acceptable, and the Moore Elliptic Flow Program (MEFP) was selected as best meeting the remaining criteria.

7.3 MOORE ELLIPTIC FLOW PROGRAM

MEFP is a fully three-dimensional, steady flow solver for compressible or incompressible, inviscid, laminar or turbulent flows with or without heat transfer. It was originally written to calculate flows in turbomachinery blade rows, and has since been used for modelling flows in internal cooling passages, disc cavities, particle separators and centrifugal impellers, (Northall, 1993). A structured, three-dimensional grid is used, the location of each grid point being specified in Cartesian or cylindrical coordinates. Grid points are assigned a type depending on whether they lie in the flow, within the solid body, or on the body surface. This approach permits a grid to pass unaltered through a solid object as well as the flow field, and is particularly amenable to modelling complex geometries. Local mesh embedding is also available, where a fine mesh is incorporated locally into a coarser, structured mesh to better define regions of interest.

The code is based on the steady Reynolds averaged conservation equations in a coordinate system rotating at speed Ω. These are given in appendix G with the rotational terms removed to reflect the use of a stationary reference frame in this investigation. Turbulence modelling is achieved using a Prandtl mixing-length model to calculate the turbulent viscosity. This is combined with the laminar flow viscosity, in a way which depends on the proximity to a fluid boundary, to give an effective viscosity for use in the momentum equation. Transition points can be specified by defining arrays which modify the laminar and turbulent viscosities.

The governing equations are discretised on the basis of upwinded control volumes, to achieve a 2^{nd} order accurate scheme which is independent of cell Reynolds number, (Moore, 1985). Rather than surrounding each grid point with its own control volume, grid cells are divided into 1/8th sub-cells as shown in figure 7.1. Each sub-cell is

then assigned to the nearest downstream grid point, which may be any of the eight points at the vertices of the original cell. The control volume for a given cell is then the accumulation of sub-cells assigned to it, and the momentum equations are discretised accordingly. This approach avoids the stability difficulties which arise from accurately evaluating absolute values for a given transported variable at the faces of a non-upwinded control volume, and ensures unconditional, 2nd order accuracy of the convection and diffusion terms in the conservation equations.

Figure 7.2 illustrates the iterative solution scheme in flow-chart form. Each stage is controlled by a file which must be edited to suit a particular problem. The per iteration change in each flow variable may be tuned by the user, but is generally large to give convergence in a relatively small number of iterations. One consequence may be that instabilities are introduced during the early iterations which cause a failure to converge, and facilities are incorporated which attempt to improve stability. Explicit smoothing may be applied to any or all of the flow variables, although 2nd order errors which compromise the solution accuracy can result if this is used over substantial areas of the flow domain. Relaxation factors can be introduced into the pressure correction and momentum equations which improve stability, but require more pass-pairs to reach convergence. MEFP does not have a built in convergence criterion, but relies on the user to review the results after a certain number of passes, and to then run more passes as required. The rms change in static pressure decreases as the calculation converges, and should ultimately reduce to a small fraction of the variation in static pressure across the flow domain. Achieving the same mass flow rate across each transverse plane is a further indication of convergence.

7.4 FLOW AROUND A CIRCULAR CYLINDER

The author had no CFD experience before commencing this project, and little background knowledge of the techniques involved. A one week training course in the subject is run annually by the company, and was attended in May 1992. This introduced

the author to the fundamentals of time-marching and pressure correction methods, but did not include any specific direction in the use of MEFP. This was achieved by practical experience, guided by members of the Rolls-Royce Aerothermal Methods group.

An important step in this learning process was the modelling of flows around circular cylinders at low Reynolds number of 40. This complex flow case has been studied extensively, and much high quality experimental data is available in the literature. Because the flow around a cylinder can be calculated without complicating factors such as compressibility and turbulence modelling, it provides a means of assessing the numerical accuracy of the basic code. A further aim was to critically compare solutions for a structured and an embedded form of mesh, with a view to adopting the more computationally efficient embedded mesh for subsequent modelling.

7.4.1 Structured Mesh Generation

Within Rolls-Royce, MEFP is used primarily for modelling turbomachinery flows, where the geometry of the blades is defined electronically as a set of x,y,z, co-ordinates in a blade file. Automated grid definition procedures have been developed which draw on the blade file data to construct a master grid. This may then be refined manually using grid manipulation software. The automated master grid generation facility could not feasibly be adapted to the cylinder geometry; the basic coordinates defining the cylinder, and the complete probe in later studies, were therefore entered by hand to form a master geometry file. This is shown for the cylinder in figure 7.3. Corner points were defined on the solid surface at the intersection of vertical (I) and horizontal (J) grid lines, to guarantee four sided grid cells in the vicinity of the cylinder. The flow boundaries were set sufficiently far away from the cylinder to avoid interactions, and to guarantee flow out of the exit plane at every J line. Because the flow was expected from the available experimental data to be symmetrically distributed about a horizontal line through the centre of the cylinder, only half of the flow domain was modelled. Two (identical) K planes were defined one above the other to limit the solution to two-dimensions.

The master grid was refined using the grid manipulation software to add I and J lines. A circular arc interpolation option was adopted to appropriately position grid points falling on the cylindrical surface. Successful convergence of the MEFP scheme is closely linked to the grid 'quality', and the following guide lines were adopted:

i) individual cell aspect ratios of less than 10 near to solid boundaries,

ii) a sufficient density of lines near the cylinder wall to resolve the boundary layer, and in other areas where strong velocity or pressure gradients were expected,

iii) expansion ratios from one cell to its neighbour of less than 5, but nearer to 2 in the boundary layer, and unity in the corners,

Achieving the second condition resulted in four sets of closely spaced grid lines which emerged horizontally and vertically from the two corner points. These gave rise to high aspect ratio cells in the flow domain, which were improved by flaring the grid lines as shown in figure 7.4. A degree of iteration was then necessary to form a grid for which a satisfactorily converged solution could be achieved. The final grid comprised 95 I lines, 56 J lines and 2 K lines, giving a total of 10,640 grid points.

7.4.2 Structured Mesh Solution

A Reynolds number of 40 was chosen as the highest value at which a steady flow solution was appropriate, (Morkovin, 1964). To have modelled this situation for a 6.35mm diameter cylinder in air would have involved freestream velocities of less than 0.1m/s, which were considered to be within the numerical uncertainty limits of the code. The option of reducing the cylinder diameter was rejected in favour of changing the working fluid properties to simulate a light oil typical of 10W50 car engine oil. Given a density and viscosity of 900kg/m^3 and 0.3Pa.s respectively, the required Reynolds number was achieved by setting a freestream velocity of 2.1m/s. These modifications

were simply achieved by changing the constants defined in the appropriate set-up files.

The solution was run under the control of a command file, which was structured to call calculation routines in accordance with figure 7.2. A total of 25 pass-pairs were required to reduce the rms change in static pressure per iteration by 2.7 orders of magnitude from start to finish. The convergence history, plotted in terms of log rms pressure and velocity change per iteration, is traced in figure 7.5. Post processing of the solution data was performed using the standard routines available on the company mainframe computer, to produce velocity vector and contour plots of the calculated parameters. A qualitative assessment of the solution was made by examining static pressure contour plots such as those shown in figure 7.6. Whilst the contours are generally smooth, some localised distortion is observed in regions of high aspect ratio cells. Convergence could probably have been improved by adding grid lines to sub-divide these cells. Velocity vectors in the wake of the cylinder are plotted in figure 7.7a), and a closed region of re-circulating flow is clearly defined. Closer inspection of the velocity vectors near the downstream corner showed that the separation point and the developing boundary layer had also been captured, (figure 7.7b).

The validity of this solution was checked by comparison with the experimental data of Coutanceau and Bouard (1976), who used a liquid flow visualisation technique to study the changes in wake structure shed from a two-dimensional cylinder at Reynolds numbers between 5 and 40. The two symmetrical eddies which form the wake structure under these conditions were defined as a set of geometrical parameters as shown in figure 7.8. Corresponding values for the CFD solution were scaled from figure 7.7, and are compared with the experimental results in table 7.1. Although the predicted separation point was 6° upstream of the experimentally observed position, agreement was otherwise very encouraging.

7.4.3 Embedded Mesh Generation

Although the cylinder test case was satisfactorily solved using a structured mesh, the number of grid points required to model this simple two-dimensional geometry suggested that a three-dimensional grid of a complete probe would be impracticaly large to run on the mainframe computer. The option of using the superior memory and processing speed of the company Cray computers was rejected due to the high risk of programme delay caused by the demands of other, higher priority users. The alternative was to adopt an embedded mesh format.

The use of embedded meshes for two-dimensional Navier-Stokes calculations is reported by Davis and Dannenhoffer (1989). This approach was extended to the third dimension, and implemented in conjunction with the MEFP flow solver, by Lapworth (1993). Embedded meshes are characterised by hanging nodes at the interfaces between fine and coarse regions. Lapworth defined a hierarchical structure in which only one hanging node per cell face was permitted. This enabled a development of the up-winded control volume technique which retained second order accuracy, and avoided the flux conservation instabilities reported in previous studies.

An embedded mesh for the flow past a cylinder case was constructed to test the accuracy of this approach against the structured mesh solution. The same master grid was taken and refined using semi-automated mesh embedding software to produce the grid shown in figure 7.9. Minimum and maximum spacing between grid lines in the freestream regions were chosen to replicate the structured grid. The cells were sub-divided in the wake and boundary layer regions partly via the automated procedure, and partly by the author to meet the same general criteria defined in section 7.4.1 above. The cylindrical surface was created using a non-uniform rational Bezier-spline (NURBS) surface definition, (Versprille, 1975). For the purposes of embedding, it was simpler to model the complete cylinder, and 98 I lines, 71 J lines and 2 K lines were required. However the total number of nodes was limited to 7,004, or 3,502 for the half cylinder case. This represented a 67% saving in the required number of nodes.

7.4.4 Embedded Mesh Solution

A solution based on the embedded mesh was calculated using the modified version of MEFP. Exactly the same flow conditions were imposed as for the structured mesh solution, but only fifteen iterations were required to achieve 3.2 orders of magnitude convergence. Inspection of the velocity vectors in the wake region (figure 7.10a) showed that a symmetrical eddy structure has been calculated as expected. The boundary layer development and separation point were again well defined, (figure 7.10b). Table 7.1 includes the geometrical parameters determined for the embedded mesh solution from figure 7.10. The separation point and the downstream position of the re-circulations were more accurately predicted with the embedded mesh. All other parameters again showed a very encouraging level of agreement with experiment, although not as good as with the structured mesh. It was considered that the slightly inferior performance of the embedded mesh was more than offset by the computational efficiency advantages of the embedded mesh approach, and embedded meshes were adopted for all the subsequent numerical modelling reported in this chapter.

7.5 MODELLING OF TWO-DIMENSIONAL WEDGE FLOWS

In a further step towards modelling a fully three dimensional probe, the flows past a narrow angle wedge shape at 0°, 4° and 8° of incidence were calculated. The specific aim of this study was to investigate the separation bubble observed on the suction side of the 24° included angle wedge model at 8° yaw during the 2-D flow visualisation experiments, (section 6.2.4). The experimental set-up was modelled as closely as possible by basing the grid master geometry on the wedge model dimensions given in figure 6.3a). Density and viscosity values appropriate for air were defined, and a freestream velocity of 4.3m/s was set to give a Reynolds number of 5.2×10^4. It had also been hoped to vary the Reynolds number and turbulence intensity to study their effect on the separation bubble formation and size; difficulties in obtaining converged solutions for

the three different yaw angle cases absorbed more time than originally anticipated, and this part of the investigation had to be curtailed.

7.5.1 Mesh Generation

Given the ultimate intention of modelling a complete probe, the wedge grid was designed to incorporate a 'U' shaped interface piece in the basic topology. This implied the use of four corner points, two on each wedge face, and the master grid shown in figure 7.11a) was defined accordingly. The area of the flow domain was made equal to the flow visualisation wind tunnel window. Coarsely distributed I and J grid lines were introduced over the entire flow domain using the structured grid manipulation software, together with more tightly packed lines through the wedge itself. These were flared to improve cell aspect ratios, and to reduce the skewness of cells near the wedge face corners. A limited amount of embedded mesh was then introduced using the automated embedding routines to further improve the grid resolution particularly in the nose and trailing edge regions where significant flow activity was expected. The resulting mesh, shown in figure 7.11b), was filed as a datum, and used as the basis for all subsequent calculations of wedge flows.

7.5.2 Calculations at 0° Incidence

Numerical instability in the highly skewed cells at the wedge leading edge caused an initial failure to converge. This was overcome by applying explicit smoothing to the static pressure in a localised region adjacent to the wedge apex. A solution for the datum mesh was then successfully computed, requiring seven pass-pairs to achieve 2.2 orders of magnitude convergence. Static pressure contours and velocity vectors at the grid nodes are plotted on the 1st K plane in figures 7.12 and 7.13a) respectively. The expected decrease in static pressure with increasing distance back from the wedge apex was observed, and the concentration of concentric contours at the base of the wedge implied

implied a closed wake comprising two symmetric eddies. No attempt to force symmetry about the wedge centre line was made in defining the boundary conditions, and some asymmetry was apparent in the solution which may have emanated from slight asymmetries in the datum mesh. The jagged nature of some of the downstream contours was further evidence of grid dependency in the solution. The re-circulatory nature of the wake is also apparent in figure 7.13a). Flow over the wedge faces separates at the rear corners and rolls-up into two counter-rotating vortices to form a closed wake which is qualitatively similar to that observed in the flow visualisation studies reported in section 6.3.4. Particularly encouraging was the well behaved nature of the flow through highly skewed cells near the grid corner regions.

In order to minimise grid dependency, and to improve flow definition in the wake region, the option of automatically adapting the mesh was exploited, (Lapworth, 1993). This option is an integral part of the mesh embedding software, and embeds grid lines to an extent depending on the first or second order difference or differential of parameter changes in an existing solution, as defined by the user. The first order difference of velocity, *du*, was used in this case as the criterion for subdividing sufficiently large cells in which *du* was greater than the rms value of *du*. A converged solution for the resulting mesh was calculated over a further 13 pass-pairs and velocity vectors are plotted in figure 7.13b). The greater density of vectors is indicative of the added grid line positions. Significantly improved definition particularly of the wake flow structure was achieved as a result of the adaption. From a comparison of figures 7.13a) and 7.13b), the length of the re-circulating wake region has increased as a result of the adaption to approximately one wedge chord. The adapted solution is therefore in better quantitative agreement with the observations made in section 6.3.4. Some regions of asymmetric flow remained however; further attempts at adapting the grid were largely unsuccessful, the tendency being to concentrate the mesh in these areas and to amplify the asymmetry.

Comparison of the wedge face static pressure distribution with that determined experimentally by Ferguson (1967) was made to check the absolute accuracy of the calculation. Static pressure coefficients at various positions, x, downstream from the

wedge leading edge were derived from the solution for the adapted mesh. These are plotted against (x/L) in figure 7.14, where L is the length of the wedge face. Ferguson's experimental data is also shown for comparison. The static pressure profiles agree to within ±6% dynamic head over the range of (x/L) for which experimental data was available.

7.5.3 Calculations at 4° and 8° Incidence

Yawed flow onto the datum wedge mesh was simulated by defining i and j-direction velocity components to give a resultant of 4.3m/s positively inclined by 4° or 8° to the horizontal, as required. Converged solutions for both cases were ultimately achieved after considerable grid refinement using the adaption and manual embedding methods described above. The mesh adaption technique proved most successful when working from a solution for the datum mesh which had converged by two orders of magnitude or more. Results are presented and compared with the two-dimensional flow visualisation results, and with experimental data for a x50 scale, 20° included angle wedge model run at 4.0×10^4 Reynolds number and reported by Ainsworth and Stickland (1992).

At 4° yaw, the flow accelerated over the wedge faces before separating at the rear corners as before. The two contra-rotating vortices were still apparent in the wake region, but that corresponding to the leeward wedge face had considerably out-grown the other, to increase the closed wake length to approximately two wedge chords. This resulted in higher momentum fluid leaving the pressure surface than the suction surface, which in-turn developed an asymmetric velocity distribution in the wake further downstream. These trends were also observed experimentally, but because the computation was purely two-dimensional and steady, the swirling motion visualised in the wake of the 2-D wedge shapes could not be modelled.

The wedge face static pressures at eleven discrete locations on both the pressure and suction surface were read from static pressure contour plots. Values of static

pressure coefficient were calculated from these, and are plotted against (x/L) in figure 7.15. The unity value of static pressure coefficient on the pressure surface for (x/L) values of less than 0.1 reflects the prediction of a stagnation point at 5% chord back from the pressure surface leading edge position. The flat static pressure profile indicated for the suction surface implies that any variation in static pressure was less than the contour intervals of the plot from which the data was taken, i.e. less than ±4.5% dynamic head in this case.

Yaw sensitivity as defined in appendix E was computed from the wedge face pressure profiles, and is plotted as a function of (x/L) in figure 7.15. Ainsworth's experimental data is included for comparison. Both experiment and prediction follow the expected trend of decreasing yaw sensitivity with increasing distance back from the wedge apex, (section 4.4). The generally higher level of yaw sensitivity predicted for the 24° wedge is to be expected, given that the experimental data relates to a 20° included angle wedge shape.

Velocity vectors calculated in the wake region of the wedge at 8° yaw are plotted in figure 7.16. The twin, contra-rotating vortex nature of the wake has been replaced by a single vortex emanating from the suction surface flow, and succeeded downstream by a complex series of eddies. The convergence history for this solution exhibited an a-periodic oscillation either side of two orders of magnitude static pressure change reduction, which persisted even after 100 pass-pairs. It was implied from this that the wake flow was unsteady, and could not be correctly resolved with a steady flow code, despite satisfactory convergence over the remainder of the flow domain. This was consistent with the 2-D flow visualisation experiments at yaw angles greater than 7°, where the unsteady nature of the wake flow was clearly visualised. Figure 7.17 shows the velocity vectors in the leading edge region; as at 4° yaw, the flow divides about a stagnation point on the pressure surface, but then separates at the wedge apex to generate a closed re-circulation or separation bubble on the suction surface. The prediction of a separation bubble is in excellent qualitative agreement with the

two-dimensional flow visualisation studies, as observed from comparison of figures 7.17 and 6.4b) for example.

The variation of static pressure over the wedge faces at 8° yaw is plotted in figure 7.18, using the same representation as in figure 7.15. The position of the minimum turning point in the suction surface pressure profile corresponds to the centre of the separation bubble. The influence of this on the predicted yaw sensitivity was to move the maximum sensitivity position back from 0.1 (x/L) at 4° yaw, to 0.2 (x/L) in this case. The experimental data was not sufficiently well resolved in the leading edge region to capture this trend, although the predicted and experimental data show similar trends at greater (x/L) values.

7.6 MODELLING OF THREE-DIMENSIONAL PROBE

The primary aim in modelling a complete wedge probe in three dimensions was to determine how the local flow field was altered by inserting the probe to various immersions. The modelled geometry was based as closely as possible on the large scale, 30° included angle wedge probe reported in section 6.3, such that the predictions could be validated against experimental data. Converged solutions for this geometry in a 25m/s flow were achieved at immersions of one, two and four probe stem diameters from a solid wall. The mesh generation procedure and a sample of results are presented below.

7.6.1 Mesh Generation

The topological arrangement of the wedge mesh was designed with corners at the intersection of the wedge faces and the 'U' shaped interface piece, (figure 7.11). Because the mesh embedding software preferentially embeds into grid corners, this resulted in a high density of embedded grid lines at these regions. Whilst acceptable in two-dimensions, extension to the third dimension would have introduced an impracticaly large number of grid nodes for handling by the mainframe computed. A revised topology

was adopted in which the interface piece was scaled down slightly to avoid contact with the wedge faces, (figure 7.19). This avoided the second set of corners. It also offered a common topology for the wedge, interface piece and cylindrical stem, the exact definition of which was achieved by appropriately setting the x,y co-ordinates of each topological node on every K plane. This can be visualised in figure 7.19 by lifting the wedge mesh (drawn on the acetate sheet) above the cylinder mesh defined on the paper page.

This topology was entered manually into a master geometry file. The size of the flow domain was made equivalent to the working section of the Sheffield wind tunnel in which the large scale probe experiments had been conducted. Each node was labelled according to its position within a solid body, on a solid surface, in the free stream, at the inlet or at the flow exit plane. Thus nodes within the cylinder where no flow calculations were performed were 'switched-on' in the flow region between the cylinder and the wedge, etc. To have modelled the pitot tube would have involved more complexity in the grid definition than was considered justified. Although the hole of introduction could have been modelled by appropriate labelling of the nodes, this was not attempted in order to minimise the ultimate size of the grid, and to avoid a potential source of numerical instability. The influence of these compromises on the final solutions is discussed in section 7.6.2.

Grid for One Stem-Diameter Immersion

An immersion of one stem diameter corresponded to fully immersing the wedge head, such that only the wedge part of the master grid was required for this case. The grid was refined by introducing a coarsely spaced structured mesh throughout the flow domain, followed by local mesh embedding around the wedge itself, (figures 7.20a) and b)). The final mesh incorporated 26,674 grid points, a saving of 68% over the equivalent structured mesh.

Grid for Two Stem-Diameters Immersion

An immersion of two stem diameters corresponded to immersing the wedge head and half of the interface piece. The semi-circular leading edge of the interface piece was modelled using a NURBS surface (section 7.4.3) which was aligned with nodes defining the leading edge position. I and J grid lines were then introduced through the leading edge region of the interface piece to define the arc before attempting any mesh embedding, (figure 7.21). A coarse structured mesh was added as before. Finer mesh was embedded in the wake region, and at the join of the wedge and interface piece to ensure adequate resolution of the flow at this discontinuity in the geometry. The final mesh incorporated 45,436 grid points, a saving of 67% over the equivalent structured mesh, but approaching the maximum feasible size for calculation on the mainframe.

Grid for Four Stem-Diameters Immersion

In this flow case, a grid defining the wedge head, all of the interface piece and a 50mm length of the cylindrical stem was required. Two NURBS surfaces were defined to describe the interface piece leading edge and the cylindrical stem. A modification to the mesh embedding software was necessary to offset the centres of these surfaces relative to each other, as required by the wedge probe geometry. The adoption of a common topology for the wedge and cylinder resulted in some skewing of grid lines in the k-direction along the length of the interface piece, (figure 7.22). The associated deformation of grid cells was small relative to cells in the wedge leading edge region however, and was not expected to influence the flow calculations. Fine mesh was embedded as economically as possible given the limit on grid points. The majority of calculations were completed with a mesh of 45,790 grid points; whilst some saving relative to the other meshes was achieved in the free-stream, the resolution of grid points local to the solid surfaces and in the wake region was inevitably poorer. K-plane sections through the wedge and cylinder in the final grid are shown in figures 7.23a) and b) respectively.

7.6.2 Calculations

Flow calculations over the three-dimensional grids were achieved using the calculation files defined for the two-dimensional geometries, with appropriately modified boundary conditions. All calculations were run at 25m/s with 0% background turbulence intensity. The appropriate boundary layer velocity profile measured in the 3-D flow visualisation experiments, (section 6.3.2), was modelled at the wall of introduction for all three cases. Calculations were completed in increments of five pass-pairs as over-night batch jobs, approximately 5½ hours of elapsed mainframe computing time being required to complete each increment with the larger grids. Because of the associated expense, (section 3.4.3), the progress of the solution was thoroughly reviewed after every five iterations for convergence of static pressure and continuity of mass flow across the flow domain before proceeding with further calculations. Typically three weeks of elapsed time was involved in achieving a satisfactorily converged solution for each grid. Standard 2-D plots of the calculated static pressure and velocity field information were supplemented with a three-dimensional representation of the flow field using the Rolls-Royce developed post processing package 'Graffiti' available only in a workstation environment.

7.6.3 Results

One Stem-Diameter Immersion

The static pressure change per pass was reduced by 1.9 orders of magnitude after 40 pass-pairs. Although the code continued to correct the static pressure field in the wake region with each additional iteration beyond this, the changes were less than 2% dynamic head. The solution was considered adequately converged after 48 pass-pairs; 'wobbles' in the static pressure contour plots are indicative of poorly converged areas. Contour maps of the static pressure distribution at the wedge surfaces and throughout the flow domain are given in figures 7.24 and 7.25. Figure 7.24 plots contours at 20Pa intervals on a vertical slice through the wedge centre-line, with flow from left to right as

indicated. The concentration of contours immediately upstream of the leading edge corresponds to a rapid deceleration as the flow approaches the wedge apex. An approximately concentric series of contour rings is observed in the probe wake, and is indicative of a re-circulating region in the plane of the paper. Horizontal slices through the wedge at three different heights above the solid wall are shown in figure 7.25. Symmetry about the wedge centre line was to be expected, and is largely observed over the wedge surfaces and in the free-stream regions outside the wake. The slight asymmetry within the wake flow reflects the failure of the solution to fully converge in this region, and may be attributed to local unsteadiness in the flow. Pressure contours in the wake region on the 'near-tip' plane are markedly different from those on planes nearer to the wall.

As with the two-dimensional modelling, the flow accelerates over the wedge-faces, resulting in an almost linear decrease in static pressure with increasing (x/L). An indication of the absolute accuracy of the prediction was obtained by comparison with the large scale wedge probe static pressure data for the same flow condition, (figure 6.15.). Numerically predicted static pressure coefficients at positions corresponding to tappings 3, 4 and 5 on the wedge face are overplotted on the experimental data in figure 7.26. Discrepancies of between 7% and 15% dynamic head are observed, depending on position. This discrepancy may be accounted for in part by numerical and experimental uncertainty, and may also be a result of simplifications in the mesh relative to the actual geometry.

A clearer representation of the static pressure variation over the wedge surfaces and the wall of introduction is given by the colour contour map of figure 7.27. Twenty five, 10Pa colour contours are defined spanning a pressure range of 99500 to 99750 Pa. The inclination of the colour contours on the wedge face implies angled flow, particularly in the tip, leading-edge region. A lifting of the streak-lines at the leading-edge, and angled flow over the wedge face towards the free-end was also observed in the flow visualisation experiments, and is shown in figure 6.18.

Velocity vectors on the wedge centre-line plane are drawn in figure 7.28. The upstream boundary layer profile and the re-circulatory region in the probe wake are clearly visualised. In figure 7.29, velocity vectors are plotted to the same scale on the near-wall, mid-height and near-tip planes *through* the wedge. Furthest from the wall, there is some evidence of the counter-rotating, twin-eddy wake structure captured in the two-dimensional modelling. This is dominated nearer the wall by a strong reverse flow component associated with the re-circulation shown in figure 7.28. Figure 7.30 is a streak-line representation of the three-dimensional flow structure in the wake region, and can be considered as a numerical version of the experimental flow-visualisation pictures. Yellow, blue and green streamlines visualised above the wedge free-end are sucked down towards the wall in the wake region, passing between the red streamlines which divide at the wake apex and proceed downstream relatively undisturbed. The purple streamlines lift sharply at the leading edge to pass over the wedge tip before re-circulating in the wake region, in good qualitative agreement with the flow-visualisation experiment result in figure 6.18.

Two-Stem Diameters Immersion

A similar degree of convergence was achieved with this grid. Static pressure contours at 40Pa intervals are plotted on a vertical slice through the probe centre-line in figure 7.31. These imply a rapid deceleration of the flow at the wedge leading edge, and complete stagnation at the front of the interface piece. The depression in the wake of the probe has intensified relative to the previous case by approximately 100Pa, or 30% dynamic head. Horizontal slices through the interface piece and the wedge at four different heights above the solid wall are shown in figure 7.32. The variation in pressure around the 'U' shape agrees generally with that expected around a cylinder at Reynolds numbers of less than 10×10^4, i.e. stagnation at the leading edge followed by a rapid pressure decrease as the flow accelerates either side of the stagnation point. Qualitatively, the static pressure variation over the wedge faces was similar to the previous case. Quantitatively, the gradient of the static pressure variation over the wedge faces was increased, resulting in lower absolute pressures towards the back of the

wedge. These features are clearly captured in the colour contour map of figure 7.33, where twenty five, 40Pa colour bands spanning a pressure range of 100000 to 99000Pa are defined. Evidence of angled flow over the wedge face in the tip region is still apparent.

Numerically predicted static pressure coefficients at positions corresponding to tappings 3, 4 and 5 on the wedge face are plotted in figure 7.26 for the two-stem diameters immersion case. The discrepancy between predicted and experimentally determined static pressure coefficients is less than 10% at all tapping positions, suggesting that this solution is more accurate than for the previous, one stem diameter immersion case.

A re-circulatory region at the back of the wedge was resolved, and is apparent from the velocity vector plot of figure 7.34. This is fed with fluid from both the free and supported ends of the wedge head. A streakline representation of the predicted flow over the probe tip is shown in figure 7.35a). As in the one stem diameter immersion case, fluid represented by the green and red streaklines is sucked into the wedge head wake re-circulation and then down the back of the interface piece towards the wall. A streakline representation of the flow around the interface piece / wedge head junction is given in figure 7.35b). The fluid which is sucked into the wedge head wake re-circulation is predominantly that which divides about the top of the interface piece, and is represented by the blue, red and green streaklines. These streaklines pass between the purple streaklines which represent flow over the wedge head itself. Again, flow is sucked down the back of the interface piece towards the wall, passing between the yellow streaklines which divide about the leading edge of the interface piece, and precede downstream relatively undisturbed. The formation of the wedge head wake re-circulation, and the stemwise flows at the back of the probe towards the wall are in good qualitative agreement with the flow visualisation results represented by figure 6.20.

A velocity vector representation of the flow around the interface piece is shown on a mid-height, cross-sectional plane in figure 7.36a). A largely stagnant region

downstream of the interface piece is observed, in which the flow structure is largely in-coherent. The wedge head wake flow structure is apparent from vector plots on three planes through the wedge in figures 7.36b), 7.36c) and 7.36d), and is qualitatively similar to the previous case. Figure 7.37 shows streaklines which originate from the three consecutive K-planes immediately adjacent to the wall, and which lie within the boundary layer. At the intersection of the wall and the interface piece, fluid immediately upstream of the leading edge is deflected towards the wall before dividing either side of the probe. The grid in this region was not sufficiently dense to resolve the horse-shoe vortex which might have been expected to form under such conditions. In the flow visualisation experiment, the hole of probe introduction prevented the initiation of a horse-shoe vortex, and failure to resolve this feature of the flow was not therefore of serious detriment to the overall solution.

Four-Stem Diameters Immersion

Despite thirty pass-pairs, no better than 1.4 orders of magnitude convergence could be achieved with this grid. Per pass adjustments in static pressure were reduced to 4% dynamic head, the largest changes being made in the probe wake region. Convergence could probably have been improved by increasing the mesh density in this area and by running the solution on an alternative computing platform. The limited time available in the project plan precluded this option, and the results presented below must be interpreted accordingly.

Failure to fully converge the solution in the cylinder wake region was also attributed to the unsteady nature of the flow at this position. Morkovin (1964) discusses the Reynolds number related changes in flow around infinitely long cylinders; at Reynolds numbers less than 10×10^4, laminar flow over the cylindrical surface up to a separation point at 100° back from the leading edge is expected, with a turbulent wake beyond that. Gould et al.(1968) investigated experimentally the flow over a cantilevered cylinder at similar Reynolds numbers in the context of buildings research. They found that the circumferential variation of static pressure coefficient was altered towards the

cylinder free-end by the formation of surface vortices which delayed the separation point. This was in such a direction as to reduce the pressure recovered at the back of the cylinder, thus increasing the local drag coefficient at the cylinder free-end. Inspection of the static pressure contours plotted on three planes through the cylindrical stem in figure 7.38 showed that this trend had been predicted despite the convergence difficulties. Velocity vectors plotted on the same planes implied a largely incoherent wake structure, although low-momentum fluid in the boundary layer apparently rolled-up into a pair of counter-rotating but asymmetric eddies, as shown in figure 7.39.

A streakline plot of the flow at the interface between the cylinder and the interface piece is given in figure 7.40. The flow lifts sharply over the free-end of the cylinder, but proceeds downstream relatively undisturbed. The streaklines which are deflected the most are those which divide at the leading edge of the cylindrical stem, i.e. the yellow and green lines.

The flow around the interface piece and the wedge was largely similar to the previous case in structure and magnitude. Figure 7.41 shows the velocity vectors plotted on a vertical plane through the probe centre line; the re-circulatory region observed in the wake of the wedge head at lesser immersions is clearly resolved, and is apparently fed from both ends of the wedge head. In the streakline representation in figure 7.42, flow over the lower part of the wedge faces is drawn into the re-circulating region, which is again bounded by flow leaving from slightly higher up the wedge faces. A stemwise flow component along the back of the probe towards the wall is clearly shown, in excellent agreement with the flow visualisation experiment result in figure 6.20.

A velocity vector representation of the flow structure in the wake of the interface piece is shown in figure 7.43a) on a mid-height cross-sectional plane. As in the two stem diameters immersion case, the wake flow adjacent to the probe is largely stagnant, although the wake extends considerably further downstream. It is not known whether this difference is a real phenomena, or a consequence of the poorly converged solution of the four stem diameters immersion case. A strong reverse flow component associated

with the wedge head wake re-circulation dominated the wedge wake flow near the supported end, (figure 7.43b). In the colour contour map of figure 7.44, the static pressure variation over the probe surface is indicated by 25, 40Pa colour bands spanning a pressure range of 100000 to 99000Pa. From comparison between this and the equivalent contour map for the two-stem diameters immersion case in figure 7.33, similarity in static pressure variation over the wedge faces is apparent. This is quantified in figure 7.26, where numerically predicted static pressure coefficients at positions corresponding to tappings 3, 4 and 5 on the wedge face are plotted with the corresponding experimental data at four stem diameters immersion. Agreement between prediction and experiment is less good than in the previous two cases, although a trend consistent with the wall proximity effect is clearly observed.

To summarise this chapter, the flow around a two-dimensional cylinder at a Reynolds number of 40 was used as a test case to successfully demonstrate the accuracy of the MEFP pressure correction code and the suitability of the mesh embedding method for numerically modelling flows around a wedge probe. The flow around a 24° included angle wedge shape at a representative Reynolds number was calculated for flow incidences of 0°, 4° and 8° relative to the wedge centre line. Good agreement with experimental data was achieved, including the resolution of a separation bubble in the leading edge, suction surface region at 8° incidence.

The large scale wedge probe used in the flow visualisation experiments was modelled, and flows calculated for immersions of one, two and four stem diameters, at a representative Reynolds number. Good qualitative agreement with the flow visualisation pictures was achieved. The quantitative agreement between measured and predicted surface static pressures at the highest immersion was less good due to limitations of the grid, and the unsteady nature of the flow in the wake of the cylindrical stem. However the wall proximity effect was reproduced in direction if not in magnitude. Time constraints precluded the study of Reynolds number and turbulence effects, and prevented numerical investigation of the facility dependence of probe calibrations. This reflects the technical time and computational effort necessary to achieve solutions for the

three-dimensional probe geometry. All other aims of the numerical modelling were achieved. In the following chapter, the way in which the CFD calculation results were used in understanding the physical mechanisms responsible for the wall proximity effect are explained.

CHAPTER 8: DISCUSSION

8.1 INTRODUCTION

In this chapter, the results of the experimental and numerical investigations are discussed with a view to meeting the project aims stated in chapter 1. In section 8.2 the findings of the factorial experiments reported in chapter 5 are discussed in the light of results from the flow visualisation and CFD calculations to develop an understanding of the physical cause of wall proximity effects. Further experimental investigation of a specific aspect of the wedge probe aerodynamic design was necessary in support of this discussion, and is reported in section 8.3. In section 8.4, a pseudo-three-dimensional, analytical model of the dominant flow structures is developed and used to predict the wall proximity effect for various geometries of wedge probe at several flow conditions.

In section 8.5, the analytical model is used to explain the static pressure coefficient discrepancy which was observed between calibrations of the same probe performed in different facilities. Possible explanations for the apparent changes in yaw sensitivity are also proposed. Procedures for avoiding calibration errors and for correcting the wall proximity dependence of existing wedge probe designs are developed in section 8.6. A new wedge probe was designed, manufactured and tested with the aim of avoiding the wall proximity effect altogether; the success of this design is discussed in section 8.7, together with proposals for further improvement.

8.2 PHYSICAL CAUSE OF WALL PROXIMITY EFFECTS

8.2.1 Discussion of Factorial Experiment Results

Of the five variables investigated in the factorial experiment described in section 5.2, the length of the interface piece was the most significant, where increasing the

interface piece length reduced the wall proximity effect both in terms of the area under the curve and the deviation of static pressure coefficient, (tables 5.3 and 5.4). This is seen directly by overlaying the results of experiments 1 and 2 in figure 8.1; apart from the interface piece length, the conditions between these two experiments were identical. A plateau in the curve for probe 24LS is observed between 10mm and 22mm static tapping immersion which is not apparent with the shorter interface piece probe 24SS. This feature can be related to geometric features of the 24LS probe, which is drawn to scale against the absisca in figure 8.1. The plateau begins with the wedge head and one third of the interface piece immersed in the flow, and ends as the cylindrical stem emerges through the wall. For future reference, the wall proximity curve for probe 24LS is divided into the three regions defined in figure 8.1.

The part of the curve defined as region 1 extends 10mm, or four times the boundary layer thickness from the wall. Whilst the initial decrease in static pressure coefficient could be boundary layer related, other flow mechanisms must be considered to explain this behaviour in full. An eddy at the upstream lip of the hole of introduction was noted at probe immersions of between one and three stem diameters in the large scale flow visualisation experiments, (section 6.3.4). This corresponds to actual probe immersions of between 3mm and 16mm. It was considered that low momentum fluid in the leading edge regions of the wedge and interface piece could be entrained into the re-circulation, resulting in stemwise flow along the probe towards the wall which interfered with the static tappings in some way. This was investigated further as discussed in section 8.7.

The shape of the curve in region 1 may also be explained in terms of the static pressure at the back of the wedge head. For an infinitely long element of wedge-shaped cross section, the static pressure at the back face is governed by the wake flow structure. As shown by flow visualisation, and from CFD calculation, the wake flow structure in a plane perpendicular to the wedge element axis comprises a pair of symmetric, contra-rotating re-circulations, and is purely two-dimensional, i.e. no flow component along the element. The pressure change around the element may be expressed as a

pressure drag coefficient, and does not vary along the length of the element for uniform cross-flow. At the free-end of the large scale probe wedge head, a re-circulating region in the wake of the wedge head and in the plane of the probe was observed in the flow visualisation studies, (figure 6.18), and calculated numerically, (figure 7.30). This results from a viscous deceleration of fast moving fluid passing over the free end of the probe, and gives rise to a stemwise velocity component immediately adjacent to the wedge rear face, and towards the probe free end. An associated pressure drop is to be expected, of a magnitude depending on the size and structure of the re-circulation and hence on the probe immersion. This is observed in figure 6.16; tapping no.9 was positioned on the rear face of the wedge and indicates a monotonic fall in static pressure at this position of 25% dynamic head as immersion increases between one and three stem diameters. By conservation of energy, this reduced base pressure must be accompanied by flow acceleration over the wedge faces, resulting in a reduced pressure at the static pressure tappings consistent with the wall proximity effect.

The equilibrium state reached in region 2 indicates that the wedge head is now sufficiently immersed to be free from any influence of the eddy at the hole of introduction, and that the re-circulation in the wedge head wake has attained an equilibrium diameter with a constant associated wedge base pressure. This is consistent with the flow visualisation results in section 6.3.4.

The equilibrium state is upset at the beginning of region 3 as the circular stem emerges through the wall. It is proposed that a re-circulating region similar in nature to that at the base of the wedge is established in the wake of the cylinder, which reduces the static pressure in this region below that which would be expected for an infinitely long (two-dimensional) cylindrical element. This proposition is suggested by the flow visualisation study results, and supported by experimental data in figure 6.16, where tappings 15 and 17 positioned in the cylinder trailing edge both indicate a monotonically decreasing pressure with increasing immersion. For this to cause the reduction in indicated static pressure observed through region 3 implies some interaction between the two re-circulating regions. Such an interaction was apparent in the flow

visualisation studies, (figure 6.20), where stemwise flow down the back of the probe from the wedge re-circulation towards the base of the cylinder was observed. Similarly in the CFD simulation (figure 7.42), streaklines which pass under the supported end of the wedge are sucked down into the wake of the cylinder before proceeding downstream, and are indicative of a pressure gradient down the back of the probe. This transfer of fluid occurs within an envelope the width of the interface piece, and is bounded by faster moving fluid passing either side of the interface piece. The result is to modify the wedge head wake re-circulation to further increase the momentum of fluid near the wedge faces; a more detailed consideration of this interaction is given in section 8.4 in formulating an analytical model of the probe local flow. Whilst not resolved numerically, the smoke flow visualisation indicated that the cylinder wake re-circulation also reached an equilibrium diameter at a given immersion beyond which no further growth occurred. This is consistent with a second plateau in the wall proximity curve, as observed at the end of region 3 in figure 8.1.

If the length of the interface piece were reduced, so the re-circulations behind the wedge and the cylinder would move closer together. Developing the argument above, this would intensify the stemwise static pressure gradient, and increasingly modify the wedge wake re-circulation which in turn governs the flow over the wedge faces. A greater wall proximity effect might be expected, and is observed experimentally. It follows that the different static pressure coefficients associated with probes 24LS and 24SS are determined by the relative strengths of these re-circulations. Much wedge probe research has been conducted by previous investigators using two-dimensional wedge shapes to determine characteristics which are then assumed to hold for three-dimensional probes, (section 4.2). The validity of this approach must be in doubt, since the re-circulations are not established with two-dimensional shapes. If the re-circulating regions were influenced by highly turbulent or periodically unsteady flow typical of turbomachinery, then it also follows that the static pressure coefficient would alter from that determined in a steady calibration flow. This previously un-reported idea of probe characteristics being governed by interacting regions of re-circulating flow in

the probe wake is now used in explaining other results from the factorial experiment, and is subsequently referred to as the probe vortex model.

From the factorial experiment, increasing the pitch angle from 0° to -10° resulted in a statistically significant increase in wall proximity effect, (tables 5.3 and 5.4). This is consistent with the probe vortex model; introducing negative pitch effectively reduces the separation between the two discrete re-circulations, and is analogous to reducing the interface piece length. Inclining the probe also axially displaces the two re-circulations relative to each other, which may again influence the interaction between them. This may explain why only the deviation result was influenced by the pitch angle, but why the deviation, immersion and area under the curve results were influenced by the interface piece length. No flow visualisation or numerical data is available to support this suggestion however.

From the review of previous work in section 4.5, the influence of a fillet on the wall proximity effect depended on the fillet geometry. In the factorial experiment, the fillet had a statistically significant effect at the 5% level, and increased the wall proximity effect in both sub-sets of variables, (tables 5.3 and 5.4 respectively). Considering this in terms of the probe vortex model, a re-circulating flow region is likely to form in the wake of the fillet as it emerges into the flow, which influences the flow structure in the wake of the cylinder. This in turn will alter the interaction with the wedge head re-circulation and modify the probe indicated static pressure accordingly.

This proposition is consistent with the large scale probe experimental results. Adding a fillet to the large scale probe increased the wall proximity effect as shown in figure 8.2, where the static pressure coefficients determined from the wedge face central tapping no.4, both with and without the fillet, are plotted against immersion for a Reynolds number of 8.3×10^4. In figure 8.3, the static pressure coefficients determined at the wedge head trailing edge position from tapping no.9, with and without a fillet, are plotted against probe immersion for the same Reynolds number. The curves overlay each other, within the limits of experimental uncertainty, for immersions of up to 2.5 probe

stem diameters. Beyond this, as the fillet emerges into the flow, the 'fillet fitted' curve drops below the 'no fillet' curve, and reaches a plateau at a lower level. The lower wedge base pressure with the fillet fitted is consistent with the lower wedge face pressure seen in figure 8.2, and therefore with the probe vortex model. It is reasonable to assume that the cylindrical stem wake re-circulation, and hence the wall proximity characteristic, would be directly influenced by changes in the fillet geometry as previously reported, (section 4.2); this was not investigated however.

Of the four variables investigated in sub-set 1, figure 5.6a) shows that Mach number was the second most significant. From table 5.3, the effect of Mach number was significant at the 1% level on the area, immersion and deviation results, where raising the Mach number increased the wall proximity effect. In terms of the probe vortex model, some compressibility dependence of the three-dimensional flow structures in the probe wake might be expected; this is now considered for the wedge and cylindrical component sections of a wedge probe. Hoerner (1965) considered the relationship between compressibility and drag coefficient for a 6.9° included angle wedge shape in two-dimensional flow, i.e. tested between wind tunnel walls with no free end. He assumed that the pressure drag of this wedge originated entirely at the blunt base, and that the pressure in this region was related to the wedge face static pressure at the trailing edges. It was further assumed that the static pressure fell over the wedge faces from the free stream value at the leading edge, and that the wedge face static pressure gradient, and hence the wedge pressure coefficient, increased as a function of the free stream Mach number in proportion to the Prandtl factor. An expression relating drag coefficient to Mach number was derived based on these assumptions which showed excellent agreement with experimental data; the form of this relationship is reproduced in figure 8.4. Also included in this figure is experimental data for a 30° included angle wedge shape. The CFD studies of two-dimensional flow over a 24° included angle wedge indicate that a degree of stagnation occurs in the leading edge region, (figure 7.12). This has the effect of raising the drag coefficient, and violates the assumptions on which the relationship between drag coefficient and Mach number for the 6.9° wedge were based. However the form of the curves are similar, namely a progressively rapid

increase in drag coefficient with Mach number increasing between 0.2 and 1.0. By the probe vortex model, the wall proximity effect depends directly on the wedge base pressure, and would therefore be expected to increase with increasing Mach number.

Also by the probe vortex model, the form of the wedge wake re-circulation depends on the flow structure in the wake of the cylindrical stem, which in turn is Mach number dependent. Figure 8.5 is reproduced from Hoerner (1965), and plots the variation in drag coefficient of a cylinder in two-dimensional cross flow for Mach numbers between 0.2 and 1.0. The shape of the curve agrees qualitatively with that for the wedge shapes up to a critical Mach number of approximately 0.45. Above this, the flow at the minimum pressure points on the cylinder surface locally reaches the speed of sound and the drag coefficient rises more sharply. As noted in section 7.6.3, the three-dimensional flow structure developed at the free-end of a cantilevered cylinder acts further to increase the drag coefficient in the tip region. The flow in the cylinder wake is complicated by the interface piece, and could not be calculated numerically. However the formation of a cylindrical stem wake re-circulating region in the plane of the probe, which increased in diameter as the probe immersion was increased, was visualised experimentally (section 6.3.4).

It is well known that the flow around a cylinder in cross-flow is also highly Reynolds number dependent, (Morkovin, 1964). As Reynolds number increases, so the closed wake structure modelled numerically in section 7.4 at a Reynolds number of 40 becomes unstable, forming a coherent von Karman vortex sheet which becomes fully turbulent at Reynolds numbers between 300 and 13×10^4. Above the critical Reynolds number of 13×10^4, the laminar boundary layer over the cylinder fore-body becomes turbulent, resulting in a rapid narrowing of the turbulent wake. The wake flow interacts strongly with flow over the cylinder fore-body, and influences the separation point position which in turn modifies the circumferential pressure distribution and overall drag coefficient. Although flow over two-dimensional wedge shapes separates sharply at the trailing edge corners under all flow conditions, the Reynolds number dependence of flow over two-dimensional cylinders implies that some effect of Reynolds number on the wall

proximity effect might be expected. This was not investigated experimentally or numerically for the reasons given in sections 5.2 and 7.7 respectively. Because probes used in turbomachinery applications normally operate at Reynolds numbers between $1.3x10^4$ and the critical value of $13x10^4$ where the drag coefficient is reasonably constant, the effect may not be significant. However this argument does not consider the influence of Reynolds number on the formation of wake region re-circulations. In the large scale probe experiments, the base pressure near the cylinder tip, (tapping no.13), reduced by an amount depending on the probe immersion as the Reynolds number was increased from $8.5x10^4$ to $11.5x10^4$. Further investigation is required in which the Reynolds number is varied independently of the velocity, as discussed in chapter 10.

The influence of free-stream turbulence intensity on the wall proximity effect was investigated in the factorial experiment at 0.35 Mach number only, and found to influence the immersion result at the 5% significance level. Thus turbulence is a more important effect than those which were significant at the 10% level, but less important than those effects which were significant at the 1% level. Increasing the turbulence intensity from 0.8% to 4.5% resulted in a reduction of the wall proximity effect; this is explained in terms of interactions between the turbulent eddies and the re-circulatory flow regions in the probe wake. Length scales for isotropic turbulent flow were calculated for the suction tunnel and turbulence grid geometry from correlations given by Roach (1987). These gave a micro-scale of 0.2mm, this being a measure of the average size of eddies responsible for turbulent energy dissipation, and an integral length scale of 3.3mm, where this may be taken as a measure of the largest eddy diameter. The integral length scale is of similar order to the diameter of the wedge head re-circulation, and some interaction may occur. More probable is that energy within the re-circulatory regions is dissipated by the smallest eddies, thus raising the wedge base pressure above that in laminar flow, and reducing the wall proximity effect in consequence. Again, further investigation is required as discussed in chapter 10.

In the preliminary factorial experiment referred to in section 5.2.3 as test 1, the wedge head included angle was a statistically significant variable. Increasing the wedge

angle increased the wall proximity effect, in good agreement with the literature. Hoerner (1965) presents experimental data for the drag coefficient of two-dimensional wedge shapes as a function of wedge included angle. Drag coefficients of 0.8 and 1.4 are given for wedge included angles of 24° and 60° respectively. By the same argument as used to explain the Mach number dependence of wall proximity effects, this will result in a lower pressure at the base of the 60° wedge head, and hence a more severe wall proximity effect than with the 24° probes.

Considering statistically significant interactions identified in the factorial experiment between pairs of variables, pitch angle is seen from table 5.3 to have interacted with each of the other three variables in sub-set 1. The interaction between interface piece and pitch angle is negative, indicating that the decrease in wall proximity effect which followed from increasing the interface piece length was greater at 0° than at -10°. This is consistent with the discussion above; for a given interface piece length, pitching the probe moves the two wake-region re-circulations into closer proximity, intensifying the interaction between them. The negative interaction between pitch angle and fillet indicates that the increase in wall proximity effect which results from pitching the probe is greater without the fillet than with. This result is not consistent with the probe vortex model, but represents a complex interaction. It is suggested that flow over the fillet at negative pitch influences the re-circulation in the wake of the cylinder in a manner which has not been investigated, but which contradicts the assumptions behind the probe vortex model. The positive interaction between pitch angle and Mach number indicates that the increase in wall proximity effect which follows from pitching the probe is amplified with increasing Mach number, a result which is consistent with the probe vortex model.

The only significant interaction between the variables of sub-set 2 is between interface piece length and fillet, and is in a sense consistent with the probe vortex model, (table 5.4). No significant interactions between turbulence intensity and the other three variables were identified. However at the high Mach number level of 0.75, the corresponding Reynolds number is close to the critical value at which the drag coefficient

of a cylinder changes markedly. Had it been possible to test at high turbulence intensity and high Mach number conditions, the high level of background turbulence may have resulted in transition from a laminar to a turbulent boundary layer over the cylinder surface at a Reynolds number below the critical value, with a corresponding change in the wall proximity effect. This suggests a significant but as yet un-quantified interaction between two variables which may both be at a high level under certain turbomachinery test conditions. Further work in this area is therefore required.

8.2.2 Discussion of Near Wall Calibrations for Yaw Angle

In section 5.2.4, an experiment was reported in which two narrow-angle wedge probes were calibrated against yaw angle at several immersions from the wall of introduction. The yaw sensitivity of probe 30MS increased by 12% over an immersion range similar to that over which the probe indicated static pressure was affected, (figure 5.8). This suggests a link between the yaw angle sensitivity change and the probe vortex model as discussed below.

From figure 5.10, it can be inferred that the rate of reduction of static pressure coefficient with increasing immersion at a given yaw angle is greater on the suction surface than on the pressure surface of the wedge head. A qualitative representation of this is given in figure 8.6, and two explanations are proposed. Firstly, the re-circulating region in the wake of the wedge head may be sucked into the suction surface region of the wake flow when the probe is operated at incidence. This is illustrated schematically in figure 8.7a), and would generate a pressure gradient at the base of the wedge with a minimum at the suction surface corner. As immersion was increased, so the re-circulation would grow, and reduce the base pressure differentially so as to accelerate the flow more rapidly over the suction surface than the pressure surface. Secondly, there is no physical barrier to flow migration over the free end of the wedge head from pressure to suction surface. Evidence of this was observed during the flow visualisation studies, as discussed in section 6.3.4. The over tip leakage flow may roll up into a tip vortex with its origin at the suction surface trailing edge as shown in figure 8.7b). An axial velocity is associated

with such vortices, the magnitude of which depends on the vortex diameter, its rotational velocity, and the free-stream velocity as reported by Batchelor, (1964). It is suggested that this axial velocity component may locally amplify the re-circulation in the suction surface region of the wedge wake and preferentially accelerate the suction surface flow as before. Both these explanations are speculative and require further investigation. However, both suggest that the yaw angle sensitivity, as well as the static pressure measuring ability of wedge probes depends on re-circulatory regions in the probe wake, and that modifying these flow structures can significantly influence the characteristics of a given probe.

8.3 FURTHER EXPERIMENTAL INVESTIGATION

Given the apparent importance of the re-circulatory regions, particularly in the wake of the wedge head, an experiment in which this flow structure was influenced using end-plates was conducted. The drag characteristics of elements with uniform cross-section are traditionally investigated experimentally using a model which spans the working section of the wind tunnel. This avoids three-dimensional flow effects at the free-end of a cantilevered element, but the maximum obtainable Reynolds number is usually limited either by the drag capacity of the balance or the maximum acceptable blockage in the tunnel. Cowdrey (1962) investigated the use of small end plates in place of the tunnel wall. His aim was to establish the minimum size of plate required to avoid three-dimensional flows, such that shorter elements of uniform cross-section could be used, thus minimising tunnel blockage. Cowdrey showed that a re-circulatory flow structure in the wake of a cantilevered, square section element disappeared completely when plates conforming to the dimensional criteria reproduced in figure 8.8 were fitted to the free end.

Two end plates for the 24° included angle wedge probe were designed based on Cowdrey's criteria for square section element end plates. These are shown as plates A and B in figure 8.9; the plates differ only in the lengths of the downstream overhang,

which were chosen to bracket Cowdrey's recommendation of 2.5 times the element base width. The end plates were cut from 0.25mm steel shim, and secured to the probe tip using 'Loctite' adhesive. Tests were conducted in the suction tunnel on probes 24LF and 24SF fitted in turn with plates A and B. A single flow condition of 0.35 Mach number and 0.8% free-stream turbulence intensity was used throughout. Each test involved traversing the appropriately configured probe out from the flat plate using the same procedure as in the factorial experiment, (section 5.2.3).

Results for probes 24LF and 24SF are presented in figures 8.10 and 8.11 respectively. Static pressure coefficient is plotted against probe immersion in the usual way, and the corresponding results from the factorial experiment without end-plates fitted are included for comparison. From figure 8.10, the effect of adding end-plate A was to lower the wall proximity curve of probe 24LF by a uniform 5% dynamic head at all immersions. The intent of avoiding the wedge wake re-circulation was obviously not achieved; rather the end plate would appear to have increased the wedge base depression, and hence the wall proximity effect, by increasing the diameter of the re-circulating region. Replacing end-plate A with the larger end-plate B resulted in a curve approximately mid-way between the two extremes. This implied that the wedge base pressure drop associated with the re-circulation had decreased over that with end-plate A, and that further increases in end-plate length might have reduced the wall proximity effect further. The dimensions even of end-plate A far exceeded the original requirement for a probe design which could be contained within a 6.35mm diameter cylindrical element, and larger end-plates were not pursued. Regardless of the absolute level of the three curves in figure 8.10, the plateau originally defined as region 2 in figure 8.1 was clearly resolved in the curves for end-plates A and B. Although the wedge wake re-circulation was influenced by the end-plates, the implication is that the interaction between the wedge-head and cylindrical stem wake re-circulations was not substantially altered.

In figure 8.11, the results for the three versions of probe 24SF, (i.e. with no end-plate, with end-plate A and with end-plate B), agree within the limits of experimental

accuracy for immersions up to 35mm. As discussed in section 8.2.1, the interaction between the two re-circulatory regions has a more significant effect in probes with a shorter interface piece. Because end-plates influence the wedge wake re-circulation but not that in the wake of the cylindrical stem, the result in figure 8.11 demonstrates the dominance of the stem wake re-circulation. This argument must be modified at immersions greater than 35mm, where the results for the probe with end-plates drop below the no end-plate curve by up to 9% dynamic head for end-plate A. An immersion of 35mm does not correspond to any geometrical feature of the probe. It is suggested that the end-plate acts to move the wedge wake re-circulation downstream from the probe itself as shown schematically in figure 8.12a). As the diameter of the cylindrical stem wake re-circulation grows with increasing immersion, so a point will be reached where the two re-circulations may directly interfere (figure 8.12b)) resulting in the characteristic seen in figure 8.11. No experimental or numerical evidence is available to support this suggestion however.

In summary, the introduction of end-plates influenced the wedge wake re-circulation, and hence the wall proximity effect. By applying the sizing criteria developed by Cowdrey to a wedge shaped cross-section, it was hoped to minimise the wall proximity effect by avoiding the wedge wake re-circulation. The tested end-plates were not sufficiently large to achieve this, but the wall proximity effect was influenced in a manner which was qualitatively consistent with the probe vortex model. Interaction between re-circulating regions behind the wedge head and the circular stem was clearly observed with both probes, the influence of the cylindrical stem wake re-circulation increasing as the probe interface piece was reduced in length. Despite the in-practicality of end-plates in an actual probe design for turbomachinery applications, this experiment effectively demonstrated the dependence of probe characteristics on re-circulatory flow regions established in the probe wake. This idea is extended in the following section, where a simple, analytical embodiment of the probe vortex model is developed.

8.4 ANALYTICAL MODELLING

8.4.1 Derivation of Model

In developing an analytical embodiment of the probe vortex model, the aim was to establish whether the complex structure in a probe wake could accurately be represented by simple models of isolated elements of the flow, specifically the two re-circulatory regions identified in the probe wake, and the interaction between them. The CFD solution of the re-circulatory region in the wake of the wedge head of a probe at four stem-diameters immersion was taken as a starting point, (figure 7.41). McCormack and Crane (1973) suggest that such a flow structure will comprise a central core of fluid which rotates as a solid body, such that the tangential velocity at any point on a streamline, q, is directly proportional to the radius of that streamline, r. This rotational flow structure is referred to as a forced vortex. At radii greater than a critical value, a, it can be shown that the flow becomes irrotational such that the product of q and r is a constant. This is the characteristic of a free vortex. The transition from a rotational core to an irrotational free vortex occurs at a radius which represents the balance of the rotational forces associated with each vortex structure. The critical radius therefore depends on the prevailing pressure gradient and on the action of viscosity, and is difficult to predict. However the pressure and velocity distributions through a combined forced and free vortex structure can be derived straightforwardly, for incompressible flow, from appropriate application of Bernoulli's equation and the Euler equation, (McCormack and Crane, 1973).

Modelling of Wedge Head Wake Re-circulation

In order to ascertain the prevailing structure in the wake of the wedge head, the position of the vortex centre in figure 7.41 was estimated, and taken as the origin for five circles drawn over the velocity vectors as shown in figure 8.13a). Velocity vectors tangential to any of these circles were divided by the corresponding radius and plotted in the appropriate position on the polar chart shown in figure 8.13b). Had the re-circulation

been purely a forced vortex, a polar chart comprising five circles each of radius (q/r) would have resulted. It was considered that the plot in figure 8.13b) approximated sufficiently to a circle for the wedge wake re-circulation to be modelled primarily as a forced vortex. From the CFD solution in figure 8.13a), the tangential velocity of the fully developed vortex is approximately equal to the free-stream velocity, v_o. Taking r_{we} as the equilibrium radius of this vortex, the rotational speed, ω, is then given by (v_o/r_{we}). At immersions less than r_{we} where the vortex size is restricted by the wall, it is assumed that the tangential velocity of the vortex, q_w, is also reduced in proportion, as expressed in equation 8.1. A scaling factor, F, was introduced in equation 8.1, and set to a value less than unity to reflect the deviation from a true forced vortex structure implied by figure 8.13b). The most appropriate value for F was determined by a trial and error procedure described in section 8.4.2.

$$q_w = (F \, . \, v_o \, . \, r_w \,) / r_{we} \qquad \ldots\ldots\ldots\ldots\ldots (8.1)$$

The relationship between vortex radius and probe immersion was determined through consideration of the probe geometry and the wall boundary layer thickness. Terms are defined in figure 8.14, which shows a schematic representation of the case where only the wedge head is fully immersed. It was noted from both the flow visualisation studies and the CFD solutions that the wedge wake vortex was fed from both free and supported ends of the wedge head, and was free to extend beyond the wedge head into the wake of the interface piece. From figure 8.14, the velocity at the supported end of the wedge head is governed by the boundary layer thickness and velocity profile at immersions where the probe tip is outside the boundary layer. This was reflected in the model by defining the following expressions for the vortex radius:

$$\text{For } (I + y) < (h + \delta); \qquad r = (y + I)/2 \qquad \ldots\ldots\ldots (8.2)$$
$$\text{For } (I + y) > (h + \delta); \qquad r = (h + \delta)/2 \qquad \ldots\ldots\ldots (8.3)$$

Thus it was assumed that the vortex equilibrium radius was reached once the supported end of the wedge head had moved through the boundary layer, and into the free stream.

The validity of this assumption was tested against experimental data as discussed in section 8.4.2.

In calculating the static pressure at the base of the wedge head, it was firstly assumed that the drag coefficient appropriate for an infinitely long element of wedge-shaped cross section was due entirely to pressure induced drag forces. In practice, viscous action at the wedge faces will contribute a frictional drag force component. However at zero incidence, the pressure gradient over the wedge faces was seen from the CFD calculations in section 7.5.2 to be favourable from leading to trailing edge, implying that a laminar boundary layer with no separation could be assumed, with minimal frictional drag in consequence. This assumption allowed the pressure drag to be determined without the complication of boundary layer thickness and skin friction calculations, and proved to be a good first approximation as subsequently shown in section 8.4.2; skin friction modelling could readily be incorporated in a more sophisticated model. The basis of the probe vortex model is that the velocity at the wedge faces, and hence the static pressure indicated by the probe, is governed by the wedge base pressure. Hence the base pressure in the plane of the static tappings was required. Because drag coefficient is defined in terms of the local dynamic head, and because this varies through the boundary layer, the two equations (8.4) and (8.5) were derived from the drag coefficient definition below to reflect the variation of drag force with probe position in the boundary layer.

Drag Force = Drag Coefficient x Dynamic Head x Frontal Area

For $I < (h - y)$: $F_D = C_{DW} \times (\frac{1}{2}.\rho.v_I^2) \times \{(I + y).c.\tan\varepsilon\}$ ..... (8.4)
For $I > (h - y)$: $F_D = C_{DW} \times (\frac{1}{2}.\rho.v_I^2) \times (h.c.\tan\varepsilon)$ ..... (8.5)

The drag coefficient, C_{DW}, for a two-dimensional wedge shape is taken from figure 8.4 for the appropriate Reynolds number, and the velocity, v_I, is that in the plane of the static tappings at an immersion of I. A turbulent boundary layer velocity profile modelled as a (1/7th) power law was used to determine v_I within the boundary layer. The wedge chord, c, and included wedge angle, ε, are defined in figure 8.14. Because the drag force is

attributed entirely to the pressure drop from front to back of the wedge, $(p_t - p_{bw})$, it follows that the wedge base pressure, p_{bw}, is given by:

$$p_{bw} = p_t - (F_D / A) \quad \ldots\ldots\ldots (8.6)$$

where p_t is the free stream total pressure and A the wedge head frontal area. The use of free stream total pressure inherently assumes that the flow stagnates at the wedge apex; in practice wedge head leading edges are usually radiused by 0.25mm or more as shown in figure 8.15, and this assumption should be generally applicable.

By the probe vortex model, the pressure at the base of a two-dimensional wedge shape is reduced for actual probes by the stemwise velocity associated with the forced vortex in the wedge wake. It was assumed that the ratio of p_{bw} to the reduced base pressure p_{bw}' is related to the tangential velocity of the forced vortex by the isentropic flow equation:

$$(p_{bw} / p_{bw}') = \{1 + \tfrac{(\gamma-1)}{2} (q_w / C)^2 \}^{\frac{(\gamma)}{(\gamma-1)}} \quad \ldots\ldots\ldots (8.7)$$

where C is the local speed of sound, and q_w is determined from equation (8.1). Given this modified base pressure, the static pressure gradient over the wedge faces was re-calculated by linearly interpolating between the leading and trailing edge static pressure values. From the numerically calculated wedge face pressure profile at zero incidence, (figure 7.14), the assumption of a linear pressure gradient over the wedge faces is justified for (x/L) greater than 0.2. It was also inherently assumed that the trailing edge pressure was equal to the modified base pressure, p_{bw}'; again this is justified by the numerically predicted pressure contours at one, two and four probe stem diameters in figures 7.25, 7.32 and 7.38 respectively. These assumptions were embodied in equation (8.8), which expresses the wedge face pressure as a non-dimensionalised static pressure coefficient B_{WF}:

$$B_{WF} = \{[p_{0.2} - (x / L).(p_{0.2} - p_{bw}')] - p_s \} / (p_t - p_s) \quad \ldots\ldots\ldots (8.8)$$

where $p_{0.2}$ is the wedge face static pressure at an (x/L) of 0.2. Because the value of $p_{0.2}$ is itself a function of p_{bw}', an alternative pressure datum was required for the purposes of the model. The static pressure, p_{LE}, on the wedge faces just downstream of the radiused leading edge was adopted, and defined as:

$$p_{LE} = k \,.\, (p_t - p_s) + p_s \quad \ldots\ldots\ldots (8.9)$$

where k represents the fraction of dynamic head recovered at this position. From consideration of figure 8.15, a value for k of just less than unity might be considered appropriate. However from figure 7.14, the wedge face pressure profile is not linear for $0 < (x/L) < 0.2$, and to have set k close to unity and then assumed a linear reduction in pressure from p_{LE} to p_{bw}' would have artificially raised the wedge face static pressure levels at all (x/L). A lower value of k was chosen such that a good straight line approximation to the profile in figure 7.14 was achieved for (x/L) between 0.2 and 1.0; it was then accepted that the model was not strictly valid for $(x/L) < 0.2$. The choice of k, and the sensitivity of the model to variations in k is discussed in section 8.4.2. Substituting $p_{0.2}$ for p_{LE} in equation (8.8) resulted in a final expression for B_{WF}:

$$B_{WF} = \{ [p_{LE} - (x / L).(p_{LE} - p_{bw}')] - p_s \} / (p_t - p_s) \quad \ldots\ldots\ldots (8.8a)$$

Modelling of Cylindrical Stem Wake Re-Circulation

A similar procedure was used in modelling the re-circulation in the wake of the circular cylinder. The CFD calculation of the flow structure in this region was not sufficiently well resolved to verify the assumption of a forced vortex. However, the re-circulation observed experimentally in the wake of the cylinder showed good qualitative agreement with that in the wake of the wedge, and a forced vortex structure was assumed on this basis. The radius, r_c, of this vortex was set equal to half the cylindrical stem immersion defined as 'i' in figure 8.16. The tangential velocity, q_c, at a given immersion was then calculated from the ratio:

$$q_c = (v_o . r_c) / r_{co} \quad \ldots\ldots\ldots (8.10)$$

where r_{co} was defined as the vortex equilibrium radius. The absolute value of r_{co} was determined by comparison with experimental data as discussed in section 8.4.2. The base pressure for a two-dimensional cylinder in cross-flow, p_{bc}, was calculated from the appropriate drag coefficient, neglecting any skin frictional drag component as before. Because the flow around a cylinder separates at some distance back from the stagnation point, and may also undergo laminar to turbulent transition, the use of this assumption in computing the cylinder base pressure was very much a simplification which could be refined in a development of the model. By omitting the skin friction component, too low a value of cylinder base pressure was to be expected, although in practice the assumption gave a good first approximation. The 'two-dimensional' base pressure was then modified due to the forced vortex using an equation similar to equation (8.7) to calculate p_{bc}'.

Modelling of Interaction Between Re-Circulating Regions

From the discussion in section 8.2, a complex interaction was noted between the wedge head and cylindrical stem wake vortices involving the stemwise transfer of fluid along the rear of the interface piece towards the cylindrical stem. This implied that the modified base pressure at the base of the cylinder was less than that at the base of the wedge. In deriving a simple model to describe the effect of this interaction, it was assumed that the pressure at the base of the wedge adjacent to the probe tip remained equal to the modified wedge base pressure p_{bw}' regardless of any interaction between the two vortices. The base pressure in the plane of the static pressure tappings was then modified again by linearly interpolating between p_{bw}' at the probe tip, and p_{bc}' at a plane through the cylindrical stem coincident with the centre of the vortex, to give a new value of wedge base pressure, p_{bw}'', i.e:

$$p_{bw}'' = p_{bw}' - \{ y . (p_{bw}' - p_{bc}') \} / (y + I) \quad \ldots\ldots\ldots (8.11)$$

This value of base pressure was substituted into equation (8.8a), and used in calculating the wedge face static pressure profile for immersions greater than (h + l), i.e. with the circular stem immersed into the flow. The success of the model in predicting the wall proximity effect for narrow angle wedge probes typical of those applied in turbomachinery is discussed in the following section.

8.4.2 Validation of Model

The equations established above as the basis of the probe vortex model were embodied in spreadsheet form to facilitate rapid computation of probe static pressure coefficients at probe immersions of between 0mm and 70mm. Calculated static pressure coefficients were plotted against immersion to give the conventional form of wall proximity curve, which was compared with the corresponding, experimentally determined curve in order to assess the prediction accuracy.

The model was optimised using probe 24LS at 0.35 Mach number as a test case. The probe geometry was defined in terms of six parameters entered as input data to the spreadsheet, and shown in figure 8.17. Values for the wedge and cylindrical stem drag coefficients were taken from figures 8.4 and 8.5 respectively, whilst the prevailing flow conditions were defined in terms of free stream values for velocity, total pressure and total temperature. Mach number, density, and static values of pressure and temperature were calculated from these parameters. The fit of the predicted to the experimental curve over regions 1 and 2 (as defined in figure 8.1) was then optimised by adjusting the parameters which describe the wedge head wake vortex, namely k, F, and the vortex diameter. A wedge head vortex diameter of 8.5mm, equal to the sum of the wedge head length and the boundary layer thickness, was used initially. A better fit to the experimental data was achieved using a vortex diameter of 12mm. This discrepancy may be attributable to the influence of the hole of introduction, which was not accounted for in the probe vortex model, although a degree of discrepancy is inevitable given the use of simple vortex theory to model a complex flow structure. The optimum fit to experimental data was achieved with a k value of 0.4, and with an F value of 0.8. The

shape of the predicted curve in region 3 is governed by the diameter of the vortex in the wake of the cylindrical stem, and an optimum value of 25mm, or four times the probe stem diameter was determined for this. Although the cylinder drag coefficient was originally set at the expected value of 1.2, an increased value of 1.4 gave a more accurate prediction of the absolute level of the curve in region 3.

Both the predicted and the experimentally determined wall proximity effect curves for probe 24LS at 0.35 Mach number are plotted in figure 8.18. In general, the predicted curve follows the same trends as the experimental curve through each of regions 1, 2 and 3. Static pressure coefficient is considerably overestimated near the wall. This may be indicative of the influence of the hole of introduction, but is more probably related to the assumption of a forced vortex to model the wedge head wake re-circulation. Agreement between the two curves is within 1% throughout the plateau defined as region 2. The second drop in static pressure coefficient corresponding to the emergence of the cylindrical stem is slightly over-estimated in magnitude, but occurs over the correct immersion range. Overall, the prediction is seen to be accurate to within ±2.5% for immersions greater than 1.3 probe stem diameters.

In the factorial experiment reported in chapter 5, the probe interface piece length and the flow Mach number were the two most significant variables tested. To check the general applicability of the optimised probe vortex model, a scaled down factorial experiment, in which interface piece length and Mach number were tested at the same high and low values as in the full experiment, was conducted using the model to predict the wall proximity curve. Four runs of the model were required, with interface piece length and Mach number set as indicated in table 5.2 for experiments 1, 2, 9 and 10 in turn. Only the interface piece length was altered in modelling probe 24SS at 0.35 Mach number. For the higher speed runs at 0.75 Mach number, the cylinder drag coefficient was increased to 1.6, in accordance with figure 8.5. The wedge drag coefficient was also increased to the value corresponding to Mach 0.75 in figure 8.4, but optimum results were achieved with the lower speed drag coefficient of 0.75. This anomaly is difficult to explain in terms of the simple probe vortex model and requires further investigation. The

only other parameter to be altered was F, for which an optimum value of 0.88 was determined. This result implies that the wedge head wake vortex changes in structure as free-stream velocity increases, and approximates more closely to a forced vortex at higher Mach numbers. Recognising and correcting for these anomalies, the predicted wall proximity curve proved to be accurate to within ±2.5% for immersions of 8mm or more in each of the four extreme cases.

The sensitivity of the model to the four parameters k, F, wedge drag coefficient and cylinder drag coefficient was established for each of the four cases above by varying each parameter in turn, whilst holding the other three parameters at their optimum values. Sensitivity coefficients were defined for each parameter as % error in prediction per 1% change in parameter. Values for each sensitivity coefficient were calculated at various immersions and are summarised in table 8.1. For a given probe, the sensitivity to each parameter changes little with Mach number. The model is one order of magnitude less sensitive to the cylinder drag coefficient than to the other three parameters, although the cylinder drag coefficient becomes slightly more influential in the shorter interface piece probe. This result is consistent given that reducing the interface piece length moves the two wake vortices closer together and intensifies the stemwise pressure gradient at the back of the probe. The value assigned to F was less critical with the shorter interface piece probe, whilst the sensitivity to k remained constant in all cases.

Finally, the ability of the model to predict the static pressure distribution over the wedge faces was checked against pressures measured on the large scale probe at a free-stream velocity of 25m/s. These results were presented as figure 6.15, and discussed in section 6.3.4. Two runs of the model were completed with the 'tapping displacement from the tip' set at values corresponding to the positions of tappings 3 to 5 and 6 to 8 respectively of the large scale probe. The wedge face pressure at each tapping was then calculated by appropriate choice of (x/L) in equation (8.8a). Tapping positions and all other appropriate dimensions are shown in figure 6.8. The free stream velocity was set to 25m/s, whilst values used for the actual probes at 0.35 Mach number were adopted for all other parameters. Predicted wall proximity curves for each tapping are plotted with

corresponding data points in figure 8.19. Discrepancies of up to 12% are observed between predicted and actual values for the tappings at 0.2 (x/l) back from the leading edge, i.e. tappings 5 and 8. This is to be expected given the assumption made in section 8.4.1 of a linear pressure gradient over the wedge faces. Agreement is generally better for all other tapping positions, and the trends through each of the three characteristic regions of the wall proximity curve are well predicted. An important observation from this plot is the decrease in gradient of the wall proximity curves for tappings close to the wedge leading edge, a trend which was shown experimentally and which has also been predicted. Physically, this relates to the assumption that the wedge leading edge always recovers the same fraction of the dynamic pressure head regardless of the wedge base pressure. Thus in the limit, tappings positioned immediately behind the leading edge would exhibit no wall proximity effect at all. Practically, this is impossible to achieve due to space restrictions, but a good design rule would be to position the tappings as far forward on the wedge faces as possible at least from the wall proximity effect point of view.

8.4.3 Summary of Model

Through the discussion in section 8.2, it was suggested that the complex flow structure in the wake of a cantilevered probe was responsible for the characteristics displayed by that probe in a given environment. It was further suggested that this complex flow structure could be approximated to by interacting, re-circulatory flow regions behind the wedge head and the cylindrical stem. Using simple forced vortex models to describe these re-circulations, it has been shown in this section that the wall proximity characteristics of several narrow angle wedge probe variants over a wide range of flow conditions can be predicted to within ±2.5% for immersions greater than 1.3 times the probe stem diameter. A number of areas particularly relating to the change in vortex characteristics with Mach number have been highlighted for further investigation. These include a better understanding of the flow structure at immersions of less than 1.3 probe stem diameters, where the model significantly over predicts the static pressure coefficient. Overall however, it can be concluded that the analytical probe vortex model

provides a good physical description of the flow mechanisms responsible for wall proximity effects. The model is therefore of worth in explaining wedge probe characteristics, and potentially for correcting wedge probe calibrations for wall proximity effects. This possibility is considered further in section 8.6. Indications of the geometric features to be incorporated in a new probe design were also given by the model and these are considered in section 8.7.

8.5 DISCUSSION OF FACILITY DEPENDENCE RESULTS

In the calibration facility dependence experiment described in section 5.4.4, differences between the results for both static pressure coefficient at zero yaw, and for yaw angle sensitivity were observed. Considering first the static pressure coefficient at zero yaw, that obtained in the closed tunnel was always lower, (more negative), than the value obtained in the free jet facilities, by up to 18% dynamic head in the worst case. In sections 8.2 to 8.4, the value of static pressure indicated by a wedge probe was linked to distinct regions of re-circulating flow in the probe wake. For the long interface piece probe 24LF, these two re-circulations were shown in section 8.4 to span a stemwise distance of 51mm from the probe tip. In table 8.2, the probe immersions required for the wake re-circulations to develop fully behind probes 24SS and 24LS, at the highest tested Mach number of 0.35, are compared with the immersion actually used in the two open jet calibration facilities. This shows that, at the tested immersions, the re-circulation in the cylindrical stem wake was influenced by the interface between the free jet and the surrounding stationary air, for both probes calibrated in the smaller jet 1, and for probe 24LF in jet 2. Assuming that turbulent flow at the free jet boundary acts to dissipate the re-circulating motion behind the cylinder, the probe vortex model would predict a higher value of probe indicated static pressure than that in a larger diameter jet flow where both re-circulations were fully developed. From figure 5.17a) and 5.17b), this was the case for both the 24° and 60° included angle wedge probes respectively.

In figure 8.20, comparison is made between the experimentally determined static pressure coefficients and those predicted using the probe vortex model, for probes 24SF and 24LF in the closed suction tunnel and in free jet 1, at 0.35 Mach number. The calibration in the closed tunnel was predicted using the full probe vortex model developed in section 8.4. The model was modified by omitting any contribution from the cylindrical stem re-circulation in the prediction of the open jet calibrations. In each case, agreement between experimentally determined and predicted static pressure coefficients is seen from figure 8.20 to be within ±2%. This substantiates the suggestion that the action of turbulent, largely inviscid flow at the free jet boundary is responsible for dissipating the circular stem wake vortex and influencing the probe static pressure calibration accordingly. To be consistent, this also implies that static pressure calibrations in jet 2, where there was just sufficient room for the circular stem re-circulation to develop, should agree with those in the closed tunnel. Although agreement was generally closer than between values obtained in free jet 1 and the closed tunnel, discrepancies of more than 10% static pressure coefficient remained in some cases. Probes with a short interface piece showed the largest discrepancies. Because the cylindrical stem wake re-circulation is more influential in such probes, this result implies that either the vortex equilibrium diameter is larger than the value determined in section 8.4.2, or that the cylinder wake re-circulation may also have been altered in the axial (downstream) direction. The furthest downstream edge of this re-circulation was up to 55mm away from the nozzle front face during calibrations in free jet 2, by which point entrainment of air at the free jet boundary would have reduced the axial velocity sufficiently to influence this re-circulation. This would not have occurred in the closed suction tunnel, where conditions are expected to change only gradually with increasing distance downstream of the measurement plane.

Considering the differences in yaw angle sensitivity recorded from the three calibration facilities, results for the 24° included angle wedge probes were presented in section 5.4.4 and summarised in figure 5.18. In general, the yaw angle sensitivities obtained from the two free jet facilities agree with each other, within the limits of experimental uncertainty, at both Mach numbers. The yaw angle sensitivity obtained

from the closed tunnel calibration is always higher, and in some cases double that from the free jet facilities, particularly for the short interface piece probe 24SF. Similar observations apply to the 60° included angle wedge probe results summarised in figure 5.19. In section 8.2.2, modifications to the probe vortex model were used in explaining an experimentally observed increase in yaw sensitivity with increasing immersion. Given the link established above between the probe wake re-circulations and the differences in static pressure coefficients between calibration facilities, it is suggested that the calibration facility dependence of yaw sensitivity may also be explained in terms of a similarly modified probe vortex model. To re-iterate, it was suggested that the pressures recorded at the two faces of a wedge probe operating at incidence are governed by the position and size of the re-circulating flow regions in the probe wake, which in turn might be modified by an axial flow component associated with an 'over-tip' vortex. From the CFD studies of flow around two-dimensional wedge shapes reported in section 7.5.3, it was shown that a separation bubble forms in the leading edge region of the wedge suction surface at yaw angles of 8° or more. It was also shown experimentally that the re-attachment point moved downstream with increasing yaw angle. The reduction in wedge face static pressure associated with this separation bubble was calculated numerically and plotted in figure 7.16. In the three-dimensional wedge probe geometry, the modified probe vortex model implies alterations to the suction surface flow which may in turn influence the formation and growth of the separation bubble, and change the static pressure profiles over the wedge faces in consequence. Because the probe vortex model depends fundamentally on the size of probe wake re-circulations which may be restricted from developing fully in a free jet flow, so a difference in yaw sensitivity between the closed tunnel and free jet facility calibrations might be expected. Again, further work is required as discussed in chapter 10.

8.6 MINIMISATION OF WEDGE PROBE MEASUREMENT ERRORS

8.6.1 Probe Calibration Errors

From data presented and discussed above, there is significant potential for error in wedge probe calibrations due to their facility dependence. Static pressure coefficients determined for the same probe differed by up to 19%, and yaw angle sensitivities by 100% in the worst case, depending on the type of calibration facility adopted. Considerable insight into the physical cause of such differences has been achieved and embodied in the probe vortex model. Through section 8.2 to 8.5, the various experimental and numerical results have been qualitatively explained by this model, and quantitatively predicted in the case of the wall proximity effect to within ±2.5%. It is reasonable therefore to use the probe vortex model as the basis for recommendations to significantly reduce the errors associated with calibrating and applying wedge probes.

The difficulty when calibrating in a free jet is that the probe wake re-circulations which govern the probe's calibration are interfered with in the radial direction by turbulent energy dissipation at the free jet boundary, and in the axial direction by flow entrainment. The situation improves with increasing jet size; the choice of minimum jet size depends on the jet cross-sectional shape, and on the nozzle contraction through which the flow is accelerated before exhausting to atmosphere. From consideration of the wake re-circulations, the requirement is for a near parallel jet flow of at least 150mm diameter with less than 20° contraction angle in the jet core. As illustrated in figure 8.21, this jet diameter has been based on the sum of the wedge head height, the interface piece length and the cylindrical stem re-circulation diameter, and should accommodate the wake re-circulations associated with probes built on a 6.35mm diameter stem with interface piece lengths of up to 20mm. Experimental validation of such a jet design would obviously be required. A further error associated with calibrating probes in a free jet at high Mach numbers is the assumption of uniform static pressure through the jet and the surrounding stationary fluid, which becomes invalid as the jet velocity approaches the

velocity of sound propagation. This error source may be significant in certain turbine rig applications for example.

The obvious alternative is to calibrate in a closed tunnel at a sufficiently great immersion to accommodate the fully developed cylindrical stem wake re-circulation. A minimum immersion of 55mm is recommended for a probe with 20mm interface piece length. In practice, this could be determined experimentally by traversing a given probe radially into the flow until the probe indicated static pressure reached a uniform value corresponding to region 3 defined in figure 8.1. All calibrations for Mach number and yaw angle dependence would then be completed at this immersion. Because of the uniformity of conditions at and downstream of the working section, the local turbulence and flow entrainment problems of free jet calibration would be avoided. Because the wake structure would be able to develop fully, yaw angle sensitivity should not be compromised. However these arguments only hold for probes operating in a steady flow. The effect of highly unsteady turbomachinery flows on the probe wake structure and therefore on the probe calibration has not been studied as part of this investigation, but is recommended in chapter 10 as an area for further work.

8.6.2 Wall Proximity Effect Errors

One of the originally stated project objectives was to remove wall proximity effects through probe re-design, and progress towards this goal is discussed in section 8.7. Current standards of wedge probe existing within the author's company and elsewhere are still likely to be applied to turbomachinery rig tests for some time to come however, and a procedure is required to correct the calibrations of such probes for wall proximity effects. Normal procedure within Rolls-Royce is to calibrate a given probe on the centre line of a 152mm diameter closed section tunnel for total and static pressure and yaw coefficient at various Mach numbers and over a range of yaw angles. This conforms with the recommendations made in section 8.6.1 concerning radial immersion. Probe calibrations are applied off-line to turbomachinery test data using computer based algorithms. Calibration carpets for total and static pressure and yaw coefficients as a

function of Mach number and yaw angle are used as the basis for an iterative calculation of total and static pressure, Mach number and yaw angle from the probe measured pressures P1, S2 and S3. This procedure is illustrated in flow chart form in figure 8.22; iterations continue until a pre-determined convergence criteria is reached. However the current algorithm does not recognise that the static pressure coefficient calibration carpet is also a function of probe immersion.

The probe vortex model offers a means of overcoming this shortfall. Appropriate probe dimensions could be entered into a software embodiment of the model to predict the shape and absolute level of the wall proximity curve at flow conditions corresponding to those under which calibrations were completed. A typical set of predicted curves is shown in figure 8.23a). The predicted static pressure coefficients would be spot checked against those determined experimentally at the calibration immersion to verify the accuracy of the prediction. Given the probe immersion at which a set of P1, S2 and S3 pressures were recorded, the static pressure coefficient carpet would then be adjusted upwards by an amount determined from the predicted wall proximity effect curves. Figures 8.23b) and c) illustrate this procedure with a hypothetical example. A typical static pressure coefficient calibration carpet comprising curves at three Mach numbers is shown in figure 8.23b). A set of probe indicated pressures recorded at a probe immersion of 10mm are to be analysed. The levels of static pressure coefficient appropriate for this immersion are read from the predicted wall proximity curves in figure 8.23a), and the calibration carpet corrected up to this level as shown in figure 8.23c). This revised calibration carpet is then used in the iterative procedure to calculate pressures and velocity. Had wall proximity effects been dependent on the yaw angle presented by the probe to the flow, as well as on Mach number, then this correction would itself have become iterative. However from the results of the initial factorial experiment referred to as test 1 in section 5.2.1, and from appropriate analysis of the near wall calibrations for yaw angle reported in section 5.2.4, yaw angle does not significantly influence the wall proximity effect at least up to angles of ±10°. From the probe vortex model evaluation exercise in section 8.4.2, the predicted wall proximity curves agreed with experimental data to within ±2.5% for probe static tapping immersions greater than 8mm. Thus for

narrow angle wedge probes which fall within the high and low limits tested in the factorial experiment, and over which the probe vortex model has been validated, this procedure offers a low cost and readily implemented means of correcting for wall proximity effects.

8.7 PROBE RE-DESIGN

A new three-hole pressure probe was designed to reflect the physical understanding, determined from this investigation, of wedge probe performance in steady flows . The design intent was to minimise static pressure wall proximity effects through modifications to the standard wedge probe geometry. Design constraints included the requirement that the new probe should pass through a 6.35mm diameter hole of introduction. Budget constraints dictated that the conventional fabrication method of manufacture be used, rather than more flexible but dearer micro-machining techniques. This implied designing around hypodermic tubes to transmit sensed pressures to a remote pressure transducer. Four design features were identified from consideration of the arguments in sections 8.2 to 8.4:

i) The use of end plates to avoid the wedge wake re-circulation. As explained in section 8.3, the required size of end plate was prohibitively large, but an alternative approach to minimising the effect of this re-circulation was adopted. The bluff base of the wedge was streamlined both to reduce pressure drag by recovering as much base pressure as possible, and in an attempt to break down the structure of the wedge wake vortex thus diminishing its influence.

ii) A probe of constant cross-sectional shape along its entire length. The aim of this was to avoid the second re-circulatory region associated with the cylindrical stem of the original wedge probe design. It also enabled the cavity between the hole of introduction and the probe itself to be filled thus avoiding any adverse influence of the cavity on the probe near wall characteristics.

iii) Static pressure tappings positioned as far forward on the wedge faces as possible as recommended in section 8.4.3. From calibrations of the large scale probe against yaw angle (figure 6.14), and from previous work reported in section 4.5, this offered the additional advantage of increased yaw sensitivity.

iv) A recessed pitot tube. By recessing the pitot tube into the leading edge as proposed by Ferguson (1974), and referred to in section 4.4, the probe was then free to traverse right into the wall without the pitot tube interfering with the filled hole of introduction.

Figure 8.24 shows the general arrangement of a probe designed to incorporate these features. Hypodermic tubing of 0.5mm outside diameter was chosen as the smallest practical option to minimise the danger of tube blockages. For reasons given in section 8.2, the preference was to minimise the included wedge angle; an angle of 30° was chosen against the conflicting requirements of probe size and a well forward tapping position. The bluff wedge base was streamlined by effectively adding a second, reversed wedge of 45° included angle, and by removing the sharp corners to give the cross sectional shape shown in figure 8.24. The wedge face length had to be limited to accommodate the aft-body section, and the static tappings could not be positioned forward of 0.63 (x/L). A recessed pitot tube designed in accordance with Ferguson (1974) and radially offset from the static tappings to avoid interference was designed into the wedge leading edge. To meet the second design feature identified above, a two part construction was adopted comprising a probe blade of uniform cross section sliding in a guide tube of 6.35mm outside diameter at the free end. The internal shape at the guide tube free end was the inverse of the blade cross-sectional shape defined in figure 8.24, thus effectively filling the probe hole of introduction. The guide tube free end was designed to locate in the back of the suction tunnel flat plate. The rest of the guide tube was sized at 8.0mm O.D. and 6.35mm I.D. to accommodate the probe blade when retracted.

A prototype probe was manufactured by technicians at Cranfield University using the materials identified in figure 8.24. A separate probe tip drawn in figure 8.25 was built to incorporate the pressure tappings and support the hypodermic tubes; internal passage ways were formed by spark-erosion machining. This tip was then secured onto a blade of the same cross-section which had been drilled with a single, central hole to accommodate the three hypodermic tubes. Similarly, the free-end of the guide tube was manufactured as a separate item, and spark-erosion machined to form a hole with the required cross-sectional shape. This was then glued in to the end of a length of suitable tubing before assembling the probe blade into the guide tube. The completed probe is shown in plate 8.1.

An experimental evaluation of this prototype probe was completed at zero incidence and at four Mach numbers between 0.1 and 0.75 by traversing the probe blade out from the suction tunnel flat plate. The same experimental set-up and procedure was used as in the factorial experiment reported in section 5.2.3. Results were analysed to give the usual presentation of static pressure coefficient as a function of probe static tapping immersion for each Mach number; this is shown in figure 8.26. Each of the curves is of a form characteristic of the wall proximity effect. The two lower Mach number results generally follow the same curve, where the magnitude of the total decrease in static pressure coefficient is of the same order as that observed for conventional wedge probes. However the immersion over which the effect occurs is only 25mm, or approximately half that for a conventional probe. This immersion result remains constant with increasing Mach number, but the deviation result decreases markedly. At the highest tested Mach number of 0.75, the static pressure coefficient drops by only 3% from its value at the wall, for immersions of up to 47mm. The central plateau previously described as region 2 in a typical wall proximity curve is not clearly defined in any of the four results.

The fact that this probe showed a marked wall proximity effect at lower Mach numbers indicates that the streamlined aft-body did not achieve its stated objectives. It is suggested that the flow separated at the junction of the two back-to-back wedges and

that the drag characteristics of the probe were little different from a conventional wedge. At higher Mach numbers, the flow would have been more inclined to remain attached around to a separation point somewhere on the aft-body. This would have raised the base pressure, and may partly explain the reduction of wall proximity effect at Mach 0.75. The shape of the curves adjacent to the wall differs little from conventional probe results where the cavity at the hole of introduction was not filled in. This implies that the influence of the cavity on wall proximity effect is minimal. The absence of the plateau defined as region 2 is directly attributable to the constant cross-section along the probe length, and the absence of a second re-circulatory region. It would therefore be more accurate to describe the curves in terms of regions 1 and 2, with no region 3.

The strong Mach number dependence of the wall proximity effect observed diminishes the worth of this particular probe design. However the reduction in both deviation and immersion results achieved at 0.75 Mach number is an encouraging outcome, and suggests that an alternative form of aft-body might bring reductions in the wall proximity effect at lower Mach numbers also. Bearman (1964) investigated the flow at the rear of blunt trailing edge bodies fitted with splitter plates. He showed that for splitter plate lengths greater than twice the bluff body height, the flow separating at the rear corners of the body rolled up into two counter-rotating vortices which were completely contained either side of the plate. The base pressure increased to a maximum value with this configuration. Bearman used end plates to establish two-dimensional flow over free-ended models, but found that the end plate made little difference to the base pressure for splitter plate lengths greater than 1.5 times the base height. Bearman's findings imply that the influence of a wedge wake re-circulation can be substantially avoided by fitting a suitable splitter plate. The project plan only allowed for one iteration of wedge probe re-design, and the splitter plate idea could not be pursued within this investigation. A study of wedge probe performance with splitter plates fitted at the trailing edge is recommended as an area for further work in chapter 10, where a preliminary design illustrating the critical features is included.

8.8 UNSTEADY FLOW EFFECTS

Although this investigation into wedge probe characteristics has been undertaken entirely under steady flow conditions, two points relating to the effects of unsteady flow on probe calibrations emerge directly from the discussion which are worthy of particular note. Firstly, periodic, unsteady flow typical of turbomachines may alter the probe wake flow structure such that the probe steady flow calibration for static pressure and yaw angle is no longer valid. Secondly, the suction surface separation bubble which has been shown to form at probe yaw angles of 8° or more may also be influenced by periodic unsteady flow. In certain probe designs, use is made of the depression associated with this separation bubble. The probe yaw sensitivity is maximised by positioning the static pressure tappings close to the wedge leading edge. It is possible that the yaw characteristics obtained for a such a probe in a steady calibration flow might not be valid in a turbomachinery flow environment for this reason also. Further work in this and other areas is required as discussed in chapter 10.

CHAPTER 9: CONCLUSIONS

An investigation of the aerodynamic characteristics of three-hole wedge-type pneumatic probes has been undertaken to understand two specific effects relating to the measurement of turbomachinery flows with such instruments. The first effect concerns the failure of wedge-type probes to sense the correct static pressure when operating in close proximity to a wall through which the probe is introduced, and is referred to as the wall proximity effect. The second effect relates to differences which arise between aerodynamic calibrations of the same wedge probe in a bounded flow and in an open jet. This is referred to as a calibration facility dependence effect.

With a few exceptions particularly concerning the CFD calculations, the originally planned work packages have been completed successfully. From a cost benefit analysis of the project, it has been estimated that benefits of up to £1.6million would be realised if the stated objectives were completed successfully. Although the content of the work packages was not sufficient to enable the project objectives to be achieved in full, significant progress has been made particularly towards the objectives relating to the wall proximity effect.

The main conclusions to emerge specifically from the wall proximity effect investigation can be summarised as follows:

i) An existing circular section suction wind tunnel at Cranfield University has been modified and fully characterised to realise a facility in which the ability of a given probe to measure freestream static pressure under a wide range of conditions can be tested.

ii) A data base of information quantifying the relative effects and interactions of five independent variables on the near wall characteristics of wedge-type probes has been assembled from a fully factorial experiment conducted in the suction wind

tunnel. This information shows that the wall proximity effect can be reduced by increasing the length of the interface piece, and by minimising the included angle of the wedge head. The size of the effect also depends on the flow Mach number and turbulence intensity, and on the pitch angle at which the probe is presented to the flow.

iii) The wall proximity effect has been shown to be independent of the probe yaw angle for yaw angles up to 10°. However an increase in probe yaw angle sensitivity with increasing probe immersion has been demonstrated, with associated errors in measured yaw angle of up to 0.7°. This represents a significant error source which is not normally corrected when analysing turbomachinery test data.

iv) From a series of traverses of the inlet annulus of a low speed, large scale compressor, it has been shown that the wall proximity effect does not depend on the geometry of the duct in which the probe is applied, at least for low Mach number flows.

v) Low speed smoke flow visualisation techniques have been used successfully to study flows over a three-dimensional scale model of a Rolls-Royce standard wedge probe at engine representative Reynolds numbers. Two distinct flow re-circulation regions have been identified in the plane of the probe, one behind the wedge head, and another in the wake of the cylindrical stem. Evidence of fluid transfer along the back of the probe from the probe tip towards the wall has also been observed. The size of each re-circulation has been shown to increase as the probe immersion increases.

vi) Fully three-dimensional calculations of the flow over a Rolls-Royce standard wedge probe at an engine representative Reynolds number and at three probe immersions have been completed using the full Navier-Stokes pressure correction flow solver, MEFP. Excellent qualitative agreement has been obtained

between the predicted and experimentally visualised flow structures local to the probe.

vii) From analysis of the flow visualisation and numerical calculation data, it has been shown that the static pressure sensed by a wedge-type probe depends on the structure of the wake flow, and in-particular on the two re-circulating flow regions in the plane of the probe. Altering the structure of either of these re-circulations, by traversing the probe through a wall, influences the probe indicated static pressure in a manner which is wholly consistent with the factorial experiment results.

viii) By analytically modelling the wedge head and cylindrical stem wake re-circulations as forced vortices, a procedure for predicting and correcting the wall proximity effect in conventional wedge-type probe designs has been developed, and shown to be accurate to within ±2.5% dynamic head for probe immersions of greater than 1.3 stem diameters. The analytical model is termed the probe vortex model.

ix) A new wedge probe, incorporating geometrical features designed to minimise the influence of the wake flow, has been built and tested. At 0.75 Mach number, the error in indicated static pressure arising from the wall proximity effect has been reduced from 20% dynamic head typical of current wedge probe designs, to 3% dynamic head. The performance was less good at lower Mach numbers and further work is required in this area.

The main conclusions to emerge specifically from the facility dependence of wedge probe calibrations can be summarised as follows:

i) The value of static pressure coefficient determined for a given wedge probe in a closed tunnel is lower, (more negative), than that obtained in an open jet calibration facility by up to 18% dynamic head in the worst case. It has been

shown that the immersions at which probes were calibrated in the open jet facilities were insufficient to fully immerse the wake re-circulations which govern probe characteristics. The magnitude of the discrepancy has been accurately predicted by an appropriately modified version of the probe vortex model.

ii) It has also been shown that the value of wedge probe yaw angle sensitivity determined in a closed tunnel is up to 100% greater than that obtained in an open jet calibration facility. Again this is believed to be a direct consequence of alterations to the probe wake structure when calibrations are performed in an open jet, but further investigation is required to fully understand the physical mechanisms involved.

iii) It has been shown analytically that the calibration of a standard wedge probe positioned on the centre line of a circular cross-section free jet flow of 150mm diameter or more should replicate a calibration of the same probe performed in a closed wind tunnel. This conclusion has not been validated experimentally however.

Overall, it is concluded that the characteristics of a given wedge probe are governed by the structure of the probe wake flow, and that modifications to the wake flow will change the probe characteristics. Their is potential for modifying the wake flow when a probe is traversed through a wall, or calibrated in an open jet, or operated in a highly unsteady flow environment typical of turbomachinery. Further investigation is required particularly into the influence of turbomachinery flows on wedge probe characteristics.

CHAPTER 10: RECOMMENDATIONS FOR FURTHER WORK

Throughout the preceding chapters, attention has been drawn to areas which require further investigation, and these items are summarised in this chapter.

The first objective was to understand the physical mechanisms responsible for the wall proximity effect. Whilst the probe vortex model substantially achieves this, further consideration should be given to the way in which the probe wake re-circulations are modelled. The assumption of a forced vortex in the wake of the wedge head gives a poor prediction of probe static pressure coefficient for immersions less than 1.3 probe stem diameters; this might be improved by considering the forces acting on an element of the fluid as it passes over the tip of the probe and meets the largely stagnant air in the base of the wedge head.

The second objective was to overcome the wall proximity effect through probe re-design. The idea of controlling probe wake flows by modifying the probe trailing edge geometry gave encouraging results, and should be pursued by investigating the use of splitter plates. A probe design incorporating a trailing edge splitter plate was suggested in chapter 8, and is shown in figure 10.1. It seems probable that the ideas on which the probe vortex model for wedge probes is based will also apply to some extent in other probe designs such as cobra or cylindrical probes. Since the application of cobra and cylindrical probes for turbomachinery research is widespread, it is recommended that examples of such probe designs be tested for wall proximity effects. Factorially designed experiments should be undertaken such that the relative effects of a number of variables can be determined, and compared with the wedge probe factorial experiment results reported in chapter 5.

The effect of Reynolds number on the wall proximity effect was not investigated independently, although some Reynolds number dependence was inferred from the large scale probe test results. Reynolds number may vary appreciably during a turbomachine

test, and the Reynolds number dependence of wall proximity effects should be assessed by experimental calibration in a suitable wind tunnel. Although freestream turbulence was not a highly significant effect at the levels tested in chapter 5, it is suggested in chapter 8 that appreciably higher levels of turbulence might significantly alter the probe wake flow structure, and hence the probe calibration. This should be investigated experimentally over a representative range of Mach numbers.

The yaw angle measurement characteristics of wedge probes have been shown to depend on the probe immersion in a bounded flow, and on whether the probe is calibrated in a closed flow or an open jet. These dependencies have been linked to changes in the probe wake flow structure, but further investigation is required to establish the precise mechanism. A more detailed, experimental visualisation of the flow around the large scale wedge probe should give an appreciation of the local flow structures. If access could be agreed to a more powerful computing platform than the company mainframe, then CFD calculations of the flow over a probe at incidence should also yield complementary information.

Investigation into the influence of periodic, unsteady flow on wedge probe wall proximity effects and calibrations is required. Because the interaction between freestream unsteady and probe local flows is complex, and is obscured by pneumatic averaging errors within the probe itself, such an investigation represents an extreme experimental challenge. However, fully three-dimensional CFD codes capable of resolving time dependent flows are now becoming available. Considerable insight into the interaction between periodic unsteady flow and probe wake flow structures, and hence into the effect of unsteady flows on probe characteristics might be obtained with such a code. This is strongly recommended as an area for further research.

CHAPTER 11: REFERENCES

Abernathy, R.B. et al., 1973, "Uncertainty in Gas Turbine Measurements - Handbook," AEDC-TR-73-5.

Ainsworth, R.W. et al., 1994, "The Development of Fast Response Aerodynamic Probes for Flow Measurements in Turbomachinery," ASME Paper 94-GT-023.

Ainsworth, R.W. et al., 1990, "The Use of Semi-Conductor Sensors for Blade Surface Pressure Measurements in a Model Turbine Stage," ASME Paper 90-GT-346.

Ainsworth, R.W. and Stickland, A.D., 1992, "Experimenting with Fast Response Aerodynamic Probe Geometries," Proc. 11th Symp. Measuring Techniques for Transonic and Supersonic Flow in Cascades and Turbomachines, Munich.

Al-Shamma, K.A.A., 1967, "An Investigation into the Characteristics Of Wedge-Type Pitot-Static and Yaw Probes," University of Sheffield MEng Thesis.

Anderson, J., 1992, "An Introduction to Computational Fluid Dynamics," Rolls-Royce Internal Course Notes, July 1992.

Baranson, J., 1978, "Risk Perception of Technology Decisions in Public Enterprises: A Framework for Further Research," Engineering Economist, Vol.23, No.1, pp.31-39.

Barnetson, P., 1968, "Critical Path Planning," Newness Books.

Batchelor, G.K., 1964, "Axial Flow in Trailing Line Vortices," J.Fluid Mech., Vol.20, part 4, pp.645-658.

Bearman, P.W., 1964, "Investigation of the Flow Behind a two-dimensional Model with a Blunt Trailing Edge and Fitted with Splitter Plates," J. Fluid Mech., vol.21, part 2, pp.241-255.

Benedict, R.P., 1984, "Fundamentals of Temerature, Pressure and Massflow Measurements," John Wiley and Sons, Canada.

Betts, C.J. and Stanfield, J.H., 1992, "Wind Tunnel Flow Visualisation and Measurement Techniques in Use at DRA Bedford," HMSO, London.

Bissell, D., 1989, "Taguchi Methods," The Institute of Statisticians Monograph Series.

Blottner,F.G., 1964, "Non-equilibrium Laminar Boundary-Layer Flow of Ionized Air," AIAA Journal, vol.2, no.11, pp.1921-1927.

Bosworth, R., 1989, "The Application of Taguchi Methodology to Solving Steering Wheel Niggle Vibration," IMech.E., C382/052.

Bryer, D.W., and Pankhurst, R.C., 1971, "Pressure Probe Methods for Determining Wind Speed and Flow Direction," HMSO, London.

Bubeck, H. and Wachter, Y., 1987, "Development and Application of a HIgh Frequency Wedge Probe," ASME Paper 87-GT-216.

Buck, J.R., 1989, "Economic Risk Decisions in Engineering and Management," Iowa State University Press.

Chapman, D.R., 1979, "Computational Aerodynamics Development and Outlook," AIAA Journal, vol.17, no.12.

Cherrett, M.A. et al, 1994, "Unsteady 3-D Flow in a Single Stage Transonic Fan. Part 1: Unsteady Rotor Exit Flow Field," ASME Paper 94-GT-223.

Christiansen, T. and Bradshaw, P., 1981, "Effect of Turbulence on Pressure Probes," J.Phys. E: Sci. Instrum., Vol.14.

Cohen, H. et al., 1988, "Gas Turbine Theory," 3rd Edition, Longman Singapore Publishers Ltd., Singapore.

Collins, B.J., 1992, "Performance Risk Assessment," Rolls-Royce Internal Memorandum, 30.11.92.

Cook, S.C.P.,1988,"Measurement Techniques for Unsteady Turbomachinery Flows," Phd Thesis, Cranfield University, Bedford.

Cooper, D.F. and Chapman, C.B., 1986, "Risk Analysis for Large Projects: Models, Methods and Cases," John Wiley, Chichester.

Copenhaver et al., 1994, "The Effect of Tip Clearance on a Swept Transonic Compressor Rotor," ASME Paper 94-GT-363.

Corti, G., 1973, "Risk, Uncertainty and Cost Benefit: Notes on Practical Difficulties for Project Appraisals," from 'Cost Benefit and Cost Effectiveness' by J N Wolfe.

Coutanceau, M. and Bouard, R., 1976, "Experimental Determination of the Main Features of the Viscous Flow in the Wake of a Circular Cylinder in Uniform Translation. Part 1: Steady Flow," J.Fluid Mech., vol.79, part 2, pp.231-256.

Cowdrey, C.F., 1962, "A Note on the Use of End Plates to Prevent Three-dimensional Flow at the Ends of Bluff Cylinders," NPL Aero. Rep.1025.

Davies, O.L., 1978, "The Design and Analysis of Industrial Experiments," Second Edition, Longman Group Ltd., London.

Davis, R.L. and Dannenhoffer, J.F., 1989, "Adaptive Grid Embedding Navier-Stokes Technique for Cascade Flows," AIAA-89-0204.

Depolt, Th. and Koschel, W., 1992, "Theoretical Determination of the Characteristics of Multi-Hole Pressure Probes Using Panel Methods," Proc. 11th Symp. Measuring Techniques for Transonic and Supersonic Flow in Cascades and Turbomachines, Munich.

Dominy, R.G., 1992, "Development in Flow Tracing Using Miniature Lasers," Proc. 11th Symp. Measuring Techniques for Transonic and Supersonic Flow in Cascades and Turbomachines, Munchen, Germany.

Dominy, R.G. and Hodson, H.P., 1992, "An Investigation of the Factors Influencing the Calibration of 5-Hole Probes for 3-D Flow Measurements," ASME Paper 92-GT-216.

Elder, R.L. and Tan, J., 1990, "The Measurement of Static Pressure in Gas Turbines Using Traversable Instrumentation," Research Proposal, Cranfield University.

Ewald, B., 1980, "Smoke Tunnel Development," Int. Symp. on Flow Visualisation, Bochum.

Fawcitt, N.S.J., 1991, "Getting Started with CFD," IMechE.

Ferguson, T.B. and Al-Shamma, K.A., 1967, "Wedge Type Pitot-Static Probes," BHRA SP919, 9th Members Conference, British Hydromechanics Research Association, . Cranfield.

Ferguson, T.B. et al., 1974, "The Effect of Leading Edge Geometry on the Performance of Wedge Type Pitot-Static Yawmeters," Measurement and Control, Vol.7, No.4, Paper 5.74.

Filbee, D.R., 1990, "A Study of the Aerodynamics of the Small-Scale Contra-Whirl IGV Fan," Ph.D. Thesis, Cranfield University, Bedford.

Fransson, T., 1983, "Aerodynamic Probe Calibrations - Results from the Workshop on Probe Calibrations, 1981 - 1983," Proc. of 7th Symp. on Measuring Techniques for Transonic and Supersonic Flows in Cascades and Turbomachines, Aachen.

Frenkiel, F.N., 1948, "The Decay of Isotropic Turbulence," ASME, J.Appl.Mech., pp.311-321.

Giles, M.B. and Haimes, R., 1991, "Validation of a Numerical Method for Unsteady Flow Calculations," IGTI Conference, Cologne.

Glawe, G.E. and Krause, L.N., 1975, "Miniature Probes for Use in Gas Turbine Testing," SAE 750094.

Gould, R.W.F. et al., 1968, "Wind Tunnel Tests on Chimneys of Circular Section at High Reynolds Numbers," NPL Aero Report 1266.

Gould, R.W.F., 1971, "Pitot-Stem Blockage Corrections in Uniform and Non-Uniform Flow," C.P.No.1775, H.M.S.O., London.

Grant, H.P., 1977, "Measuring Time-Averaged Stagnation Pressure in Pulsatile Air Flow," ISA, ISBN 87664-362-4, pp.425-438.

Hall, H.G. et al., 1962, "Blunt-Nose, Inviscid Airflows with Coupled Non-equilibrium Processes," Journal of the Aerospace Sciences, vol.29, no.9, pp.1038-1051.

Hoerner, S.F., "Fluid-Dynamic Drag," Published by the author, USA.

Hollis, E.J., 1971, "An Investigation into the Effects of Plain Leading Edge Geometry Upon the Yaw Characteristics of Wedge-Type Probes," University of Sheffield BEng. Thesis.

Howard, M. et al., 1993, "Endwall Effects at Two Tip Clearances in a Multi-Stage Axial Flow Compressor with Controlled Diffusion Blading," ASME Paper 93-GT-299.

Huey, 1978, "A Yaw-Insensitive Static Pressure Probe," J. Fluid Eng., Transactions of the ASME, Vol.100, pp.229-31.

Humm, H.J., 1991, Private Communication.

Humm, H.J. et al., 1994, "On Fast-Response Probes: Part 2 - Aerodynamic Probe Design Studies," ASME Paper 94-GT-27.

Keast, F.H., 1951, "High Speed Cascade Testing Techniques," ASME Paper 51-SA-31.

Kennewell, R.J., 1988, "Examination of a Wedge Type Airflow Sensor," prepared for Royal Aircraft Establishment, September 1988.

King, 1993, "Risk Management Guidelines," Rolls-Royce Engineering Audit Department.

Kopal, Z., 1947, "Tables of Supersonic Flow Around Cones," Dept. of Electrical Engineering, Centre of Analysis, Massachusetts Institute of Technology, Cambridge, USA.

* Lewis, R.I., 1963, "Annular Cascade Wind Tunnel," The Engineer, February 1663, pp.341-344.

Loftus, P. et al., 1993, "Component Efficiency Determination Working Party - Final Report," Rolls-Royce Internal Report EIR01475.

Massey, B.S., 1988, "Mechanics of Fluids," Fifth edition, Van Nostrand Reinhold (International) Co. Ltd., London.

McCormack, P.D. and Crane, L., 1973, "Physical Fluid Dynamics," Academic Press, New York and London.

McKenzie, A., 1952, "An Investigation of Flare Dimensions for Standard and Annular Air Meters," Rolls-Royce Internal Report RCR90087.

Meldrum, M.J. and Millman, A.F.,1991, "Ten Risks in Marketing High-Technology Products," Industrial Marketing Management 20, pp.43-50.

Meyer, C.A. and Benedict, R.P., "Instrumentation for Axial Flow Compressor Research," ASME 52-SA-31.

Mishan, E.J.,1988, "Cost Benefit Analysis," 4th Edition, Unwin Wyman Press, London.

Moore, J.G., 1985, "Calculation of 3-D Flow Without Numerical Mixing," AGARD Lecture Series No.140, '3-D Computational Techniques Applied to Internal Flows in Propulsion Systems.'

Morkovin, M.V., 1964, "Flow Round Circular Cylinder - A Kaleidoscope of Challenging Fluid Phenomena," ASME Symp. on Fully Separated Flows.

Morris, R.E., 1961, "Multiple Head Instrument for Aerodynamic Measurements," The Engineer.

Mueller, T.J., 1983, "Smoke Visualisation in Wind Tunnels," Astronautics and Aeronautics, January edition.

Nakayama, Y., 1988, "Visualised Flow," Pergamon Press plc., Oxford.

Norris, K.P., 1971, "The Accuracy of Project Cost and Duration Estimates in industrial Research and Development," R. and D. Management 2, no.1.

Northall, J.D., 1993, "Introduction to the Computational Fluid Dynamics System (CFDS)," Rolls-Royce Internal Report, TSG0689.

Prandtl et al., 1934, "Applied Hydro- and Aerodynamics," McGraw Hill Book Co., Inc.

Roach, P.E., 1986, "The Generation of Nearly Isotropic Turbulence by Means of Grids," Journal of Heat and Fluid Flow, Vol.8, No.2, pp.82-92.

Robinson, C.J., 1991, "End-wall Flows and Blading Design for Axial Flow Compressors," Ph.D. Thesis, Cranfield University, Bedford.

Rolls-Royce, 1969, "The Jet Engine."

Rossow, V.J., 1991, "Probe Systems for Measuring Static Pressure and Turbulence Intensity in Fluid Streams," U.S.Patent No.5233865, 24th April 1991.

Ruffles, P., 1993, "ECOM User Manual," Rolls-Royce Internal Document issued by Engineering Systems and Methods, Bristol.

Sassone, P.G. et al.,1978, "Cost Benefit Analysis, A Handbook," Academic Press.

Schlichting, H., 1960, "Boundary Layer Theory," Fourth Edition, McGraw-Hill Book Co. Inc., New York.

Seyb,N.J.,1992,"Compressor Performance Bid Risk Assessment - A Suggested Method," Rolls-Royce Internal Report GN31027.

Shaw, R., 1960, "The Influence of Hole Dimensions on Static Pressure Measurements," J.Fluid Mech., 7, page 550.

Shreeve, R.P.,1976, "Calibration and Application of Multiple Sensor Pneumatic Probes for Velocity Determination, with Corrections for Boundary Effects," AIAA 76-373.

Smith, A.M., and Bauer, A.B., 1970, "Static Pressure Probes that are Theoretically Insensitive to Pitch, Yaw and Mach Number," J. Fluid Mech., vol.44, part 3, pp.513-528.

Smout, P.D., 1989, "The Measurement of Static Pressure in Gas Turbines Using Traversable Instrumentation," Rolls-Royce Internal Report EIR01162.

Smout, P.D., 1990, "The Problem of Static Pressure Measurement in Turbomachinery Annuli Using Traversable Instrumentation," Proc. 10th Symp. Measuring Techniques for Transonic and Supersonic Flow in Cascades and Turbomachines, VKI, Brussels.

Smout, P.D., 1991 ,"High Accuracy Interstage Measurements in Multi-Stage Turbomachines," Rolls-Royce Internal Research Brochure PVK1-61D.

Smout, P.D., 1992, "Experimental Determination of Wedge Probe Behaviour in the Near Wall Region: Brochure PVK1-61D First Year Report," Rolls-Royce Internal Report EIR01407.

Smout, P.D., 1993, "Experimental Determination of Wedge Probe Behaviour in the Near Wall Region: Brochure PVK1-61D Second Year Report," Rolls-Royce Internal Report EIR01538.

Strazisar,A.J., 1994, "The Changing Roles of Experimental and Computational Fluid Mechanics," August edition of IGTI 'Global Gas Turbine News.'

Sullivan, W.G. and Or, R.G.,1982, "Monte-Carlo Simulation Analyses Alternatives in Uncertain Economy," Industrial Engineering, vol.14 No.11, pp.43-49.

Takagi, T., 1986, "Experiments and Performance Evaluation of a Transonic Axial Flow Turbine With Variable Nozzle," ASME Paper 86-GT-214.

Thomas, H., 1973, "The Assessment of Project Worth and Applications to Research and Development," from 'Cost Benefit and Cost Effectiveness,' by J N Wolfe.

Townsend, A.A., 1976, "The Structure of Turbulent Shear Flow," Second Edition, Cambridge University Press, Cambridge.

Versprille,K.J., 1975, "Computer Aided Design Applications of the Rational B-Spline Approximation Form," Dissertation, Syracuse University.

Vlay, G.J. and Brekka, L.T.,1990, "Risk Management Integration with System Engineering and Program Management," AIAA Paper 90-3773-CP.

Walpole, R.E. and Myers, R.H., 1989, "Probability and Statistics for Engineers and Scientists," 5th edition, MacMillan Publishing Co., New York.

APPENDIX A: RISK ANALYSIS SOFTWARE

The following list of software packages is not intended to be exhaustive, but indicates the diverse range of risk analysis support programs currently available commercially. In each case, an indication of the necessary computing hardware and the name of the software publisher or supplier is included. An approximate price guide is also given, where prices were correct at the end of 1993. All information was taken from 'The Software Users Yearbook - 1993.'

CRAMM CCTA Risk Analysis and Management Method

This package provides a risk analysis and management methodology supported by documentation and training. It gives a basis for Information Technology staff without security experience to identify and justify all counter-measures to ensure security of all types of current and future IT systems and networks.

HARDWARE: IBM PC and compatibles
PUBLISHER: BIS Information Systems
PRICE: £4000 to £7500

GOALFIX PROFIT PLANNER PLUS

This management planning tool is designed to appraise the financial implications of different business strategies. Using a pre-built model which requires no programming, several analyses may be performed including sensitivity, what-if, goalseek and ratio analysis.

HARDWARE: IBM PC and Compatibles.
PUBLISHER: Goalfix Marketing Ltd.
PRICE: Not available.

INTANET Corporate Project Management System

This is a corporate project management and modelling system which addresses operational planning, performance monitoring and financial forecasting, including bid modelling and risk analysis options.

HARDWARE: UNIX based workstation platforms.
PUBLISHER: Computation Research and Development Ltd.
PRICE: £100000 to £120000

MONTE CARLO

The package is designed for analysing the risks in large-scale projects modelled in software. It evaluates the impact of high-risk elements such as inflation, the weather, and technological change. Difficult go/nogo decisions can be modelled through alternative branching. Contingency plans to mitigate uncertainty can also be developed. Schedule, resource and cost aspects of the project model are taken as input data.

HARDWARE: IBM PC and compatibles.
PUBLISHER: Forge Track (UK) Ltd.
PRICE: £4500

OPERA

This is a risk analysis extension to the 'Open Plan Project Management System.' It allows the user to modify the durations and costs of projects using a variable distribution profile. A Monte Carlo simulation is then performed to find percentage probability of milestones being achieved and costs met, as well as identifying critical activities.

HARDWARE: IBM PC and Compatibles plus most UNIX based machines.
PUBLISHER: Welcome Software Technology International.
PRICE: From £1250

PLANTRAC-MARSHAL

This risk analysis system uses Monte-Carlo simulation techniques to assess the impact on projects of risk items such as bad weather, resource limitations and late delivery of items.

HARDWARE: IBM PC and Compatibles.
PUBLISHER: Computerline Ltd.
PRICE: From £450

XASSIST

This package is intended to assist in reducing the risks associated with new business computer procurement. It aims to reduce short to long term costs, and supports policy decision making.

HARDWARE: IBM PC and Compatibles.
PUBLISHER: XIS Ltd.
PRICE: £975 to £1750

APPENDIX B: **PARTICIPANTS IN EUROPEAN SYMPOSIUM ON MEASURING TECHNIQUES FOR TRANSONIC AND SUPERSONIC FLOWS IN CASCADES AND TURBOMACHINES**

PARTICIPANT:	COUNTRY:	AREA OF INTEREST:
D.L.R.	Germany	i) Probe development for transonic compressor cascade testing
R.W.T.H. - Aachen	Germany	i) Thermal anemometry and pressure probe measurements in transonic linear cascade testing ii) Minimisation of multi-hole pressure probe blockage effects in transonic flow
University of Federal Armed Forces - Munich	Germany	i) Pressure probe developments for measurements in high speed cascades ii) Development of pressure data acquisition systems
Polytechnic of Milan	Italy	i) Investigation of influence of unsteady flow and pressure gradients on pressure probe performance
University of Cagliari	Italy	i) Measurement uncertainties associated with pressure probe calibration methodologies
E.T.H. - Zurich	Switzerland	i) Silicon pressure sensor characteristics and packaging technology for application to high response pressure probes. ii) Aerodynamic characteristics of pressure probe designs in steady and unsteady flow - experimental investigation.
Onera	France	i) Transonic pressure probe calibration facility development
Oxford University	U.K.	i) Experimental investigation of 2-D and 3-D pressure probe characteristics in steady flow ii) Experimental and numerical investigation of probe performance in unsteady flow
D.R.A. - Farnborough	U.K.	i) Thermal anemometry, pneumatic and high response pressure probe applications to fan and multi-stage compressor rigs.

APPENDIX C: TRAINING COURSES ATTENDED IN PARTIAL FULFILMENT OF TOTAL TECHNOLOGY Ph.D. SCHEME REQUIREMENTS

Technical Courses

COURSE TITLE	DATE ATTENDED	COURSE ORGANISERS
Turbomachinery Compressors and Fans	May 1992	Cranfield University
Introduction to Computational Fluid Dynamics	August 1992	Rolls-Royce
IGTI Conference - The Hague	June 1994	A.S.M.E.

Non-Technical Courses

COURSE TITLE	DATE ATTENDED	COURSE ORGANISERS
Programme Management	May 1992	Rolls-Royce (Learning Resource Centre)
Introduction to Management	October 1992	Rolls-Royce (Management Training Department)
Financial Awareness	November 1992	Rolls-Royce (Adult Training Department)
Marketing of Technological Products	March 1993	Cranfield School of Management

APPENDIX D: TOTAL TECHNOLOGY Ph.D. SUPPORT PANEL MEETINGS

Members of Support Panel

SUPPORT PANEL MEMBER	REFERENCE	ORGANISATION	ROLE ON SUPPORT PANEL
Prof. R.L.Elder	RLE	Cranfield University	Chairman
Dr. P.C.Ivey	PCI	Cranfield University	Academic Supervisor
Mr. J.Mapes	JM	Cranfield School of Management	Management Advisor
Mr. P.Loftus	PL	Rolls-Royce	Industrial Supervisor
Mr. J.Carlin	JC	Rolls-Royce	Training Advisor
Dr. J. W. H. Chivers	JWHC	Rolls-Royce	Sponsoring Manager
Mr. P. D. Smout	PDS	Rolls-Royce	Student

Support Panel Meetings

DATE	RLE	PCI	JM	PL	JC	JWHC	PDS
6.12.91	✓	✓	✓	✓		✓	✓
30.3.92	✓		✓	✓	✓		✓
6.7.92	✓	✓		✓			✓
20.10.92	✓	✓		✓			✓
9.12.91	✓	✓	✓	✓			✓
15.3.93	✓	✓		✓		✓	✓
7.6.93		✓	✓	✓			✓
11.10.93	✓	✓	✓	✓		✓	✓
20.12.93	✓	✓		✓			✓
21.3.94	✓	✓		✓			✓
6.6.94	✓	✓	✓	✓			✓
3.10.94	✓			✓			✓

APPENDIX E: PROBE CALIBRATION COEFFICIENTS AND UNCERTAINTY ANALYSIS

Definition of Coefficients

Total Pressure Coefficient;

$$C_t = \frac{(P1 - p_t)}{(p_t - p_s)}$$

Static Pressure Coefficient;

$$B = \frac{Sm - p_s}{(p_t - p_s)}$$

Yaw Angle Coefficient;

$$C_{yaw} = \frac{(S2 - S3)}{(p_t - p_s)}$$

Yaw Angle Sensitivity;

$$S_{yaw} = \frac{C_{yaw}}{\beta}$$

where: P1 = probe indicated total pressure

ps = tunnel reference static pressure

pt = tunnel reference total pressure

S2 = probe indicated static pressure (Left hand tapping)

S3 = probe indicated static pressure (Right hand tapping)

Sm = $\frac{(S2 + S3)}{2}$

α = Probe yaw angle

Uncertainty Analysis

The instrumentation arrangement for the actual probe tests reported in chapter 5 is shown schematically in figure E.1. Various transducers were selected for sensing the probe and wind tunnel reference pressures, in order to match the range of each instrument to the measured pressure as closely as possible. The instruments used for each measurement parameter are summarised in table E.1 with associated ranges and uncertainty limits quoted by the instrument manufacturer.

The absolute uncertainty, X, in each calibration coefficient was taken to be the root sum square of the partial derivatives of the coefficient with respect to each dependent variable, in accordance with the industry standard uncertainty analysis technique proposed originally by Abernethy, (1973). This gave the following expressions for the uncertainty in each coefficient, where uncertainties are expressed as absolute values:

$$X_{C_t} = \sqrt{(dC_t)^2_{p_t} + (dC_t)^2_{p_s} + (dC_t)^2_{P1}}$$

where:

$$(\delta C_t)_{P1} = \frac{\delta p_t}{(p_t - p_s)}$$

$$(\delta C_t)_{p_s} = \delta p_s \left\{ \frac{P1 - p_t}{(p_t - p_s)^2} \right\}$$

$$(\delta C_t)_{p_t} = -\delta P1 \left\{ \frac{P1 - p_s}{(p_t - p_s)^2} \right\}$$

$$X_B = \sqrt{(\delta B)_{p_t}^2 + (\delta B)_{p_s}^2 + (\delta B)_{Sm}^2}$$

where:

$$(\delta B)_{p_t} = -\delta p_t \left\{ \frac{Sm - p_s}{(p_t - p_s)^2} \right\}$$

$$(\delta B)_{p_s} = \delta p_s \left\{ \frac{Sm - p_t}{(p_t - p_s)^2} \right\}$$

$$(\delta B)_{Sm} = \frac{\delta p_{Sm}}{(p_t - p_s)}$$

$$X_{C_{yaw}} = \sqrt{(\delta C_{yaw})_{p_t}^2 + (\delta C_{yaw})_{p_s}^2 + (\delta C_{yaw})_{(S2-S3)}^2}$$

where:

$$(\delta C_{yaw})_{p_t} = -\delta p_t \left\{ \frac{S2 - S3}{(p_t - p_s)^2} \right\}$$

$$(\delta C_{yaw})_{p_s} = \delta p_s \left\{ \frac{S2 - S3}{(p_t - p_s)^2} \right\}$$

$$(\delta C_{yaw})_{(S2-S3)} = \frac{\delta(S2 - S3)}{(p_t - p_s)}$$

The following error sources were considered in calculating the total uncertainty, δp_x, in each pressure, p_x.

i) *Transducer uncertainty* - assumed to be a precision (random) error. These are summarised in table E.1 for each type of transducer

ii) *Error due to turbulent flow* - a bias error of less than 0.07% dynamic head at 0.35 Mach number. Because all the pressure coefficients defined above are expressed as pressure differences, this error source was ignored.

iii) *Static tapping related errors*, including damaged or dirty tappings, and minor imperfections in the solid wall upstream or downstream of the tapping. All the wind tunnel and probe static pressure tappings were regularly cleaned and inspected, such that these error sources could be neglected.

iv) *Static tapping diameter* - a bias error of upto 0.3% dynamic head at 0.75 Mach number was to be expected for the 0.5mm diameter tappings in the wind tunnel, (Shaw, 1960). This error cancelled where the difference between two static pressure tappings was taken, and was allowed for when static pressures were used in isolation.

v) *Pitot tube total pressure recovery* - the reference pitot tube was mechanically aligned with the rig axis. The laser anemometry traversing demonstrated axial flow to within ±2° yaw, over which range the pitot tube was expected to be insensitive to yaw angle.

Overall, the only significant remaining error was that introduced by the transducers, and the δp_x values in each case were simply taken to be the uncertainty values associated with each instrument. Error bars of length equal to the overall uncertainty in each pressure coefficient were calculated, and drawn through experimental data points as appropriate.

EXPERIMENT	THESIS SECTION	MACH NO	PARAMETER	INSTRUMENT	UNCERTAINTY
Factoral Experiment	5.2)	0 TO 0.5	Pl)	DRUCK DPI 140	
	)		Pr)	(80 to 115 kPa	± 15.0 Pa
	)		Ps)	Range)	
	)		S2)		
Compressor Tranversing	5.3)		(S2 - S3)	FC014 Micro-Manometer	± 2.50 Pa (0.2 kPa range) ± 25.0 Pa (2.0 kPa range) ± 250 Pa (20 kPa range)
	)	>0.5	P1)	As above	As above
	)		Pt)		
	)		(S2 - S3))		
	)				
Open Jet/Closed Tunnel Comparison	5.4)		Ps)	DRUCK DPI 140	± 0.02% reading
	)		S2)	(3.5 to 115 kPa	± 0.01% full scale
	)			range)	
Large Scale Wedge Probe	6.3	All	All	DPI 140 (80 to 115 kPa range) + 30° Inclined Water Manometer	± 15.0 Pa + ± 2.5 Pa

TABLE E.1 SUMMARY OF PRESSURE INSTRUMENT UNCERTAINTIES

APPENDIX F: WIND TUNNEL SPECIFICATION FOR LOW SPEED FLOW VISUALISATION

1. Working Section Arrangement

   1.1 Horizontally arranged working section
   1.2 Square or rectangular cross-section
   1.3 Optimum size: Height, h = 1.0 meter
   Width, w = 1.0 meter
   Minimum size: h = 0.5 meter
   w = 0.5 meter
   1.4 Openings in the top and rear tunnel walls required through which to traverse the probe model. Probe model to be constructed with a probe stem diameter, d, where d = (h/16).
   1.5 Both top and rear tunnel walls should be illuminated from the front and from beneath.
   1.6 Perforated top and rear tunnel walls for boundary layer control would be desirable but not essential.

2. Flow Conditions at Working Section

   2.1 The Reynolds number achievable at the working section must be variable over a minimum range of $0.2x10^4<Re<5x10^4$, where Reynolds number is based on the probe stem diameter, d.
   2.2 The free stream velocity required to achieve the above Reynolds number range must be sufficiently low to permit smoke flow visualisation, (i.e. less than 15m/s).

3. Upstream Flow Conditions

   3.1 The upstream flow conditioning must be such that smoke filaments injected into the flow upstream of the contraction do not undergo laminar to turbulent transition before reaching the probe model. This implies:
      a) a large upstream contraction in the horizontal plane,
      b) an upstream settling chamber, and
      c) upstream damping screens.
   3.2 A multi-element smoke rake should be mounted vertically in the contraction. Ideally this should be traversable laterally.

4. Other Requirements

   4.1 A suitable smoke generator will be required
   4.2 Suitable instrumentation for measuring the free stream air velocity will also be required.

APPENDIX G: GOVERNING FLOW EQUATIONS USED IN CFD CODE MEFP

In general, steady Reynolds averaged conservation equations are used in a coordinate system rotating at speed Ω. For the applications discussed in chapter 7, a stationary frame of reference was required, and Ω was set to zero to give the following:

Mass Conservation:

$$\nabla.\rho u = 0$$

Momentum Conservation:

$$\rho u.\nabla u - \nabla\mu_{eff}\nabla u = \nabla\mu_{eff}(\nabla u)^T - \nabla p$$

Energy Conservation:

$$\rho u.\nabla I - \nabla.\left\{\frac{\mu_l}{Pr_l} + \frac{\mu_T}{Pr_T}\right\}\nabla I = 0$$

$$I = C_p T_s + \frac{1}{2}u^2$$

In applications (such as this) where heat transfer calculations are not required, then it is assumed that the product $C_p T_s$ is constant.

Equation of State:

$$p = \rho R T_s$$

Nomenclature:

C_p	=	Specific heat at constant pressure
I	=	total internal energy
p	=	static pressure
Pr	=	Prandtl number
R	=	gas constant
T	=	temperature
$\underline{u}$	=	velocity vector ($u\underline{i} + u\underline{j} + u\underline{k}$)
ρ	=	density
μ	=	viscosity

Subscripts:

eff:	effective
l:	laminar
s:	static
T:	turbulent

ITEM	ADDITIONAL COST PER TEST (£)
1. ADDITIONAL 50 HOURS TECHNICAL SUPPORT TIME	1615
2. ADDITIONAL 4 HOURS RIG RUNNING TIME:	2647
3. ADDITIONAL POST TEST ANALYSIS TIME:	1000
4. PROVISION OF LASER WINDOW:	2000 (One off cost)
5. LASER EQUIPMENT CAPITAL DEPRECIATION	1500
TOTAL:	6762

Table 2.1: Summary of Additional Costs Involved in Adopting Laser Anemometry Approach to Static Pressure Determination

TEST FACILITY	MOTIVE POWER	AVERAGE UNIT FUEL COST	AVERAGE HOURLY FUEL USE	AVERAGE HOURLY MAN COST	NO OF MEN PER TEST	TOTAL HOURLY RATE
COMPRESSOR TEST RIG NO.6	INDUSTRIAL AVON GAS TURBINE	£0.13 PER LITRE	2640 LITRES	£79.61 PER MAN	4	£662
COMPRESSOR TEST RIG NO.3	ELECTRIC MOTOR	£69.10 PER MW	4.8 MW	£79.61 PER MAN	4	£650
TURBINE TEST RIG NO.4	ELECTRIC MOTOR	£69.10 PER MW	5.5 MW	£79.61 PER MAN	4	£698
LP TURBINE TEST RIG	ELECTRIC MOTOR	£69.10 PER MW	32.0 MW	£79.61 PER MAN	10	£3000

Table 2.2: Hourly Rates for Testing on Rolls-Royce Derby Facilities Averaged Over 1993

PROJECT BUDGET		MAN POWER RESOURCE	
RANGES: (£1000'S)	**'B' VALUE:**	**RANGES: (HOURS)**	**'R' VALUE**
0 TO 0.4	1	0 TO 40	1
0.4 TO 1.0	2	40 TO 100	2
1.0 TO 4.0	3	100 TO 400	3
4.0 TO 10	4	400 TO 1000	4
10 TO 40	5	1000 TO 4000	5

Table 2.3: Criteria for Assessing Appropriate Level of Risk Assessment

ITEM	RISK	LIKLIHOOD	CONSEQUENCES			TOTAL RISK SCORE:	OVERALL RATINGS (L/M/H)
			TIME:	COST:	SPEC:		
TECHNICAL							
1	Steady code to model unsteady flow	3 H	3 H 9	3 H 9	3 H 9	27	H
2	3-D geometry griding	2 M	3 H 6	1 L 2	2 M 4	12	M
PEOPLE							
3	No prior experience	3 H	3 H 9	2 M 6	1 L 3	18	M
4	Reliant on TSG support	3 H	1 L 3	1 L 3	1 L 3	9	L
EQUIPMENT							
5	Terminal access	1 L	2 M 2	1 L 1	1 L 1	4	L
6	Printer quality	2 M	1 L 2	1 L 2	2 M 4	8	L
PROCEDURAL							
7	Dept CPU time allocation	3 H	1 L 3	2 M 6	1 L 3	12	M
8	Interuptions from other work	2 M	3 H 6	1 L 2	2 M 4	12	M
PROGRAMME							
	None						
	SUM OF RISK SCORES BY COLUMN		40	31	31		
	SUMS AS FRACTION OF TOTAL (%)		39.2	30.4	30.4		

Table 2.4: CFD Numerical Modelling

Likelihood Definitions:

LOW: < 10% Probability

MEDIUM: 10% < Probability < 33%

HIGH: > 33% Probability

Consequence Definitions:

	TIME:	COST:	SPEC:
LOW:	< 1 ADDITIONAL DAY	< 1% OVER BUDGET	INSIGNIFICANT CHANGE
MEDIUM:	1 DAY ➲ 1 WEEK EXTRA	1% ➲ 5% OVER	SMALL NON-RECOVERABLE CHANGE
HIGH:	> 1 ADDITIONAL WEEK	5% OVER BUDGET	MANY NON-RECOVERABLE CHANGES

Table 2.5: Likelihood/Consequences Grid Criteria

STAGE	MEAN (DAYS)	S.D (DAYS)
TRAINING COURSES	5	0
TRAINING EXERCISES	24	4
MODELLING OF 2-D CYLINDERS:	15	3
MODELLING OF 2-D WEDGES:	19	4
MODELLING OF 3-D PROBES:	23	5
TOTALS:	86	8.12

Table 2.6a): Time Estimates for Each Stage of CFD Numerical Modelling

WORK PACKAGE (WP) IMPLEMENTATION STAGE (IS)	MEAN (DAYS)	S.D (DAYS)
WP1: CFD NUMERICAL MODELLING	86	8.12
WP2: 3-D FLOW VISUALISATION	6.6	0.43
WP3: HIGH SPEED PROBE CALIBRATIONS	19.5	1.48
WP4: OPEN JET CALIBRATIONS	43.0	4.92
WP5: 4-STAGE RIG PROBE TRAVERSES	2.5	0.31
IS1: PROBE DESIGN	17	1.25
IS2: PROBE MANUFACTURE & EVALUATION	10.5	1.10
IS3: DOCUMENTATION	100	7.07

Table 2.6b): Summary of Timescale Estimates for All Work Packages

RESEARCH AIMS	CONTRIBUTING WORK PACKAGES	MEAN: (DAYS)	S.D (DAYS)	ALLOCATION (DAYS)	PROBABILITY (%)
1. NEAR WALL STATIC PRESSURE MEASUREMENT	1,2,3 and 5	114.6	8.27	130	96.9
2. NEAR WALL ANGLE MEASUREMENT	1 and 3	105.5	8.25	120	96.1
3. CALIBRATION DISCREPANCIES	1, 3 and 4	148.5	9.61	165	95.7
IMPLEMENTATION STEPS					
1. PROBE DESIGN	-	17	1.25	20	99.2
2. PROBE MANUFACTURE & EVALUATION	-	10.5	1.10	20	100.0
3. DOCUMENTATION	-	100	7.07	130	100.0

Table 2.6c): Summary of Probabilities of Achieving Originally Allocated Timescales

DATE	A.P.	ITEM	INTERNAL SPEND (£k)	EXTERNAL SPEND (k)
Feb.'92	2	Research probe manufacture	5.8	
Feb.'92	2	Low speed testing in suction tunnel		1.0
May'92	5	Pitot tube manufacture	1.0	
June'92	7	High speed testing in suction tunnel		0.5
July'92	8	Modifications to suction tunnel		1.0
Sep.'92	10	2-D flow visualisation		0.8
Jan.'93	1	Large scale probe manufacture	2.4	
Feb.'93	2	Sheffield wind tunnel modifications	0.6	
Feb.'93	2	Hire of Sheffield wind tunnel		0.3
Feb.'93	2	Manufacture of smoke rake		1.5
May'93	5	Sheffield wind tunnel modifications	0.3	
May'93	5	Modifications to suction tunnel		1.0
July'93	8	High speed testing in suction tunnel		1.0
Aug.'93	9	Construction of open jet 1 facility	0.4	
Sep.'93	10	Hire of Sheffield wind tunnel		0.3
Nov.'93	12	High speed testing in suction tunnel		0.5
Nov.'93	12	4-stage compressor rig testing		1.0
Jan.'94	1	Smoke generator parts		0.2
Feb.'94	2	Probe calibrations on No.5 rig	7.9	
May'94	5	Prototype probe manufacture		1.0
June'94	7	Prototype probe evaluation		1.0
		TOTALS:	18.4	11.1
		OVERALL TOTAL:	29.5	

TABLE 3.1: Itemised Project Spend

TEST NUMBER	WEDGE ANGLE	LENGTH 'l'	MACH NUMBER	TURBULENCE	YAW ANGLE	PITCH ANGLE	FILLET
1	√	√	X	√	√	√	X
2	X	√	√	√	X	√	√

KEY:

Variable Tested: √
Variable Not Tested: X

TABLE 5.1: Variables Used in Tests 1 and 2

TEST NO	PROBE WEDGE ANGLE	TURBULENCE		MACH NUMBER		FILLET		PITCH ANGLE		INTERFACE		PROBE IDENT
		0.8%	4.5%	0.35	0.75	NO	YES	0 deg	-10 deg	SHORT	LONG	
1	24 deg	✔		✔		✔		✔		✔		24SS
2		✔		✔		✔		✔			✔	24LS
3		✔		✔		✔			✔	✔		24SS
4		✔		✔		✔			✔		✔	24LS
5		✔		✔			✔	✔		✔		24SF
6		✔		✔			✔	✔			✔	24LF
7		✔		✔			✔		✔	✔		24SF
8		✔		✔			✔		✔		✔	24LF
9		✔			✔	✔		✔		✔		24SS
10		✔			✔	✔		✔			✔	24LS
11		✔			✔	✔			✔	✔		24SS
12		✔			✔	✔			✔		✔	24LS
13		✔			✔		✔	✔		✔		24SF
14		✔			✔		✔	✔			✔	24LF
15		✔			✔		✔		✔	✔		24SF
16		✔			✔		✔		✔		✔	24LF
17			✔	✔		✔		✔		✔		24SS
18			✔	✔		✔		✔			✔	24LS
19			✔	✔		✔			✔	✔		24SS
20			✔	✔		✔			✔		✔	24LS
21			✔	✔			✔	✔		✔		24SF
22			✔	✔			✔	✔			✔	24LF
23			✔	✔			✔		✔	✔		24SF
24			✔	✔			✔		✔		✔	24LF

TABLE 5.2: Factorial Experiment Design - Summary of High and Low Value Combinations

VARIABLE(S)		AREA	IMMER'N	DEVIATION
EFFECT	Length (L)	1% (-ve)	5% (-ve)	1% (-ve)
	Pitch (P)			1% (+ve)
	Fillet (F)		5% (+ve)	
	Mach No.(M)	1% (+ve)	1% (+ve)	1% (+ve)
INTERACTION	(L+P)			10% (-ve)
	(L+F)			
	(P+F)	10% (-ve)		
	(L+M)			
	(P+M)			5% (+ve)
	(F+M)			

TABLE 5.3: Summary of Significance Levels for Test 2, Sub-Set 1 Variables

VARIABLE(S)		AREA	IMMER'N	DEVIATION
EFFECT	Length (L)	1% (-ve)		1% (-ve)
	Pitch (P)			5% (+ve)
	Fillet (F)	5% (+ve)		5% (+ve)
	Turbulence (T)		5% (-ve)	
INTERACTION	(L+P)			
	(L+F)	5% (-ve)		10% (-ve)
	(P+F)			
	(L+T)			
	(P+T)			
	(F+T)			

TABLE 5.4: Summary of Significance Levels for Test 2, Sub-Set 2 Variables

WEDGE MODEL	5.2×10^4 REYNOLDS No.	9.5×10^4 REYNOLDS No.	12.2×10^4 REYNOLDS No.
24°, Sharp Nose	0° to 44° Yaw	0° to 44° Yaw	0° to 44° Yaw
24°, Round nose	0° to 44° Yaw	0° to 44° Yaw	x
24°, Blunt nose	0° to 44° Yaw	0° to 44° Yaw	x
60°, Sharp nose	0° to 44° Yaw	0° to 44° Yaw	0° to 44° Yaw
60°, Round nose	0° to 44° Yaw	0° to 44° Yaw	x
60°, Blunt nose	0° to 44° Yaw	0° to 44° Yaw	x

TABLE 6.1: Summary of Two-Dimensional Flow Visualisation Test Results

LOCATION	WORKING SECTION DIMENSIONS	CONTRACTION INTO WORKING SECTION	VELOCITY RANGE (m/s)	BOUNDARY LAYER CONTROL	VIEWING WINDOWS	FLOW VISUALISATION EQUIPMENT	COST PER DAY (£)
D.R.A. Farnborough	1.22 x 0.91m	30:1	6 to 25	None	2 sides and bottom	Traversable single point smoke wand	750
Sheffield University	0.30 x 0.30m	9:1	5 to 23	None	2 sides and bottom	Smoke rake and helium bubble equipment	50
Sheffield University	0.61 x 0.61m	18:1	3 to 35	None	2 sides only	None fitted	50
Cranfield University	2.50 x 2.50m	6:1	5 to 25	Variable Suction	2 sides, top and bottom	Smoke rake and helium bubble equipment	600
Rolls-Royce Hucknall	0.76 x 0.76m	9:1	5 to 25	None	Circular windows - 2 sides only	Smoke rake but no generator	742

TABLE 6.2: Flow Visualisation Wind Tunnel Summary Table

FREE STREAM VELOCITY (m/s)	BOUNDARY LAYER THICKNESS CALCULATED FROM EQUATION (5.1) (mm)	BOUNDARY LAYER THICKNESS MEASURED AT TRAVERSE PLANE (mm)
5.0	21.9	23.0
11.3	18.6	20.0
15.2	17.5	18.0
24.0	16.0	15.5

TABLE 6.3: Comparison Between Predicted and Measured Boundary Layer Thicknesses at Traverse Plane of Sheffield University Wind Tunnel

VELOCITY (m/s)	REYNOLDS No.	FILLET ?	CAL'N for YAW ANGLE	CAL'N for IMMERSION	FLOW VIS'N?
10	$3.3x10^4$	x	✓	✓	✓
15	$5.0x10^4$	x	✓	✓	✓
15	$5.0x10^4$	✓	✓	✓	✓
25	$8.3x10^4$	x	✓	✓	x
25	$8.3x10^4$	✓	✓	✓	x

TABLE 6.4a): Original Test Schedule for Large Scale Probe Tests

VELOCITY (m/s)	REYNOLDS No.	FILLET ?	CAL'N for YAW ANGLE	CAL'N for IMMERSION	FLOW VIS'N?
5	$1.7x10^4$	x	x	✓	✓
25	$8.3x10^4$	x	✓	✓	x
25	$8.3x10^4$	✓	✓	✓	x
34	$11.3x10^4$	x	x	✓	x
34	$11.3x10^4$	✓	x	✓	x

TABLE 6.4b): Modified Test Schedule for Large Scale Probe Tests

VORTEX DESCRIPTIVE PARAMETER	COUTANCEAU AND BOUARD EXPT. DATA	MEFP CFD: STRUCTURED MESH	MEFP CFD: EMBEDDED MESH
L/D	1.9	2	2.1
a/D	0.7	0.8	0.7
b/D	0.55	0.54	0.58
a/L	0.36	0.4	0.31
Theta	53°	59°	54°

TABLE 7.1: Comparison Between Experimental and Calculated Flow Around a Two-Dimensional Cylinder at a Reynolds Number of 40

PROBE	MACH No.	C_{DW} at 15mm	C_{DW} at 30mm	C_{DW} at 50mm	C_{DC} at 15mm	C_{DC} at 30mm	C_{DC} at 50mm	F	k
24LS	0.35	-0.56	-	-	-	-0.06	-0.04	-0.86	+0.39
24LS	0.75	-0.45	-	-	-	-0.06	-0.04	-0.70	+0.39
24SS	0.35	-0.48	-0.50	-	-0.08	-0.08	-	-0.38	+0.40
24SS	0.75	-0.35	-0.40	-0.40	-0.13	-0.05	-0.08	-0.60	+0.40

TABLE 8.1: Sensitivity Coefficient Values for C_{DW}, C_{DC}, F and k at Several Immersions

PROBE	REQUIRED IMMERSION (mm)	ACTUAL IMMERSION IN JET 1 (mm)	ACTUAL IMMERSION IN JET 2 (mm)
24SF	37	28	54
24LF	51	28	54

TABLE 8.2: Comparison Between Actual Probe Immersions and Immersions Required to Fully Immerse Probe Wake Flow Structures

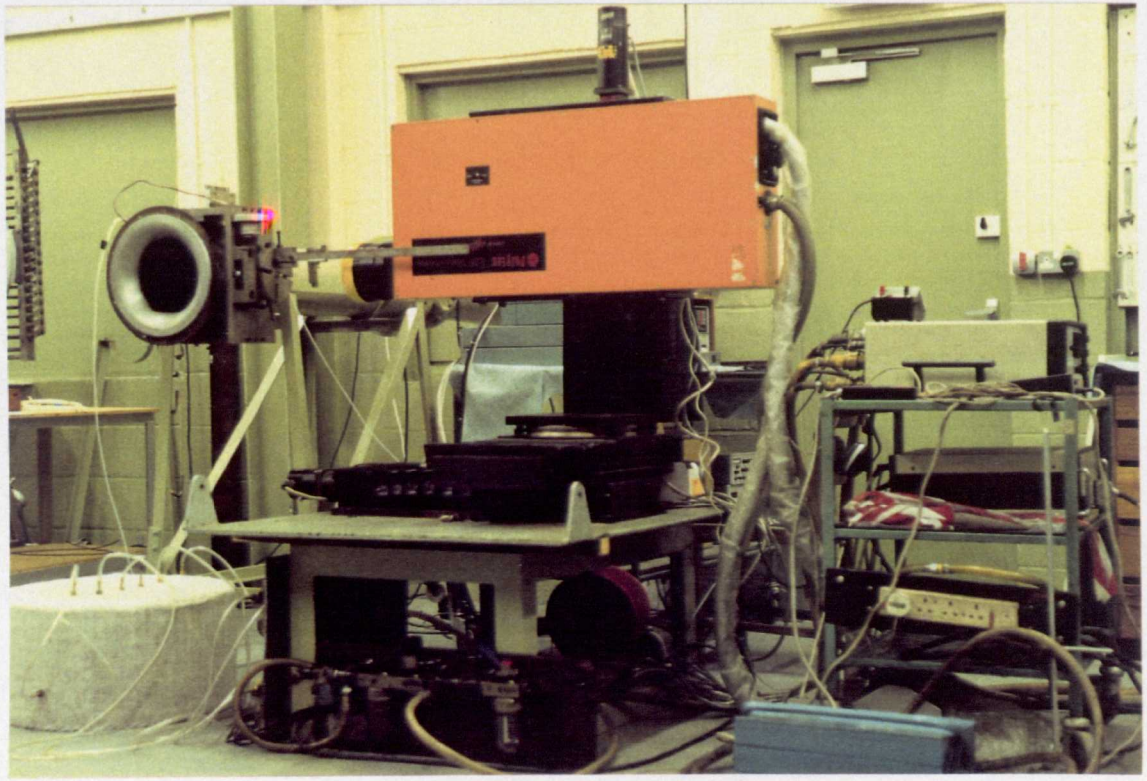

PLATE 5.1: Cranfield University Suction Wind Tunnel (With Inlet Filter Removed and Showing Laser Anemometer)

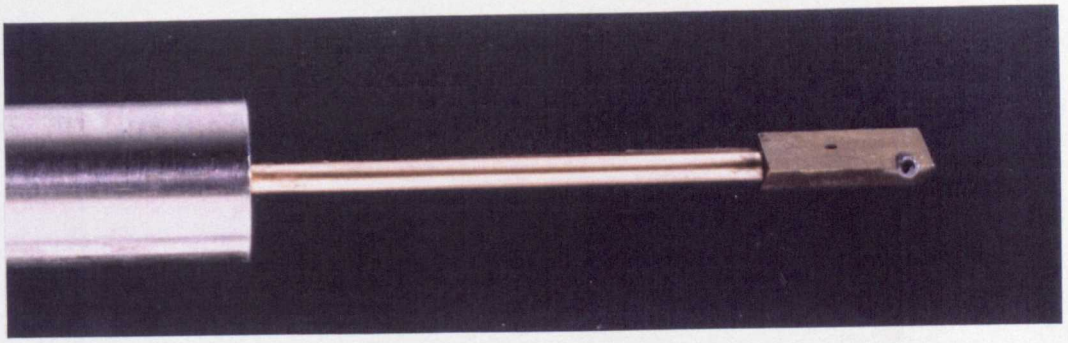

PLATE 5.2a): 24° Wedge Probe with Long Interface Piece - Probe 24LS

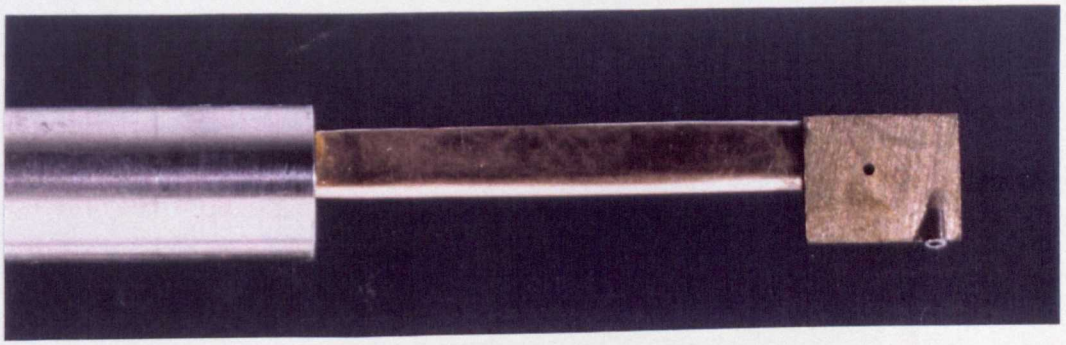

PLATE 5.2b): 24° Wedge Probe with Long Interface Piece - Probe 24LS

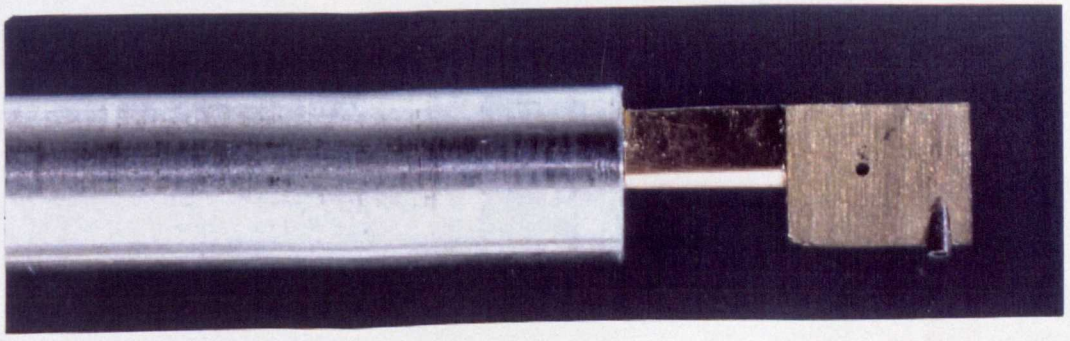

PLATE 5.2c): 24° Wedge Probe with Short Interface Piece - Probe 24SS

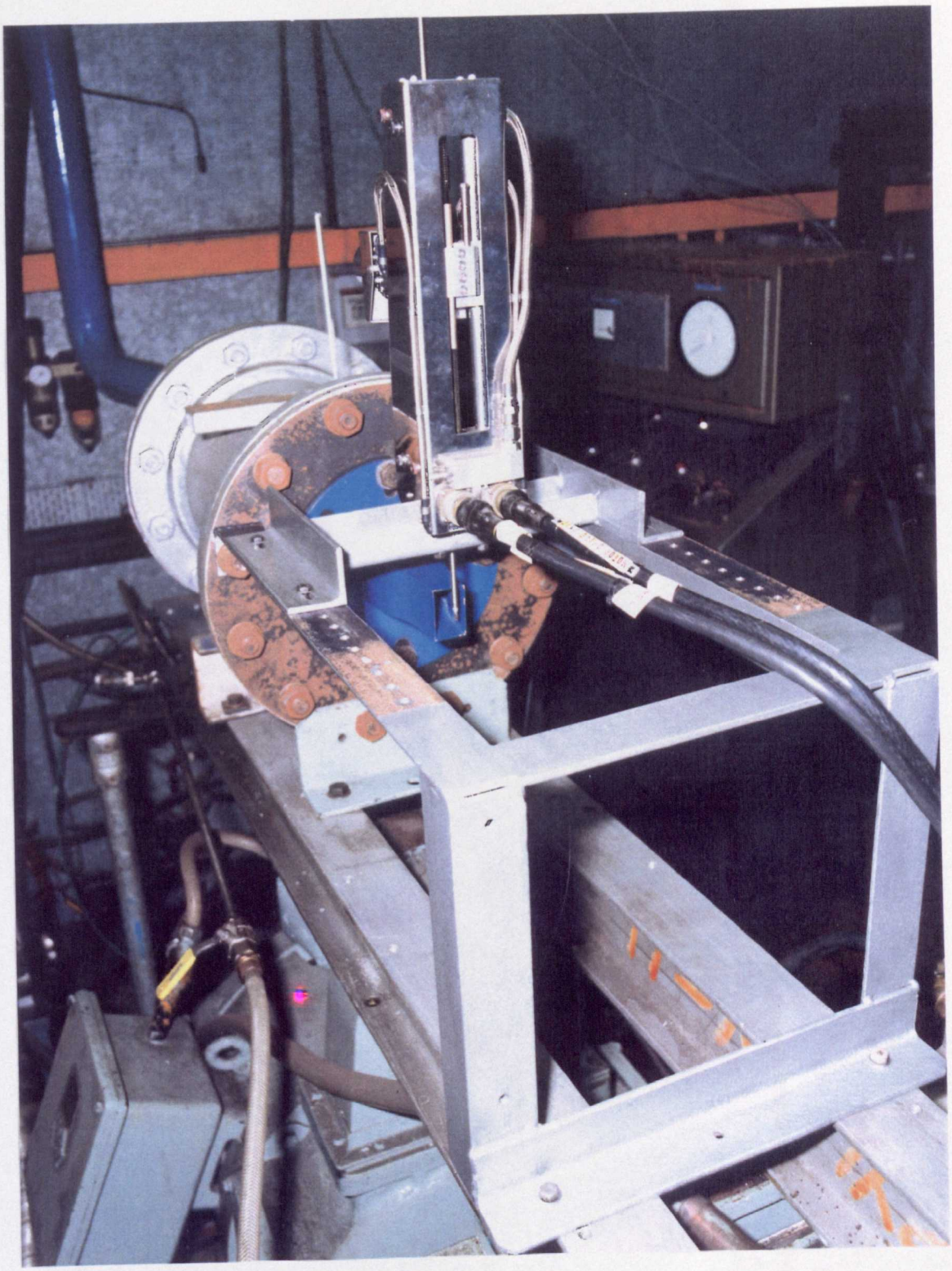

PLATE 5.3: 'Jet 1' Open Jet Probe Calibration Facility, Showing Probe Traverse Gear and Rectangular Nozzle

Neg No: 93.1623.4

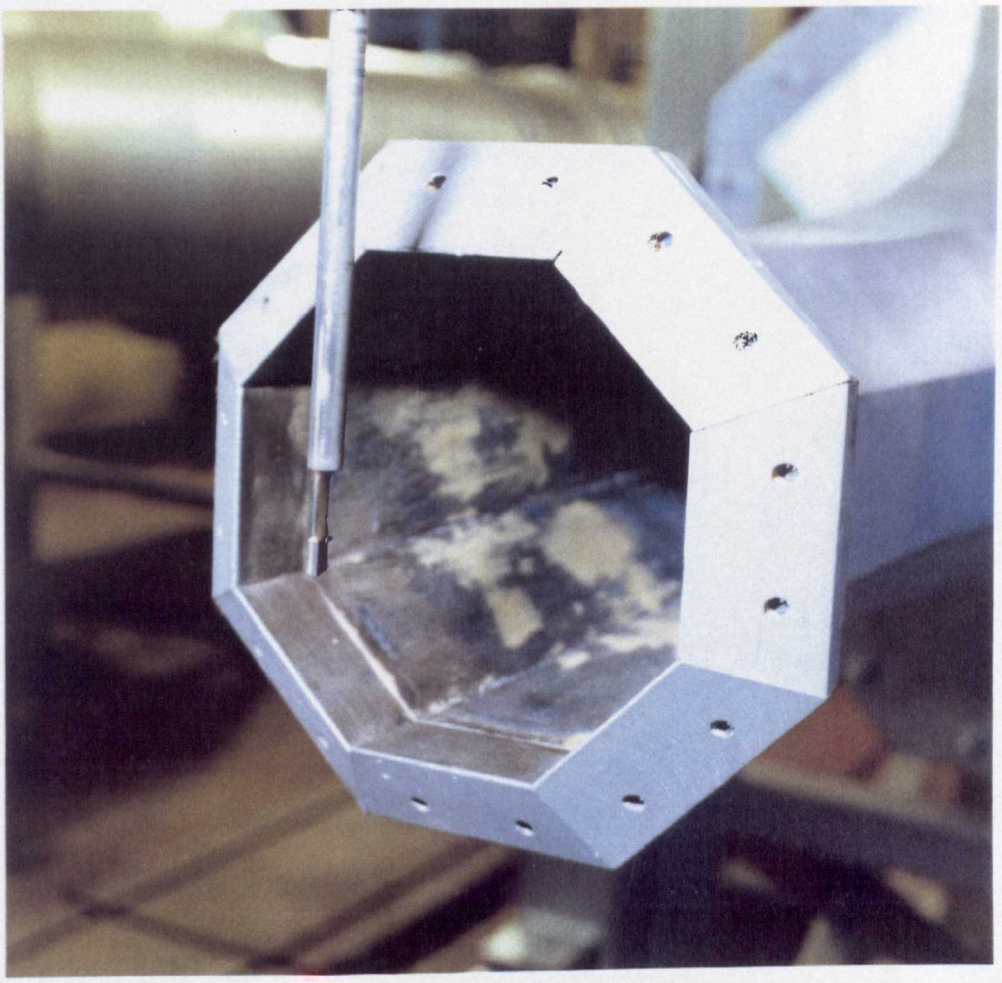

PLATE 5.4: Octagonal Nozzle of 'Jet 2' Open Jet Probe Calibration Facility

Neg No: 88.2491.7

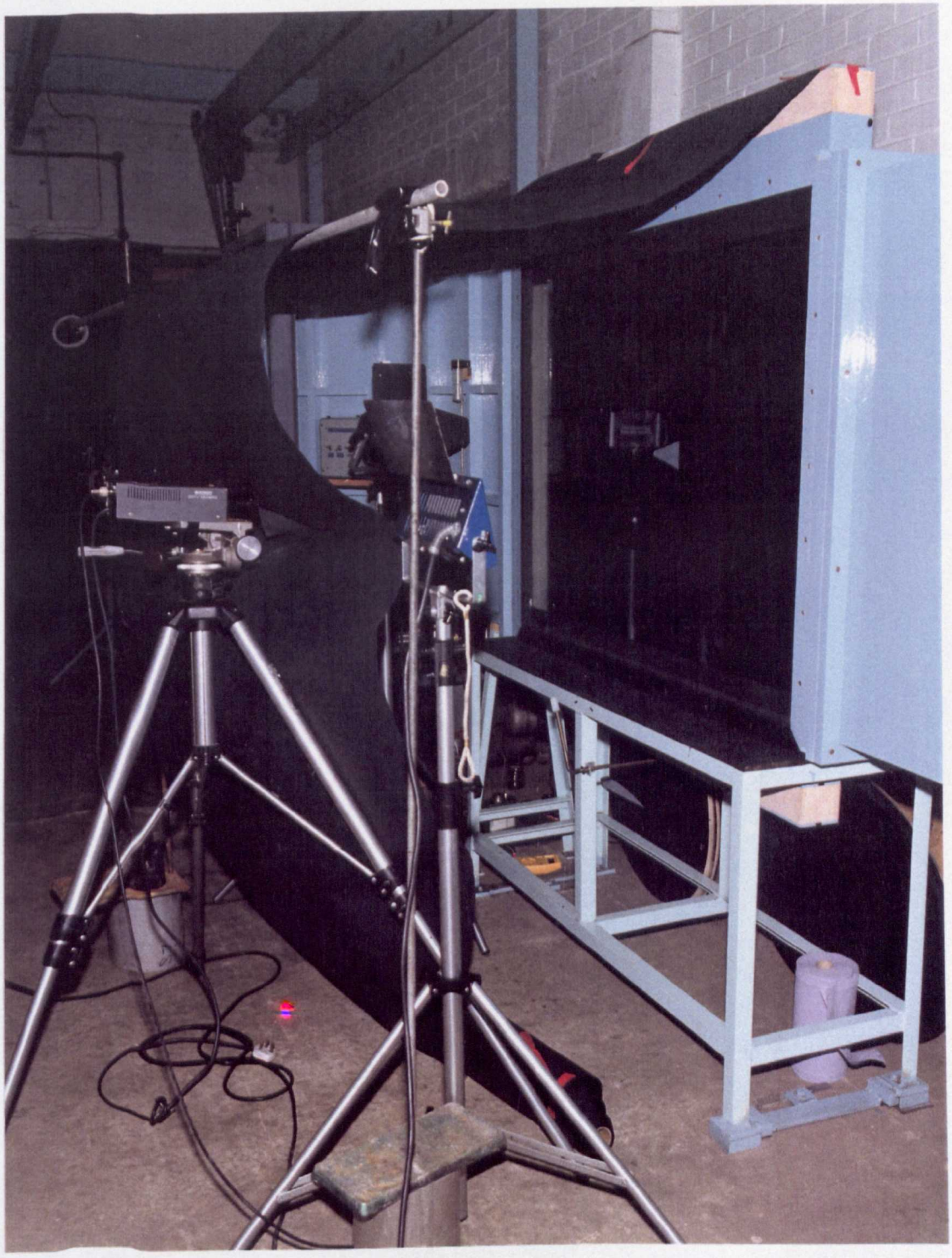

PLATE 6.1: Cranfield University 2-D Flow Visualisation Wind Tunnel, Showing Video Camera and Lighting Arrangement

Neg No: 92.1346.1

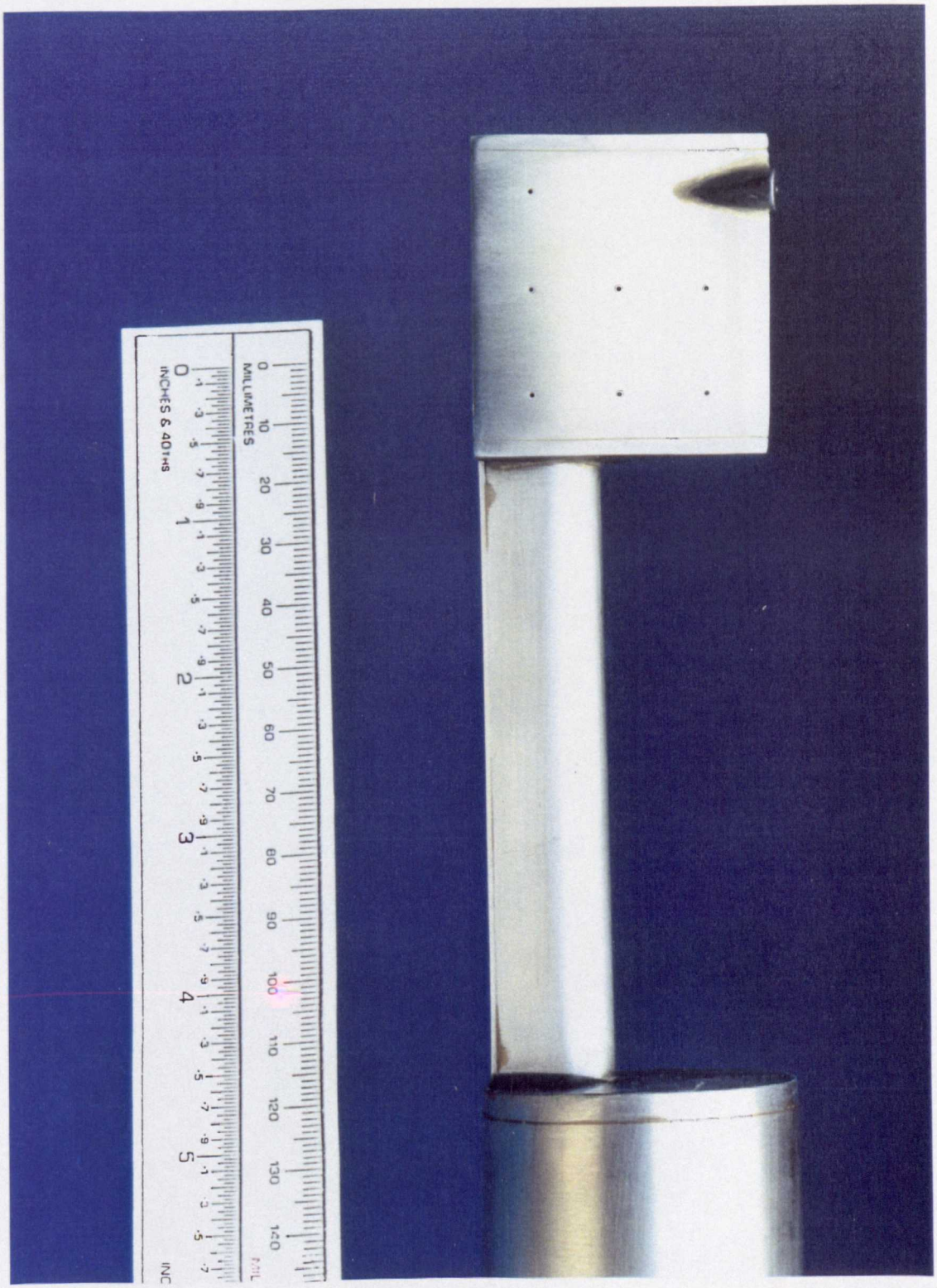

PLATE 6.2a): Side View of Large Scale Probe Showing Wedge Face Static Pressure Tappings

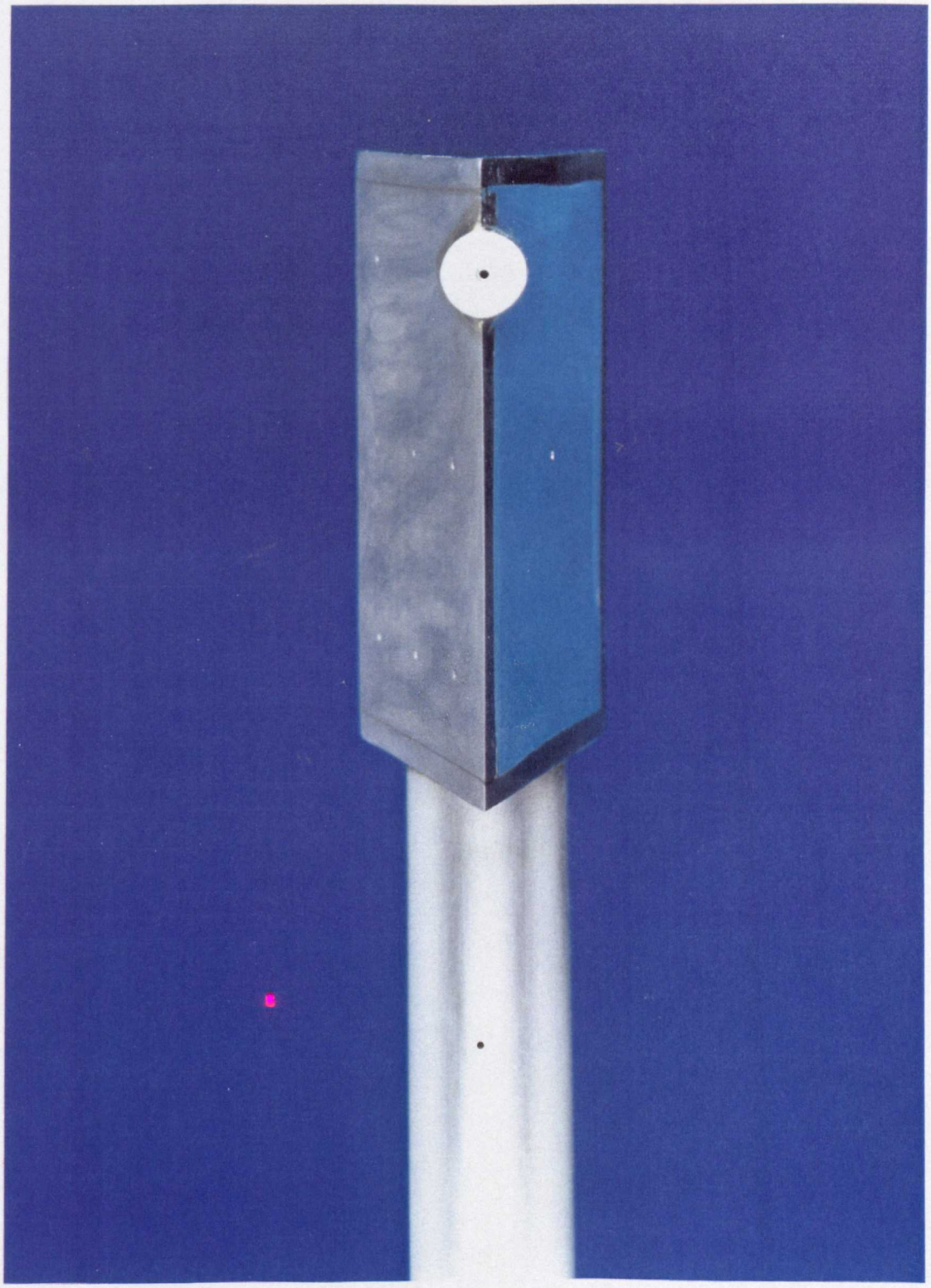

PLATE 6.2b): View on Leading Edge of Large Scale Probe Showing Wedge Head and Interface Piece Static Pressure Tappings

PLATE 6.3: Sheffield University 3-D Flow Visualisation Wind Tunnel with Large Scale Probe Installed, Showing Video Camera and Lighting Arrangement

Neg No: 93.1401.7

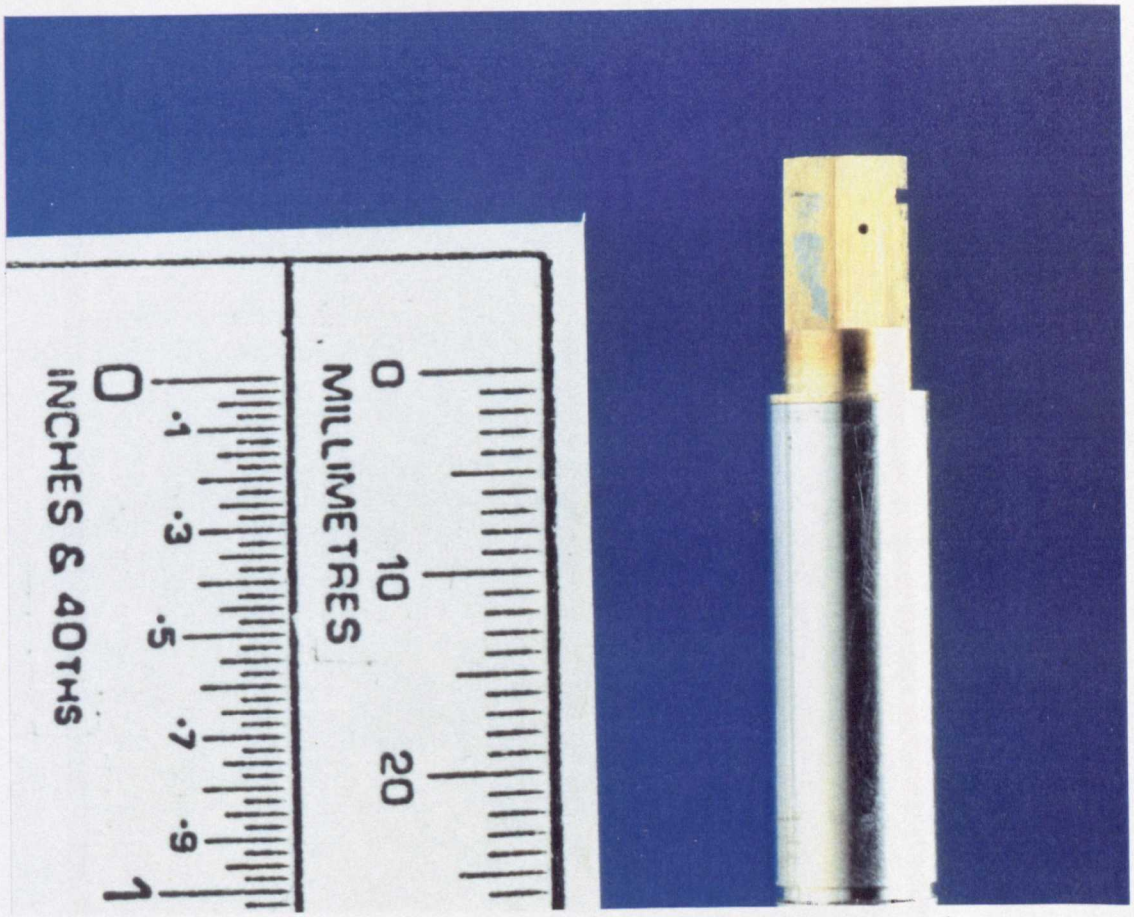

PLATE 8.1a): Re-Designed Wedge Probe Partially Retracted into Guide Tube

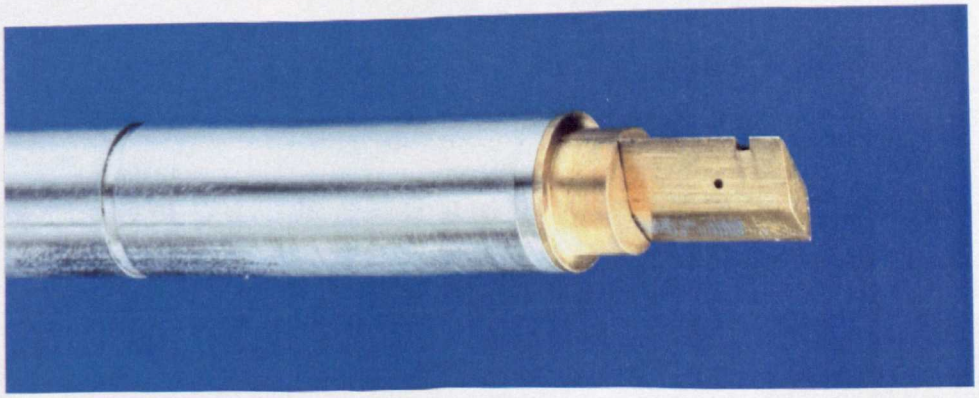

PLATE 8.1b): View of Re-Designed Wedge Probe Showing Probe Blade and Stepped End of Guide Tube

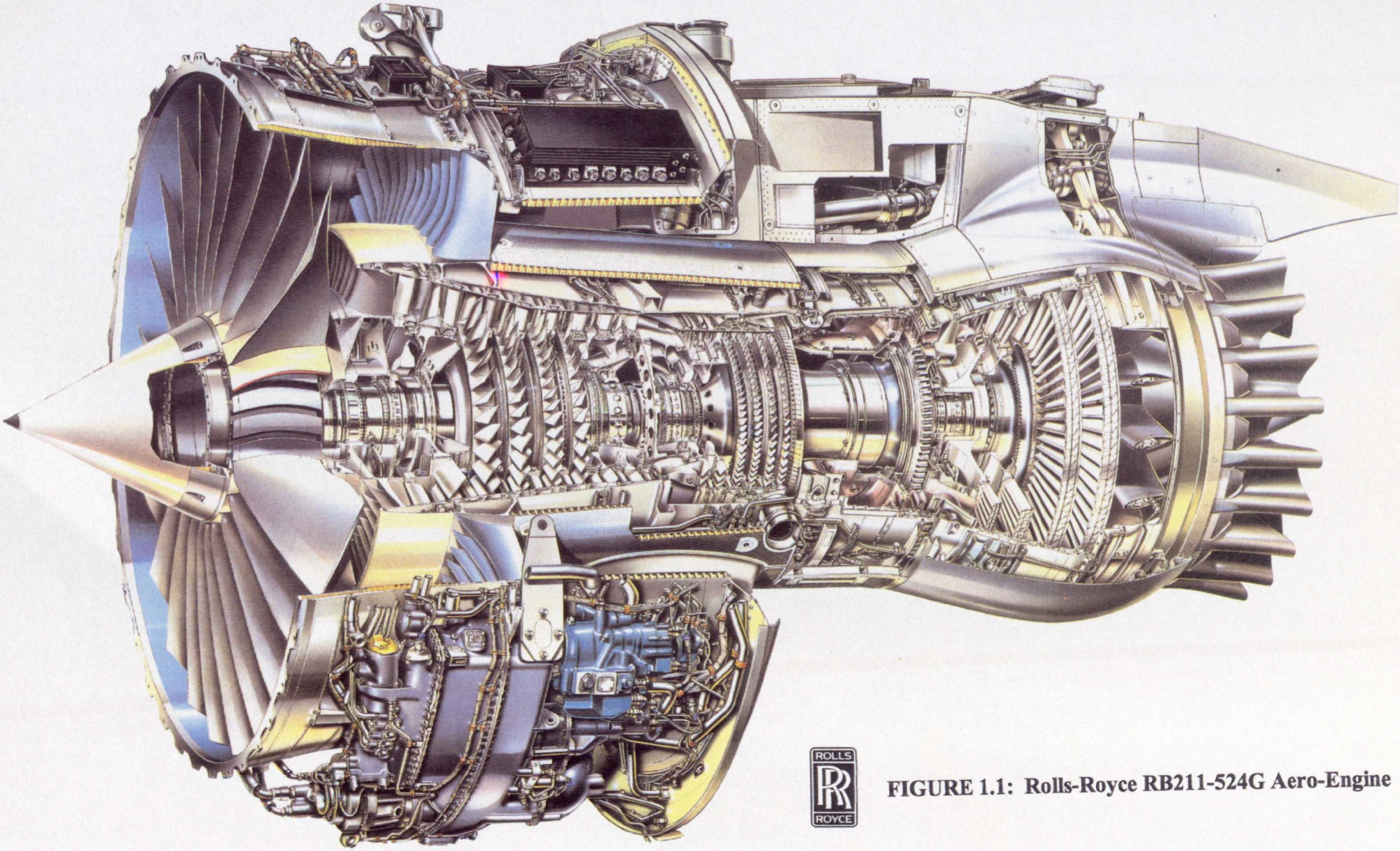

FIGURE 1.1: Rolls-Royce RB211-524G Aero-Engine

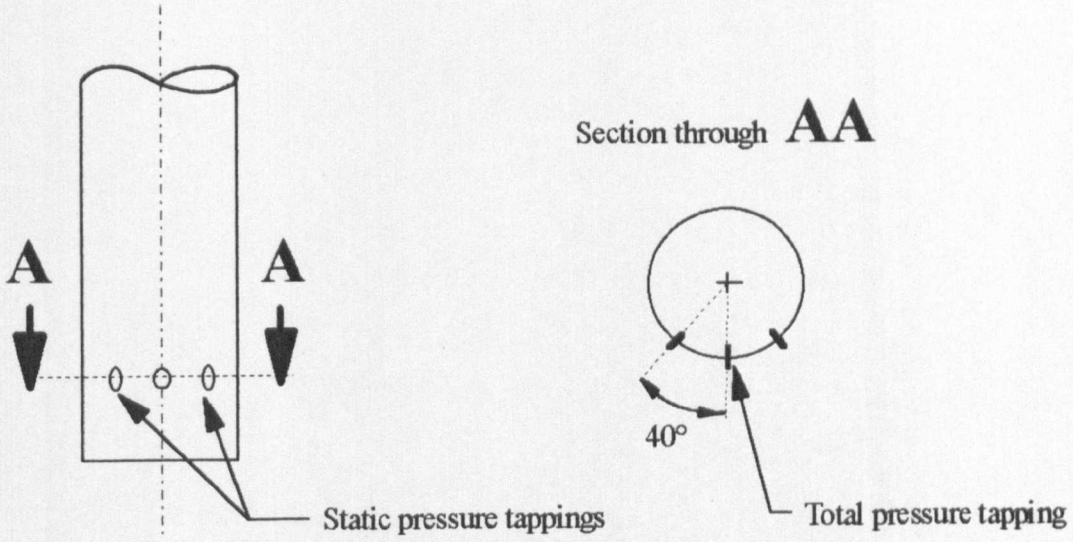

FIGURE 1.2a): Cylindrical Type Pneumatic Pressure Probe

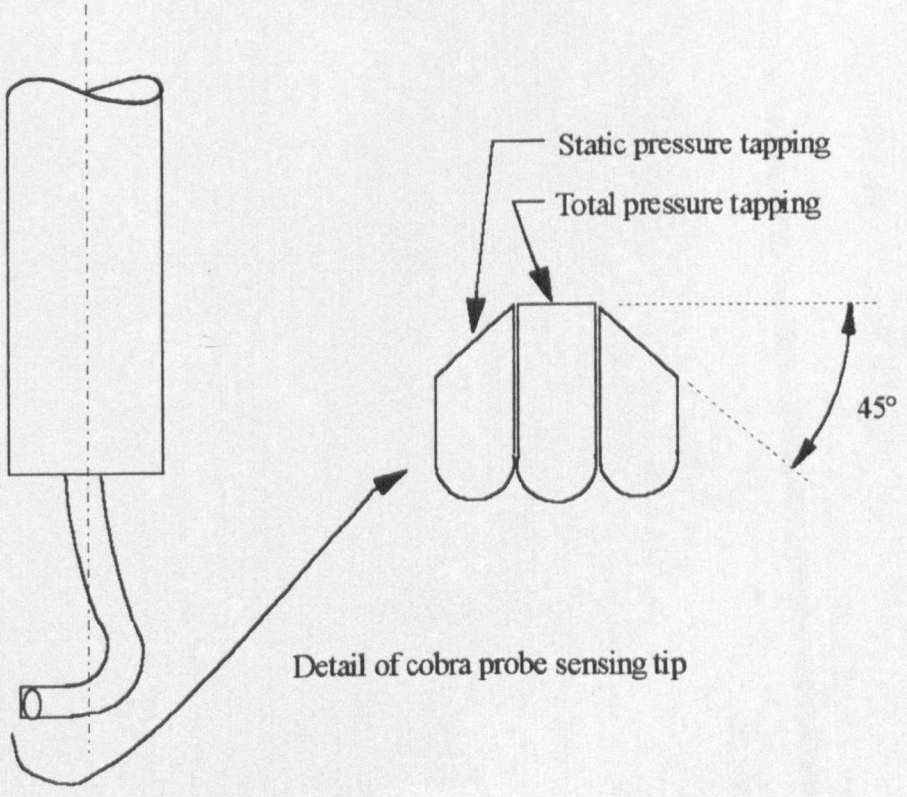

FIGURE 1.2b): Cobra Type Pneumatic Pressure Probe

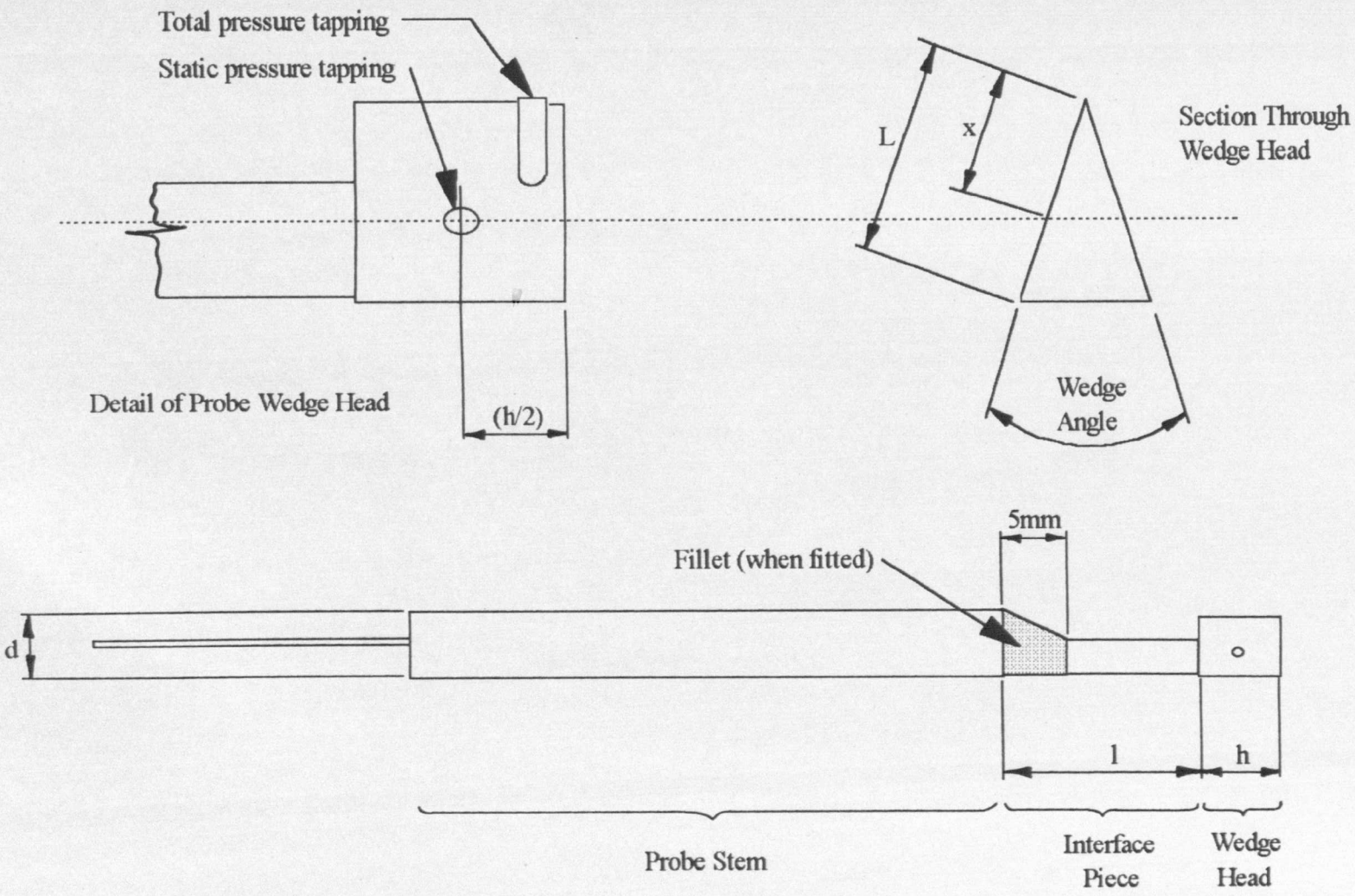

FIGURE 1.2c): Wedge Type Pneumatic Pressure Probe

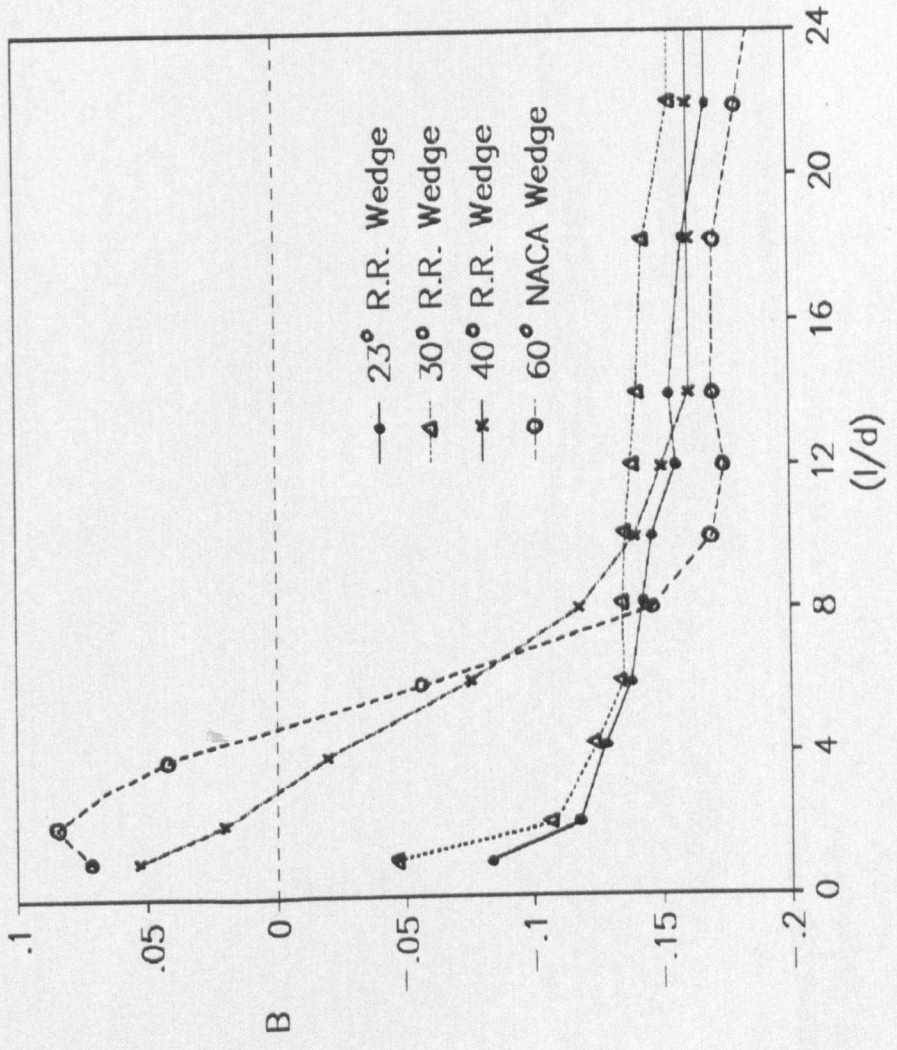

FIGURE 1.3: Wedge Probe Wall Proximity Effect

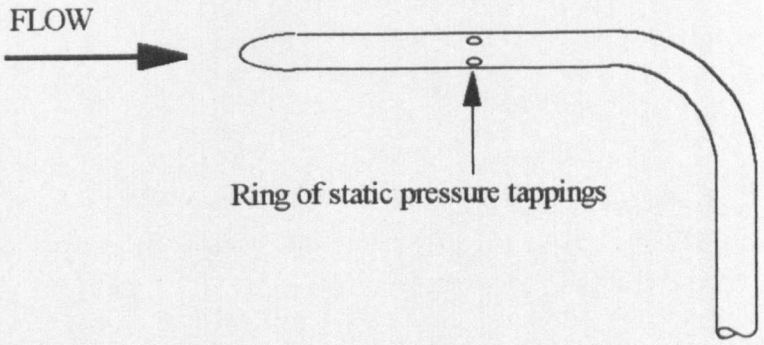

FIGURE 1.4a): 'Prandtl' Static Pressure Tube

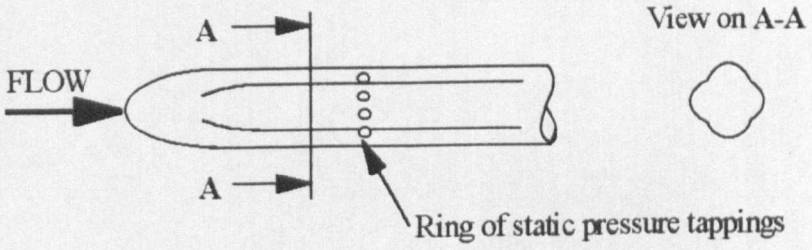

FIGURE 1.4b): 'Smith and Bauer' Static Pressure Probe Head

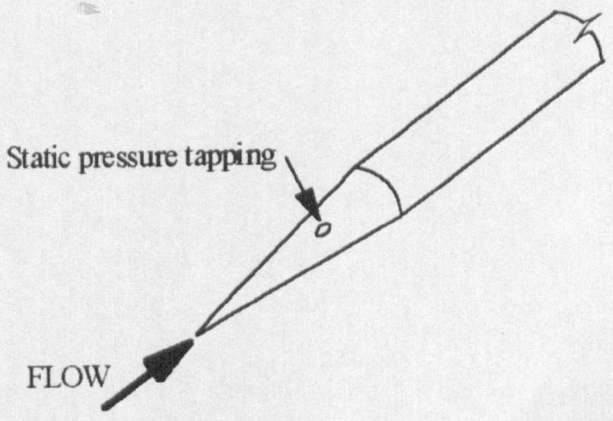

FIGURE 1.4c): Needle Static Pressure Probe

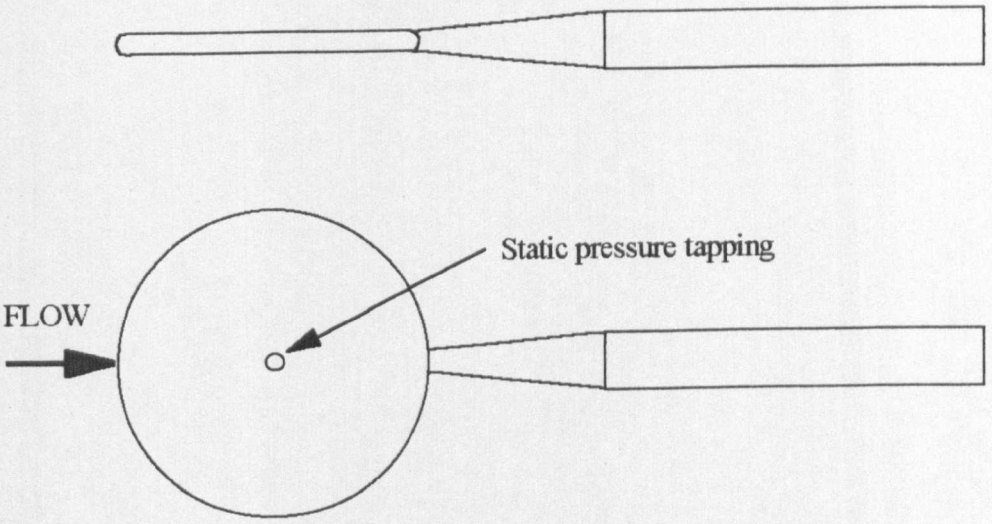

FIGURE 1.4d): Disc Static Pressure Probe

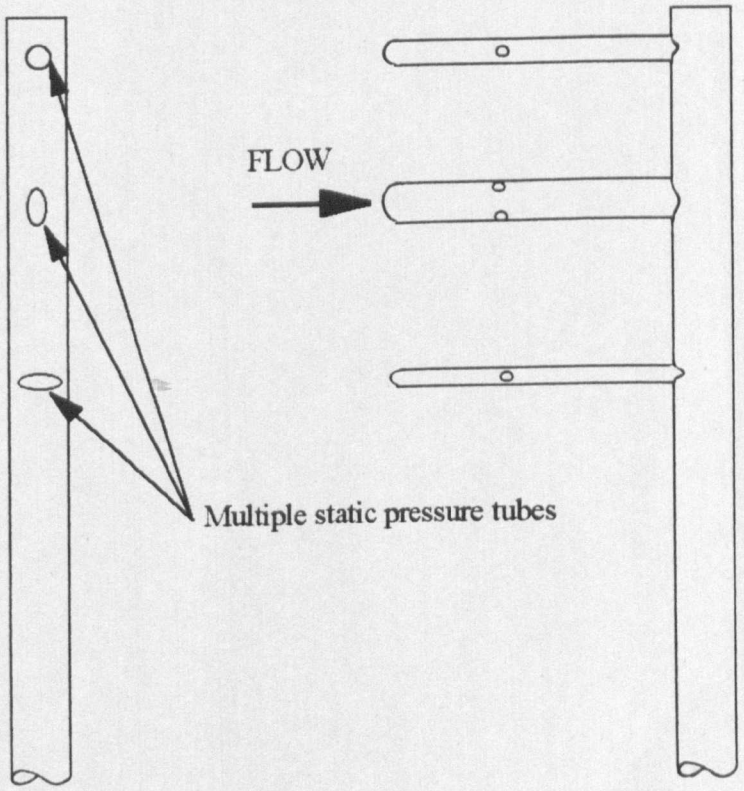

FIGURE 1.4e): 'Rossow' Static Pressure Probe

Rolls-Royce plc
Derby

ADVANCED ENGINEERING PROGRAMME
TECHNICAL OBJECTIVE AND PROGRAMME SUMMARY

PVK1-61D
High Accuracy
Interstage Measurement

1 **Statement of Work**

Theoretical modelling and wind tunnel calibration to design and demonstrate an aerodynamic probe for near wall static pressure measurements in turbomachinery annuli. Further theoretical and experimental work to develop instrumentation for measurement in unsteady flows. The work will be performed by a Rolls-Royce employee doing an Industrial Studentship.

2 **Technical Objectives**

i) To produce robust aerodynamic instrumentation which performs in a fully understood manner in flows typically encountered in turbomachines.

ii) To demonstrate that this instrumentation may routinely be applied to multistage turbomachines to make interstage measurements from which the performance of individual embedded stages may be determined.

3 **Engine Applicability**

The probes will be applied to compressor and turbine aerothermal rigs, enabling increased understanding of traverse data from instrumented rig builds, thus potentially avoiding additional rig builds. Higher data acquisition rates associated with dynamic instrumentation imply a reduction in traverse time. These benefits would also reduce overall engine development times.

4 **Resources**

Funding: Private Venture. External Agencies: Cranfield Institute of Technology. Business Agreement: RR/AEP 78/2

5 **Estimated Timing and Costs**

Timescales/Years	1991	1992	1993	1994	TOTAL	
Workstage:	Review and Static Pressure Investigation (Part 1)		Unsteady Flow Investigation (Part 2)			
Costs (£k/year):						
internal:	3.0	4.0	11.0	-	18.0	29.5
external:	1.0	2.5	7.0	1.0	11.5	
Engineering Time (Manyears/Year):	0.2	0.8	0.8	0.6	2.4	

* Least expensive option shown. Further EAA to be raised if more expensive option actually chosen.

6. Brochure Owner: P. D. Smout. Date: 24.9.91.
7. Assistant Chief Engineer: Date: 1 Oct 91

PDS.51

FIGURE 2.1: Research Brochure PVK1-61D Front Sheet

COSTS:	1991	1992	1993	1994
M.,F.& T.:	.00	10.10	9.30	10.10
Man Hours:	11.30	41.80	41.80	20.90
Computing O/heads:	.00	1.00	3.00	19.10
TOTAL:	11.30	52.90	54.10	50.10
DISCOUNT RATE (%):	5	5	5	5
DISCOUNTED COST:	11.30	50.38	49.07	43.28

PROB'Y OF ACHIEVING AIMS:	(P)
Near Wall ps Measurement:	1
Near Wall Angle Measurement	1
Calibration Discrepancies:	1
NET PROBABILITY:	1

BENEFITS:	1994	1995	1996	1997	1998	1999
Alternatives Avoided:	.00	136.00	136.00	136.00	136.00	136.00
Reduced Uncertainty:	.00	300.00	300.00	300.00	300.00	300.00
TOTAL:	.00	436.00	436.00	436.00	436.00	436.00

DIS-BENEFITS:

a):
b):
TOTAL:

NET BENEFITS:	.00	436.00	436.00	436.00	436.00	436.00
DISCOUNT RATE (%):	5	5	5	5	5	5
DISCOUNTED BENEFIT:	.00	358.70	341.62	325.35	309.86	295.10

IMPLEMENTATION COSTS:	1994
M.,F.& T.:	2.00
Man-Hours:	14.00
TOTAL:	16.00
DISCOUNT RATE (%):	5
DISCOUNTED IMPLEMENT'N:	13.82

IMPLEMENTATION PROBABILITY:	(P)
Probe Manufacture:	1
Probe Evaluation:	1
Reporting:	1

NET IMPLEMENTATION COST =	13.82

NET BENEFIT VALUE =	.00	358.70	341.62	325.35	309.86	295.10

SUMMARY

Total Benefit Value =	1630.62
Implementation Cost =	13.82
Total Research Cost =	154.03
BENEFIT-COST RATIO:	9.496711

FIGURE 2.2: Cost Benefit Analysis Summary Sheet

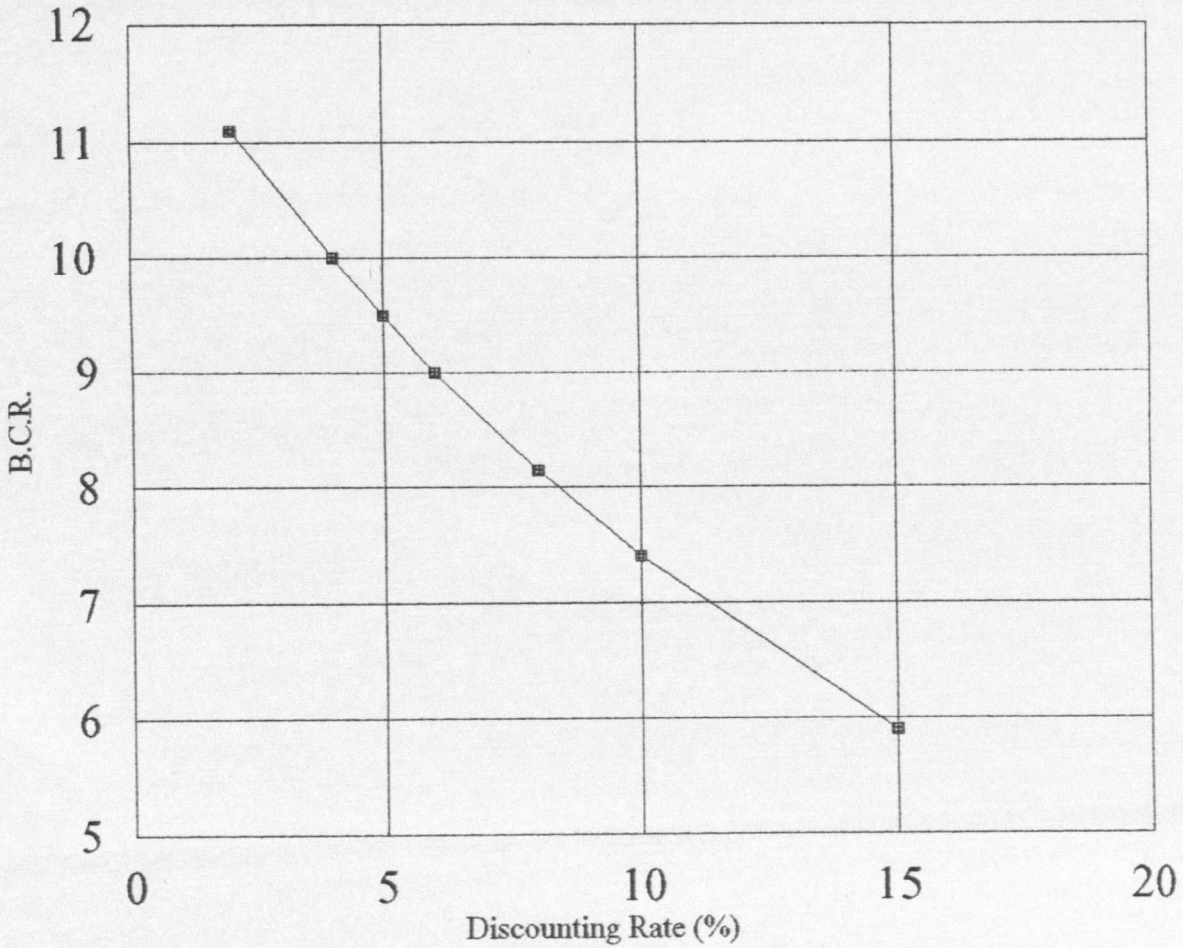

FIGURE 2.3: Sensitivity of B.C.R. to Discounting Rate Assuming 100% Success in Achieving Objectives

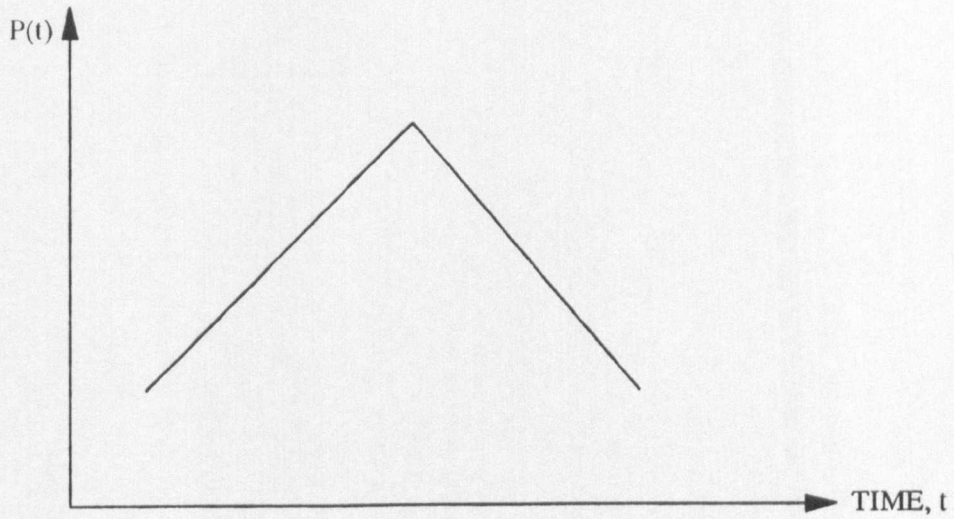

FIGURE 2.4a): Triangular Distribution

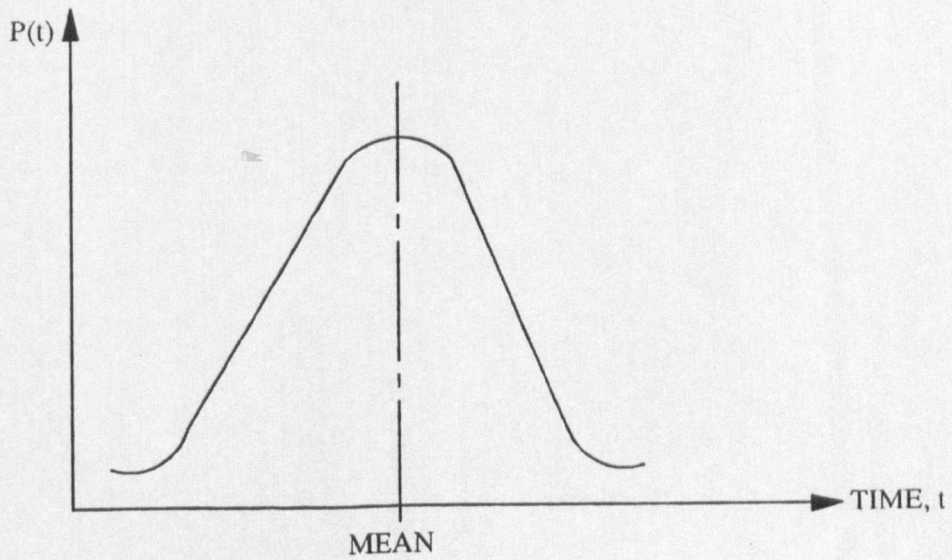

FIGURE 2.4b): Gaussian (Normal) Distribution

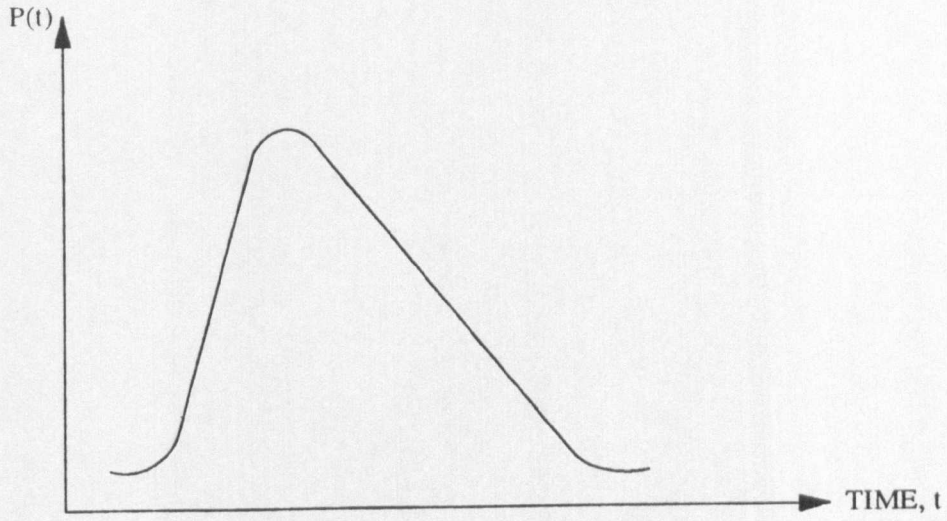

FIGURE 2.4c): Skewed Normal Distribution

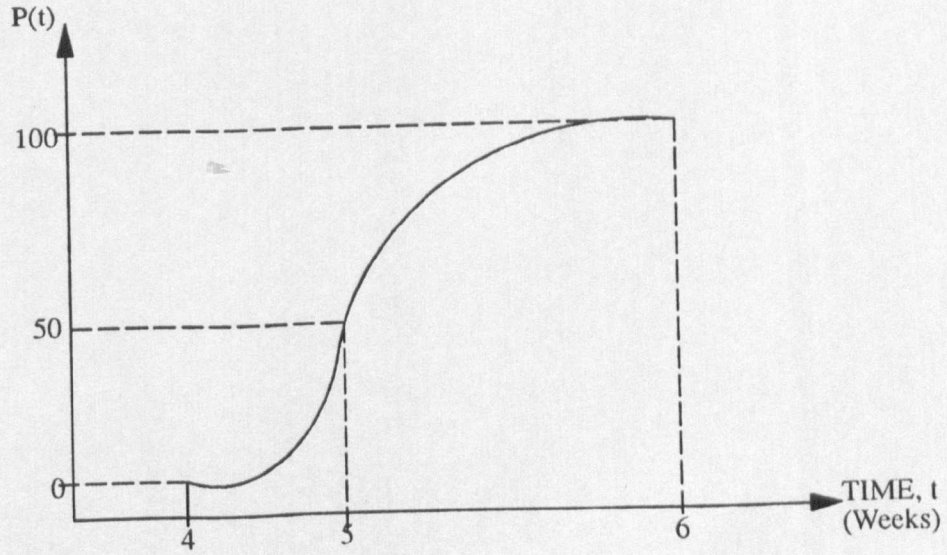

FIGURE 2.4d): Cummulative Probability Distribution

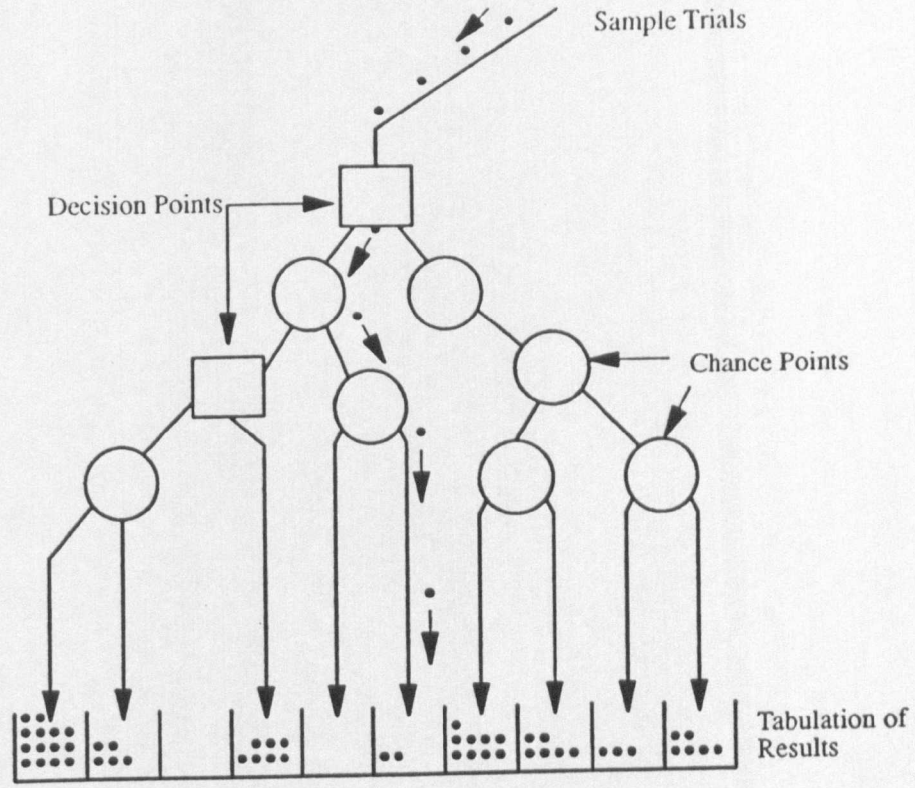

FIGURE 2.5: Simulation Model of a Given Project For Subsequent Monte-Carlo Analysis (Buck, 1989)

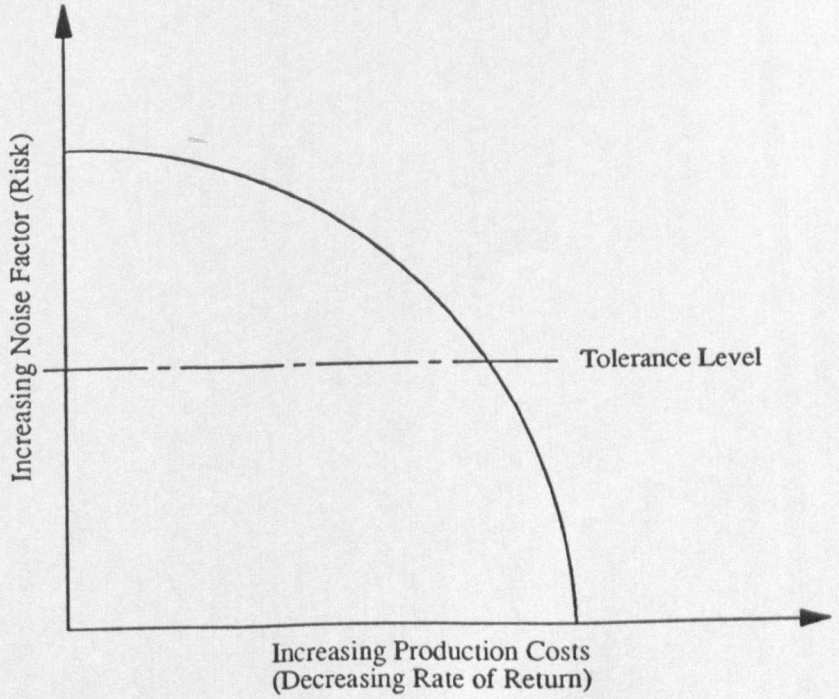

FIGURE 2.6: Noise Factor vs. Production Costs Trade-off Curve (Baranson, 1978)

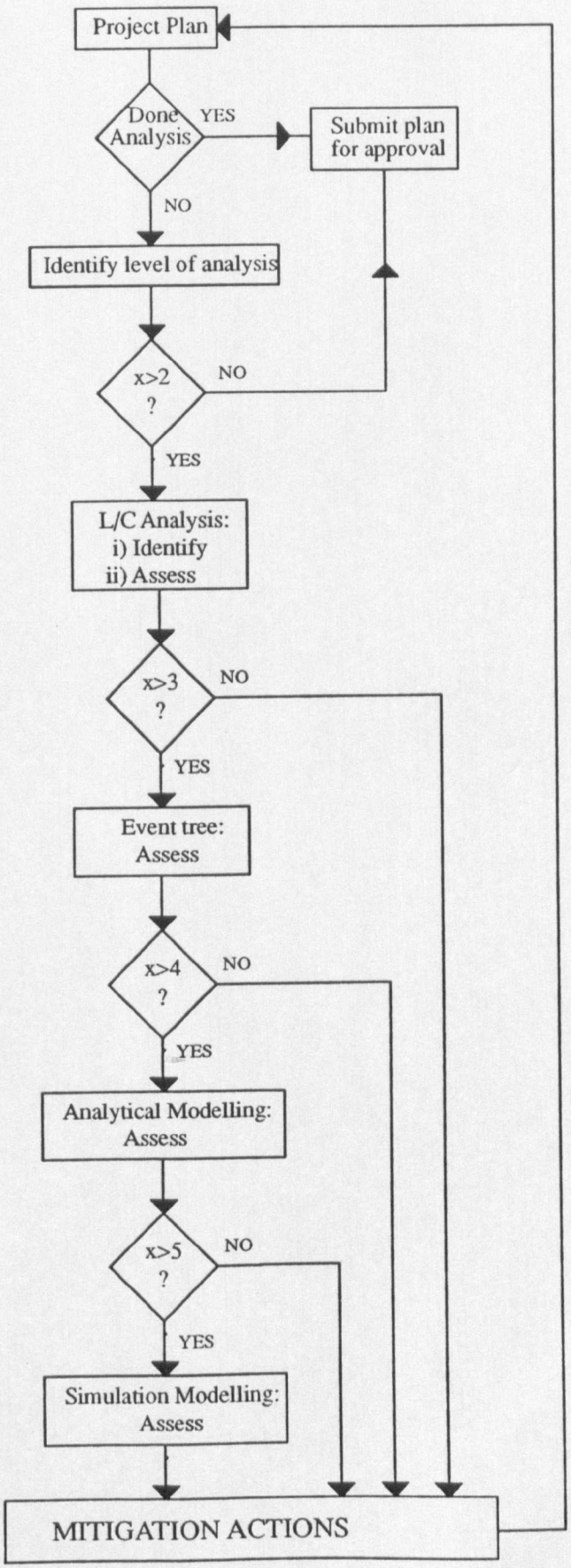

FIGURE 2.7: Risk Analysis Guids Line Flow Chart

FIGURE 2.8: Project Plan for Years 2 and 3

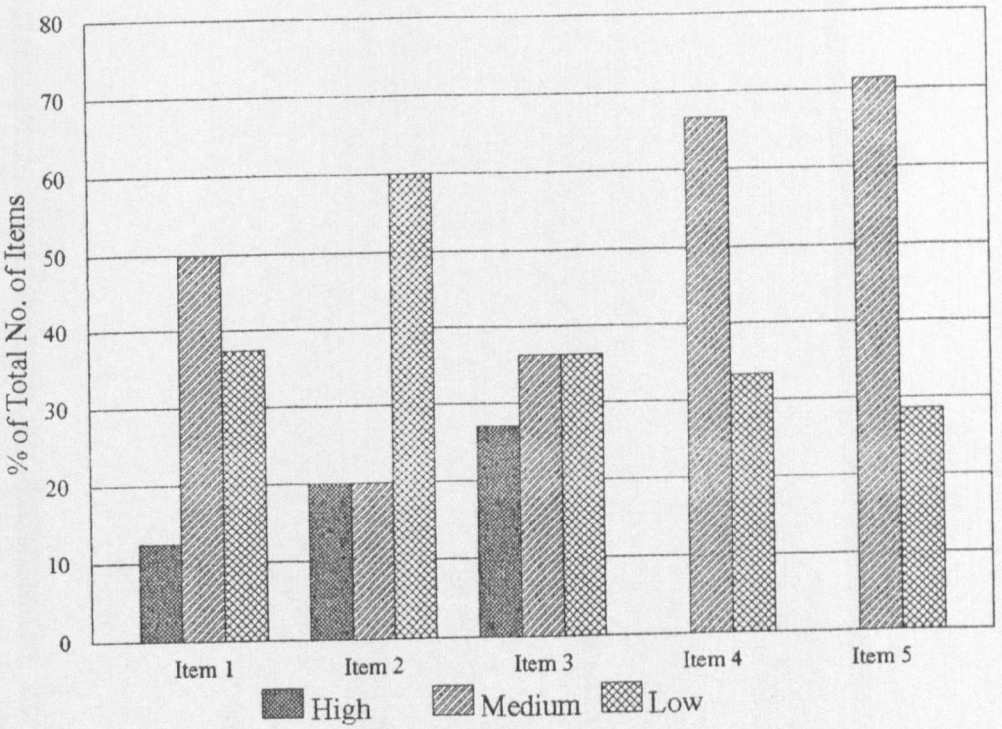

FIGURE 2.9: Likelihood/Consequence Analysis - Risk Distributions by Work Package

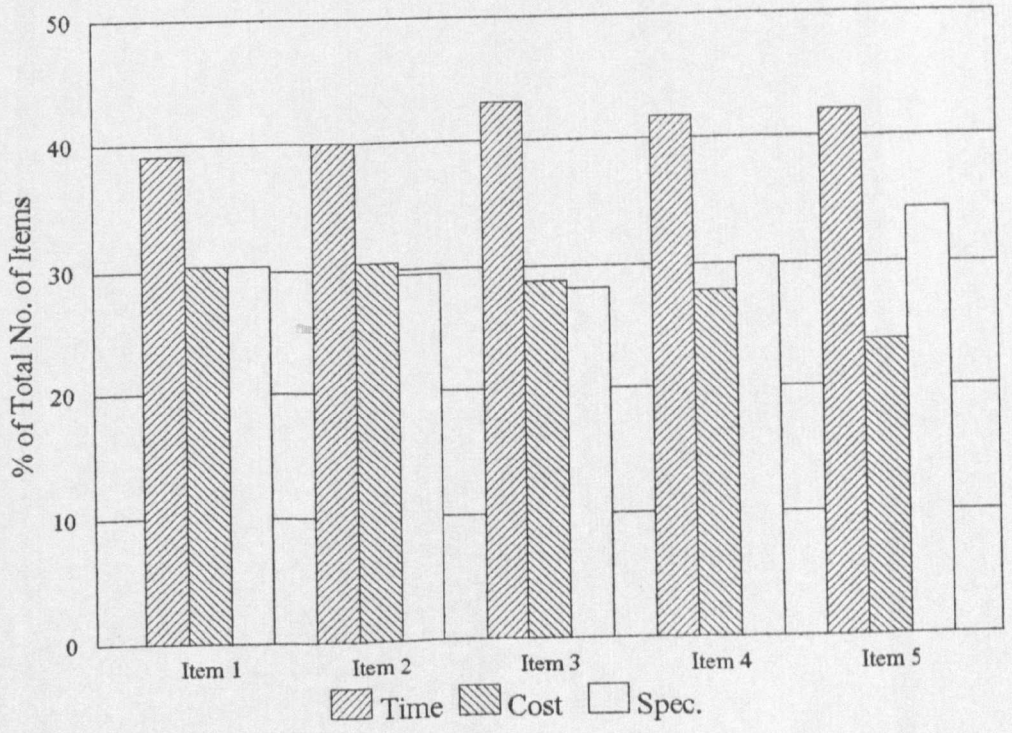

FIGURE 2.10: Likelihood/Consequence Analysis - Breakdown of Consequences

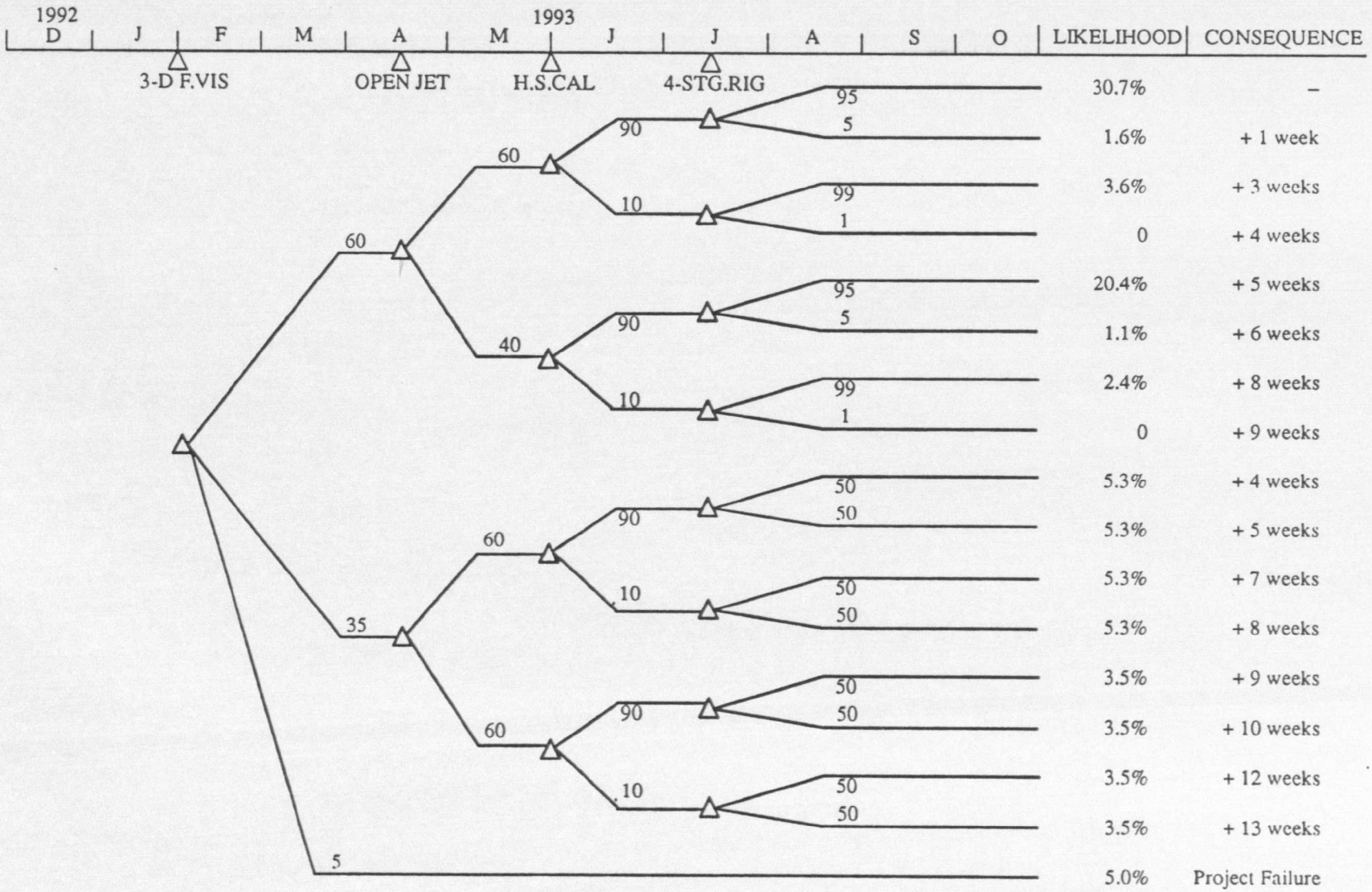

FIGURE 2.11: C.F.D. Numerical Modelling Event Tree

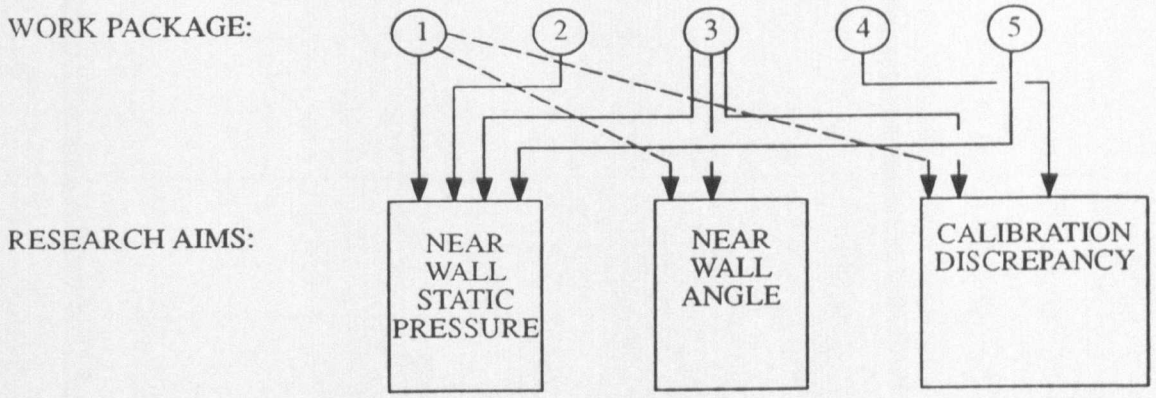

FIGURE 2.12: Relationship Between Work Packages and Research Aims

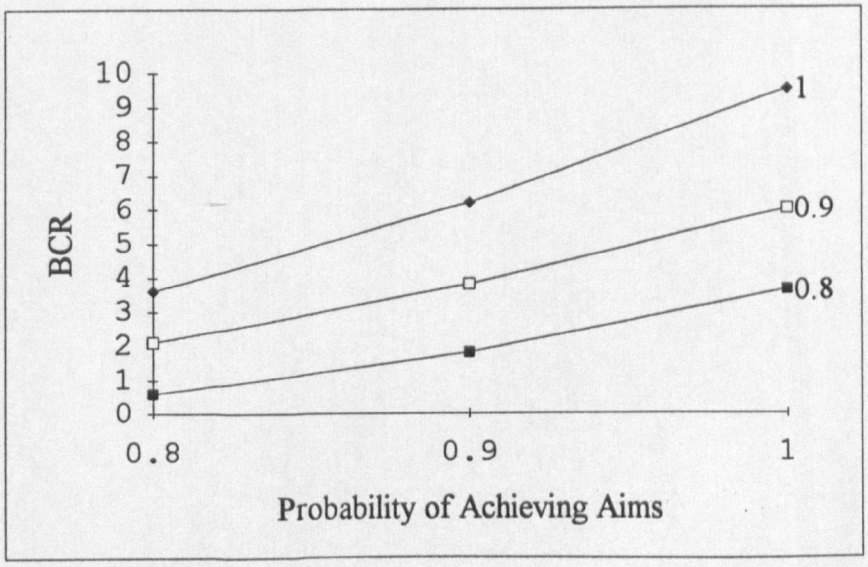

FIGURE 2.13: Relationship Between Probability of Success and BCR

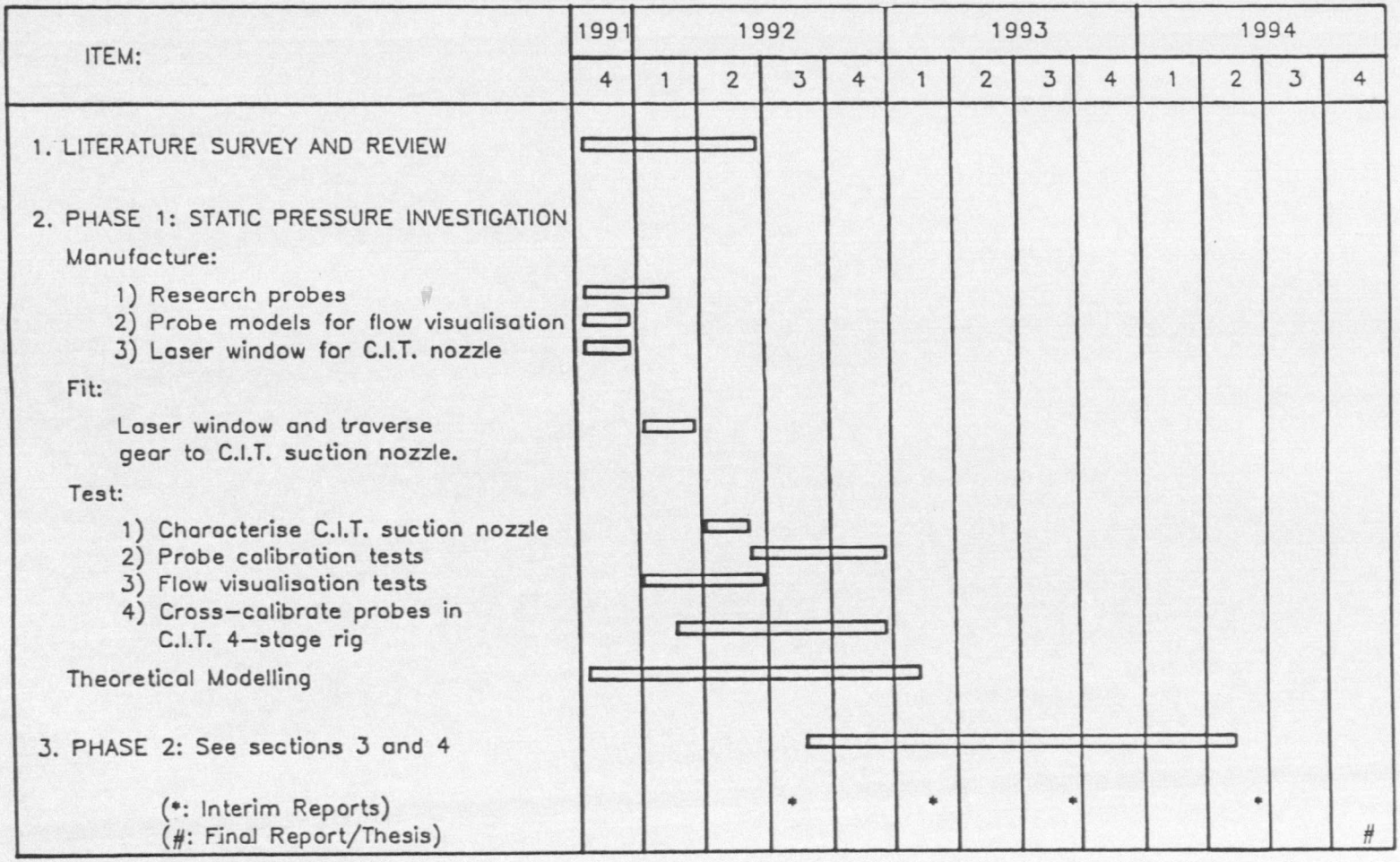

FIGURE 3.1: Original Overall Project Plan for Brochure PVK1-61D

OPTIONS	OBJECTIVES					OBJECTIVE WEIGHTINGS		DECISION MATRIX
	High Response	Correct Mean	Result in 3 Years	Robust				
WALL PROXIMITY	0	0.9	0.9	0.9	x	0.1	=	**0.81**
DYNAMIC YAWMETER	0.8	0.5	0.7	0.8		0.3		0.68
REVERSE KIEL PROBE	0	0.7	0.9	0.9		0.3		0.75
DYNAMIC TEMP. PROBE	0.7	0.5	0.6	0.6		0.3		0.58

FIGURE 3.2: APPLICATION OF CHURCHMAN-ACKOFF DECISION ANALYSIS TECHNIQUE IN DETERMINING PROJECT DIRECTION FOR YEARS 2 AND 3.

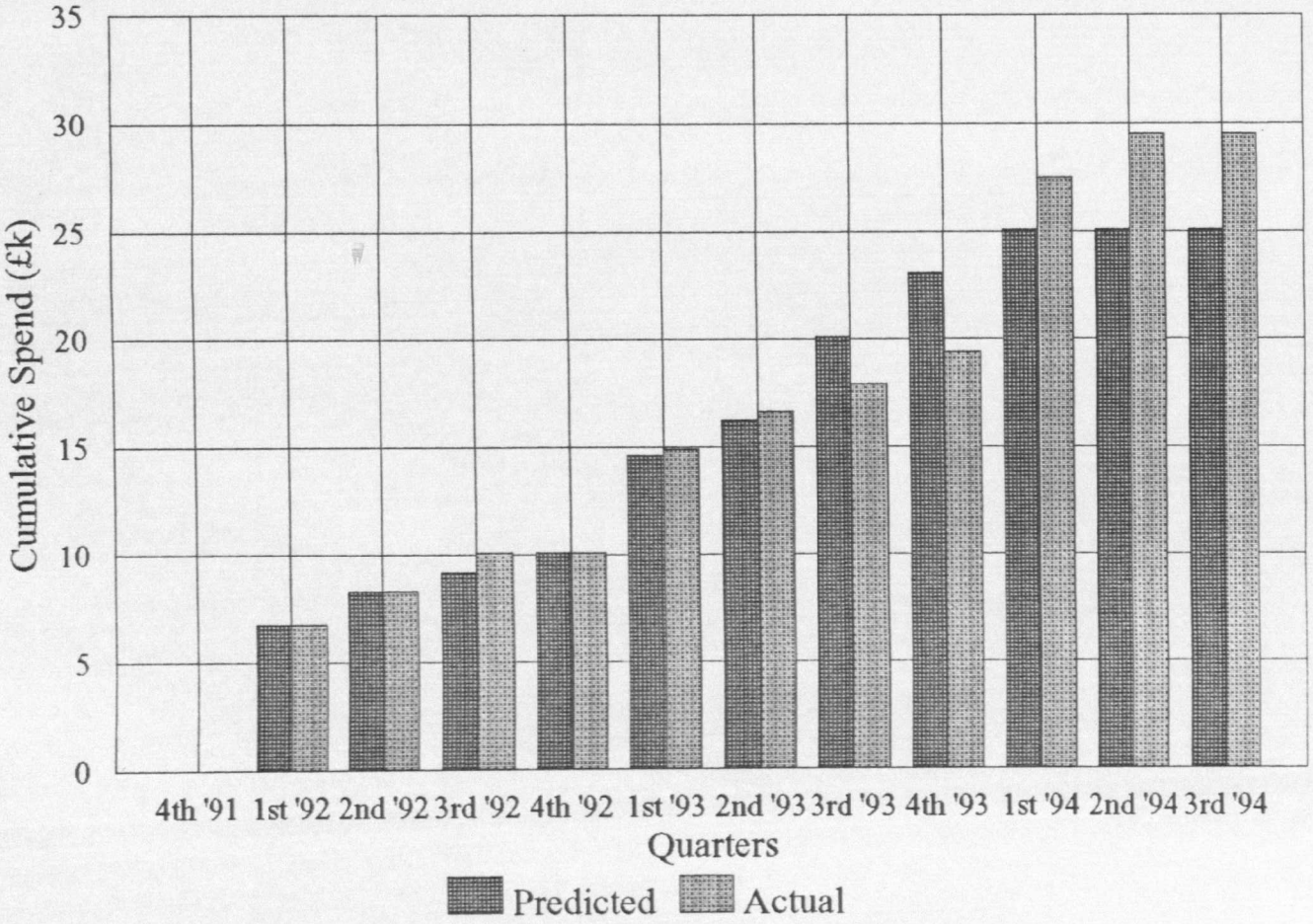

FIGURE 3.3: Brochure PVK1-61D Spend Summary

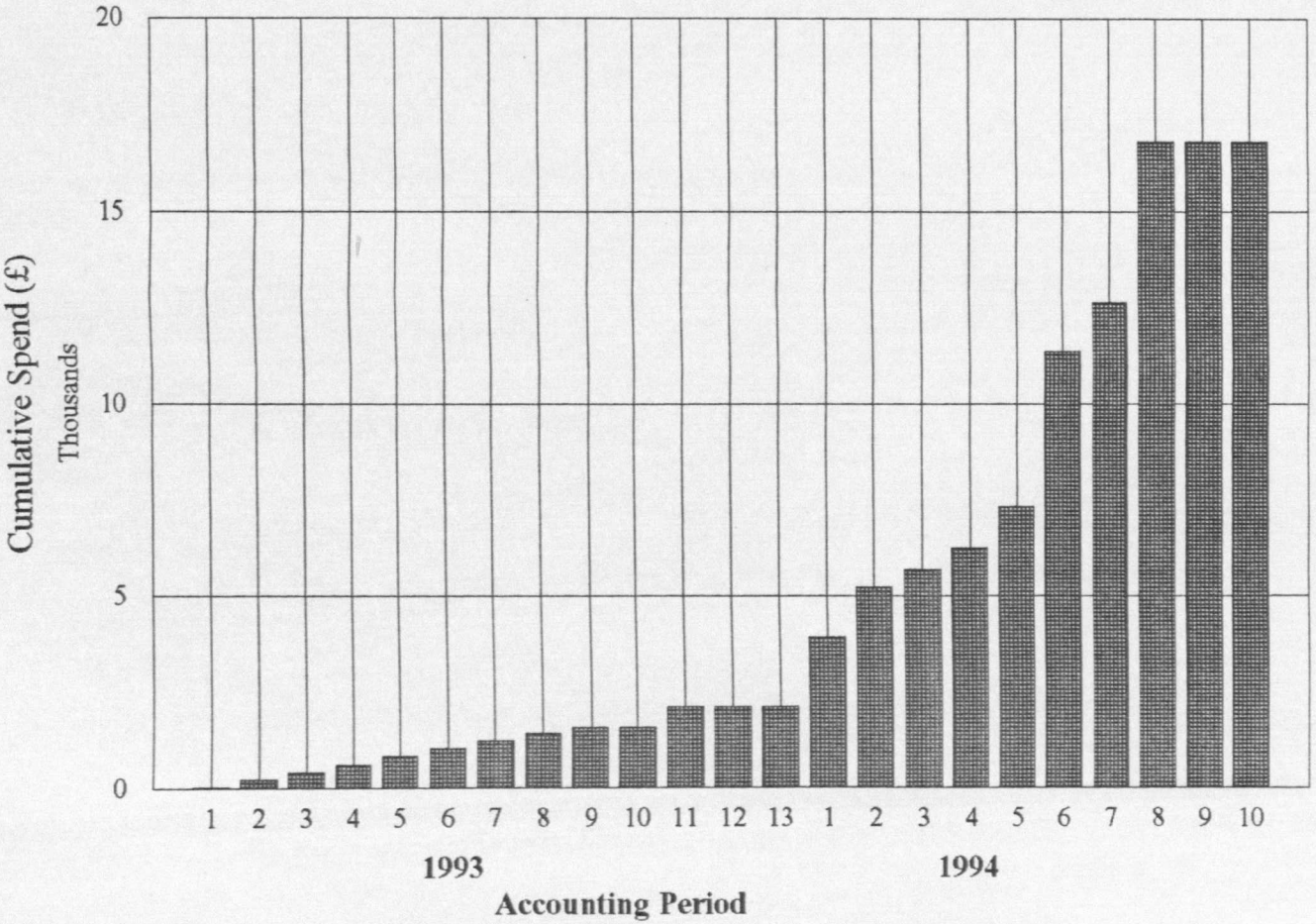

FIGURE 3.4: Computing Overhead Costs (Mainframe Useage for CFD)

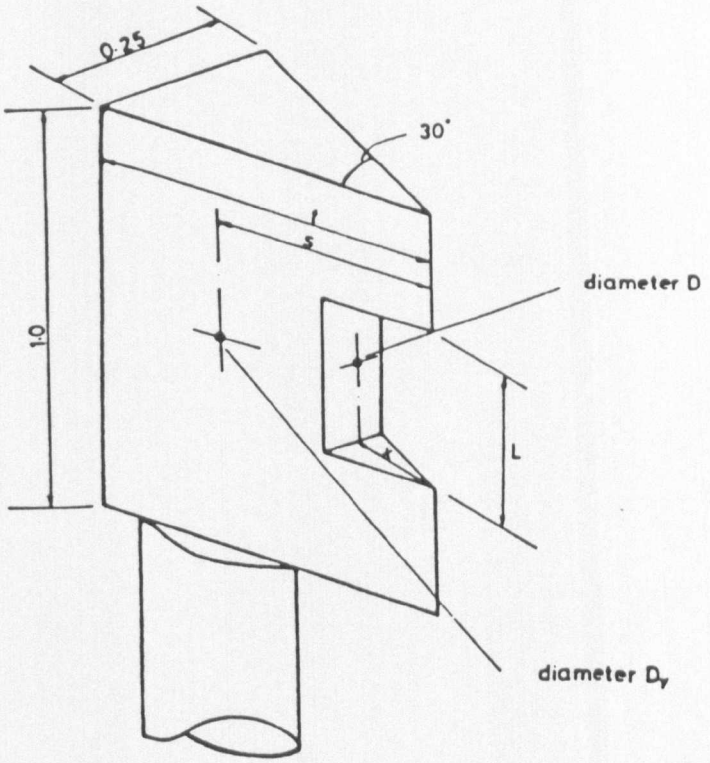

FIGURE 4.1a): Optimum Geometry of Single-Stepped Pitot Tube (Ferguson, 1974)

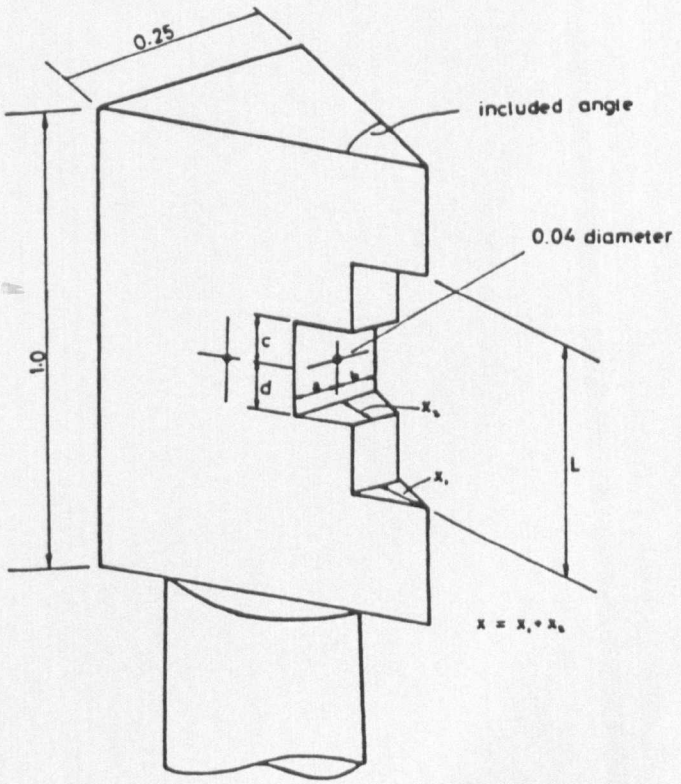

FIGURE 4.1b): Optimum Geometry of Double-Stepped Pitot Tube (Ferguson, 1974)

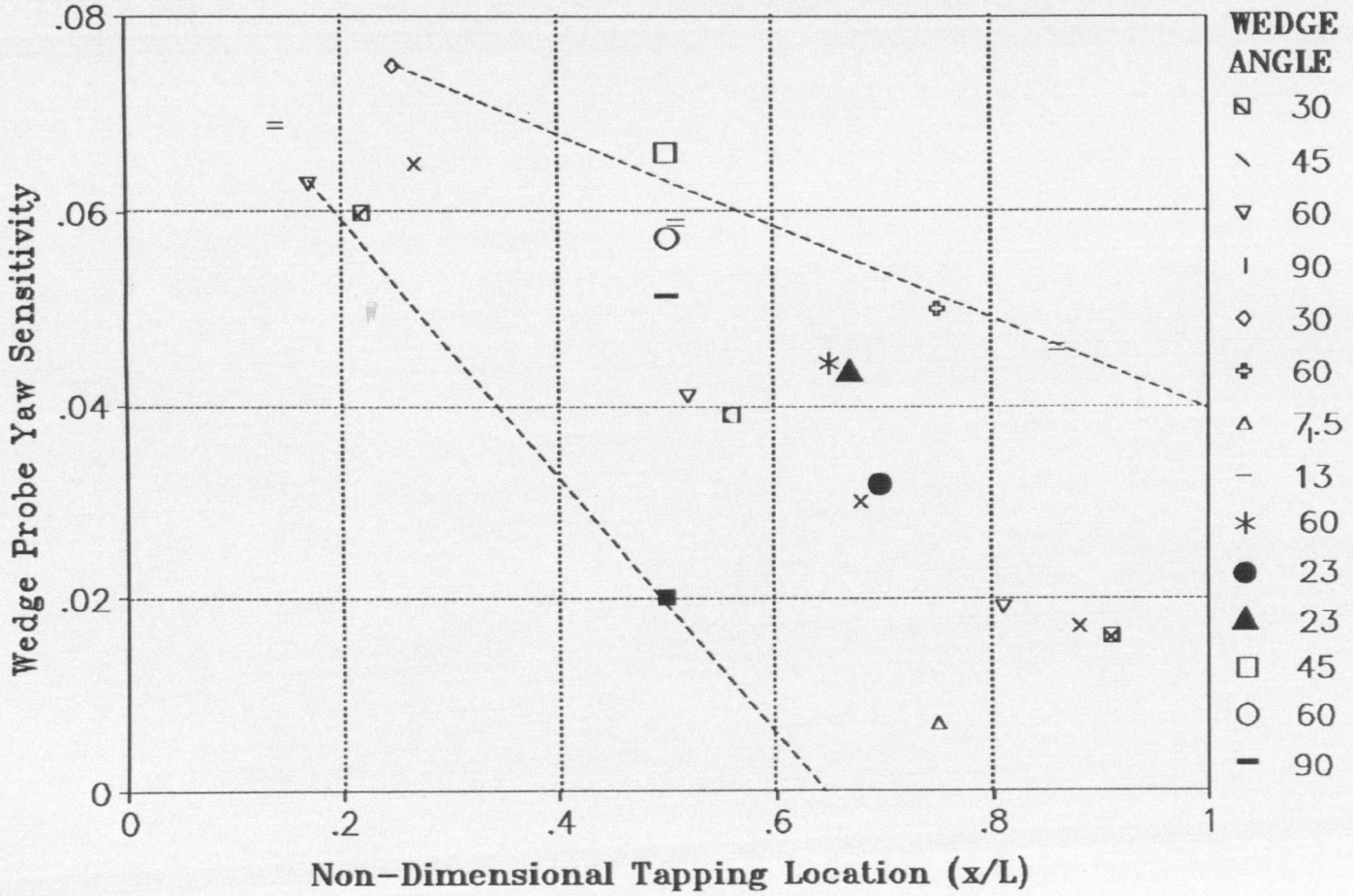

FIGURE 4.2: Collation of Results for Wedge Probe Yaw Angle Sensitivity Dependence

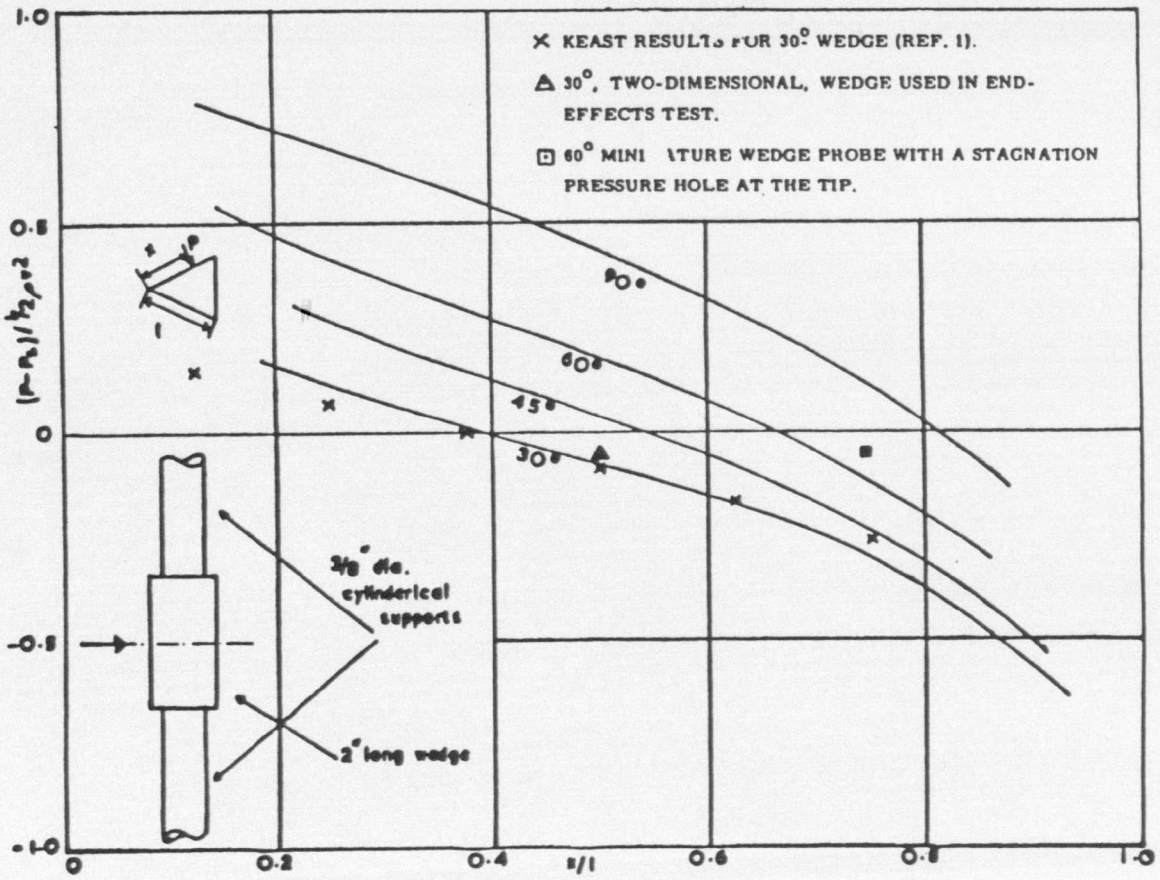

FIGURE 4.3: Wedge Face Pressure Distribution for Four Different Included Angle Wedge Shapes at 0° Yaw and Pitch

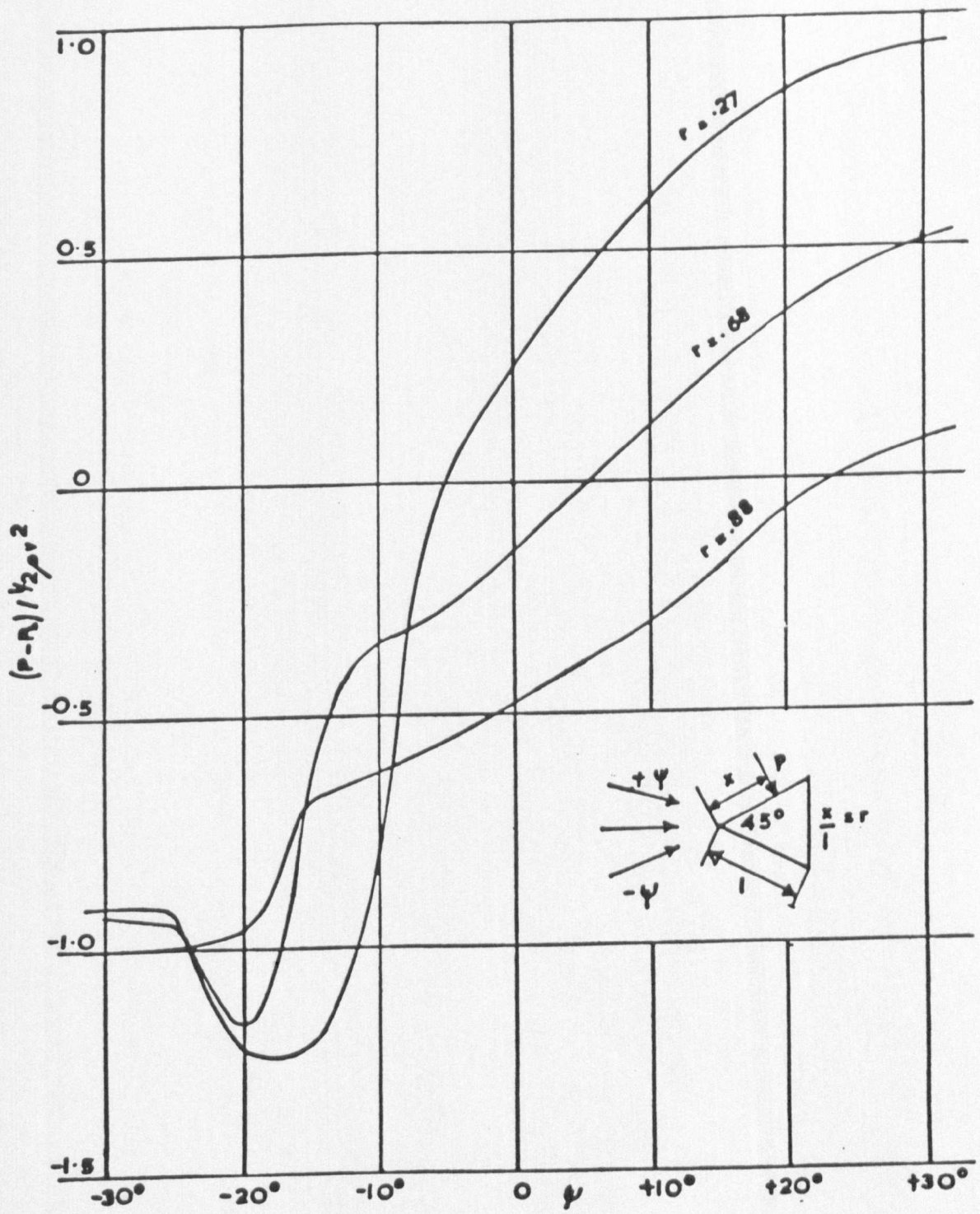

FIGURE 4.4: Variation of Wedge Face Static Pressure with Yaw Angle for a 45° Included Angle Wedge Shape

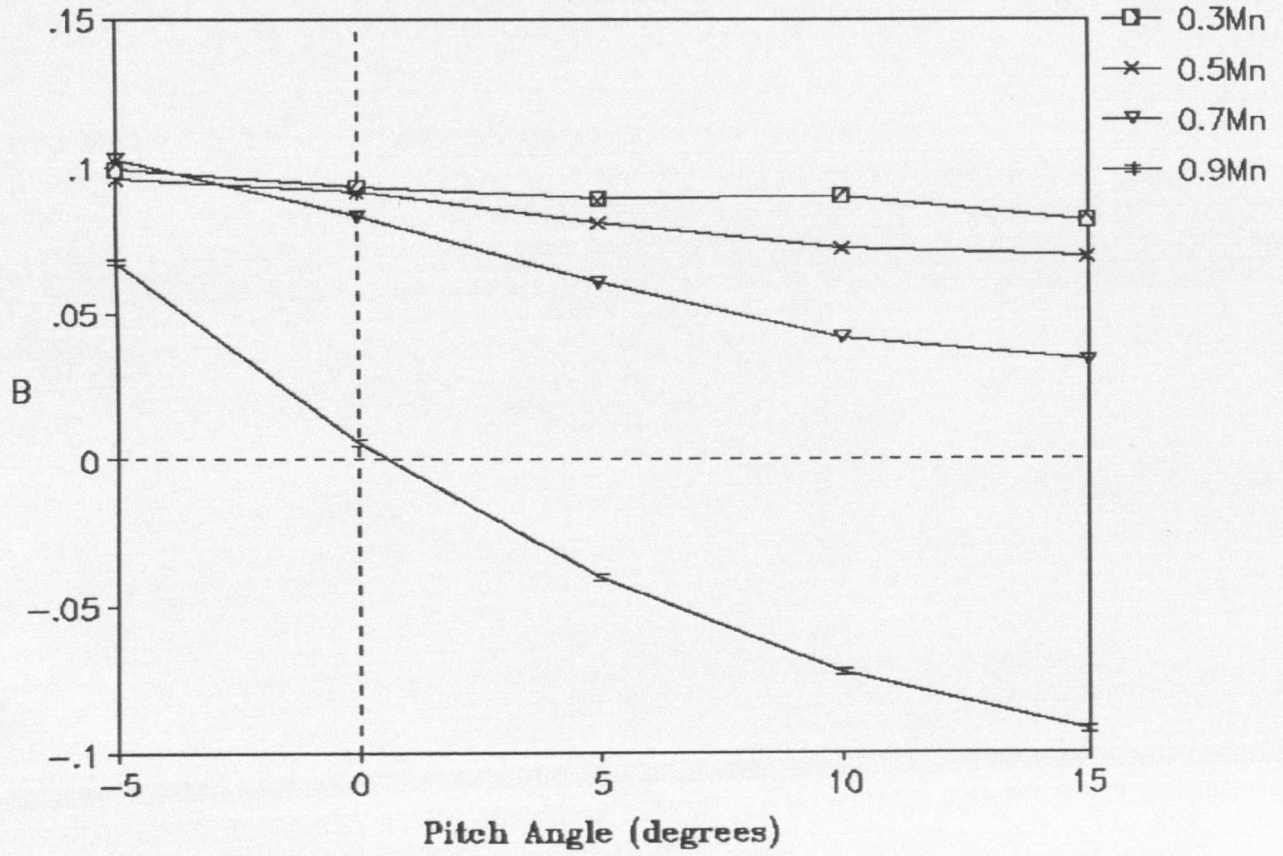

FIGURE 4.5: Variation of Pitch Sensitivity with Mach Number for a 30° Wedge Probe (Hodson, 1989)

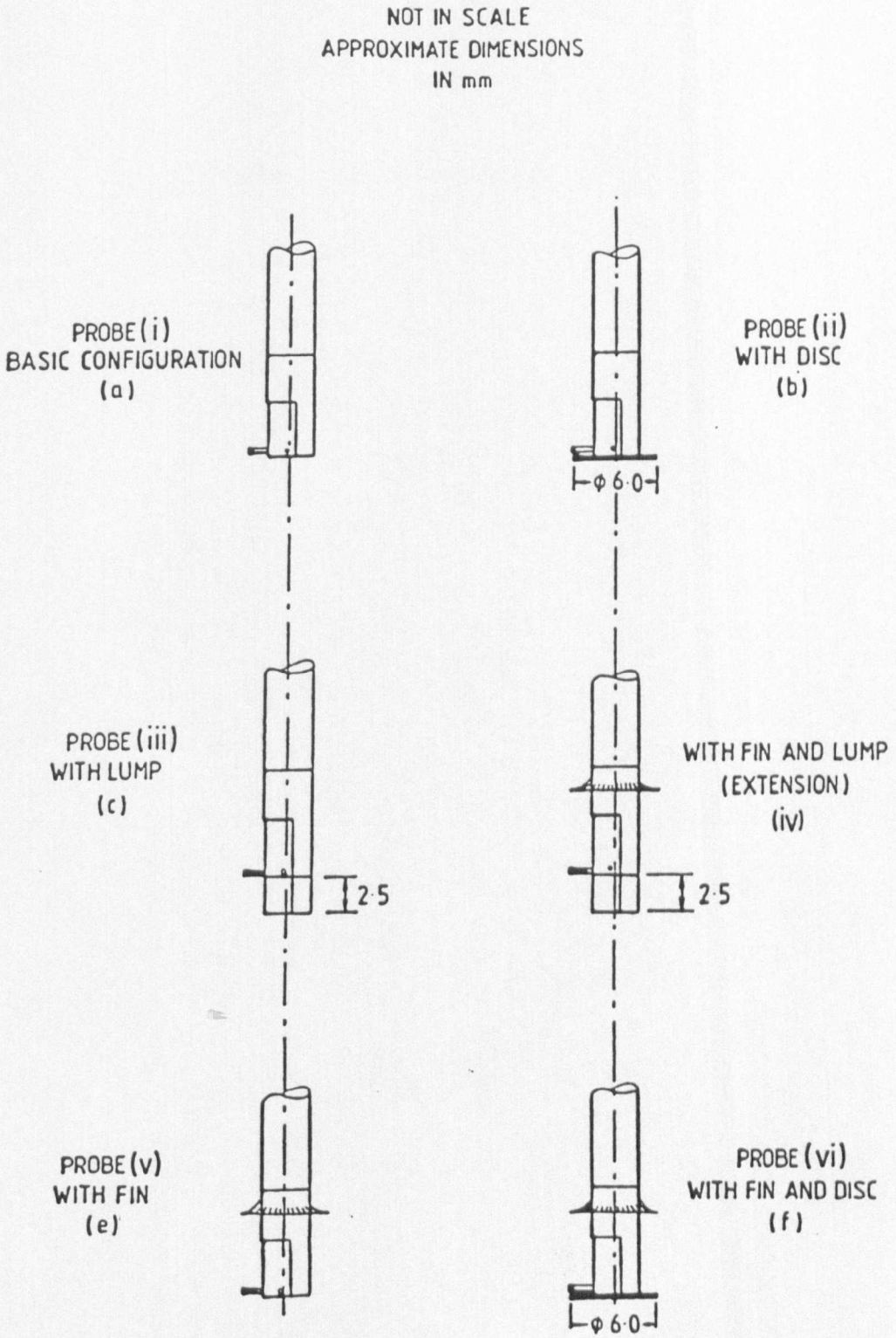

FIGURE 4.6: Wedge Probe Modifications Aimed at Improving Near Wall Performance (Filbee, 1990)

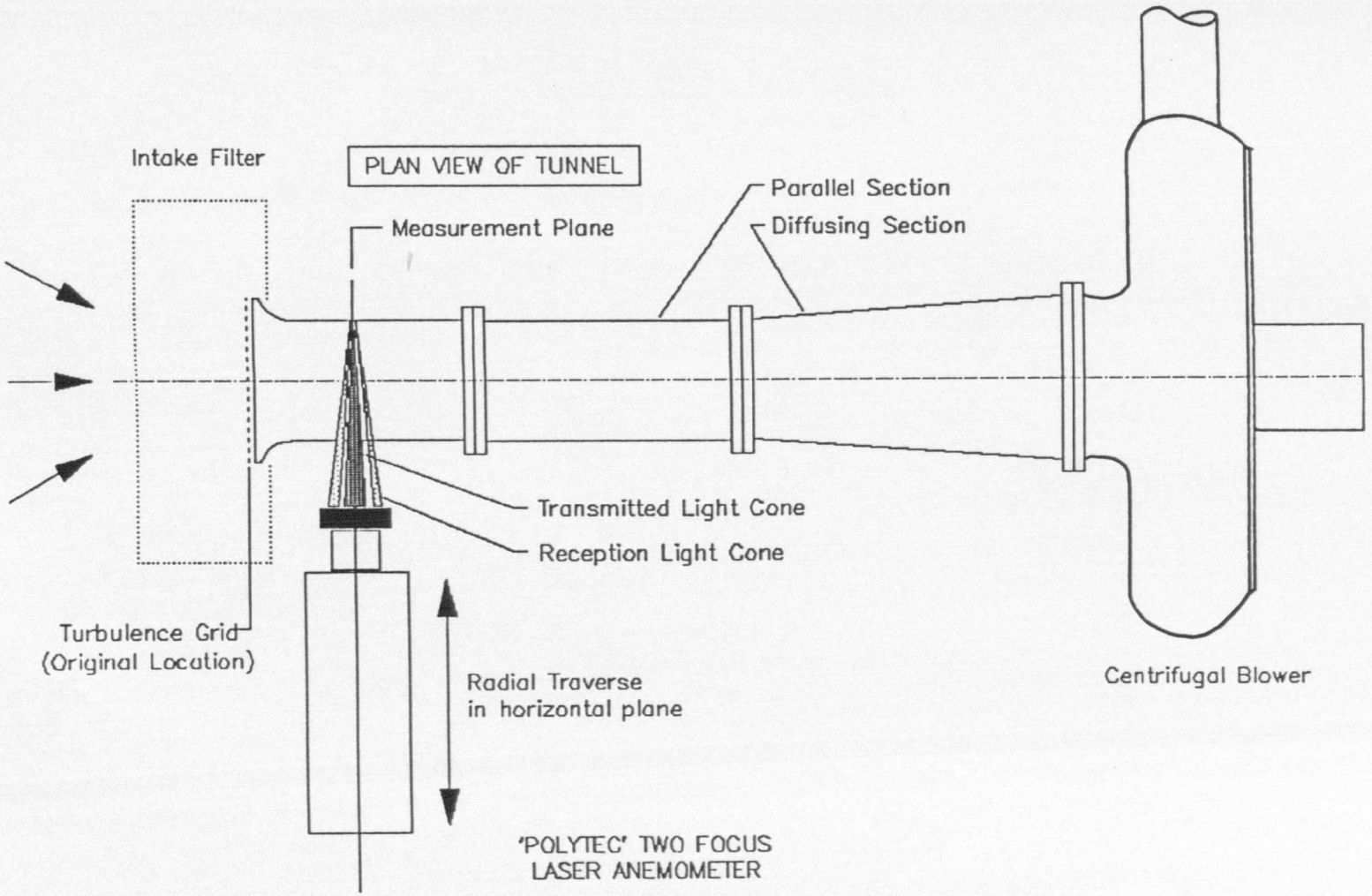

FIGURE 5.1: Cranfield University Suction Wind Tunnel - Plan View

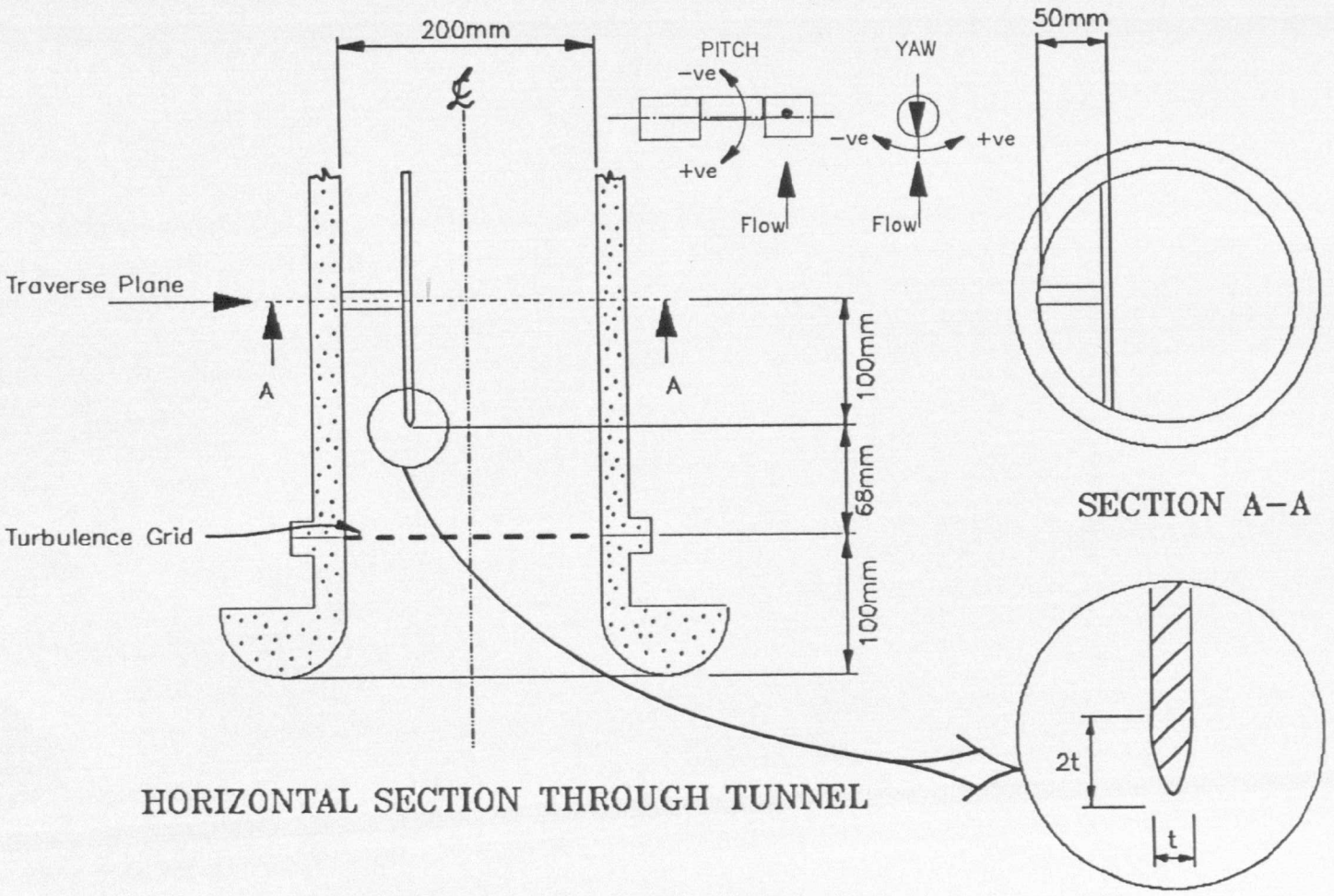

FIGURE 5.2: Installation of Vertical Plate and Arrangement of Suction Wind Tunnel Intake Bellmouth

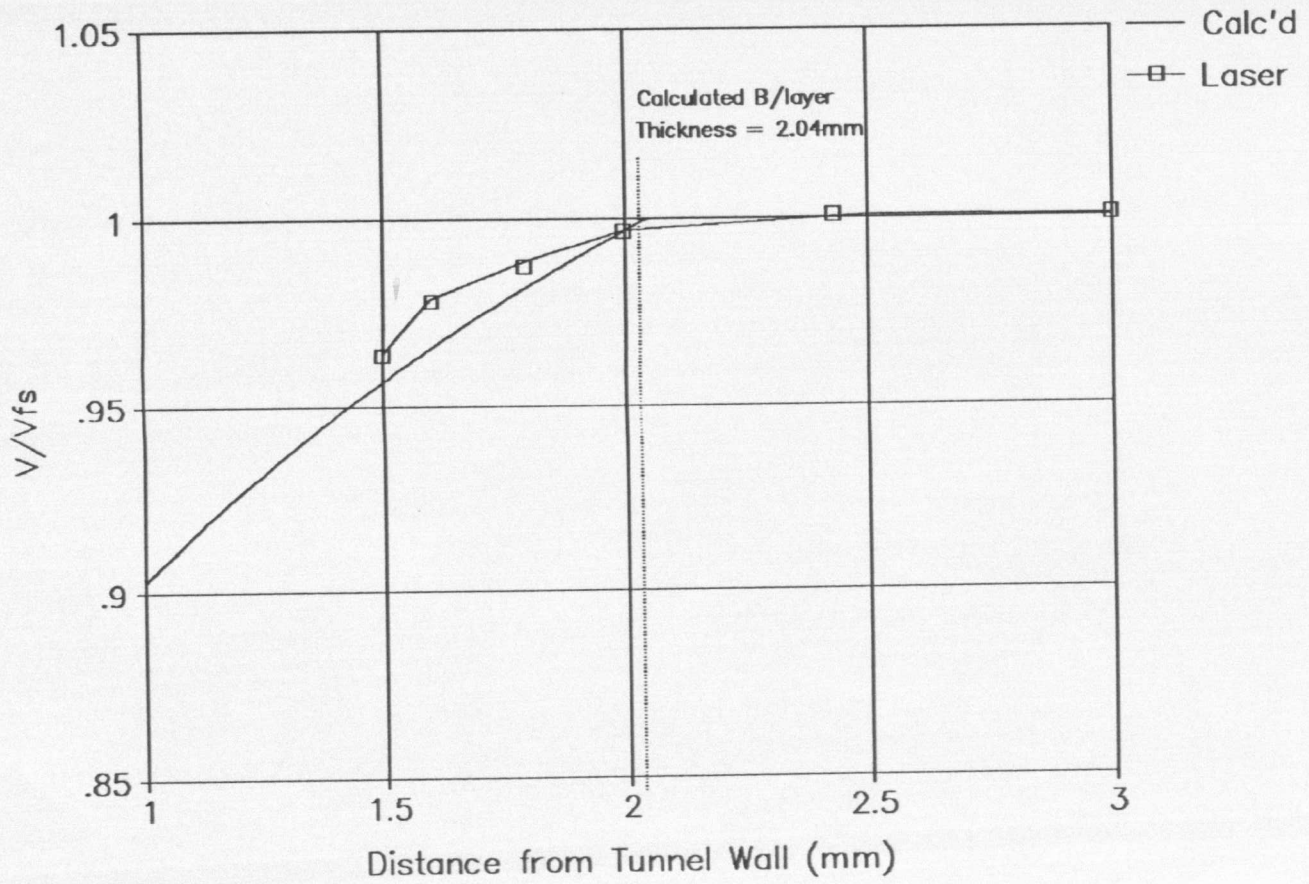

FIGURE 5.3: Measured and Calculated Boundary Layer Profiles Adjacent to Suction Wind Tunnel Vertical Plate at 0.75 Mach Number and 0.8% Freestream Turbulence Intensity

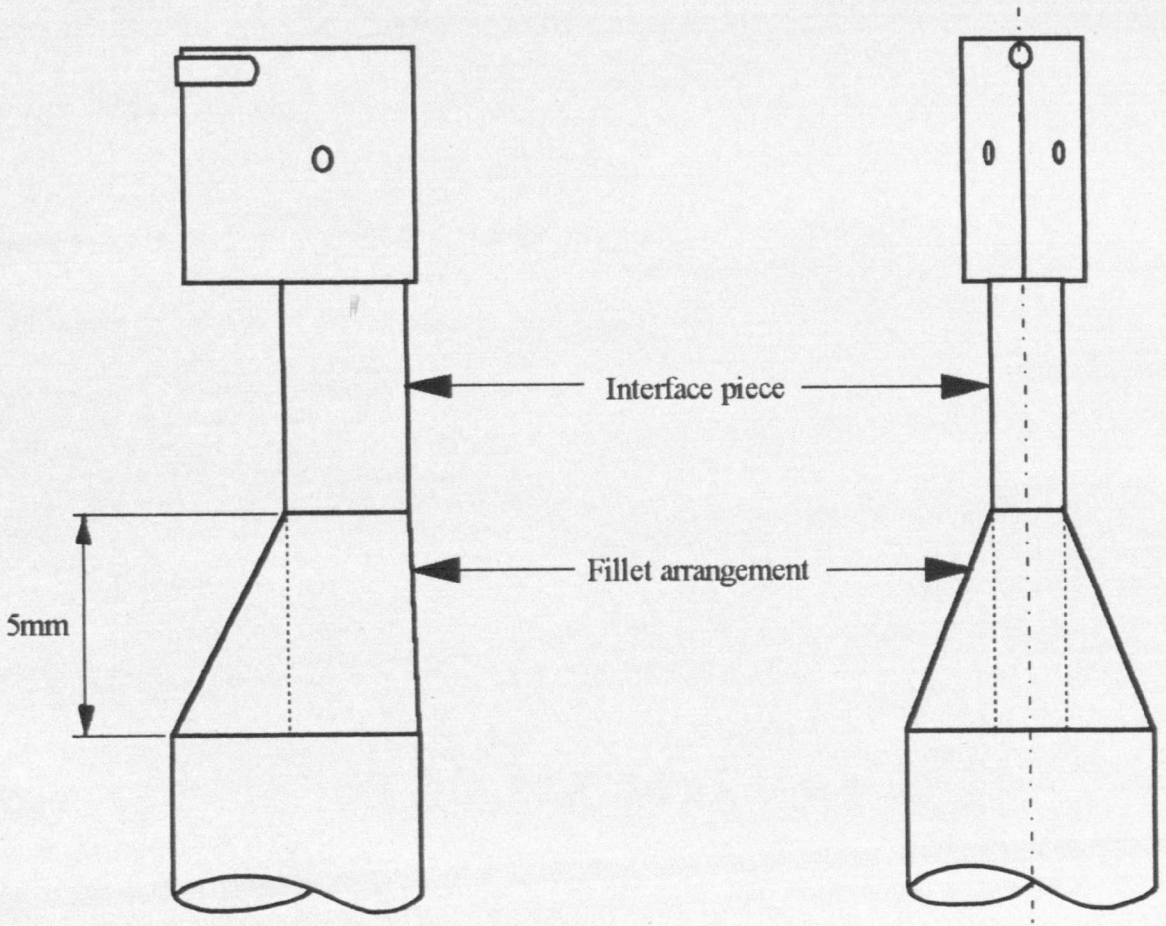

FIGURE 5.4: Fillet Arrangement in Factorial Experiment

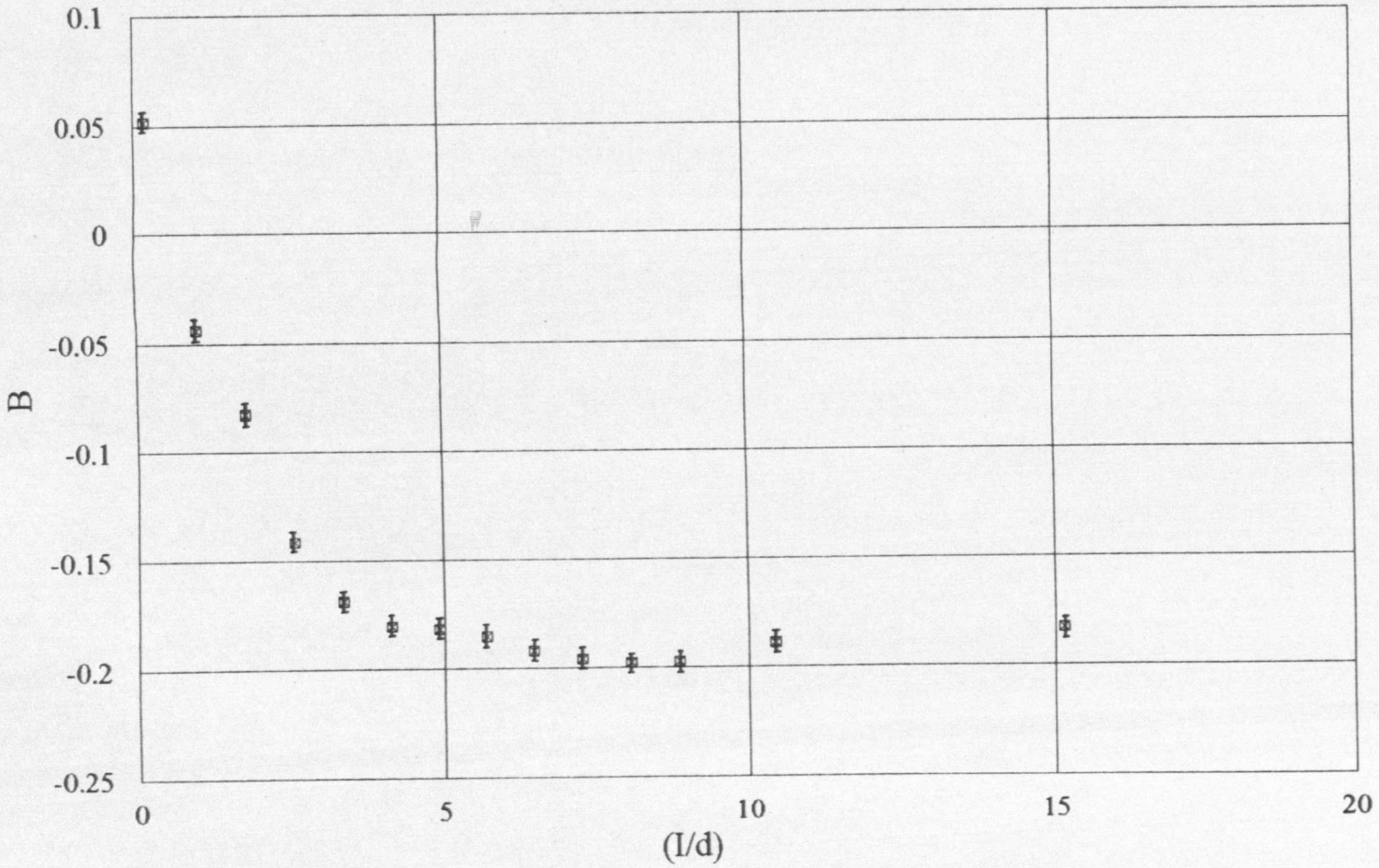

FIGURE 5.5: Wall Proximity Effect Result for Expt.9 of Factorial Experiment

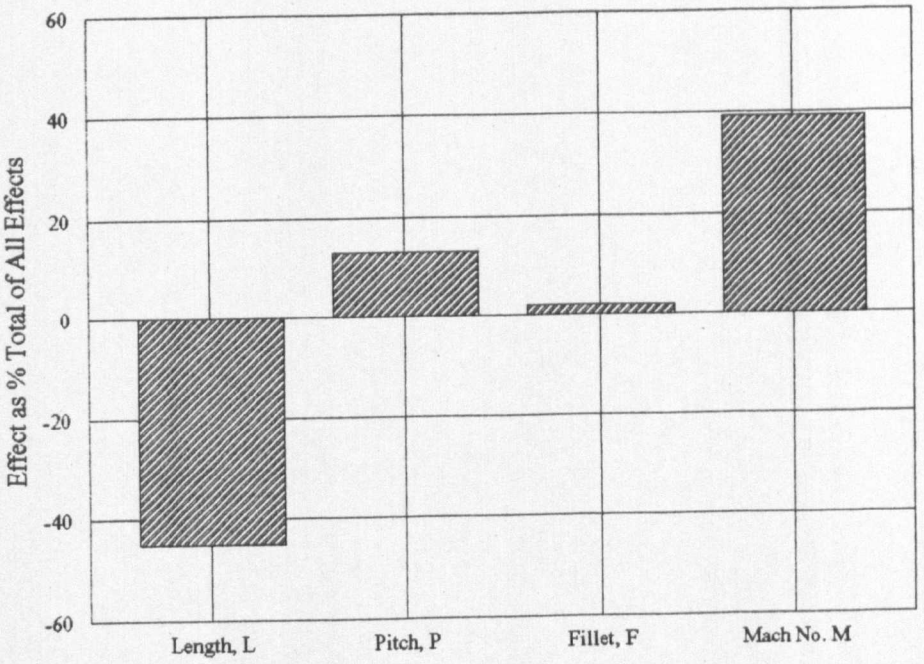

FIGURE 5.6a): Relative Effects of Four Variables of Sub-set 1

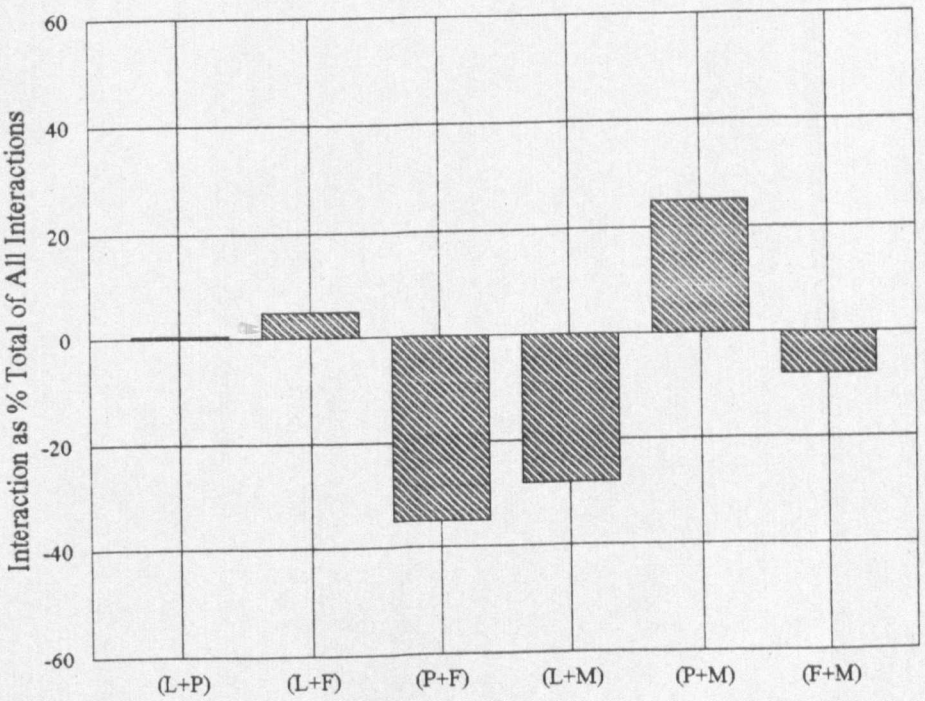

FIGURE 5.6b): Relative Interactions Between Four Variables of Sub-set 1

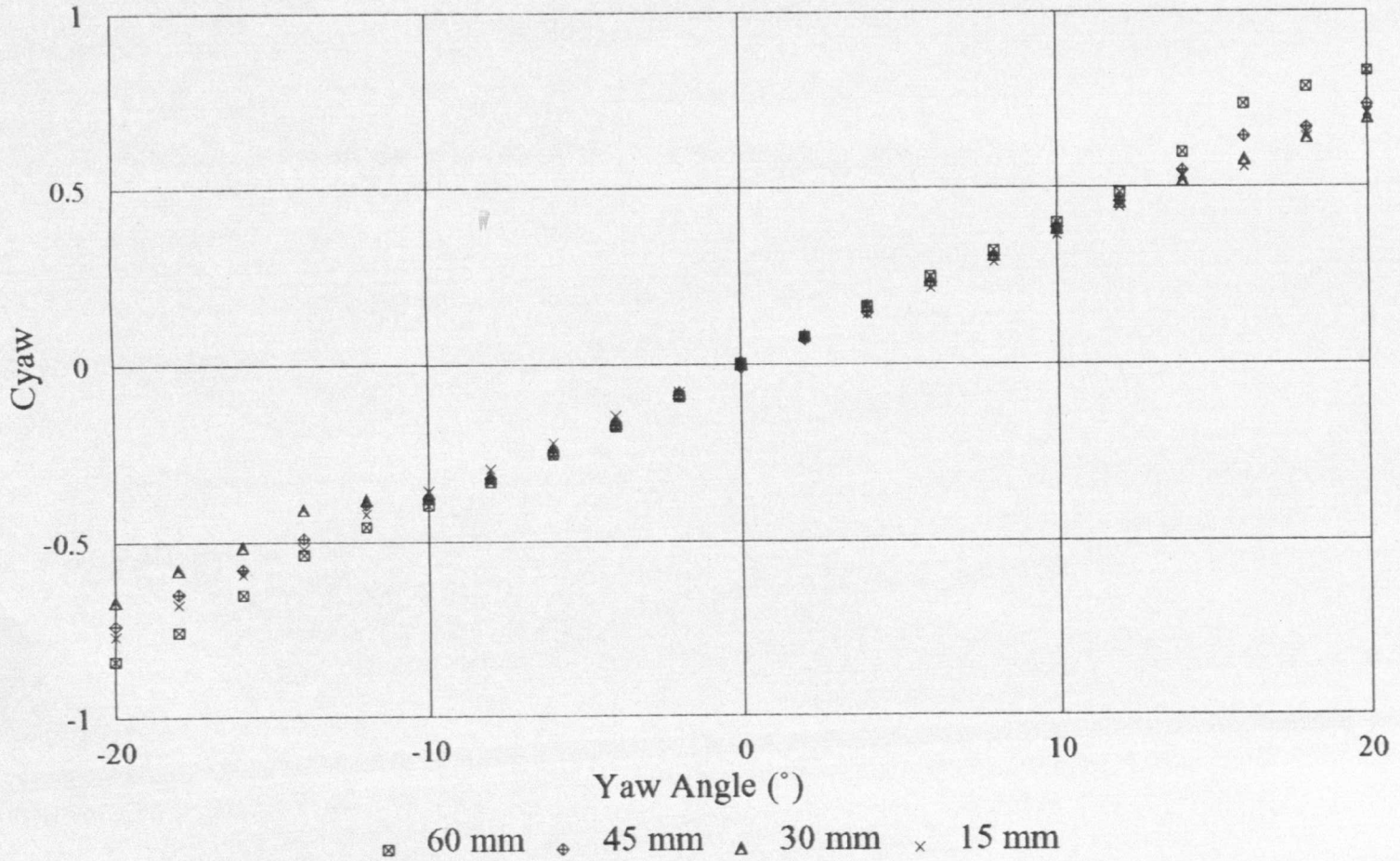

FIGURE 5.7: 30° Wedge Probe Calibration at 0.1Mach No. and Four Immersions

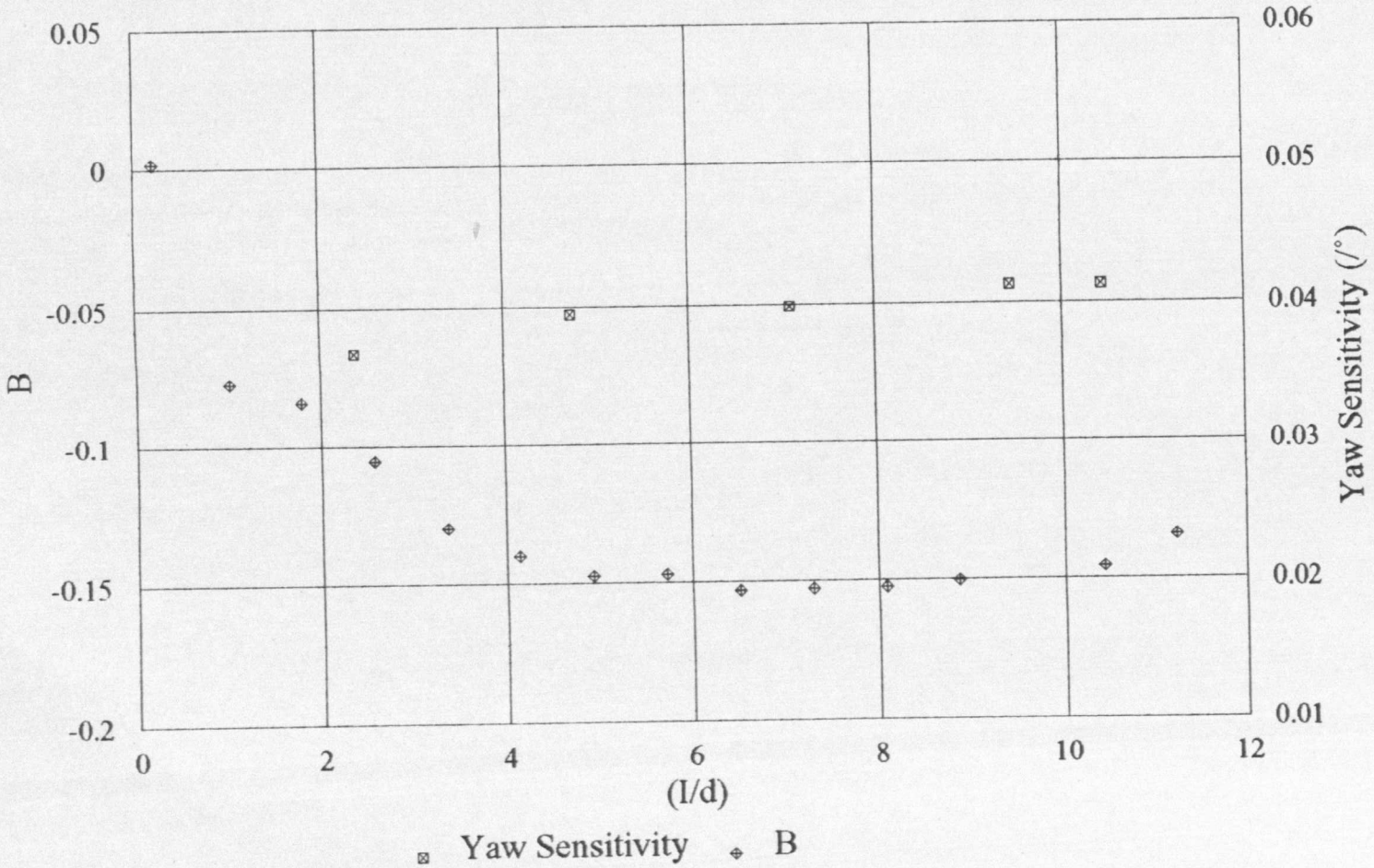

FIGURE 5.8: 30° Wedge Probe Calibration Against Immersion at 0.1 Mach No.

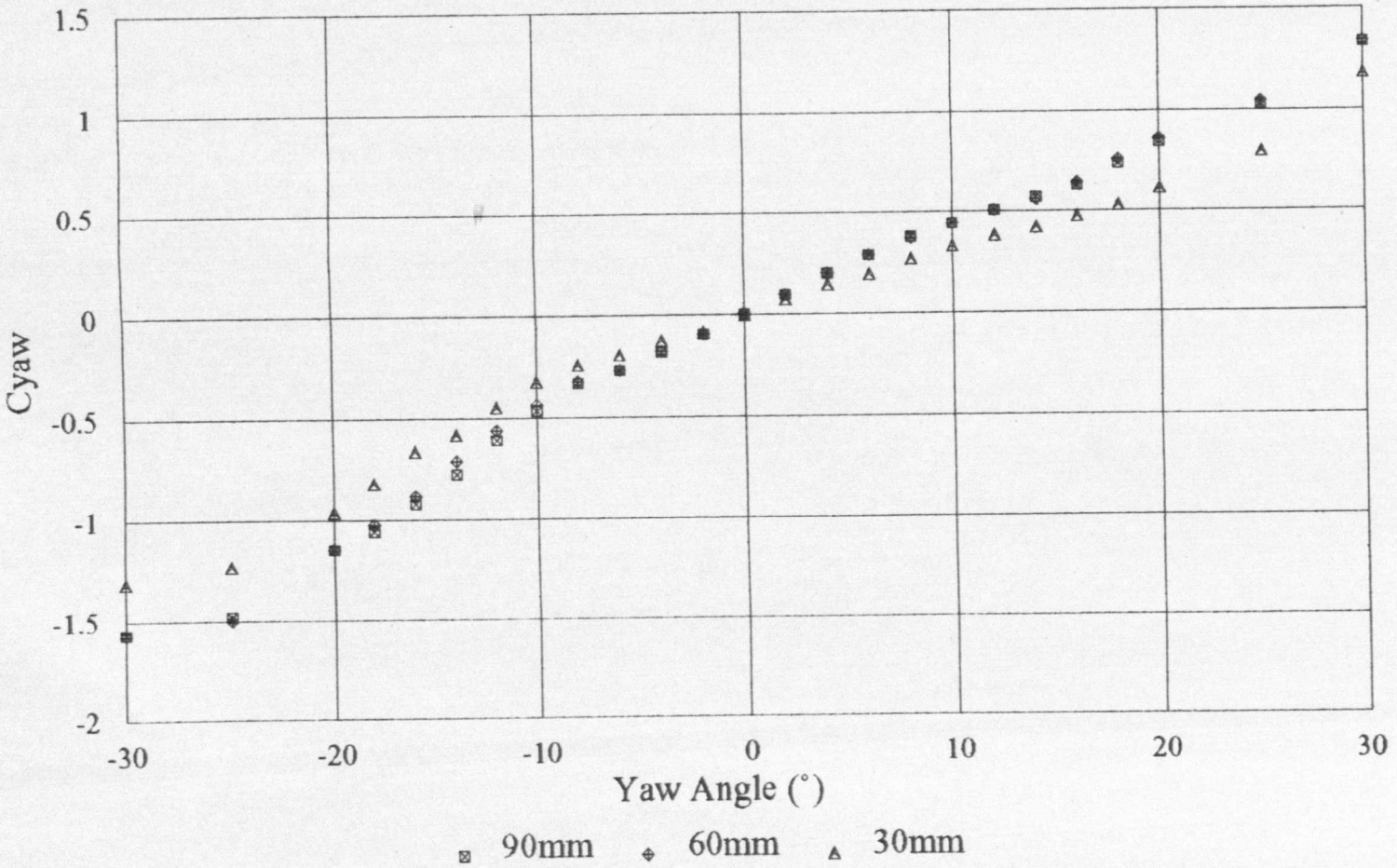

FIGURE 5.9: Wedge Probe 24SF Calibration at 0.35Mach No. and Three Immersions

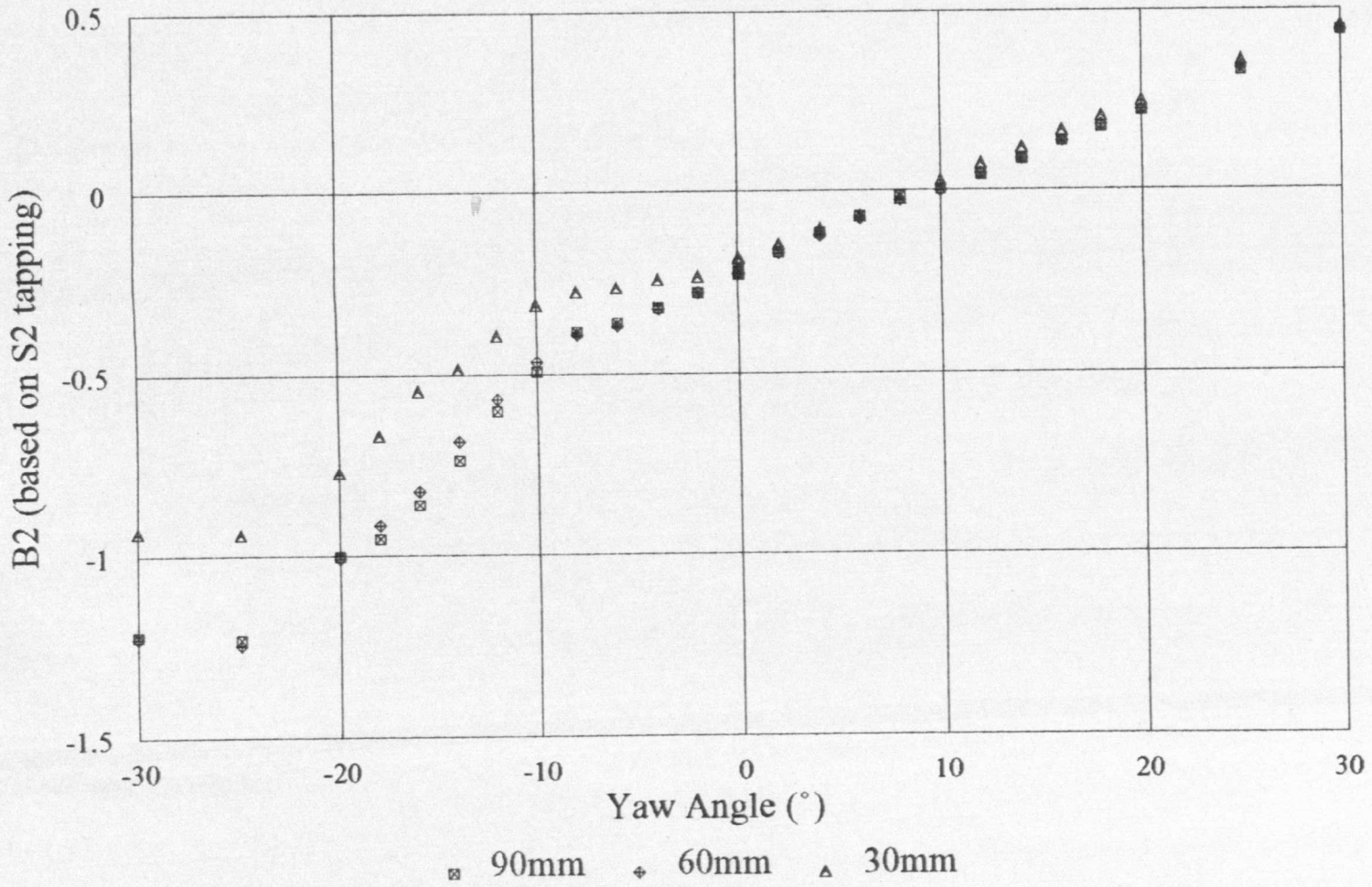

FIGURE 5.10: Wedge Probe 24SF Calibration at 0.35Mach No. and Three Immersions

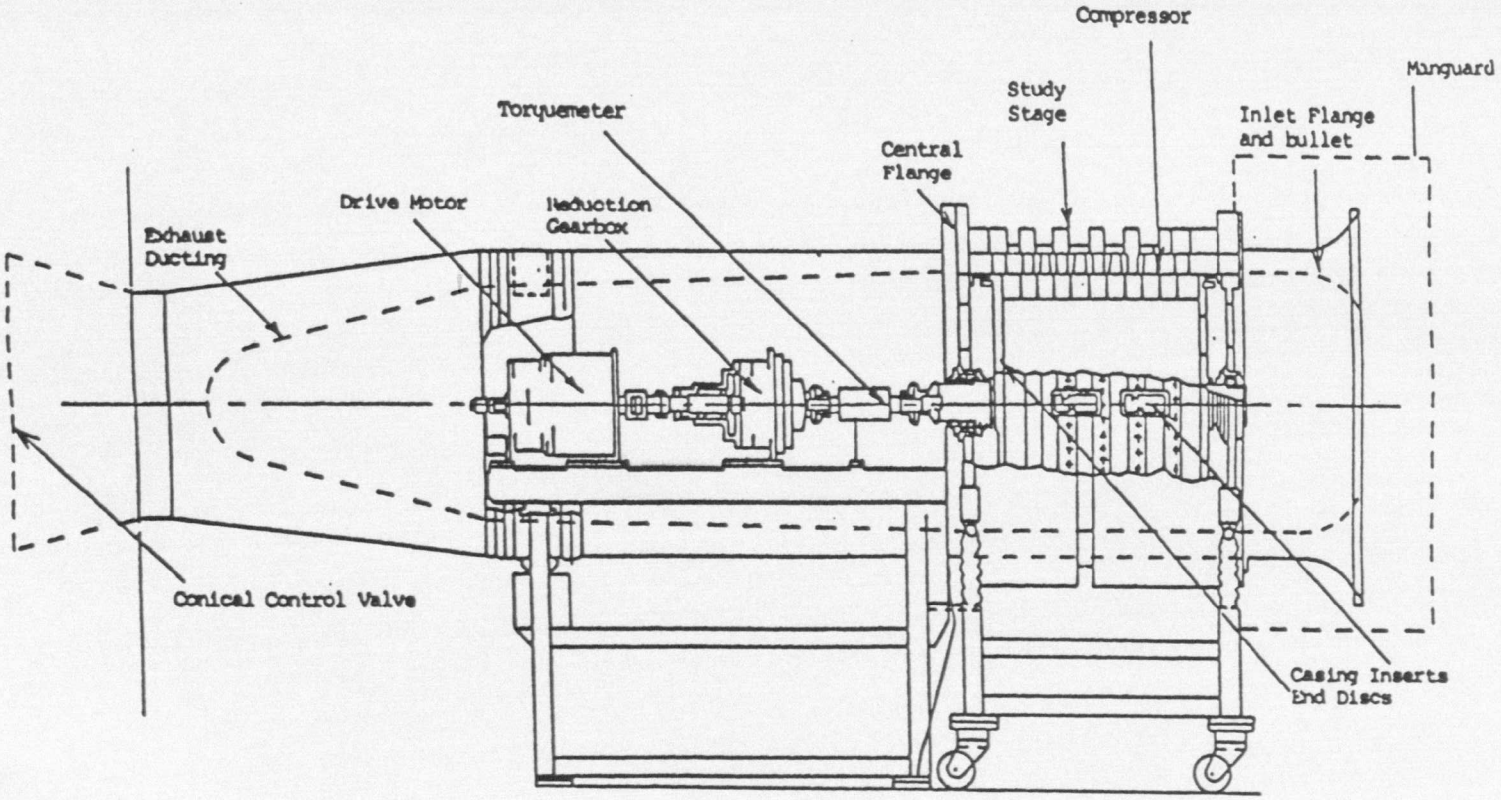

FIGURE 5.11: Cranfield University 4-Stage, Low Speed Large Scale Compressor Rig

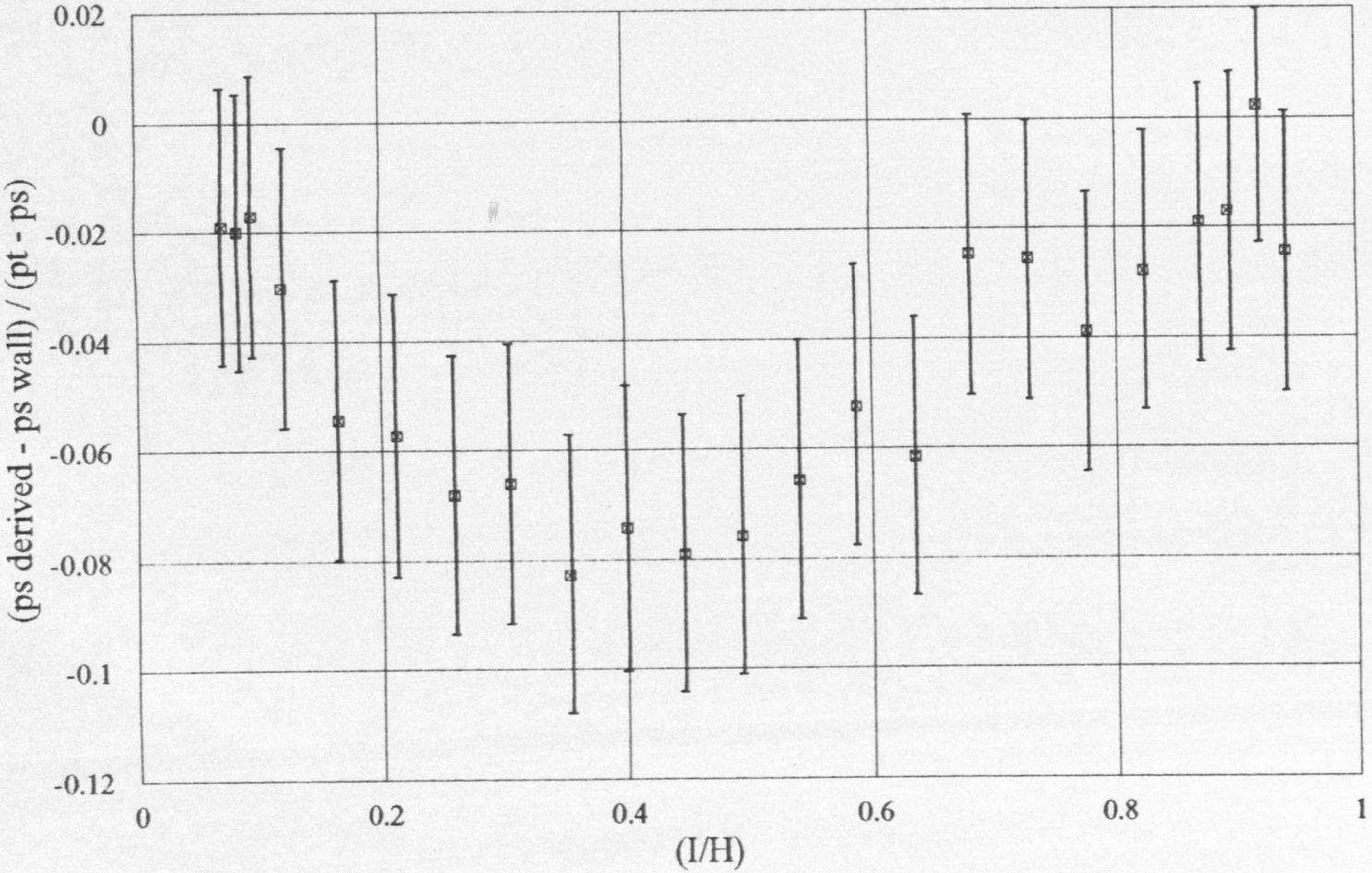

FIGURE 5.12: Derived Static Pressure Profile at IGV Inlet Plane of 4-Stage Rig

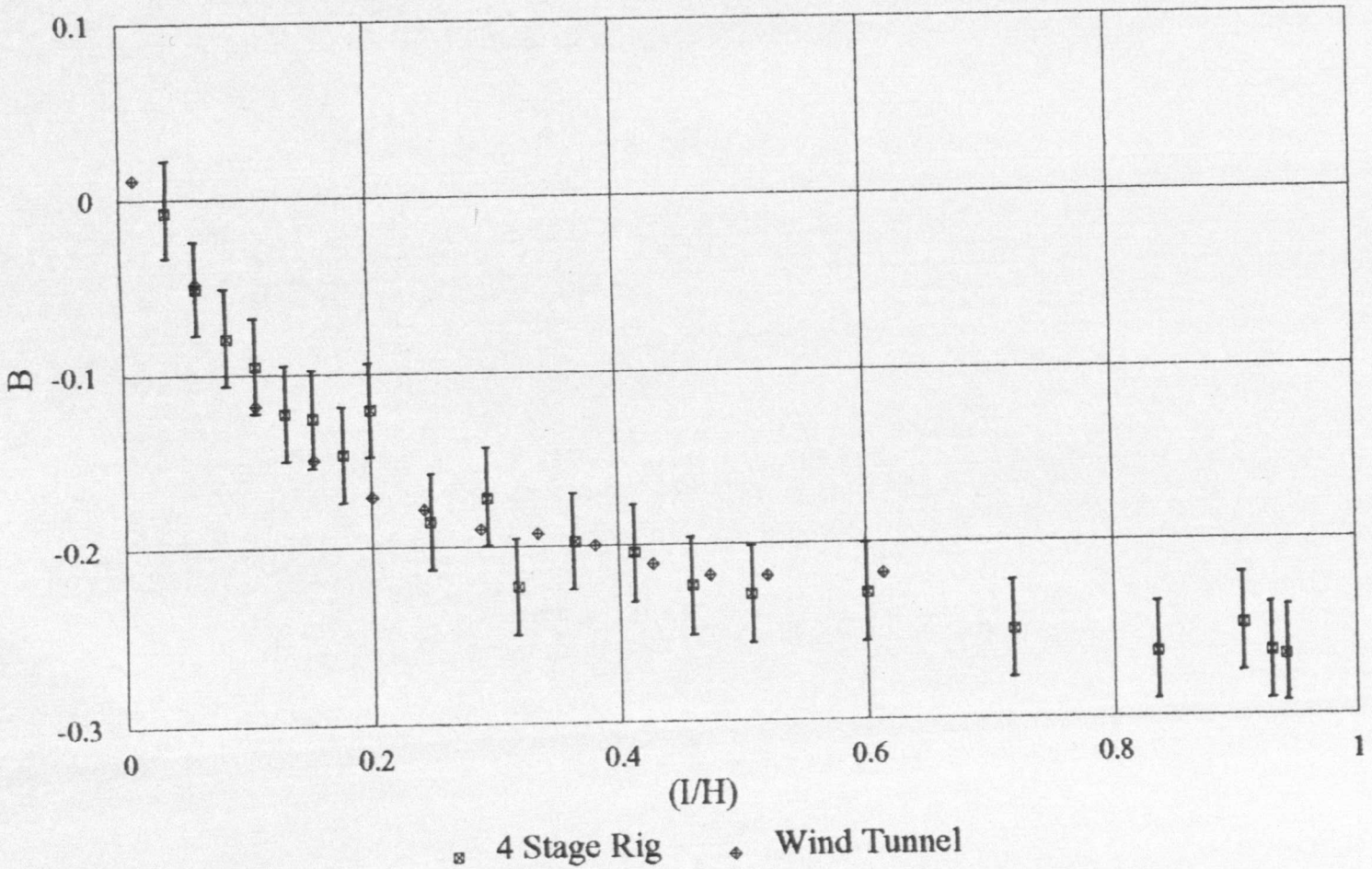

FIGURE 5.13: Comparison Between Wall Proximity Curves for Probe 24SF in Circular and Annular Ducts

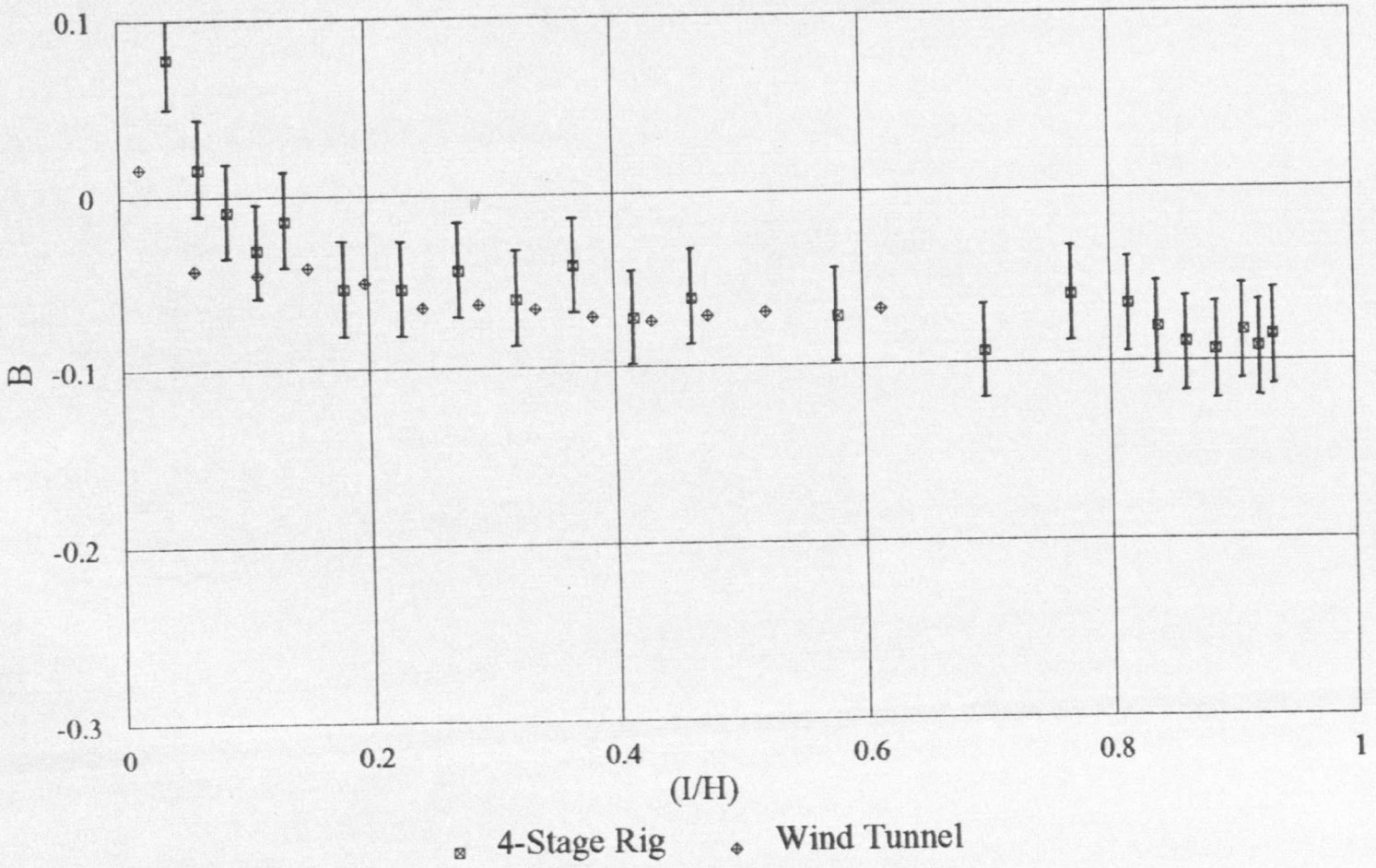

FIGURE 5.14: Comparison Between Wall Proximity Curves for Probe 24LF in Circular and Annular Ducts

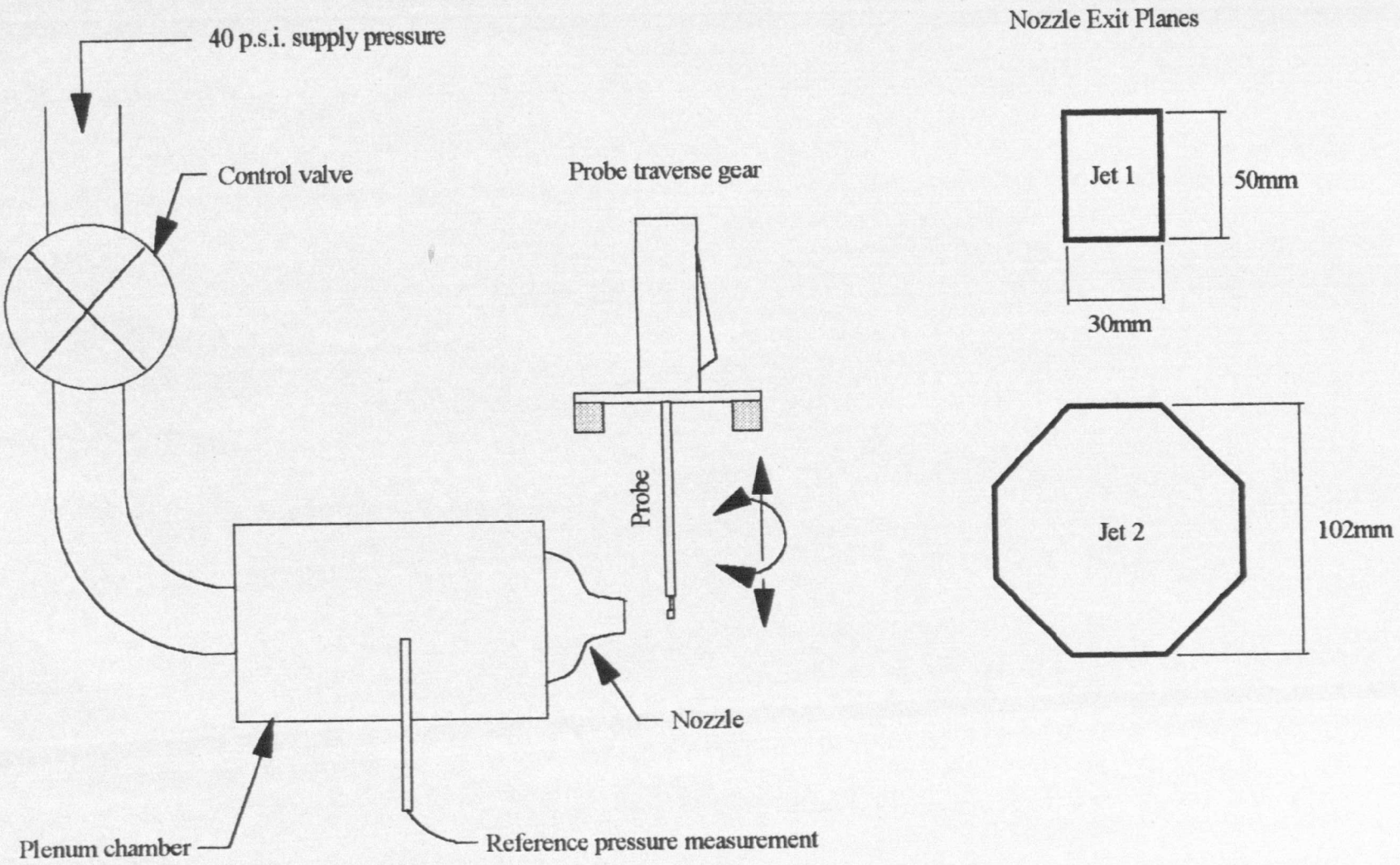

FIGURE 5.15: Arrangement of Open Jet Probe Calibration Facilities

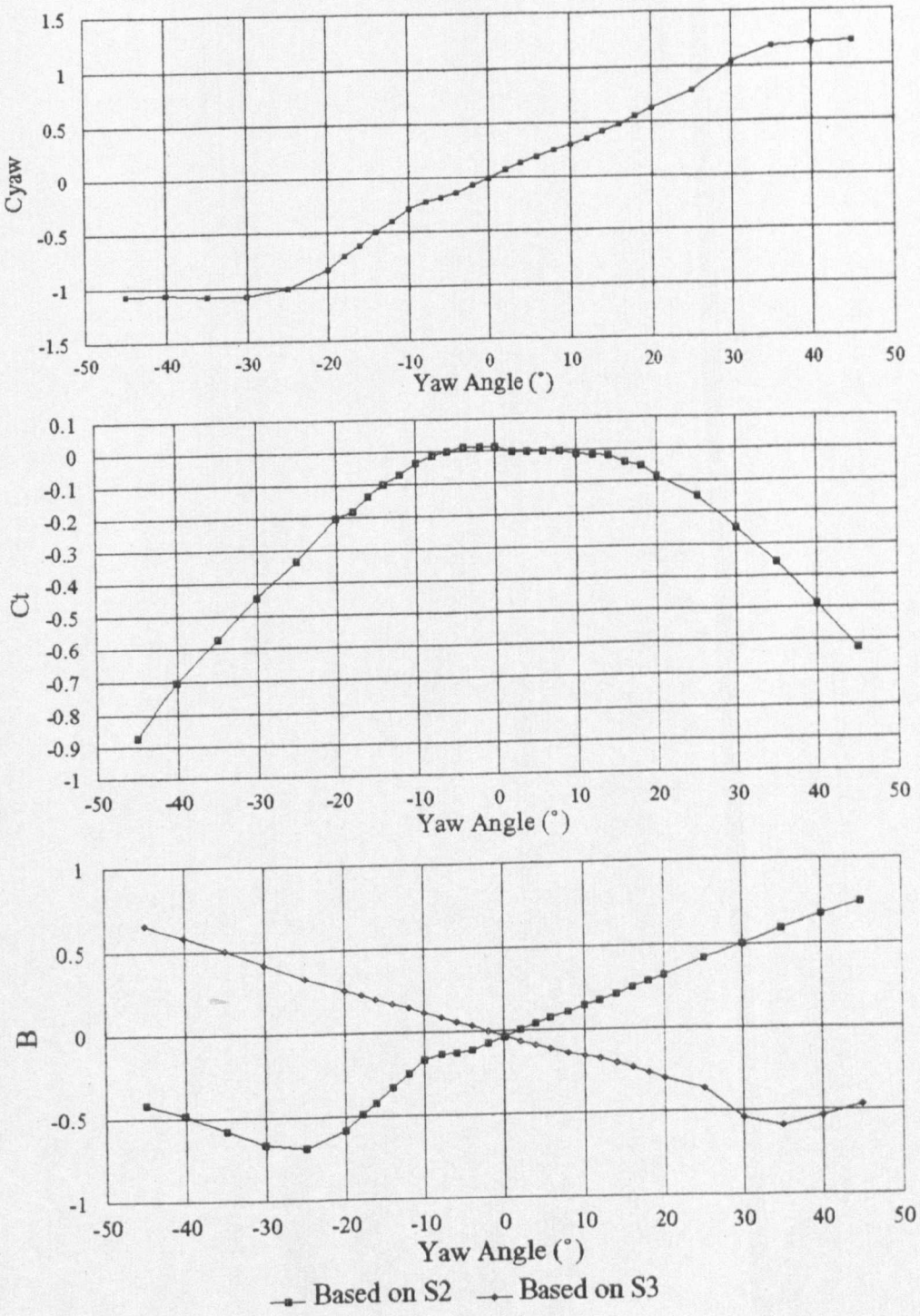

FIGURE 5.16: Calibration of Probe 24LF in Jet 1 at 0.35 Mach Number

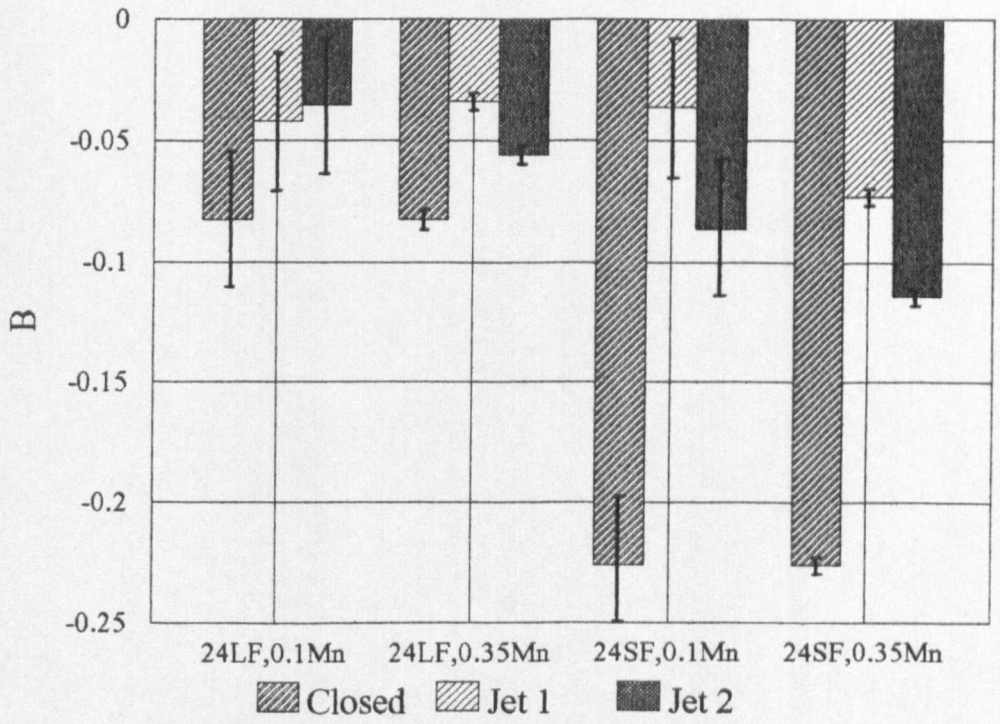

FIGURE 5.17a): Comparison Between B Values for 24° Probes in Open and Closed Flows

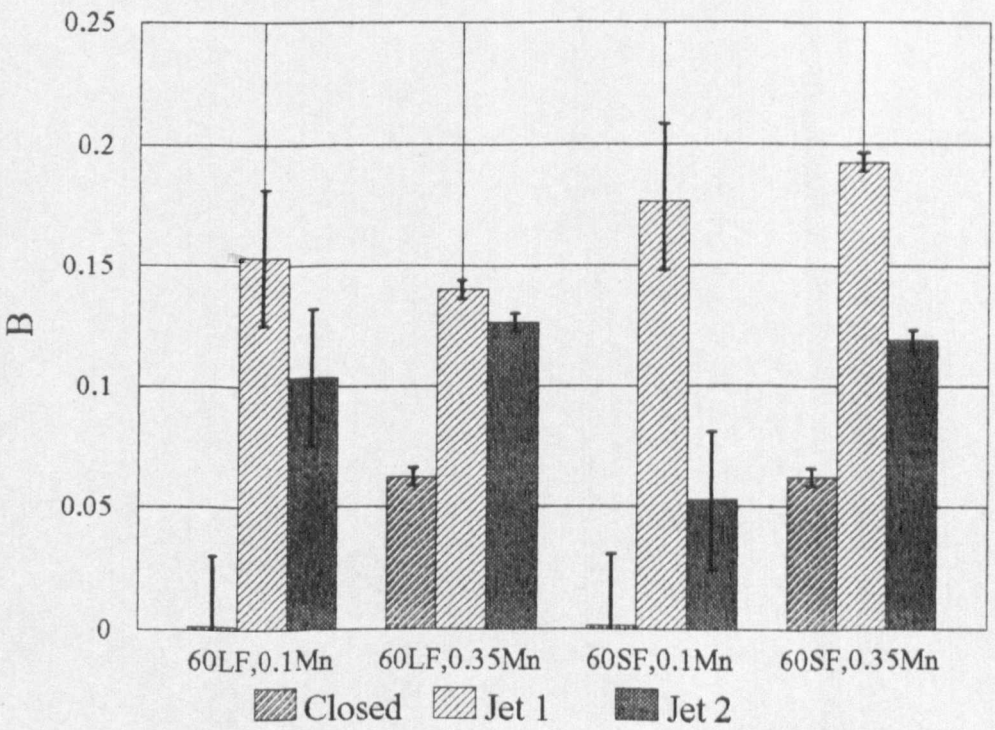

FIGURE 5.17b): Comparison Between B Values for 60° Probes in Open and Closed Flows

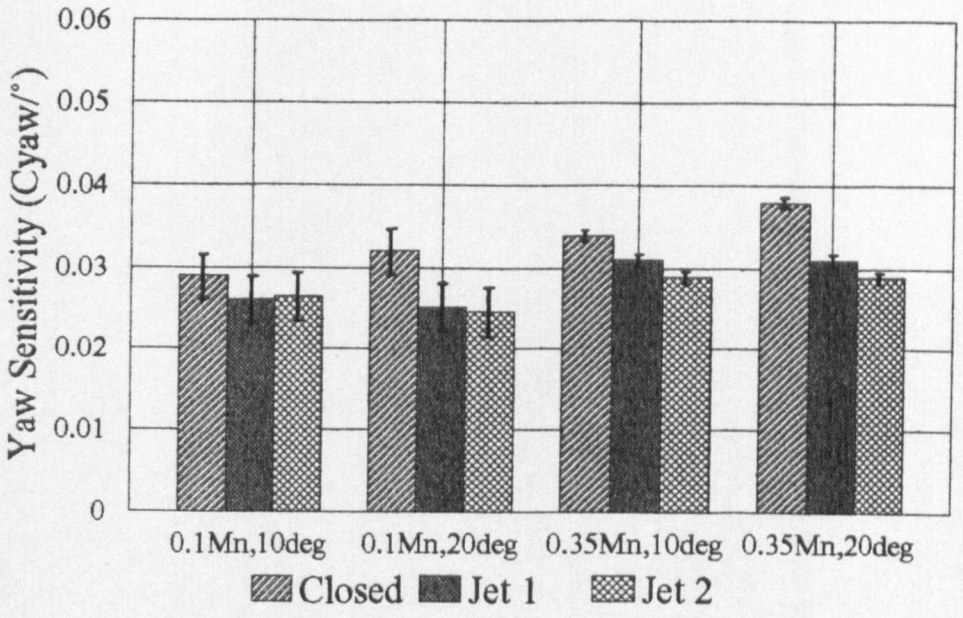

FIGURE 5.18a): Comparison Between Yaw Sensitivities of Probe 24LF In Open and Closed Flows

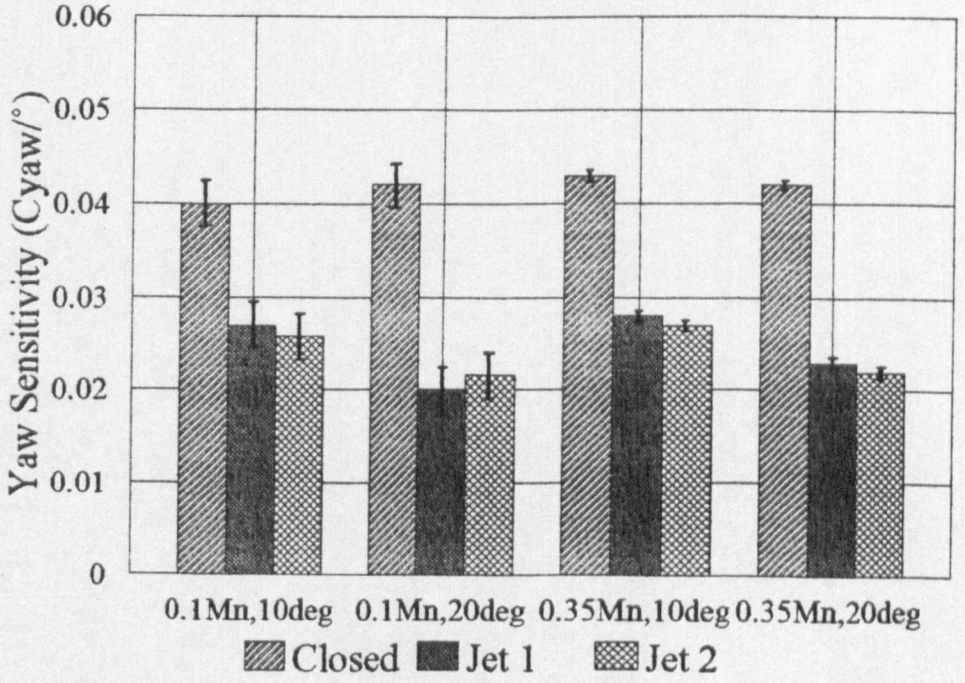

FIGURE 5.18b): Comparison Between Yaw Sensitivities of Probe 24SF In Open and Closed Flows

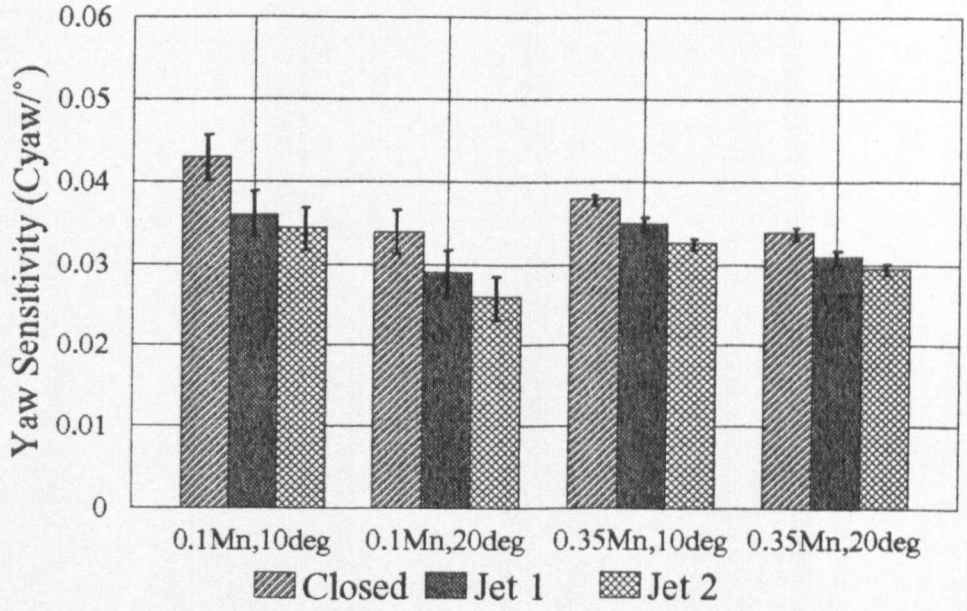

FIGURE 5.19a): Comparison Between Yaw Sensitivities of Probe 60LS In Open and Closed Flows

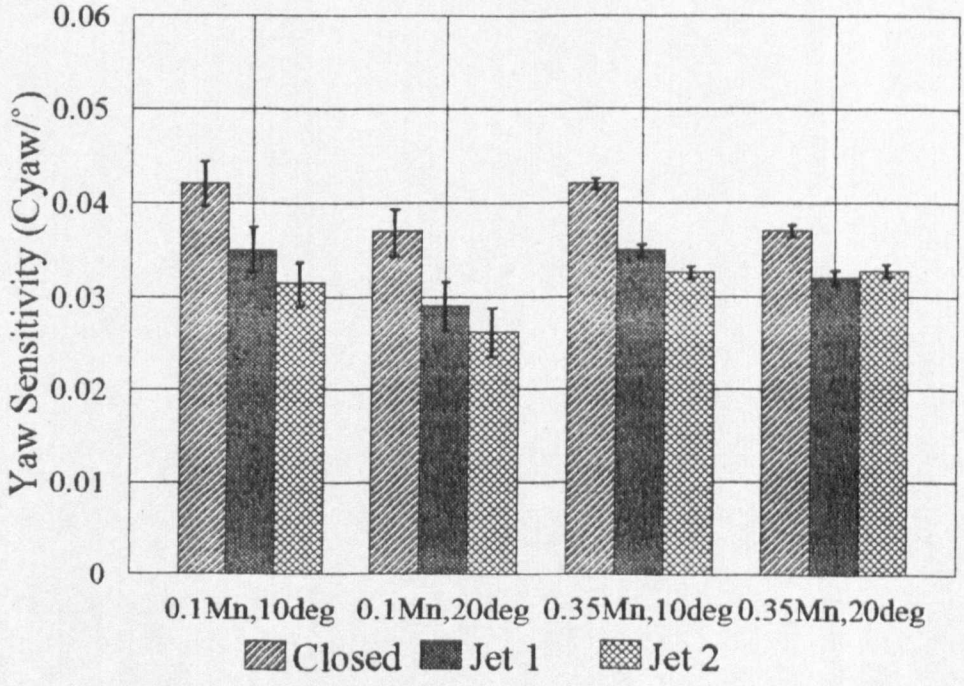

FIGURE 5.19b): Comparison Between Yaw Sensitivities of Probe 60SS In Open and Closed Flows

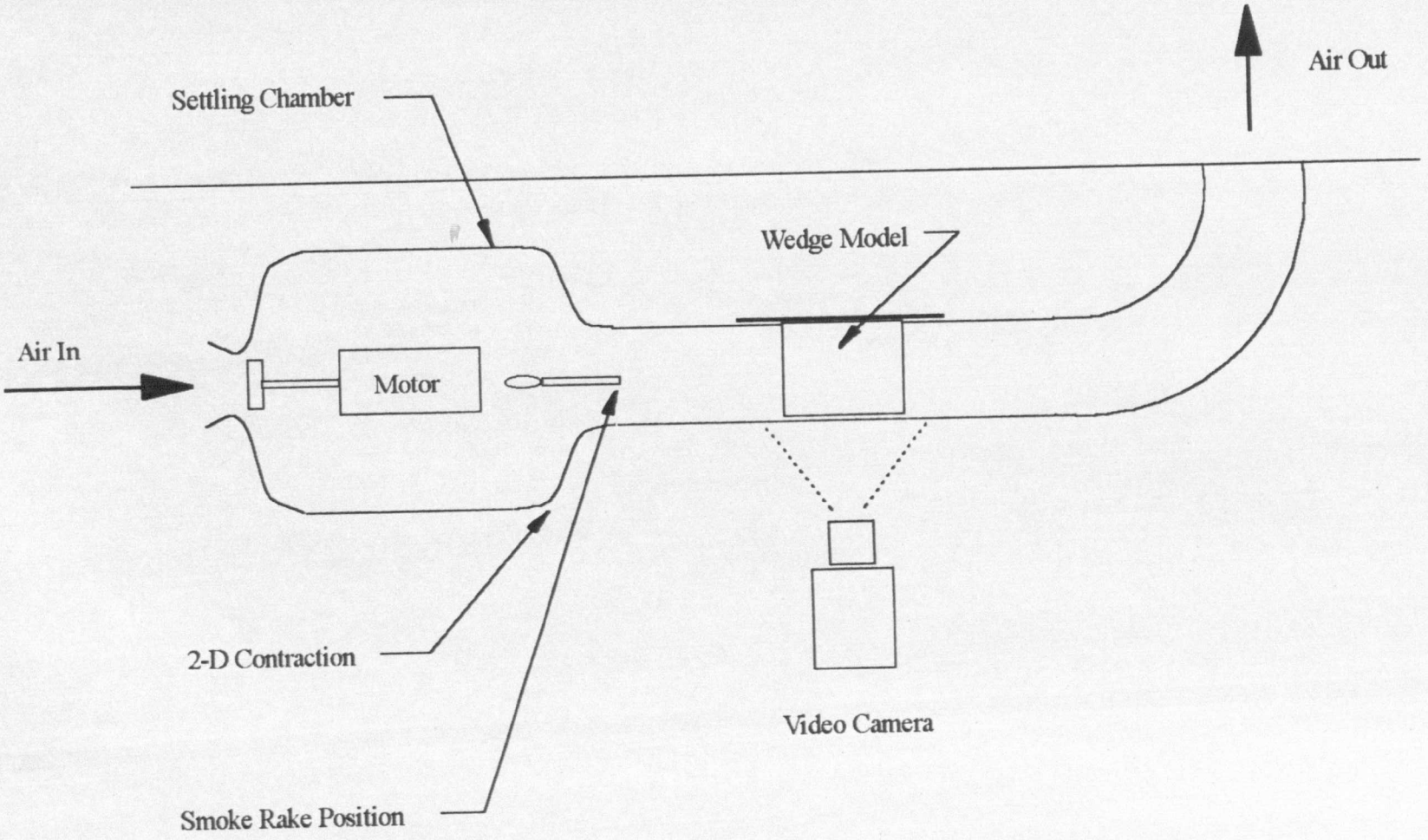

FIGURE 6.1: Cranfield 2-D Flow Visualisation Wind Tunnel

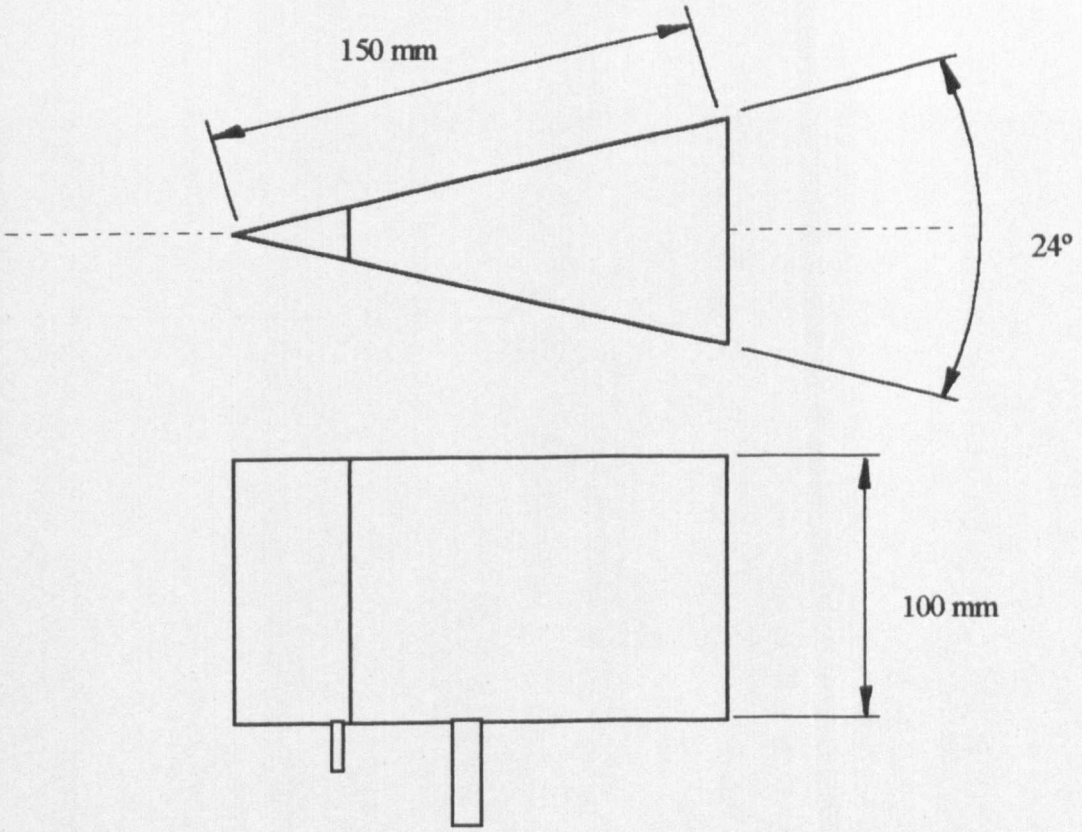

FIGURE 6.3a): 24° Wedge Model for 2-D Flow Visualisation Studies

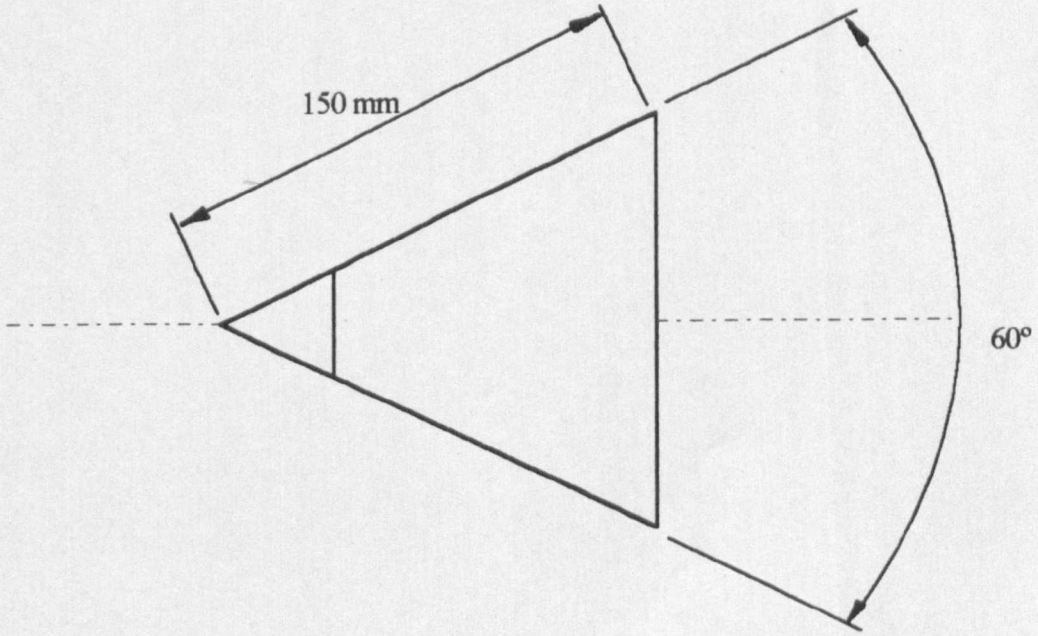

FIGURE 6.3b): 60° Wedge Model for 2-D Flow Visualisation Studies

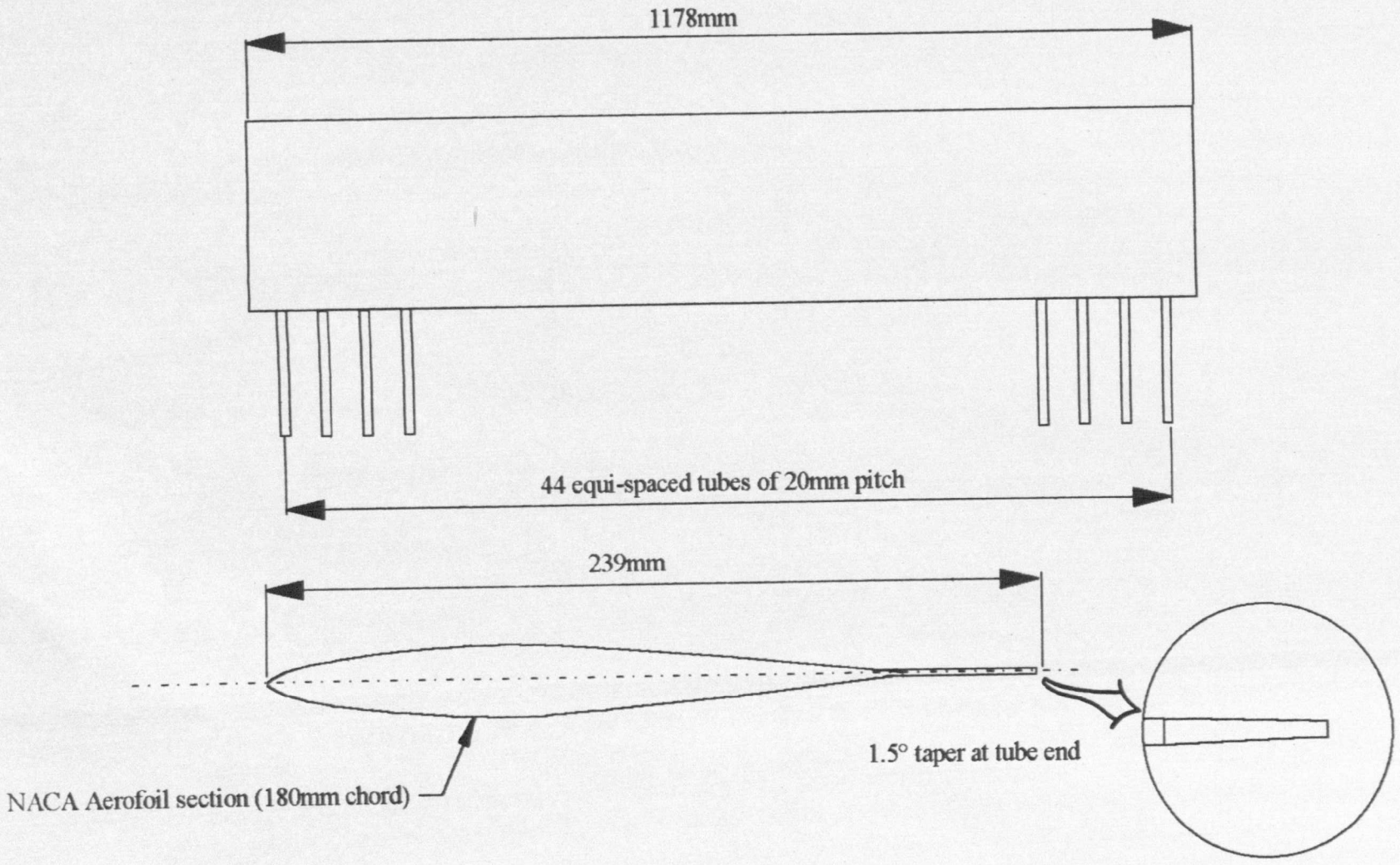

FIGURE 6.2: Cranfield 2-D Flow Visualisation Wind Tunnel Smoke Rake

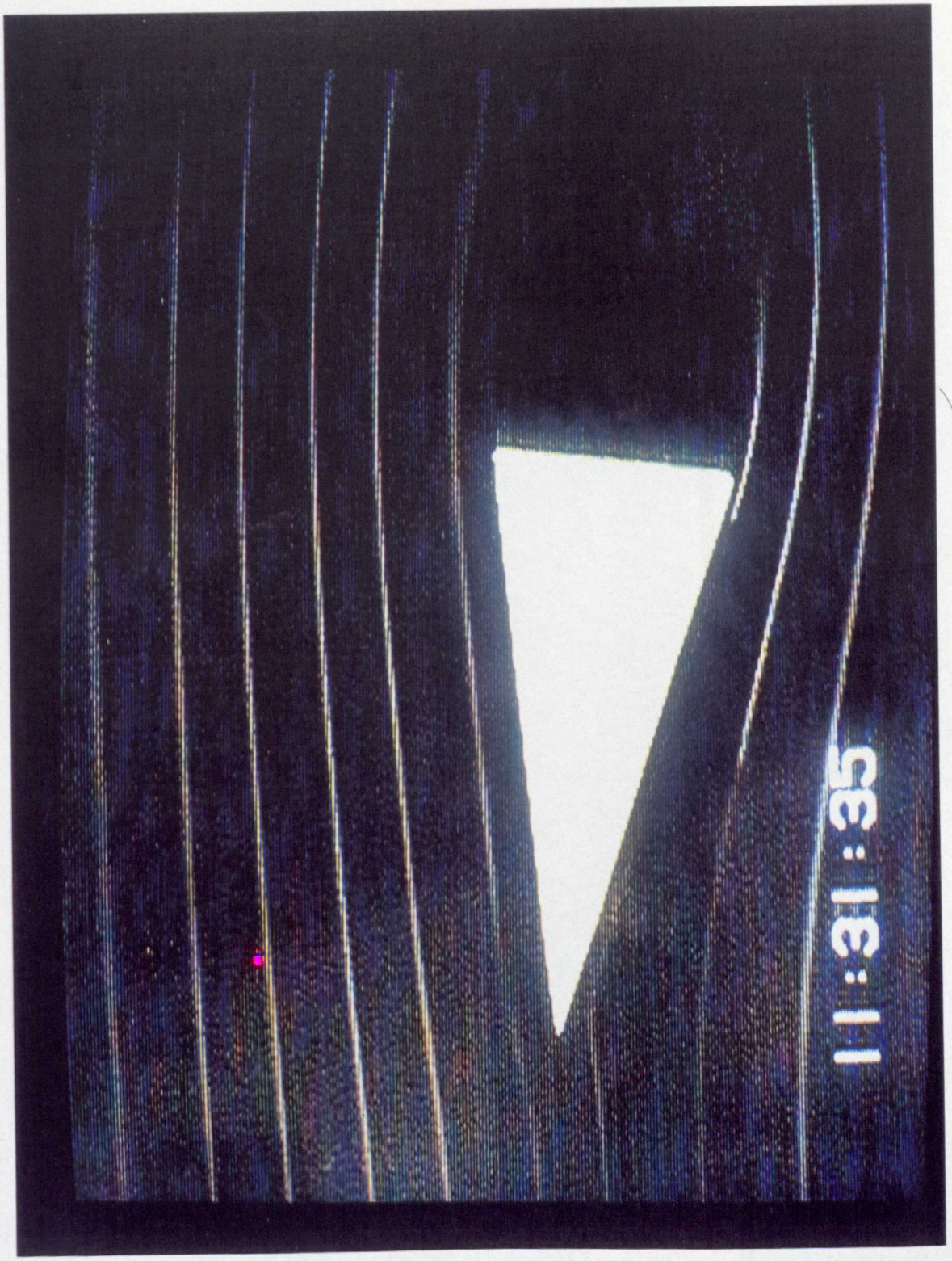

FIGURE 6.4a): Visualisation of Flow Over Two-Dimensional, Sharp Nosed, 24° Wedge Model at 4° Yaw and 5.2×10^4 Reynolds Number

Neg No: 94.2357.9

FIGURE 6.4b): Visualisation of Flow Over Two-Dimensional, Sharp Nosed, 24° Wedge Model at 8° Yaw and 5.2×10^4 Reynolds Number

Neg No: 94.2357.10

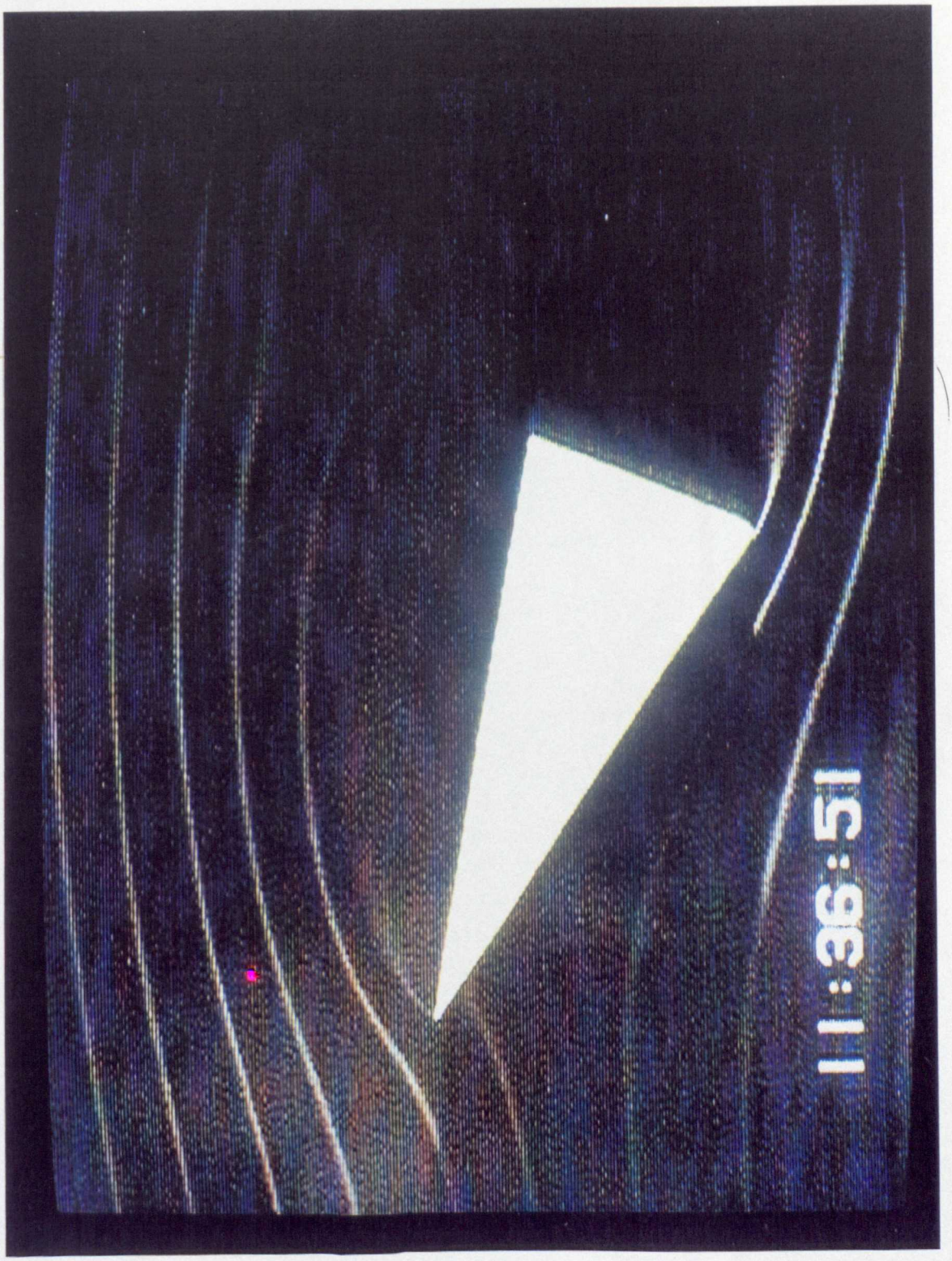

FIGURE 6.5: Visualisation of Flow Over Two-Dimensional, Sharp Nosed, 24° Wedge Model at 20° Yaw and 5.2×10^4 Reynolds Number

Neg No: 94.2357.11

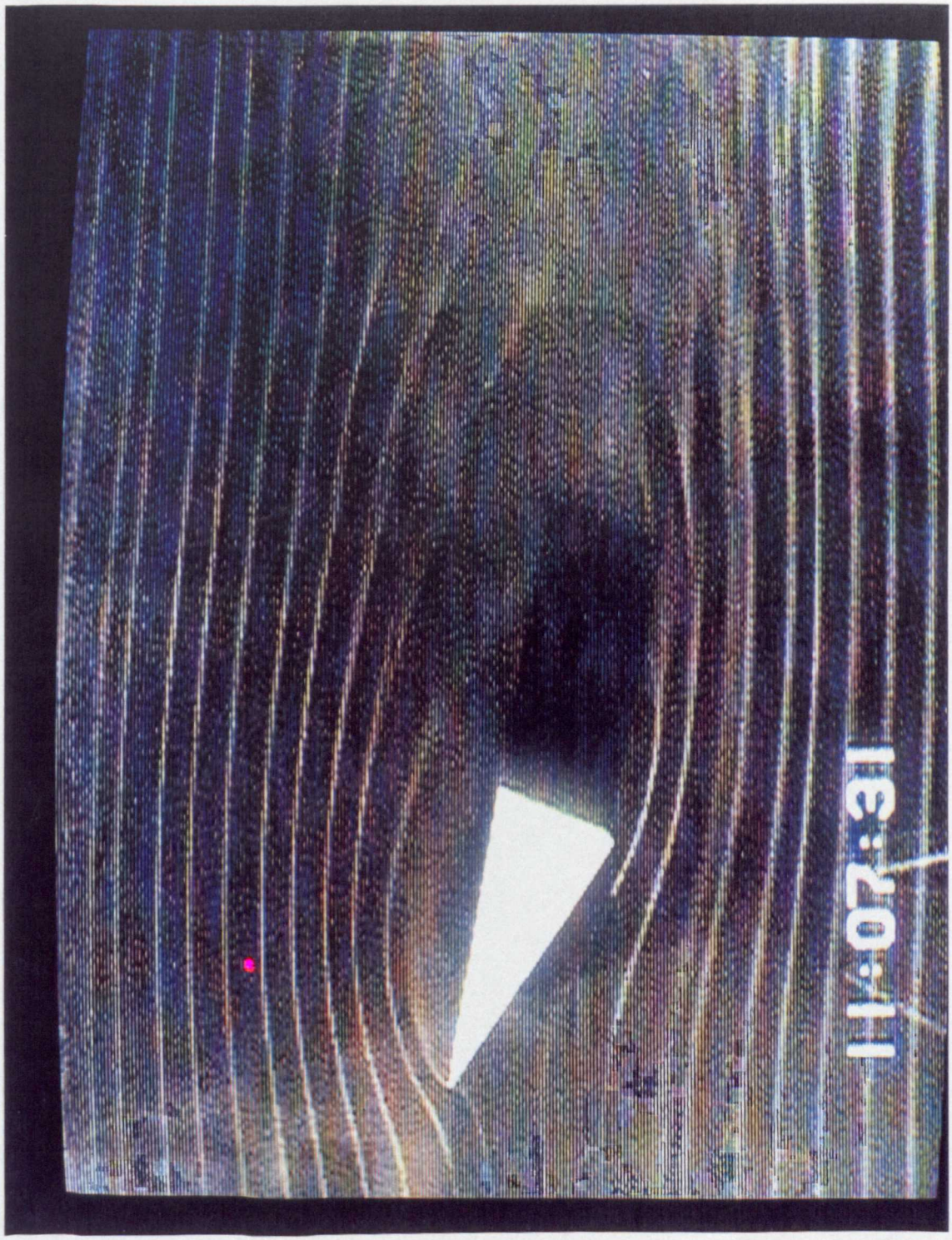

FIGURE 6.6: Visualisation of Flow Over Two-Dimensional, Sharp Nosed, 24° Wedge Model at 20° Yaw and 5.2×10^4 Reynolds Number - Far Field View

Neg No: 94.2357.8

FIGURE 6.7: Visualisation of Flow Over Two-Dimensional, Rounded Nose, 24° Wedge Model at 8° Yaw and 5.2×10^4 Reynolds Number

Neg No: 94.2374.2

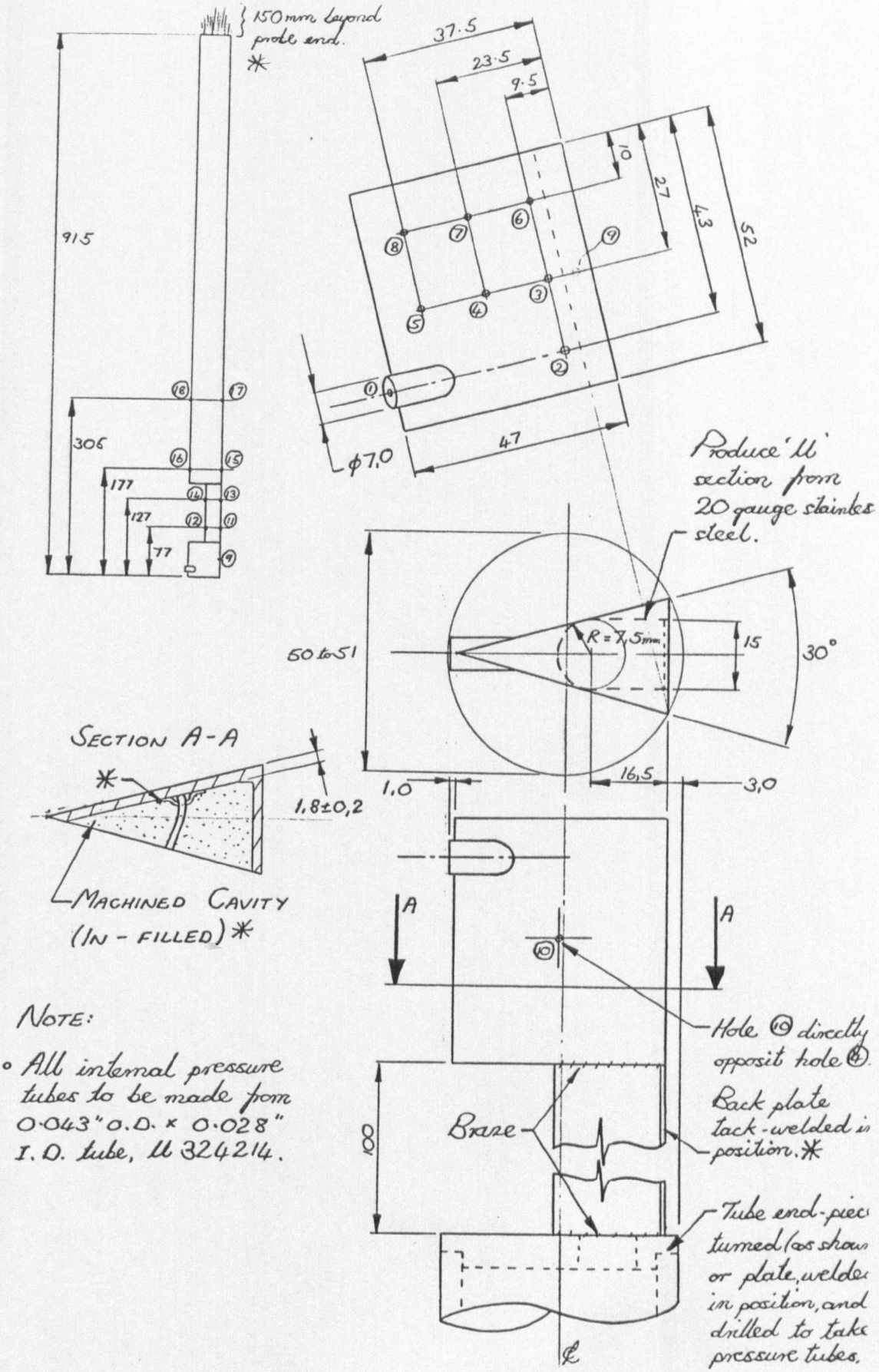

FIGURE 6.8: Large Scale Wedge Probe

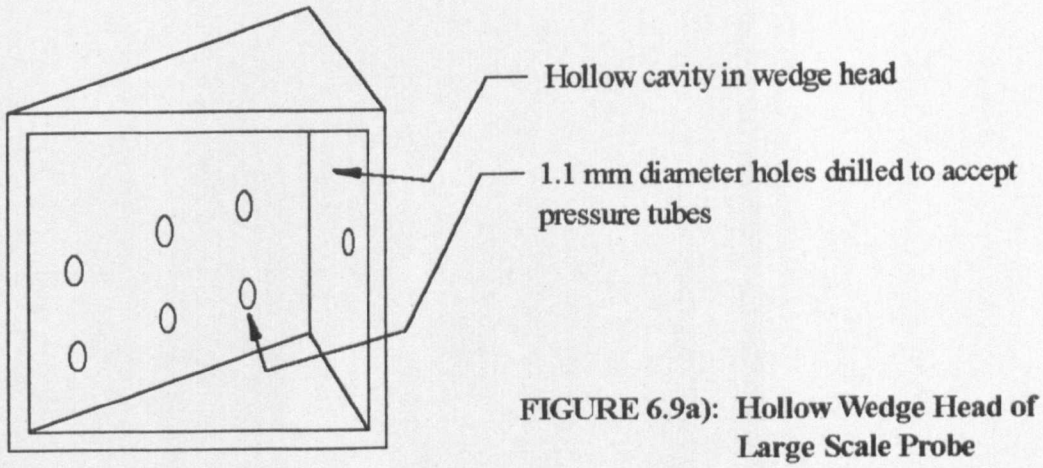

FIGURE 6.9a): Hollow Wedge Head of Large Scale Probe

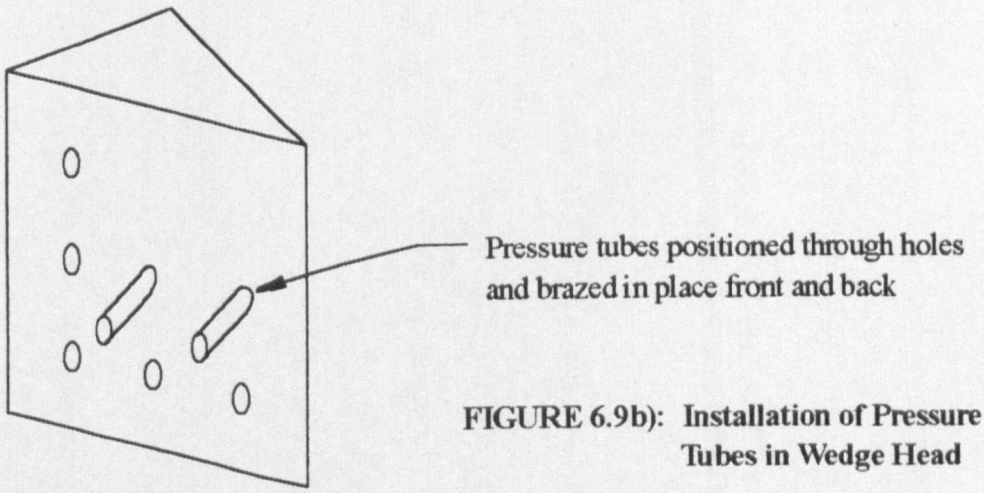

FIGURE 6.9b): Installation of Pressure Tubes in Wedge Head

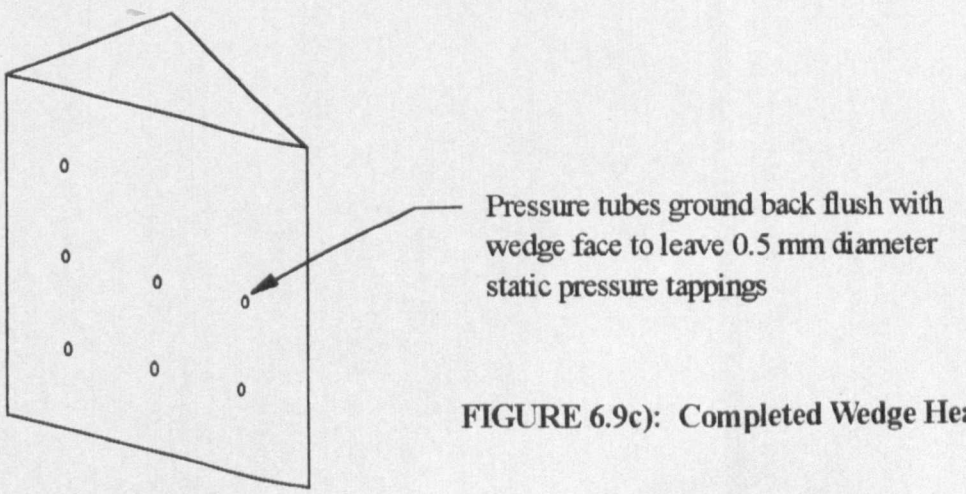

FIGURE 6.9c): Completed Wedge Head

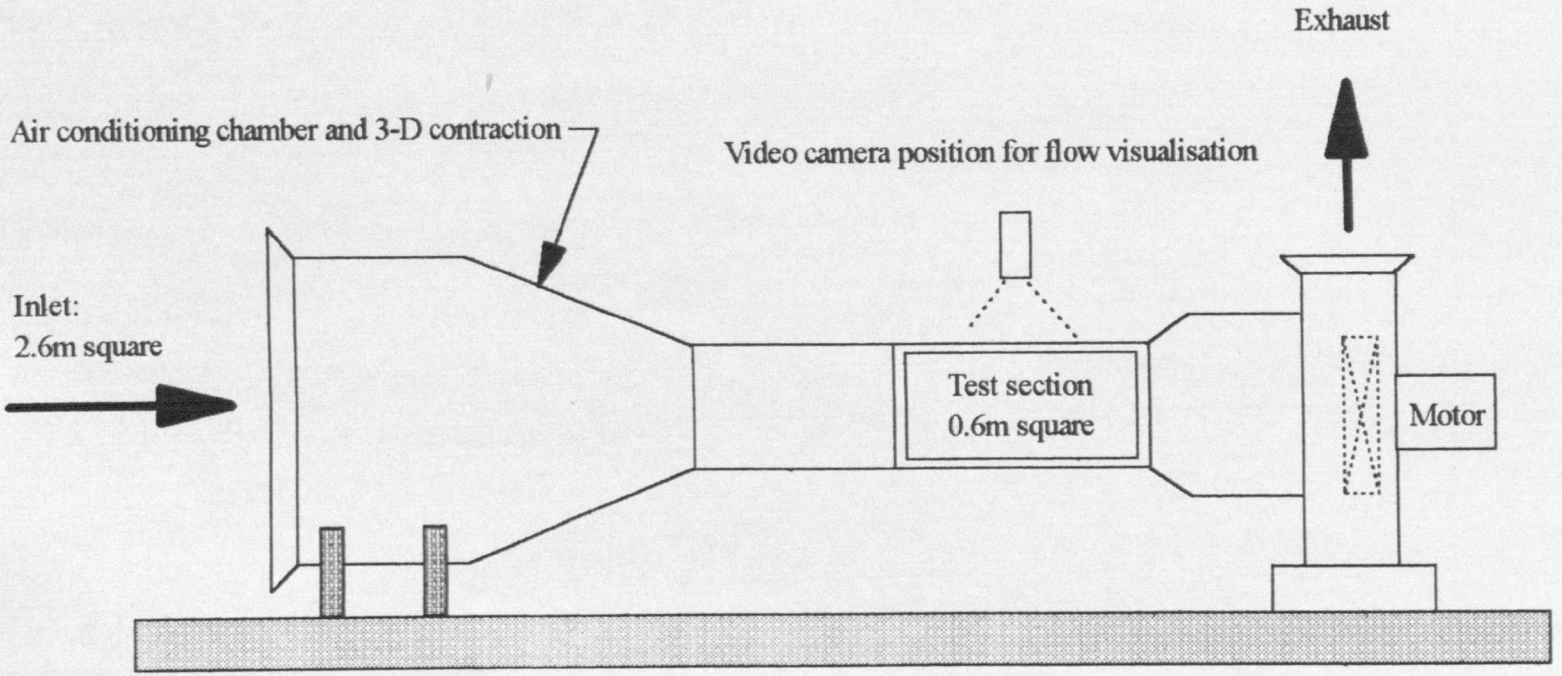

FIGURE 6.10: Sheffield University 3-D Flow Visualisation Wind Tunnel

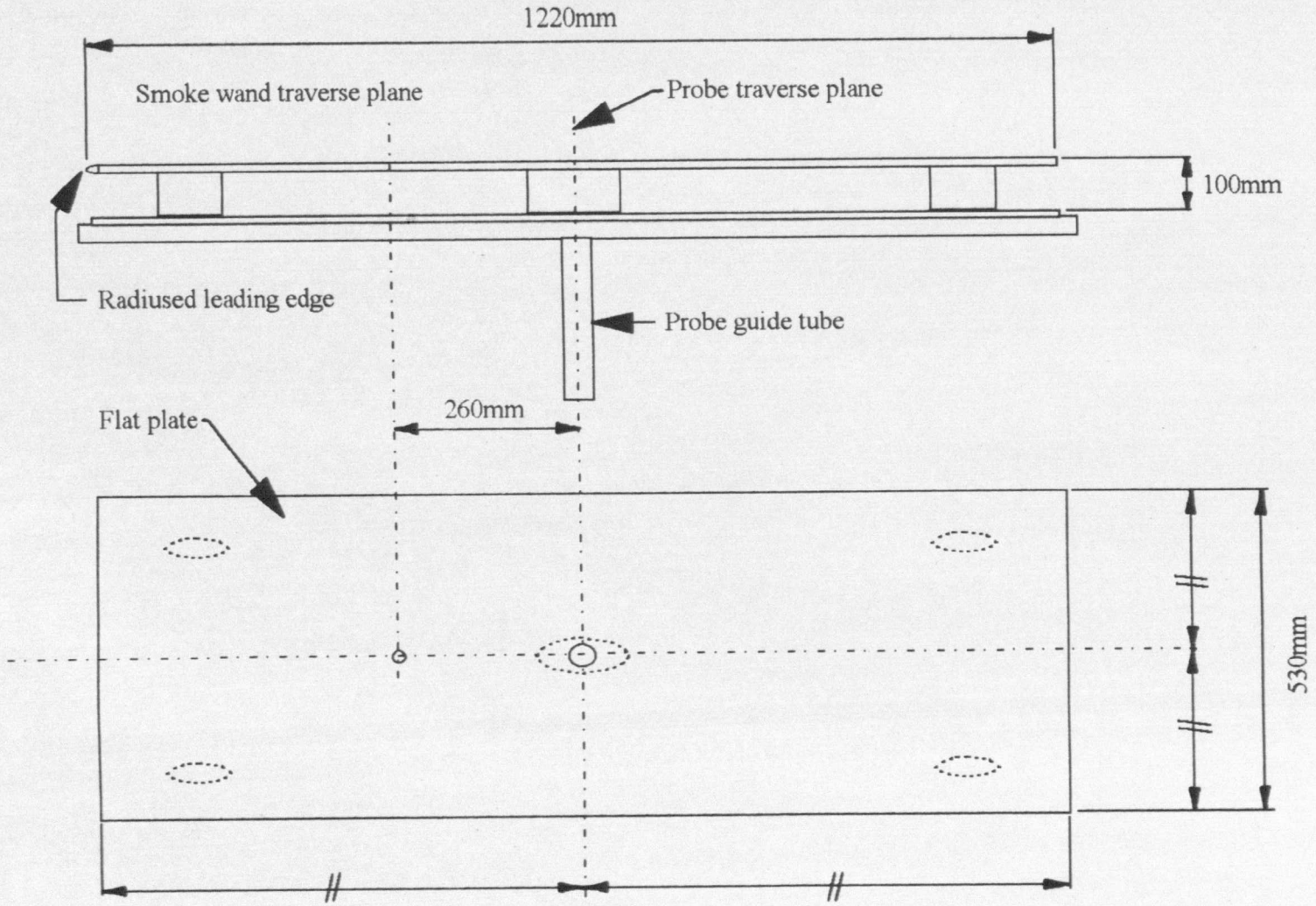

FIGURE 6.11: Detailed Drawing of Flat Plate Installed in Sheffield University Wind Tunnel

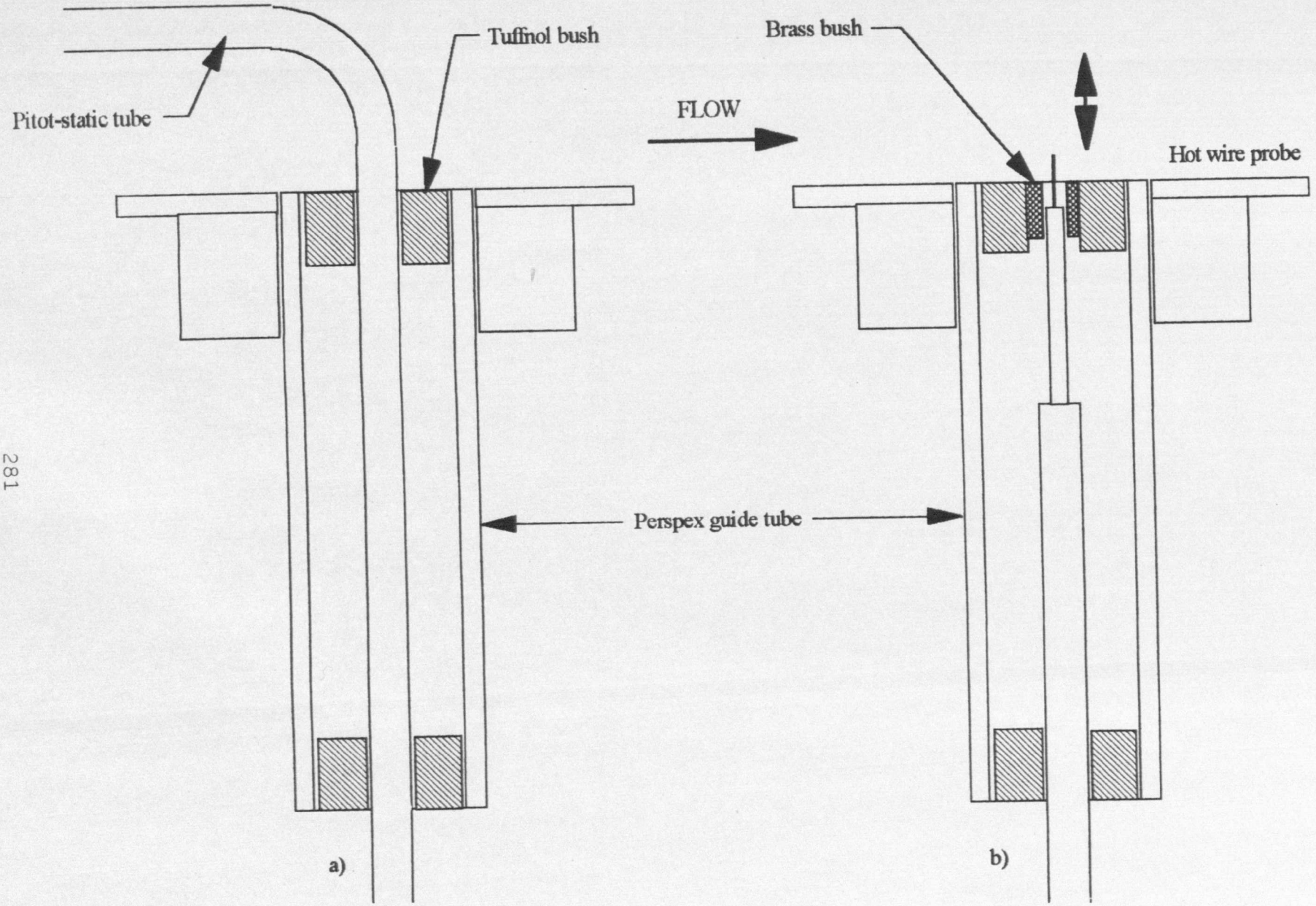

FIGURE 6.12: Traverse Probe Mounting Arrangements: a) Tuffnel bushes to support pitot-static tube, b) Brass bush to support hot wire probe

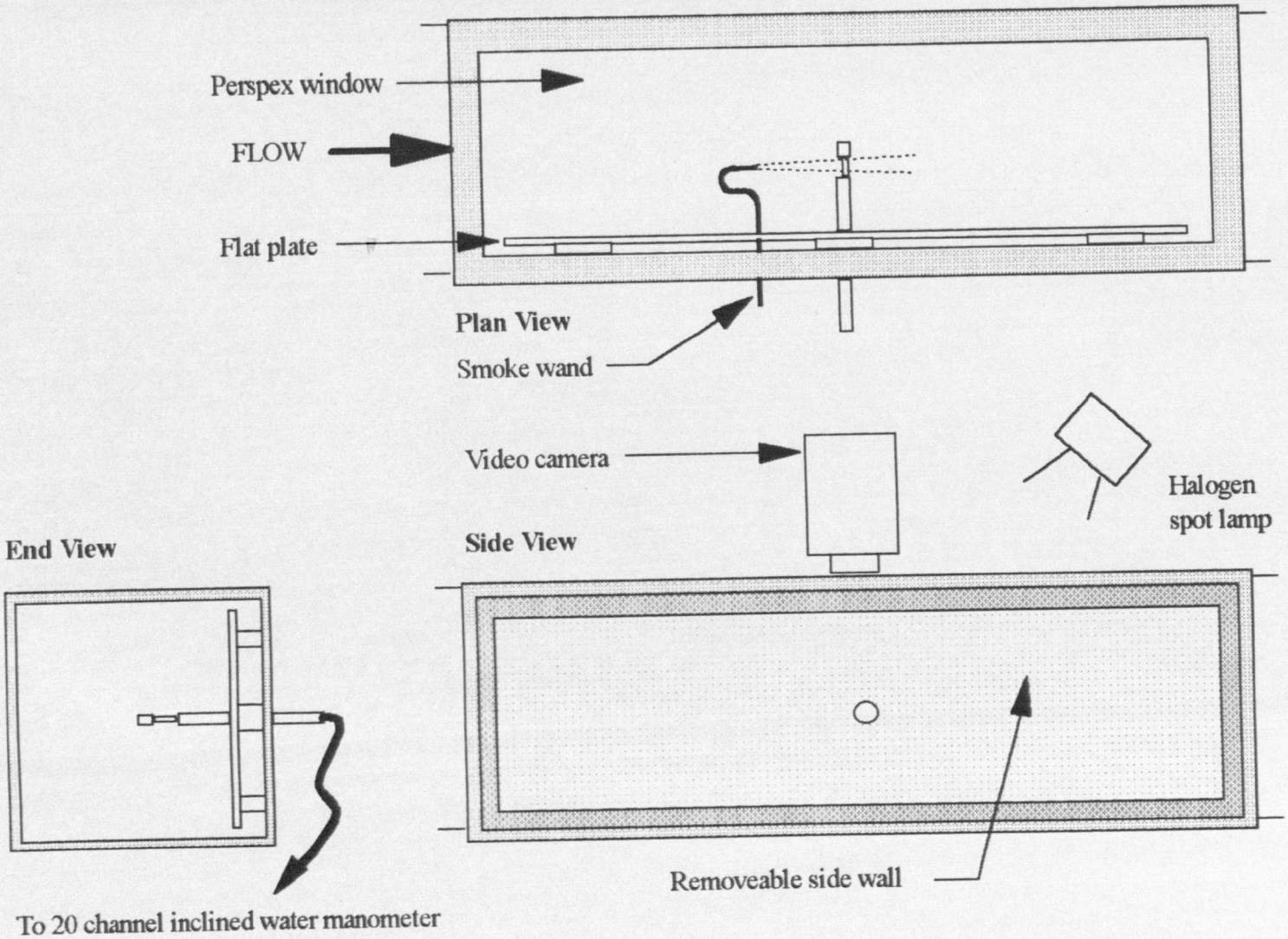

FIGURE 6.13: Arrangement of 3-D Flow Visualisation Experiment

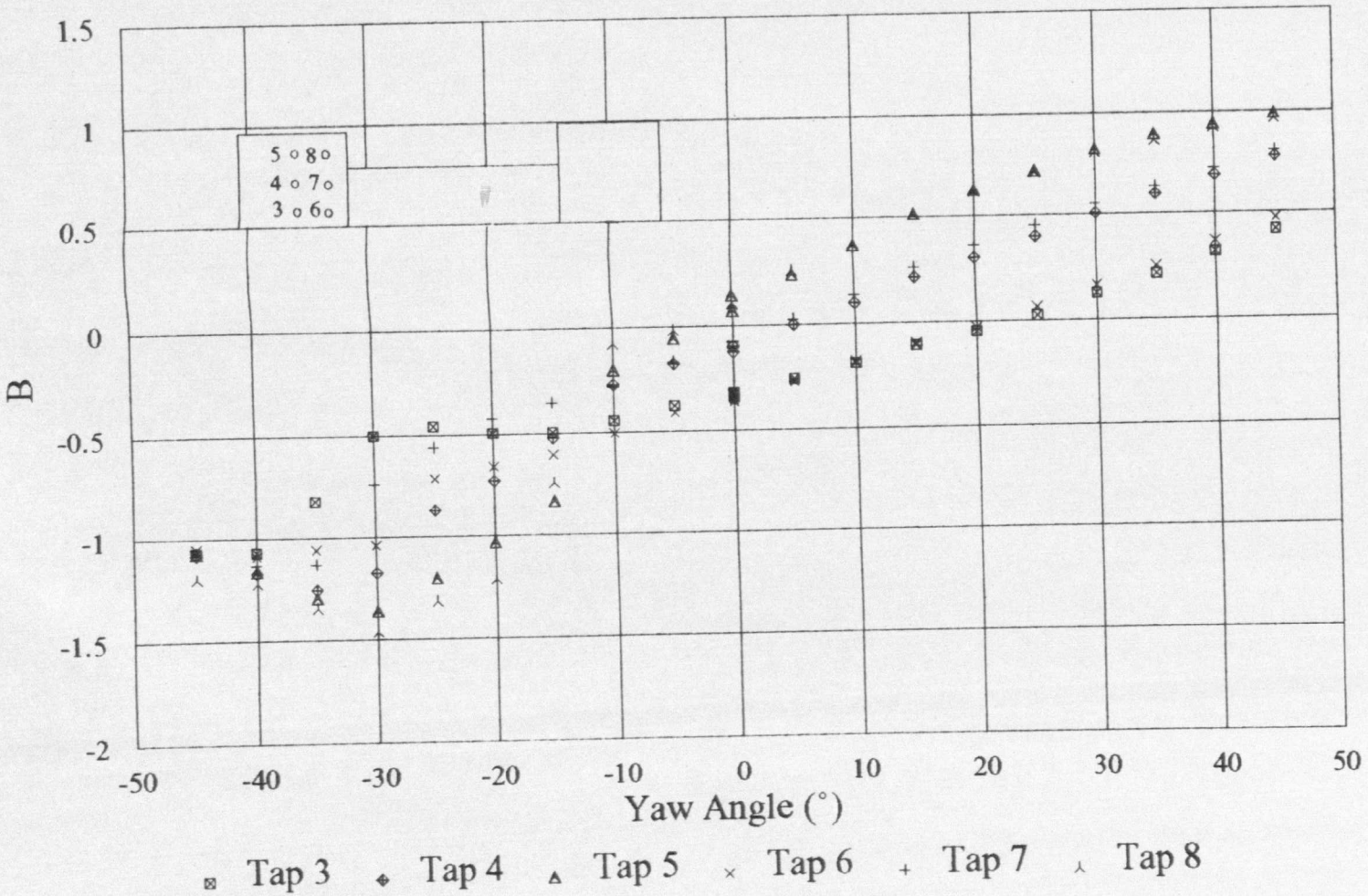

FIGURE 6.14: Large Scale Wedge Probe Calibration Against Yaw Angle at 25m/s

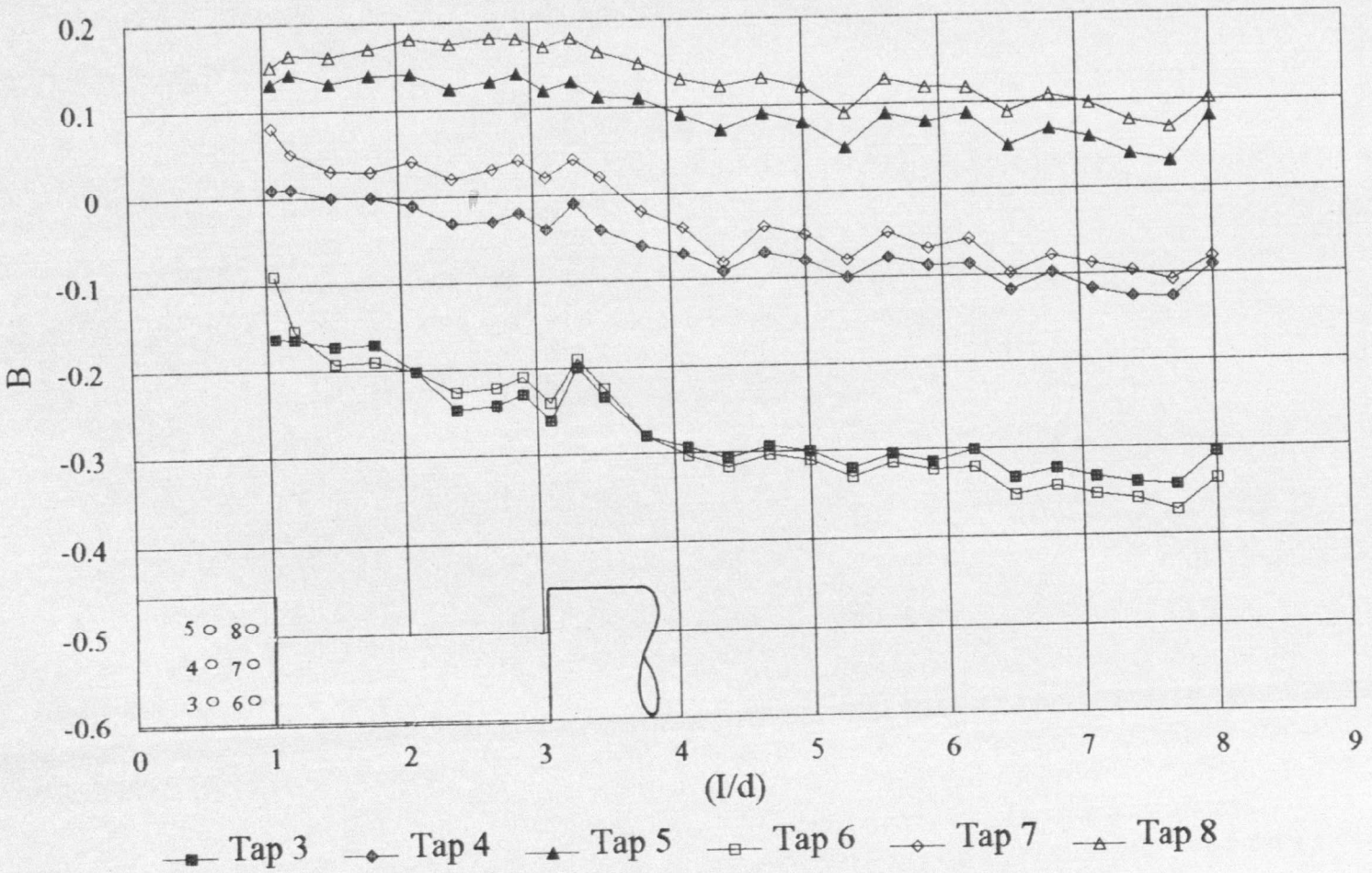

FIGURE 6.15: Large Scale Wedge Probe Radial Traverse at 25m/s Flow

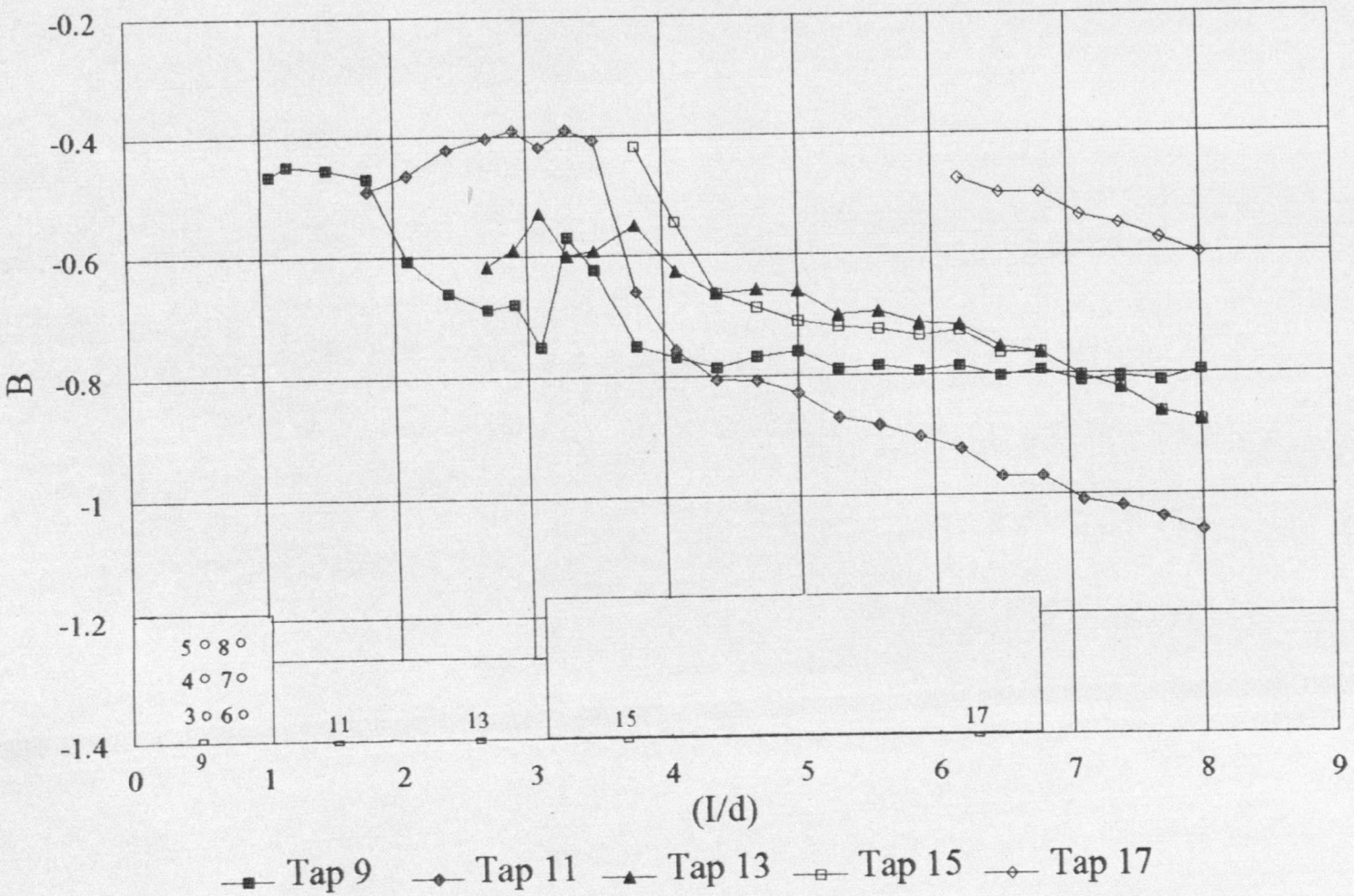

FIGURE 6.16: Large Scale Wedge Probe Radial Traverse at 25m/s

FIGURE 6.17: Visualisation of Flow Over Three-Dimensional Probe at 2.5d Immersion, 0° Yaw and 1.7×10^4 Reynolds Number - Formation of Re-Circulating Region at Lip of Probe Hole of Introduction

Neg No: 94.2374.3

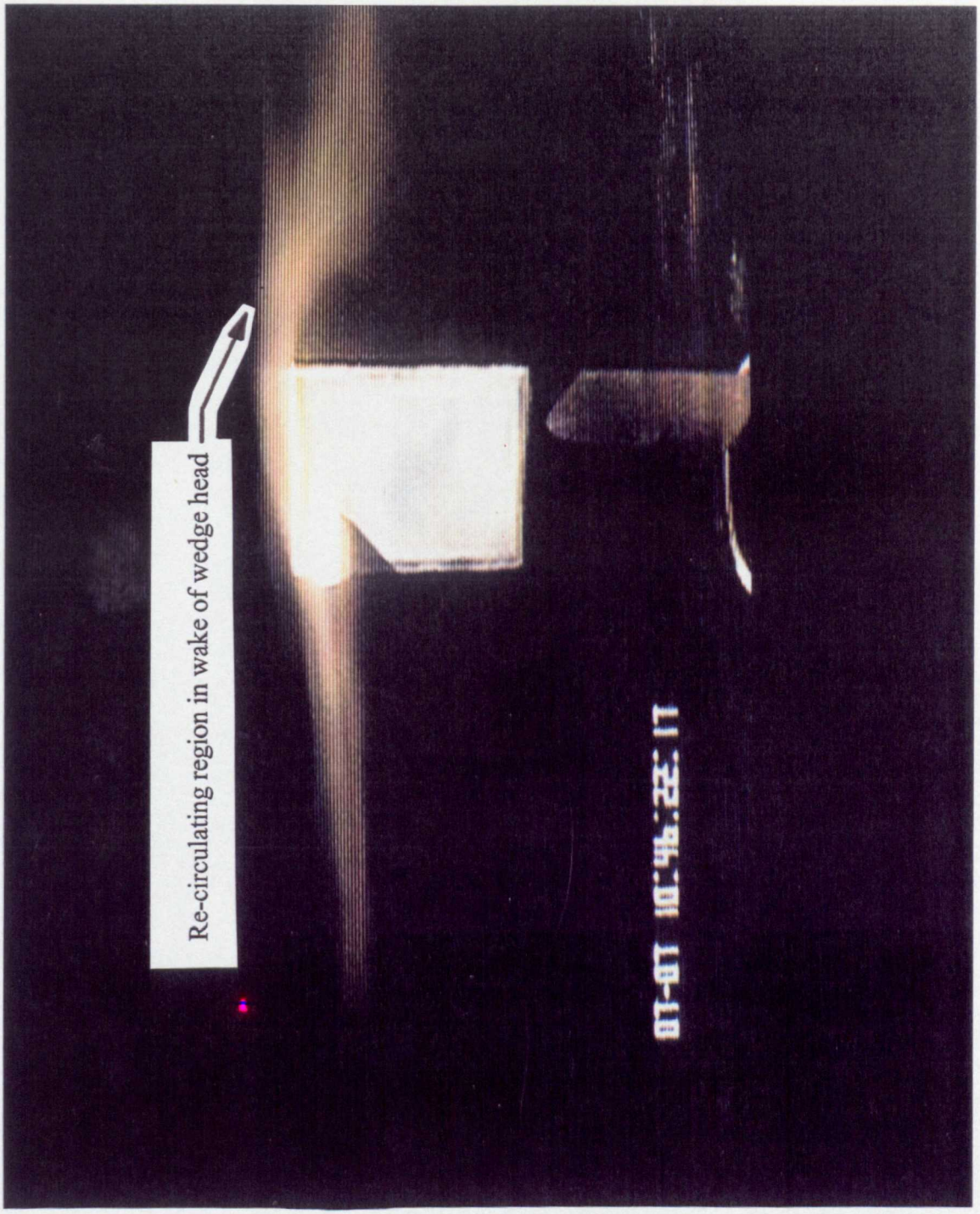

FIGURE 6.18: Visualisation of Flow Over Three-Dimensional Probe at 2.0d Immersion, 0° Yaw and 1.7×10^4 Reynolds Number - Formation of Re-Circulating Region in the Wake of the Wedge Head and in the Plane of the Probe

Neg No: 94.2374.5

FIGURE 6.19: Visualisation of Flow Over Three-Dimensional Probe at 3.5d Immersion, 0° Yaw and 1.7×10^4 Reynolds Number - Formation of Horse-Shoe Vortex Around Interface Piece

Neg No: 94.2374.9

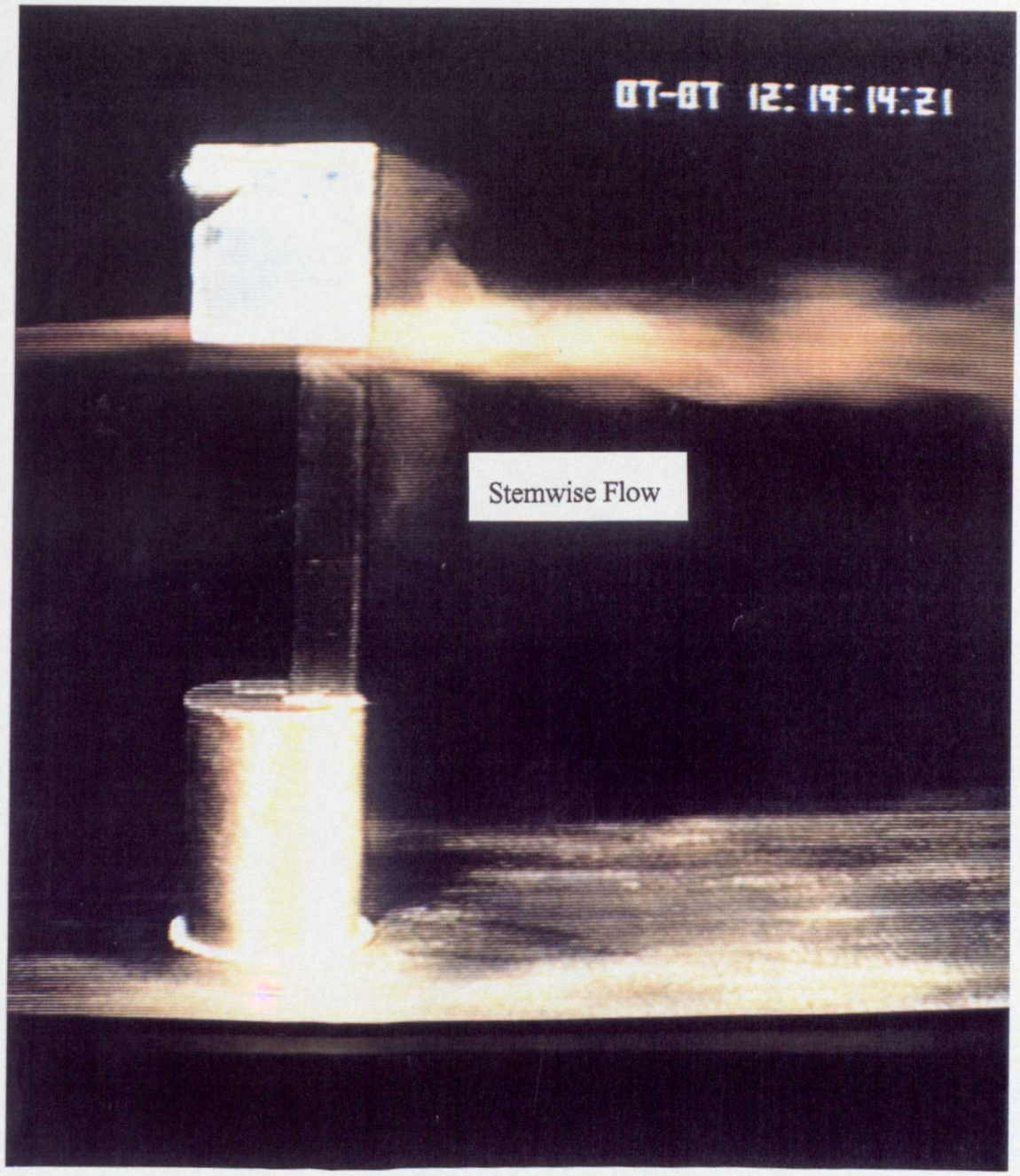

FIGURE 6.20: Visualisation of Flow Over Three-Dimensional Probe at 4.5d Immersion, 0° Yaw and 1.7×10^4 Reynolds Number - Stemwise Flow in Wake of Wedge Head and Interface Piece

Neg No: 94.2374.11

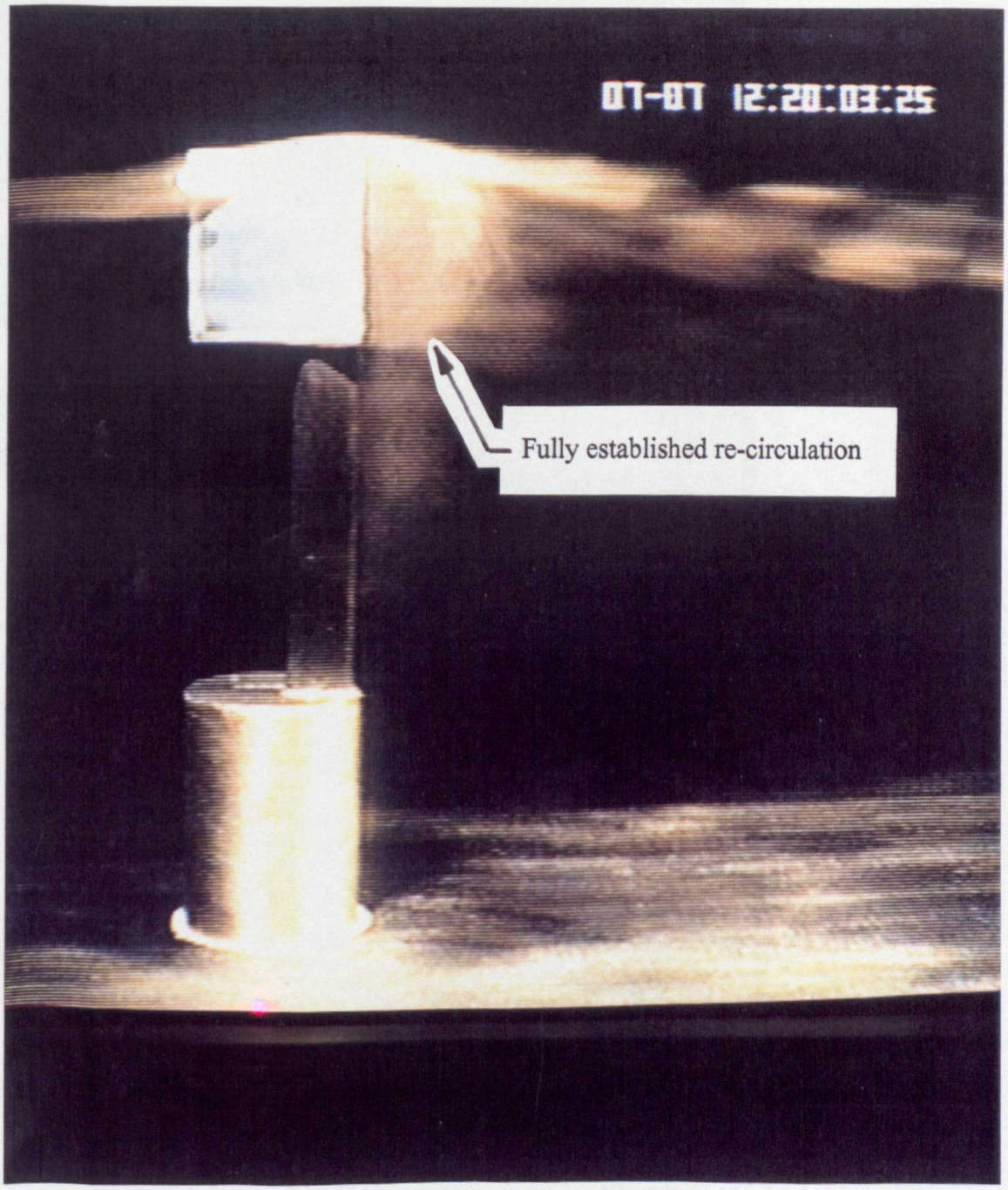

FIGURE 6.21: Visualisation of Flow Over Three-Dimensional Probe at 4.5d Immersion, 0° Yaw and 1.7×10^4 Reynolds Number - Stabilised Re-Circulating Region in Wake of Wedge Head, With Evidence of Stemwise Flow in Wake of Interface Piece

Neg No: 94.2374.12

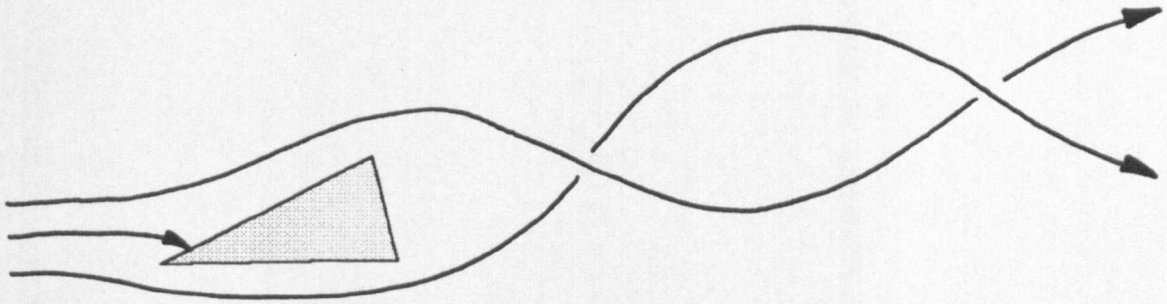

Spiraling flow in probe wake at incidence

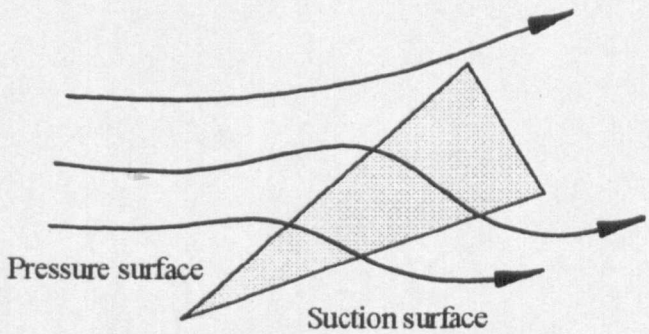

Over-tip flow at higher incidence angles

FIGURE 6.22: Flow Visualisation On Large Scale Probe at Incidence

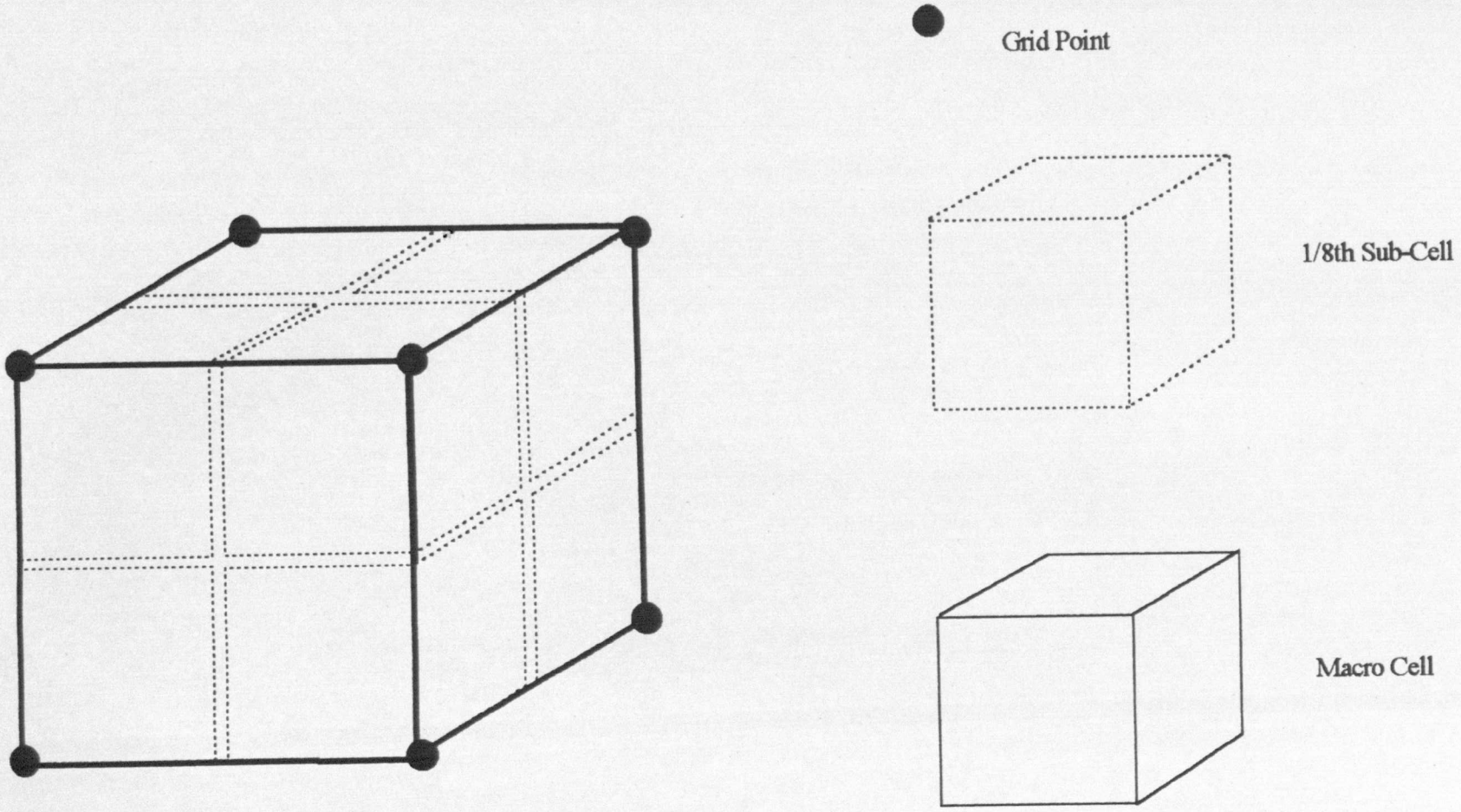

FIGURE 7.1: Division of MEFP Grid Cells into Sub-Cells for Control Volume Upwinding

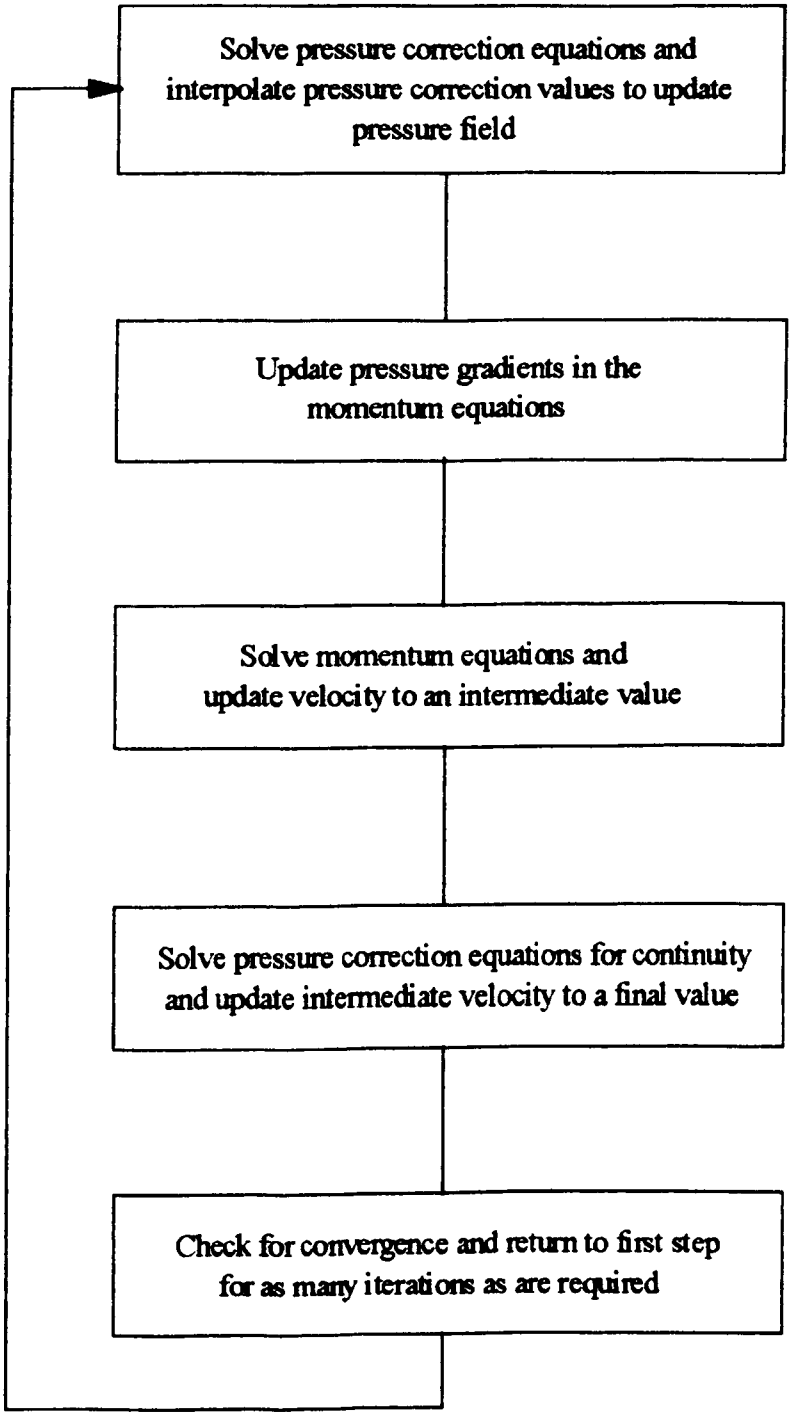

FIGURE 7.2: Calculation Scheme for MEFP Pressure Correction Code

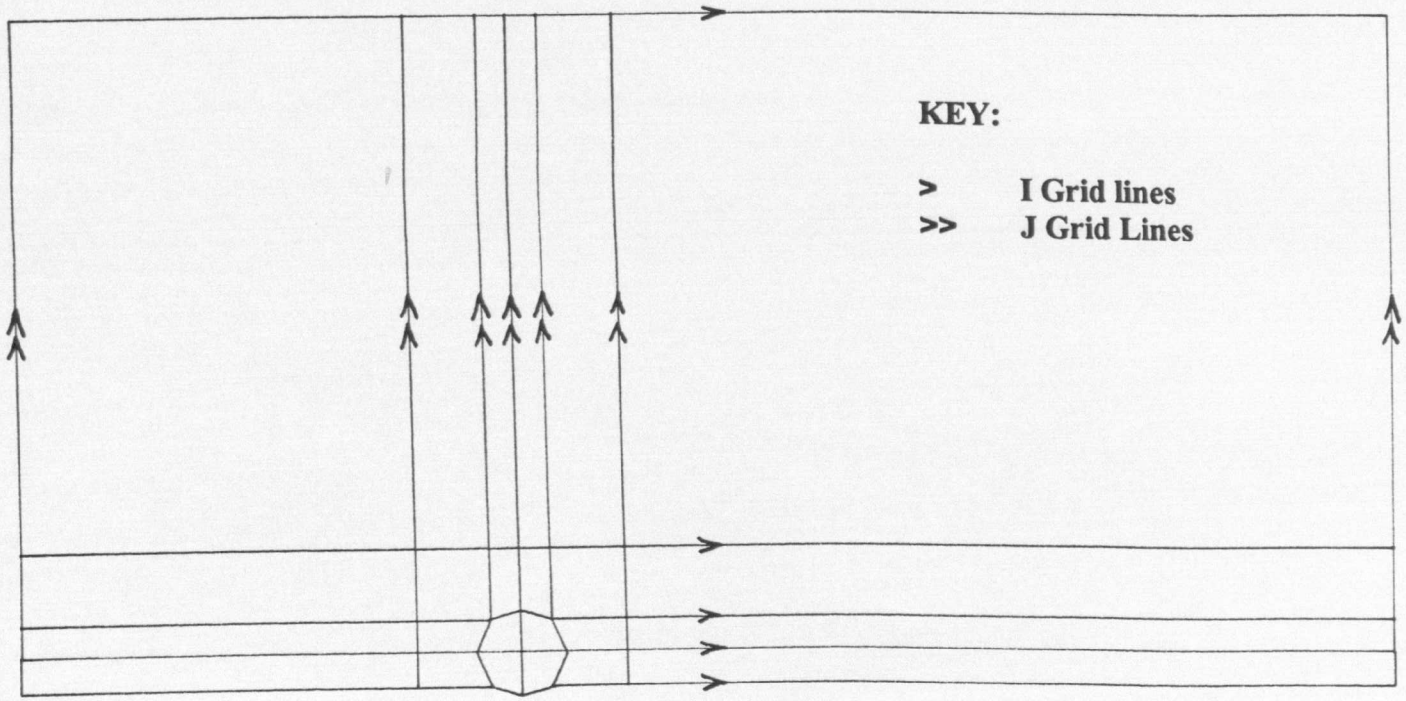

FIGURE 7.3: Master Geometry for Structured Mesh of 2-D Cylinder.

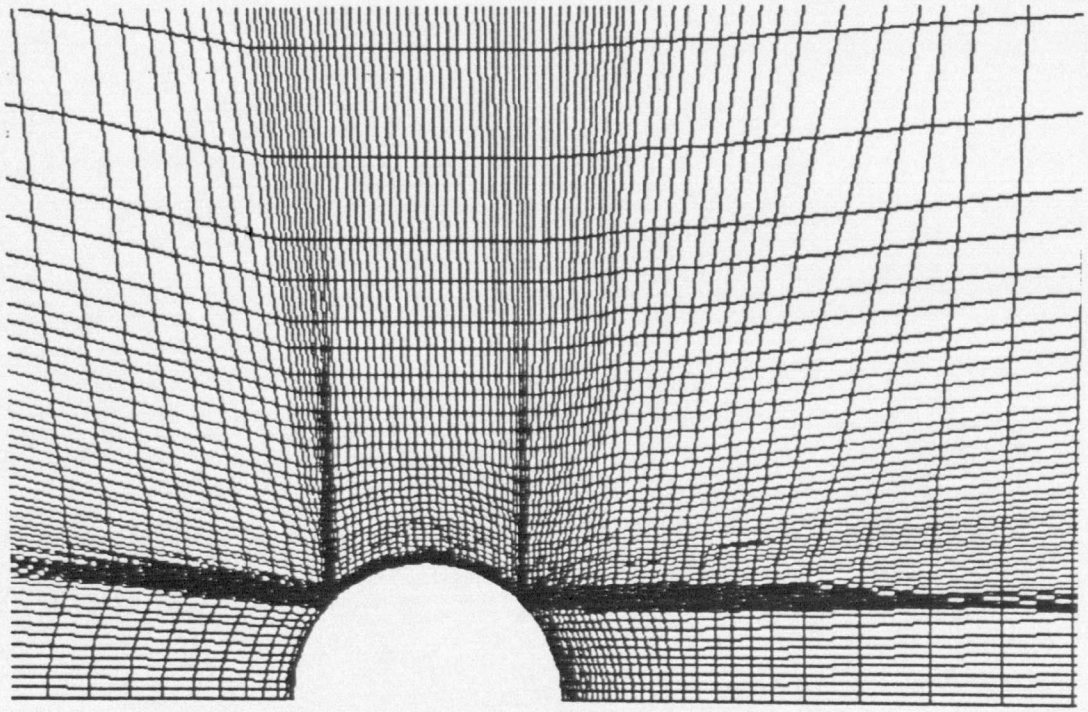

FIGURE 7.4: Flaring of Closely Packed Grid Lines to Reduce Individual Cell Aspect Ratios

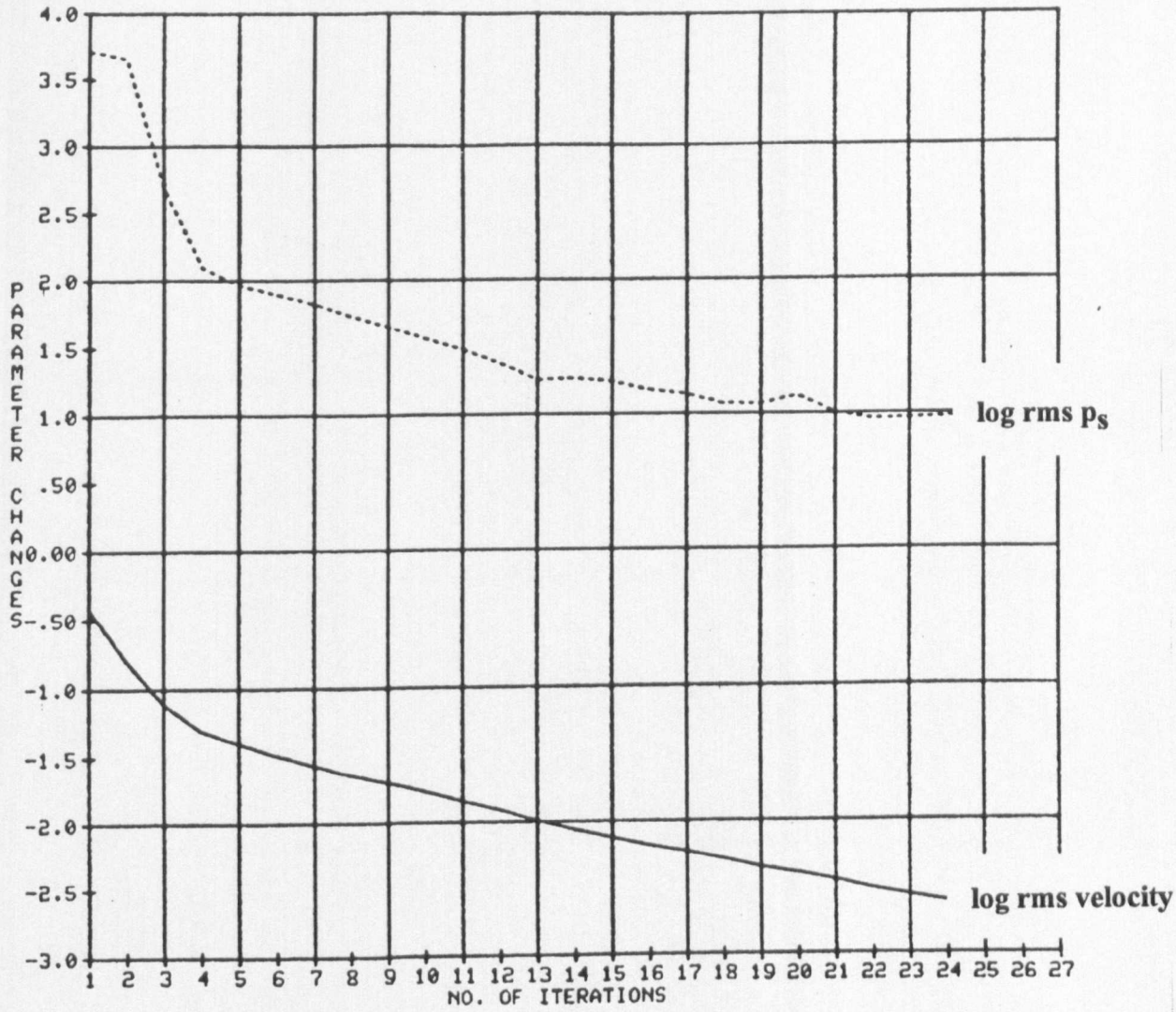

FIGURE 7.5: Convergence History for Calculation of Flow On Structured Cylinder Mesh

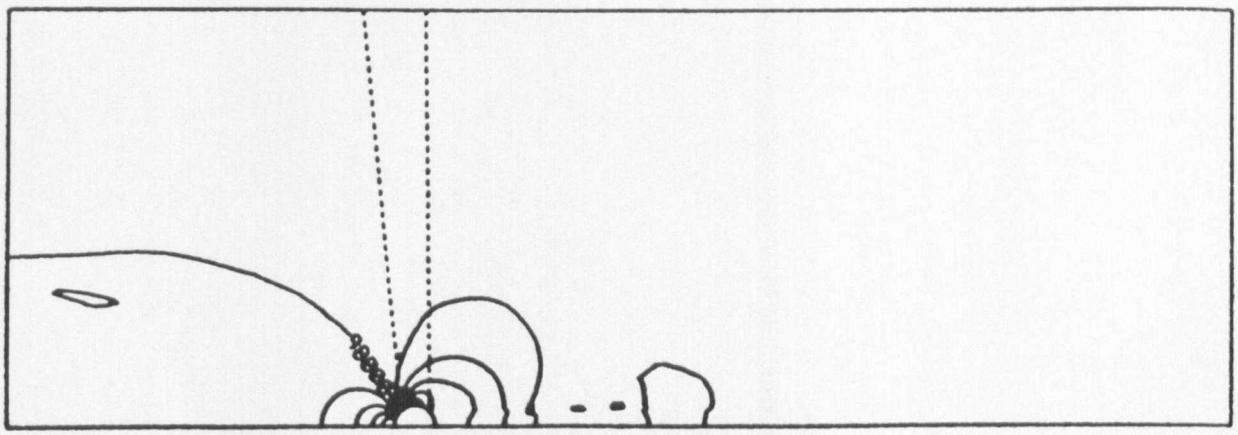

FIGURE 7.6: Static Pressure Contour Map for Re = 40 Solution of 2-D Cylinder Flow (Structured Mesh)

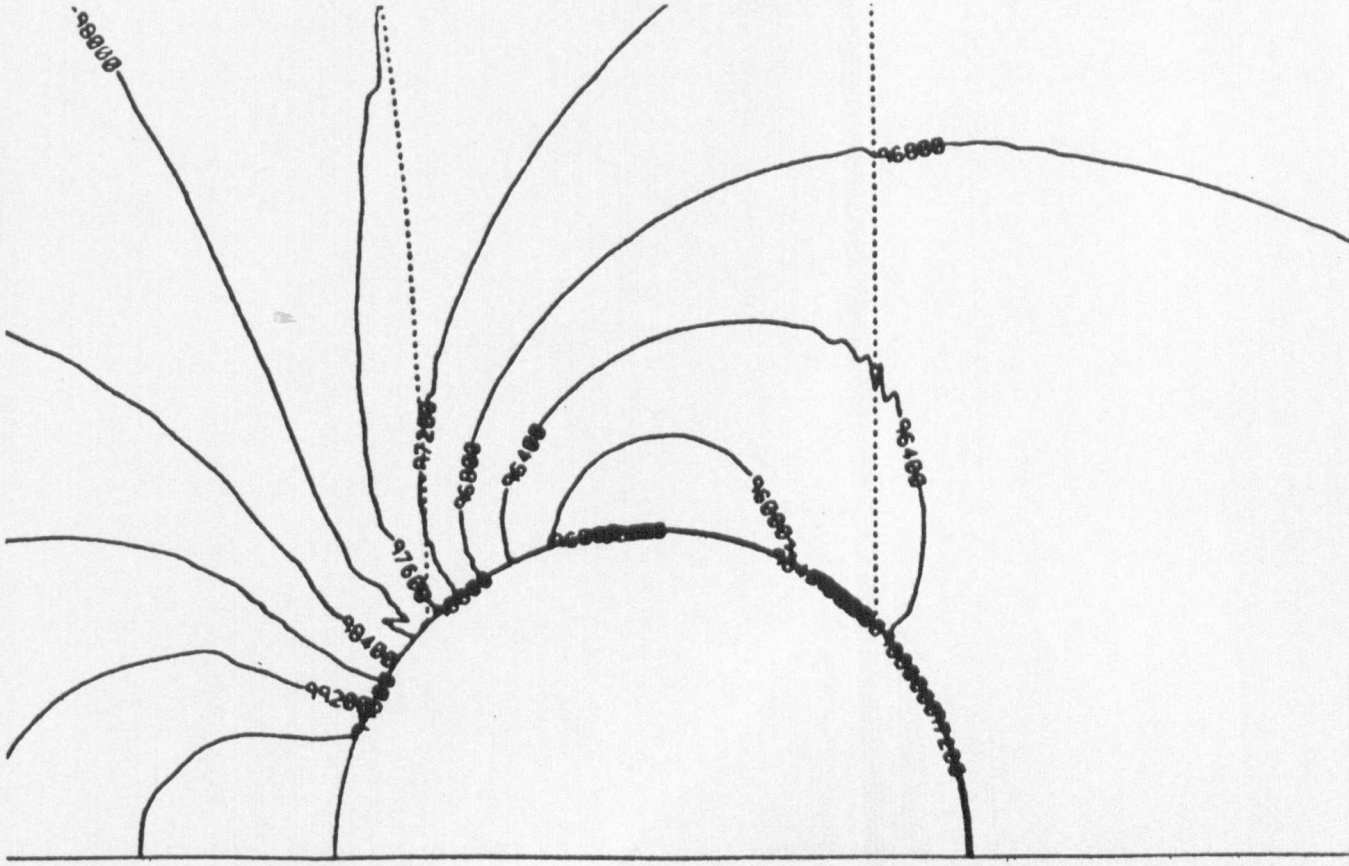

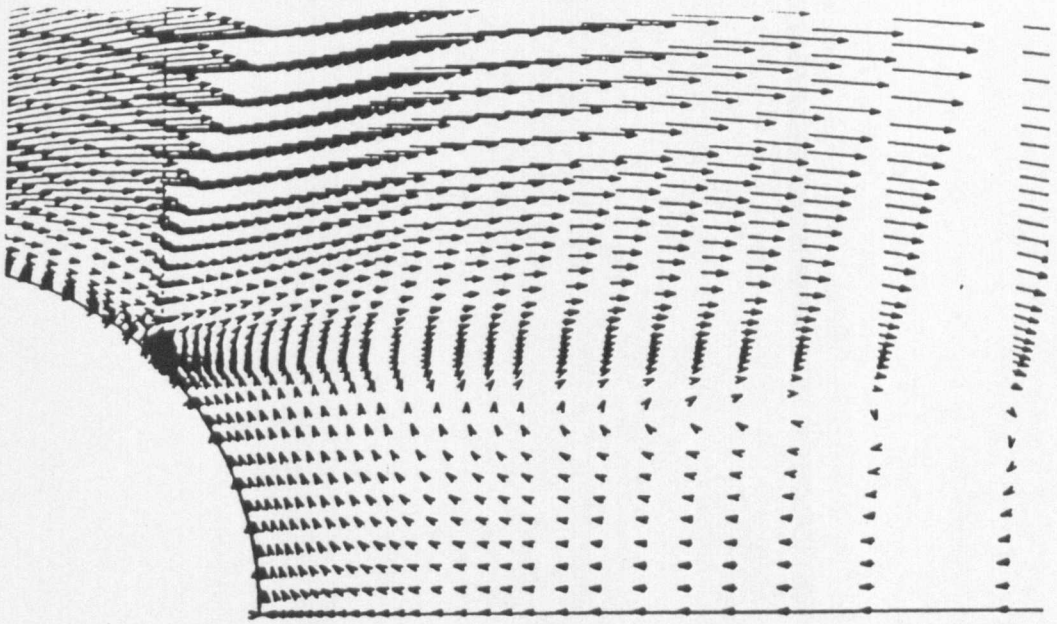

FIGURE 7.7a): Velocity Vectors in Wake of 2-D Cylinder at Re = 40 (Structured Mesh)

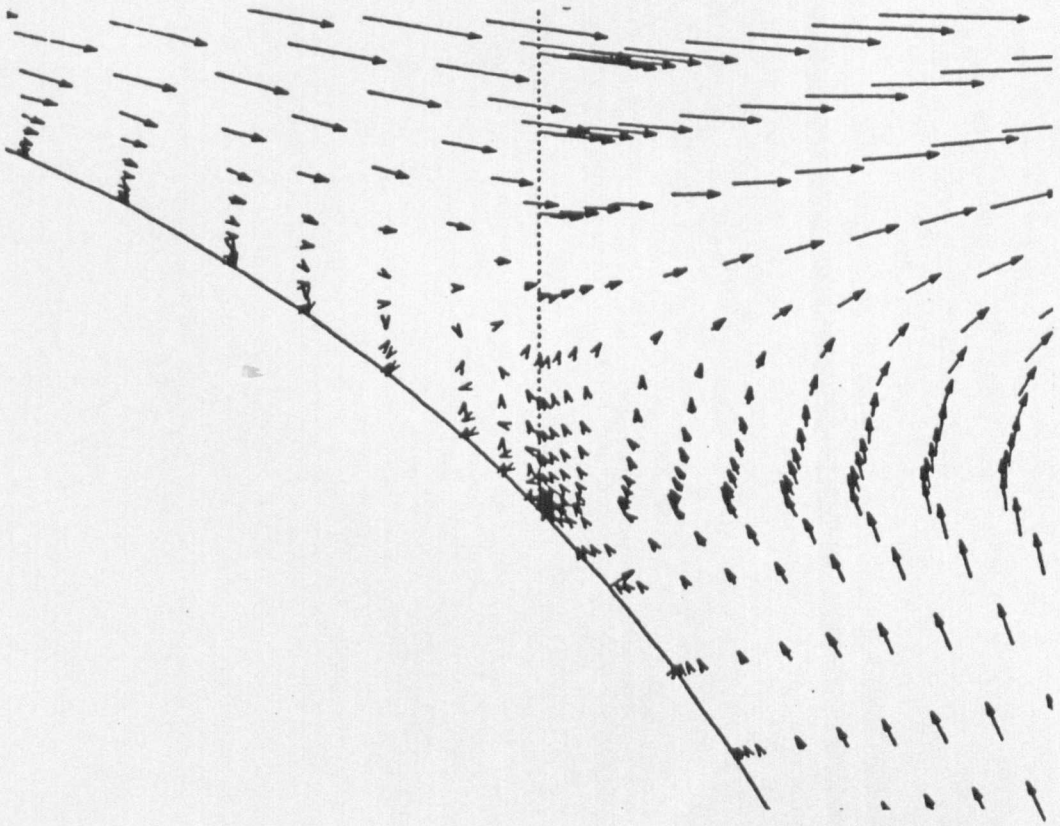

FIGURE 7.7b): Detail of Separation Point at Re = 40 (Structured Mesh)

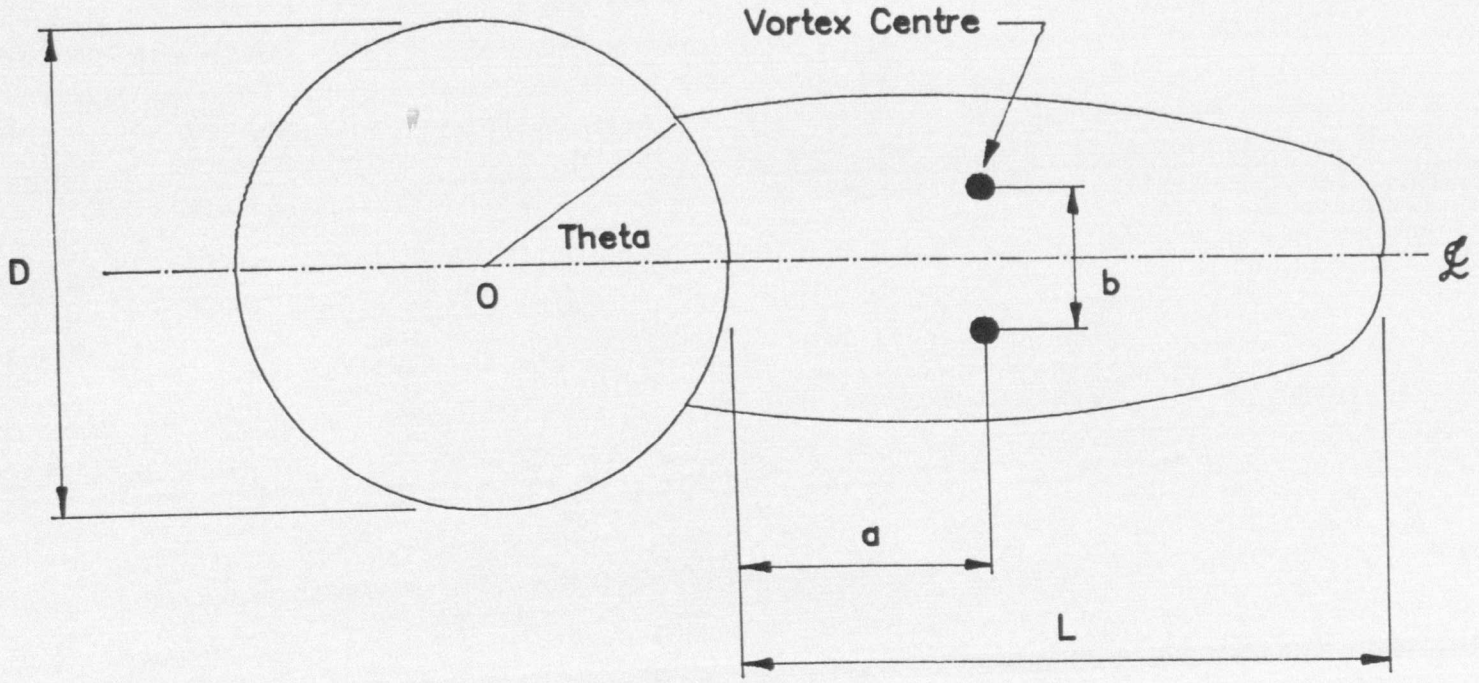

FIGURE 7.8: Definition of Geometrical Parameters for the Closed Wake Behind a Cylinder in Cross-Flow

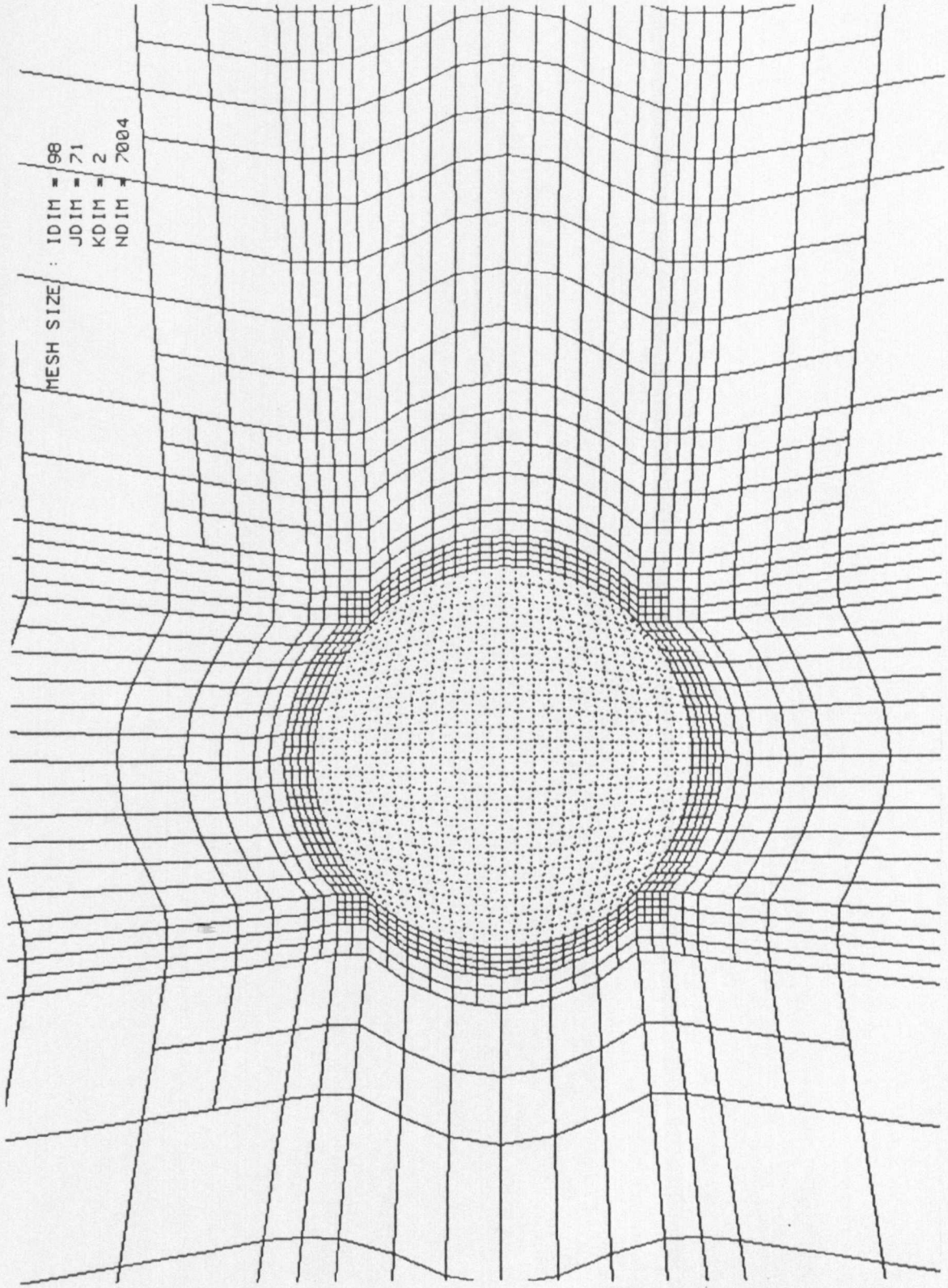

FIGURE 7.9: Embedded Mesh of 2-D Cylinder

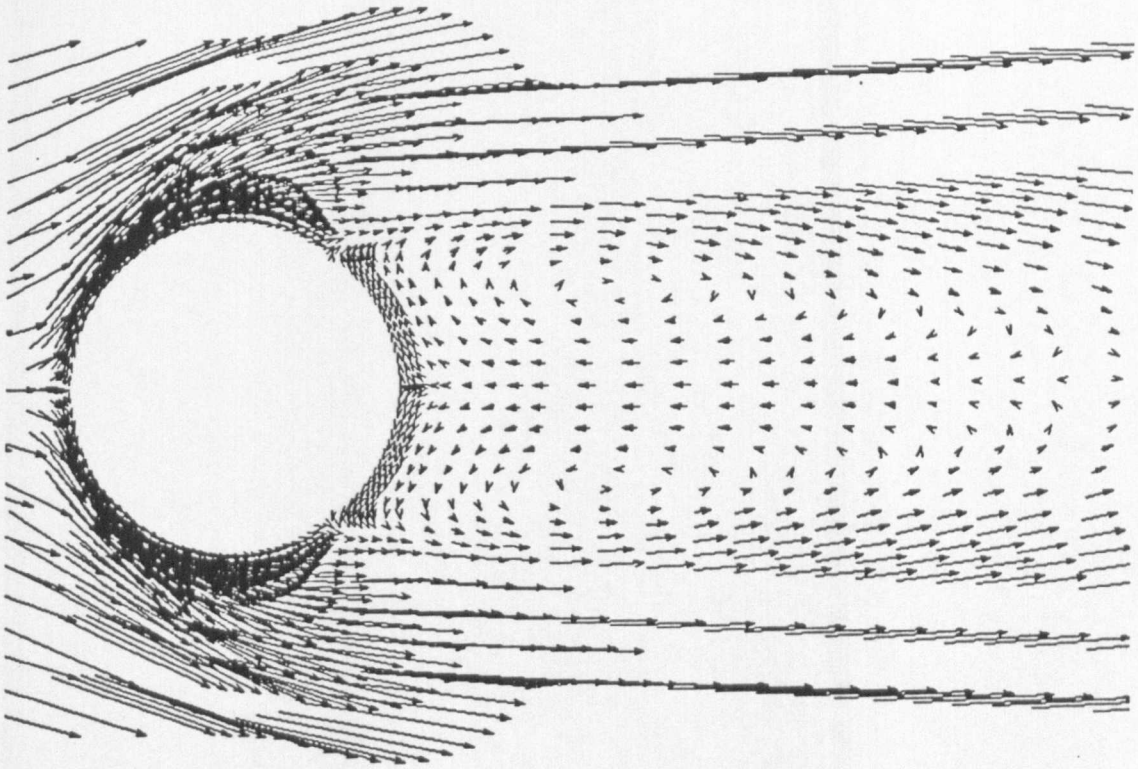

FIGURE 7.10a): Velocity Vectors in Wake of 2-D Cylinder at Re = 40 (Embedded Mesh)

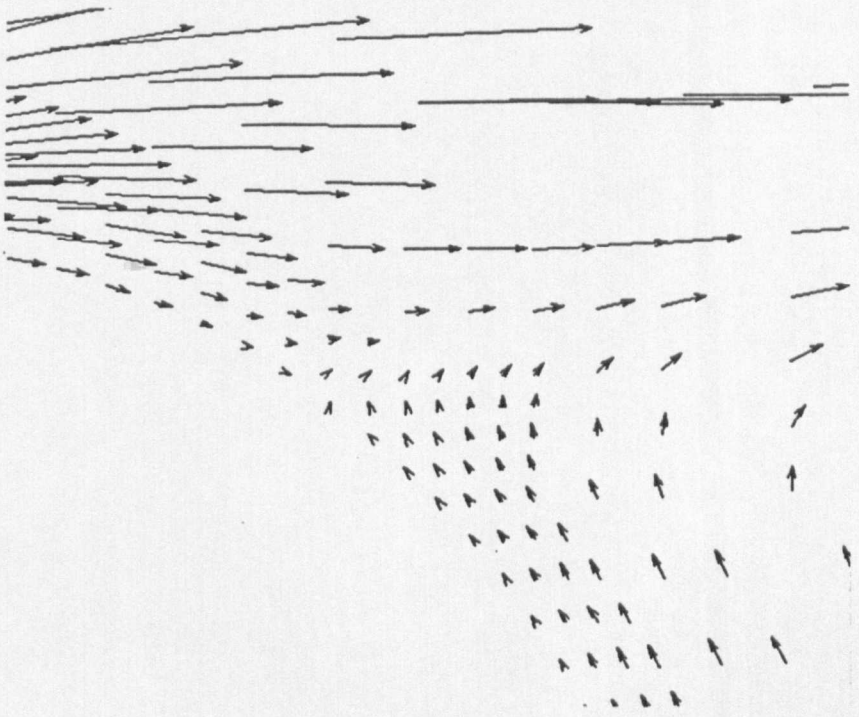

FIGURE 7.10b): Detail of Separation Point at Re = 40 (Embedded Mesh)

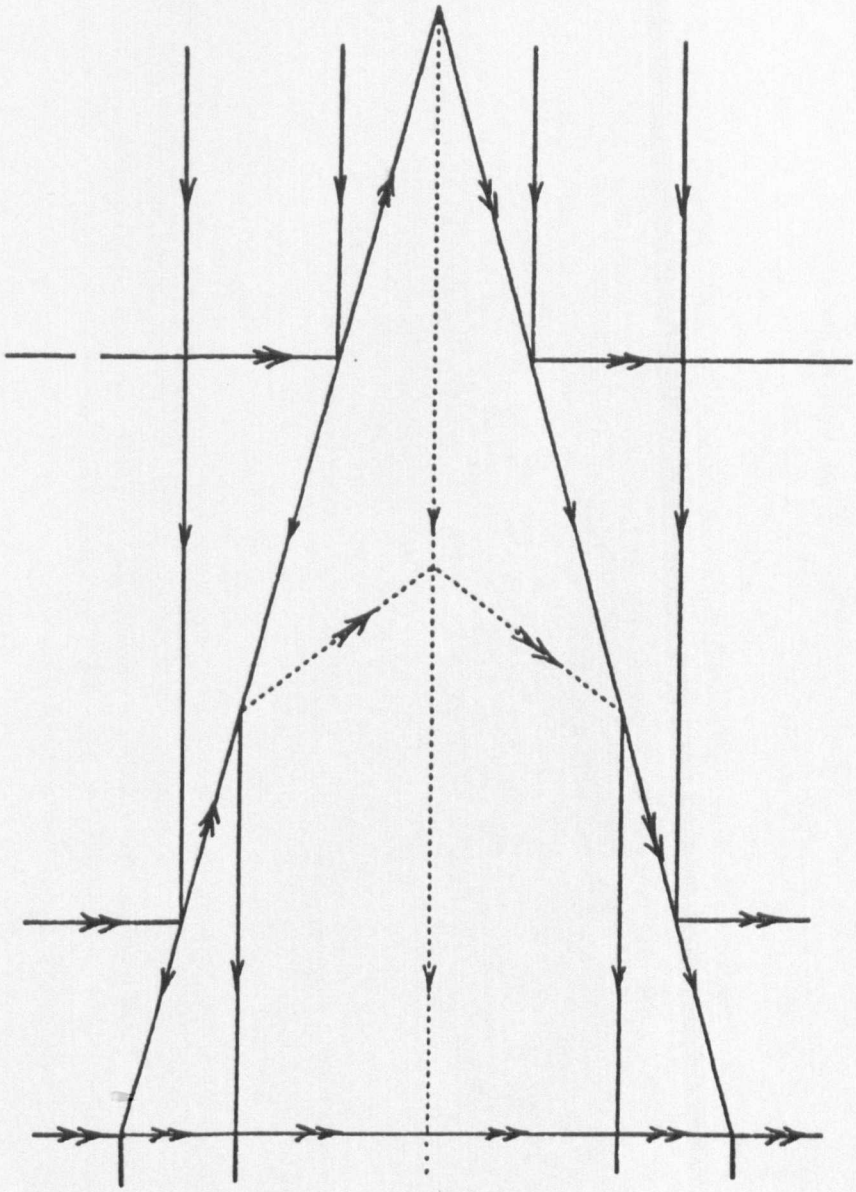

KEY:

> **I Grid lines**
>> **J Grid Lines**

FIGURE 7.11a): Master Geometry for 24º Included Angle, 2-D Wedge

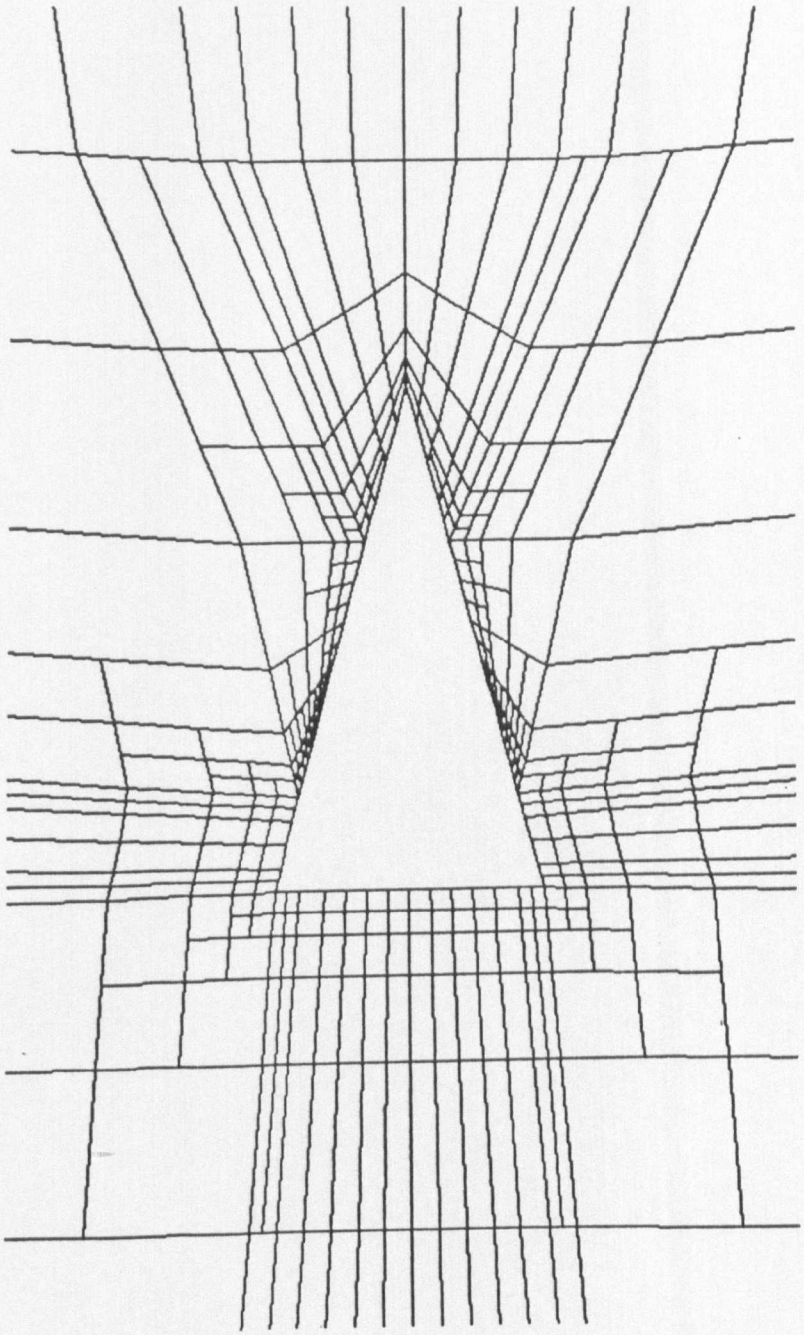

FIGURE 7.11b): Final Grid for 2-D Wedge

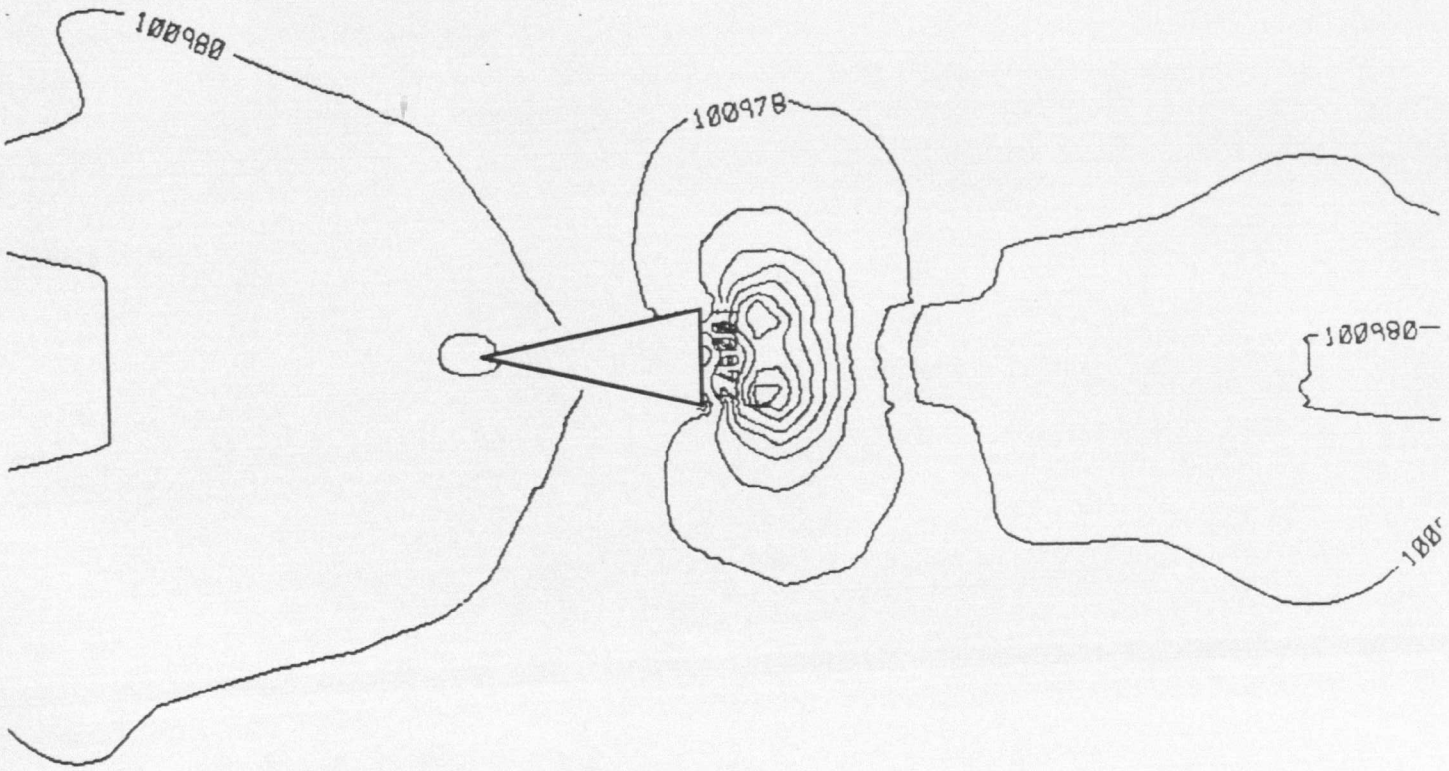

FIGURE 7.12: Static Pressure Contour Map for Re = 5.5×10^4 Solution of 2-D Wedge

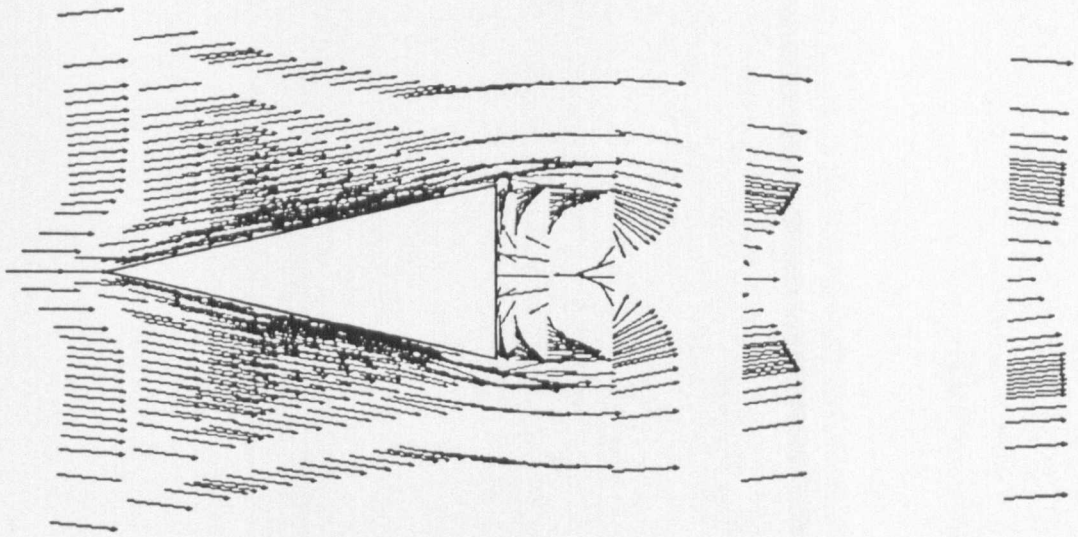

FIGURE 7.13a): Velocity Vector Representation of Flow Around 2-D Wedge at 0º Yaw (Before Mesh Adaption)

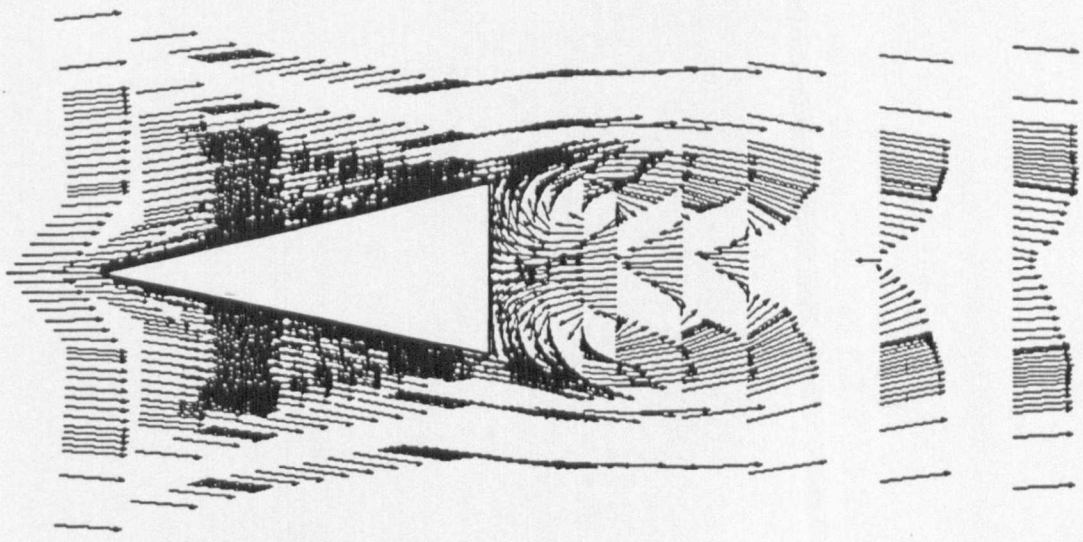

FIGURE 7.13b): Velocity Vector Representation of Flow Around 2-D Wedge at 0º Yaw (After Mesh Adaption)

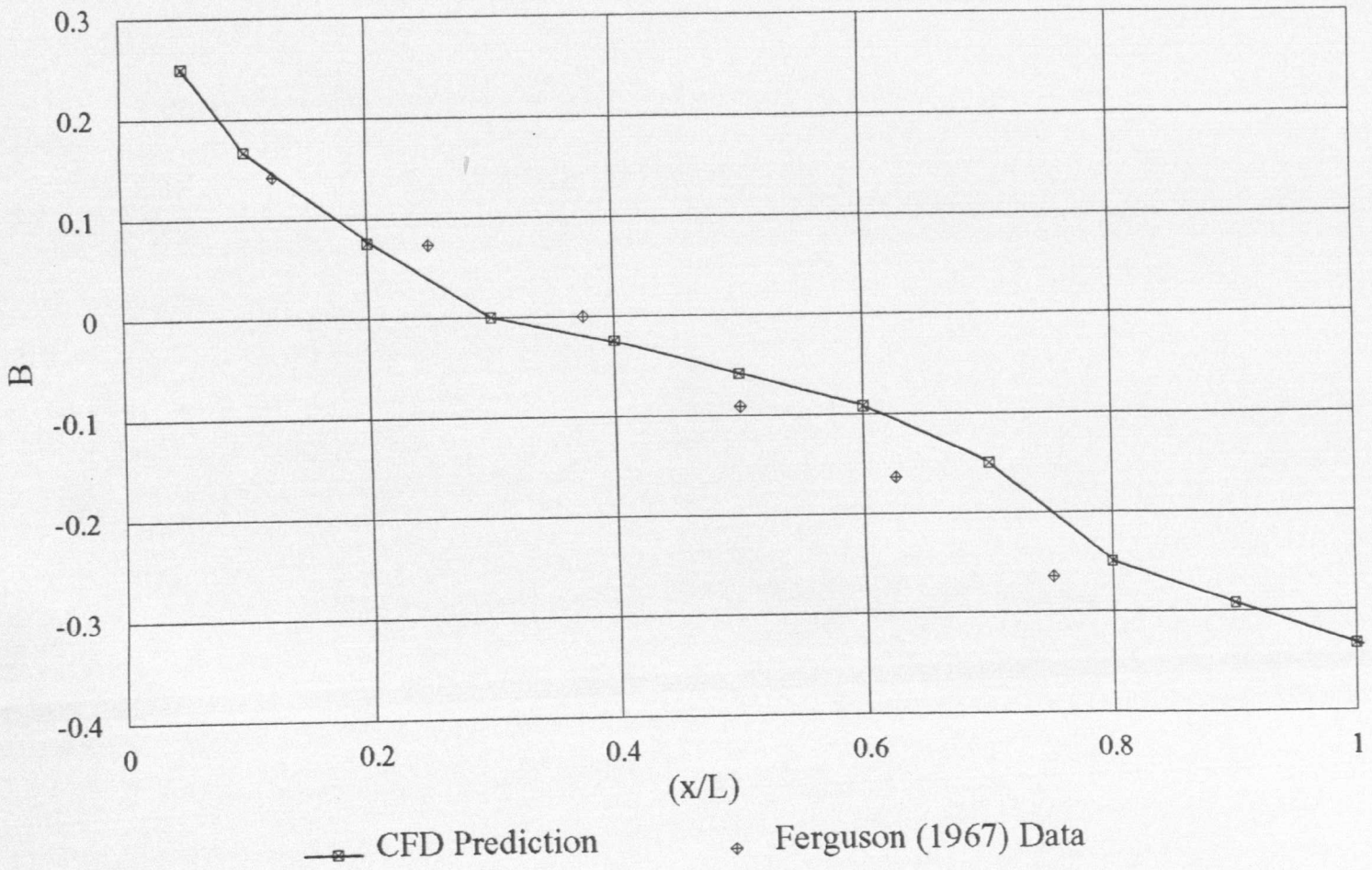

FIGURE 7.14: Predicted Wedge Face Static Pressure Distribution at 0° Yaw (24° Wedge at 52000 Reynolds Number)

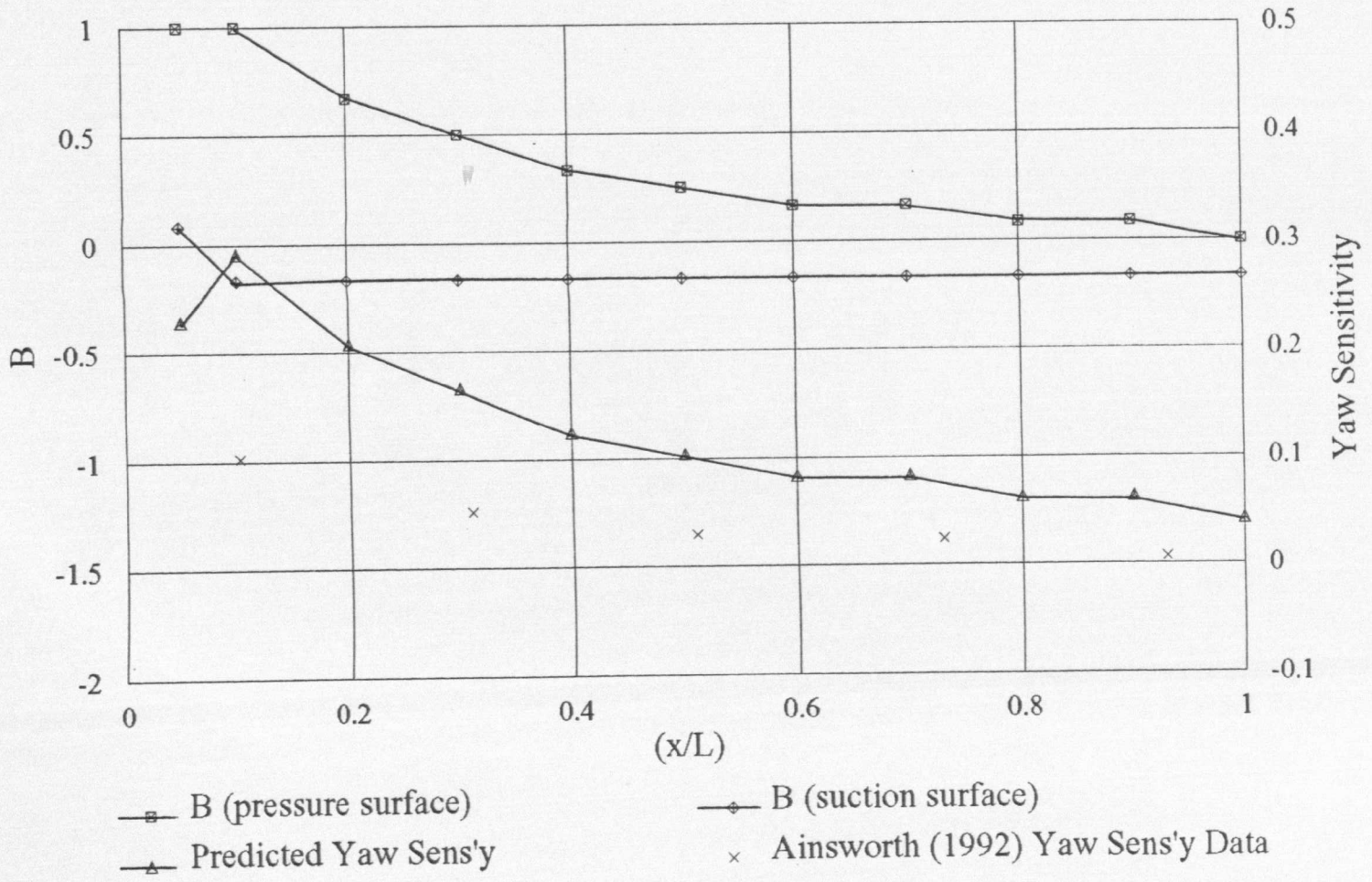

FIGURE 7.15: Predicted Wedge Face Static Pressure Distribution at 4° Yaw (24° Wedge at 52000 Reynolds Number)

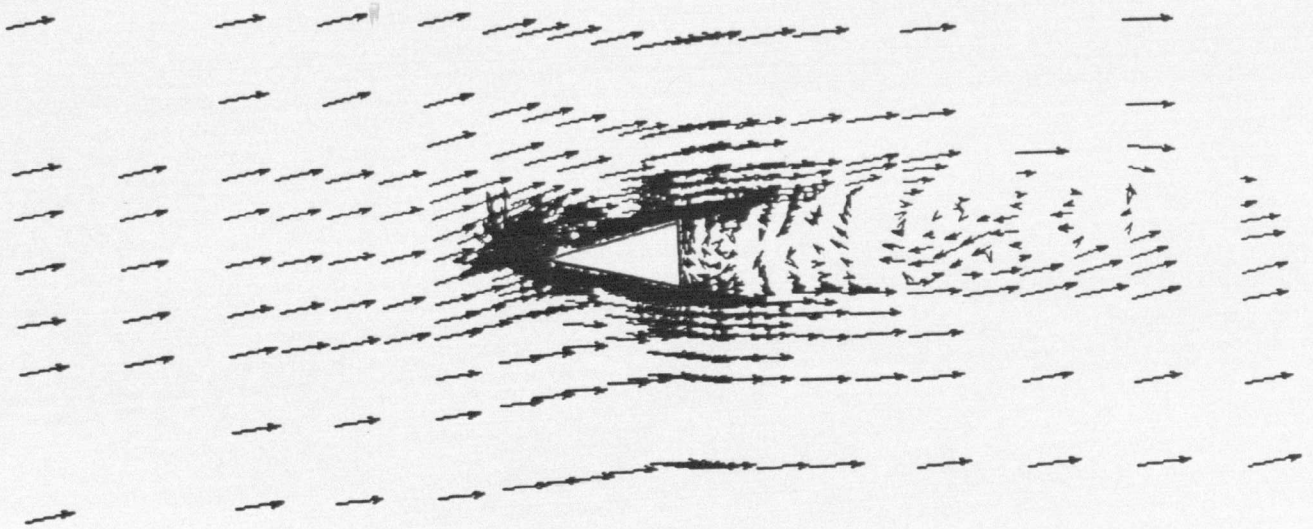

FIGURE 7.16: Velocity Vector Representation of Flow Around 2-D Wedge at 8º Yaw

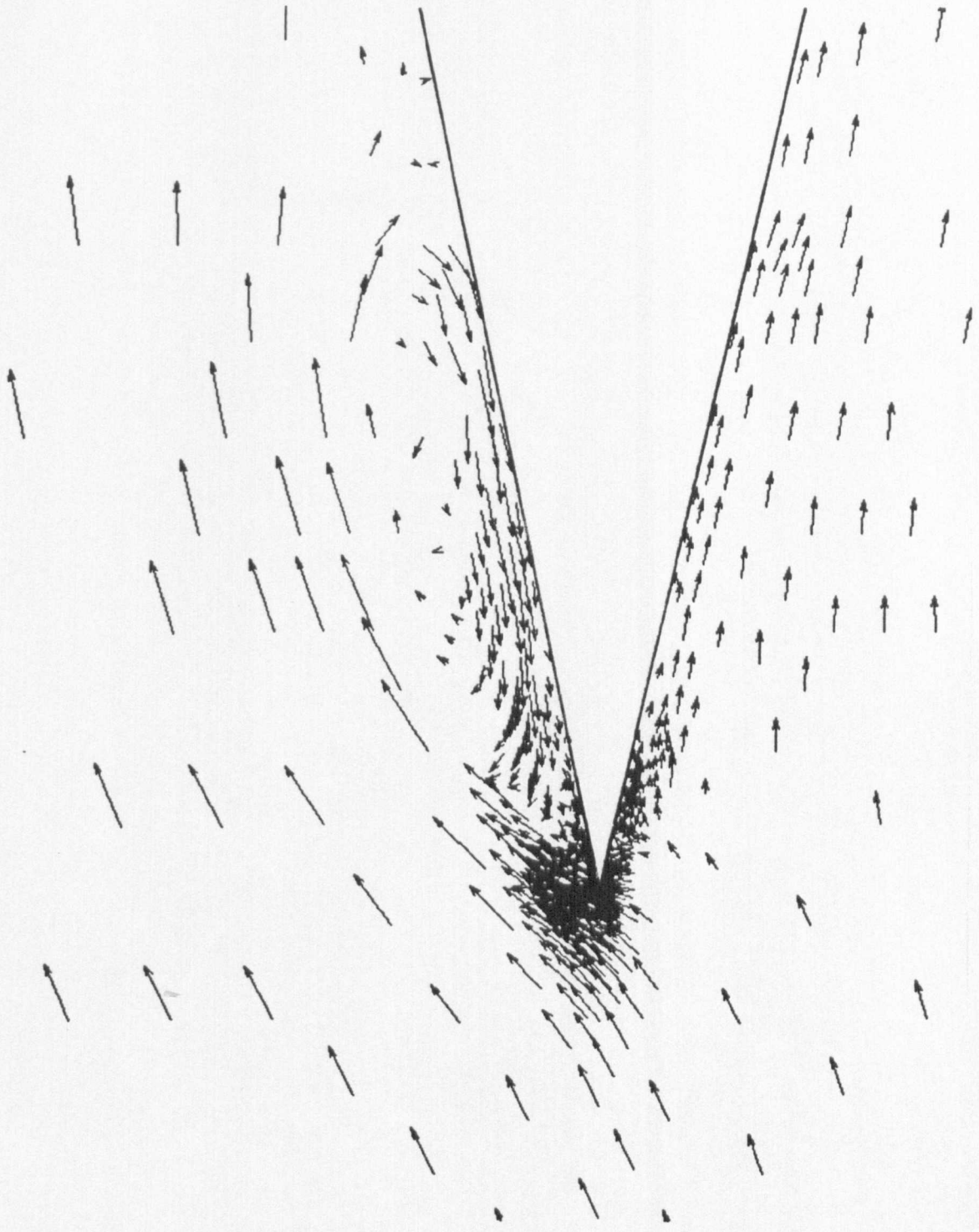

FIGURE 7.17: Separation Bubble in Suction Surface Leading Edge Region at 8º Yaw

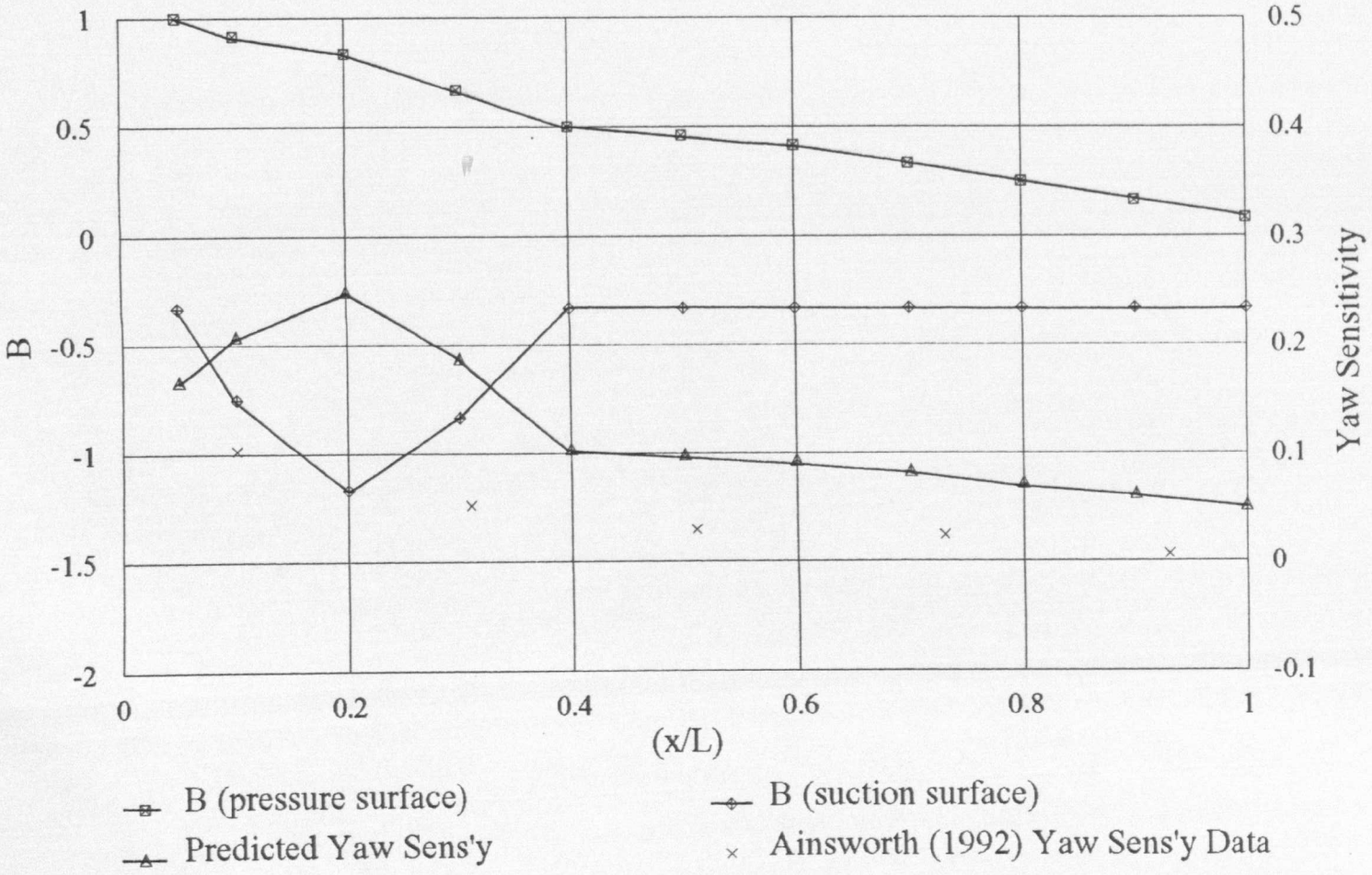

FIGURE 7.18: Predicted Wedge Face Static Pressure Distribution at 8° Yaw (24° Wedge at 52000 Reynolds Number)

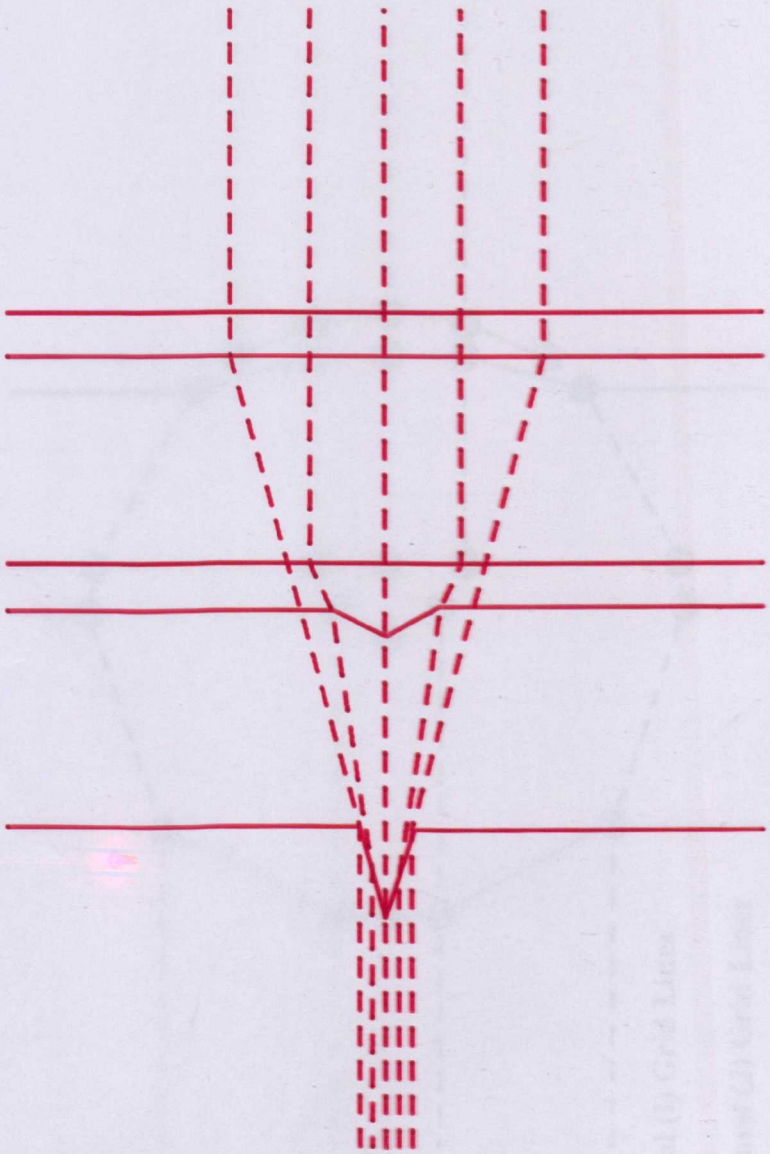

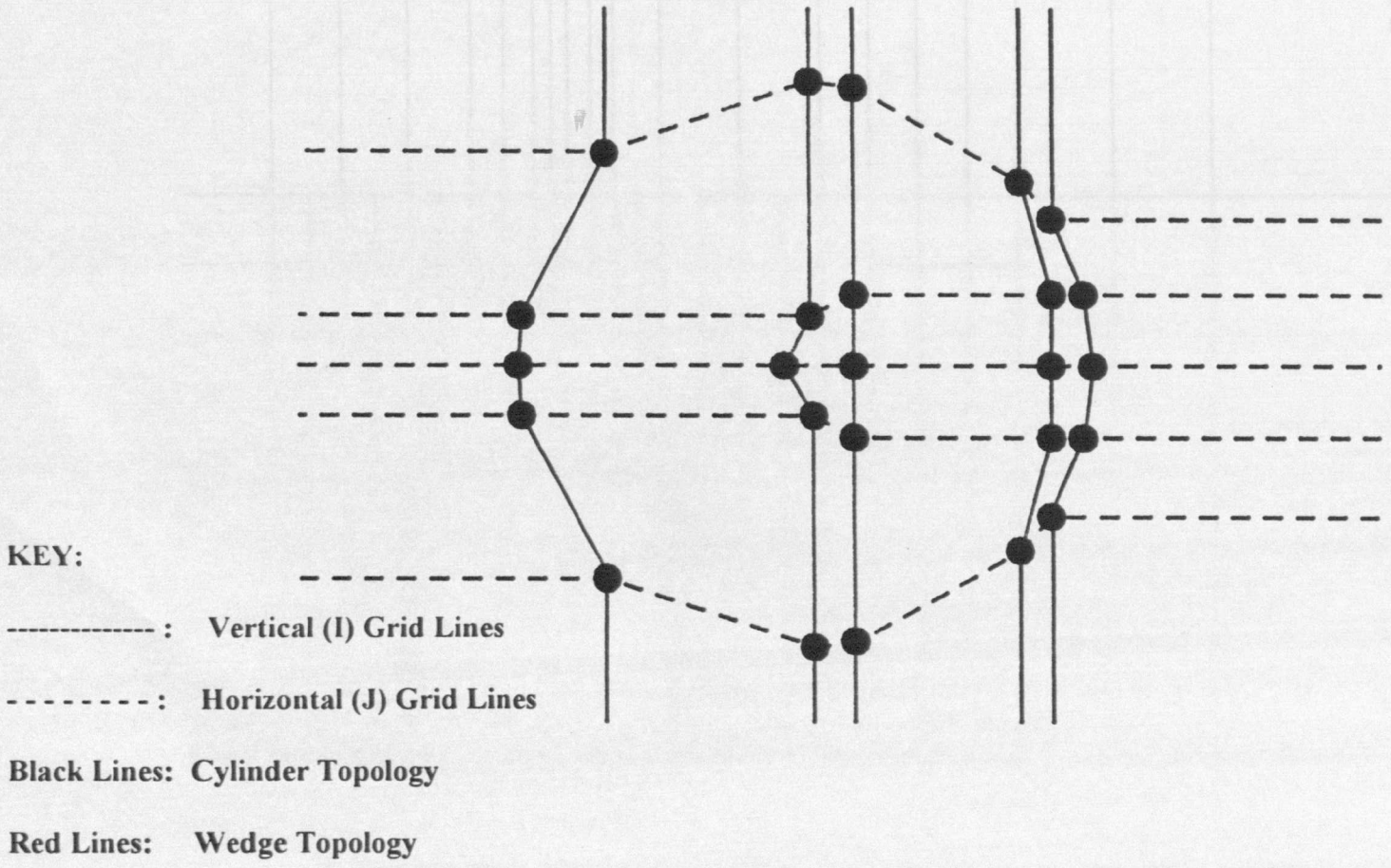

FIGURE 7.19: Topology for Three-Dimensional Wedge Probe Mesh

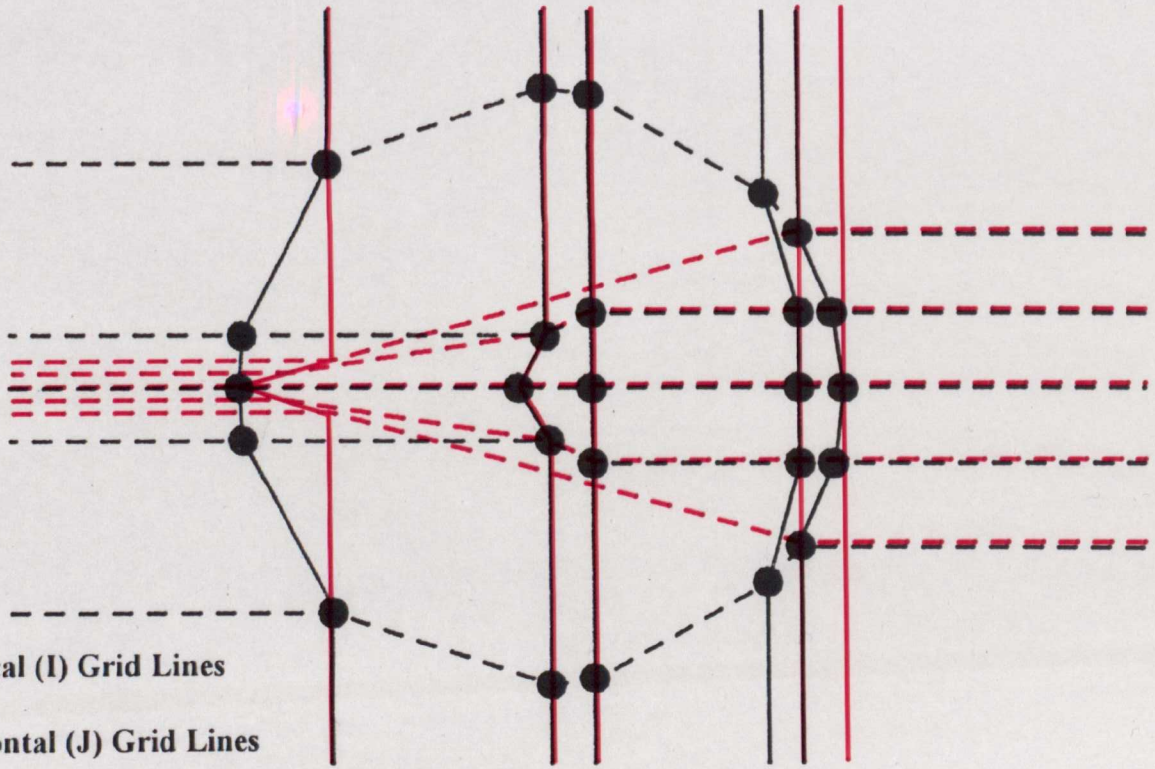

KEY:

---------- : Vertical (I) Grid Lines

- - - - - - - - : Horizontal (J) Grid Lines

Black Lines: Cylinder Topology

Red Lines: Wedge Topology

FIGURE 7.19: Topology for Three-Dimensional Wedge Probe Mesh

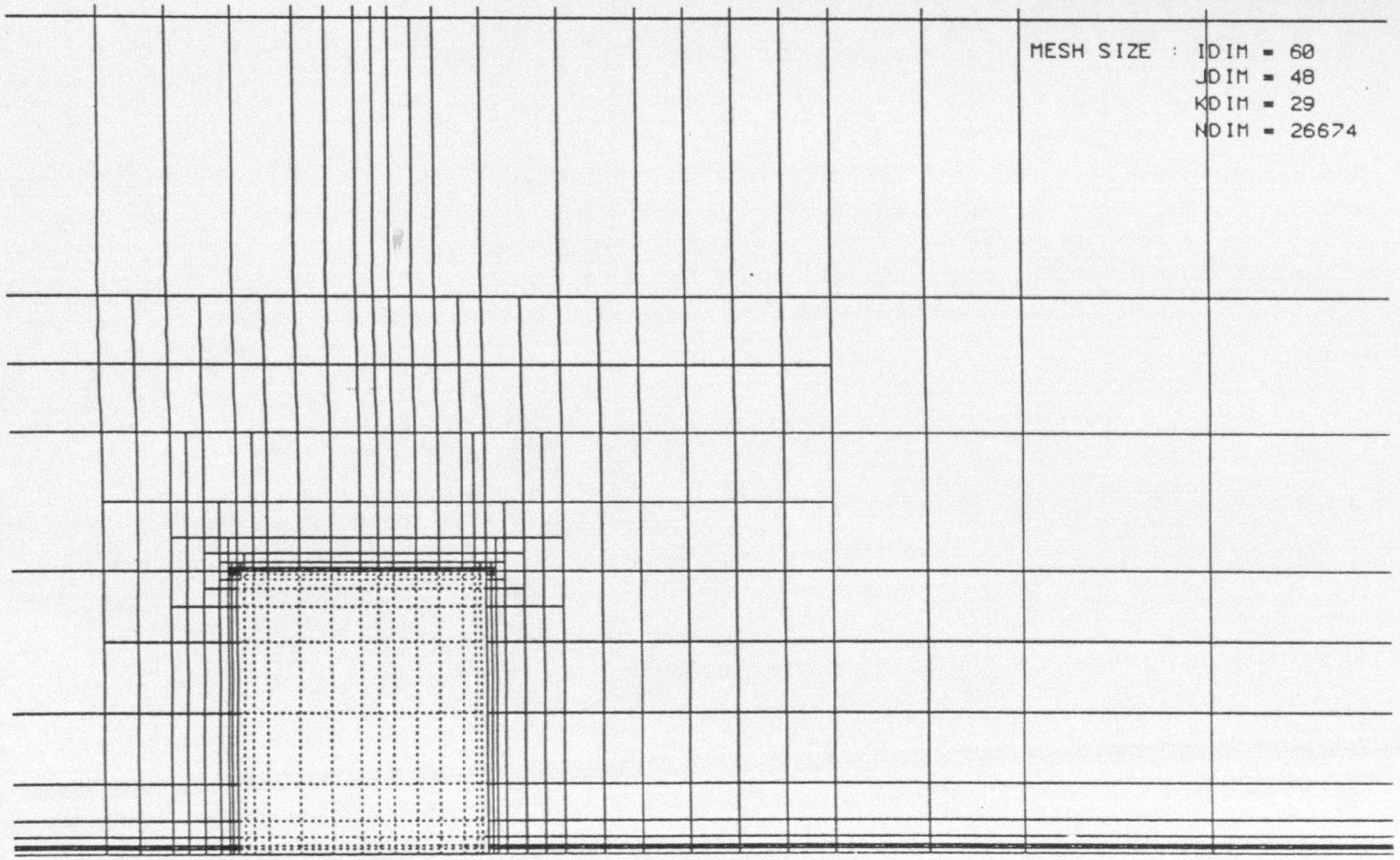

FIGURE 7.20a): Final Mesh for 3-D Wedge Probe at One Stem Diameter Immersion (Meridional View)

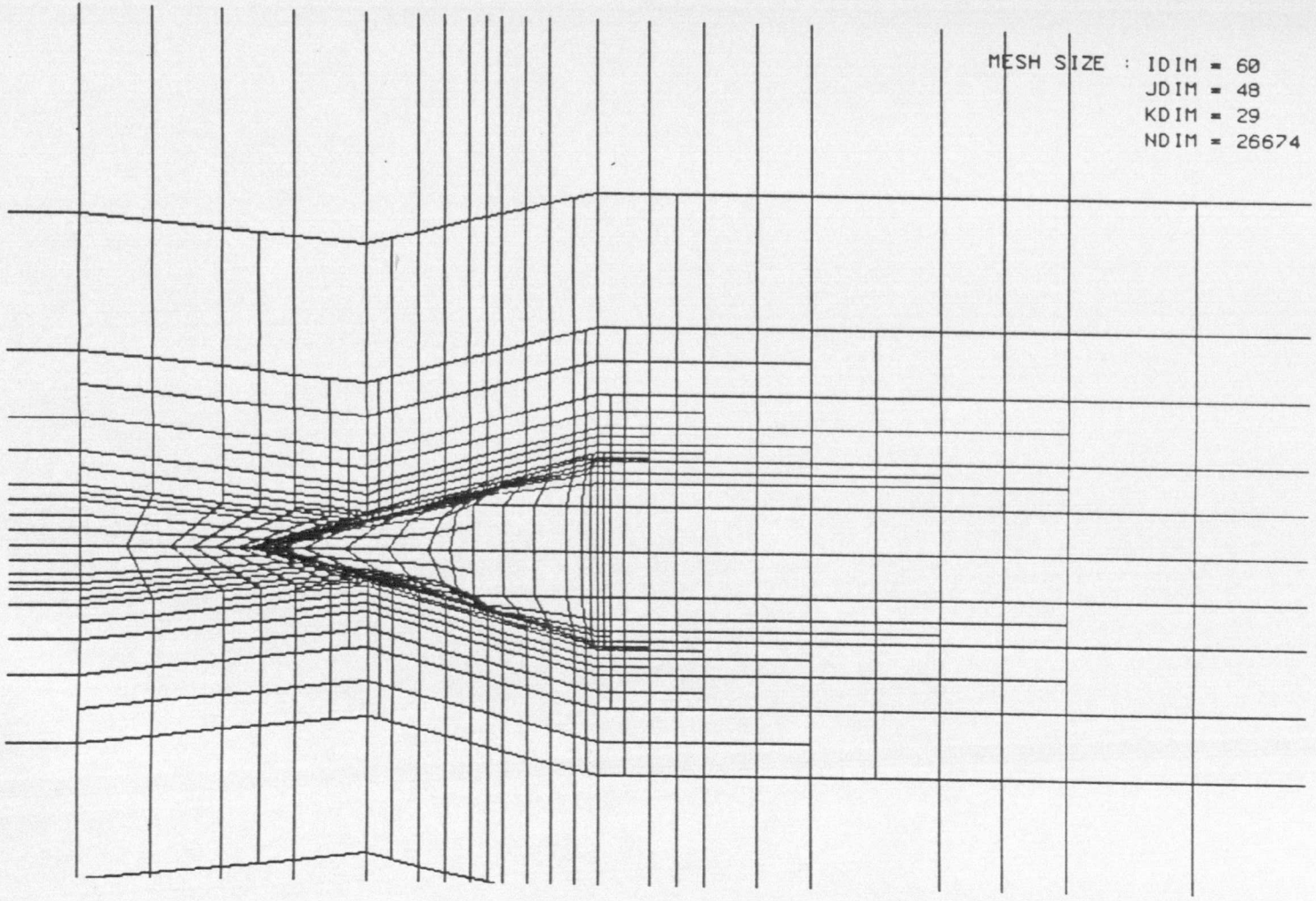

FIGURE 7.20b): Final Mesh for 3-D Wedge Probe at One Stem Diameter Immersion (Cross-sectional View)

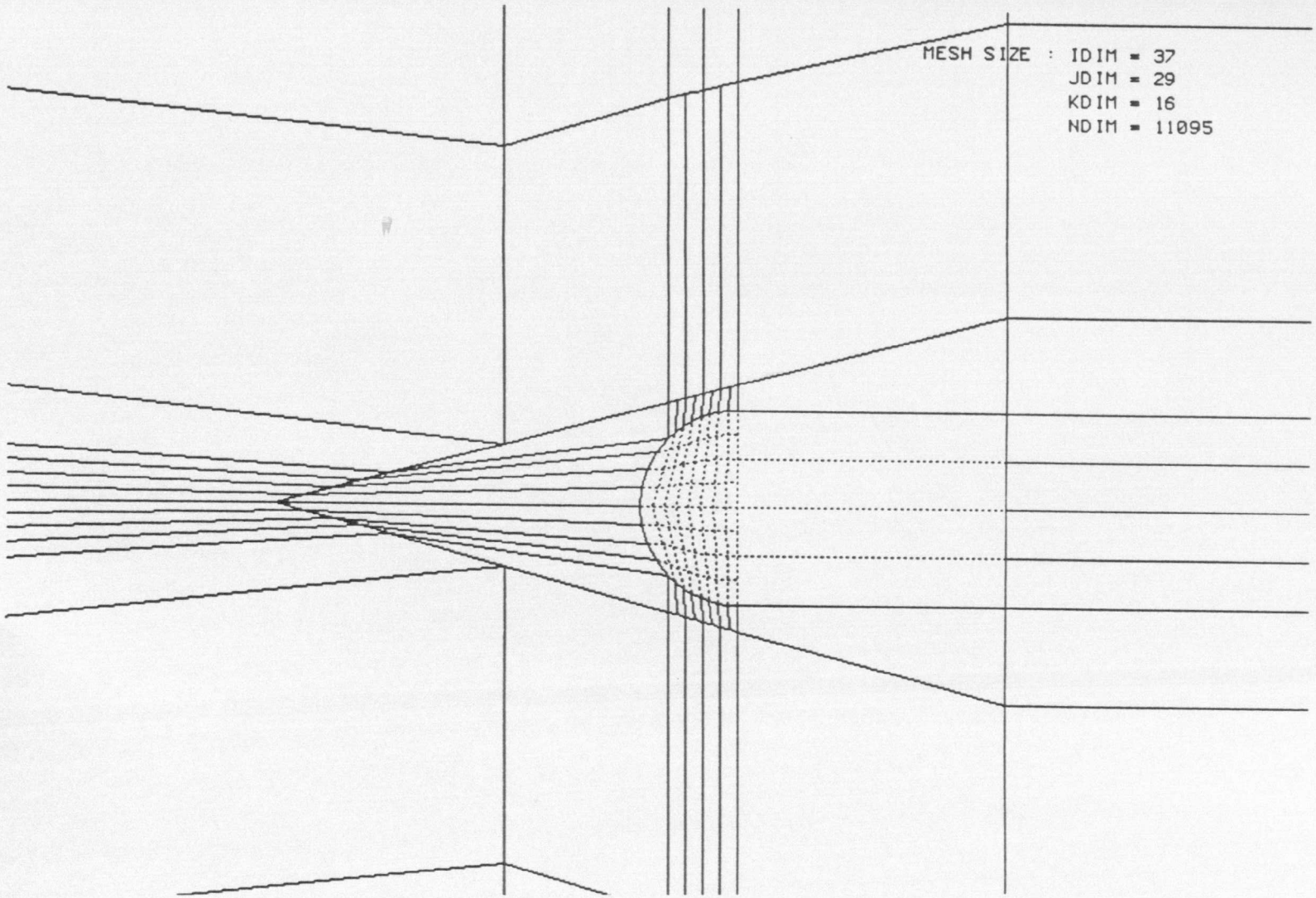

FIGURE 7.21: Preliminary Step in Constructing the 3-D Wedge Probe Interface Piece Mesh - Embedding of Lines to form Semi-circular Leading Edge.

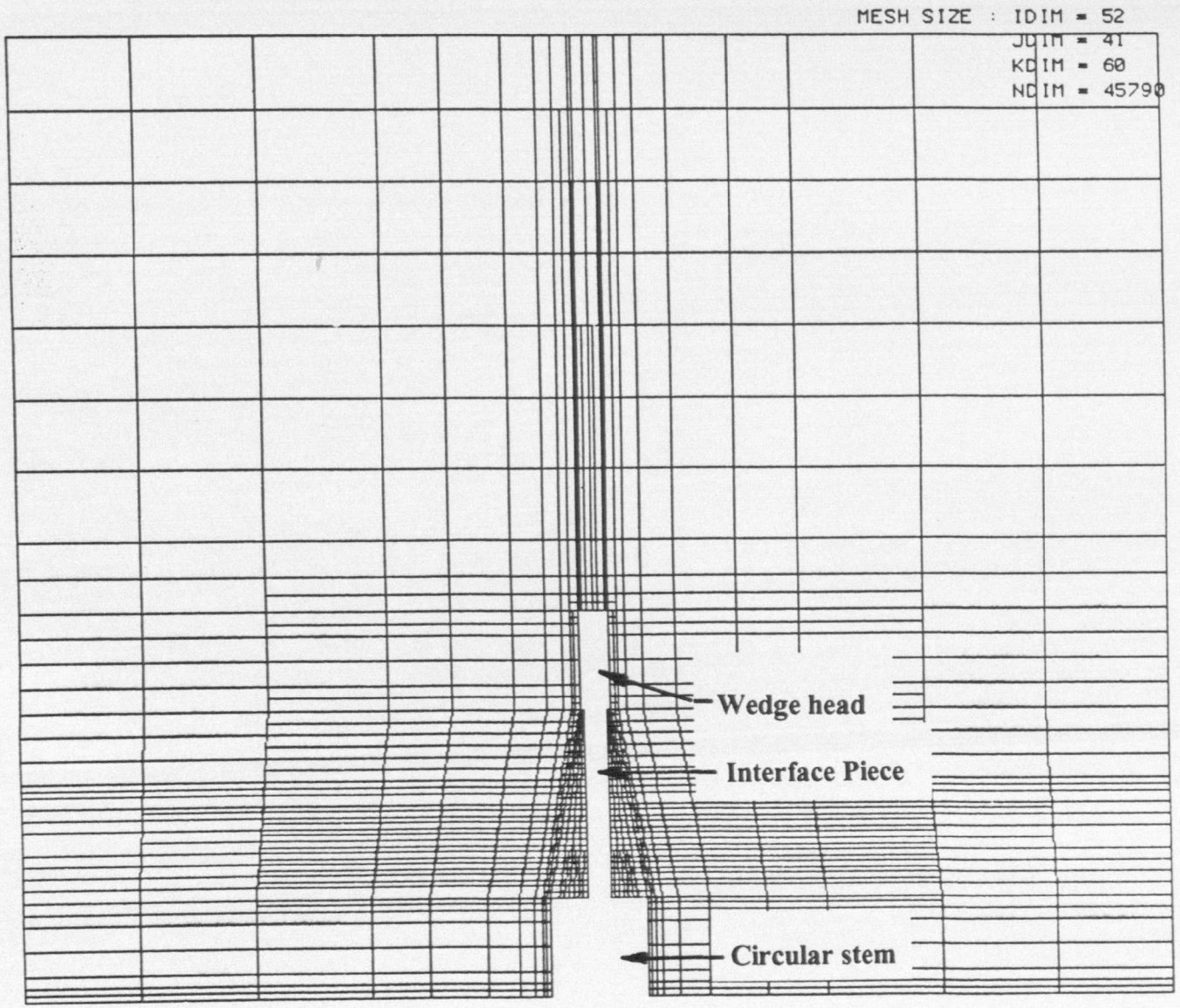

FIGURE 7.22: Skewing of Grid Lines to Enable Common Wedge and Cylindrical Grid Topologies

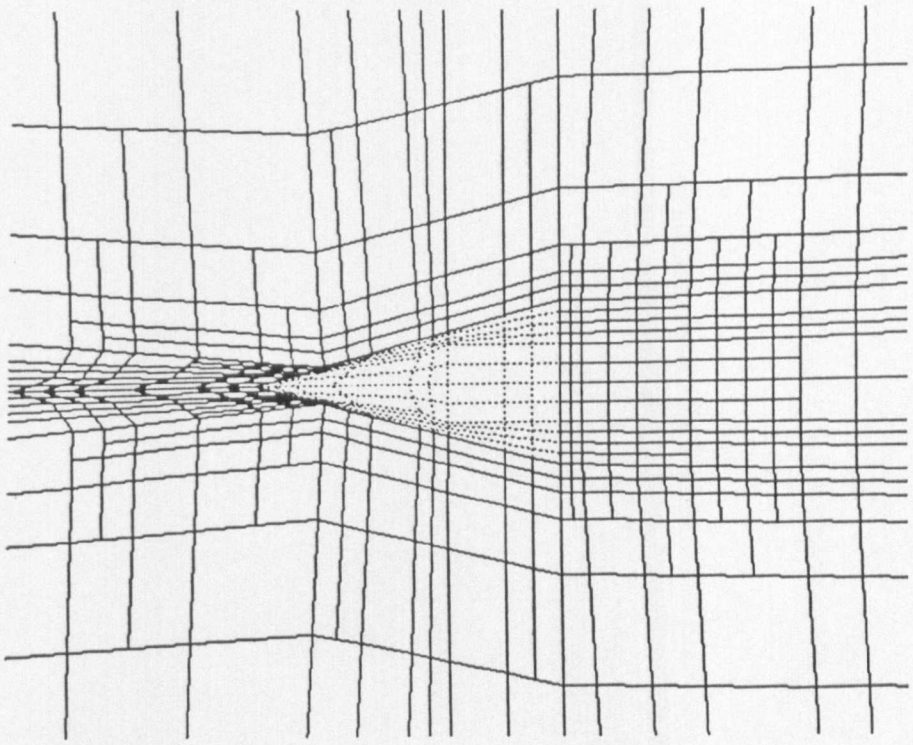

FIGURE 7.23a): Final Mesh for 3-D Wedge Probe at Four Stem Diameters Immersion (Cross-sectional View Through Wedge)

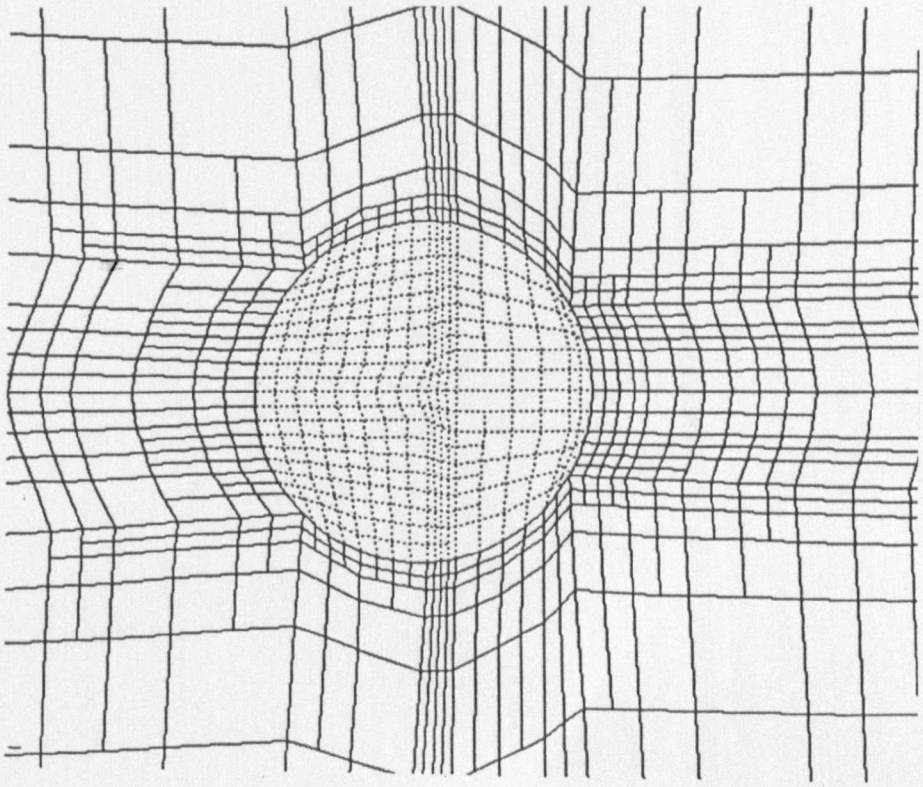

FIGURE 7.23b): Final Mesh for 3-D Wedge Probe at Four Stem Diameters Immersion (Cross-sectional View Through Cylinder)

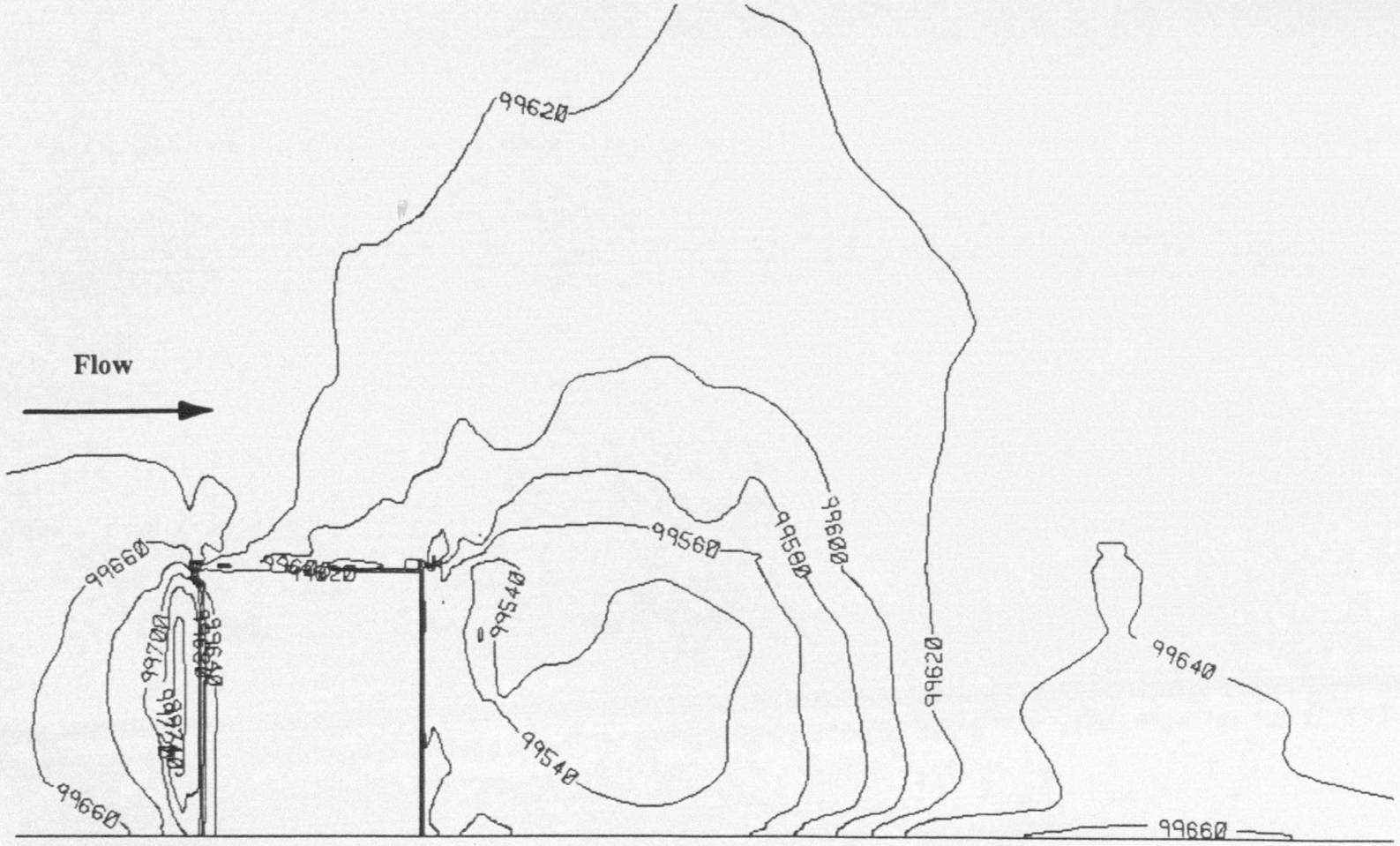

FIGURE 7.24: Static Pressure Contours for Solution of One Stem Diameter Immersion Case at Re = 8.3×10^4 (Meridional View)

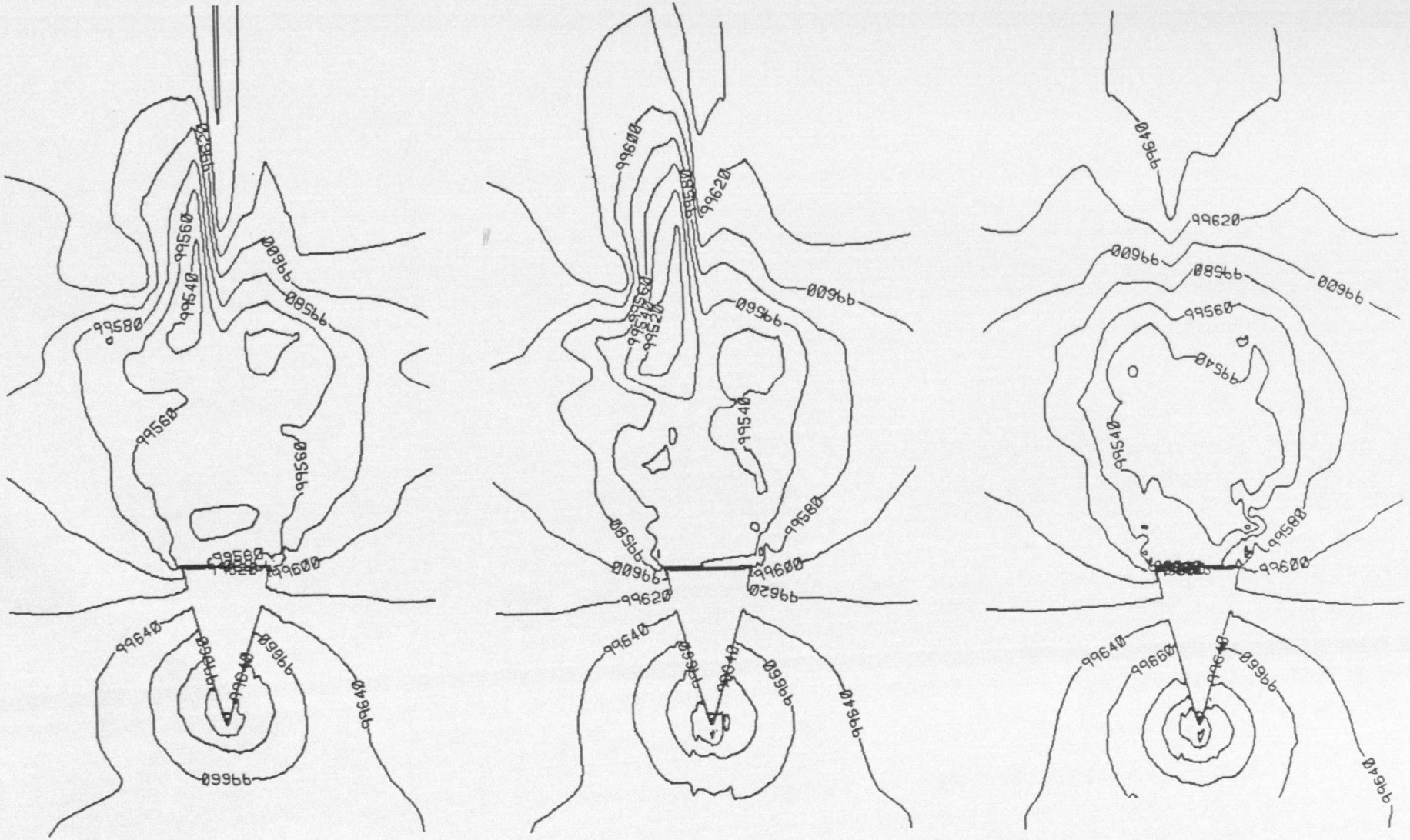

a): Near Wall b): Mid-Span c): Near Tip

FIGURE 7.25: Static Pressure Contours for Solution of One Stem Diameter Immersion Case at Re = 8.3×10^4 (Cross-Sectional Views)

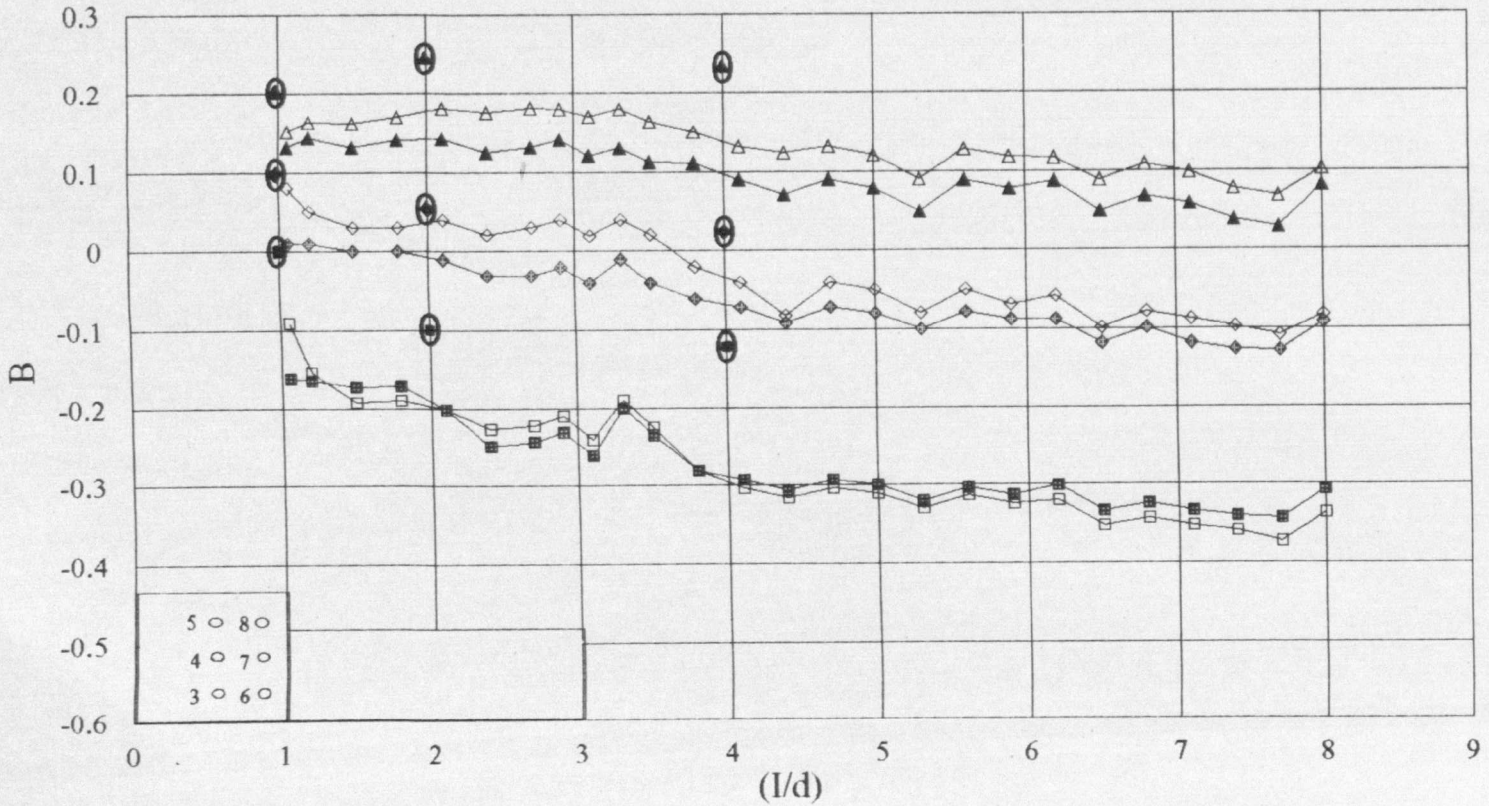

FIGURE 7.26: Comparison of CFD Calculated and Experimentally Determined Static Pressure Coefficients for Larg Scale Probe

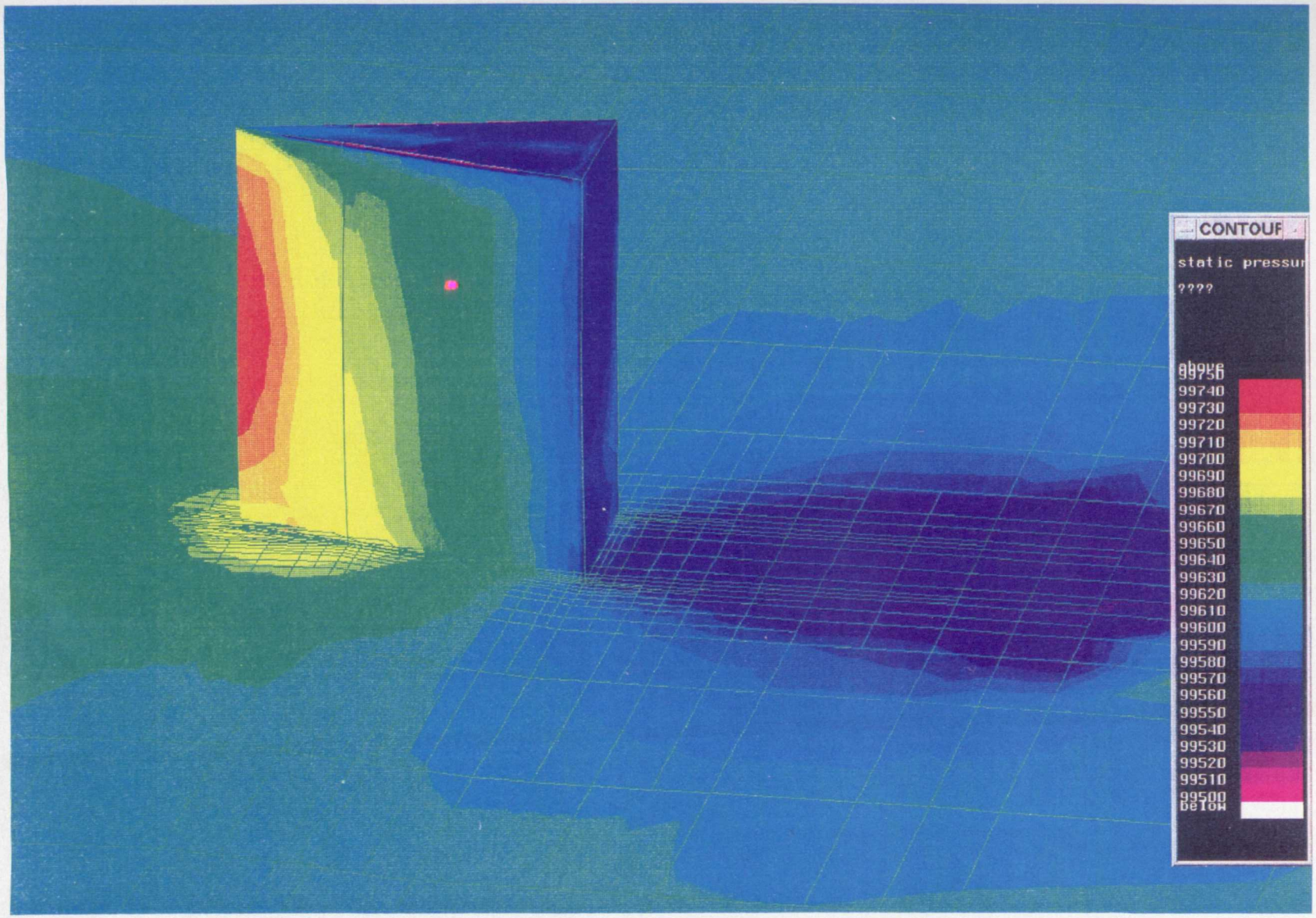

FIGURE 7.27: Surface Static Pressure Variation for Solution of One Stem Diameter Immersion Case at Re = 8.3×10^4

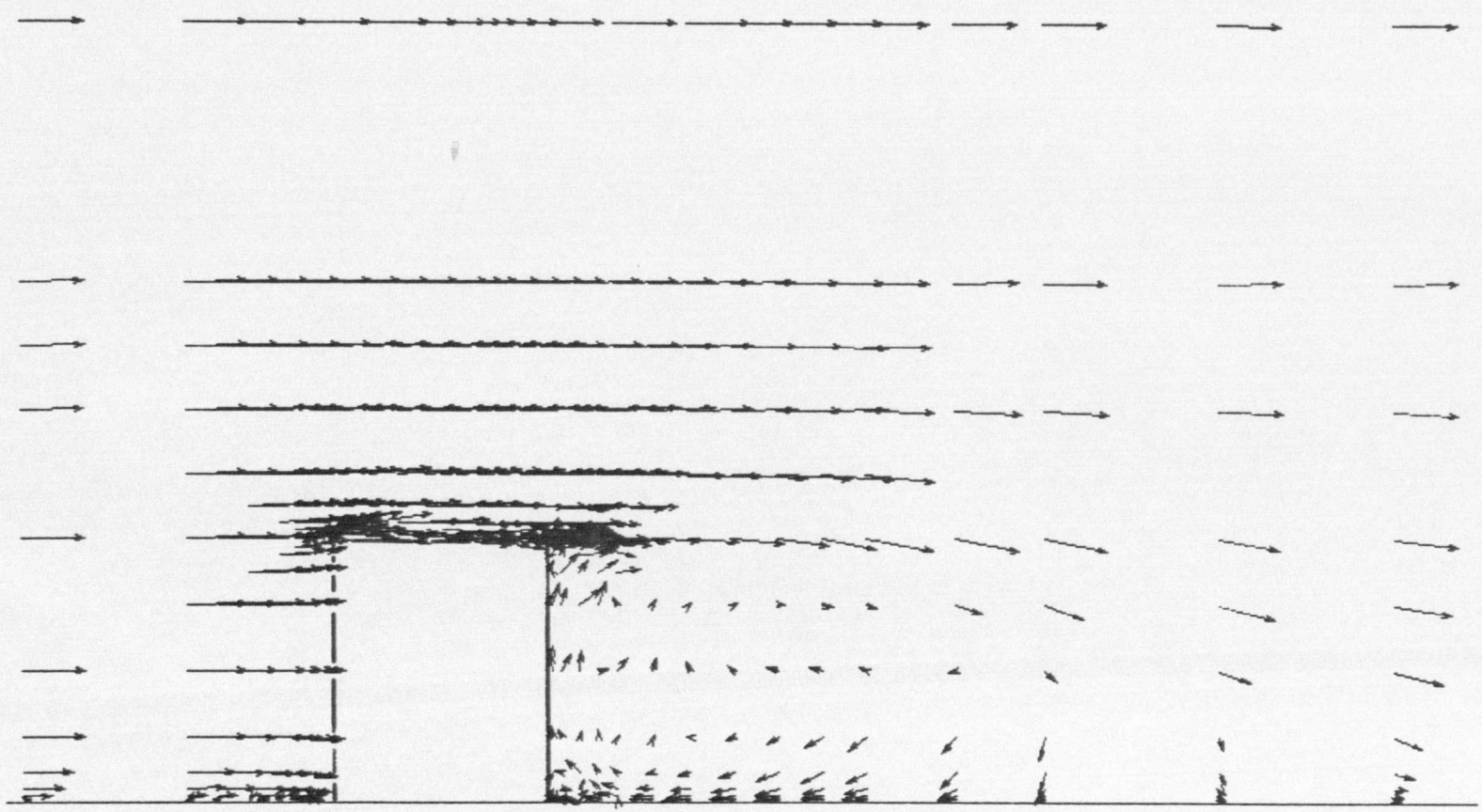

FIGURE 7.28: Velocity Vectors for Solution of One Stem Diameter Immersion Case at Re = 8.3×10^4 (Meridional View)

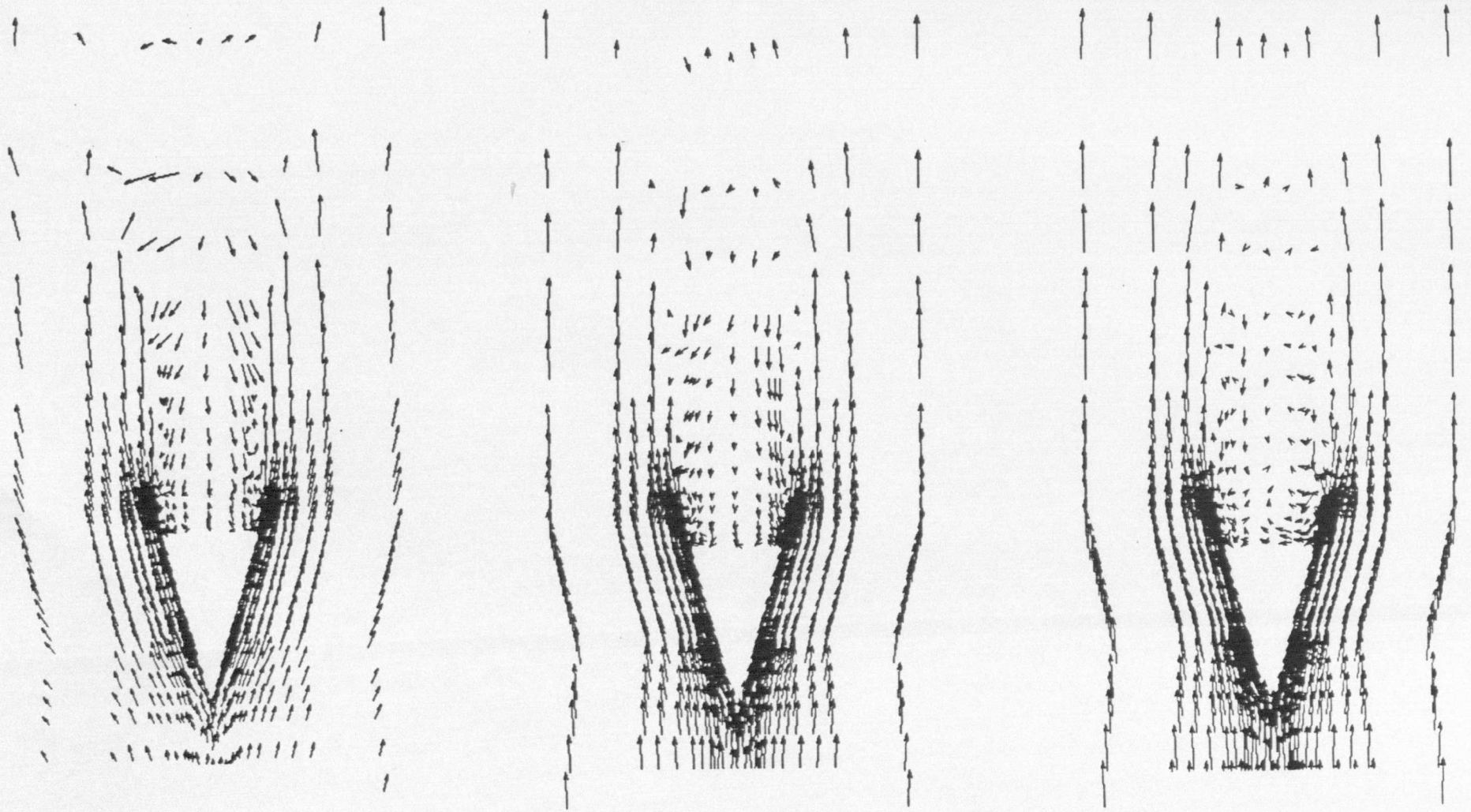

a): Near Wall

b): Mid-Span

c): Near Tip

FIGURE 7.29: Velocity Vectors for Solution of One Stem Diameter Immersion Case at Re = 8.3×10^4 (Cross-Sectional Views)

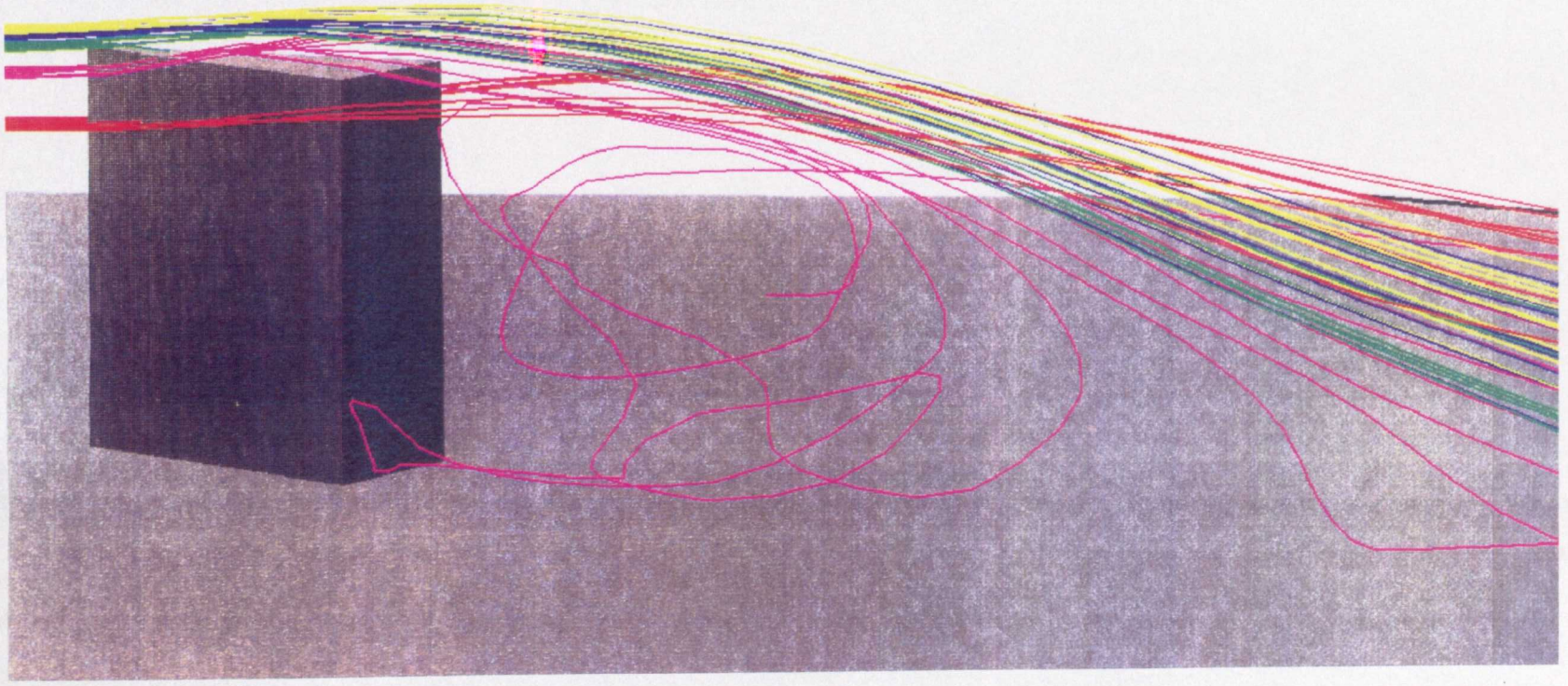

FIGURE 7.30: Streakline Representation of Flow Over Probe Tip at One Stem Diameter Immersion, ($Re = 8.3x10^4$)

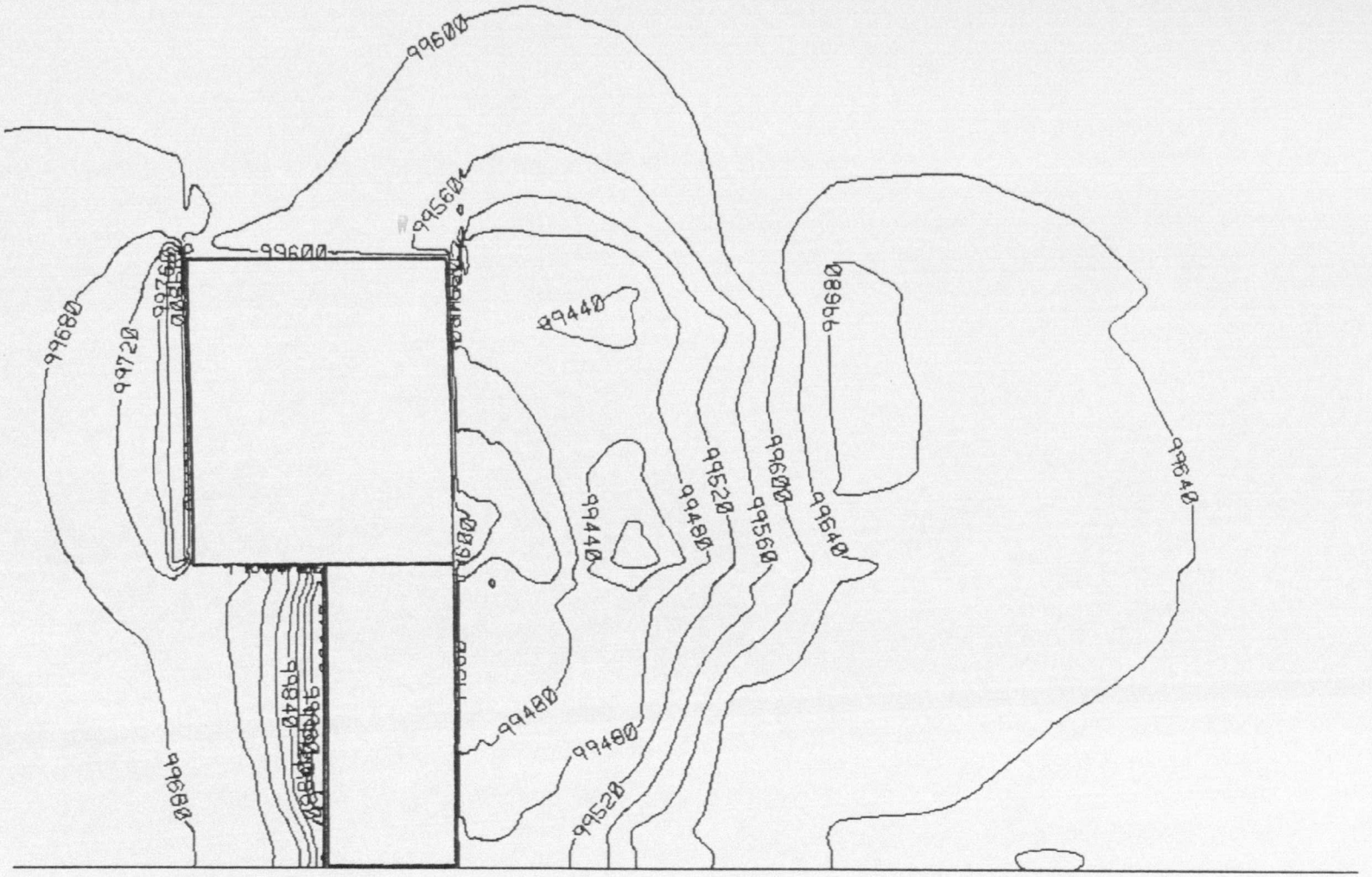

FIGURE 7.31: Static Pressure Contours for Solution of Two Stem Diameters Immersion Case at Re = 8.3×10^4 (Meridional View)

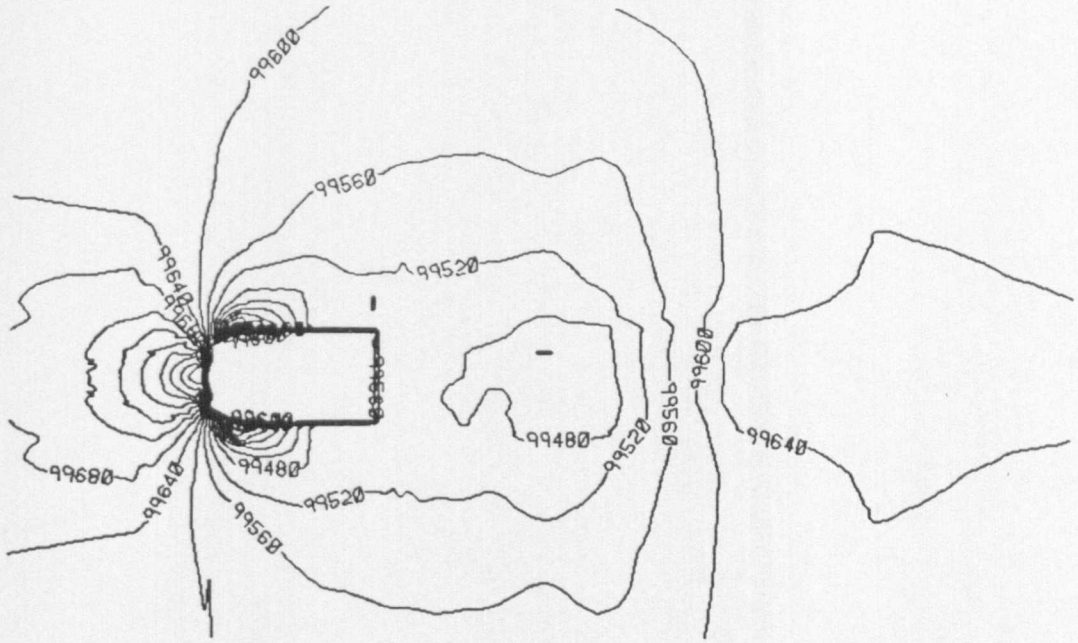

a): Interface Piece -
Mid-height

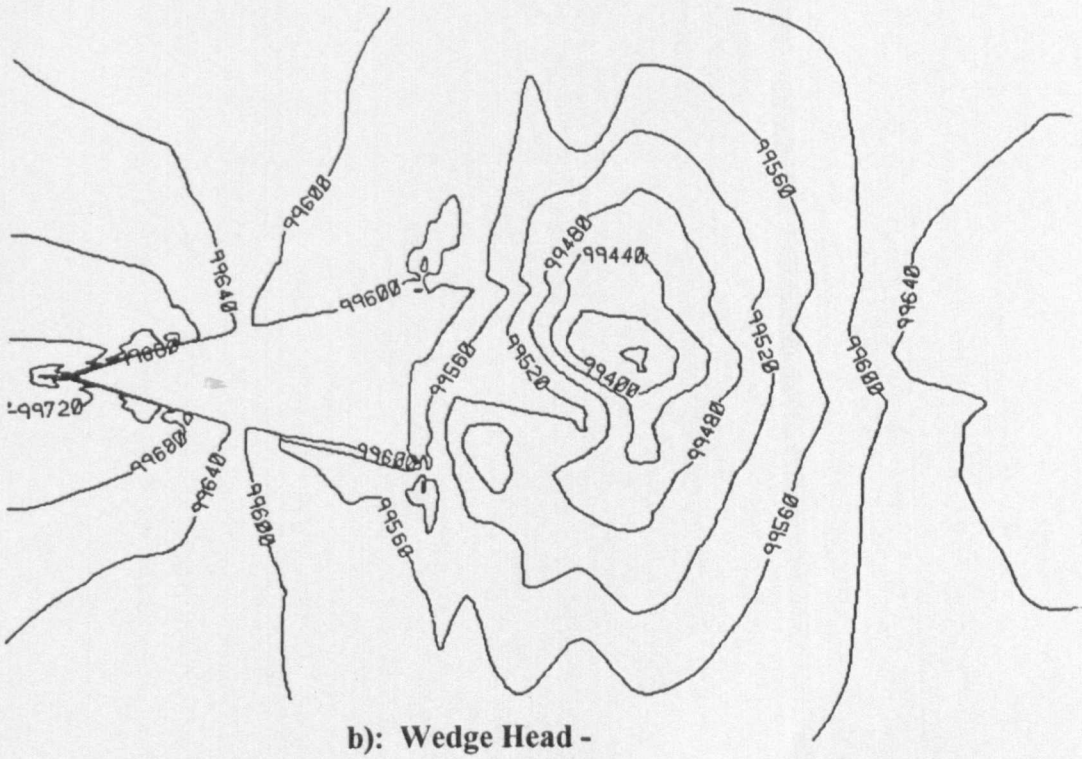

b): Wedge Head -
Supported End

FIGURE 7.32: Static Pressure Contours for Solution of Two Stem Diameters Immersion Case at Re = 8.3×10^4 (Cross-Sectional Views)

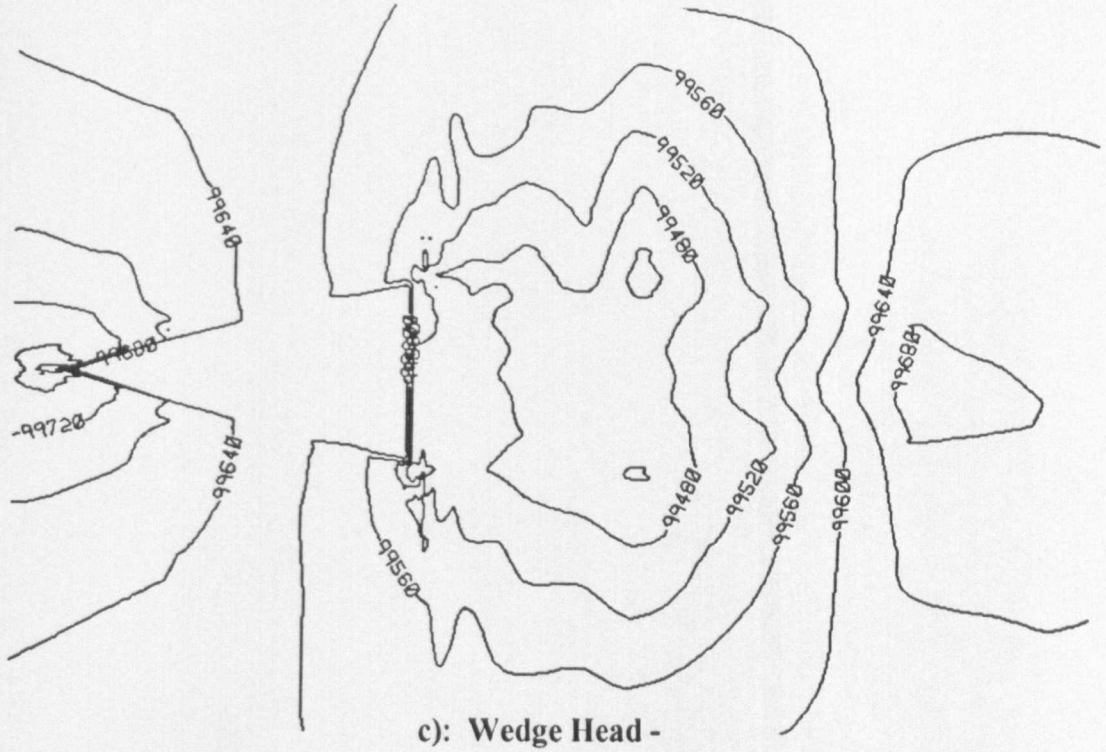

c): Wedge Head - Mid-Span

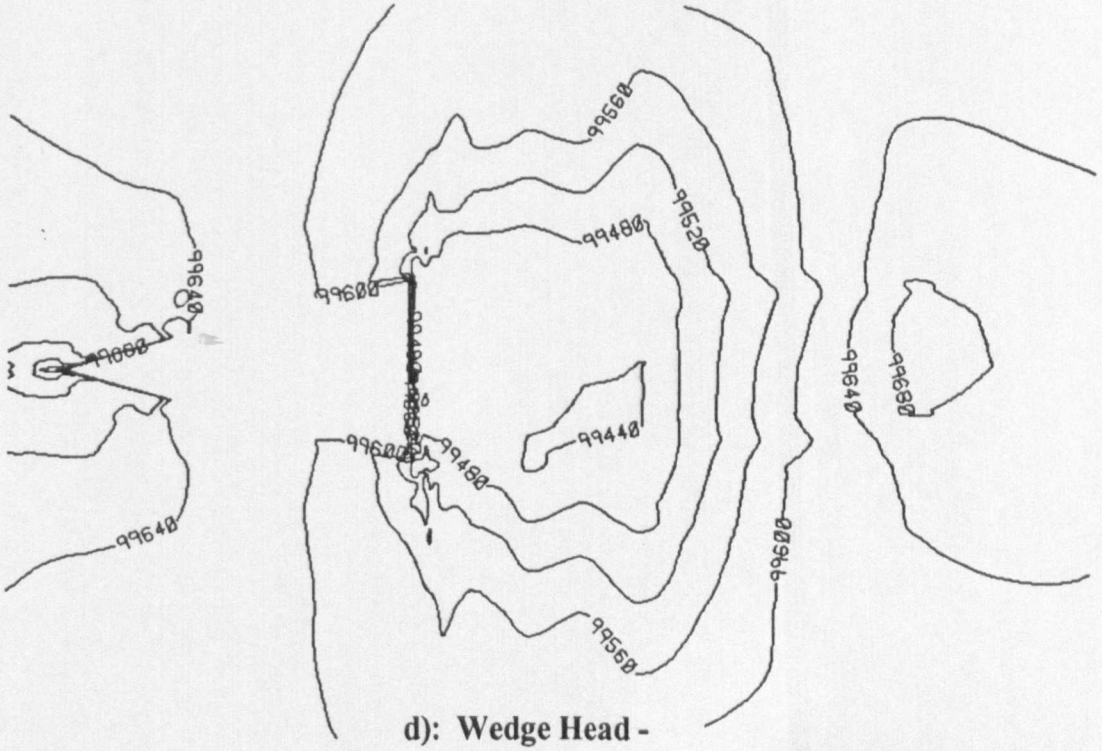

d): Wedge Head - Near Tip

FIGURE 7.32: Static Pressure Contours for Solution of Two Stem Diameters Immersion Case at Re=8.3x10^4 (Cross-Sectional Views)

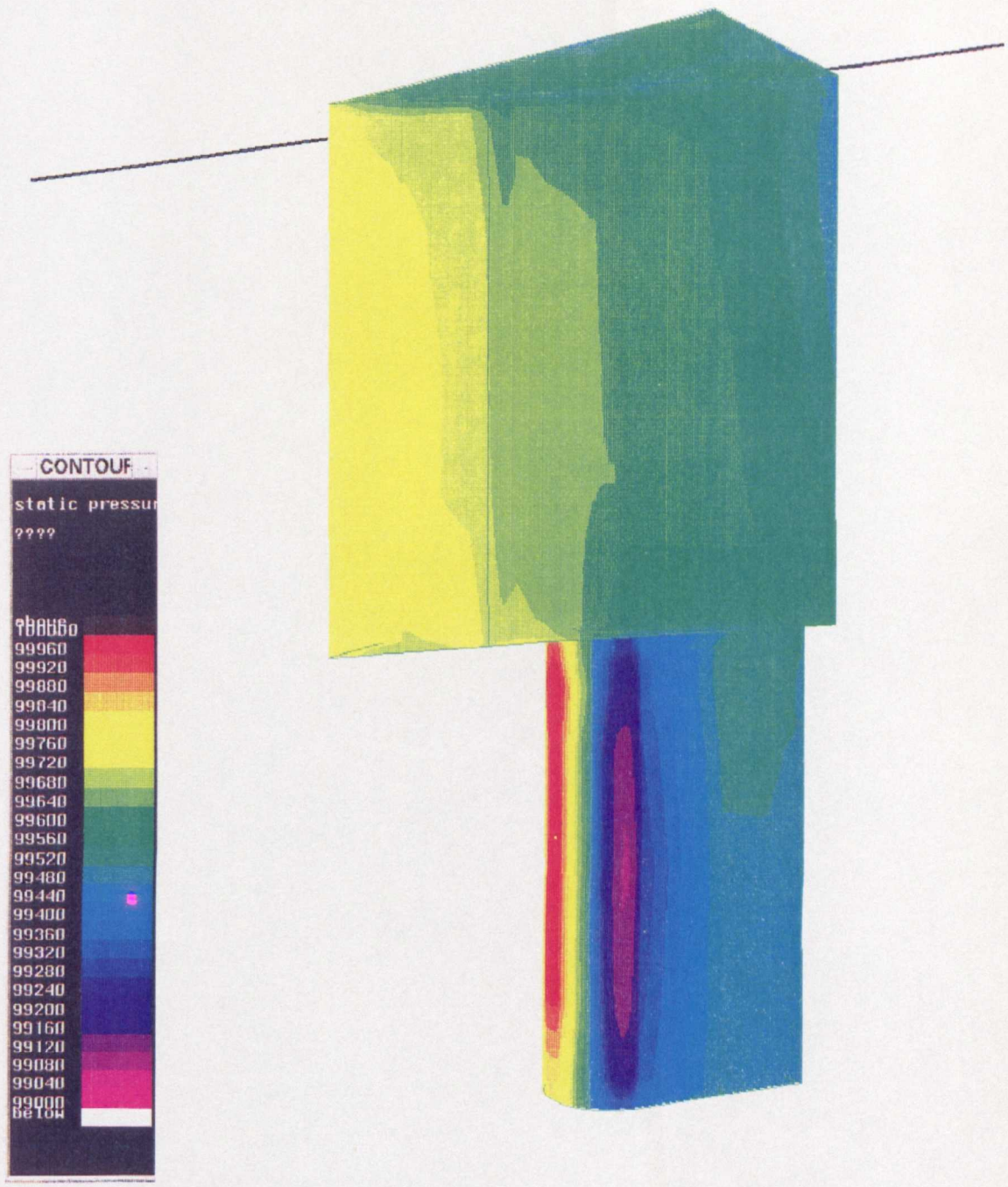

FIGURE 7.33: Surface Static Pressure Variation for Solution of Two Stem Diameters Immersion Case at Re = 8.3×10^4

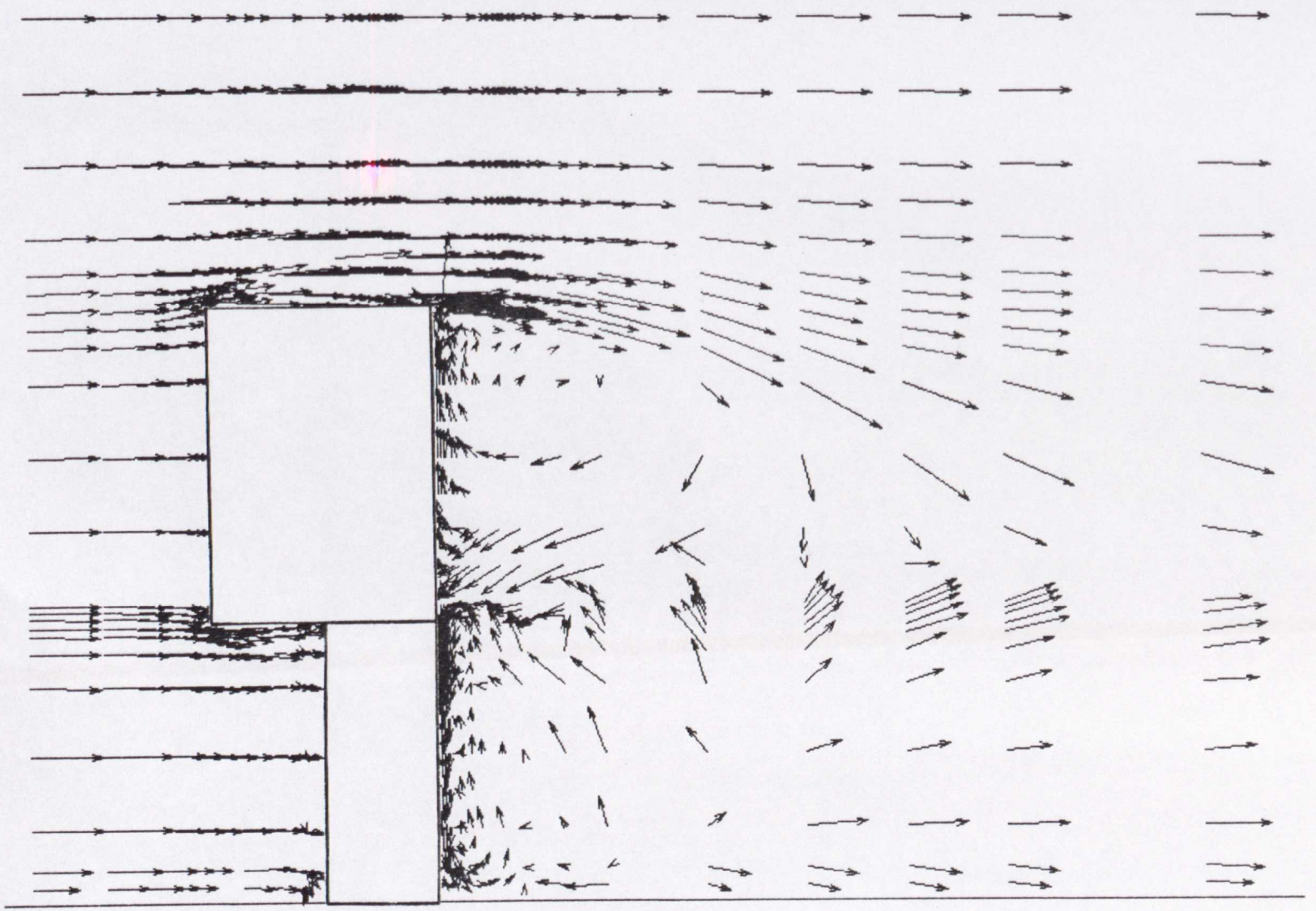

FIGURE 7.34: Velocity Vectors for Solution of Two Stem Diameters Immersion Case at Re = 8.3×10^4 (Meridional View)

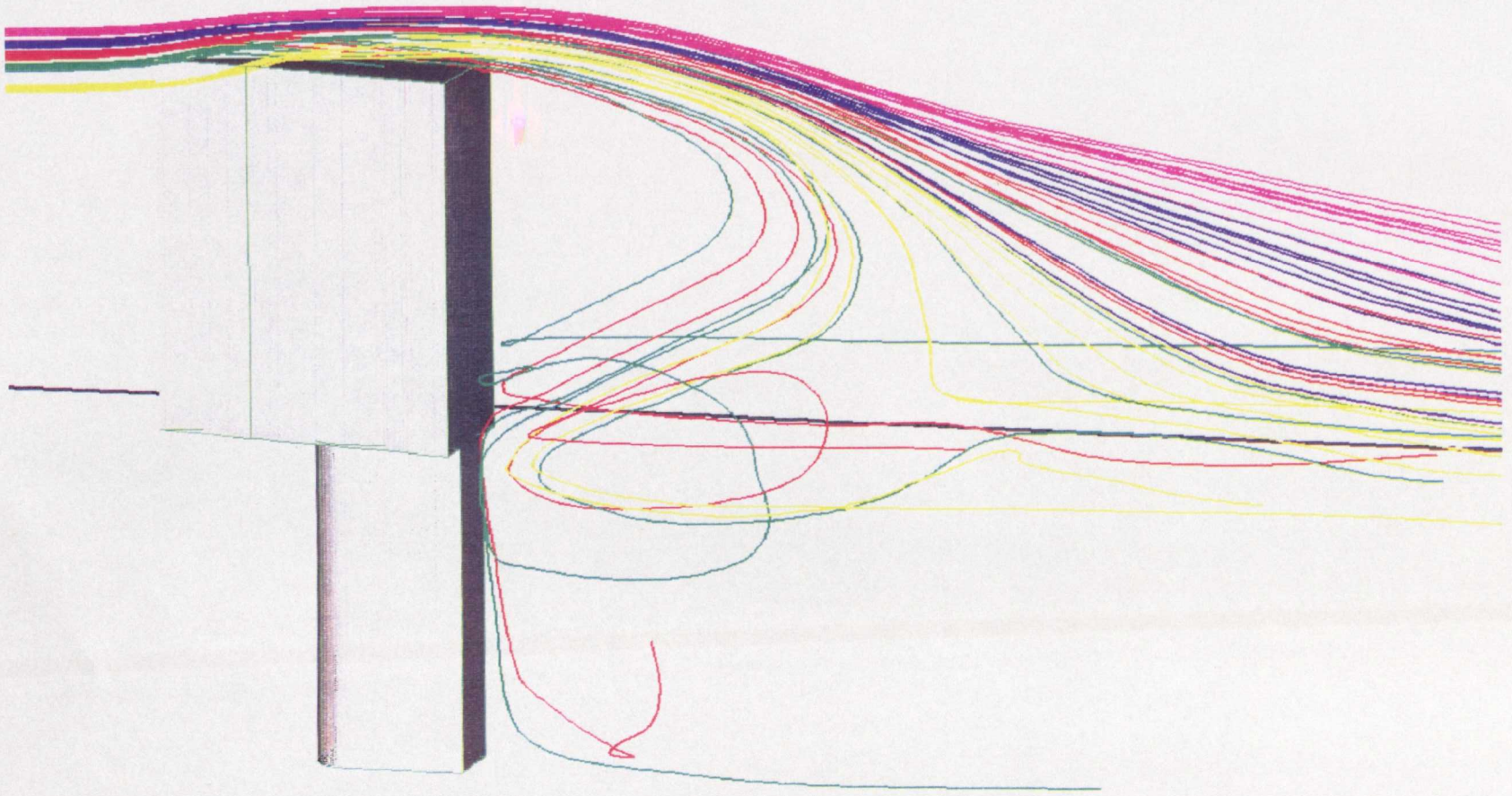

FIGURE 7.35a): Streakline Representation of Flow Over Probe Tip at Two Stem Diameters Immersion, ($Re = 8.3x10^4$)

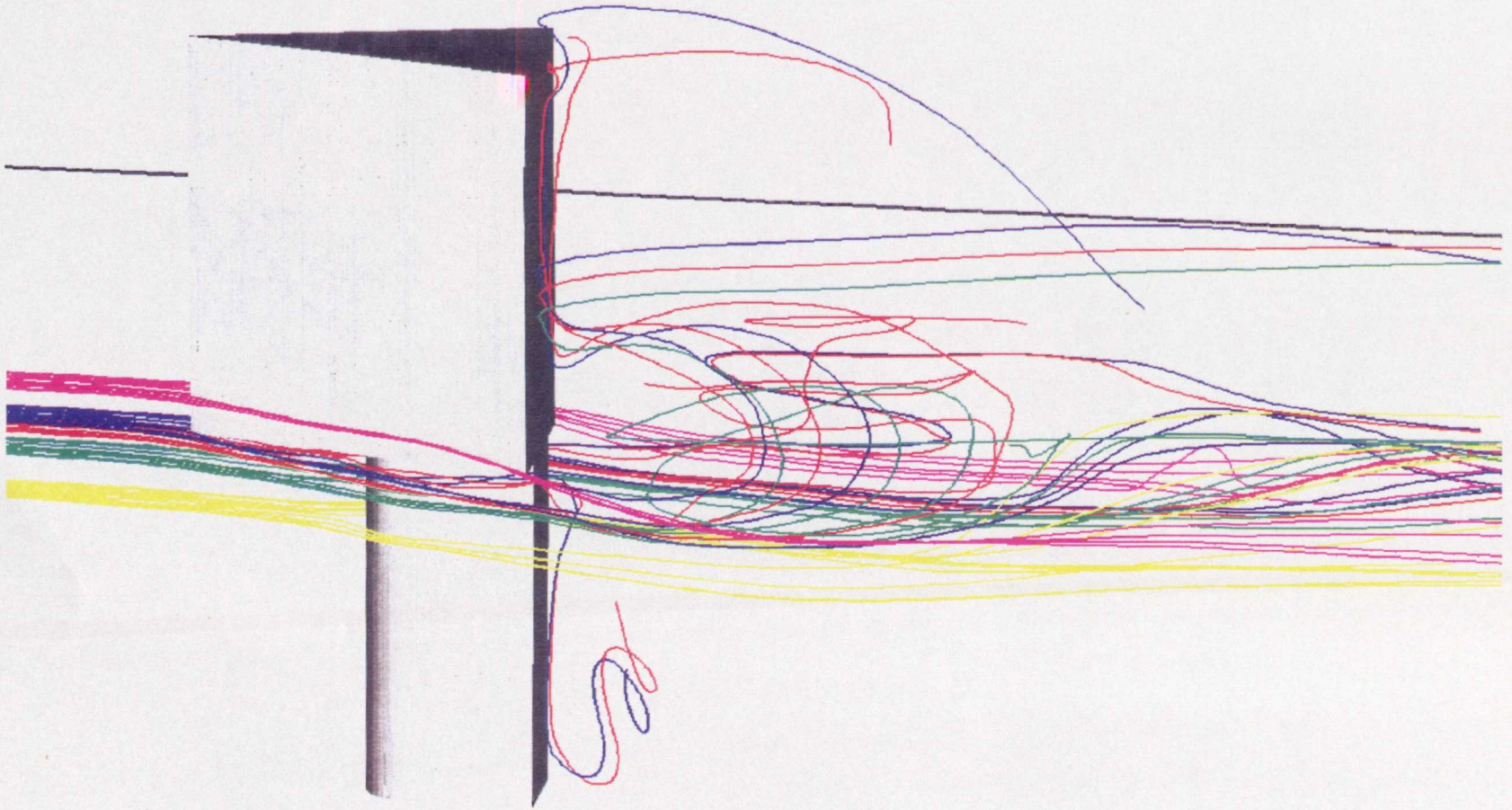

FIGURE 7.35b): Streakline Representation of Flow Under Wedge Head Supported End at Two Stem Diameters Immersion, ($Re = 8.3x10^4$)

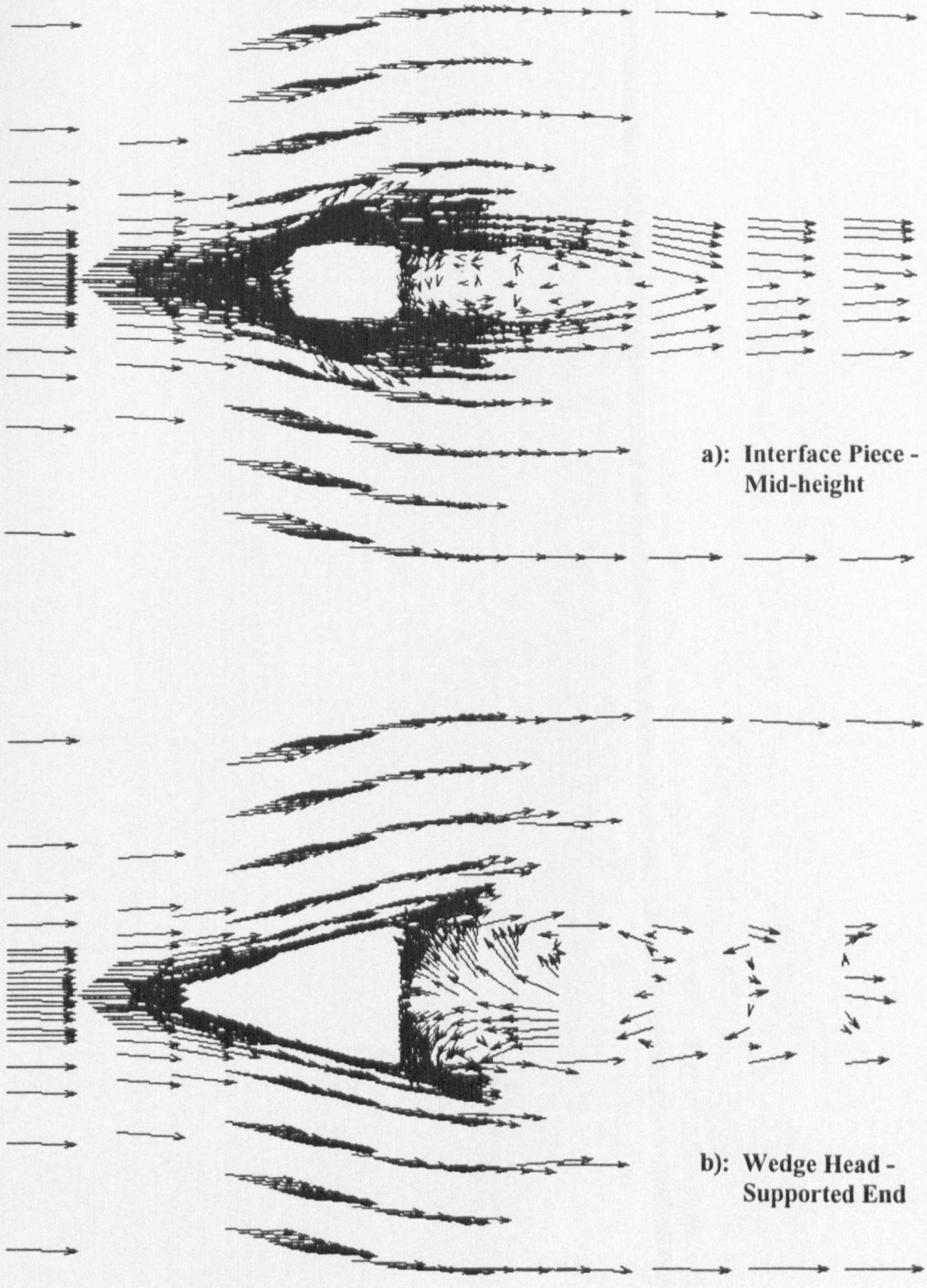

FIGURE 7.36: Velocity Vectors for Solution of Two Stem Diameters Immersion Case at Re = 8.3×10^4 (Cross-Sectional Views)

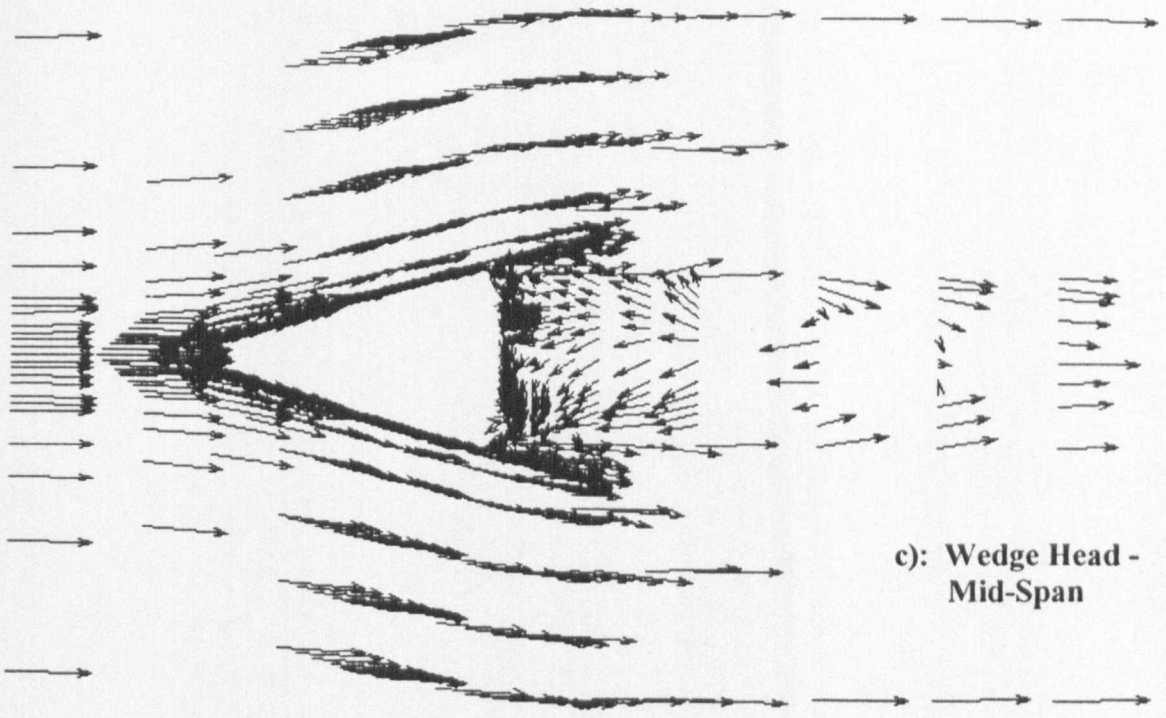

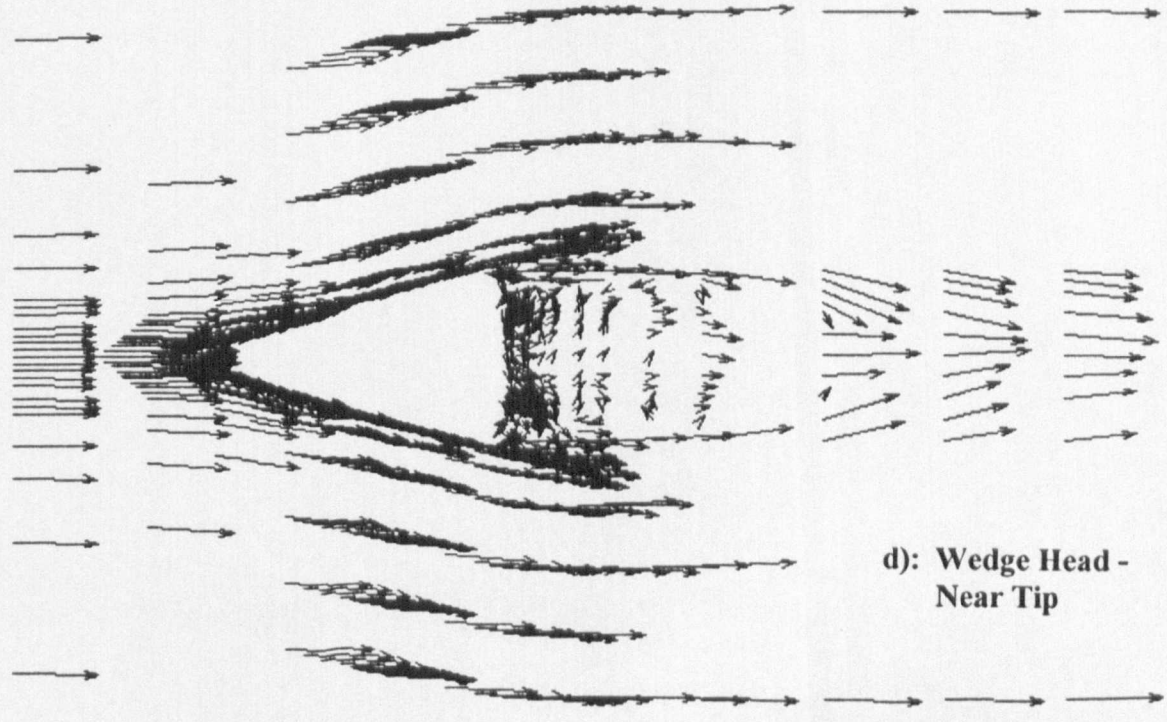

FIGURE 7.36: Velocity Vectors for Solution of Two Stem Diameters Immersion Case at Re=8.3x10^4 (Cross-Sectional Views)

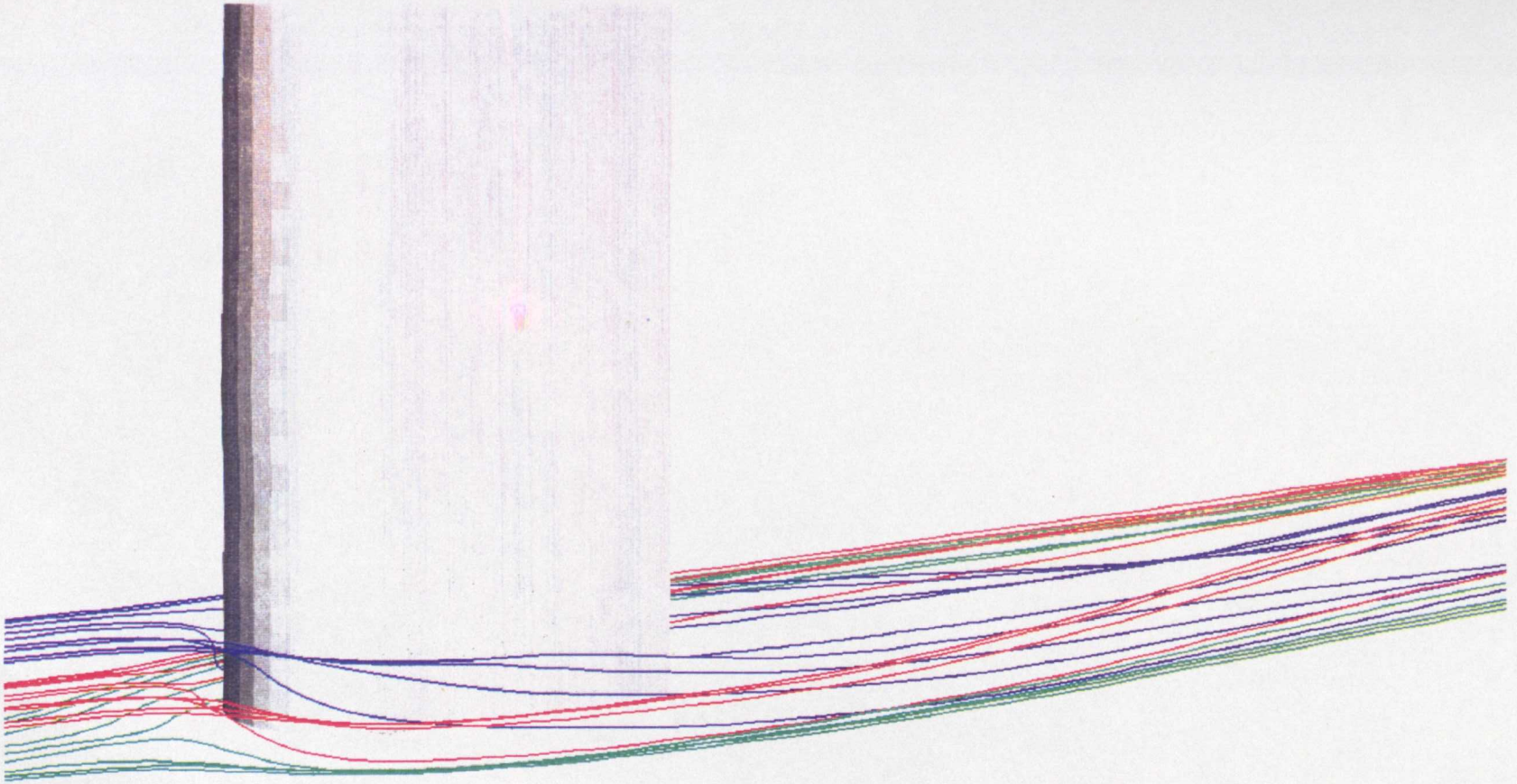

FIGURE 7.37: Streakline Representation of Flow at Base of Interface Piece at Two Stem Diameters Immersion, ($Re = 8.3x10^4$)

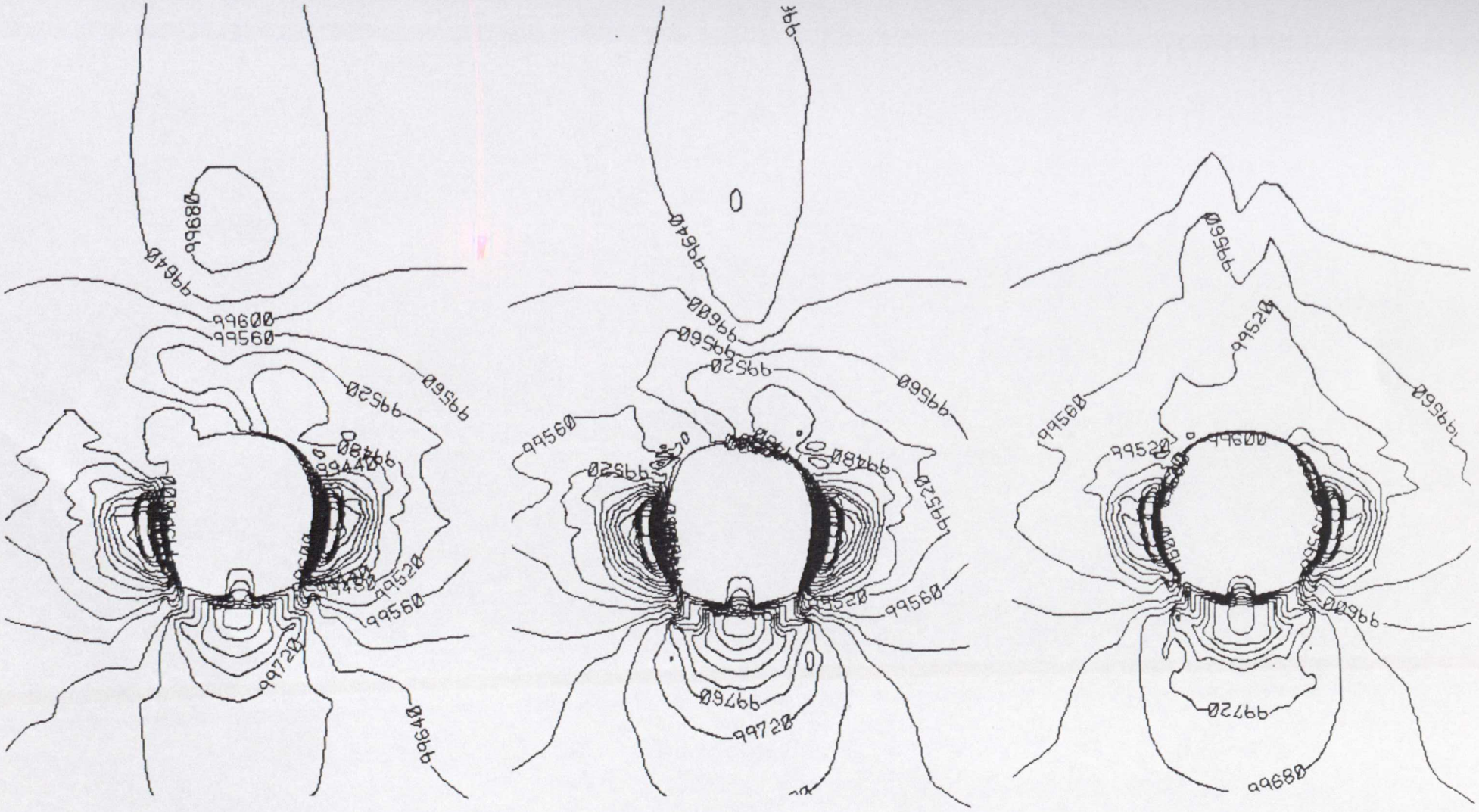

a): Near Wall b): Mid-Height c): Near Free End

FIGURE 7.38: Static Pressure Contours for Solution of Four Stem Diameters Immersion Case at Re = 8.3×10^4 (Cross-Sectional Views Through Cylindrical Stem)

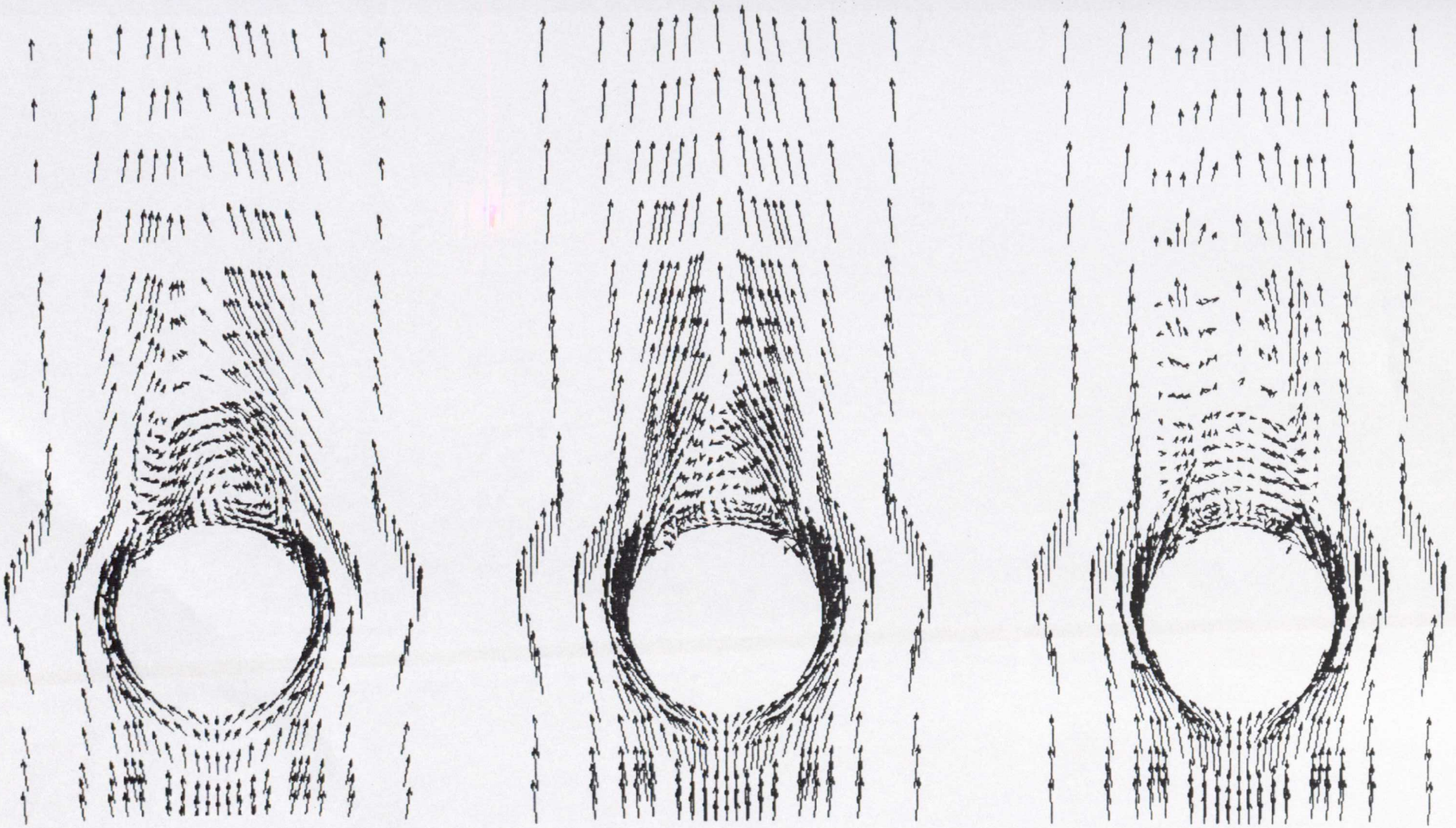

a): Near Wall

b): Mid-Position

c): Near Free-End

FIGURE 7.39: Velocity Vectors for Solution of Four Stem Diameters Immersion Case at Re = 8.3×10^4 (Cross-Sectional Views Through Cylindrical Stem)

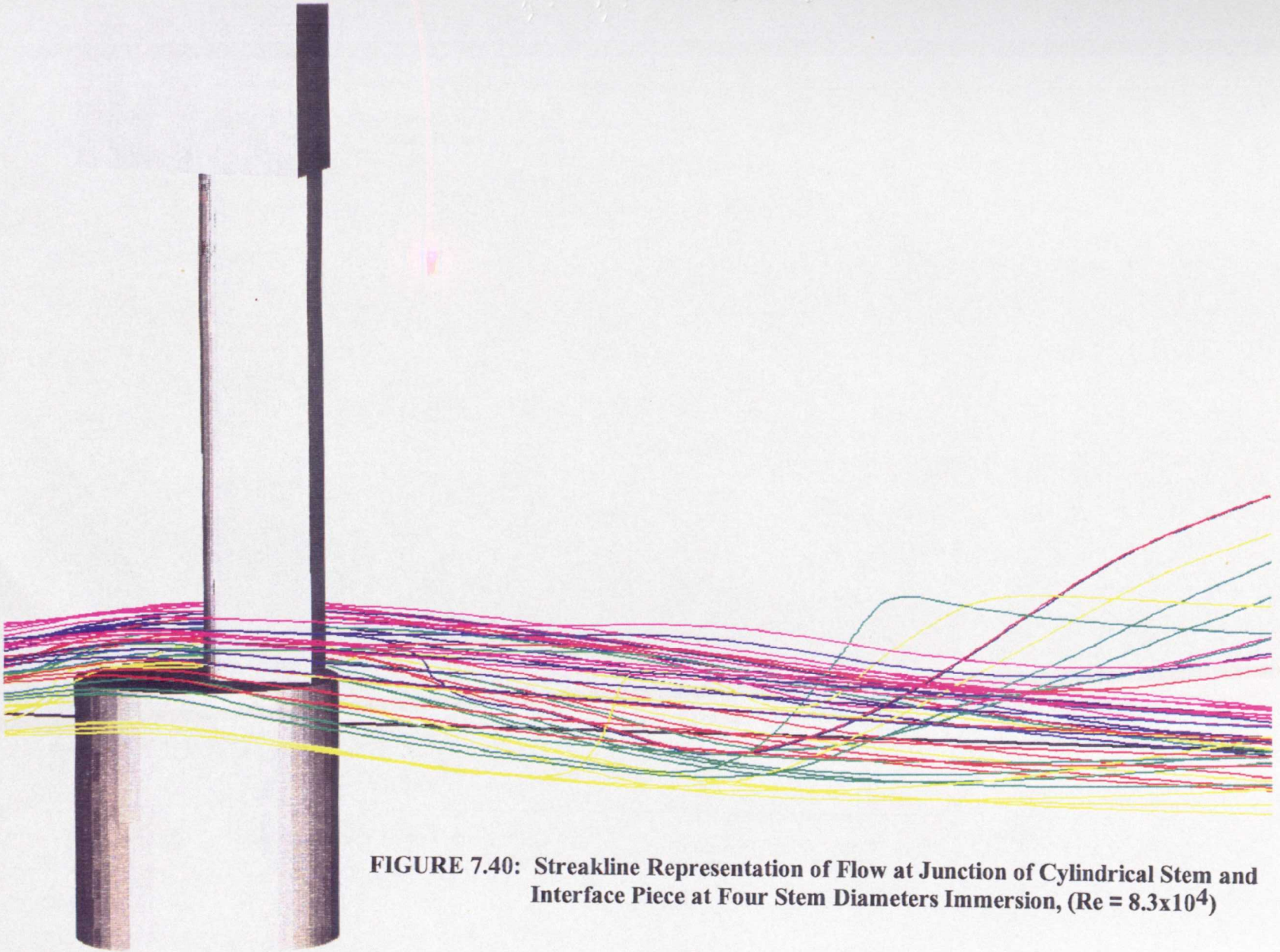

FIGURE 7.40: Streakline Representation of Flow at Junction of Cylindrical Stem and Interface Piece at Four Stem Diameters Immersion, ($Re = 8.3x10^4$)

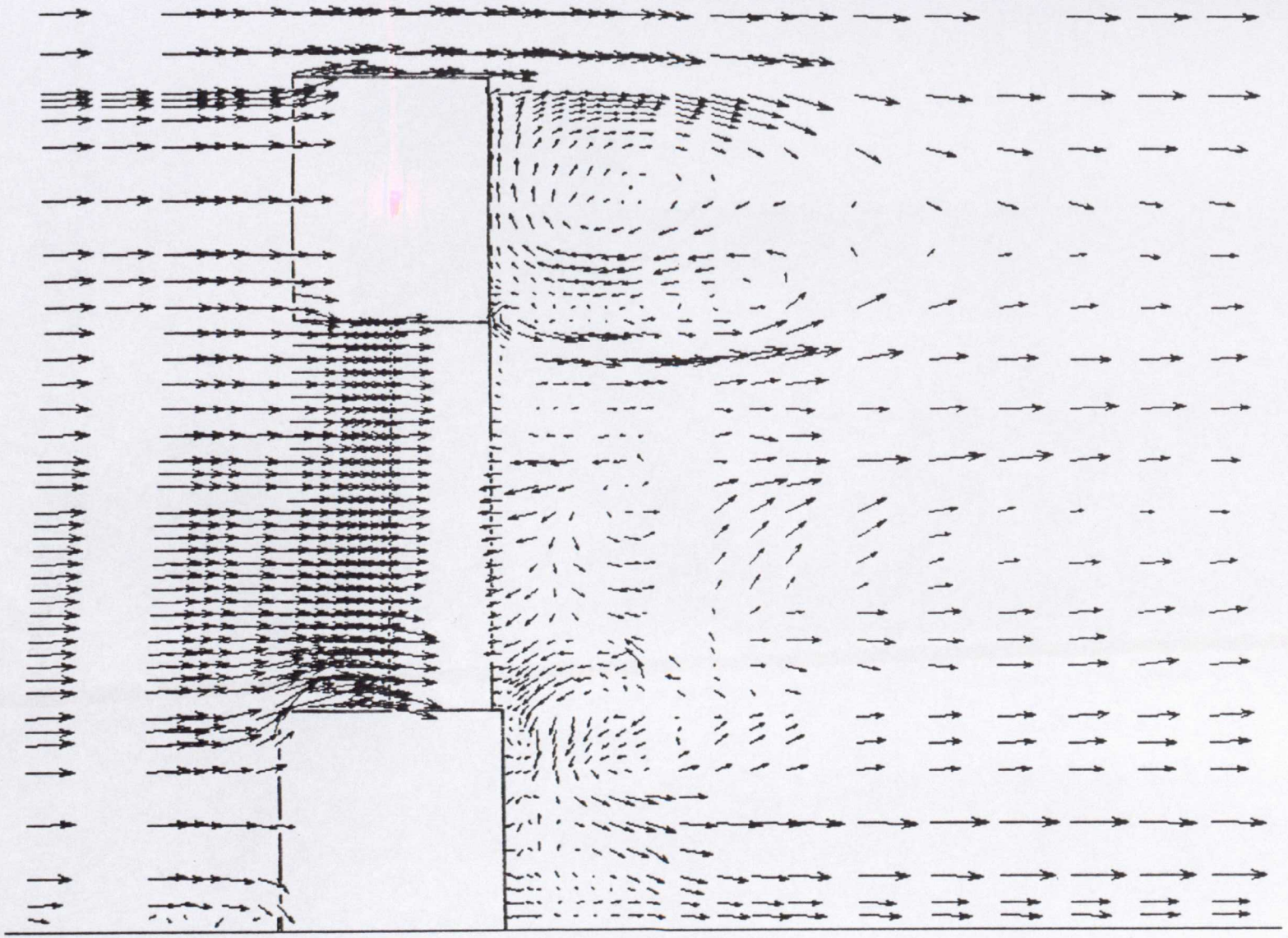

FIGURE 7.41: Velocity Vectors for Solution of Four Stem Diameters Immersion Case at Re = 8.3×10^4 (Meridional View)

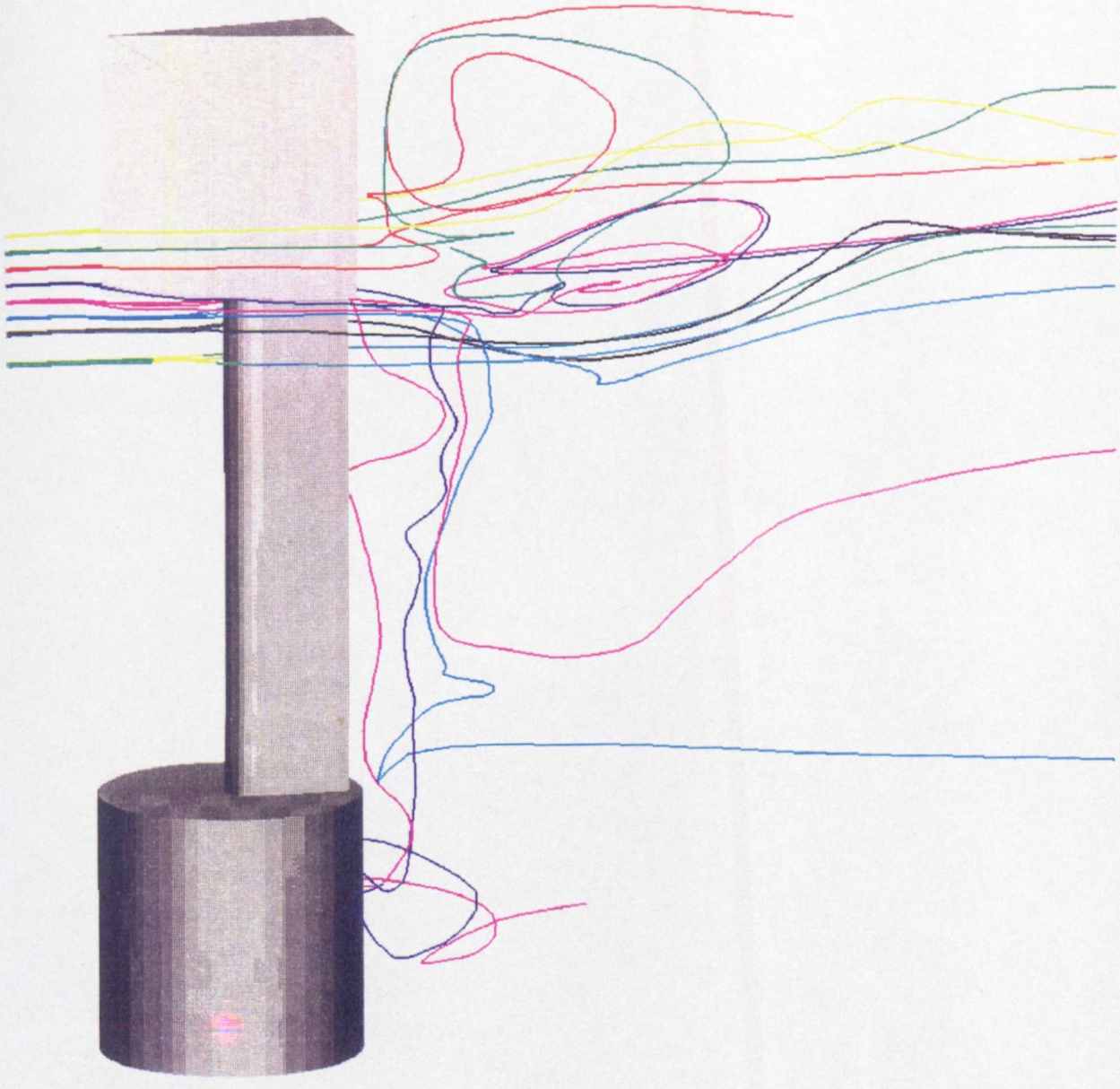

FIGURE 7.42: Streakline Representation of Flow at Junction of Interface Piece and Wedge Head at Four Stem Diameters Immersion, ($Re = 8.3x10^4$)

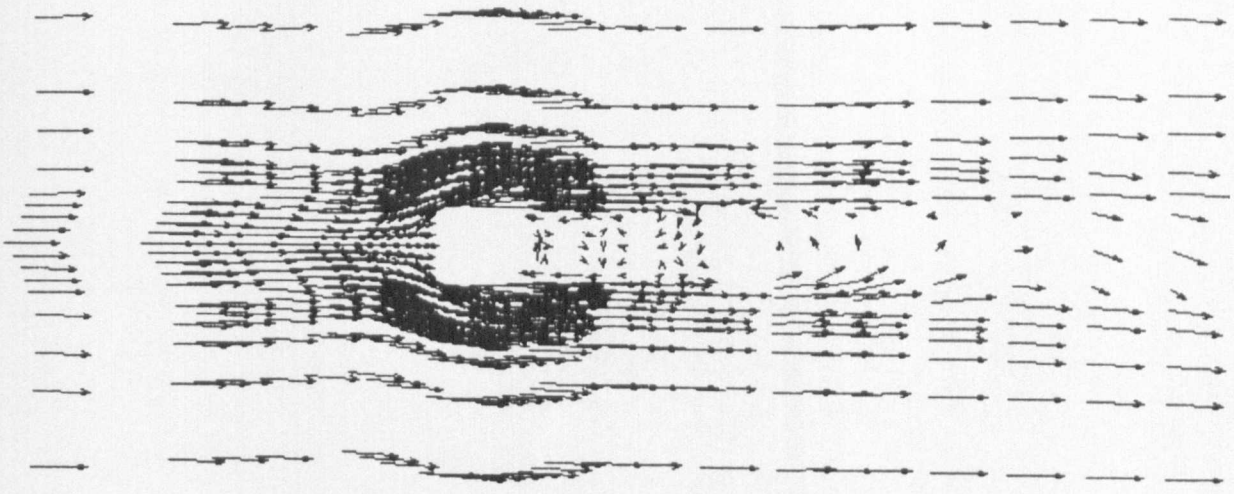

a): Interface Piece -
Mid-height

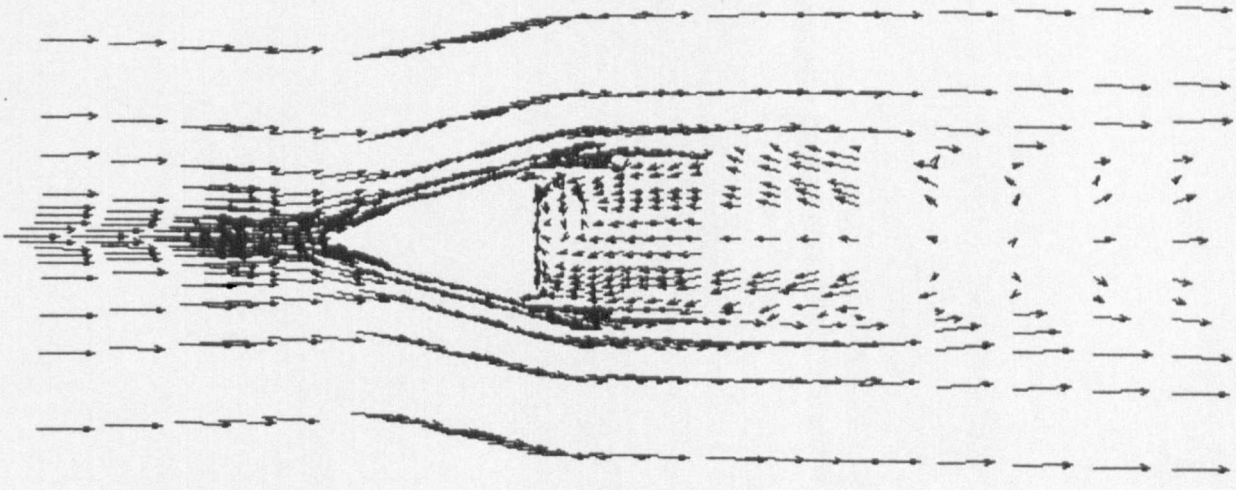

b): Wedge Head -
Supported End

FIGURE 7.43: Velocity Vectors for Solution of Four Stem Diameters Immersion Case at Re = 8.3×10^4 (Cross-Sectional Views)

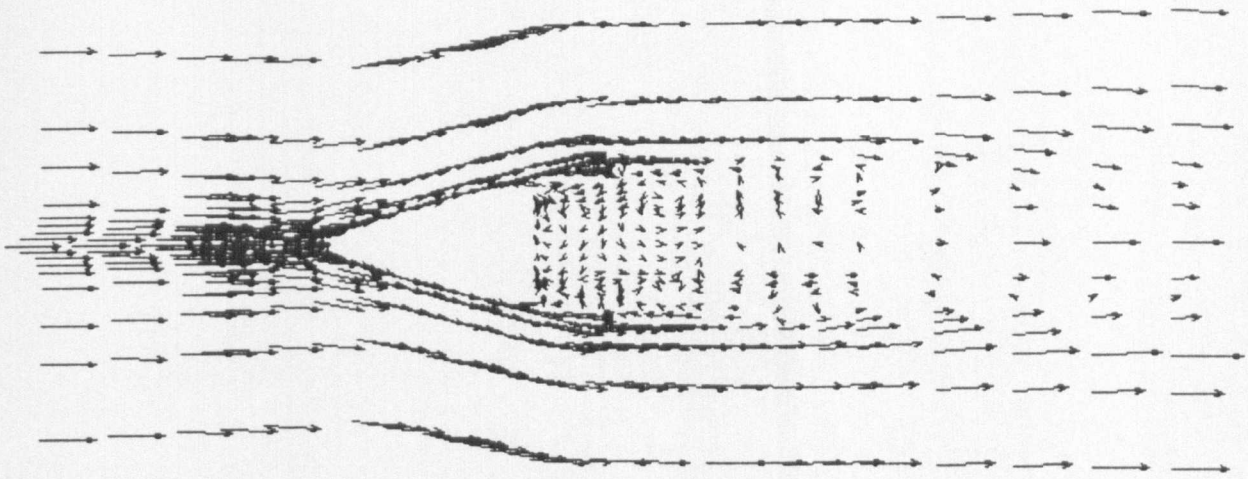

c): Wedge Head -
Mid-Span

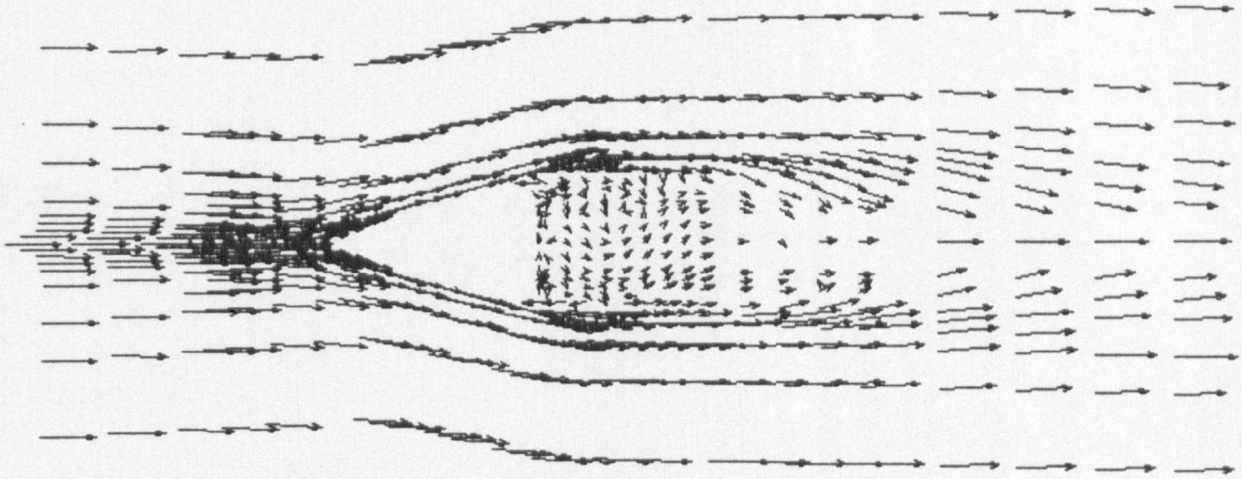

d): Wedge Head -
Near Tip

FIGURE 7.43: Velocity Vectors for Solution of Four Stem Diameters Immersion Case at Re=8.3x10^4 (Cross-Sectional Views)

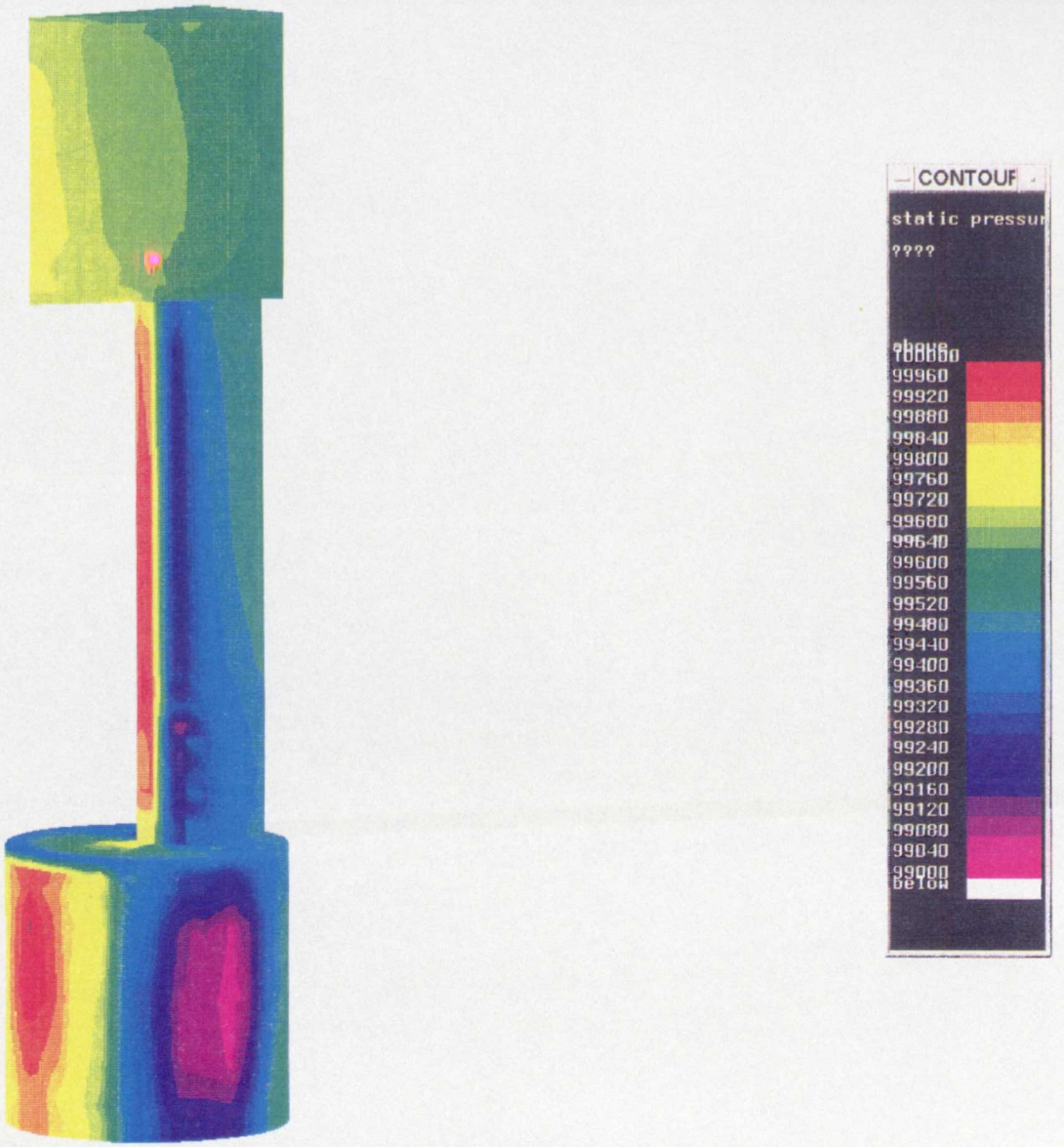

FIGURE 7.44: Surface Static Pressure Variation for Solution of Four Stem Diameters Immersion Case at Re = 8.3×10^4

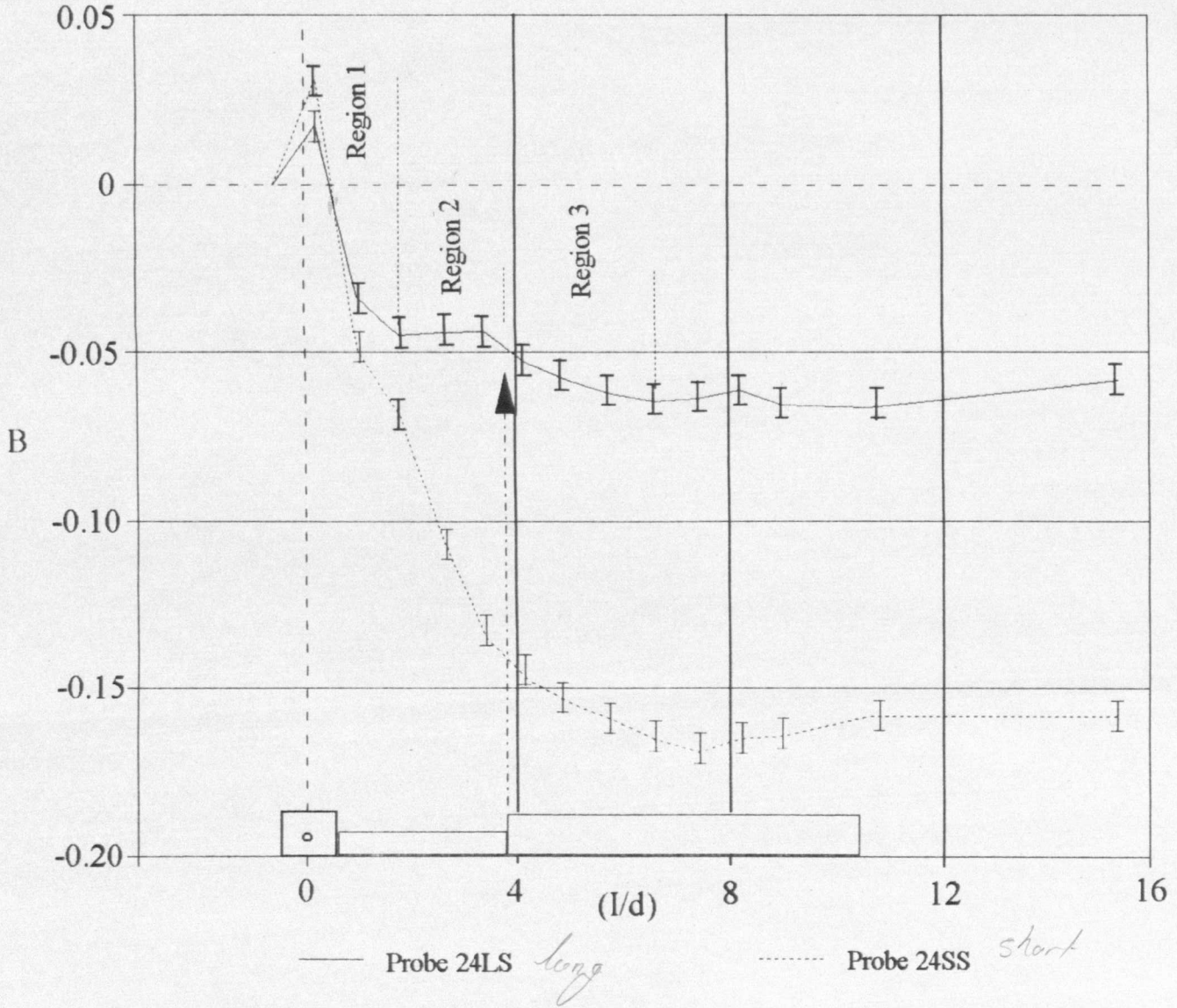

FIGURE 8.1: Influence of Interface Piece Length on Wall Proximity Effect

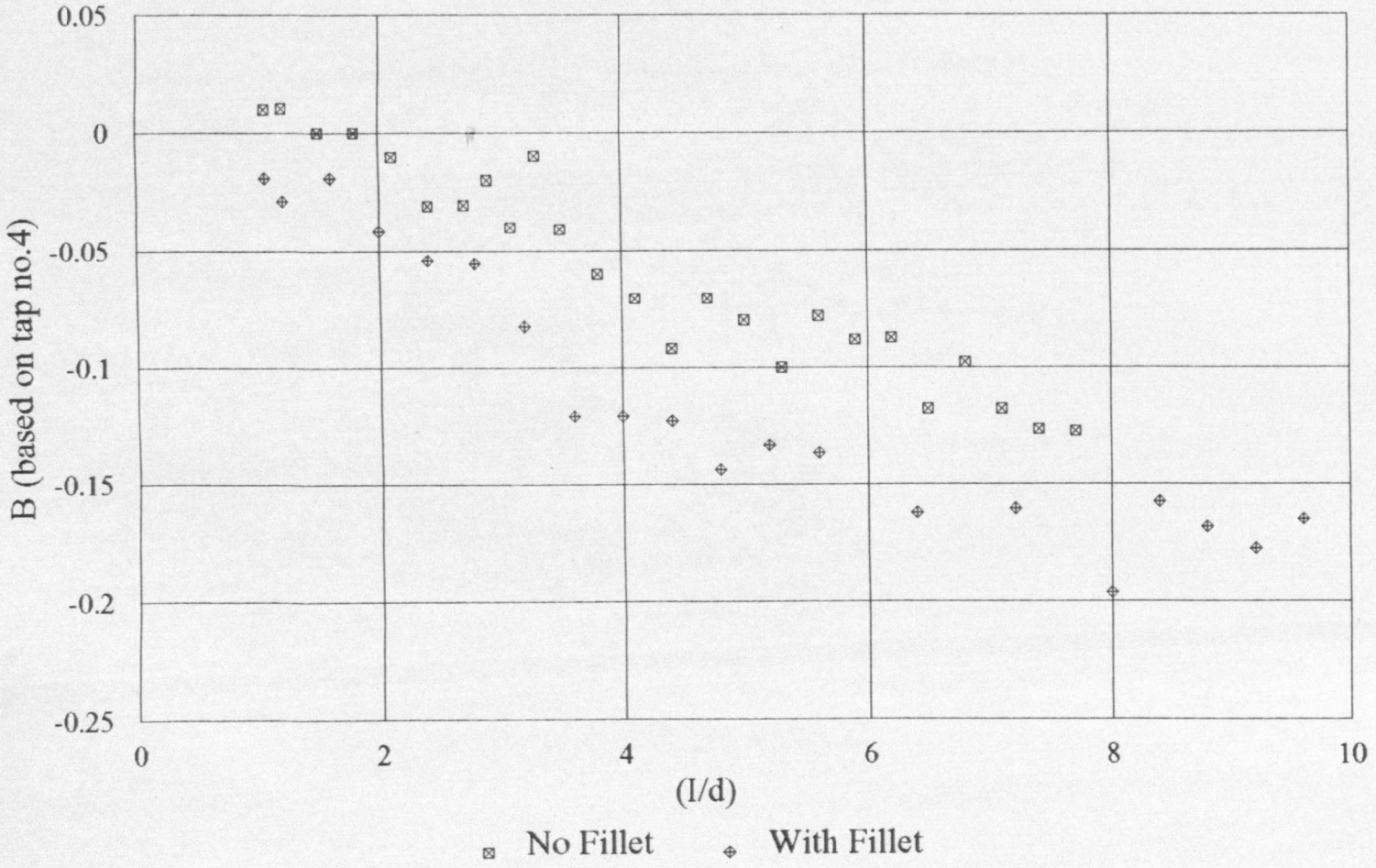

FIGURE 8.2: Wall Proximity Effect for Large Scale Probe Tapping No.4 at 25m/s - With and Without Fillet

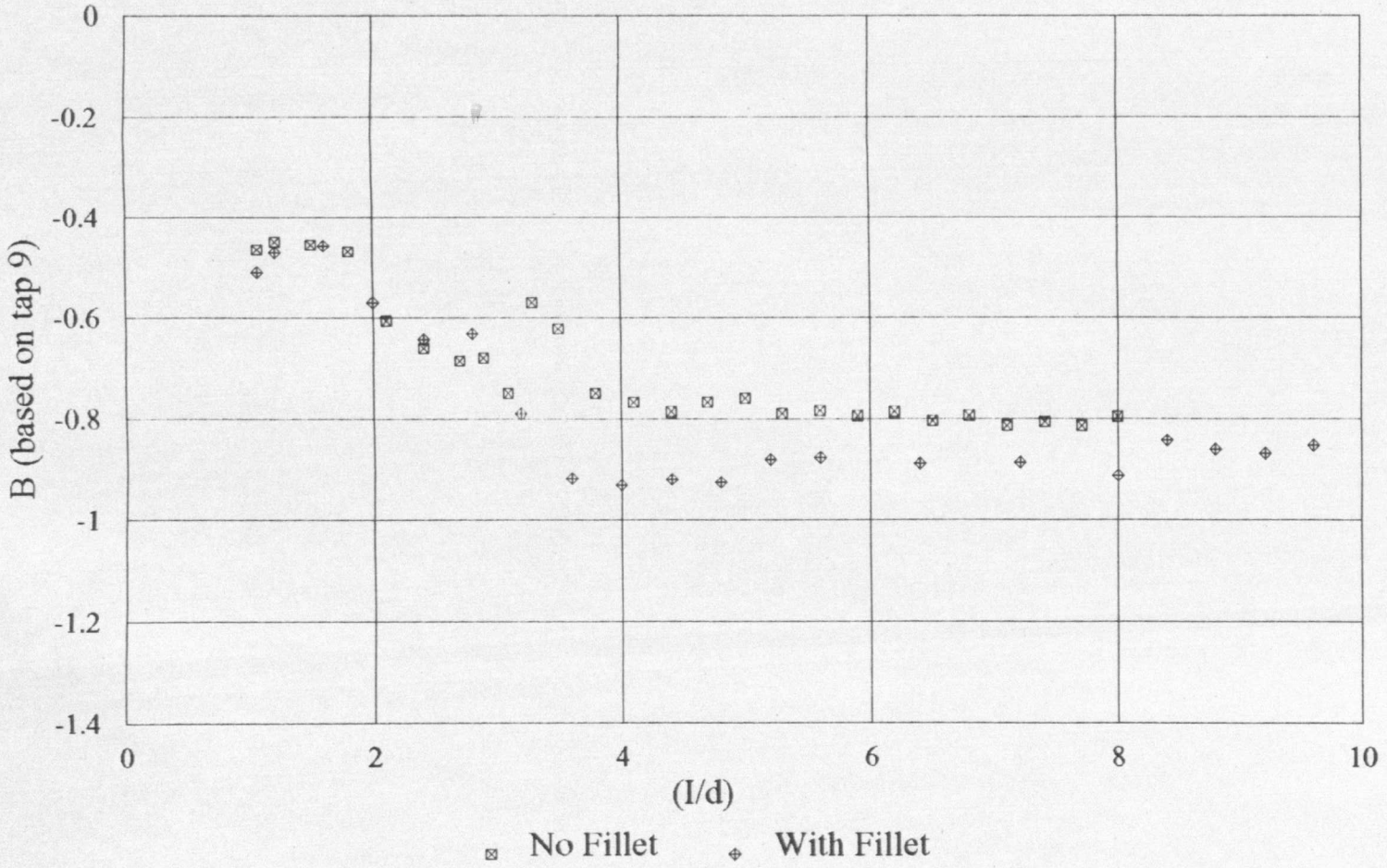

FIGURE 8.3: Wall Proximity Effect for Large Scale Probe Tapping No.9 at 25m/s - With and Without Fillet

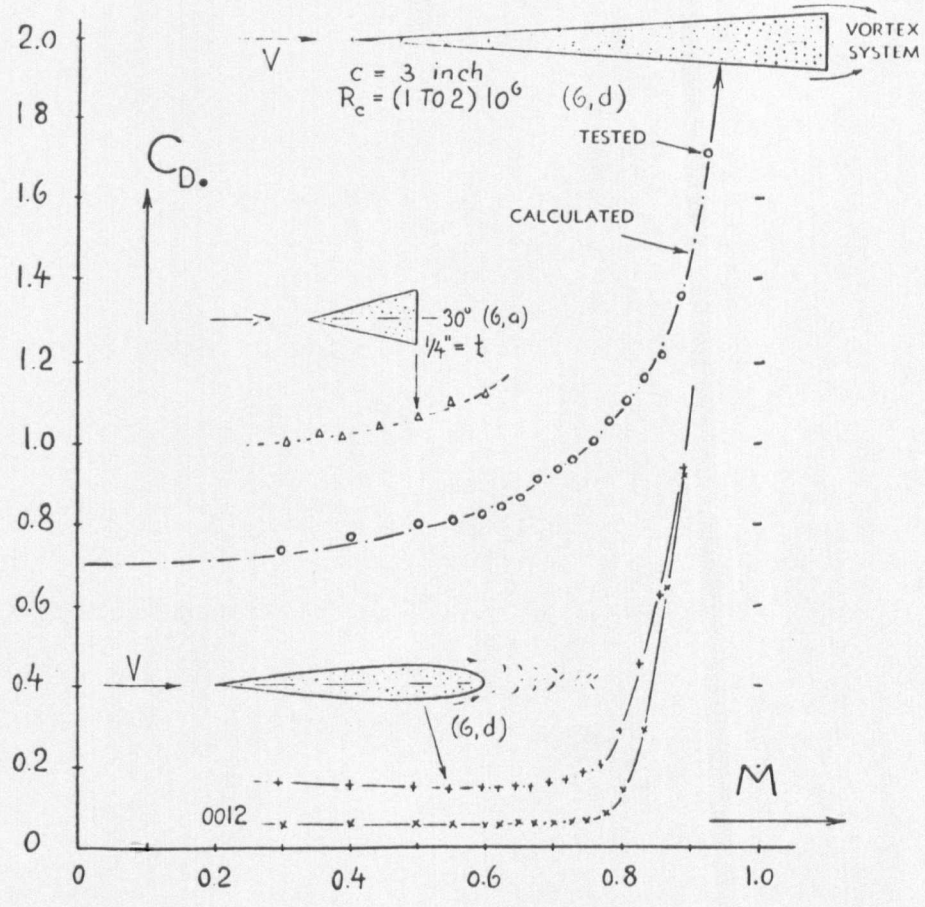

FIGURE 8.4: Wedge Shape Drag Coefficients as a Function of Mach Number (Hoerner, 1965)

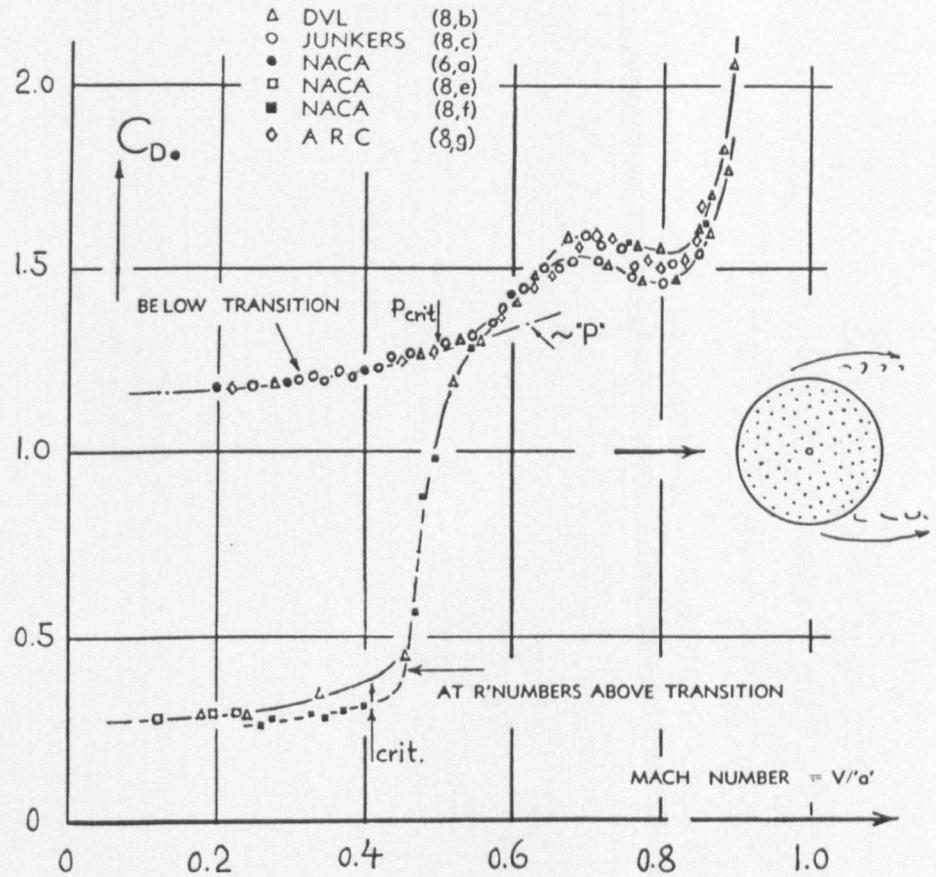

FIGURE 8.5: Circular Cylinder Drag Coefficients as a Function of Mach Number (Hoerner, 1965)

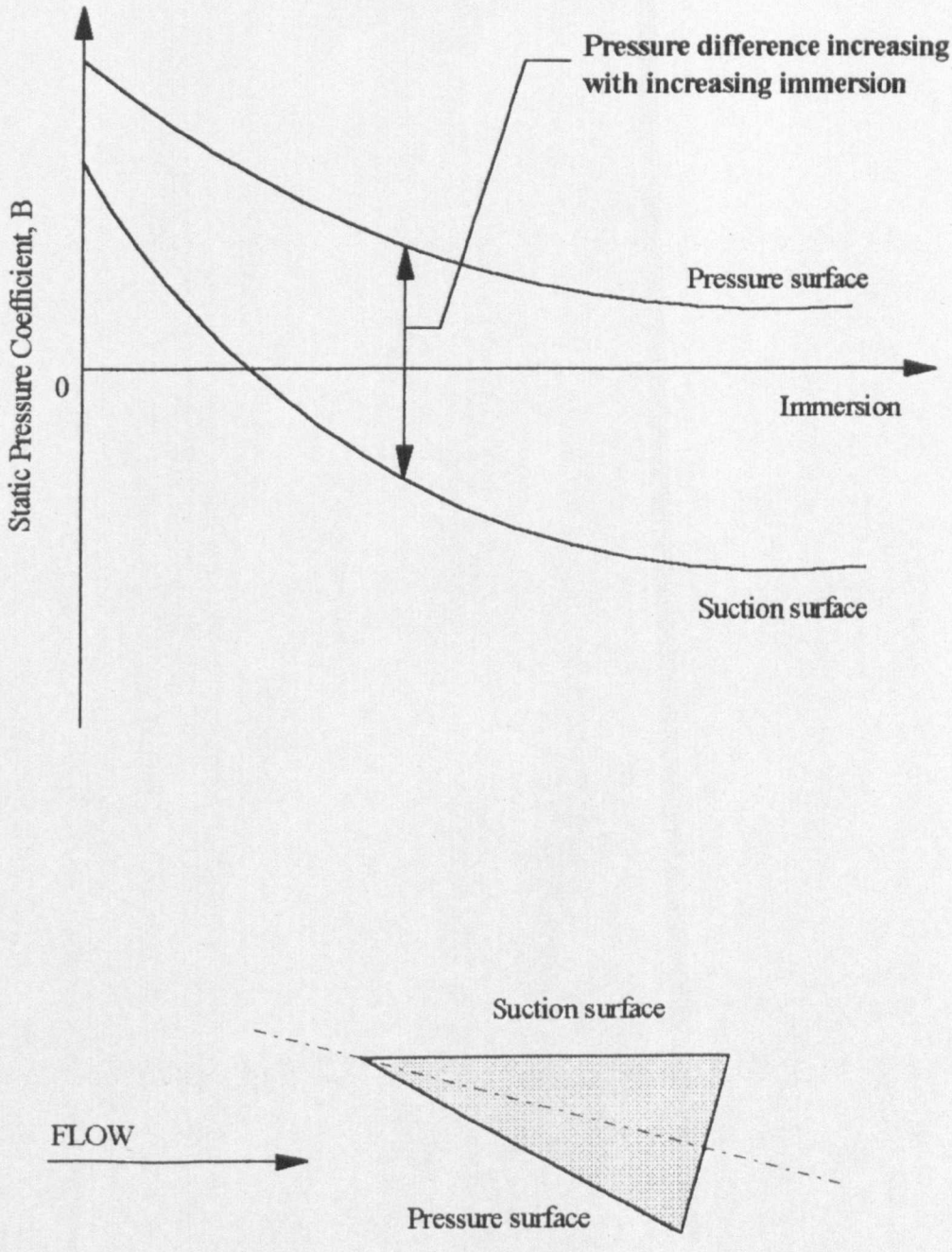

FIGURE 8.6: Static Pressure at Wedge Face Centres; Schematic Representation of Change of Pressure with Immersion

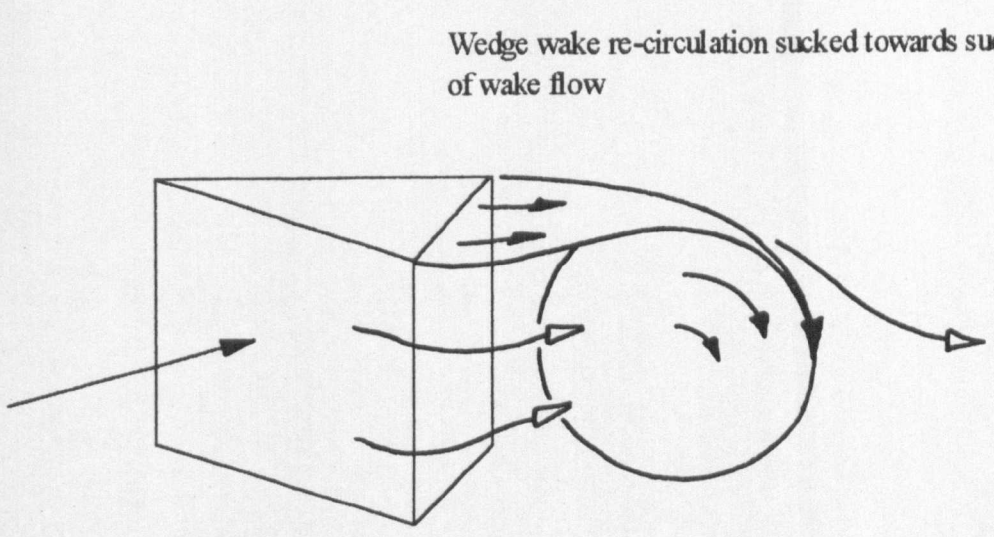

FIGURE 8.7a): Yaw Angle Sensitivity Variation with Immersion - Movement of Wedge Wake Re-circulation

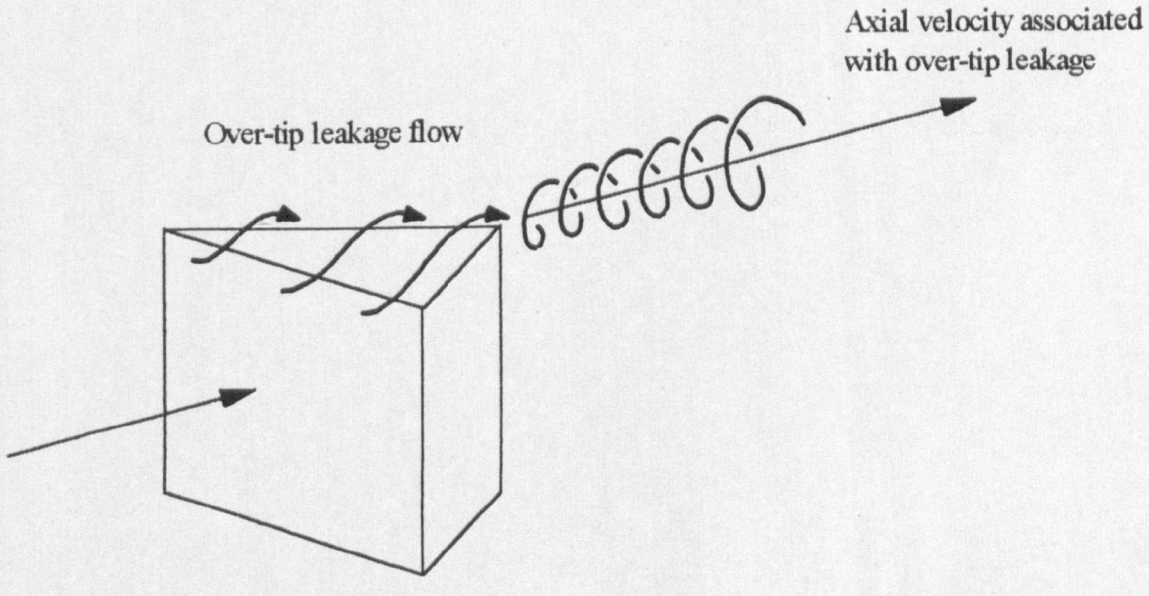

FIGURE 8.7b): Yaw Angle Sensitivity Variation with Immersion - Over-tip Leakage Vortex Formation

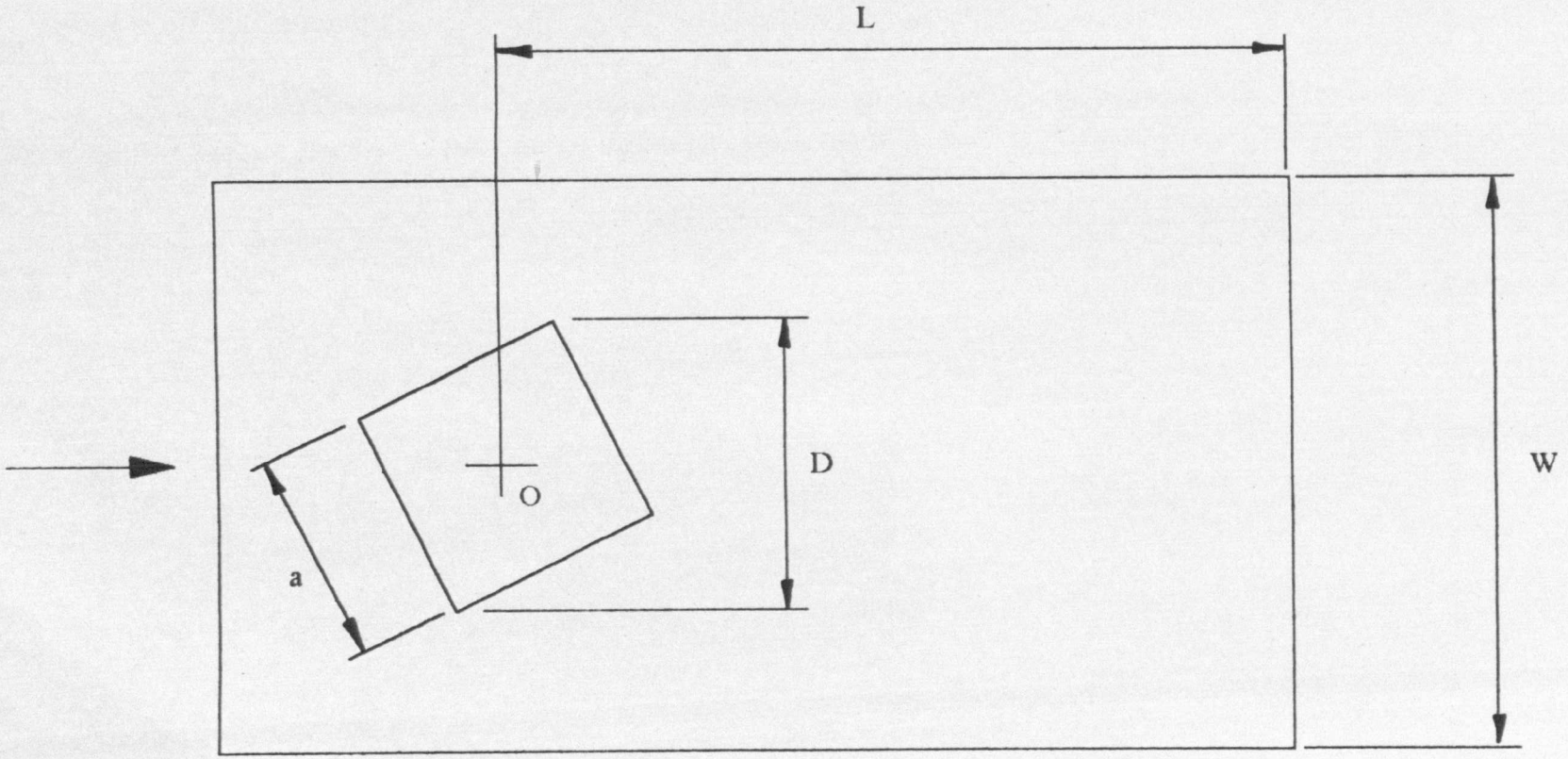

L = 2.5 x Dmax
W = 2.0 x Dmax

FIGURE 8.8: Dimensions Given by Cowdrey (1962) for Square 'Cylinder' End Plates

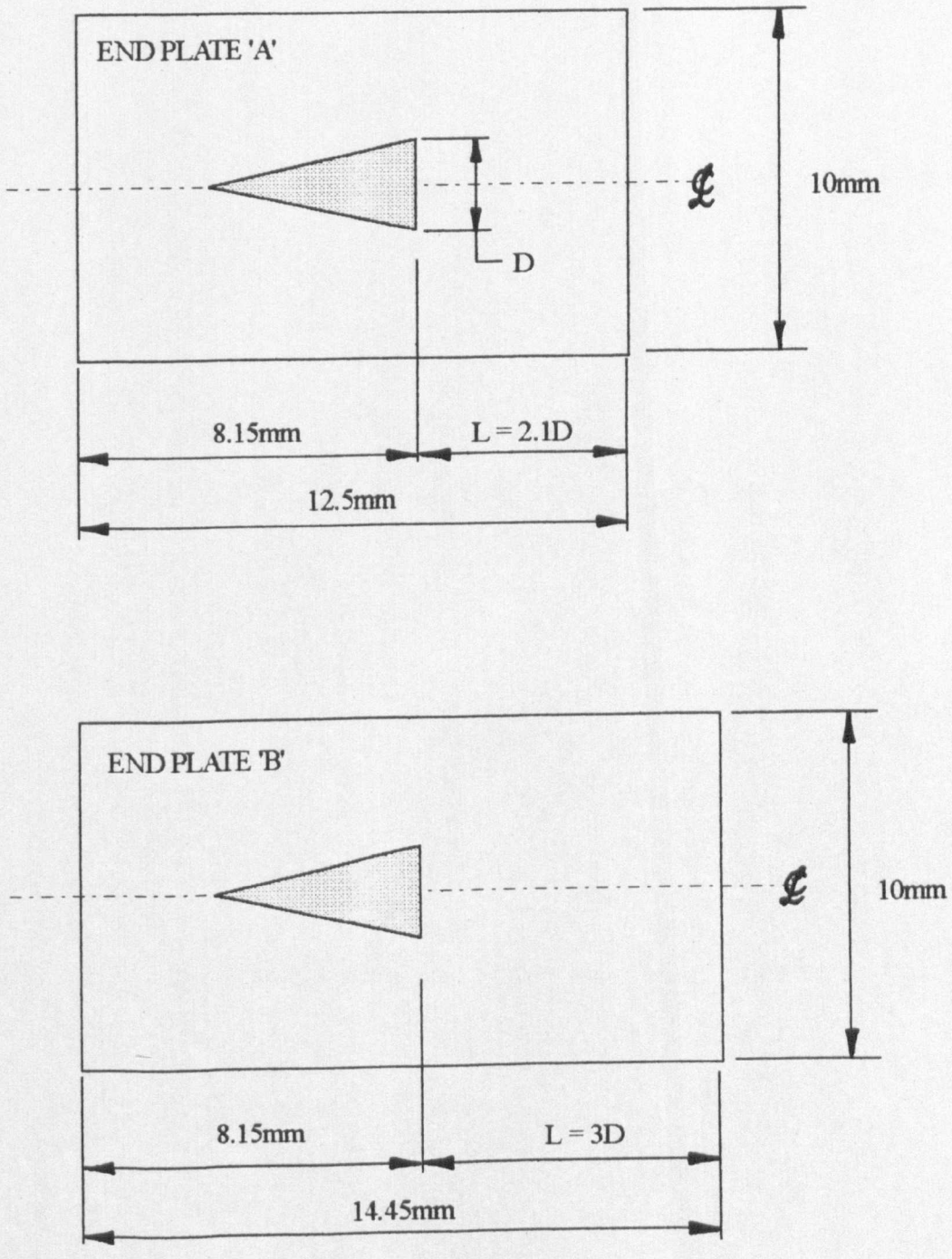

FIGURE 8.9: End Plates 'A' and 'B' used in Actual Probe Tests

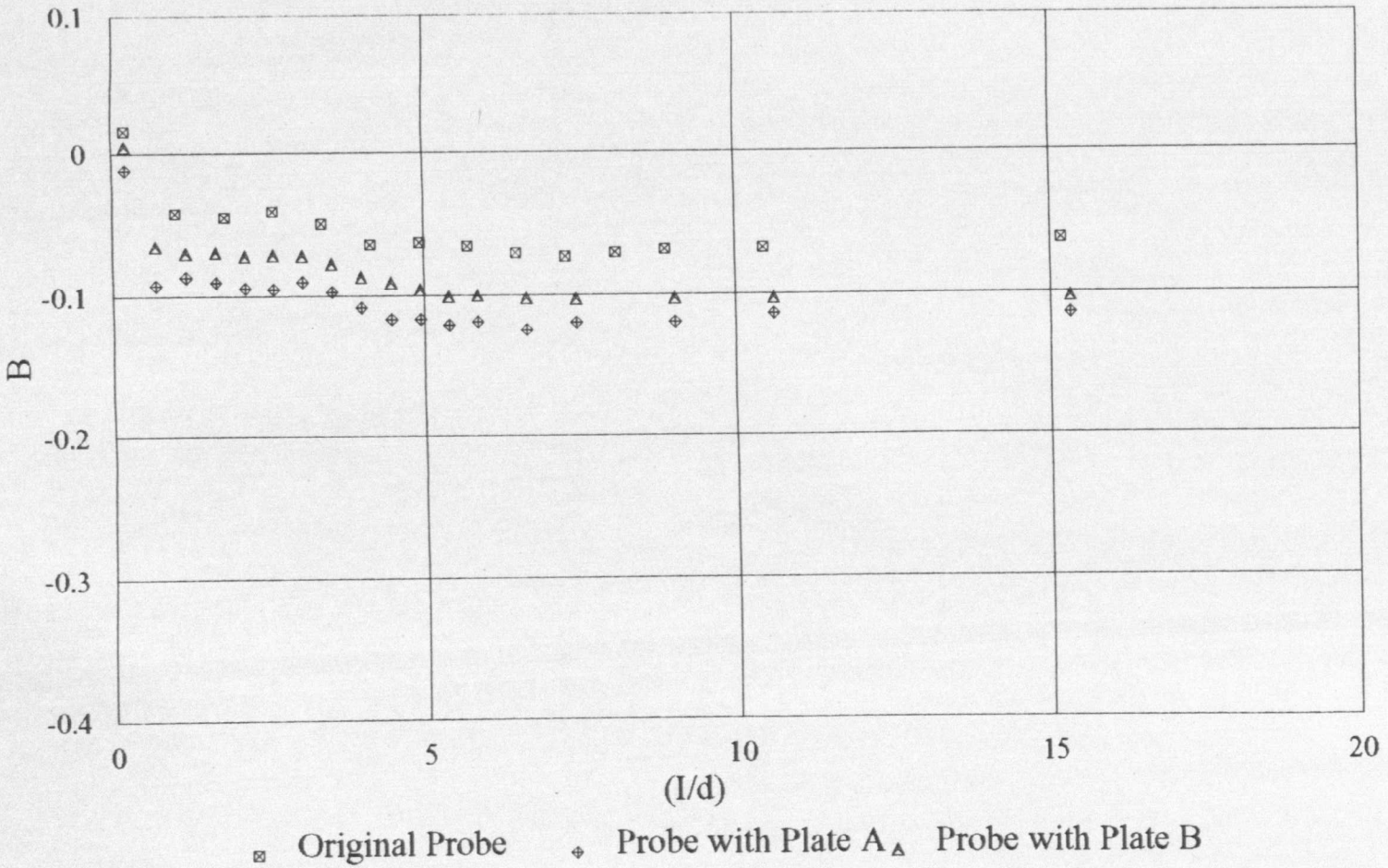

FIGURE 8.10: Result of Applying End Plates to Probe 24LF at 0.35 Mach Number

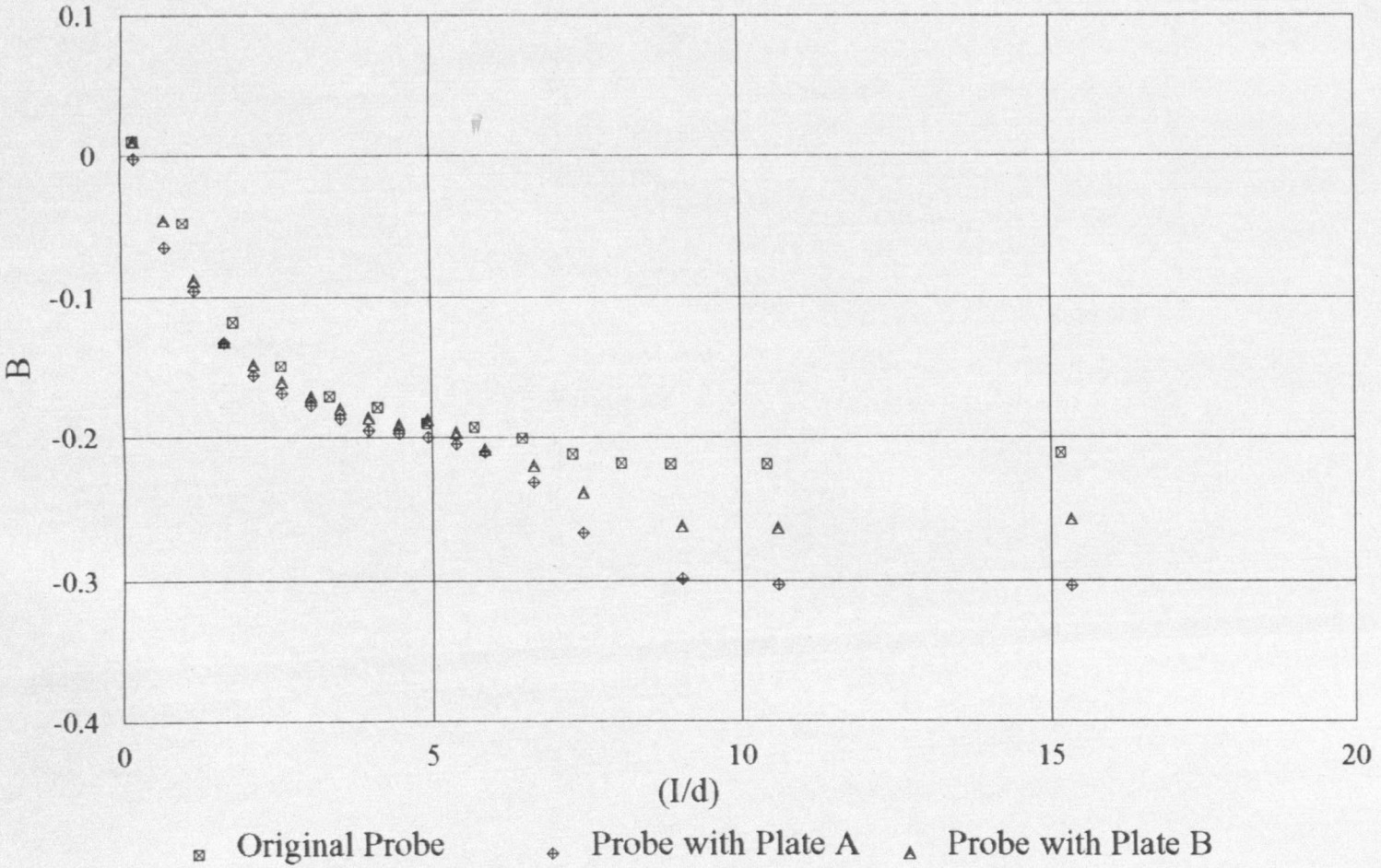

FIGURE 8.11: Result of Applying End Plates to Probe 24SF at 0.35 Mach Number

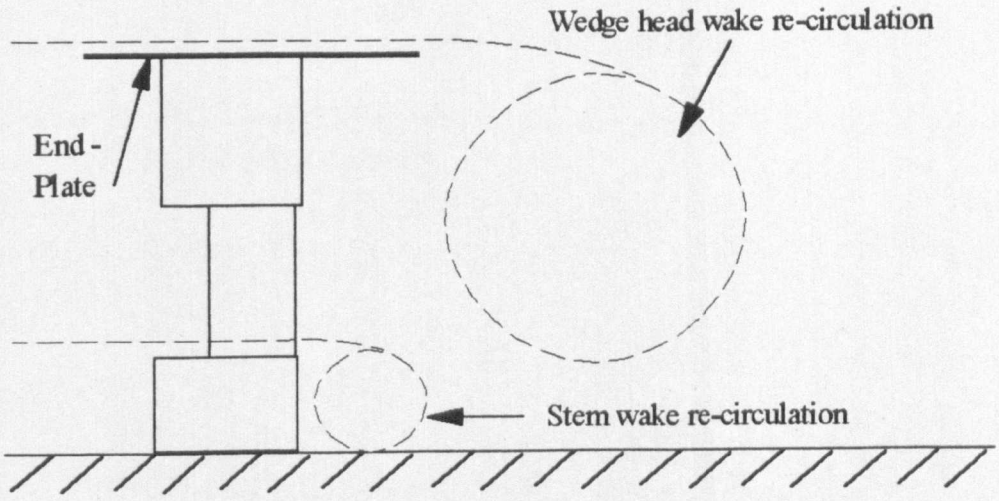

FIGURE 12a): Influence of End Plates on Wedge Head Wake Re-circulation Regions - Low Probe Immersions (<35mm)

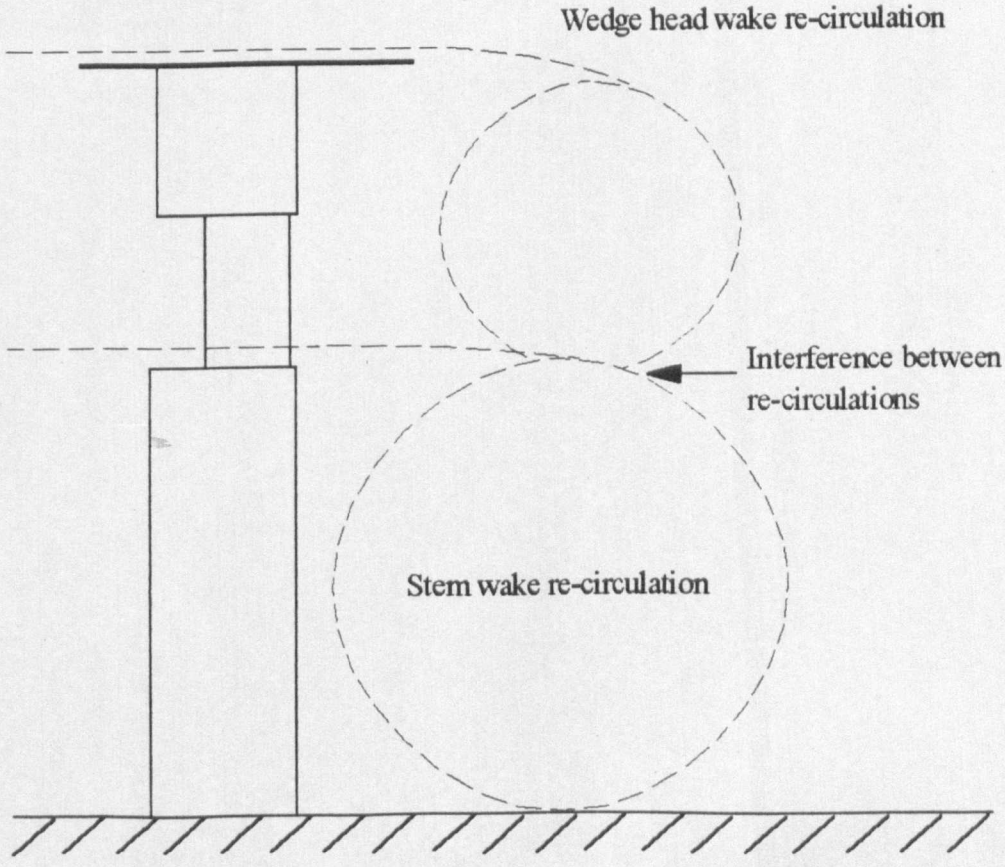

FIGURE 12b): Influence of End Plates on Wedge Head Wake Re-circulation Regions - Higher Probe Immersions (>35mm)

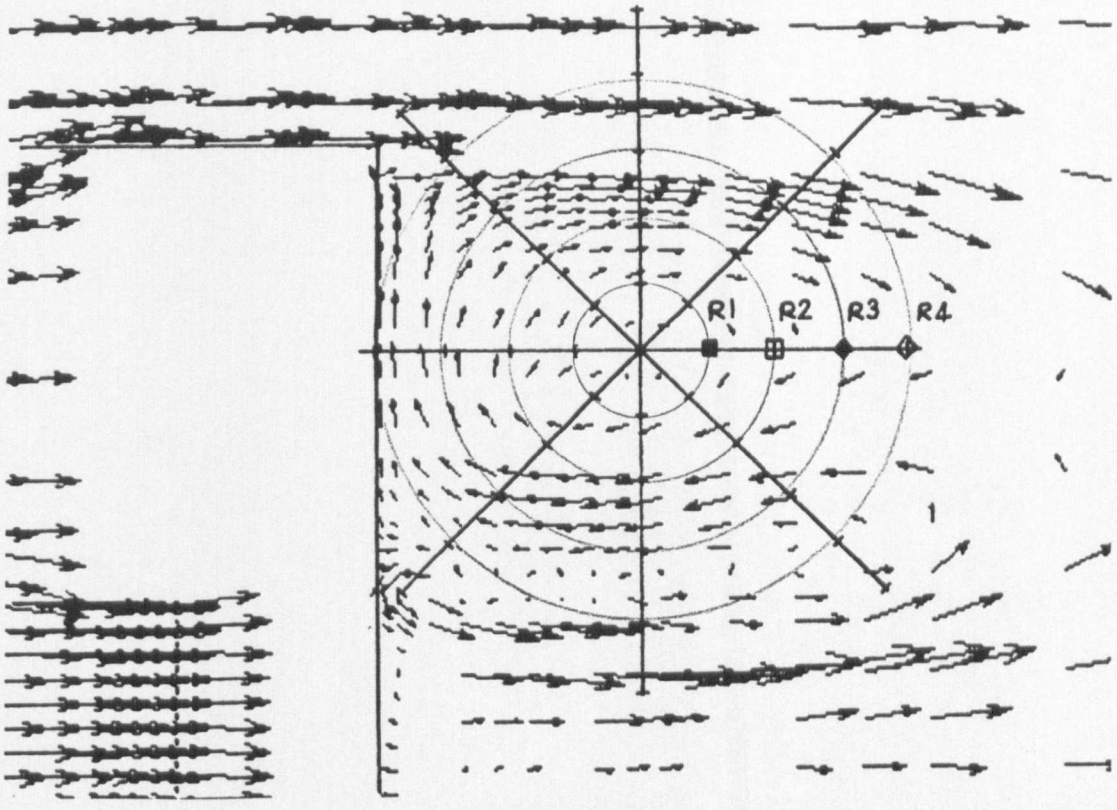

FIGURE 8.13a): Numerically Calculated Velocity Vectors in Wake of Wedge Head

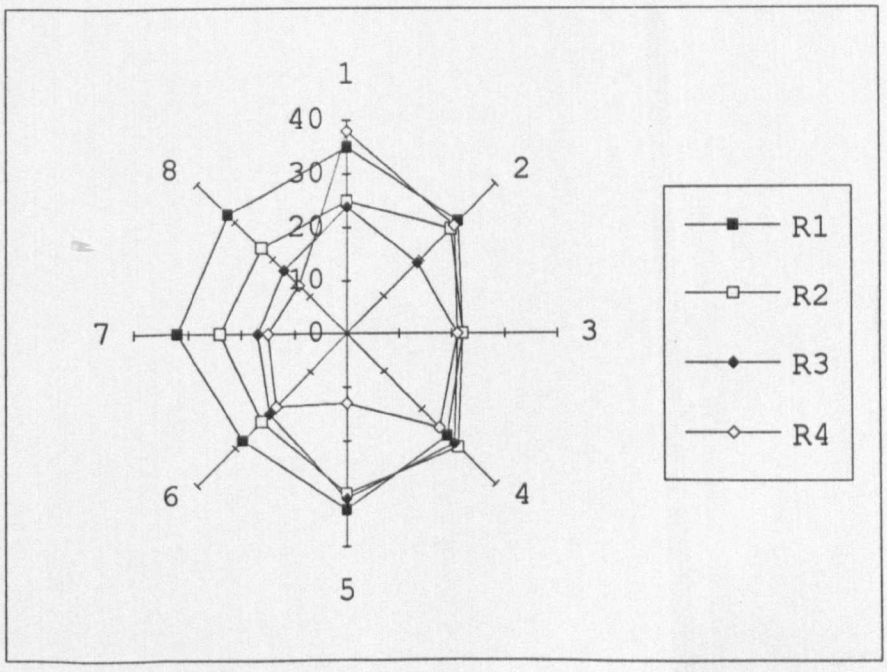

FIGURE 8.13b): Polar Plot of ω on Four Circles Through Re-Circulation

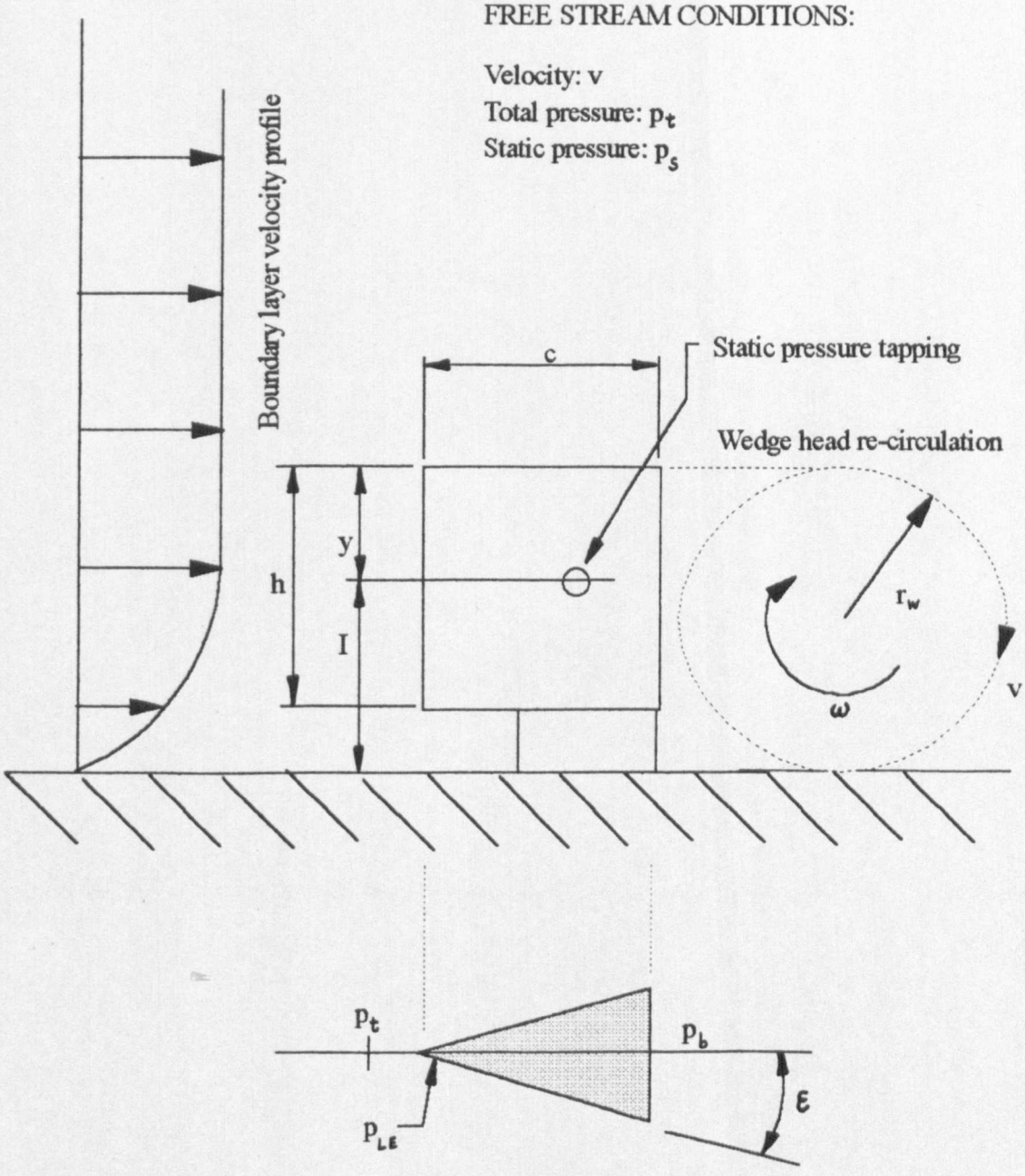

FIGURE 8.14: Schematic Representation of Probe Wedge Head Immersed Through Wall of Introduction

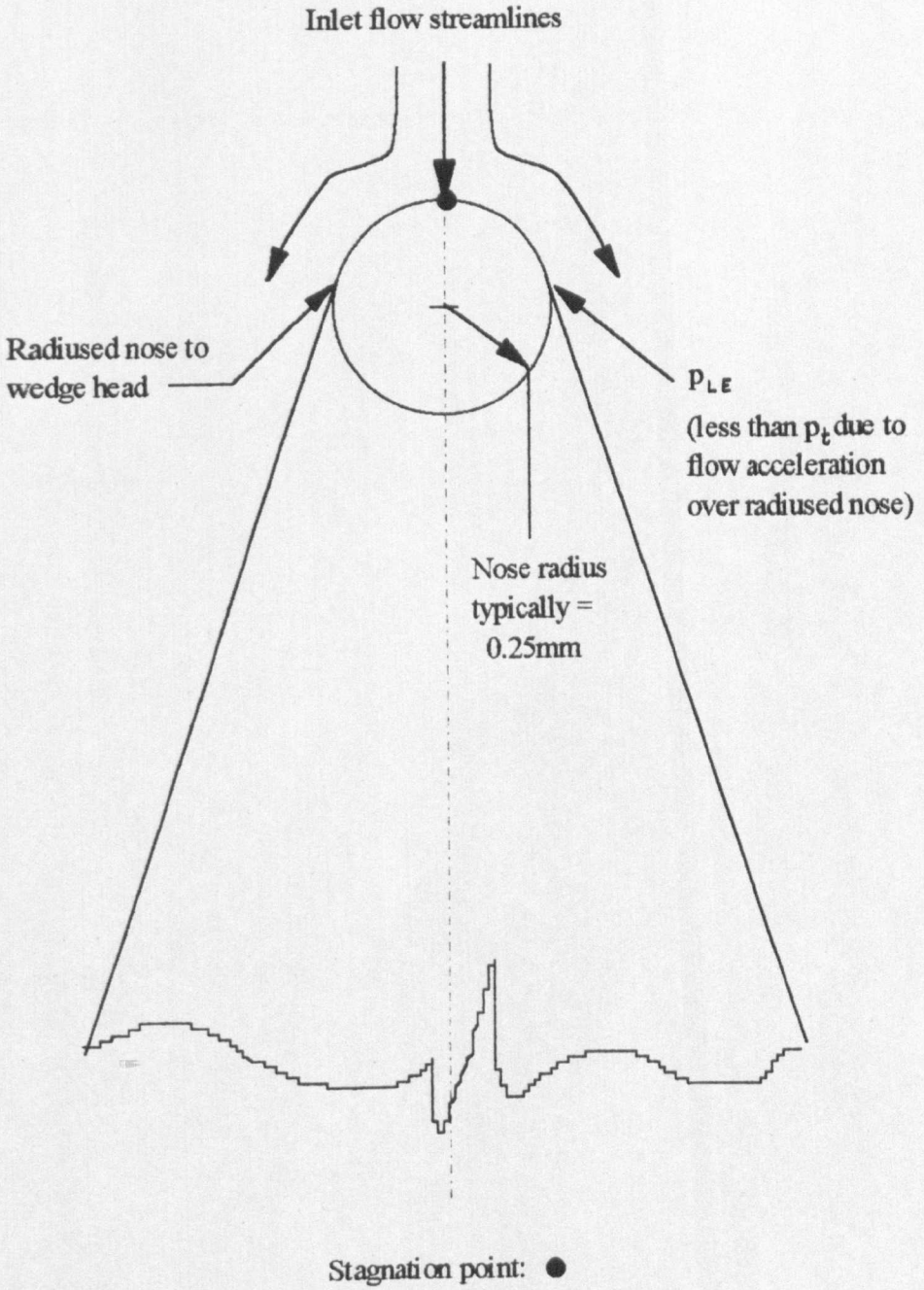

FIGURE 8.15: Detailed View of Wedge Head Leading Edge

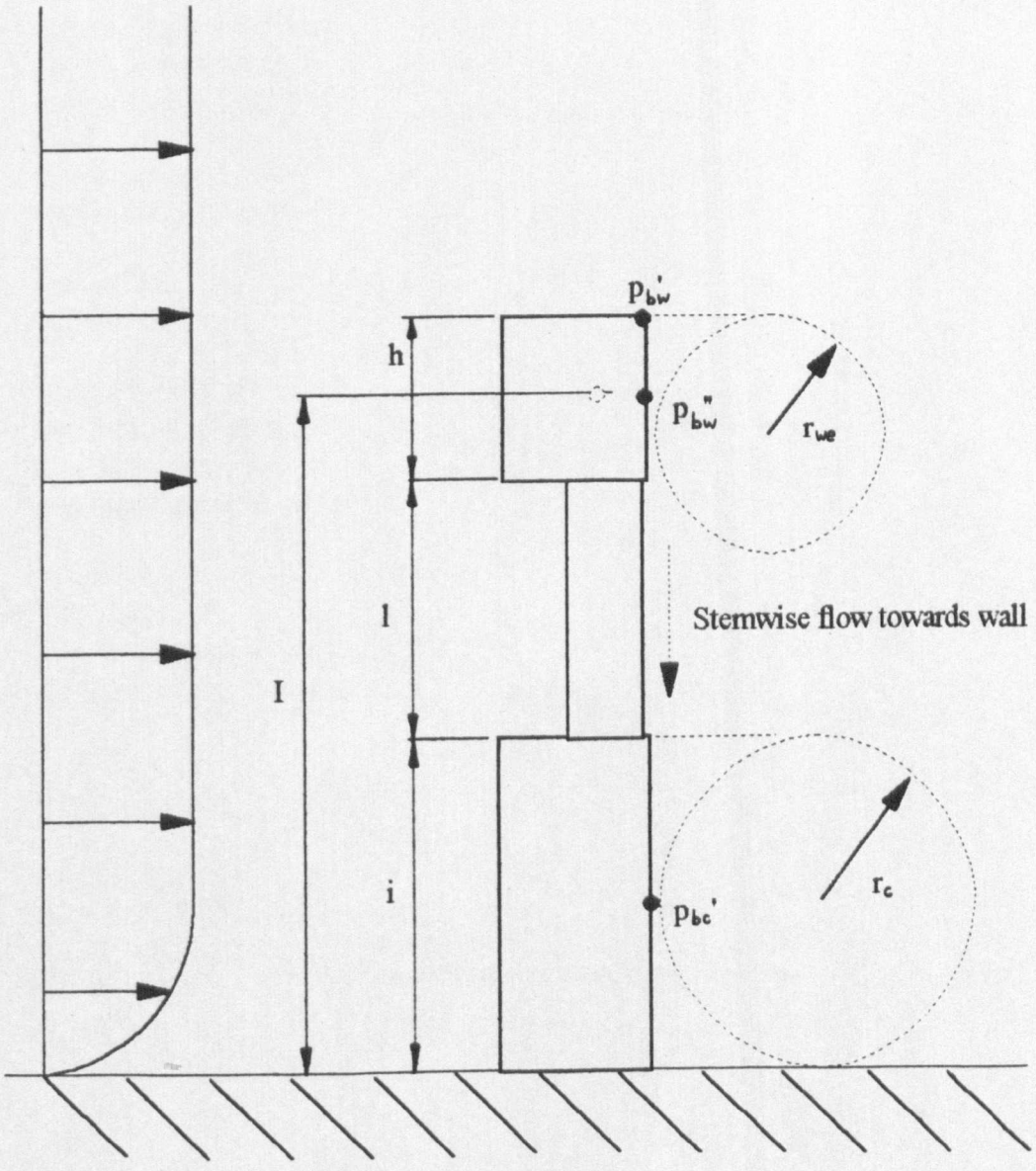

FIGURE 8.16: Schematic Representation of Re-circulating Flow in Wake of Wedge Head and Cylinder

INPUT DATA for Probe 24LS:

Wedge Angle (deg):	24
Wedge Length (mm):	6
Wedge Chord (mm):	5
ps Tap Disp't from Tip (mm):	3
Stem Diameter (mm):	6.35
Interface Length (mm):	20
Wedge Cd:	0.75
Cylinder Cd:	1.4
Free Stream Vel'y (m/s):	119
Free Stream pt (Pa):	100000
Free Stream Tt (K):	288
Boundary Layer d (mm):	2.5
'k' Value:	0.4
'F' Value	0.8
Wedge Vortex Diameter (mm):	12
Cyl. Vortex Diameter (mm):	25

INITIAL CALCULATIONS:

Speed of Sound:	340.23333
Mach Number:	0.34976
Free Stream ps (Pa):	91887.825
Free Stream Ts (K):	281.12196
Density (kg/m3):	1.1384921
Dynamic Head (Pa):	8061.0932

FIGURE 8.17: Example of Input Data to Spreadsheet Embodiment of Analytical Probe Vortex Model

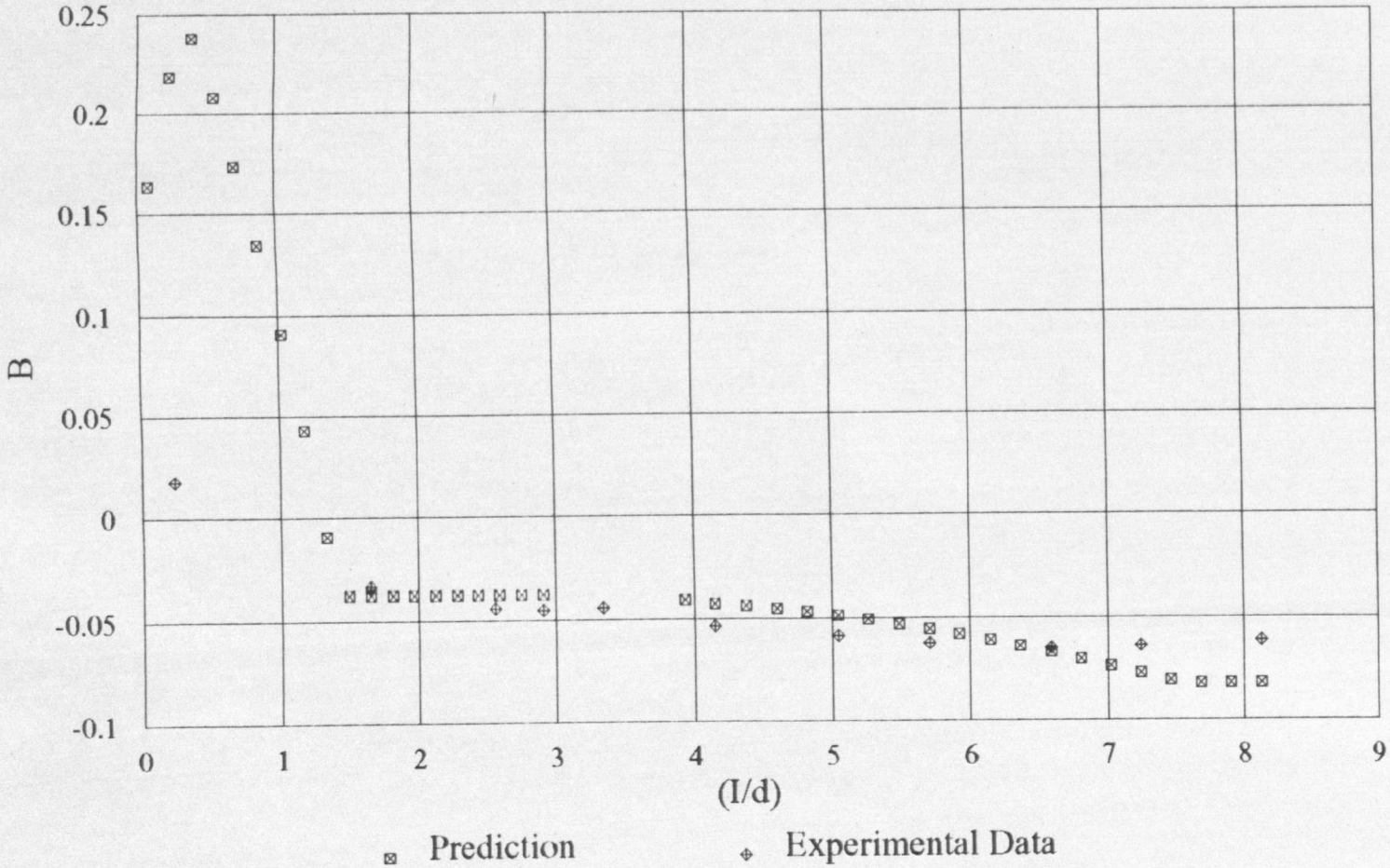

FIGURE 8.18: Comparison Between Analytically Predicted and Experimentally Determined Wall Proximity Curves for Probe 24LS

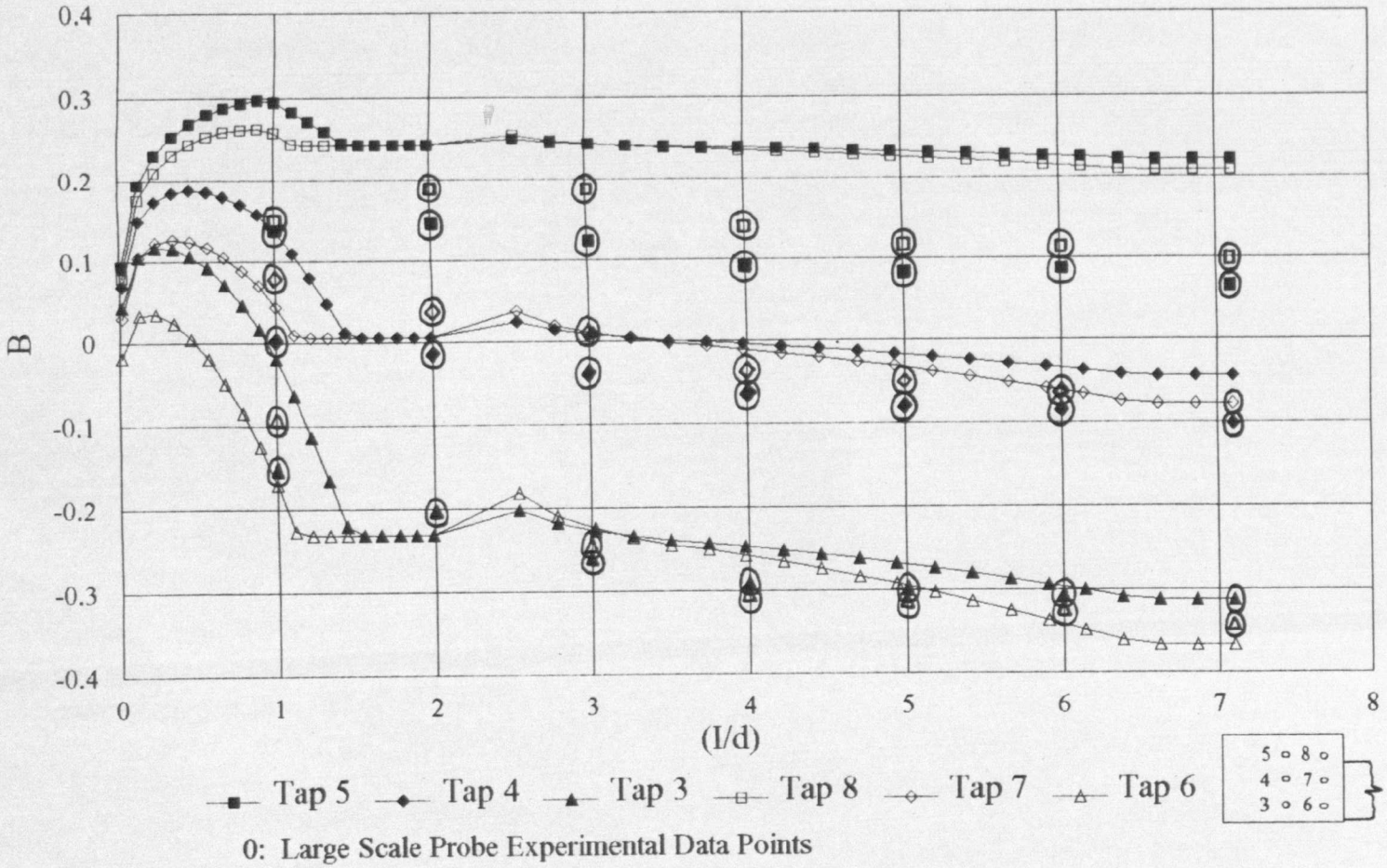

FIGURE 8.19: Comparison Between Analytically Predicted and Experimentally Determined Wall Proximity Curves for Large Scale Probe

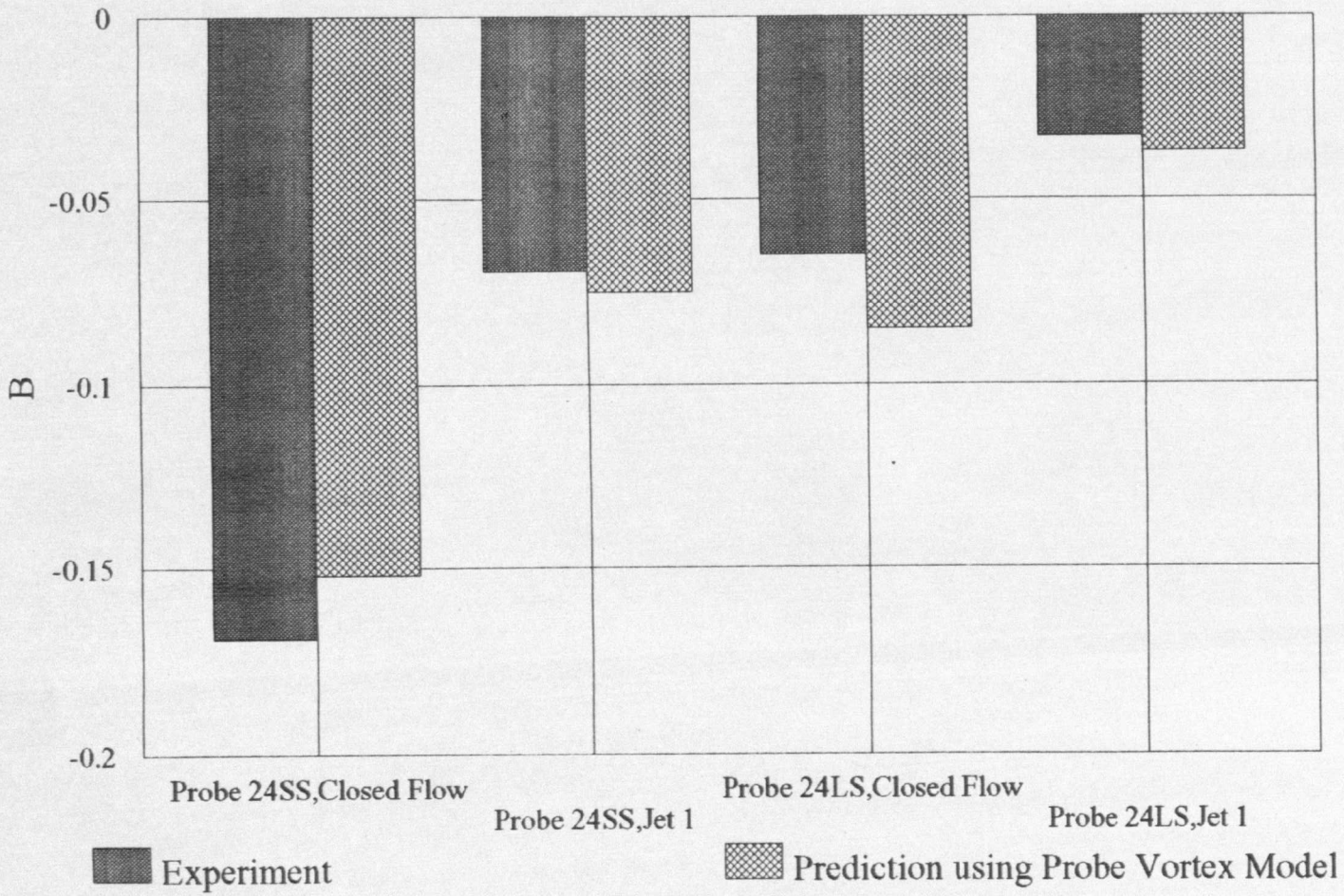

FIGURE 8.20: Comparison Between Analytically Predicted and Experimentally Determined Static Pressure Coefficients for 24° Probes at 0.35 Mach Number

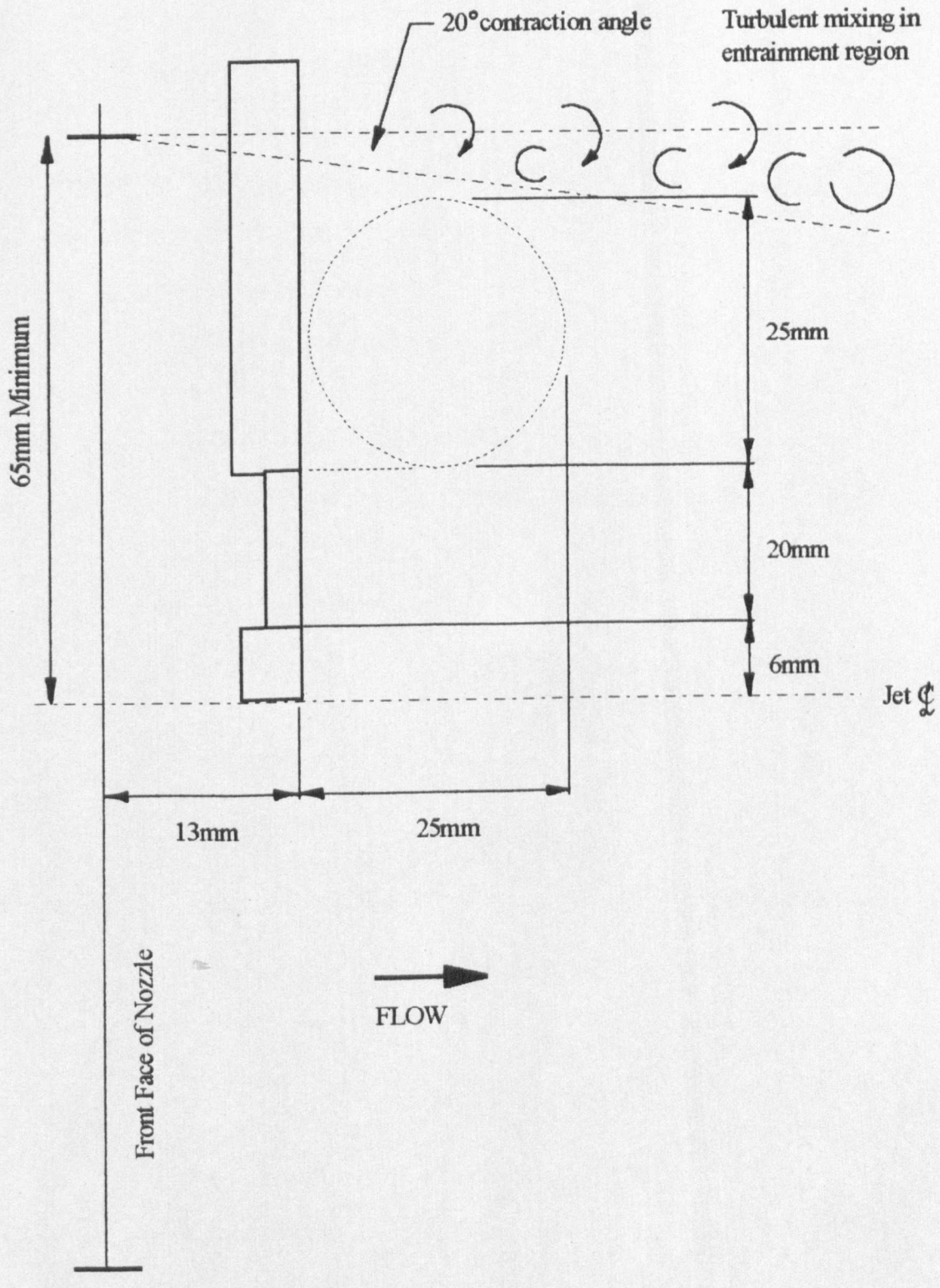

FIGURE 8.21: Sizing of Open Calibration Jet

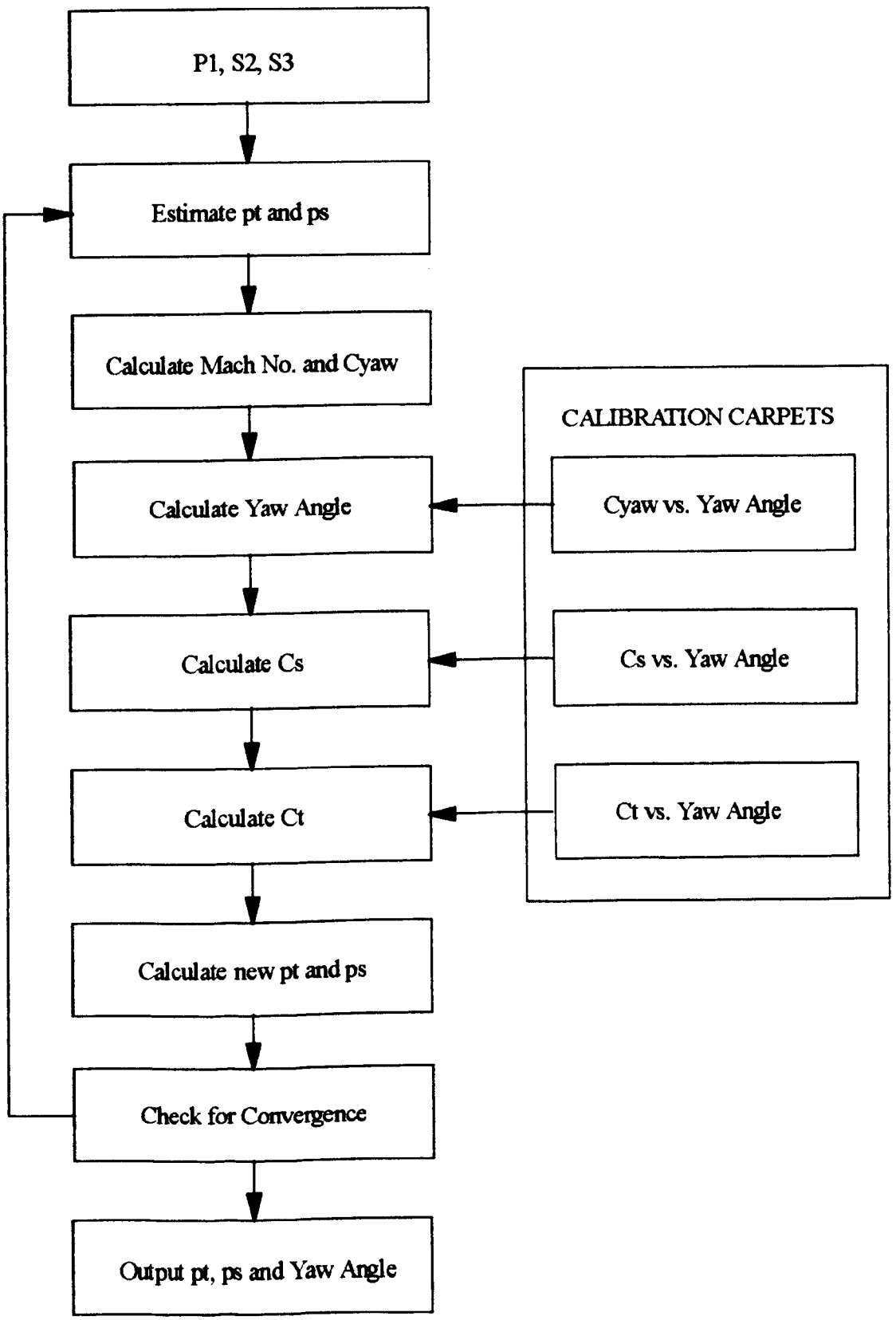

FIGURE 8.22: Wedge Probe Iterative Data Reduction Algorithm

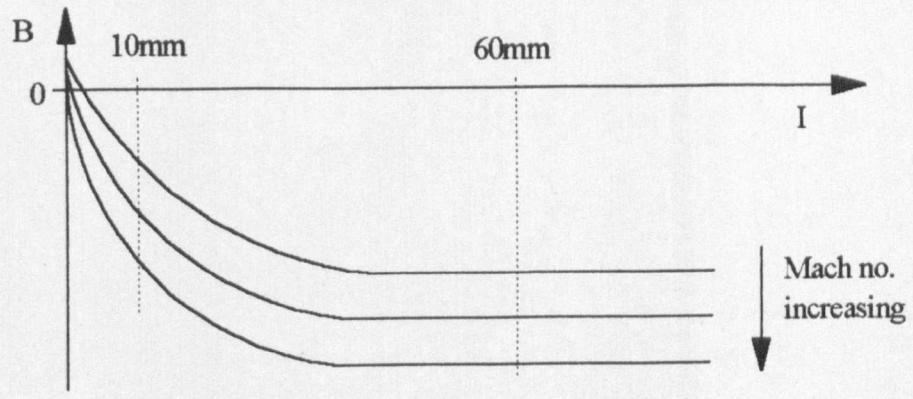

8.23a): Predicted variation of B with immersion at appropriate Mach nos.

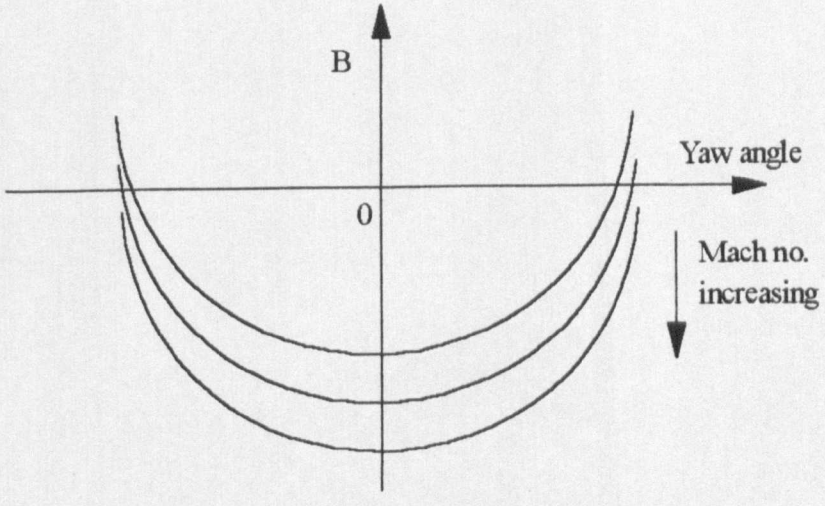

8.23b): Probe calibration against yaw angle at 60mm immersion

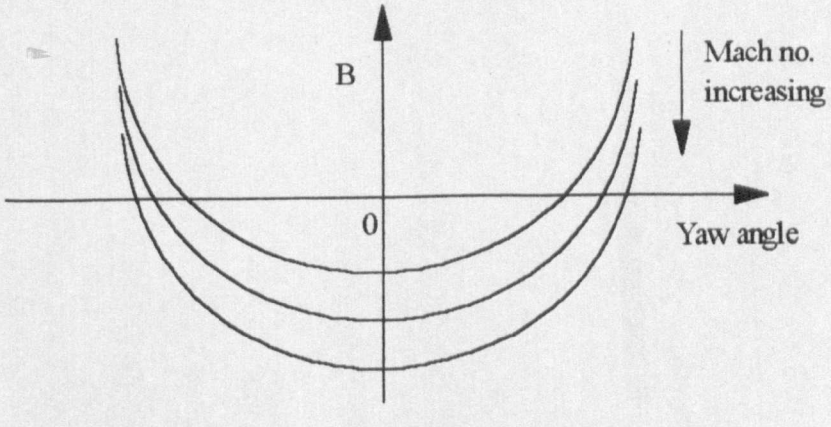

8.23c) Probe calibrations moved up in accordance with figure 8.23a) to appropriate levels for 10mm immersion

FIGURE 8.23: Wall Proximity Effect Correction Method

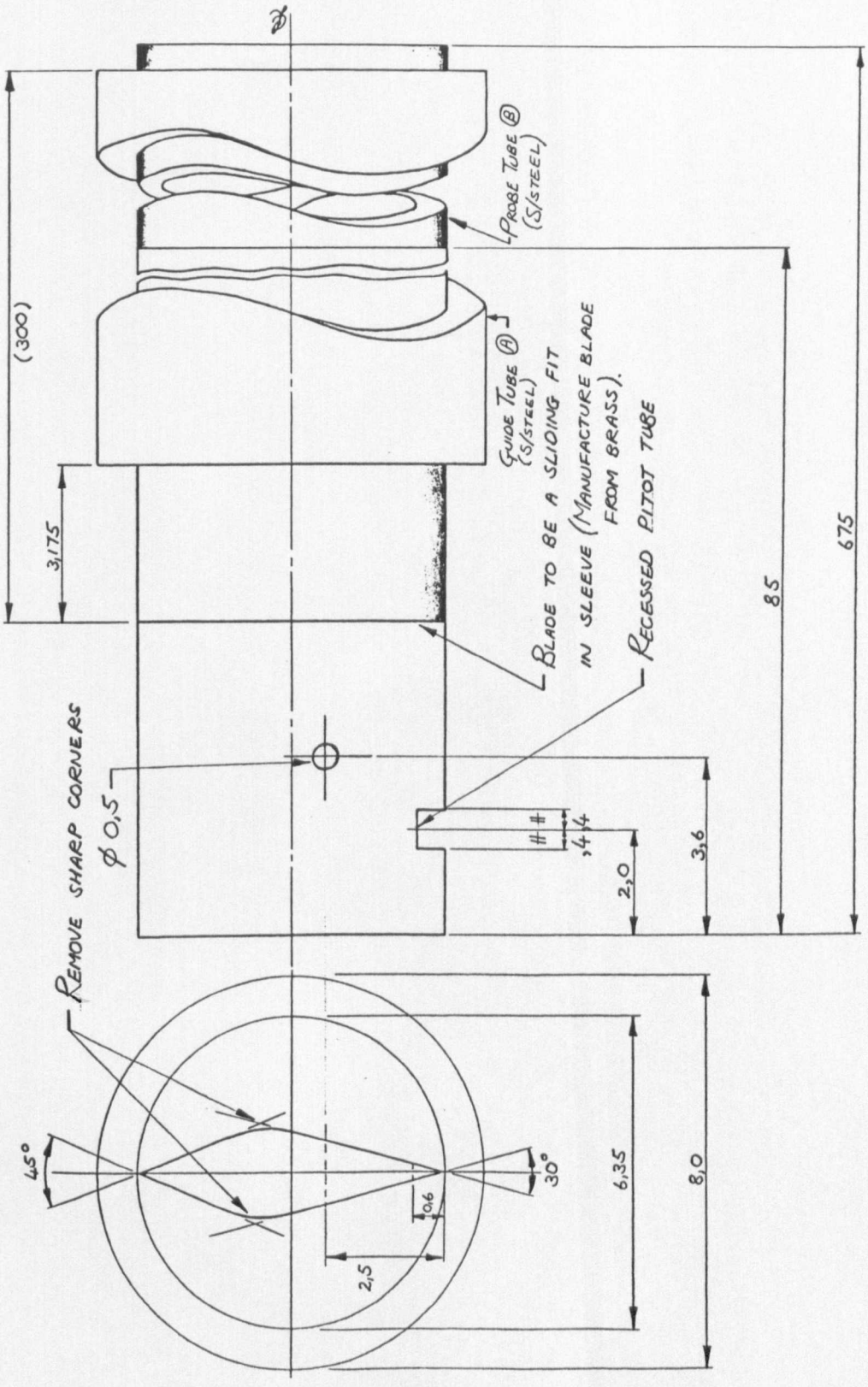

FIGURE 8.24: General Arrangement of New Wedge Probe Design

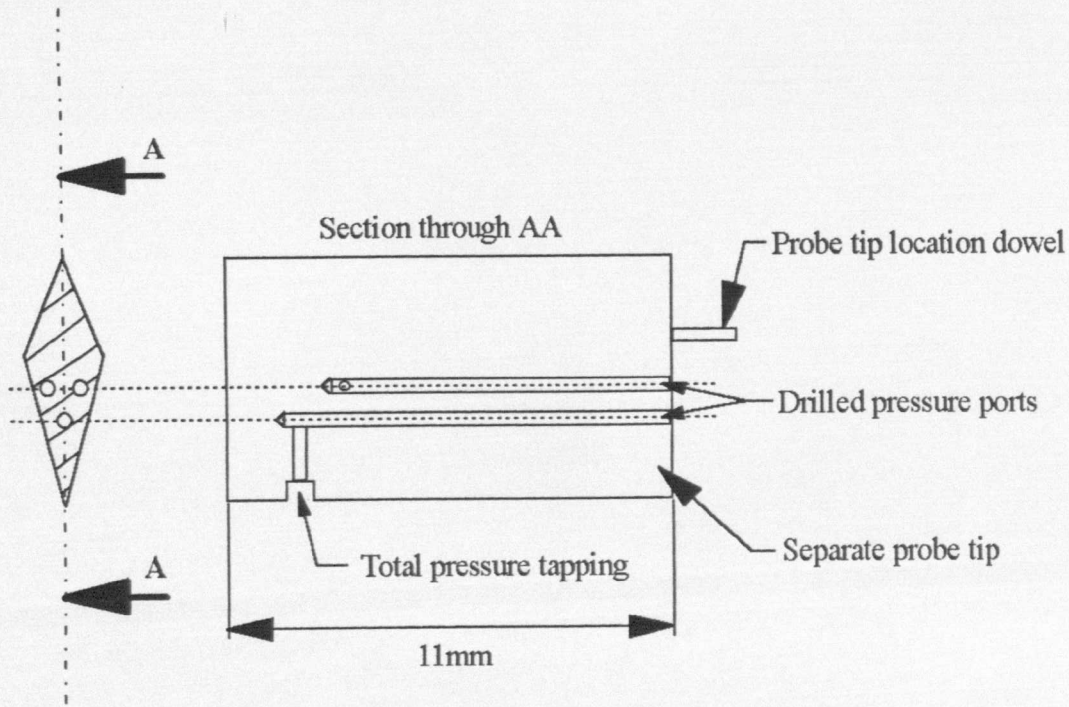

FIGURE 8.25: Detail of New Wedge Probe Tip Design

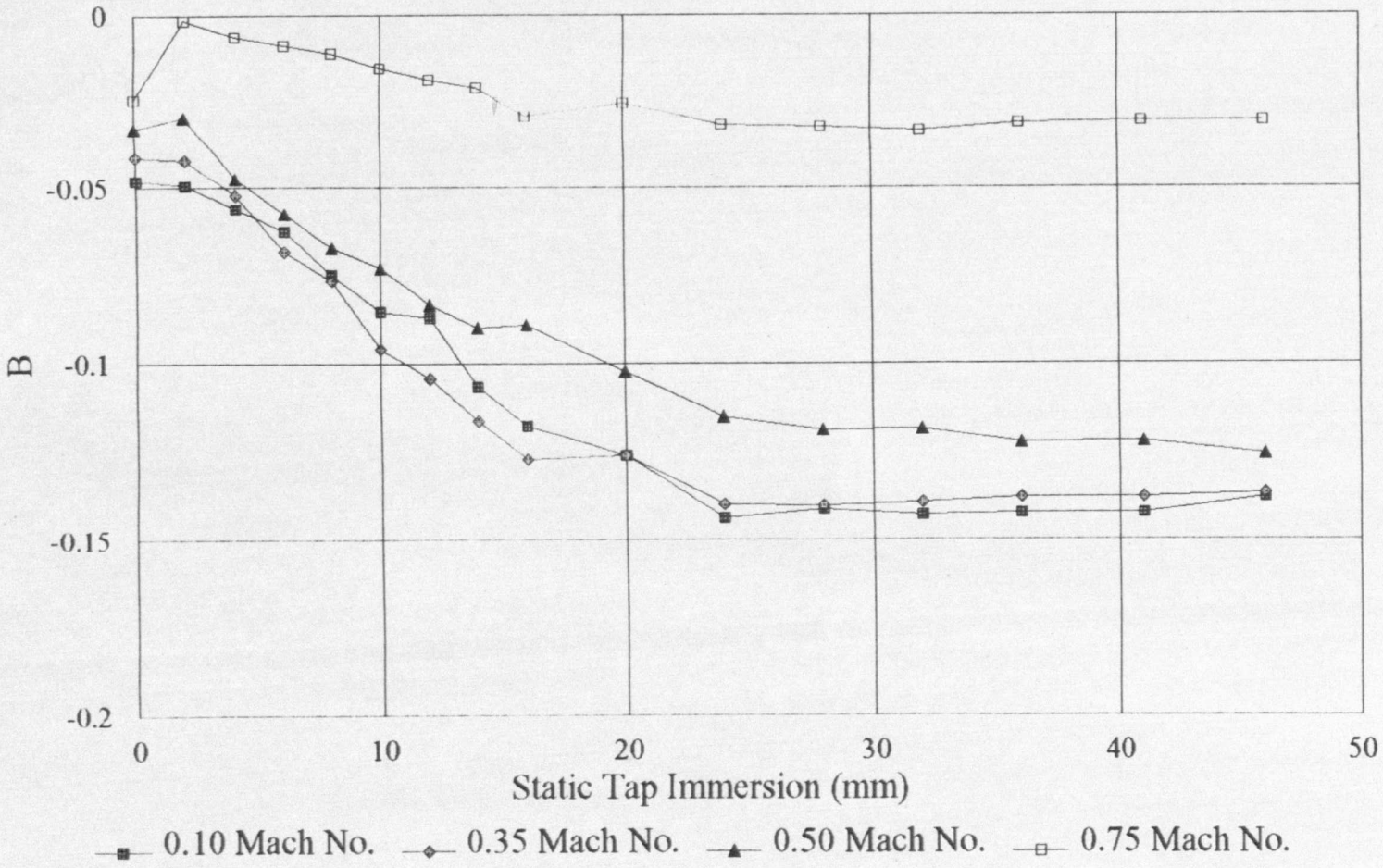

FIGURE 8.26: New Wedge Probe Design Characterisation at Four Mach Numbers

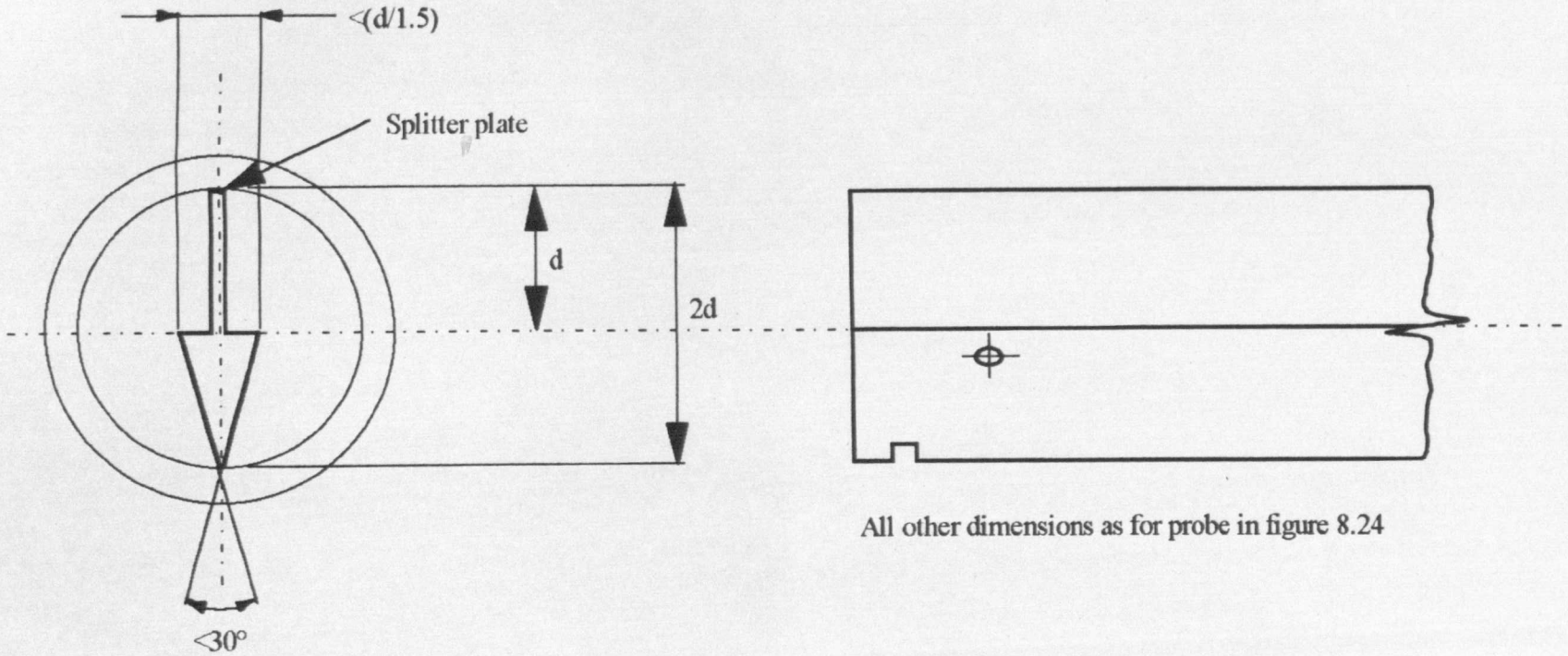

FIGURE 10.1: Alternative 'Splitter-Plate' Wedge Probe Design Proposal

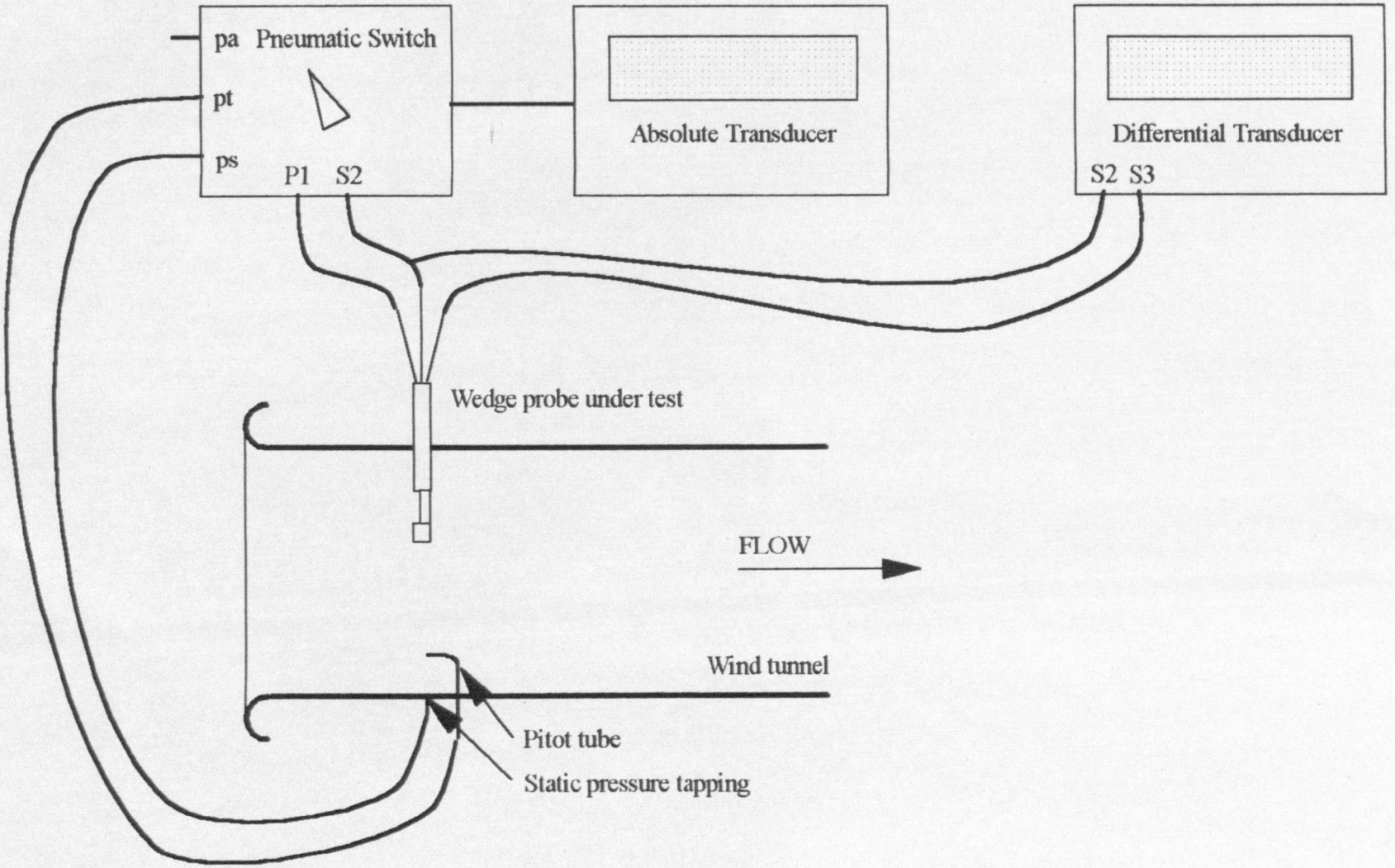

FIGURE E.1: Experimental Arrangement of Transducers for Test Reported in Chapter 5.